SENSORLESS FIELD ORIENTED CONTROL OF BRUSHLESS PERMANENT
MAGNET SYNCHRONOUS MOTORS

by

JAMES ROBERT MEVEY

B.S., Kansas State University, 2006

A REPORT

submitted in partial fulfillment of the requirements for the degree

MASTER OF SCIENCE

Department of Electrical and Computer Engineering
College of Engineering

KANSAS STATE UNIVERSITY
Manhattan, Kansas

2009

Approved by:

Major Professor
James E. DeVault

Abstract

Working with the subject of sensorless motor control requires an understanding of several topical areas; this report presents an understanding that was gained during this research work. The fundamentals of electric motors (particularly brushless motors) are developed from first principles and the basic models are discussed. The theory of sinusoidal synchronous motors is reviewed (phasor analysis of the single phase equivalent circuit). The concept of a complex space vector is introduced and developed using a working knowledge of the sinusoidal synchronous motor. This leads to the presentation of the space vector model of the permanent magnet synchronous motor, in both the stationary and rotor reference frames. An overview of the operation of three-phase voltage source inverters is given, followed by an explanation of space vector modulation and its relationship to regular sinusoidal pulse width modulation. Torque control of the permanent magnet synchronous machine is reviewed in several reference frames and then rotor-flux-field-oriented-control is explained. Finally, some schemes for sensorless operation are discussed.

Table of Contents

List of Figures

List of Tables

List of Symbols

Symbol	Meaning	Units
D	diameter	[m]
Y	length	[m]
G	airgap length	[m]
b	friction	[N·m·s/(rad)]
J	inertia	[kg·m^2]
v	applied voltage	[V]
g	total induced EMF	[V]
e	back-EMF	[V]
i	current	[A]
R	reluctance	[A(·turn)/Wb] = [1/H]
R	resistance	[ohm]
L,M	inductance	[H] = [Wb/ A(·turn)]
f,F	MMF	[A(·turn)]
λ	stator flux linkage	[Wb(·turn)]
ψ_S	component of stator flux linkage due to stator current (stator self flux linkage)	[Wb(·turn)]
ψ_R	component of stator flux linkage due to rotor flux (rotor-stator flux linkage)	[Wb(·turn)]
φ, Φ	flux	[Wb]
B	flux density	[Wb/m^2] = [T]
H	magnetic field strength	[A/m]
μ	magnetic permeability	[H/m]
T	torque (developed electromechanical)	[N·m]
T$_L$	load toque	[N·m]
t	time	[s]

Symbol	Meaning	Units
δ	torque angle	[(rad)] or [deg]
ξ	angle of arbitrary space vector	[(rad)] or [deg]
θ_r	rotor angle	[(rad)] or [deg]
θ	angle around stator	[(rad)] or [deg]
ω	angular velocity	[(rad)/s]
f_e	electrical frequency	[Hz]
P	poles (= P/2 pole pairs)	
N_{rpm}	mechanical shaft speed	[rev/min]
N	total number of winding turns	[(turns)]
N_e	number of effective winding turns for sinusoidal winding	[(turns)]
k	space vector scaling constant	
K_t	per-phase torque constant	[N·m/ A_{peak}]
K_e	per-phase back-EMF constant	[V_{peak}/ (rad)/s]
K_T	total torque constant	various dimensions
x	general quantity; dynamic state	

Units in parenthesis are implied. In general, functions are represented by a lowercase letter; constant and total values are represented with an uppercase letter, though some exceptions must exist.

Abbreviations

ACIM   AC induction motor

BPMS   brushless permanent magnet synchronous

ECM   electronically commutated motor

PM   permanent magnet

DTC   direct torque control

FOC   field oriented control

SV   space vector

SVM   space vector modulation

VVVF   variable voltage variable frequency

VSI   voltage source inverter

PWM   pulse width modulation

SPE   single-phase equivalent

MSC   method of symmetrical components

LTV   linear transformation of variables

bEMF   back electromotive force

MMF   magnetomotive force

PS   positive-sequence

NS   negative-sequence

ZS   zero-sequence

Nomenclature

Notation

$\tilde{V}_a$	phasor
$\vec{v}_A$	space vector
$\overline{V}$	average quantity
V_A	DC quantity
v_A	total instantaneous quantity
V_p	peak quantity; amplitude of sinewave
$\hat{V}$	magnitude of space vector
$\mathbf{V}$	matrix
$\mathbf{v}$	vector
$\hat{\mathbf{v}}$	estimated vector
$\mathbf{d},\mathbf{q}$	unit vectors for rotating reference frame
$\boldsymbol{\alpha},\boldsymbol{\beta}$	unit vectors for stationary reference frame
$\mathbf{a},\mathbf{b},\mathbf{c}$	unit vectors for phase-variables
$\boldsymbol{\mu}$	unit vector for general magnetic axis

Operators

$(\cdot)^*$	complex conjugation
j	imaginary unit sqrt(−1)
ρ	time-derivative operator d/dt; also denoted with superscribed •
a	spatial or time advance operator ($a = e^{j\frac{2\pi}{3}} = e^{j120^\circ} = e^{j\gamma}$)
$(\cdot)^{\mathrm{T}}$	transpose

<u>Superscripts</u>

*	commanded value
ref	reference value
R	variable described in the rotor reference frame
S	variable described in the stator reference frame

<u>Subscripts</u>

N	neutral (star) point of motor
M	midpoint of DC bus
R	quantity related to the rotor
S	quantity related to the stator
s	synchronous
ℓ	leakage
mag	magnetizing
d,q	**d** (direct) axis component, **q** (quadrature) axis component
α,β	**α** axis component, **β** axis component
a,b,c, A,B,C	**a** axis component, **b** axis component, **c** axis component

<u>Matrices</u>

$\mathbf{C},\mathbf{C}^{-1}$	Clarke transform, inverse Clarke transform
$\mathbf{C}_0$	Clarke transform with zero sequence (i.e., αβ0 transform)
$\mathbf{P}$, $\mathbf{P}^{-1}$	Park transform, inverse Park transform (i.e., Givens rotation)
$\mathbf{Z}$	impedance matrix
$\mathbf{Q}$	phase interference matrix
$\mathbf{A}$	symmetrical component transformation matrix
$\mathbf{A},\mathbf{B},\mathbf{C}$	state space matrices: system, input, output
$\mathbf{K},\mathbf{L}$	state space gain matrices: feedback, observer

Acknowledgements

I am greatly indebted to my major professor Jim DeVault for offering his guidance through the various challenges encountered in completing this degree, handling each situation with candor and tact. His organizational skills and technical thoroughness are second to none, and his labs and lectures have served as an exemplary model of true engineering brilliance whose importance to me cannot be described. I am grateful to John Devore for his gusto and originality in teaching and for his endeavors to constantly improve lectures, even though they are already tops. With every lecture or discussion I learn that there is always a simpler and better algorithm than what I have in mind, and that there is always one more trick in bit twiddling that I would have never discovered on my own. I am very appreciative of Chris Lewis for understanding that asking 'dumb questions' is sometimes the best way to learn, and for having the patience to endure countless such questions about controls. I had already taken the controls course prior to his joining our department, but in seeing some of his material and in knowing that he teaches real-world controls backed by experience, I cannot help but be a bit envious of his students. I am thankful to all of these professors for their dedication to quality engineering instruction, for serving on my graduate committee, and for tying up the ends of the degree on such short notice.

I am also thankful to the great folks at ICE Corporation of Manhattan, KS, for sponsoring part of this research and for their cooperating and understanding as the trajectory of the research continuously changed. The practical insights gained and the many 'whiteboard discussions' are much appreciated. Their commitment to quality engineering and their concern for employees are remarkable to say the least.

Finally, I am thankful to everyone involved for being patient, understanding, and willing to work with me through the tough spots and delays in the research as well as those in my own life.

CHAPTER 1 - Introduction

Historically (c. 1900–) the three major types of electric machines have been the brush-commutator DC, synchronous, and induction machines. From the earliest times variable speed operation of motors was desired. This was not possible with the synchronous machine; its primary function has been to generate grid power. The DC motor is amenable to controlled speed operation and a great many schemes have been devised over the years. Early methods were characterized by low efficiency or complexity. One of the most widely adopted was the Ward Leonard system (essentially an adjustable DC voltage source produced mechanically). The speed of the induction motor is not as easily controlled, since it is essentially a synchronous motor with the field replaced by a cage that allows self-starting. Simple schemes consisted of tap or pole-changing switches, yielding a few discrete speeds. Continuous control could be had with a wound-rotor machine but at the expense of efficiency. Elaborate multi-machine speed control systems were employed to change frequency or to recover slip-energy. Alongside the simple mechanical means and multi-machine schemes appeared those that employed the first controlled power devices of type and function too numerous to mention. Additional information on this rich history can be found in [91], [90], [23, vols.1,2,4,5].

Although progress was continuous it was primarily along the same lines it had always been, until the "second electronics revolution" that came when the commercial thyristor was introduced around 1958. The principles of speed control in the machines obviously did not change, only the means by which it could be achieved. With the solid-state controlled rectifier came the inverter, which originally used originally load- or force- commutated thyristors. Variable frequency operation was thus finally achieved by solid-state means but only at large power levels. The possibility of pulse width modulation (PWM) came as self-turn-off thyristors and power transistors were developed, allowing variable frequency operation at lower power levels. The thyristor was used to build chopper drives for DC motors and variable-voltage variable-frequency (VVVF) adjustable speed drives for induction motors (both six-step and PWM). The inverter could have also been used to achieve variable speed operation of the synchronous machine but this was not common.

As the ability to control motors progressed, so did the types of motors that could be controlled. One of the many variations that arose was the brushless permanent magnet synchronous (BPMS) motor, which is the subject of this report. Although there were many paths of development that occurred around the world, according to Jahns [108] the BPMS motor evolved from at least two distinct application areas. The first type (call them type-A) were BPMS motors with a rotor cage that would start across the line and then pull into synchronism. In the 1970s integral-horsepower versions were designed that offered excellent efficiency but their high cost prevented widespread acceptance. In the second path of development, permanent magnet (PM) brushed DC servos (call them type-B) began to replace those with field coils in the 1960s, thus eliminating the field loss.

According to Jahns, these two development paths converged in the 1970s, where for the first time PM-rotor synchronous motors were driven by solid-state inverters. Before the merger, rotor losses (type-A) and field losses (type-B) had been eliminated, but now rotor inertia was decreased due to the elimination of the starting cage (type-A) and of the armature on the rotor (type-B); this enabled faster maximum acceleration rates. Further, the problems associated with a brush-commutator system (outgassing, mechanical and electrical inefficiency, required maintenance, voltage and current limits, and the impossibility of operating submersed or in explosive environments) of type-B machines were eliminated. According to Jahns, electronically-commutated motors (ECMs) were developed first, simply because of the simplicity of the control required. Later (late 1970s and 1980s) the sinusoidal variety was developed; this was a significant advancement because it required the phase of the VVVF output waveforms to be controlled in addition to amplitude and frequency (whereas for the induction motor, control of the phase was unnecessary). More about the differences between the ECM and the sine motor will be discussed at the end of Chapter 2.

Return again to the beginning of the century to examine modeling. André Blondel introduced *two-reaction* (or *two-axis*, or *d-q*) *theory* in France before 1900 which was translated into English in 1913 [1]. In the United States this was extended by R.E. Doherty and C.A. Nickle in late 1920s ([2]-[6]) and was more-finalized by R.H. Park in 1929 [7], [8]. Two-reaction theory allowed salient machines to be analyzed and was important in studying machine stability and transient operation (today, almost all such analysis uses the transform). In the middle of the century the "generalized theory of electric machines" ([18], [37, ch.9]) was gaining ground and Kron's tensor analysis ([13], [14]) was causing a stir, although the author is unsure of the influence of these two theoretical areas. It seems that the "final" step in modeling was the idea of using complex space

vector theory to model a machine, which was formalized in 1959 by Kovács and Rácz in Hungary [15]. (Transient phenomena in AC machines had already been documented [16], [17]—it seems that it was the space vector's complex-valued notation and ability to combine electrical and mechanical quantities that made it of value.)

Regardless of any gains in theoretical understanding of the induction motor, it seems that the motor continued to be controlled as described earlier, until the late 1960s when Germans Blaschke and Hasse made some key innovations [19], [20], [21]. It seems that their efforts led to the first control systems that attempted to control the induction motor based on its transient model instead of the steady-state equivalent circuit—they were the first form of "vector control." Instead of simply generating three-phase voltages of varying frequency and amplitude in order to achieve variable speed operation, the vector control also controlled the phase of the output waveforms. This was the beginning of a revolution that would allow the induction motor to be used in speed control applications requiring dynamic performance, eliminating the need to oversize motors to achieve satisfactory transient performance. Vector control is also known as field oriented control (FOC). FOC can be applied to other AC machines as well and there is benefit in doing this. However, the benefits obtained in applying FOC to a synchronous machine are not the same as those obtained with the induction motor. At the simplest level, vector control of a synchronous machine provides a control structure that makes decoupling control and arbitrary control schemes easier to implement. Due to the fact that the structure performs inherent synchronous frame current regulation, it also affords better steady-steady control at high speeds where traditional "stationary frame" regulators begin to lose gain and phase. In contrast, FOC control tames the dynamics of the induction motor (which are more sluggish than those of the synchronous machine). It seems as if the drastic benefits provided by FOC of an induction motor have been ascribed to the synchronous machine as well, causing some general misunderstanding as to the benefits of FOC. It is interesting to note that according to [100] most major servo drive manufacturers use FOC for sinusoidal drives (as opposed to non-FOC sinusoidal commutation), yet very few advertise this fact. In this case, the servo manufacturers are not contributing to the confusion between FOC of a BPMS motor and FOC and induction motor; it seems that most of the confusion has been caused by the other articles in the popular literature. Additional information on AC motor drives can be found in [64], [75], [81], [92], [93], [94], [95], [96], [97], [99].

From the summary above, it can be understood that the history of motor control spans more than a century and is very multifaceted. To understand where the material in this report fits into the overall picture, some points should be summarized. The realization of AC motor control via the generation of variable voltage and frequency current (using solid-state devices) was a landmark achievement. This was followed by the development of power devices that could be turned off at will, which allowed PWM to become a reality. In the beginning this was used to create VVVF induction motor drives. At some time, a line-start permanent magnet synchronous motor was introduced but it was not used in variable-frequency applications. In addition, an electronically-commutated (thus brushless) permanent magnet machine was devised. Eventually the concept of a sinusoidal permanent magnet synchronous machine was combined with an inverter to yield an adjustable-speed AC drive without brushes, capable of servo-like performance. The electronically commutated motor also served in this capacity, with the distinct advantages of using less expensive shaft position sensors and power electronics; due to the lower cost and simplicity of the system, the technique is still used today. Separate from all of this, vector control allowed linear control over the torque produced by an induction motor; this eventually allowed the induction motor to be used in servo-like applications as well where it was previously not possible. The vector control scheme can be applied to other motors and it provides distinct benefits, but these benefits are not the same as those achieved with the induction motor. All methods of synchronous machine control and all methods of vector control (of any machine) require knowledge of the rotor flux, which can be obtained directly or indirectly from a shaft sensor. There are many benefits to eliminating the shaft sensor, yielding so-called *sensorless control*.

The original purpose of the research that led to this report was to investigate the advantages and disadvantages of the sensorless FOC of a BPMS motor. This involved learning the fundamentals of brushless motor operation; since this is not taught in most curricula the initial sources of information were application notes written by servo motor and servo drive manufacturers, and by manufacturers of silicon devices (ASICs, MCUs, DSPs) involved in motor control. The motor drive literature was naturally lacking on the details of how the controls were implemented internally, and the silicon device literature was geared toward the implementation in a particular device and was lacking in theory. All of that literature would be useful for practical applications of the manufacturer's product, but it is not useful to learn theory. In addition, this literature is very lacking in performance data. Manufacturers are quick to list benefits of using their products, but often these claims are misleading at best. This literature (as well as all articles in trade

publications and magazines, and Internet articles) will be called the *popular literature* in this report.

The popular literature was abandoned in hopes of finding more detailed information in the *academic literature* (which is defined here to consist of textbooks, conference proceedings, and technical journals). However, it was quickly discovered that textbooks in motor control are generally written at an advanced level and most articles investigated such advanced or detailed topics that they were of little help in learning the theory.

The bulk of the research then was learning the fundamental theory of brushless motor operation and control in order to be able to interpret the academic literature to gain a better understanding and to find answers to specific questions. Therefore, the first purpose of this report is to summarize what has been learned in terms simple enough that the average technical person can gain an understanding of the field. The second purpose has been to establish a collection of useful references.

In addition to investigating the fundamentals mentioned, it was found that the modern academic literature is written in terms of space vector theory, thus this had to be learned as well. Additional topics of importance were found to be the Clarke and Park transforms, reference frame theory, the modifications that must be made to traditional synchronous machine theory in order to describe BPMS motors, state-space control systems, state observer theory, and three-phase inverter control techniques. The report is meant to highlight the pertinent issues and present the author's present understanding; it is not meant to be a comprehensive treatment that is complete. As each topical area is brought to a close, additional references are listed so that the reader can resume study where the author left off.

Organization

This report is organized into the following chapters and appendices.

Chapter 2 – "Fundamentals of Electric Motors" – presents some fundamentals of electric motors and their models, eventually narrowing the focus to the brushless permanent magnet (BPMS) motor that is the subject of this report. The basics of motor structure and terminology are discussed, followed by a fundamental examination of the physical laws that govern motor operation; this leads to the general per-phase electrical model for a winding that will be used throughout the report. In addition, the derivation provides a foundation for understanding inductance in a motor winding and demonstrates the significance of the magnet's leakage permeance on the magnetic circuit. Then torque production and back-EMF generation are investigated on a per-phase basis. This forms a basis for understanding polyphase motor operation and enables the full phase-variable electromechanical model of the polyphase motor to be developed. In the last section, the two theoretical types of BPMS motors are discussed and torque and back-EMF are then investigated for these two motors. This examination of torque production forms a natural introduction to current commutation.

Chapter 3 – "Sinusoidal BPMS Motors" – is the most important chapter and comprises the bulk of the report. Its ultimate purpose is to develop a space vector model for the sinusoidal BPMS motor because that model and its understanding (reference frame theory) are the basis for all modern motor modeling and control schemes. In order to achieve this goal the chapter is split into three parts. In Part I the standard analysis of sinusoidal synchronous machines is presented in the time and phasor domains. Part II introduces and discusses the space vector definition, notation, and interpretation by building on the understanding of the synchronous machine presented in Part I. Finally, Part III applies the space vector concepts from Part II to the modeling material from Part I to yield the space vector model of a BPMS motor.

Chapter 4 – "Inverters and Space Vector Modulation" –reviews inverter topologies and basic principles, concentrating on the voltage-source inverter (VSI). Space vector modulation (SVM) is introduced by building on the six-step 180° squarewave inverter. The

relationship between SVM and other PWM methods is discussed and some detailed aspects of SVM are presented.

Chapter 5 – "Field Oriented Control of BPMS Motors" – develops the concept of field oriented control as applied to the brushless PM synchronous motor. The concept is introduced by building on the per-phase torque production described in Chapter 2. It is then shown that FOC implements current regulation in the synchronous frame. The stationary and synchronous regulators are compared, then the synchronous regulator is studied in greater detail and decoupling control is introduced.

Chapter 6 – "Sensorless Techniques" – describes some techniques used to achieve control of a synchronous machine without using physical shaft sensors.

Chapter 7 – "Concluding Remarks" – makes some final comments regarding the topics investigated in this report.

Appendix A – "Elementary Electromagnetics" – reviews some basic electromagnetic concepts of a general machine in order to clarify terms that are sometimes incorrectly defined in the literature. Then the general case is specialized for the permanent magnet brushless motor in order to define the terminology used in this report.

Appendix B – "Phase-variable BPMS Motor Model" – derives the phase-variable model of a BPMS motor. Particular attention is given to the concepts of magnetizing, leakage, and synchronous inductance of a three-phase machine and the influence of the wye connection on the phase-variable model.

Appendix C – "Sinusoidal and Nonsinusoidal Motors" – elaborates the distinction between sinusoidal and nonsinusoidal motors.

Appendix D – "Three-Phase Concepts and Transformations" – is a collection of various topics related to three-phase systems that appear throughout the report. Topics include harmonics, sequence components, the method of symmetrical components, the relationship between the Clarke and αβ0 transforms, the linear dependence of the phases

in a wye-connected load, and some important implications of the zero-sequence component.

Appendix E – "Park Transforms" –discusses a few forms of the Park transform and the issues related to their axis and angle conventions.

Appendix F – "Useful Mathematical Results" – lists some useful identities and provides a table of Fourier series coefficients for some waveforms commonly encountered when working with brushless permanent magnet synchronous motors.

CHAPTER 2 - Fundamentals of Electric Motors

This chapter presents some fundamentals of electric motors and their models, eventually narrowing the focus to the brushless permanent magnet synchronous (BPMS) motor that is the subject of this report.

To begin, the general physical structure of some common motors is presented. The major types of motors are organized using various classification schemes in order to provide some perspective on the types of motors discussed in this report. A basic definition of saliency is used to extend these classifications and this is followed by the introduction of concept of the armature and field.

The bulk of the chapter is concerned with establishing a generalized electrical and mechanical model for an individual winding in a brushless permanent magnet motor (the "per-phase model"). The two most fundamental aspects of an electric machine (the induction of voltage and the production of force) are a recurrent theme. The second section develops these using an elementary physics-based approach (the laws of Faraday and Lorentz). The basic magnetic structure of the brushless permanent magnet motor is shown and is used to develop notions of inductance and flux linkage. Together with the two laws, this understanding allows the development of the per-phase (scalar) electrical model.

In the third section, the per-phase back-EMF generation and torque production are examined for each of two simple conceptual machines (sinusoidal and trapezoidal). This will show the equivalence between back-EMF generation and torque production on a per-phase basis. Equally importantly, it is shown that that their equivalence is innately related to the rotor-to-stator flux linkage that will be important in later chapters.

In section four, the general per-phase electromechanical model is given and is extended to form the "phase-variable" time-domain model of a three-phase brushless permanent magnet synchronous (BPMS) motor.

Finally, the fifth section examines the similarities and differences between three-phase sinusoidal and trapezoidal motors. The phase-variable model is used to examine torque production in the
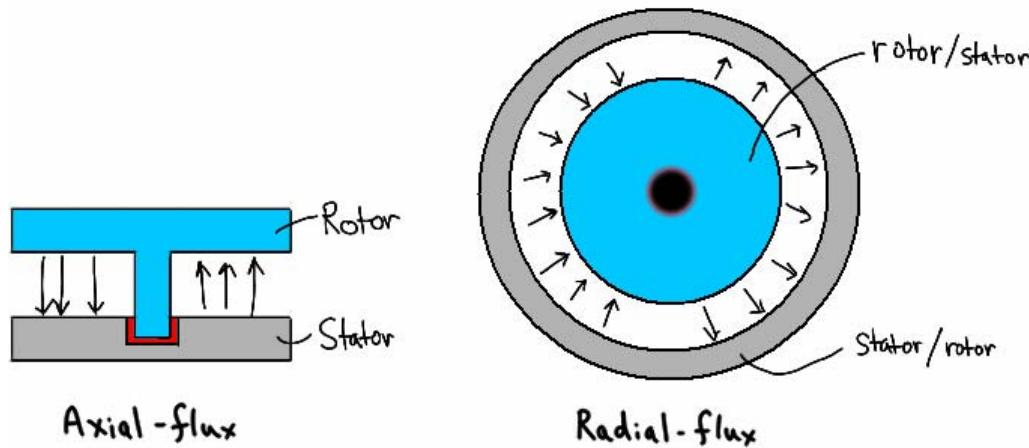
two motors and this leads into a discussion of whole-motor torque constant and line-line back-EMF constants. The control of the two motors is introduced from the perspective of the motors' requirement to achieve ideal torque production (electronic commutation). The chapter ends with an important discussion of the differences between the two motors; the conclusions will introduce and motivate Appendix C, which explains how sinusoidal and trapezoidal motors will be treated throughout the remainder of the report.

Preliminaries

In reading the literature on motor control a number of different motor configurations will be encountered, along with terminology that describes them. While some of that material is only a few decades old, the "motor scene" has changed significantly from the presentation contained in most textbooks. Therefore, some preliminaries about modern motor types and construction are presented to give the reader some perspective as to where BPMS motors fit into the overall picture. In addition, this information is requisite to understanding the various schemes that have evolved to control these motors.

Motor Structures
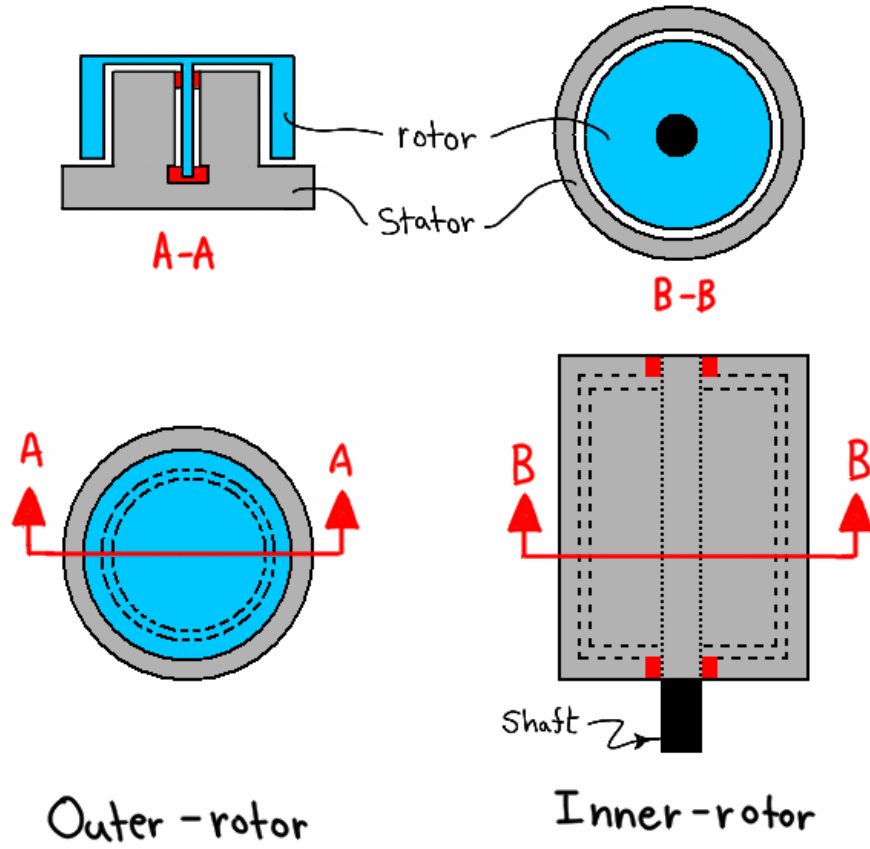
Both linear and rotational motors are in common use in servo applications. A rotational motor consists of a physical member that is stationary (the stator) and a physical member (the rotor) that rotates with respect to the stator. There are two general configurations of rotational motors: radial flux and axial flux. Axial flux motors [66] are an active area of research but are not nearly as common as radial flux motors in servo applications. A comparison between the two is shown in Figure 2.1.

Figure 2.1 – Radial- and axial- flux motors.

Of the radial flux motors, there are two common configurations: inner-rotor and outer-rotor. There exist motors that have a rotor that is both inside and outside of the stator but they are not in common use. The inner-rotor configuration offers the possibility of a smaller overall motor diameter, lower rotor inertia, and possibly better winding heat dissipation. These characteristics make it suitable for applications that require small size, low mechanical time constant, and high

power (or lower operating temperature), respectively. In contrast, the outer-rotor configuration can provide a larger inertia that may be desirable in constant-speed applications. An inherent feature of this motor is that the rotating rotor is exposed, which allows a load to be easily secured to (or manufactured as part of) the rotor assembly. A common form of each type is shown in Figure 2.2. Note the similarity between the axial flux and outer-rotor radial flux motors; the direction of the flux that is the distinguishing feature.
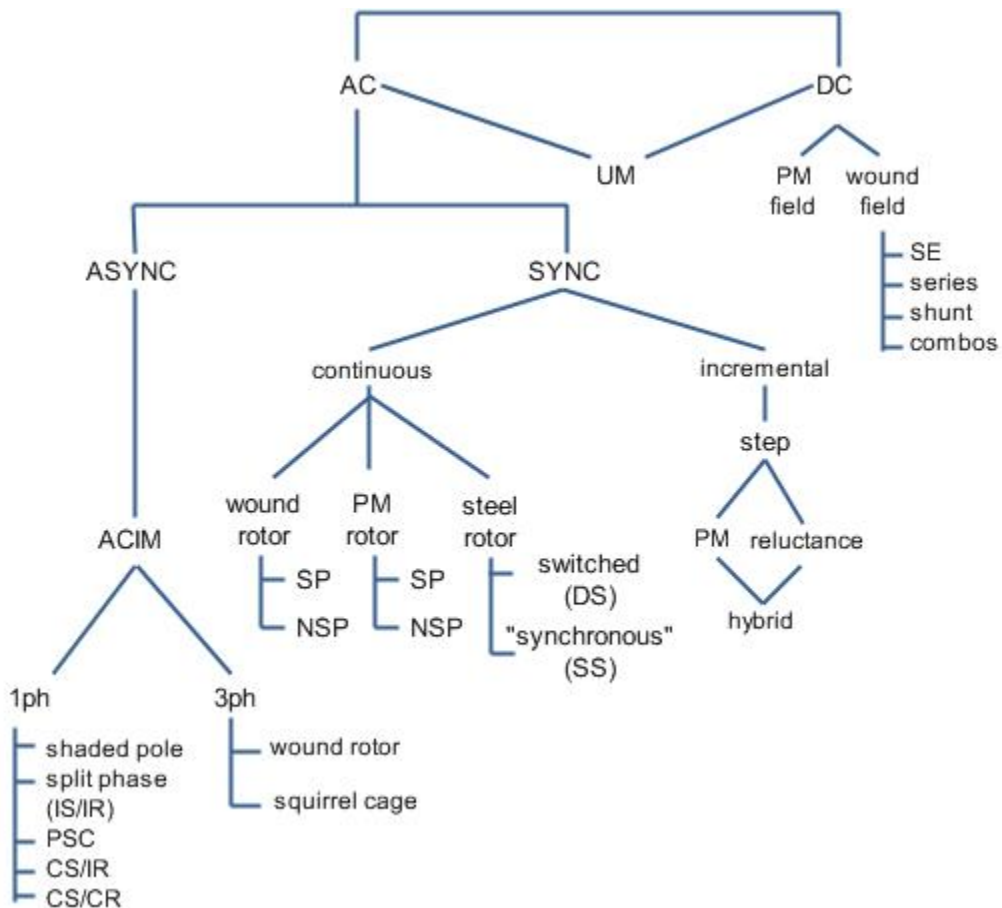
Figure 2.2 – Outer- and inner- rotor radial flux motors.

Motors used for "servo" applications (robotics, manufacturing, high-performance control), energy conversion applications (machine tool spindle drives, conveyors, pumps, fans, compressors, HVAC, traction motors), and general purpose applications are usually of the inner-rotor type. In contrast, cooling fans and magnetic and optical data storage systems may use the outer-rotor configuration. Additionally, the outer-rotor configuration has found application in "gearless" or "direct drive" machine tools and in vehicle propulsion, where the rotor is integrated into the wheel hub. *All subsequent discussion is directed toward radial-flux inner-rotor motors*, though many concepts apply to outer-rotor, axial-flux, and linear motors.

Taxonomy of Motors
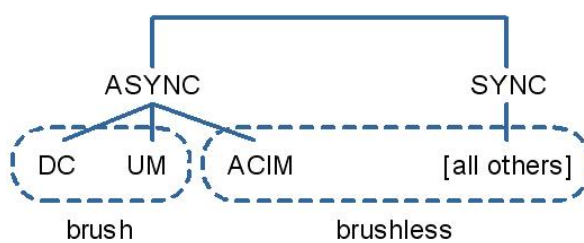
There is any number of ways to categorize electric motors and these different categorization methods are useful in different areas of motor applications. Many presented in the literature contain glaring errors but even the correct ones must be interpreted carefully (including those found in this report). For this report it makes the most sense to categorize motors according to the requirements for controlling them but it is hard to discuss such a categorization without being able to relate it to the physical construction and operation of motors. Therefore several classification schemes will be presented, beginning with a top-level overview and working toward the control-oriented taxonomy used in this report. This discussion concerns only the motor itself (not the motor together with a motor controller). The first categorization is shown in Figure 2.3. It is a general, broad categorization that shows common types of machines and is included only to provide perspective. Older motors (such as repulsion and two-phase), specialty motors (such as electrostatic and PCB types), and very low-power motors (such as hysteresis and self-starting reluctance) are excluded.

Figure 2.3 – General categorization of machines.

13

In the popular literature there are many opinions, much confusion, and even debates regarding the distinction between AC and DC motors. *In this report, the descriptors AC and DC refer to the type of ideal supply current (through the machine terminals) required to operate a motor from a supply without the use of any type of motor controller. Therefore any motor that will not turn continuously when connected to a battery is defined as an AC motor.* Among the many definitions of AC and DC motors, the reason for the above definition is that all (non-homopolar) machines have alternating flux linkage and induced voltage and require a current source that alternates in polarity in order to produce useful torque. Even the commutator DC machine has this property— it is the only the half-cycle-reversing action of the commutator that allows it to operate from a DC source. This distinction is clear in Figure 2.3, with the exception that the universal motor (and other brushed/"series AC" types) can operate from either source. The distinction between AC and DC motors will be revisited at the end of the chapter.
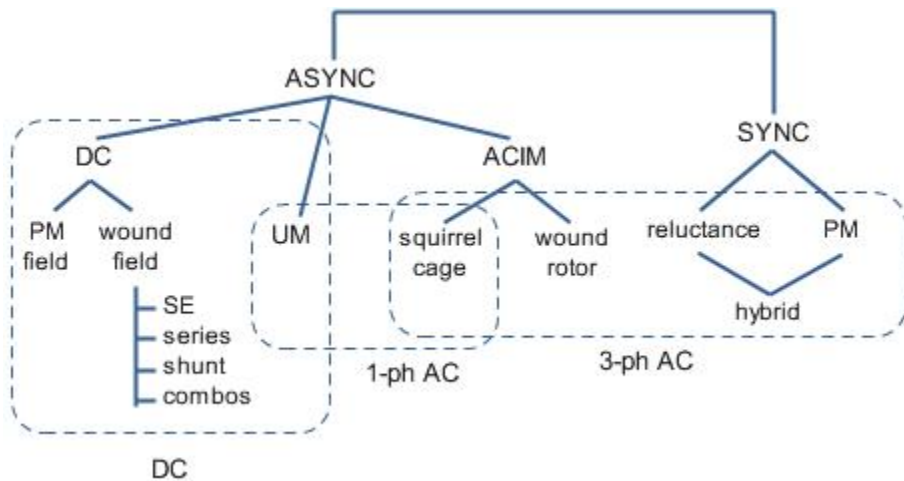
A second categorization (based on the presence or absence of a brush-commutator system) is shown in Figure 2.4. Both the induction and synchronous motors do not have brushes and thus do not have the limitations and problems associated with brushes. Essentially all modern synchronous motors are brushless, including wound-field machines since brushless exciters have replaced the slip ring and brush systems in most machines. (An exception could be made for low-cost, low-power applications, such as residential/consumer gasoline generator sets, but even a portion of these use brushless exciters.) That the induction motor does not require a brush-commutator system is one reason for the induction motor's robustness, although it should be noted that the induction motor is not usually called a "brushless motor."

Figure 2.4 – Motors categorized by presence or absence of brushes.

A third categorization is one based on power supply type; this is shown in Figure 2.5. Only continuous motors are shown (thus stepper motors are excluded). Loosely, the three types of ideal voltage/current supplies are DC, single-phase AC, and three-phase AC. Motors using DC supplies can be controlled by controlling the average voltage; the counterpart technique for single-phase AC supplies is phase angle control (phase chopping). Both DC and single-phase AC control is accomplished by "adjusting" or "limiting" the power supply without markedly changing its
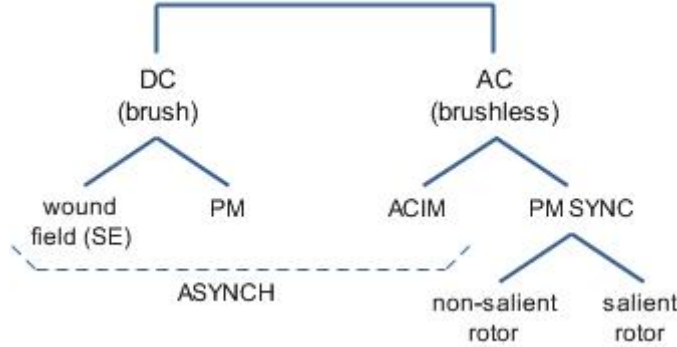
characteristics (the DC load current still a constant average value and the phase-chopped AC supply voltage is still at the line frequency and though no longer continuous, it retains the sinusoidal form over the continuous portions). Three-phase induction and synchronous motors require a completely different form of control wherein the supply waveforms are not simply "adjusted" but are instead "synthesized." Both the frequency and amplitude of the waveform are changed. Supplies of this type are often called a VVVF (variable voltage, variable frequency) drive, VFD (variable frequency drive), or ASD (adjustable speed drive). If the drive can adjust the phase of the output then the drive is called a vector drive. These distinctions will be covered later—for now it is sufficient to understand that three-phase drives differ from single-phase AC drives and DC drives. Small (perhaps up to 10 h.p.) adjustable speed drives are available for single-phase induction motors but all other modern AC motor drives are of the three-phase variety. *Thus, only three-phase AC machines are considered from this point forward.*

Figure 2.5 – Motors categorized by power supply type.

A final categorization is shown in Figure 2.6. This taxonomy shows only the most common motors used in servo and in medium-power energy conversion applications, with possible exception of the separately excited DC motor. It appears to the author that these are used primarily in traction applications, but it is included here because the control model of an AC synchronous motor under FOC is very similar to that of a separately exited DC motor. The taxonomy excludes universal motors because they are typically not used in servo and energy conversion applications (they find extensive use in consumer products such as vacuum cleaners and power hand tools). Wound-rotor induction motors seem to have fallen out of use due to the advent of variable/adjustable speed drives, solid state "soft" starters, and vector drives; they are therefore excluded. Step (stepper, stepping) motors are in common usage but are typically used in open-loop incremental motion control rather than continuous-motion servo and energy conversion

applications in which a wide speed range, smooth motion, and fast response are desired; they are therefore excluded. Finally, reluctance motors (both switched-reluctance and continuous synchronous-reluctance) have been the subject of much research in recent decades but are not a common type of off-the-shelf servo motor; they are therefore excluded.

Figure 2.6 – General motor taxonomy used in this report.

The taxonomy shown in Figure 2.6 is the one that will be used throughout this report (a more detailed discussion of the types of PM synchronous motors is deferred until the end of the chapter). Given the previous definitions of DC and AC motors—and the exclusion of the universal motor—all motors in this report can be classified as either DC or AC. Note that DC motors employ brushes (and accompanying commutator) whereas AC motors do not. A brief reasoning behind the selection of this taxonomy is as follows, proceeding from left to right in Figure 2.6. DC motors have historically been used when variable speed is required; only in the past several decades have they begun to be replaced by AC variable speed and servo drives [87], [78], [73]. The wound-field separately excited (SE) DC motor is important in the industry because it has field-weakening capability and it is important in this report because its control model is similar to that of a motor operating under field oriented control (FOC). The permanent magnet (PM) brush DC motor is important because of its simplicity and its power density (as compared with that of the wound-field DC motor); many (most?) brushed PM servo motors are of this type. PM DC motors do not need compensating windings, do not suffer field losses, are less susceptible to armature reaction, and have simpler torque-speed characteristics when compared to wound-field motors that are not separately excited (namely, motors wound in series, shunt, or any combination thereof). The dominant AC motors are the asynchronous AC induction motor and the permanent magnet synchronous motor. Presently, it seems that most PM synchronous motors (i.e. commercially available servo motors) use non-salient rotors, though salient rotors have been heavily researched, can be controlled satisfactorily, and are in use in certain applications. Salient rotor motors have the advantages of better field-weakening capability, an additional reluctance

torque component, sturdily constructed rotors that can operate at very high speed, and some advantages over non-salient-rotor designs when used in certain sensorless applications.

Magnetic Saliency

Most aspects of machine operation (such as torque production, inductance, and armature reaction) are influenced by the magnetic structure of the machine. The most general aspect of this structure is its *saliency*, which describes the reluctance of the main flux paths in the machine. Before introducing saliency it is necessary to describe some assumptions used in magnetic modeling (these will be used throughout the report).

Flux in a motor travels through the rotor, across the airgap, through the stator, then across the opposite airgap to arrive at the point from which it started. As a particular flux path is traced one will encounter various media such as air, steel (traditionally called "iron" [33, p.11]), permanent magnet material, nonferrous winding material (copper, insulation, varnish), and nonferrous structural material (such as aluminum, polymer, composite). To a certain approximation, all of the nonferrous material in the motor has a relative permeability of air, which in elementary machine analysis is taken to be the permeability of free space (μ_0). The steel in the motor has a relative permeability of several thousand. Since everything in the flux path except the steel is assumed to have a permeability of μ_0, often the reluctances of these components are lumped and considered to be the "effective" airgap reluctance. When this is done the only other permeability of concern is that of the steel. In basic motor analysis the permeability of the steel is assumed to be so much larger (sometimes infinitely larger) than μ_0 that the reluctance of the steel is negligible compared to that of the effective airgap. Ignoring leakage, the MMF generated by the stator winding drives a flux (called the *magnetizing flux*) through the airgap and the steel. Since the reluctance of the steel is assumed negligible, the MMF developed across the steel is negligible and it is therefore ignored in the magnetic circuit. (The electrical analogue is that voltage produced by a source drives current through the resistance of the supply conductors and the load, but the supply conductors have a resistance much smaller than the load, thus a negligible voltage is developed across them and they may generally be ignored.) Further, since there is a negligible amount of MMF in across the steel it is assumed that the field strength is negligible as well. Assuming that the airgap is "small" compared to the radius of the rotor the boundary conditions are then such that it can be assumed that the field is perpendicular to the steel surfaces at the airgap [27]. There are always nonlinear fringing effects and this assumption is perhaps not a good one for PM motor analysis since the effective airgap of a PM synchronous machine is much

larger than that of the synchronous machines treated in [27]. Nonetheless, this assumption is good enough to understand the basic principles of motors and will be used throughout this report, which is concerned with machine analysis not from a design perspective but from the perspective of basic understanding and control.

Using these assumptions we can trace flux paths through the machine and know that the length or shape of the path through the stator and rotor steel does not affect the reluctance of that path— only the length of the path through the effective airgap is important. Since every machine has a certain cross section that will yield diametrical symmetry it is easiest to trace these flux paths through the center of the rotor shaft. Finally, this idea allows a basic definition of saliency: when stator and rotor slotting is ignored a machine is non-salient if all flux paths through the center of the rotor have the same reluctance; any machine that is not non-salient is salient. The cross sections of some generalized stators and rotors are shown in Figure 2.7.
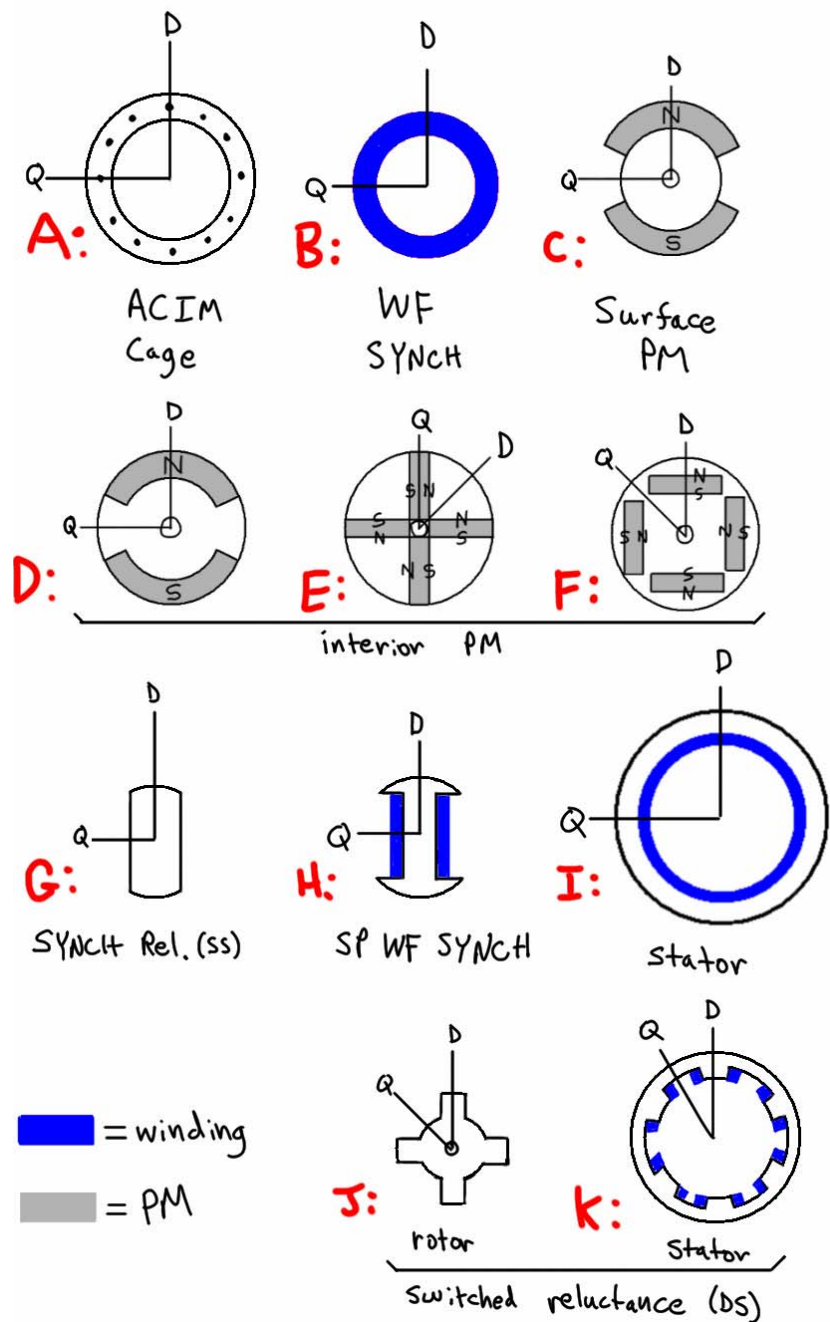
Figure 2.7 – Cross sections of some generalized synchronous motors.

For each rotor and stator type two axes are drawn: one marked D and one marked Q. The eight rotors (A-H) are used with the stator (I). The first three rotors (A-C) are nonsalient because the two paths are of equal reluctance. The other rotors (D-H) are salient because the two paths encounter different reluctances. In the switched reluctance machine (J-K) both the rotor and stator are salient. The topic of saliency will be revisited in Chapter 5.

Motors can produce torque using two independent principles: the first is to use two interacting magnetic fields and the second is to use one magnetic field and a magnetic circuit whose reluctance is a function of rotor position. Some motors use only the first principle, some use only the second, and some motors use a combination of the two. When discussing torque production (and hence, motor control) it is necessary to make these distinctions.

Some observations about common existing motors are useful to learn how to categorize them according to saliency. When torque is produced only by the interaction of two fields (called *mutual torque*), one field is produced by the stator and the other is produced by the rotor; these machines are called *non-salient machines*. When torque is produced only by the interaction of one field and a variable reluctance element (called *reluctance torque*), that field is produced by the stator; these machines are called *reluctance machines*. When a motor uses a combination of these principles (producing both mutual and reluctance torque) it is called a *salient-pole machine*. For salient-pole machines an additional observation is that the rotor is always salient and the stator may or may not be salient. If only the rotor is salient it is called a *singly-salient machine*; when both the rotor and stator are salient it is called a *doubly-salient machine*.

To summarize, non-salient machines produce only mutual torque, reluctance machines produce only reluctance torque, and the torque produced by salient-pole machines has both mutual and reluctance components. Induction motors are non-salient; synchronous machines may be salient or non-salient (this is true for both wound-field and PM types); a salient machine generally has a salient rotor; and the only common doubly-salient machine is the switched reluctance motor. In the literature, a *cylindrical rotor*[1] is one that is non-salient, *smooth bore* describes a non-salient stator, and *smooth airgap* describes a non-salient machine (rotor and stator).

DC motors have been excluded from this discussion because of the concentration on synchronous machines. There is indeed a difference in saliency between the wound-field and PM types and this saliency does affect operation, although the nature is different because the saliency is in the stator field poles. Many of these aspects have direct parallels to AC machines but cannot be included here. Something else to note is that slotting has been ignored in this discussion. If slotting is considered it is clear that it contributes to saliency because flux paths through the teeth will have lower reluctance than those through the winding slots. One must question where to

---

[1] *Cylindrical rotor* is found in the literature to mean a non-salient rotor but is also used to refer to a radial-flux machine (as opposed to an axial-flux machine, which has a flat "pancake" rotor).

draw the line between the solenoidal windings and large slot widths of the switched reluctance machine (whose stator is intended to be salient) and the slots of a non-salient machine (such as a sinusoidal PM synchronous machine) where the slotting causes undesired parasitic effects. Those effects are minimized when the width of the slots are "small" compared to those of the teeth or when there are many slots per pole. As far as the author can tell, for the non-salient PM brushless motors considered in this report, the only effect of slotting that needs to be considered is the cogging torque that results as the rotor magnets attempt to align with the teeth.

Armature and Field

The categorization based on saliency was presented primarily to discuss torque production and circuit models later in the report. However that categorization also helps illustrate the fact that motors from all three groups must have at least one winding. As a consequence of the mechanical motion of the rotor this winding will have a voltage induced in it—this is the armature winding. It is the induction of a voltage that makes this winding different the other winding that a motor may have (as both windings will create a field).

If the motor has a second magnetic field, that field is produced by either a permanent magnet or another winding; this field is usually called the field. If a magnet is used it is called a PM machine; if a winding is used it is called a wound-field machine. In a brush DC motor, the field is produced by the stator; in a synchronous motor, the field is produced by the rotor. (Induction motors are not well described by the words armature and field so the circuits are generally called the stator and rotor circuits, respectively.)

Brush DC machines always have the armature wound on the rotor; the armature winding is always called the armature winding (or simply, the armature). Contrarily, all traditional (grid-tied) synchronous machines and all brushless machines have the armature wound on the stator. For this reason, the armature winding is often called the stator winding (or simply, the stator). This misnomer is as widely accepted in the vernacular as the phrase "the flow of electric current" and thus will be used in this report.

Elementary Physics and Modeling

This section examines the fundamental physics of electromechanical energy conversion. The laws of Faraday and Lentz are developed. The basic magnetic structure of a brushless motor is introduced to derive the electrical model and discus flux linkage.

Faraday's Law

Faraday's law of induction describes the voltage induced in a coil of wire in relation to the sum of flux linked by that coil. This is the first of two fundamental concepts that describe the operation of electric motors and must be understood to create an electrical model of a motor. Physics texts often define this law as Equation (2.1), where φ represents the flux through a loop of wire in a plane perpendicular to the flux.[2]

$$g(t) = -\frac{d}{dt}\varphi \tag{2.1}$$

This idealized situation is not practical when the coil consists of multiple turns which are potentially displaced in space, in which case the flux through each turn may not be the same for every turn. To account for this condition, φ must be replaced with something that accounts for the additional turns of the coil. Namely, it must be replaced with the total flux linkage given by Equation (2.2), where φ_n is the flux that links the nth turn and N is the total number of turns. This can be interpreted as considering each turn of the coil to be a separate, single-turn coil connected in series with the other turn.

$$\lambda = \sum_{n=1}^{N} \varphi_n \tag{2.2}$$

For a concentrated winding (where all the turns are grouped together in two slots 180° electrical degrees apart) the assumption can be made that the same flux links each of the N turns of the coil. With this assumption, Equation (2.2) is reduced to Equation (2.3). If φ in Equation (2.1) is replaced with λ in Equation (2.3), Equation (2.1) becomes Equation (2.4). Later on, λ will be identified as the coil's "flux linkage."

$$\lambda = N \cdot \varphi \tag{2.3}$$

$$g(t) = \frac{-d\lambda}{dt} = -N\frac{d\varphi}{dt} \tag{2.4}$$

---
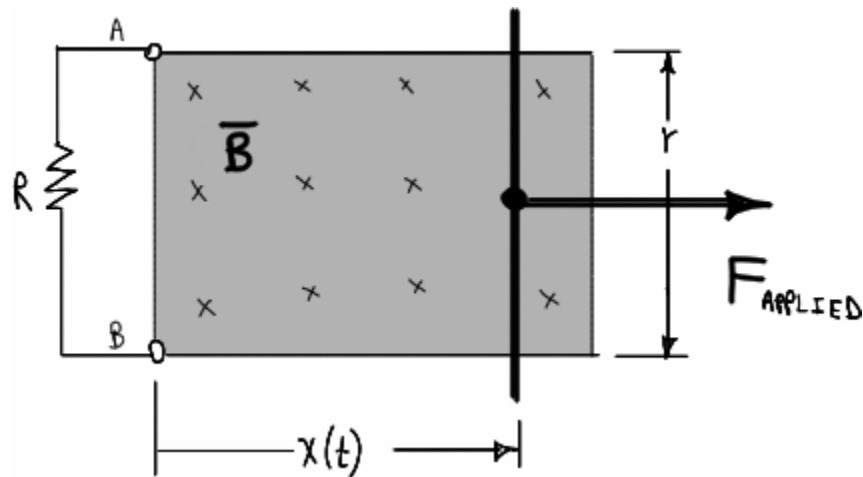
[2] Generally this induced voltage is denoted by $e(t)$ or $\varepsilon(t)$ but this report will use $g(t)$.

These texts generally attribute the minus sign to Lenz's law, but many of them do not even graphically depict a coil with labeled terminals. It is impossible to describe the polarity of a voltage of a coil if there are no terminals or if the terminals are not distinguished from one another; this can lead to considerable confusion. Even if polarities are stated, greater confusion can result when trying to apply Equation (2.4) to electrical machines because Lenz's law is stated in terms of current and the polarity convention for current depends on whether the machine is taken to be a motor or a generator. Equation (2.4) is for a generator sign convention. Since this report concerns only motors, the motor sign convention will be defined shortly. Lenz's law could be stated as follows:

> When the flux linkage in a coil of wire changes, it will induce an EMF whose magnitude is given by Faraday's law. The polarity of the EMF is such that—if the coil were shunted by a resistance—a current would flow in the direction required to generate a flux that would counter the change in flux linkage that induced the EMF in the first place.

To understand these two laws, examine the "classic" demonstration circuit with two terminals shown in Figure 2.8. The vertical conductor is a movable rod that maintains continuous contact with the horizontal conductors. The entire circuit is taken to be of zero resistance; the external resistor connected to the terminals exists only so that a current can flow in the circuit (this is required since Lenz's law is specified in terms of the direction of current). The circuit is contained in a plane that is perpendicular to a **B** field that is constant in both time and space.

Figure 2.8 – Demonstration of Faraday & Lentz laws; generator.

Using conventional current (as opposed to electron current), the "right hand rule" for a coil states that if the fingers of the right hand point or curl in the direction of current, the MMF produced will be in the direction of the thumb. The magnetic axis of the coil (sometimes denoted **μ**) is then
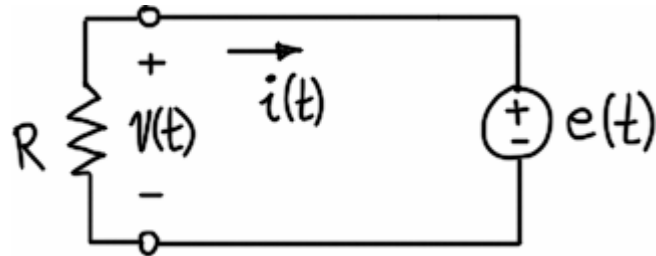
defined to be in the direction of the thumb; flux in this direction is taken to be positive. Since this report adopts the motor (load) sign convention, this will be defined as the direction of positive current and the terminal into which the current is flowing is the positive terminal. In reference to Figure 2.8, positive current is that which flows into terminal A and the magnetic axis of the loop is into the page, thus positive flux will be of the same polarity as the **B** external field (all magnetic quantities in this report share the same polarity conventions).

The **B** field shown is into the page. If an external force $\mathbf{F}_{applied}$ is applied to the rod and pulls it to the right, the area of the loop in the **B** field will increase which will in turn increase the flux linkage. By Lenz's law and the right hand rule, a current will flow in the circuit in the **counter**clockwise direction, producing a flux which points out of the page. Current flow in this direction creates a potential across the resistor such that terminal A is more positive than terminal B; since A is defined as the positive terminal, this shows that *an increase in flux linkage generates a positive EMF*. Therefore, it is best to define Faraday's law according to the motor (load) sign convention, Equation (2.5).

$$g(t) = \frac{d\lambda}{dt} \tag{2.5}$$

To summarize the convention, if the thumb of the right hand points in the direction of the magnetic axis, then the fingers will wrap in the direction that (positive) current must flow in order to produce positive flux along the magnetic axis. When the flux linkage of the coil increases, the EMF produced will be of positive polarity and have a magnitude given by Equation (2.5).

Finally, this ideal coil can be modeled electrically as shown in Figure 2.9. Note that although the circuit has thus far acted as a generator, we have selected the motor sign convention; therefore, the voltage polarity and current direction are correct.

Figure 2.9 – Electrical model of ideal coil shunted by an external resistance.

Given this convention, the EMF induced in the apparatus of Figure 2.8 can be calculated as follows. Since this is a one-turn coil, $N=1$ and the flux linkage is simply equal to the flux through the loop as shown by Equation (2.6).

$$\lambda = N \cdot \varphi = B \cdot A = B \cdot Y \cdot x(t) \tag{2.6}$$

The induced voltage is given by the application of Equation (2.5) to Equation (2.6), yielding Equation (2.7).

$$g(t) = \frac{d\lambda}{dt} = \frac{d(B \cdot Y \cdot x \cdot (t))}{dt} = B \cdot Y \cdot \frac{dx(t)}{dt} \tag{2.7}$$

The term $\frac{dx(t)}{dt}$ is by definition the instantaneous velocity v; thus, Equation (2.7) can be written as Equation (2.8). This is often called the "BLv law," where L represents the conductor length; here Y is used to avoid confusion with inductance).

$$g(t) = B \cdot Y \cdot v \tag{2.8}$$

The magnitude of the EMF is directly proportional to conductor speed and is independent of the presence or value of the resistance shown, although the size of the resistor will determine the amount of force needed to move the bar. This concept will now be examined.

Lorentz Force Law

The Lorentz Force law is the second of the two fundamental concepts that describe the operation of electric motors and must be understood in order to create an electrical model of a motor. The law is generally defined [44] as Equation (2.9),

$$\mathbf{F} = q \cdot (\mathbf{E} + \mathbf{v} \times \mathbf{B}) \tag{2.9}$$

where $\mathbf{F}$ is the force on the particle of charge q moving at velocity $\mathbf{v}$ in the electric field of potential $\mathbf{E}$ and magnetic field of flux density $\mathbf{B}$; all bold terms are vector quantities and $\times$ is the vector cross product. In a motor the contribution from $\mathbf{E}$ is irrelevant thus Equation (2.9) is reduced to the more familiar Equation (2.10).

$$\mathbf{F} = q \cdot \mathbf{v} \times \mathbf{B} \tag{2.10}$$

When $\mathbf{v}$ and $\mathbf{B}$ are perpendicular, the vector cross product reduces to a scalar product and yields Equation (2.11).

$$F = q \cdot v \cdot B \tag{2.11}$$
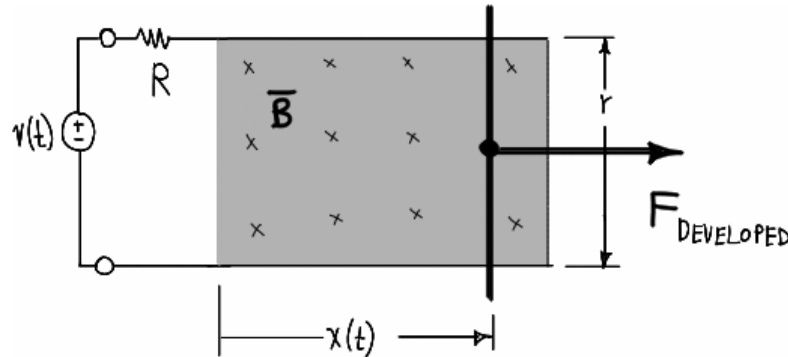
When Y is perpendicular to $\mathbf{B}$ over its entire length and when $\mathbf{B}$ is constant over the entire length Y, Equation (2.11) can be manipulated [68, p.61] to into the equivalent form Equation (2.12), where Y is the length of the conductor carrying current i; (usually L is used for the length and it is known as the "BLi law"). It is clear that the force is directly proportional to current.

$$F = B \cdot Y \cdot i \tag{2.12}$$

Returning to Figure 2.8, when an external force is applied to the rod, a voltage is induced according to Faraday's law. Since an external resistance is connected, a current flows and dissipates heat in the resistor. To satisfy conservation of energy Equation (2.13) must be satisfied (the mechanical work input must equal the electrical energy dissipated in the resistor).
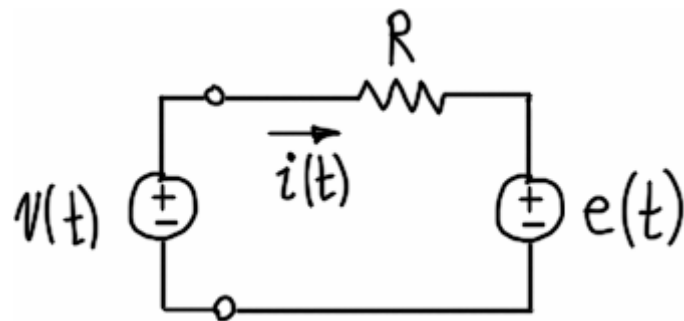
$$F \cdot v = g \cdot i \tag{2.13}$$

The apparatus in Figure 2.8 is an elementary, ideal linear generator with a load: mechanical energy is converted into electrical energy which is then dissipated as heat energy. Now, instead of the resistance serving as a kludge to allow the application of Lenz's law, let the resistance represent the distributed resistance of a real coil lumped into one element and let this coil be driven by an external voltage source. The apparatus now functions as a linear motor, converting electrical energy into mechanical work. Whereas previously $F_{APPLIED}$ was exerted to generate a current, here a current is made to flow and it produces $F_{DEVELOPED}$, as shown in Figure 2.10.

Figure 2.10 – Demonstration of the Lorentz Force law; motor.

In the same way that an electrical model (Figure 2.9) was created to represent the apparatus of Figure 2.8, an electrical model (Figure 2.11) can be created to represent the apparatus of Figure 2.10.

Figure 2.11 – Electrical model of coil connected to voltage source.

The above discussion demonstrates that any time the flux linkage of a coil changes, a voltage is induced in the coil. The mechanism responsible for the induced voltage is the same mechanism responsible for the applied (or developed) force acting on the coil itself. This result will be

26

extended to the rotational case later. It is important to note that there is no inductance in the simple models here because the flux linkage of the coil is controlled by the rod (inductance is a measure of the flux linked by a coil due to the coil's current; here, we assumed that the **B** field was fixed by an external source, thus there can be no inductance).
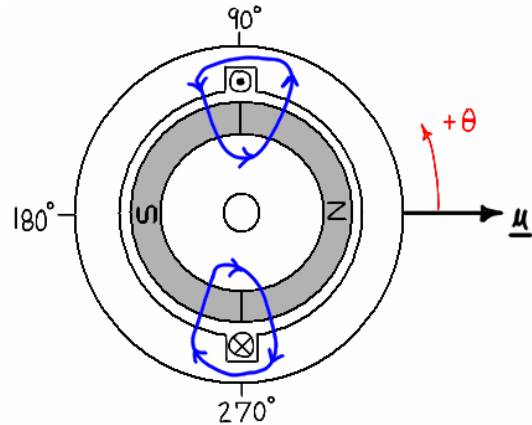
Per-Phase Electrical Model for Generalized Brushless PM Motor

The previous two sections discussed the two most fundamental concepts in electric machine operation and showed that they are inseparable. This section seeks to apply that information to develop a general electrical model of a motor with one phase winding. Since the magnetic medium is the coupling between the electrical and mechanical portions of the model, it is necessary to first introduce the basic magnetic structure of the brushless motor. From there we can obtain an expression for flux linkage and employ Faraday's law to find the induced voltage. The resulting equation and circuit will be used to discuss the concepts of stator inductance, stator flux linkage, back-EMF, and their relationships. It is obvious that the interaction between rotor flux and the stator winding is spatial in nature (as the magnetic quantities in the motor are distributed in space), yet the voltage induced in the coil is a scalar quantity. The spatial aspect is important to understand and will be analyzed later. But in this section, attention is restricted to the scalar electrical result in order to derive the per-phase electrical model for a winding in a BPMS motor.

We seek an electrical circuit model with as few mechanical and spatial dependencies as possible. It is representative of one winding in a three-phase motor and will be called the *per-phase model*. But it is important to note that this is *not* the familiar "single-phase *equivalent*" model found in most texts (which sometimes called "per-phase *equivalent*"). Single-phase *equivalent* analysis is concerned with the electrical phasor diagram of one phase (which is representative of the other two balanced phases) and the torque of the entire machine. In contrast, the per-phase model developed here is concerned with the time-domain representation of one phase and the torque produced *per-phase*. This distinction will be revisited and elaborated upon several times later on.

Since real motors employ coils in a magnetic circuit, the flux linkage expression is more complicated than that of the previous section. To extend the concepts to a real motor, the coil from the previous section is now placed inside a motor and a more detailed model is derived using [42], [27], and [68] as guides.

The general form of an inner-rotor brushless permanent magnet motor is shown in Figure 2.12. The rotor and stator are constructed of laminated electrical steel with a solid shaft. Two magnets encircle the rotor steel. The magnets are radially magnetized (they have magnetic domains aligned in a radial fashion) such that the flux density in the airgap is constant over the face of the magnet. Obviously, the North and South magnets cannot exist as monopoles; the convention used here is that the magnet is labeled with polarity of the flux entering the airgap (for example, the magnet labeled N has the North pole facing the airgap and the South pole facing the rotor steel). Likewise, flux traveling from the rotor to the stator is considered positive and therefore the flux density is also positive. Finally, the $\otimes$ and $\odot$ represent the direction of armature winding; its definition is deferred until later. For now simply note that when current flows in the directions indicated, positive flux will be generated in the direction of the magnetic axis μ per the right-hand rule.

Figure 2.12 – Section view of a general brushless PM motor.

The magnets on the rotor push flux across the airgap and through the rotor and stator following the general flux paths shown in the figure; this defines a magnetic circuit. Again, analysis of this magnetic circuit requires that the space distributions be accounted for. However, since the reluctance of all flux paths are the same (that is, the machine is nonsalient) we can examine the magnetic circuit in terms of total flux by aligning the rotor with the magnetic axis of the stator as shown. Later the spatial dependency can be introduced to develop the simplest possible electrical model. Similarly, in the figure discussed below the rotor flux cannot ever attain the shape shown because of rotor flux leakage but all practical rotors will produce a flux density with quarterwave symmetry. Thus the results derived here apply to the peak of any waveform that exists in practice.

Given the assumptions presented earlier, the lines of flux are nearly perpendicular to the steel surfaces (they are radial in the airgap) so long as the stator slotting is ignored (as it is in the

present analysis). When this is true, the motor in Figure 2.12 can be "unwrapped" into a linear version that is qualitatively equivalent (called the *developed view*) as shown in Figure 2.13. Like cross-section detail views, developed views are rarely drawn to scale; in particular, the airgap length and slot sizes are usually greatly exaggerated for clarity.
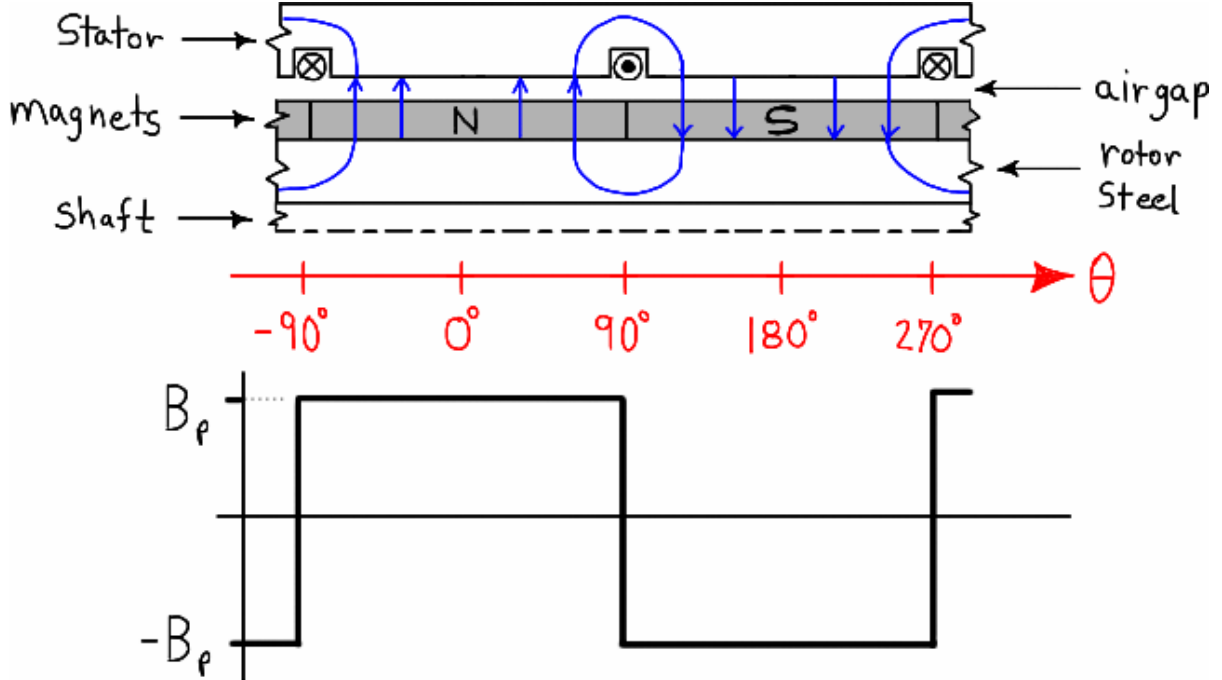
Figure 2.13 – Developed view showing only ideal rotor flux density.

The angle θ is measured beginning at zero and increasing as the airgap is traversed counter-clockwise. It is worthwhile to mentally verify that the flux paths are equivalent between the two figures. The graph below the developed view shows the "impossibly ideal" air gap flux density B (which cannot be attained in practice due to fringing effects, rotor leakage flux, and core nonlinearity).

Now that the magnetic structure has been introduced, the magnetic circuit will be developed. This will lead to some important observations about how the magnet sets up flux in the airgap, the meaning of flux linkage, and the meaning of inductance.

When the rotor is fixed in the position shown in Figure 2.12, the magnetic circuit can be modeled schematically as shown in Figure 2.14 ([68], [42]), which ignores leakage flux (flux that links only the stator or only the rotor, but does not cross the airgap). R_S, R_R, and R_{ag} represent the effective reluctances of the stator, rotor, and airgap, respectively. The magnets are represented as a source of flux in parallel with a reluctance R'_m, as in a Norton current source. R'_m is shown as a

reluctance for compatibility with the derivation but it is known as the *internal* or *leakage* *permeance* of the magnet [69, p.4.12]. The flux shown in Figure 2.14 corresponds to the flux path in the center of Figure 2.13.
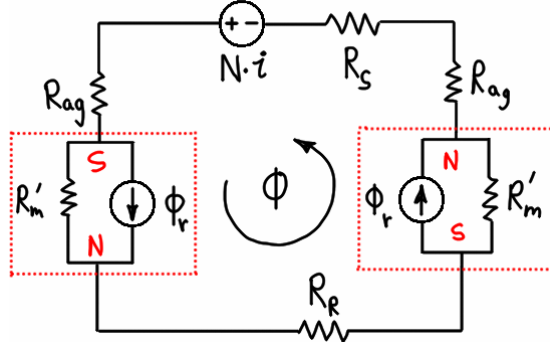
Figure 2.14 – Magnetic circuit of Figure 2.12.

The two magnets can be combined ($R_m = 2R'_m$) and the two airgap reluctances can be combined as $R = 2 \cdot R_{ag}$. Per the assumptions given earlier the rotor and stator reluctances are ignored. The reduction yields the circuit shown in Figure 2.15.
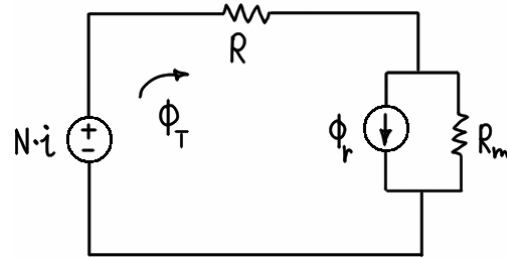
Figure 2.15 – Simplified magnetic circuit of Figure 2.12.

The flux linking the turns of the coil is from two sources: the coil (Φ_C) and the permanent magnet (Φ_M). Ignoring hysteresis, superposition applies and the total flux (Φ_T) is given by Equation (2.14). Since leakage flux is ignored here, this total flux crosses the airgap, thus it could be called the airgap flux.

$$\Phi_T = \Phi_C + \Phi_M \tag{2.14}$$

Φ_C and Φ_M are found by standard circuit analysis techniques using the circuits shown in Figure 2.16Figure 2.16 and are given by Equation (2.15) and Equation (2.16).

$$\Phi_C = \frac{N \cdot i}{R + R_m} \tag{2.15}$$

$$\Phi_M = \Phi_r \frac{R_m}{R + R_m} \tag{2.16}$$
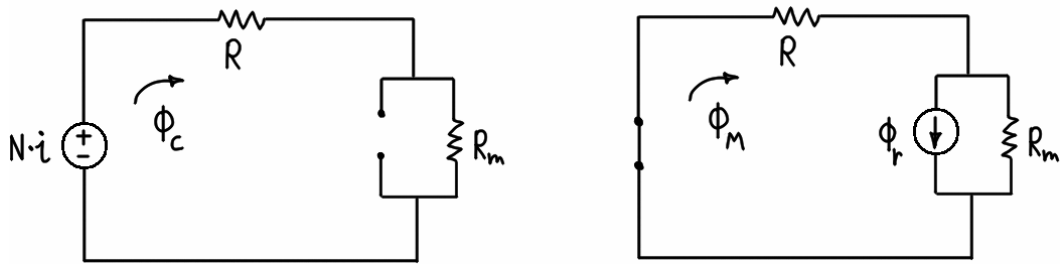
Figure 2.16 – Components of total flux (cf. Figure 2.15).

This simple analysis is not valid in practice but is good enough to illustrate some key points. First, notice that the airgap flux due to the magnet is controlled by the properties of both the magnetic circuit and the magnet—the magnetic circuit loads the magnet to an operating point. Further modeling or understanding is not necessary but it is useful to understand the general idea that the airgap flux due to the magnet is set by the magnetic circuit. Examining Figure 2.15 from a circuit-theory point of view, if the magnet was an ideal flux source ($R_m = \infty$) the airgap flux would be dominated by the "current source" of magnet flux. If the magnet was not magnetized but the magnet material kept in place ($\Phi_r = 0$ =open circuit) the airgap flux would be comprised of only coil flux. Also examine these two cases in light of Figure 2.16: it is clear that if the magnet is ideal the coil cannot influence airgap flux, or if the magnet is not magnetized the coil completely controls the airgap flux. This is an oversimplified analysis but is useful to know that real motors are somewhere in between these extremes.

Equally importantly, this model can be used to gain a better understanding of flux linkage. Flux linkage describes the total flux linked by a winding. A winding in a magnetic circuit can be linked by lines of flux that were produced by a means external to the winding (mutual flux linkage) and it can also be linked by lines of flux produced by its own current (self flux linkage). Thus, *flux linkage* is an expression that describes the total flux linked by the winding and this expression is written in terms of the winding's own current and in terms of the variables that describe the external source(s) of flux. It follows that a winding's flux linkage expression will take on a form consistent with the type of magnetic equipment containing the winding. Two familiar examples are the standard inductor and the transformer. For the inductor, the flux linkage expression involves only the flux produced by its own current; there is only one term. For the transformer, the simplest (ideal) flux linkage expression for a winding would contain a term describing the flux linkage due to that winding's current and one term for each additional winding of the transformer. For a brushless permanent magnet motor, the expression for a winding's flux linkage will contain the term describing the flux produced by the winding current, a term describing the

flux linkage produced by the rotor magnets, and a term for each additional winding present describing the flux linkage due each of those windings' current. For the present analysis, only one winding and the rotor magnets will be considered; inclusion of the other windings is deferred until the next chapter.

Assuming that all of the flux links each turn of the winding, the flux linkage is given by Equation (2.17), where Equation (2.14) has been used. The subscript 'S' could be added to λ to denote that this is the flux linkage of a stator winding, but the is no rotor winding in a BPMS motor thus the flux linkage is understood to be the stator's flux linkage (see Appendix A).

$$\lambda = N \cdot \Phi_T = \frac{N^2 \cdot i}{R + R_m} + N \cdot \Phi_M \tag{2.17}$$

By definition, an inductance is a constant of proportionality that indicates the amount of flux produced in a magnetic circuit per unit of current. The reluctance of the circuit is constant (not a function of rotor position) so a constant inductance can be defined as Equation (2.18). In this ideal analysis where leakage flux is ignored, the inductance is a function of the total reluctance of the circuit as seen by the MMF source of the coil. Since this reluctance is dominated by the airgap, it is often called the airgap inductance.[3]

$$L \equiv \frac{N^2}{R} = \frac{N^2}{R + R_m} \tag{2.18}$$

Using Equation (2.18), the flux linkage expression can be written as Equation (2.19). The first term in Equation (2.19) is by definition the self flux linkage of the winding. The second term is a flux linkage due to rotor flux.

$$\lambda = L \cdot i + N \cdot \varphi_M \tag{2.19}$$

In a real machine, L may be a function of rotor position (due to saliency) and N may be a function of the angle around the stator (a "stator winding distribution"), and φ_M will always be a function of both the angle around the rotor (a "rotor flux distribution" described relative to the stator) and the rotor position with respect to the stator. These dependencies are shown explicitly in Equation (2.20).

$$\lambda = L(\theta_r) \cdot i(t) + N(\theta_s) \cdot \Phi(\theta_r, \theta_s) \tag{2.20}$$

---

[3] Comparing Equation (2.17) with Equation (2.6) shows why the electrical model of the simple apparatus in Figure 2.8 had no inductance: because the B field was assumed to be held constant by an external source. In a real motor there is a similar source (the magnet) but it is not ideal, thus the current creates a flux linkage and therefore the coil has inductance.

As aforementioned a spatial analysis is required, but we can generalize the spatial relationships to a degree in order to gain an understanding of the basic electrical model. First, this report is only concerned with non-salient machines and therefore L will not be a function of rotor position. With this simplification the expression for stator flux linkage becomes Equation (2.21).

$$\lambda = L \cdot i(t) + N(\theta_s) \cdot \Phi(\theta_r, \theta_s) \tag{2.21}$$

Second, regardless of the nature of the last two terms (the distributions of stator winding and rotor flux) their interaction defines a flux linkage that will be a cyclic function of rotor position. From an electrical standpoint it makes sense to disregard the details of the two distributions and represent only the resulting flux linkage, which will be denoted by a new variable, $\psi_R(\theta_r)$. This new variable represents the component of total stator flux linkage that is due to the rotor flux. Since it is flux linkage due to the magnets it is sometimes called the "magnet flux linkage," but this report will use "rotor-stator flux linkage" because the former term sounds as if we are trying to describe the flux linking the magnet as opposed to the coil. Using this new variable, the expression for stator flux linkage becomes Equation (2.22).[4]

$$\lambda = L \cdot i + \psi_R(\theta_r) \tag{2.22}$$

To recapitulate, Equation (2.22) is the flux linkage of a stator winding. It has two components: flux linkage due to stator self inductance and flux linkage due to the rotor magnets.

Now, to finish the development of the general electrical model the dependence on rotor angle in $\psi_R(\theta_r)$ will be ignored until the next section. In the meantime we will use the generalized stator flux linkage expression given by Equation (2.23).

$$\lambda = L \cdot i + \psi_R \tag{2.23}$$
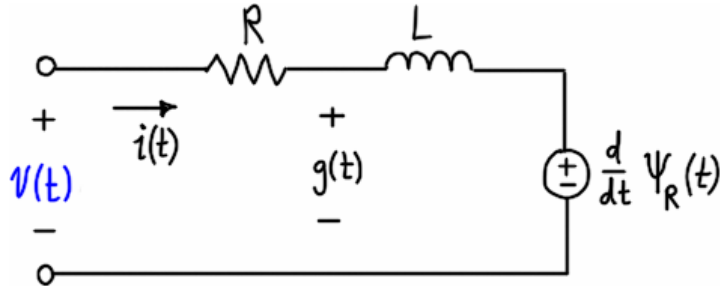
Faraday's law can be applied to Equation (2.23) to find an expression for the voltage induced in the coil, Equation (2.24).

$$g(t) = \frac{d\lambda}{dt} = L\frac{di}{dt} + \frac{d\psi_R}{dt} \tag{2.24}$$

Equation (2.24) suggests that the induced voltage in the winding of a general BPMS motor could be modeled as an inductor in series with a voltage source, as shown in Figure 2.17. (To

---
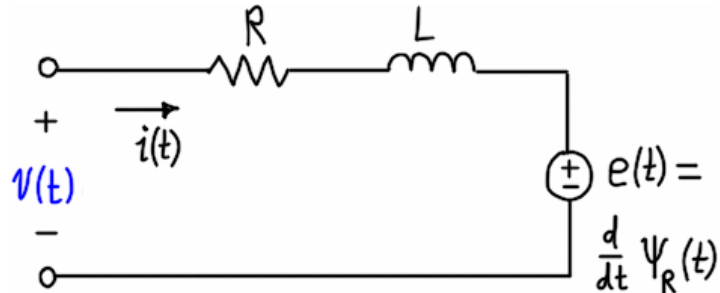
[4] Unfortunately, the variable identified here as ψ_R is sometimes referred to as the "rotor flux linkage" or the "rotor flux" in the popular literature. It is neither, thus these terminologies are incorrect and misleading. The reader unfamiliar with the distinction may find Appendix A helpful.

emphasize that $v(t)$ is the *applied voltage* (not a modeled source) it will be indicated by a polarity instead of a source.)
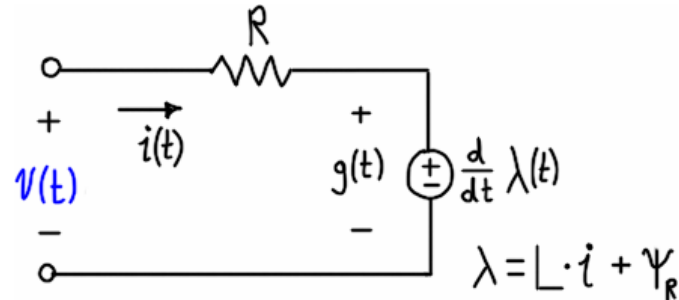
Figure 2.17 – Per-phase electrical model of general brushless PM motor; explicit inductor.

Readers familiar with the synchronous machine will likely identify the last term in Equation (2.24)—which corresponds to the voltage source in Figure 2.17—as the back-EMF (bEMF). In this report this bEMF term will be labeled e(t) as shown in Figure 2.18.

Figure 2.18 – Per-phase electrical model of general brushless PM motor; explicit inductor.

In much of the literature, the total induced voltage is represented as a voltage source equal to the time derivative of the flux linkage as shown in Figure 2.19.

Figure 2.19 – Per-phase electrical model of general brushless PM motor; implicit inductor.

The circuits in Figure 2.18 and Figure 2.19 are the two most prevalent models for an armature winding in a non-salient-pole synchronous machine. (At this point we have still neglected the effects of the other windings and the effect of flux leakage; later it will be shown that both of these effects can be accounted for by modifying the simple inductance defined earlier.) This discussion has made careful distinction between g(t) and e(t), but much of the literature uses the explicit "e(t)" to mean what has here been denoted g(t). The context of an article should make

clear the meaning, but the reader is cautioned that there are many different terms used to describe a voltage induced in a coil and the various components of that voltage. Some of the common terms are: *speed voltage*, *transformer voltage*, *motional EMF*, *counter-EMF*, *back-EMF*, *rotational voltage*, *armature reaction voltage*, *magnetizing EMF*, *airgap voltage*. While there is some common agreement as to the specific meaning of each term they are often used interchangeably, especially *back-EMF*. In the sense that all components of an induced voltage act to counter changes in flux, identifying any of them as the back-EMF or counter-EMF could be etymologically reasonable. But to be clear, *this report defines back-EMF to be the component of induced stator voltage produced only by a change in the stator flux linkage due to the position of the rotor*. This means that any change in the stator circuit that occurs while the rotor is locked cannot be called the bEMF. This approach has some circuit-theory appeal in that the distributed inductance of a real winding can be modeled as a lumped element in series with an ideal voltage source. On the other hand, the entire stator flux linkage plays an important role in the modeling presented in the next chapter, thus the total induced voltage $g(t)$ is often used. In addition, $g(t)$ has a physical meaning that will be examined in the next chapter.

The KVL equations for the circuits shown in Figure 2.18 and Figure 2.19 are Equations (2.25) and (2.26), respectively, with the stator flux linkage is defined as Equation (2.27). It should now be clear that when Equation (2.27) is substituted into Equation (2.26), the result is equivalent to Equation (2.25). The distinction between $e(t)$ and $g(t)$ and the connection between these equations will be revisited in the next chapter and should become clearer at that time.

$$v(t) = i(t) \cdot R + L \frac{di(t)}{dt} + \frac{d\psi_R}{dt}, \text{ where } \frac{d\psi_R}{dt} = e(t) \tag{2.25}$$

$$v(t) = i(t) \cdot R + \frac{d\lambda}{dt} \tag{2.26}$$

$$\lambda = L \cdot i + \psi_R \tag{2.27}$$
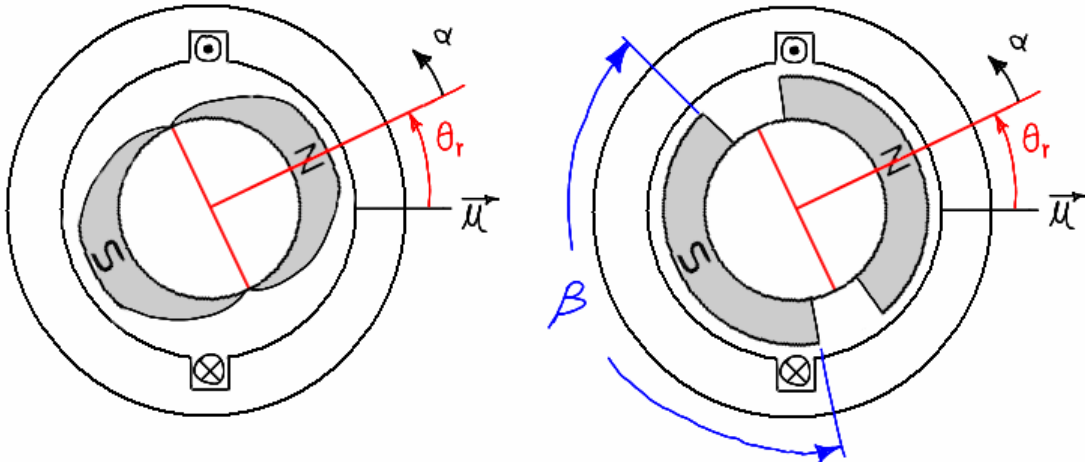
Per-Phase Back-EMF Generation & Torque Production

The electrical model of a motor has been developed with as little dependence on the mechanical model as possible, although it was mentioned that the bEMF is a function of rotor position. As discussed at the beginning of the chapter, the induction of voltage and the production of force in a motor are inseparable. Since the bEMF generated is a function of rotor position it is therefore expected that the torque produced will also be a function of rotor position. This section will elaborate on the nature of bEMF generation and torque production.

The discussion of the Faraday and Lorentz laws concluded that in the elementary linear machine studied, the induced voltage was linearly proportional to the velocity of the moving conductor (relative to the field) and that force was linearly proportional to the current in the conductor. It is not difficult to demonstrate how the BLi and BLv laws can be modified for the rotational case and applied to simple motor structures. Expressions for torque and bEMF could be obtained by allowing the flux density to be a function of rotor position, B(θ), appropriate to the machine. This approach becomes complicated for all but the simplest windings.
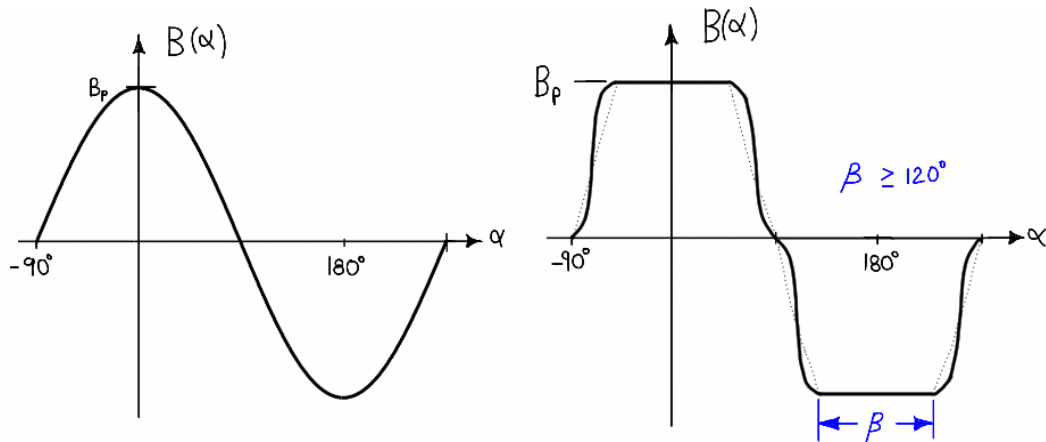
In fact, academicians hold different opinions as to whether either law is applicable in a machine in which the conductors are contained in slots in the iron since most of the flux will pass through the teeth, avoiding the slot where the conductor lies (most motors use slotting). The actual mechanisms at work producing torque and bEMF are likely not exactly those described by the laws [42, p.93], [33, p.20], but many of the results obtained by classical methods agree with those obtained using the BLi and BLv laws [69]. There are better methods to find the bEMF and torque and these will eventually be discussed at the end of this section. Although the BLi and BLv laws are not always practical for study of real machines, they can be employed to analyze simplified machines to gain an important perspective about their operation.

Studying the torque and bEMF of a single winding will prove useful in the analysis of three-phase motors, particularly non-sinusoidal motors. It can be demonstrated that the torque and bEMF produced by a winding in any brushless permanent magnet machine is a function of rotor position by considering two elementary motors shown in Figure 2.20. The windings of both motors consist of N turns that are contained in the slots shown. Obviously the results we obtain will be specific to this construction, but the principles will be applicable to any winding.

Figure 2.20 – Elementary brushless PM motors with concentrated full-pitch winding.

The rotor magnets produce airgap flux densities as shown in Figure 2.21. The motor on the left has magnets that produce an airgap flux density that is a sinusoidal function of the angle around the rotor, α. The motor on the right has magnets that produce an airgap flux density that is also a function of the angle around the rotor but whose shape is difficult to describe. However, it has the notable feature that the magnitude is constant over an angular pitch of β≥120°; note that β has correspondence between Figure 2.20 and Figure 2.21. If these segments are centered about α=0° and α=180°, the airgap flux density could be approximated by the trapezoid shown in dashed lines. These two elementary models are *representative* of the two most common types of non-salient BPMS motors (real motors are not always constructed as shown). The motor on the left is a sinusoidal motor and the motor on the right is an arbitrary trapezoidal motor.

Figure 2.21 – Airgap flux density profiles for two BPMS motors.

The airgap flux densities shown in Figure 2.21 are defined in terms of the angle α around the *rotor*. But since the coilsides that compose the winding have fixed positions it is possible to

describe the flux density directly over a conductor of the $\otimes$ coilside[5] in terms of the rotor position (per the previous discussion, the flux takes the tooth and the wire is not actually in the field but we use the equations anyway). For the sinusoidal motor the description is simple and is given by Equation (2.28). Describing the flux density seen by the conductors of the trapezoidal motor is best accomplished by considering the trapezoid approximation and using discontinuous functions, but for simplicity the result is derived only graphically. In all of the following, the analytical result will be provided for the sinusoidal case only; the results for the trapezoidal case will be found graphically using the sinusoidal case as a guide.

$$B(\theta_r) = -B_p \sin(\theta_r) \tag{2.28}$$

This result will be used to examine first the torque production and then the bEMF generation.

Torque Production

The torque exerted on the rotor is found from first principles and the BLi law. Torque is produced by both coilsides (each having N conductors) and is given by Equation (2.29), where F is the force per coilside and D is the diameter of the coil centers. Substituting in the BLi law gives Equation (2.30), where Y is the length of the conductors in the stator lamination stack and $i(t)$ is the current in the winding.

$$T = 2F\left(\frac{D}{2}\right) \tag{2.29}$$

$$T = 2\left(N \cdot B \cdot Y \cdot i\right)\left(\frac{D}{2}\right) \tag{2.30}$$

Substituting Equation (2.28) for B in Equation (2.30) yields Equation (2.31),

$$T(\theta_r) = -N \cdot D \cdot Y \cdot B_p \cdot \sin(\theta_r) \cdot i(t) \tag{2.31}$$

Since the terms premultiplying the sine are constant, Equation (2.31) can be rewritten as Equation (2.32), where K_t is called the torque constant.

$$T(\theta_r) = -K_t \sin(\theta_r) \cdot i(t) \tag{2.32}$$
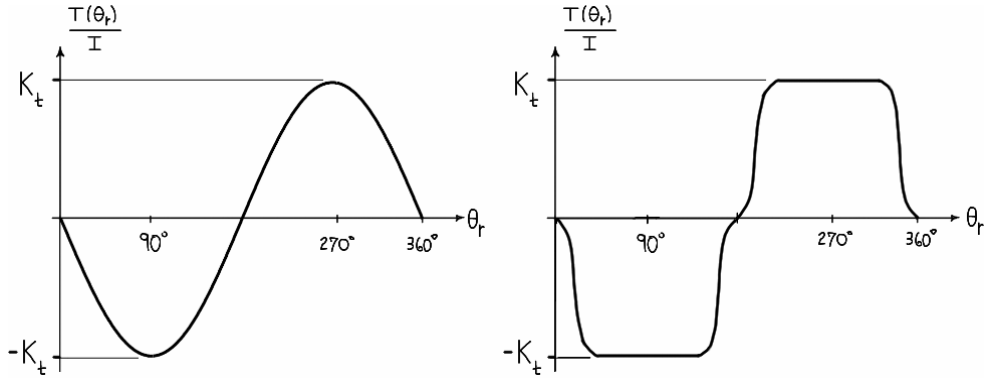
The torque produced in the sinusoidal motor, Equation (2.32), is seen to scale linearly with the current, as expected from the discussion of the Lorentz force law. The current may vary arbitrarily with time. To remove this dependence from the magnitude, Equation (2.32) can be rewritten as the ratio of torque produced per unit current to yield Equation (2.33), which may be

---

[5] This coilside is selected because the BLi law describes force on a conductor so the force on the rotor is in the opposite direction. The stator is fixed thus the rotor rotates. Torque is written in terms of the force on the rotor and its sign convention is the same as that for angles (Figure 2.12).

called the *per-phase torque function*. As usual, the uppercase K represents a constant and the lowercase k represents a function.

$$\frac{T(\theta_r)}{i(t)} = k_t(\theta_r) = -K_t \sin(\theta_r) \tag{2.33}$$
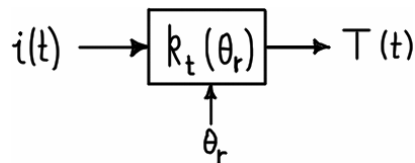
Equation (2.33) is plotted in Figure 2.22; current is held constant. Since it is obvious that the torque function takes the same shape as the airgap flux density,[6] the torque produced by the trapezoidal motor is found graphically as shown in the figure. Clearly the polarity of current will need to match the polarity of the torque function to produce useful torque; this is discussed at the end of this chapter.

Figure 2.22 – Torque functions of sinusoidal and arbitrary trapezoidal motors.

Expressing torque in terms of the torque function allows easy manipulation of the expression, even if the torque function is not easily described mathematically. This is demonstrated in Equation (2.34) and the corresponding simulation diagram is shown in Figure 2.23.

$$T(t) = k_t(\theta_r) \cdot i(t) \tag{2.34}$$

Figure 2.23 – Simulation diagram for per-phase torque function.

---

[6] To be clear, in this case the torque (a function of rotor position as measured with respect to the stator) takes on the shape the rotor flux density (a function of the angle *about* the rotor axis), i.e. replace α with θ_r. This is true for the simple concentrated full-pitch winding but is not true in general, as will be discussed later.

Back-EMF Generation

As the torque was developed using the BLi law the bEMF will now be developed using the BLv law along with first principles. Using the conventions established earlier in the chapter the voltage induced in the winding could be given by Equation (2.35).

$$e(t) = 2N \cdot B \cdot Y \cdot v \tag{2.35}$$

Substituting in Equation (2.28) for B and simplifying yields Equation (2.36), where ω is the rotational velocity.

$$e(\theta_r) = 2N \cdot [-B_p \sin(\theta_r)] \cdot Y \cdot [\frac{D}{2}\omega]$$

$$e(\theta_r) = -N \cdot D \cdot Y \cdot B_p \sin(\theta_r) \cdot \omega(t) \tag{2.36}$$

Since the terms multiplying sine are constant, Equation (2.36) can be rewritten as Equation (2.37).

$$e(\theta_r) = -K_e \sin(\theta_r) \cdot \omega(t) \tag{2.37}$$

The bEMF produced in the sinusoidal motor, Equation (2.37), is seen to scale linearly with the velocity, as expected from the discussion of the Faraday's law. The velocity may vary arbitrarily with time. To remove this dependence from the magnitude, Equation (2.37) can be rewritten as the ratio of torque produced per rotational velocity, yielding Equation (2.38), which may be called the *per-phase bEMF function*.

$$\frac{e(\theta_r)}{\omega(t)} = k_e(\theta_r) = -K_e \sin(\theta_r) \tag{2.38}$$

Equation (2.38) is plotted in Figure 2.24; velocity is held constant. As with the torque function, the bEMF function takes the same shape as the airgap flux density, the torque produced by the trapezoidal motor is found graphically as shown in the figure.
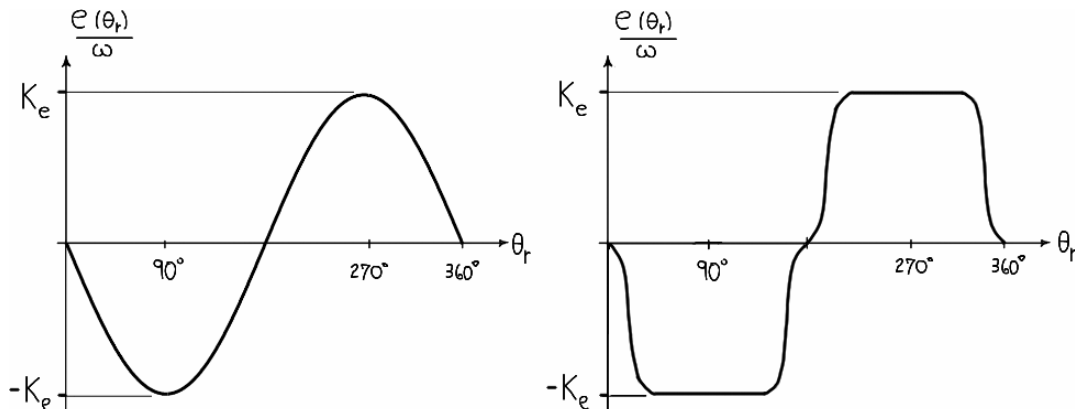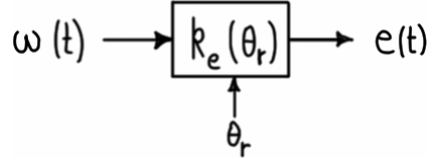
Figure 2.24 – Back EMF functions of a sinusoidal and arbitrary trapezoidal motor.

Expressing bEMF in terms of the bEMF function allows easy manipulation of the expression, even if the bEMF function is not easily described mathematically. This is demonstrated in Equation (2.39) and the corresponding simulation diagram is shown in Figure 2.25.

$$e(t) = k_e(\theta_r) \cdot \omega(t) \tag{2.39}$$

Figure 2.25 – Simulation diagram for per-phase bEMF function.

The torque and bEMF functions will be examined together in the next two subsections.

Equivalence of Per-Phase Back-EMF and Torque Functions

Now that the per-phase bEMF generation and torque production have been examined a very important fact is stated. *The per-phase bEMF and torque functions have the same waveshape. In addition, when SI units are used, the per-phase bEMF and torque functions are numerically equal and the units of each function ($\left[\text{volt} \cdot \text{s}/(\text{rad})\right]$ and $\left[\text{N} \cdot \text{m}/\text{A}\right]$) are dimensionally equivalent ($\left[\text{kg} \cdot \text{m}^2 \cdot \text{s}^{-2} \cdot \text{A}^{-1}\right]$).* For the simple coil studied earlier, the expression for the conservation of energy was given as Equation (2.13). For the rotational case this becomes Equation (2.40), which can be derived using several different methods of differing rigor [68], [69], [27]. For example, an intuitive method is to solve the BLi and BLv laws for the product BL and equate the result.

$$e \cdot i = \tau \cdot \omega \tag{2.40}$$

Equation (2.40) holds for transient and steady state conditions, but it is important to note that the equation only governs the part of energy conversion process that involves flux that links both the field and the armature. It describes only the energy that crosses the airgap. When the instantaneous values of bEMF and torque are replaced with their general descriptions given by Equation (2.34) and Equation (2.39), the result is Equation (2.41).

$$\left[k_e(\theta) \cdot \omega\right] \cdot i = \left[k_t(\theta) \cdot i\right] \cdot \omega \tag{2.41}$$

Regardless of the type of motor or motor controller, the current and velocity on each side of the equation will be the same and may be cancelled, leaving the all-important result shown as Equation (2.42). Naturally, any equation is only true if the variables are expressed in compatible units and in SI base units this is automatically the case.

$$k_e(\theta) = k_t(\theta) \tag{2.42}$$

That the two functions are equivalent is readily apparent when Figure 2.22 and Figure 2.24 are compared. It must be noted that K_t and K_e are per-phase values. These are not necessarily the torque and bEMF constants found on a motor datasheet. This will be discussed toward the end of this chapter.

Back-EMF and Torque in Terms of Rotor-Stator Flux Linkage

Earlier, the concept of flux linkage was developed in order to obtain an electrical model and gain an understanding of inductance in a BPMS motor. The connection between stator-rotor flux linkage and bEMF was shown. And previously, the bEMF and torque functions were derived using simple first principles for the case of a concentrated full-pitch winding. Now the bEMF and torque functions will be derived again, this time using the flux linkage. The understanding provided by this derivation will be requisite to further understanding the difference between motor types and in understanding FOC.

Returning to Figure 2.20, it is clear that the amount of flux linked by the winding of either motor will be a function of rotor position. As before, the sinusoidal case will be derived analytically and the trapezoidal case will be analyzed graphically. The flux linkage for the sinusoidal motor is found as follows, where α and θ_r are defined in Figure 2.20,

Y is length of the rotor and stator lamination stack, and D is the diameter of the N-turn winding. Since the motor uses a concentrated full-pitch winding, N is simply a constant.

$$
\begin{aligned}
\psi_R(\theta_r) &= N \cdot \varphi = N \cdot B \cdot A \\
&= N \int B(\alpha) \cdot dA \\
&= N \int_{\alpha=-\pi/2}^{\pi/2} \left[B_p \cos(\alpha - \theta_r) \right] \cdot \left[Y \cdot (D/2) \cdot d\alpha \right] \\
&= N \cdot (D/2) \cdot Y \cdot B_p \sin(\alpha - \theta_r) \Big|_{\alpha=-\pi/2}^{\pi/2} \\
&= N \cdot (D/2) \cdot Y \cdot B_p \cdot [\sin(\pi/2 - \theta_r) + \sin(\pi/2 + \theta_r)]
\end{aligned}
$$

$$\psi_R(\theta_r) = N \cdot D \cdot Y \cdot B_p \cos(\theta_r) \tag{2.43}$$

$$\psi_R(\theta_r) = \Psi_R \cos(\theta_r) \tag{2.44}$$

Equation (2.44) is the component of stator flux linkage due to the rotor (the rotor-stator flux linkage) and Ψ_R is the peak value.[7] It is easy to verify that the peak value given in terms of the parameters in Equation (2.43). The area of the pole face of the coil is given by Equation (2.45). When the rotor is aligned to zero degrees the total flux is the average flux given by Equation (2.46). Then, the total flux linkage (which is the peak value at zero degrees) is given by Equation (2.47).

$$A = (D/2)\pi Y \tag{2.45}$$
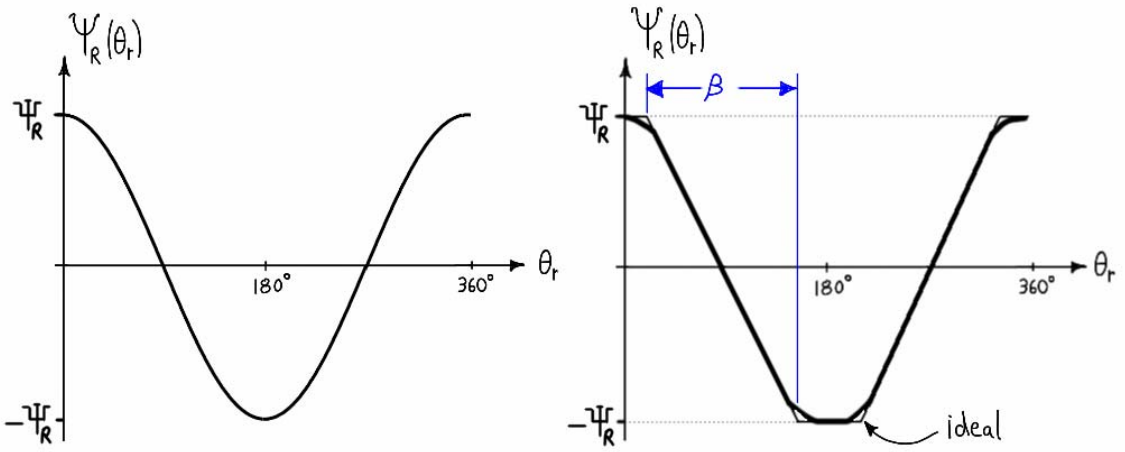
$$\overline{\Phi} = \int_0^\pi B_p \sin(\theta)d\theta = \frac{2}{\pi} B_p \tag{2.46}$$

$$\Psi_R = N\Phi_p = N \cdot D \cdot Y \cdot B_p \tag{2.47}$$

The rotor-stator flux linkage in the trapezoidal motor can be found graphically by considering the flux density as a function of the angle around the rotor, α, as shown in Figure 2.21. The plots of rotor-stator flux linkage as a function of the rotor position θ_r are given in Figure 2.26. The sinusoidal case is simple but the trapezoidal case is more complicated. If the airgap flux density of the trapezoidal motor in Figure 2.21 was a rectangular wave (with zero segments corresponding to the gaps between rotor magnets), the rotor-stator flux linkage would be the lighter trapezoid shown below. Due to fringing effects and the hysteretic B-H curve of the iron the actual flux density deviates from the ideal, as shown in Figure 2.21, thus the actual rotor-stator flux linkage differs, as shown in Figure 2.26. Note that the angle β (which defines the ideal case) has correspondence between Figure 2.20, Figure 2.21, and Figure 2.26.

---

[7] Notice that the peak value is denoted by the uppercase Ψ. This should perhaps be denoted only the subscript 'p' as with other variables, but the notation adopted here is used to better align with space vector notation in the rest of the report.

Figure 2.26 – Rotor-stator flux linkage for a sinusoidal and arbitrary trapezoidal motor.

The expressions for torque and bEMF were derived previously as Equations (2.31)-(2.32) and Equations (2.36)-(2.37).

(2.31): $T(\theta_r) = -N \cdot D \cdot Y \cdot B_p \cdot \sin(\theta_r) \cdot i(t)$

(2.32): $T(\theta_r) = -K_t \sin(\theta_r) \cdot i(t)$

(2.36): $e(\theta_r) = -N \cdot D \cdot Y \cdot B_p \sin(\theta_r) \cdot \omega(t)$

(2.37): $e(\theta_r) = -K_e \sin(\theta_r) \cdot \omega(t)$

Comparing Equations (2.43)-(2.44), (2.31)-(2.32), and (2.36)-(2.37) makes clear the equivalence shown in Equation (2.48).

$$\Psi_R = K_e = K_t = N \cdot D \cdot Y \cdot B_p \tag{2.48}$$

Equation (2.48) shows that the units of K_e and K_t are the units of flux linkage, $\left[\text{Wb}(\cdot\text{turns})\right]$. Further, the derivative of Equation (2.44) with respect to rotor position is Equation (2.49).

$$\frac{d}{d\theta_r}\psi_R(\theta_r) = -\Psi_R \sin(\theta_r) \tag{2.49}$$

Comparing Equation (2.49) with Equations (2.32) and (2.37) makes clear the relationships shown in Equations (2.50) and (2.51).

$$T(t) = \frac{d}{d\theta_r}\psi_R(\theta_r) \cdot i(t) \tag{2.50}$$

$$e(t) = \frac{d}{d\theta_r}\psi_R(\theta_r) \cdot \omega(t) \tag{2.51}$$

Similar to Equation (2.48), these can be written as Equation (2.52).

44

$$\frac{d}{d\theta_r}\psi_R(\theta_r) = k_e(\theta_r) = k_t(\theta_r) = -\sin(\theta_r)$$ (2.52)

To recapitulate, the torque and bEMF were previously found via the BLi and BLv laws, respectively. Then the rotor-stator flux linkage was derived (Equations 2.43-2.44) and its position derivative was computed (Equation 2.49). By comparing the former expressions for torque and bEMF it was seen that they could be rewritten in terms of the position derivative of rotor-stator flux linkage (Equations 2.50 and 2.51). These two derivations demonstrate the two common perspectives from which we usually think about motor operation. The BLi and BLv laws focus on the conductors (of the coilsides) and how much flux they "cut" as the rotor moves, whereas use of the flux linkage focuses on the entire winding. Obviously both interpretations are useful but it is the flux linkage method that is most used in modern analysis (and thus, in this report).

That Equations (2.32) and (2.37) are identical to Equations (2.50) and (2.51) (with Equation 2.52) is not a coincidence. When the circuit model was developed earlier, the bEMF was given in Equation (2.25) as the *time* derivative of the rotor-stator flux linkage ψ_R, which was left general at that stage in the development. Now that we have found an expression for ψ_R in a sine motor (Equation 2.44), Faraday's law can be invoked to yield Equation (2.53).

$$e(t) = \frac{d}{dt}\psi_R(\theta_r(t))$$

$$= \frac{\partial\psi_R(\theta_r)}{\partial\theta_r} \cdot \frac{d\theta_r}{dt}$$

$$e(t) = \frac{d\psi_R(\theta_r)}{d\theta_r} \cdot \omega$$ (2.53)

Equation (2.53) is seen to be identical to Equation (2.51). This shows that the latter is valid and is just a restatement of Faraday's law. Similarly, Equation (2.50) is simply a restatement of another result (although there is no associated surname). For the nonsalient machines considered here, Equation (2.50) is the same as the torque determined by taking the partial derivative with respect to rotor position of the energy (flux held constant) or of the coenergy (current held constant) stored in the magnetic circuit [68, pp.59-60], [69, p.5.36]. The topic of stored energy and coenergy is useful to study but is far beyond scope; it can be found in many older machine texts such as [27], [42], [26], [38]. Aside from highlighting the duality between torque and bEMF that we have come to expect, this derivation shows how each is related to the rotor-stator flux linkage, which is a key idea in the SV model.

45

Rotor-stator flux linkage is a result of the spatial interaction of the rotor flux density distribution and the stator winding. Its determination requires an integral evaluation of an analytic expression, a simulation, or measurement in the lab. For the simple concentrated winding, the relationships are easy to visualize, but motors are often constructed such that the rotor-stator flux linkage does not have these simple relationships with the rotor flux distribution. Fortunately, the torque and bEMF functions will always be related to the rotor-stator flux linkage as shown here. Thus the take-away from this subsection is that there are different ways to build sinusoidal and trapezoidal motors but as far as torque production and bEMF generation are concerned, those differences are irrelevant and all that matters is the rotor-stator flux linkage (or the bEMF/torque function) as a function of rotor position. This will be made clear at the end of this chapter.

General Electromechanical Models

There are essentially only two pieces missing from the complete electromechanical model of a three-phase motor: the contribution of the other two phases and the mechanical model. First, we only consider a single phase, as the earlier parts of this chapter have done. The electromechanical simulation diagram for a motor with only one phase, plus its mechanical load, can be obtained by examining Figure 2.18 (Equation 2.25), Figure 2.23 (Equation 2.34), and Figure 2.25 (Equation 2.39). This is shown in Figure 2.27, where the variables are as follows:

R	armature resistance
L	self inductance (Figure 2.27)
L_s	synchronous inductance (Figure 2.28)
b	friction (rotor & load)
J	inertia (rotor & load)
v	applied terminal voltage
i	armature current
T	developed electromagnetic torque
T_L	load torque (rotor & load)
ω	rotational velocity

In all block diagrams in this report, the polarity of a vector or signal is always shown to the arrow's own left.
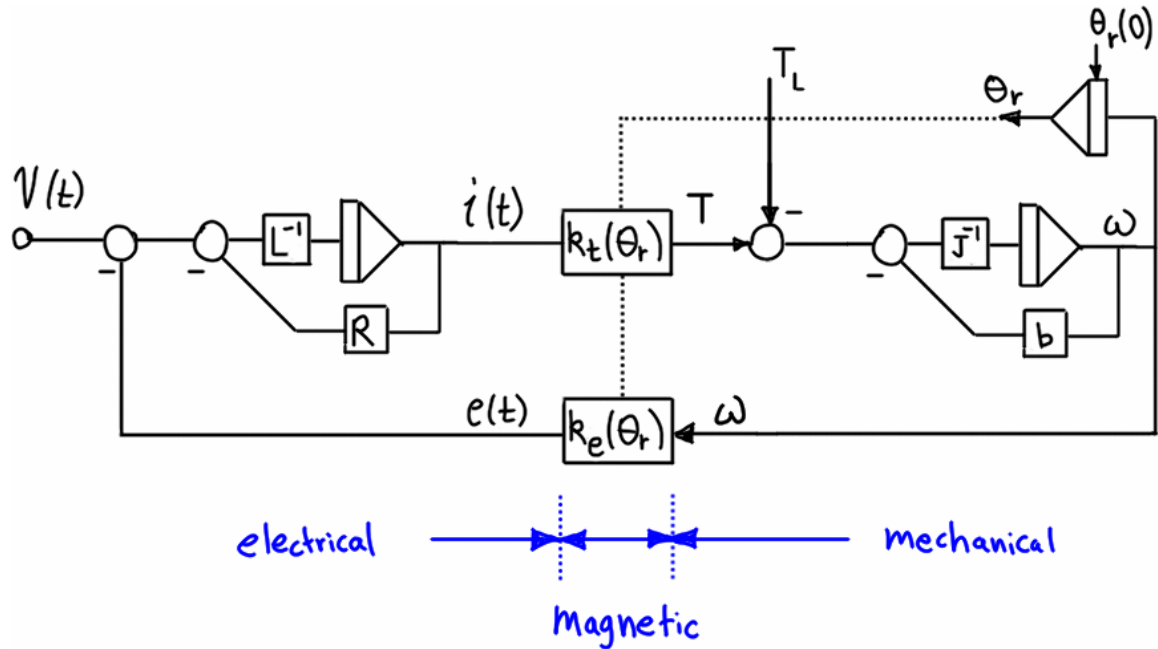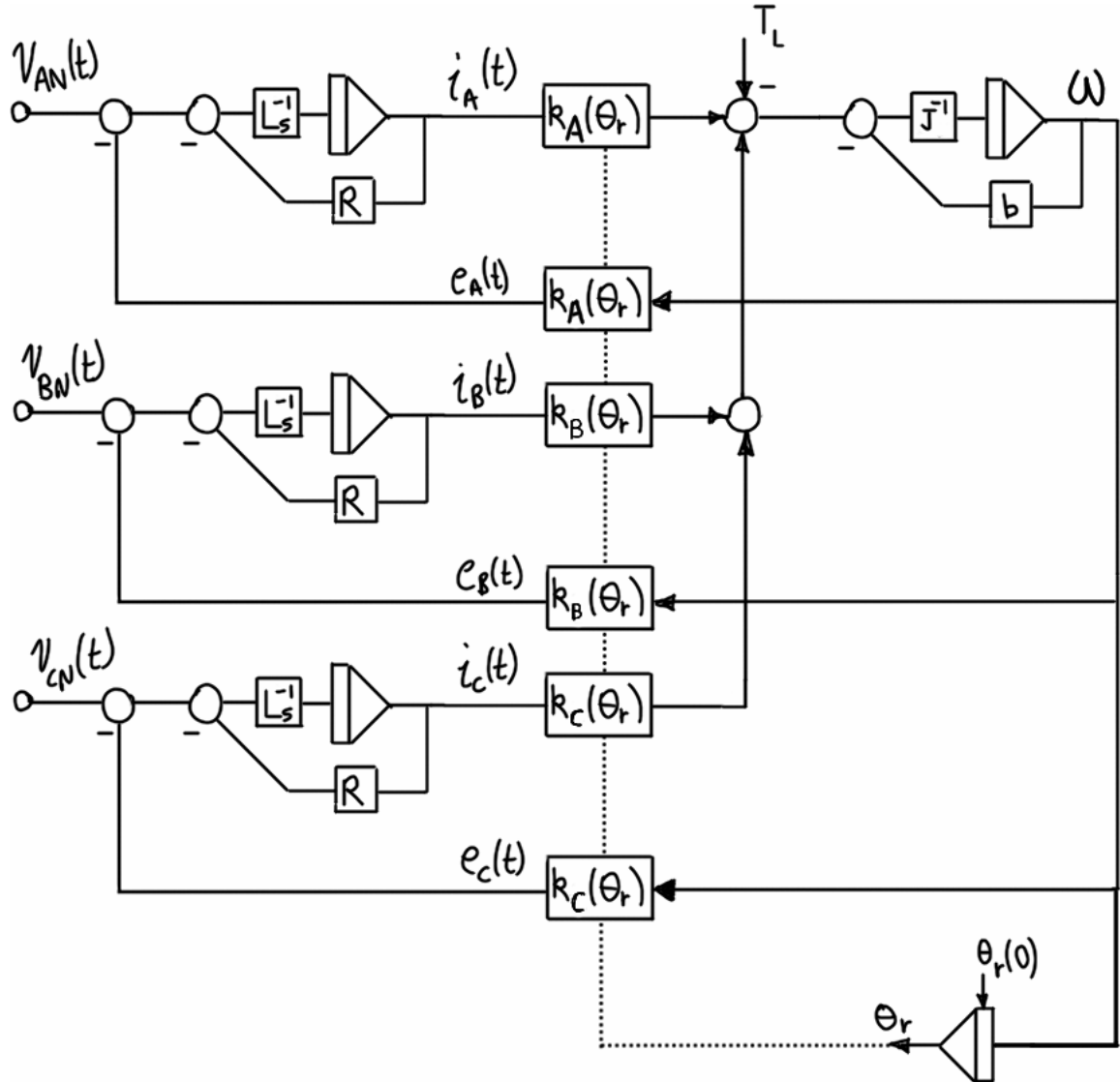
Figure 2.27 – Simulation diagram of general motor.

The figure shows the relationships developed in this chapter. The torque function is the "cascade connection" and the bEMF function is the "feedback connection" between the electrical portion and the mechanical portion. The coupling exists via the magnetic medium (rotor-stator flux linkage). Note that the bEMF acts as a disturbance in the voltage-to-current conversion and the load torque acts as a disturbance in the electromagnetic-torque-to-velocity conversion. These relationships are derived from first principles so there is essentially no simpler model of a motor. That is, the torque production, bEMF generation, and their relationship will exist in any motor in a way very similar to that shown.

Thus, this model could represent a brush DC motor (in that case the torque and bEMF functions would be constants). Here, it will be used to represent a single winding in a BPMS motor and it will be called the "phase model." If a per-phase model is used for each phase, three of them combined can be used to represent a three-phase motor; this is called the "phase-variable model" and is shown in Figure 2.28.

Figure 2.28 – Phase-variable simulation diagram of general motor.

Clearly, each phase contributes to the overall torque production, thus torque production of a three-phase motor cannot be investigated unless all three phases are considered. Additionally, each winding has mutual inductive coupling with the other windings. The duality between torque and bEMF would then suggest that the circuit of each phase could not be investigated unless all three phases are considered. This is true but for a wye-connected motor it turns out that this coupling can be removed by replacing the simple inductance with the "synchronous inductance" L_s (Appendix B). Thus, the phase-variable model shows that torque is produced by all three phases but the electrical circuits are not coupled. However, it is vital to note that the applied voltages are the *line-neutral* voltages (this directly follows from the previous electrical model; combining three models (such as that shown in Figure 2.18) the "$v(t)$" is by definition the line-neutral voltage). This means that the model is correct only for applied three-phase voltages that

do not contain a common-mode component. In the next section the ideal waveforms do not contain a ZS component so this is no harm, and in the next chapter, the space vector model will take care of this.

The phase-variable simulation model will be used to develop concepts and to compare torque production in sinusoidal and trapezoidal motors. A summary of the models used in this report is as follows.

- The *single-phase equivalent* (SPE) model (introduced in the next chapter) represents one phase of the machine in operation. It is likely the most familiar model of a three-phase machine but it is valid only for a sinusoidal motor driven by sinusoidal currents and operating in steady-state. The SPE model cannot be used with salient machines.

- The *phase-variable model* described above can describe a nonsinusoidal machine in transient conditions but it is difficult to work with and does not provide very intuitive results unless solved on a computer. The form shown above is useful for basic torque analysis (shown in the next section) but will be most useful for deriving the space vector model.

- The *space vector* model incorporates the combined action of each phase, like the three-phase simulation model, but it is condensed into a two-phase equivalent version that is easier to work with. It is valid for arbitrary currents, even in transient operation, but can only describe sinusoidal motors. The space vector model is simply the complex-valued representation of the traditional "two-axis synchronous" model; both will be examined in the next chapter.

Trapezoidal and Sinusoidal BPMS Motors

This chapter has developed the per-phase model of a motor and the previous section described how three of these can be combined to give the complete model of a three-phase motor. Now that we have this model, the torque production of three-phase trapezoidal and sinusoidal motors will be examined. This provides an explanation of each motor's operation, which facilitates a discussion of whole-motor torque constants and the ideal type of winding current control (electronic commutation) required of each motor. Finally, the chapter concludes with a commentary regarding the differences between the trapezoidal and sinusoidal motor. While that discussion may not be useful to the general reader the conclusions are crucial to the remainder of the report.

Torque Production

The per-phase torque functions for the sinusoidal and trapezoidal motor types were shown in Figure 2.22. The per-phase torque produced as a function of rotor position will match the torque function in shape when a DC current is forced through the winding. In this case if a hand crank were attached to the shaft and rotated through one revolution, the operator would have to **exert** positive (CCW) torque on the crank from 0°-180°, whereas the operator would have to **resist** the force of the crank (by applying negative (CW) torque) from 180°-360° as it seeks to return to the equilibrium point from which it started (both the 0° and 180° positions are equilibrium points). The force would vary with position according to Figure 2.22, depending on the type of motor. The concept of a torque function is an important one because it shows this bipolar symmetry that is present in every PM or wound-field machine. Since the product of bEMF and current divided by speed is torque, this makes it clear that both DC and AC motors require the polarity of the armature current to reverse each electrical cycle in order to produce always-positive (but not constant) torque.

In a traditional brush DC motor the torque function of each winding is made to look something like that of the trapezoidal motor. The commutator reverses the current flow in each armature winding every 180°. There are several armature windings, so as one winding is energized another is de-energized, thereby producing a nearly-constant torque. AC motors do not have a brush-commutator system and therefore require that the terminal current be reversed every half cycle by electrical or electronic means. For this reason the action of controlling the current relative to the shaft position in a brushless motor is sometimes called *electronic commutation*. There are two

common schemes in use and they differ significantly from one another. But one thing they have in common is that each they seek to drive current in a winding with the same polarity as the bEMF/torque function.

Equation (2.40) describes the energy balance for one phase acting alone. Since the three-phase motor has three phases and each phase contributes to torque (per Figure 2.28), the energy balance for the three-phase motor is Equation (2.54), where all quantities are instantaneous functions of time. This equation is valid for transient and steady-state conditions and is valid for any bEMF and current waveshape; it holds even if the phase bEMFs are asymmetrical or displaced by an angle other than 120°.

$$\tau \cdot \omega = e_A i_A + e_B i_B + e_C i_C \tag{2.54}$$

If the bEMF terms are expanded according to Equation (2.39), each side of Equation (2.54) could be divided by ω, leaving the bEMF function on the right-hand side, Equation (2.55).
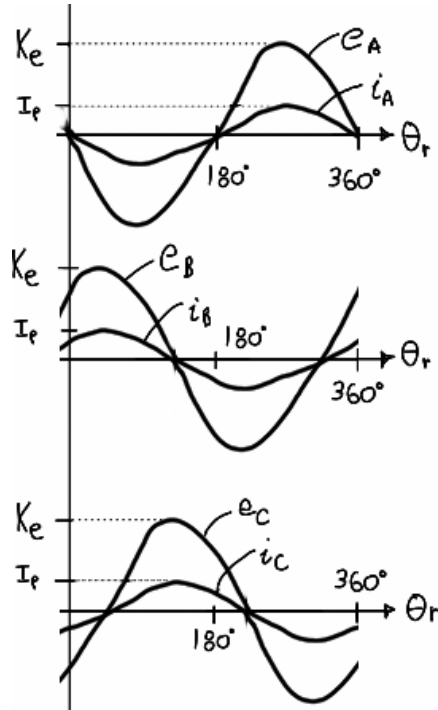
$$\tau = k_{eA}(\theta_r) \cdot i_A + k_{eB}(\theta_r) \cdot i_B + k_{eC}(\theta_r) \cdot i_C \tag{2.55}$$

Each winding of a sinusoidal motor will have a torque function like the one shown in Figure 2.22, but since each winding is displaced from the other windings by 120°, each winding's torque function will be similarly displaced by 120°. Assuming balanced bEMF waveforms, this is expressed as Equation (2.56) and is shown in Figure 2.29.[8]

$$\tau = -K_e \sin(\theta_r) \cdot i_A - K_e \sin(\theta_r - 120^\circ) \cdot i_B - K_e \sin(\theta_r + 120^\circ) \cdot i_C \tag{2.56}$$

---

[8] The math is less cumbersome if cos(θr) or +sin(θr) is used and the figures are clearer if an arbitrary rotor angle is used. Most of the literature takes advantage of this and as a result, plots such as Figure 2.29 (and especially Figure 2.31) look very different in each reference. Additionally a single article will often use several different references for θr and never mention the change nor discuss its importance. While each approach is perhaps acceptable it has been the author's experience in learning that using arbitrary references and divorcing the plots from the actual rotor position is a detriment to properly visualizing synchronous motor operation and FOC in particular. Thus it is strictly avoided in this report in faith that a less-simple introduction can be endured in exchange for a more accurate understanding in the long run. Finally, there are two common choices in defining an absolute θr and they are 90° apart, thus there are two valid versions of the "actual" waveforms shown here; the alternate version will be discussed in Appendix E.
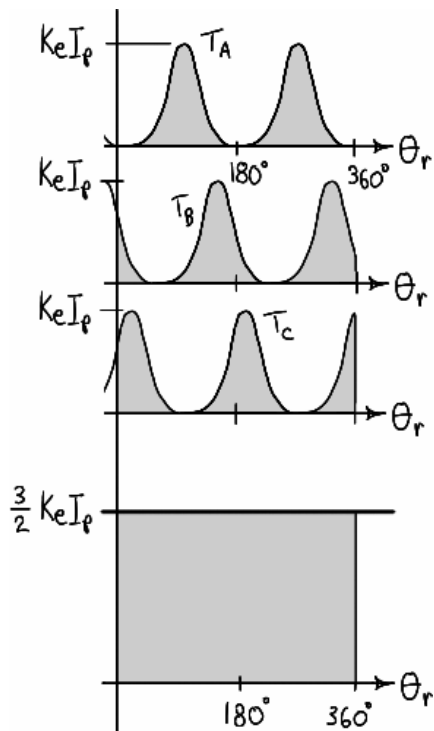
Figure 2.29 – Back-EMF and drive current for sinusoidal BPMS motor.

If sinusoidal currents of amplitude I_p are forced into the windings and kept in phase with the bEMF, the torque produced is given by Equation (2.57).

$$\tau = \left[-K_e \sin(\theta_r)\right] \cdot \left[-I_p \sin(\theta_r)\right] + \left[-K_e \sin(\theta_r - 120°)\right] \cdot \left[-I_p \sin(\theta_r - 120°)\right]$$

$$+ \left[-K_e \sin(\theta_r + 120°)\right] \cdot \left[-I_p \sin(\theta_r + 120°)\right]$$

$$\tau = K_e \cdot I_p \left[\sin^2 \theta_r + \sin^2(\theta_r - 120°) + \sin^2(\theta_r + 120°)\right]$$

$$\tau = \frac{3}{2} K_e \cdot I_p \tag{2.57}$$

Thus, each phase's contribution is a $\sin^2$ term displaced 120° from the other phases' and the result is a constant torque, as shown in Figure 2.30. When the drive currents are kept in phase with the bEMFs, it is seen that the torque is linearly proportional to the peak of phase current. Since $K_e = K_t$, it makes sense that the per-phase torque would be proportional to $K_e \cdot i(t)$.

Figure 2.30 – Torque production in sinusoidal BPMS motor.

Torque production in a three-phase sinusoidal motor is not usually visualized on a per-phase basis; rather the motor is analyzed as a whole using the single-phase *equivalent* or vector descriptions. Both methods will be developed in the next chapter, but the per-phase analysis here will more easily facilitate comparison with the trapezoidal motor. When sinewave currents are driven into the windings (in synchronism with the shaft position) the motor drive is called a sinewave drive (or "sinusoidal commutation").

Each winding of a trapezoidal motor will have a torque function like the one shown in Figure 2.22, but that of each phase will be displaced by 120° as in the sinusoidal motor; this is shown in Figure 2.31 along with the typical drive currents.
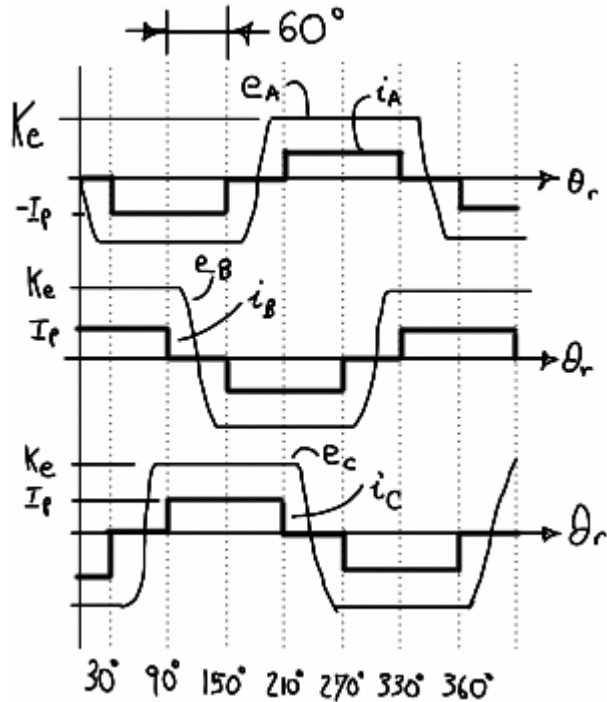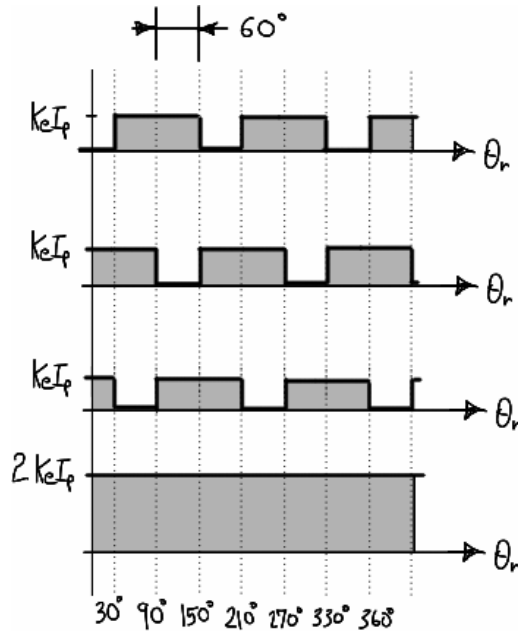
Figure 2.31 – Back-EMF and drive current for trapezoidal BPMS motor.

Unlike the sinusoidal motor, it is seen that the trapezoidal motor is driven with discontinuous currents, again with magnitude I_p. This current control scheme goes by various names (such as trapezoidal drive, six-step commutation, squarewave current drive) but these are all misleading because each can carry several different meanings depending on context. Thus, this report will call this *120° six-step* commutation. Torque is produced by a phase winding only when the bEMF and current are both nonzero, thus we do not need any analytical expression for the bEMF—as long as it is constant over the 120° "commutation period" it can be considered a DC value in the torque equation. This is why the trapezoidal motor described earlier in the chapter was called an "arbitrary" trapezoidal motor—in the ideal case it does not really matter what shape the bEMF takes on between commutation periods as long as there is at least 120° of flat-topped bEMF.[9] Only two windings contribute to torque at any given instant, thus the torque can be expressed as Equation (2.58).

$$\tau = 2 \cdot K_e \cdot I_p \tag{2.58}$$

The per-phase torque and total torque for a trapezoidal motor are shown in Figure 2.32. Similar to the sine motor, it makes sense that the per-phase torque is equal to $K_e \cdot i(t)$.

---

[9] Real trapezoidal motors rarely achieve this 120° flat top. Additionally, when a trapezoidal motor is driven with non-ideal currents (whether intentionally or as a result of operation with motor-drive mismatch or at the edge of normal operation) the waveshape between the flat segments *does* matter because it interacts with the bEMF to produce torque ripple.

Figure 2.32 – Torque production in trapezoidal BPMS motor.

Although the exact same mechanism is responsible for torque production in the two types of motors, comparing Figure 2.30 and Figure 2.32 makes it clear that the interaction of the current and the torque function in each motor causes a very different per-phase *contribution* to torque in the two types of motors. These are the desired modes of operation that typify sinusoidal and trapezoidal motors.

Torque & Back-EMF Constants

In earlier subsections, Equations (2.42) or (2.52) demonstrated that the per-phase torque and bEMF functions $[k_t(\theta_r), k_e(\theta_r)]$ are identical for a given motor and thus the per-phase torque and bEMF constants (K_t, K_e) are identical (Equation 2.48). Regardless of the motor type, the per-phase K_e is defined as the peak value of line-neutral bEMF per unit angular velocity and the per-phase K_t is defined as the peak value of torque per unit peak current. These definitions are always true, but they are defined in terms of line-neutral quantities which are not always measurable when a neutral connection is not available; they are rarely found on motor datasheets. The previous section analyzed torque production of the overall motor and it was observed that when the current is properly controlled, total torque in a sinusoidal and trapezoidal motor were given as Equations (2.57) and (2.58), respectively. Since in practice one is only concerned with the total torque, an "overall torque constant" can be defined for each motor by dividing each equation by the peak of the phase current, I_p. These torque constants are defined by Equation (2.59), where $K_e = K_t$. The uppercase subscript indicates that the constant describes total torque, not per-phase torque.

$$K_T = \frac{3}{2} K_e \quad \text{(sinusoidal)}$$

$$K_T = 2K_e \quad \text{(trapezoidal)}$$

(2.59)

Since there is no such thing as "overall" bEMF, there is no corresponding constant K_E. However, since the motor neutral is not usually available, only line-line parameters can be measured and the bEMF constant is often specified as a line measurement, $K_{e,LL}$. Due to the way in which the two motors are typically controlled, for the sinusoidal motor the line-line voltage is $\sqrt{3}$ larger than the line-neutral voltage but for the trapezoidal motor the line-line voltage is twice as large as the line-neutral voltage. Using these relationships and Equation (2.59), the torque constants in terms of line quantities can be found and are given by Equation (2.60).

$$K_T = \frac{\sqrt{3}}{2} K_{e,LL} \quad \text{(sinusoidal)}$$

$$K_T = K_{e,LL} \quad \text{(trapezoidal)}$$

(2.60)

These values of K_T are valid when the proper type of current is fed to each motor. Later the case will be examined when improper current is fed to the motors. Finally, it must be noted that there are several variants of these values used throughout the literature and this seems to be a large point of confusion. Those given here have been selected to provide technically-accurate continuity between the per-phase and three-phase discussions. Most variants in the literature can be resolved but there have been a few which the author could not decipher. [69] gives the most detailed coverage of the subject of these constants.

Electronic Commutation

The trapezoidal motor can theoretically produce ripple-free torque when driven with ideal rectangular currents, though this is not completely achievable in practice (discussed later). Since the current in a trapezoidal motor is DC over the flat-topped bEMF, since it is switched full-on over the commutation period, and since the polarity of the current is reversed once per electrical cycle, this motor *resembles* a brush DC motor without the brushes. For this reason it is sometimes called a Brushless DC Motor (BLDC), although claims in the literature that it is simply a brush DC motor "turned inside out" are false, as should be apparent from prior discussion. Further, since the current is controlled by only electronic means, it is sometimes referred to as an Electrically-Commutated Motor (ECM) or electronically switched motor. As mentioned, the process of controlling the current relative to shaft position is often called electronic (current) commutation. For a trapezoidal motor the current changes only six times per revolution so Hall-effect sensors are often used with simple logic circuits to determine which windings should carry

which polarity of current at what time (i.e., they are used with logic to "commutate the motor"). Notice that the commutation scheme need only perform the traditional role of the commutator: to reverse polarity and to interrupt current flow—the magnitude of the current is controlled independently according to the torque demanded of the motor. A conceptual diagram of a trapezoidal motor controller is shown in Figure 2.33, where the required current is given by Equation (2.61) and K_T is that for a trapezoidal motor. The commutation logic depends on the placement of the Hall effect sensors but is always found in conjunction with Figure 2.31. For this simple case the commanded current is a DC value given by Equation (2.62) and is equal to the reference current since an ideal source is assumed.

$$\tau = K_T I_p \quad \Rightarrow \quad I_p^{ref} = \frac{\tau^{ref}}{K_T} \tag{2.61}$$

$$i^* = I_p \tag{2.62}$$
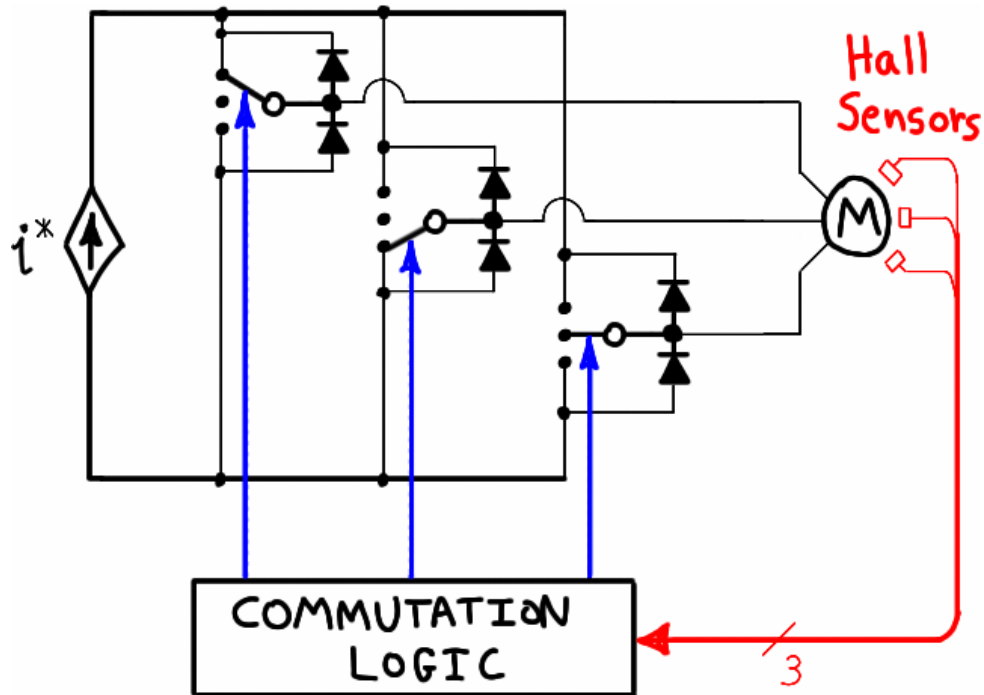
Figure 2.33 – Torque control of trapezoidal BPMS motor.

Though less fitting, *electronic commutation* is also used to describe current control in the sinusoidal motor; sometimes it is called *phasing*. It is clear that the sine motor is capable of producing ripple-free torque when driven with properly-phased sinusoidal currents. It is sometimes called a Permanent Magnet Synchronous Motor (PMSM) since it is just like the "classic" synchronous motor, with the wound-field rotor replaced by a PM rotor. The current

control scheme must keep sinusoidal currents aligned in time with the rotor position. In its most basic form, this requires a continuous position sensor (resolver) or near-continuous sensor (absolute encoder). While the rotor is rotating the required instantaneous value of phase current changes continuously, even when the commanded torque is constant. Thus for the sinusoidal motor, current control cannot be separated from the commutation or phasing as it can for the electronically switched motor. A conceptual diagram of a sinusoidal motor controller is shown in Figure 2.34, where the peak reference current is again given by Equation (2.61) and the commanded currents of each phase are given by Equation (2.63), where K_T is that for a sinusoidal motor.

$$\begin{cases} i_A^* = I_p^{ref} \cdot \left[-\sin(\theta_r) \right] \\ i_B^* = I_p^{ref} \cdot \left[-\sin(\theta_r - 120^\circ) \right] \\ i_C^* = I_p^{ref} \cdot \left[-\sin(\theta_r + 120^\circ) \right] \end{cases} \qquad (2.63)$$
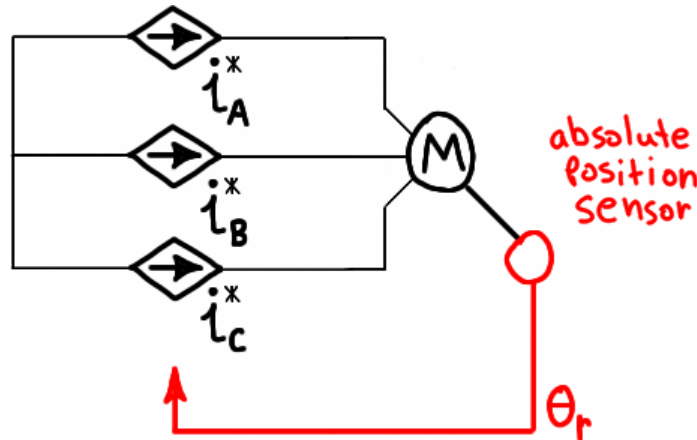
Figure 2.34 – Torque control of sinusoidal BPMS motor.

The actual circuitry to accomplish the conceptual torque control presented here will be discussed in Chapter 4 (for the case of sinusoidal motors).

Types of Brushless Permanent Magnet Motors

A ridiculous number of acronyms are found in the literature to describe BPMS motors, such as the following:

- BACM   brushless AC motor
- BDCM   brush/brushless DC motor
- BLDC   brushless DC
- BLSM   brushless servo/synchronous motor

59

- BPM   brush/brushless PM
- ECBM   electronically commutated brushless motor
- ECDCM   electronically commutated DC motor
- EDCM   equivalent DC motor
- PMAC   permanent magnet AC
- PMBDC   permanent magnet brush/brushless DC
- PMDC   permanent magnet DC
- PMSM   permanent magnet synchronous motor
- SPM   sinusoidal/surface/synchronous PM
- SPMSM   surface PM synchronous motor
- SMPMSM   surface mounted PM synchronous motor

Most of these acronyms are unsuitable because they are ambiguous or contradictory. There seems to be an emerging trend in the popular literature: BLDC is used to refer to a trapezoidal motor and; PMSM is used to refer to a sinusoidal motor. But even within that trend there is much inconsistency. Additionally there is little consistency among motor manufacturers, but it is sometimes observed that motors meant to be driven with 120° currents are called "brushless DC" (BLDC) motors whereas motors meant to be driven with sinewave currents are called "brushless AC" (BLAC) servos. In surveying several motor manufacturers' websites, some have two separate links (akin to BLDC and BLAC) that do point to two separate product lines, indicating the possibility of two different motors. Others have two separate links (akin to BLDC and BLAC) that point to the same product; in this case there is obviously only one motor type. Others have a single link, indicating that there is only one motor type offered by that manufacturer. As mentioned in the section on taxonomy, the motors considered in this report are all synchronous, brushless, AC, and they all employ permanent magnets. Thus this report has used *trapezoidal* and *sinusoidal* (or the shorter *trap* and *sine*) to describe the two common variants of the BPMS (brushless permanent magnet synchronous) motor, with the understanding that both types are synchronous and AC. There are many alternative definitions of AC and DC motors that have advantages (a good example is [69, p.1.3]), but most tend to unnecessarily segregate the brushless motors into the trap or sine types.

It is the author's opinion that the difference between trap and sine BPMs is surrounded by more misunderstanding and confusion than any other subject in the field of brushless motor control (the second-place award goes to the distinction between vector- and field-oriented- control). Magazine and online articles, internet discussion forums, datasheets, and application notes are often filled

with misconceptions. The primary issues are machine construction, current control, and "torque ripple," with secondary issues being efficiency, "harmonics," and audible noise. While some references are weakly worded (as if the authors are uncertain of their claims), it is not difficult to find sources with clear wording from both extremes of each issue. For example, "there is absolutely no difference between sine and trap motors," and "sine and trap motors are entirely different machines." Or, "sine and trap machines require different types of current commutation," versus "either motor may be driven by similar means." Or, "motor and drive types may be mixed," versus "mixing motor and control types may cause serious issues." Without field experience it is difficult to determine the truth regarding each issue. The largest difficulty seems to be that the amount of popular literature exceeds the amount of academic literature (concerning this issue). The author has found that although there are excellent resources to help a newcomer distinguish the difference, it takes a steady research effort to locate these resources, it takes time to work through and comprehend these resources, and it is very difficult to "unlearn" solid misconceptions. Some references include [68], [69], [63], [65], [76].

The author's understanding is summarized here. Sine and trap motors may be constructed a number of different ways but as far as torque production and bEMF generation is concerned, the motors differ only in the shape of the rotor-stator flux linkage. This difference can be created by changing the way the winding is distributed in the stator slots, by adjusting the magnetic design (airgap and tooth/slot dimensions), by adjusting the construction of the rotor and physical shape of the rotor magnets, and by adjusting the magnetization profile of the magnets [68], [69]. As shown earlier, the bEMF/torque function is the derivative of the rotor-stator flux linkage with respect to rotor position and in the general case torque is produced as shown in Figure 2.28 and Equation (2.54). It is clear that the fundamental mechanism by which torque is produced is identical regardless of the type of motor. If a motor can be categorized as trap or sine—and ideal drive currents are forced into it—the motor will produce "ideal" torque. There is much misinformation about the possibility or impossibility of driving a motor with non ideal current waveforms. Quite simply, either type of motor (or any arbitrary motor not fitting either classification) can be driven by any arbitrary current waveform. The torque produced in each case will be different, the efficiency will be affected, and the performance of the current controller will be affected; these issues will be discussed later.

CHAPTER 3 - Sinusoidal BPMS Motors

The ultimate purpose of this chapter is to develop a space vector model for the sinusoidal BPMS motor because that model and its understanding (reference frame theory) are the basis for all modern motor modeling and control schemes. In order to achieve this goal the chapter is split into three parts. In Part I the standard analysis of sinusoidal synchronous machines is presented in the time and phasor domains. Part II introduces and discusses the space vector definition, notation, and interpretation by building on the understanding of the synchronous machine presented in Part I. Finally, Part III applies the space vector concepts from Part II to the material from Part I to yield the space vector model of a BPMS motor.

It must be emphasized that this chapter concerns only sinusoidal motors. (Appendix C clarifies the definition of a sinusoidal motor.) Part I considers only *sinusoidal currents*. In Parts II and III, sinusoidal and arbitrary currents will each be considered as required.

Part I – Sinusoidal BPMS Motors with Sinusoidal Currents

Part I reviews the nonsalient sinusoidal synchronous machine operating on *balanced sinusoidal current in the steady state*. It is similar to the standard treatment found in most machine texts except that the field winding has been replaced with a permanent magnet and there are no damper/amortisseur windings or starting cage. First the general physical structure of the PMSM is presented including conventions for winding directionality and magnetic axes. A brief discussion of wye and delta connections is given next. The rotating stator MMF distribution is then developed, both graphically and mathematically; this includes a discussion of the relationship between electrical and mechanical angular measures. A common expression for electromagnetic torque is formulated and the phasor-based electrical model (the single-phase equivalent) is developed.

Physical Construction and Windings

The general structure of the three-phase brushless permanent magnet synchronous machine is exactly like that presented in the previous chapter except that there are two additional phase windings on the stator as shown in Figure 3.1. Per the convention given in Appendix C, the buried coilsides are used to indicate the center of the sinusoidal windings. Note that the phase order of the axes increases in a counter-clockwise direction. This convention is not universal in the literature but it is by far the most convenient mathematically and graphically thus is used here.
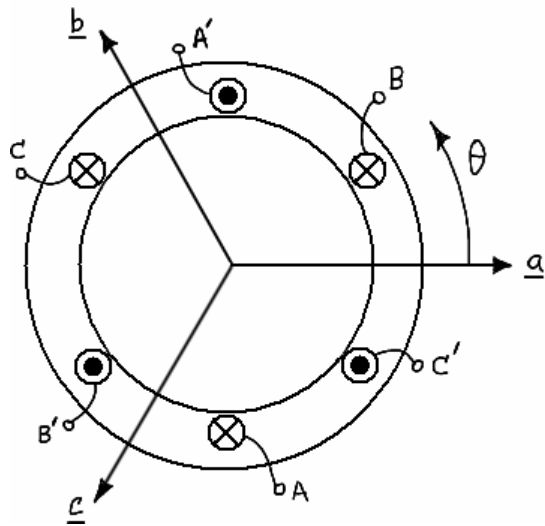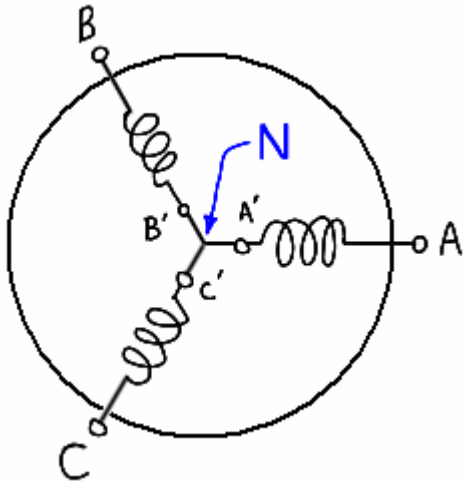
Figure 3.1 – Stator of three-phase sinusoidal synchronous machine.

Similar to any general three-phase load, the windings of a three-phase motor may be connected in wye (Y) or delta (Δ); if connected in wye the center connecting point (the *neutral*) may or may

not be brought out of the motor housing for connection purposes. It appears to the author that most brushless permanent magnet synchronous motors are connected in a wye configuration with no neutral terminal available, as shown in Figure 3.2. When no neutral terminal is provided, it is said that the neutral is *inaccessible*, *disconnected*, *floating*, or *isolated*. The traditional terminal designations ABC are used in this report, but XYZ and RST are found in the literature also and UVW is widely used in the motion control industry.

Figure 3.2 – Three phase wye-connected stator with three phase terminals.
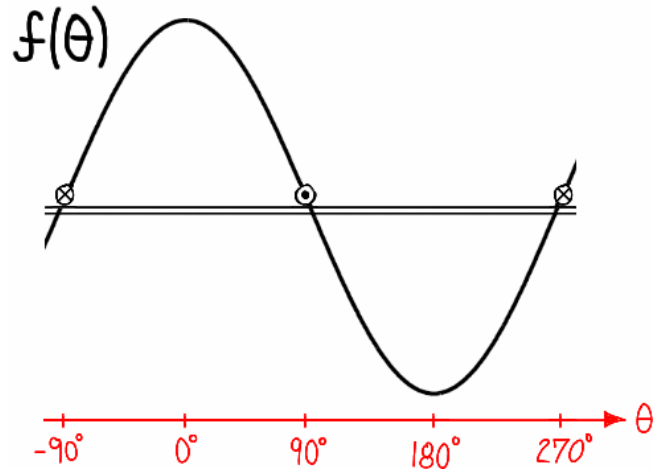
As far as the author can deduce, the most significant advantage that can be gained by using a delta connected winding in a BPMS motor is the possibility that the armature may be wound less expensively or more easily than a wye connected winding [69, p.5.21]. However, since the operation of a delta connected motor can be significantly different than that of a wye connected motor, the delta winding may provide certain benefits in special applications.[10] Further, if the bEMF contained the third harmonic it would cause current to circulate in a delta connected winding, contributing to copper losses without producing torque and this may potentially overheat the motor. Therefore, the delta connection can only be used efficiently when certain conditions are met [68], [69]. Although similarities exist, some of the analysis and control techniques applicable to a wye connected motor with isolated neutral will not hold for a

---

[10] In standard line-connected induction motors, the delta connection can provide some advantages. For this reason, 6-, 9-, and 12- terminal stators are available to allow the motor to be wired as a delta or wye, or one winding in delta and one winding in wye; the configuration can be either hard-wired or changed dynamically via contactors. Advantages include the ability to use a single motor with various supply voltages, the reduced starting current provided by a wye-start/delta-run configuration, and the ability to change the torque characteristic, perhaps among others [24, ch.20], [27, ch.10]. Permanent magnet synchronous motors are always used with a motor drive that supplants these older techniques so the delta connection offers no obvious advantage in these regards.

grounded-neutral wye or delta connected motor. *All subsequent discussion is directed toward wye-connected stators with an isolated neutral.*

The remainder of this report assumes that unless otherwise stated in a particular discussion, the windings are effectively sinusoidally distributed such that the airgap MMF is sinusoidally distributed in space as shown in the developed view of Figure 3.3.

Figure 3.3 – Developed view showing sinusoidal stator MMF distribution.
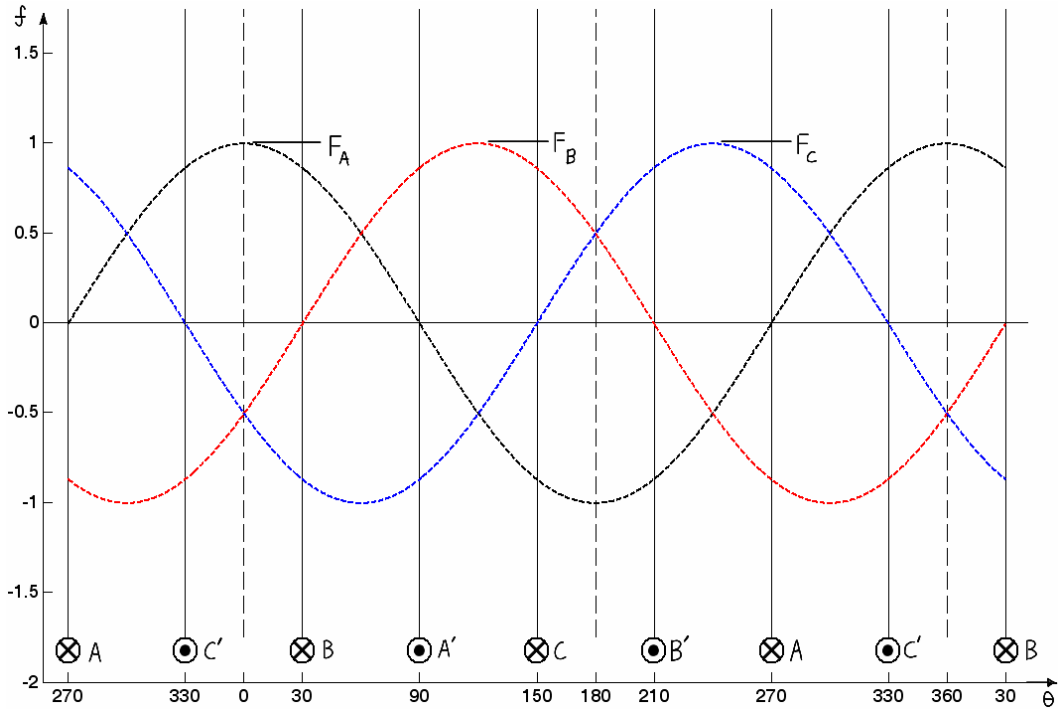
Recall that positive flux in the airgap is defined as that which travels from the rotor to the stator; additionally, flux density, magnetic field strength, and MMF share the same polarity.

The Rotating Field

The most fundamental aspect of a sinusoidal synchronous machine is the stator's rotating MMF wave (this MMF wave is the same as that produced by the stator of the polyphase induction machine). It will be developed graphically and then mathematically.

Graphical Illustration

To illustrate this concept a three-phase wye connected two-pole synchronous motor with sinusoidal MMF distribution is shown in developed form as Figure 3.4. To simplify illustrations, from this point forward the stator is understood to be on the top of the abscissa, the rotor is on the bottom, and the coilsides are drawn anywhere convenient. Further, it is essential to understand that this discussion regards the MMF produced by the stator alone—that is, the development proceeds as if the rotor magnets are not present (but the rotor steel is still in place).

Figure 3.4 – Developed view showing superimposed MMF distributions of all phases.
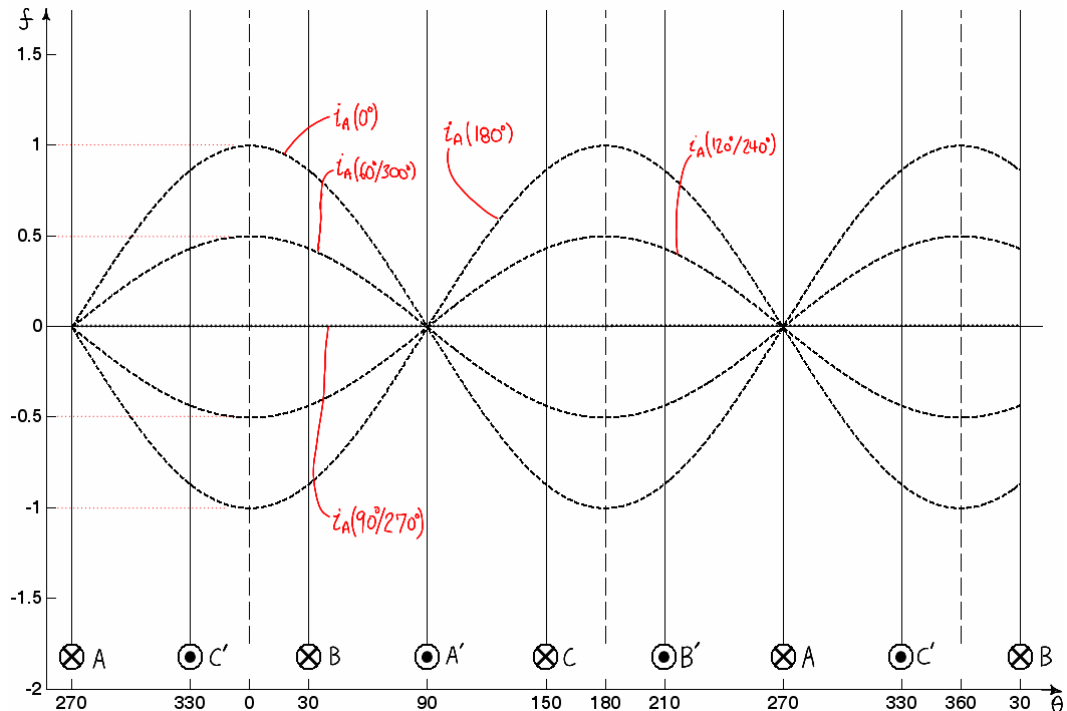
Figure 3.4 shows three plots of MMF (one for each phase) superimposed on a common axis. These are the MMFs that would be produced if each phase were separately excited by a DC current of unit-amplitude. The MMFs shown are therefore the maximum that each phase can contribute.[11] In actual operation the component MMFs will sum together and since all three phases cannot simultaneously carry full positive current, the per-phase components of MMF will never peak at the same time; the lines are dashed to serve as a reminder of this. The purpose of this figure is to graphically illustrate the MMF's sinusoidal distribution in space. Although the amplitude of the per-phase MMF peak will scale linearly with the current, the spatial distribution will remain sinusoidal. The per-phase MMF components can be represented by Equation (3.1), where N_e represents the effective number of winding turns (as defined in Appendix C) and θ represents the angle around the periphery of the machine, as shown in Figure 3.1.

---

[11] A current of unit-amplitude (1.0[A]) would produce an MMF of amplitude $(N_e / 2)$ [A-turn]; since this is the peak value of MMF produced for unit-amplitude current it is called the unit-amplitude value of MMF, as shown in the figure. Thus "unit-amplitude" does not refer to a numerical value of 1.0. This terminology is used to emphasize the relationship between current and MMF. In addition, it is not meant to indicate a value in the "per-unit" measurement system, which is *not* used in this report.
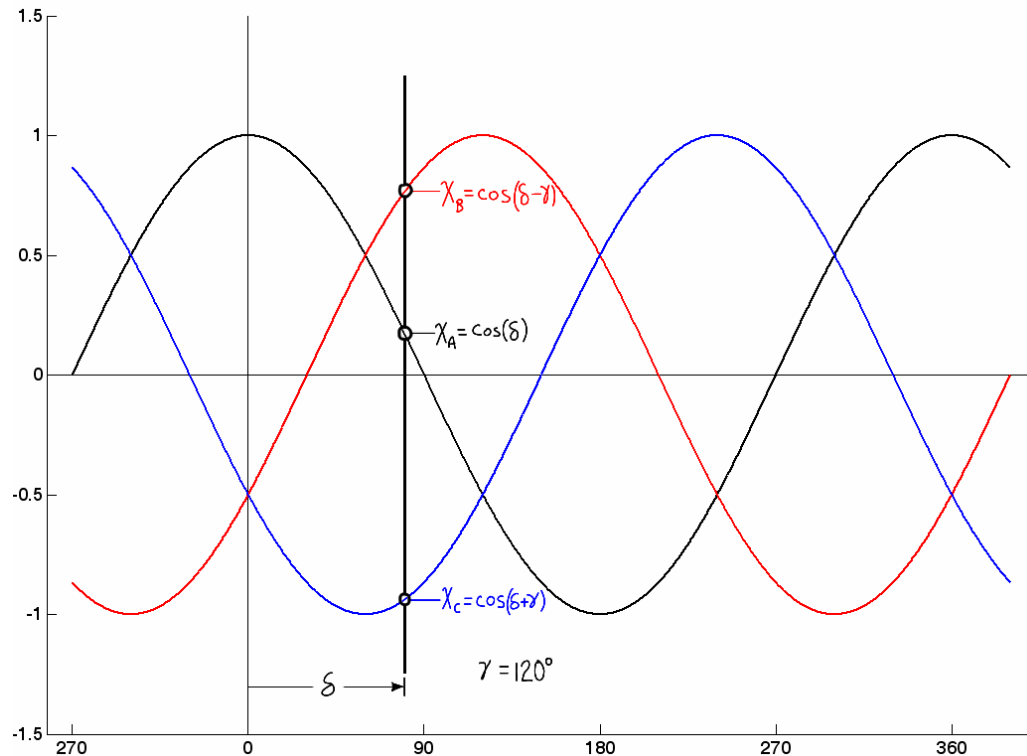
$$f_A(\theta) = \frac{N_e}{2} i_A \cos(\theta)$$

$$f_B(\theta) = \frac{N_e}{2} i_B \cos(\theta - 120°)$$ (3.1)

$$f_C(\theta) = \frac{N_e}{2} i_C \cos(\theta + 120°)$$

To further illustrate that the per-phase MMF space distribution is always sinusoidal, Figure 3.5 shows the component of MMF due to phase-A current at different electrical positions ωt=(0°, 60°, 90°, 120°, 180°, 240°, 270°, 300°), assuming $i_A(t) = 1.0\cos(\omega t)$. Each phase's component of MMF is a standing wave in space.

Figure 3.5 – Stator MMF distribution of phase-A at various electrical positions in time.

Figure 3.6 shows one complete electrical cycle of unit-amplitude balanced cosinusoidal three-phase general quantities (notice that the ordinate is not at the far left-hand side). At any given electrical angular position δ, a vertical reference line will intersect all three phase plots. The instantaneous value of each phase quantity is that value at the intersection with the reference line. As a mathematical property, the sum of all instantaneous phase values will always be zero.
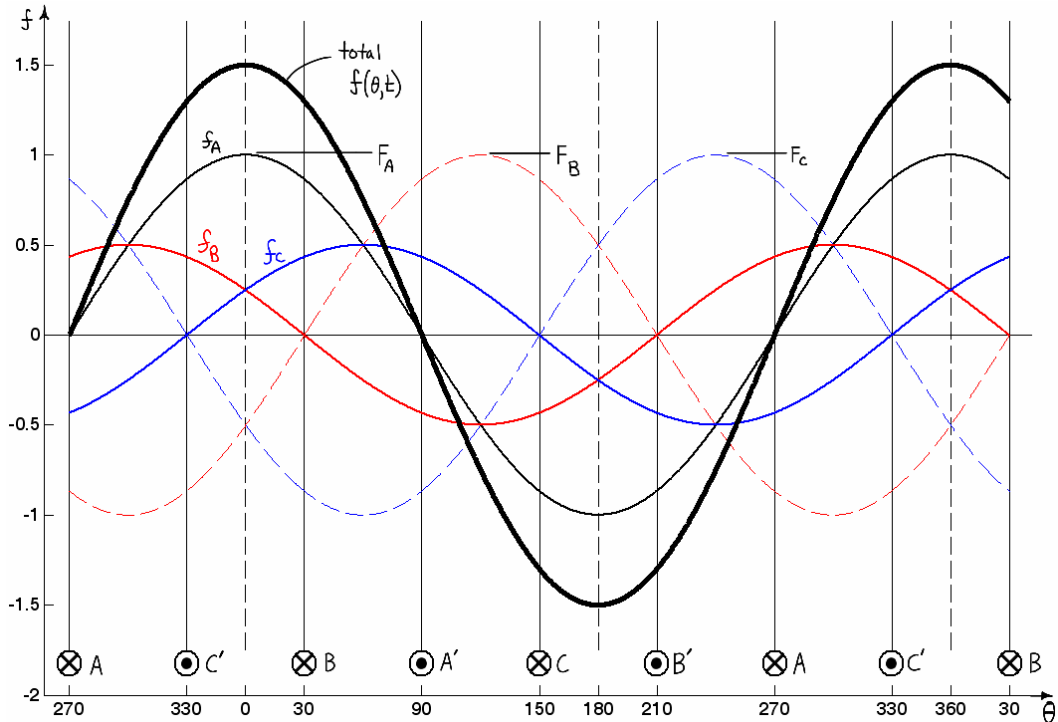
Figure 3.6 – One electrical cycle of unit-amplitude, balanced sinusoidal general quantities.

Now let Figure 3.6 represent the phase currents of a wye-connected stator with an isolated neutral. As a first example, use the ordinate as a reference line ($\delta = 0°$) and determine the three phase currents: I_A is equal to 1.0 while I_B and I_C are both equal to –0.5. Since I_A is positive and unity, its MMF component is exactly that shown in Figure 3.4. Since I_B and I_C are both negative and half-unity, their MMF components are of opposite polarity and are half the amplitude of those shown in Figure 3.4. At this position (zero electrical degrees), the component of MMF in the airgap due to each phase is shown in Figure 3.7. Also shown is the overall ("total"[12]) MMF in the airgap; the peak of the total MMF is coincident with the electrical position of the three-phase currents (zero electrical degrees).

---
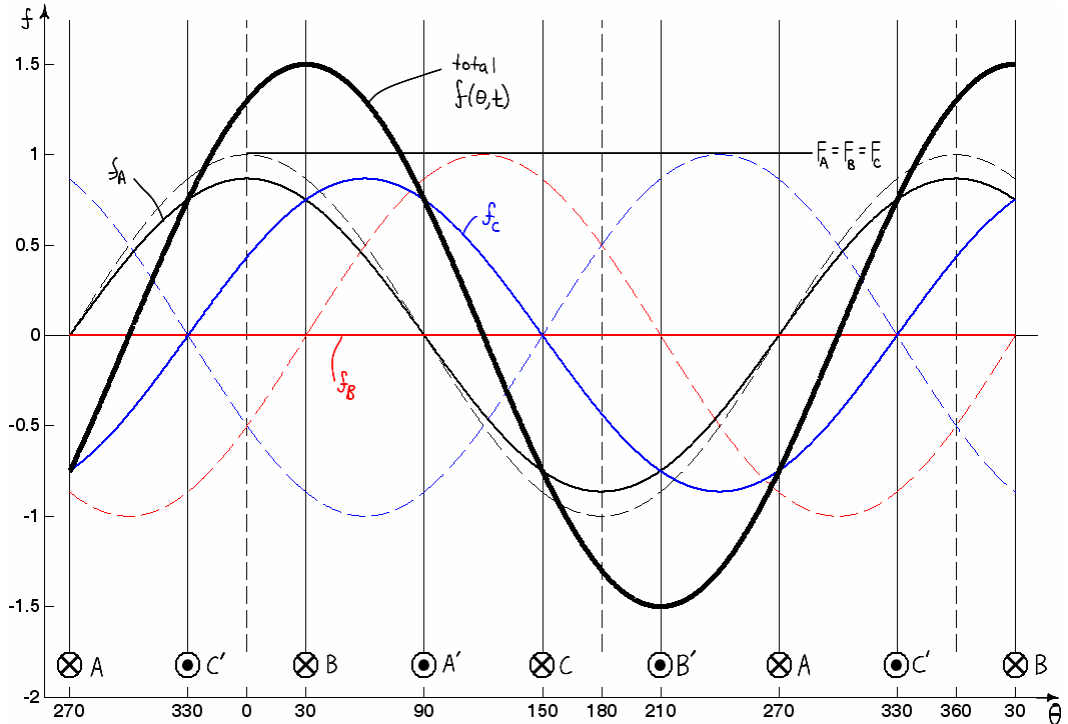
[12] "Resultant" would be a more appropriate term but it is nearly always reserved to describe the combination of stator and rotor magnetic fields and these will be discussed later.
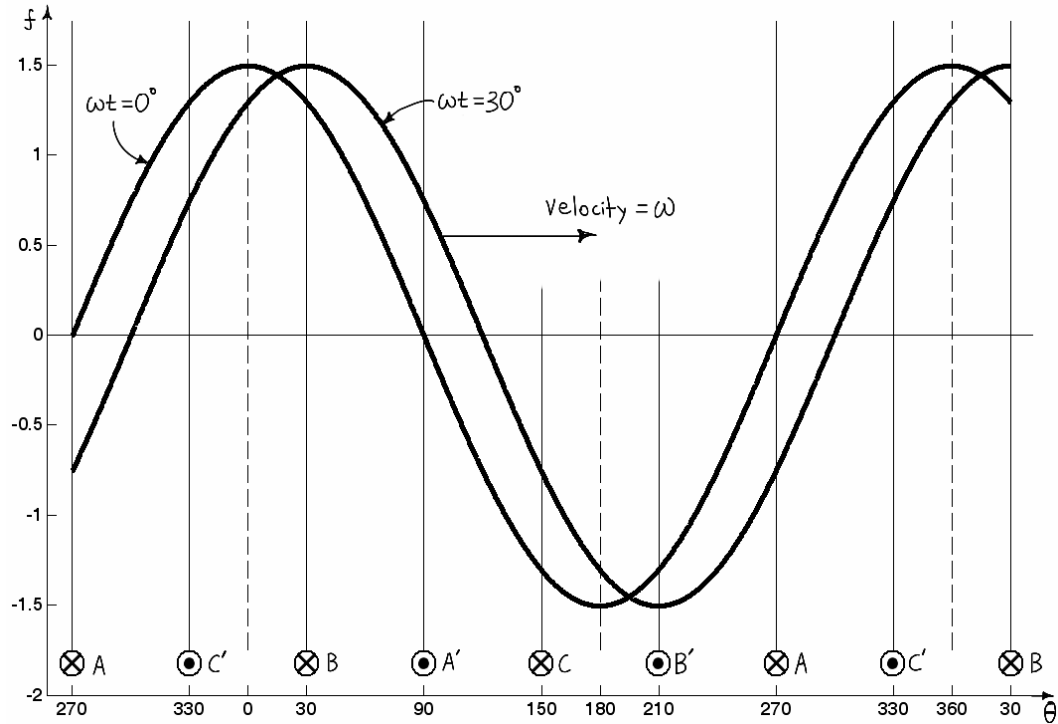
Figure 3.7 – Developed view at zero electrical degrees.

As the reference line in Figure 3.6 moves forward in electrical angular position, the current in each phase will increase or decrease and the component MMF of that phase will increase or decrease proportionally. The component MMF of each phase maintains a cosinusoidal shape in space—that is, with respect to the stationary stator conductors. As the current in a phase varies cosinusoidally this space distribution does not change in shape. Rather, the magnitude increases and decreases cosinusoidally with time; that is, the amplitude of the cosinusoidal space distribution is modulated cosinusoidally in time. For any given electrical angle, the *total* MMF will also be cosinusoidally distributed in space (it is a general property that when two or more cosine waves of the same period are added, the result is another cosine wave of the same period). Further, as the component MMFs (with their fixed spatial axes) increase and decrease, the peak of this *total* cosinusoid will move in *space*. Figure 3.8 is the same as Figure 3.7 except the electrical reference line in Figure 3.6 has been moved to $\delta = 30^\circ$. Here, $I_A = \sqrt{3}/2$, $I_B = 0$, and $I_A = -\sqrt{3}/2$. Again compare (the instantaneous MMF of each phase with the maximum possible) in conjunction with the values of current at this instant.

Figure 3.8 – Developed view at thirty electrical degrees.

To recapitulate, a phase current will produce a component of airgap MMF that is cosinusoidally distributed in space. The amplitude of this space-cosinusoid scales linearly with the phase current. Since a phase current is itself cosinusoidal with time, the amplitude of the component MMF due to a phase will be cosinusoidally modulated in time; for each phase alone, this creates a standing MMF wave in space. When balanced cosinusoidal currents are forced into the stator, the component MMFs from the phase windings will sum to produce a total airgap MMF that is cosinusoidally distributed in space along the periphery of the airgap, just as the component MMFs were. But unlike the component MMFs, this resulting distribution is a traveling wave that rotates around the stator periphery with time. Figure 3.9 shows two traces of the resulting airgap MMF at two different times: one corresponds to three-phase current at 0° (Figure 3.7) and the other corresponds to three-phase current at 30° (Figure 3.8). The figure is the developed view, thus the abscissa represents the angle around the stator and the figure is a snapshot of the traveling MMF wave at two different times.

70

Figure 3.9 – Developed view showing stator MMF waves of Figure 3.7 and Figure 3.8.

Prior to the development of controlled drives, synchronous machines were line-connected and operated at line frequency and induction motors were driven by variable frequency drives. In the synchronous machine, torque production requires that the rotor and stator fields maintain a fixed relationship in space but it was sufficient to think about the constant rotation of the rotating field and let the torque angle vary slowly as determined by the load and the controller.[13] In the induction motor, the steady-state equivalent circuit was all that was considered and the drive varied frequency and voltage to control speed but had poor transient performance. In contrast to both, a modern synchronous machine drive (or vector induction motor drive) seeks to control the *instantaneous position* of the rotating MMF of the stator with respect to the position of the rotor field. Thus instead of visualizing the constant synchronous rotation, it is essential to develop a mental connection between the instantaneous position of current (the reference slider of Figure 3.6) and the position of the peak of the stator MMF wave. The instantaneous angular position of the MMF is always the same as that of the current. This means that if the current is stationary the stator MMF will also be stationary, yet retains its cosinusoidal distribution in space. This concept

---

[13]   The load angle (and thus the power factor) can be controlled by adjusting field current and this is an important aspect in synchronous machine control. However, in large machines the angle is varied by a compensator to ensure stability. It is a "slow-changing" steady state control problem where (aside from the controller dynamics required to ensure stability) it is the time-average value that must be controlled.

is crucial to the understanding of FOC and is illustrated again in the mathematical derivation and then again in the development of the space vector.

Mathematical Derivation

The presented graphical depiction of the rotating MMF wave is now developed mathematically. Equation (3.1) describes each phase's component MMF as a function of the angle around the stator periphery. The total MMF as a function of the angle around the stator is given by their sum, Equation (3.2).

$$f(\theta,t) = f_A(\theta) + f_B(\theta) + f_C(\theta)$$
$$= \frac{N_e}{2}\left[i_A(t)\cdot\cos(\theta) + i_B(t)\cdot\cos(\theta - 120°) + i_C(t)\cdot\cos(\theta + 120°)\right] \tag{3.2}$$

The currents form a balanced sinusoidal set given by Equation (3.3), where I_p is the amplitude and $\omega t = \theta_e$ is the electrical position.

$$i_A = I_p \cos(\omega t)$$
$$i_B = I_p \cos(\omega t - 120°) \tag{3.3}$$
$$i_C = I_p \cos(\omega t + 120°)$$

Substituting Equation (3.3) into Equation (3.2) yields Equation (3.4).

$$f(\theta,t) = \frac{N_e}{2}\begin{bmatrix} I_p \cos(\omega t)\cos(\theta) \\ +I_p \cos(\omega t - 120°)\cos(\theta - 120°) \\ +I_p \cos(\omega t + 120°)\cos(\theta + 120°) \end{bmatrix} \tag{3.4}$$

The amplitude of each cosine term is a function of ωt—that is, each cosine term is a standing wave in θ with peak that is always located at 0°, 120°, and 240°. Equation (3.4) can be reduced by the trigonometric identity in Equation (3.5) to give Equation (3.6). Equation (3.6) is the standard result provided by any machine text (it is valid only for balanced sinusoidal currents).

$$\cos(A)\cos(B) = \frac{1}{2}\left[\cos(A - B) + \cos(A + B)\right] \tag{3.5}$$
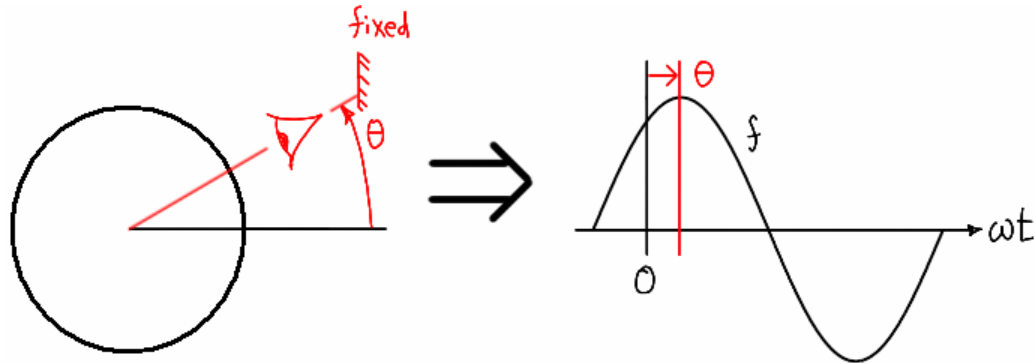
$$f(\theta,t) = \frac{3}{2}\left(\frac{N_e}{2}\right)I_p \cos(\omega t - \theta) \tag{3.6}$$

It can be noticed that the order in which (A and B) in Equation (3.5) are assigned to (ωt and θ) is arbitrary, thus Equation (3.6) could also be written as Equation (3.7). This also follows from the fact that cosine is an odd function; both equations are found in the literature.

$$f(\theta,t) = \frac{3}{2}\left(\frac{N_e}{2}\right)I_p \cos(\theta - \omega t) \tag{3.7}$$

Although Equations (3.6) or (3.7) are a standard result, the argument of the cosine is one of the more interesting aspects of AC machine theory. The angle θ is a spatial angle around the stator and the angle ωt is an electrical angle of a scalar circuit variable, yet the two appear together in the argument. The MMF exists in the airgap around the stator so the cosine describes the MMF as a function of this angle, irregardless of the ωt term.

In Equation (3.6) ωt is usually thought of as the independent variable along the abscissa and the variable in the position of θ is a delay. If an observer were stationed at the position θ, the equation would describe the magnitude of MMF at that position as a function of time, as shown in Figure 3.10. The observer at θ sees the peak θ / ω seconds later than an observer at zero (black line); hence the delay. It is helpful to mentally verify this result. Assume the currents are at zero so the peak of MMF wave is at zero as well. If the currents increase in angle the peak will move CCW with time. It can be seen that the observer at θ will indeed see the peak at a time greater than zero.

Figure 3.10 – Observing MMF value at fixed position.

In contrast to the interpretation of Equation (3.6), in Equation (3.7) the independent variable is θ and the delay is ωt. Instead of fixing the observation point, the point in time is fixed and the equation describes the traveling wave shown in Figure 3.9. As ωt increases the wave is delayed in θ. A delay makes the peak occur later in θ (at a larger positive value) thus this correctly describes the traveling wave (rotating CCW). Equation (3.6) describes the peak MMF from at an observation point and Equation (3.7) describes the instantaneous distribution at a point in time, yet they are the same equation and describe the same MMF. This concept seems universally accepted in the literature without consequence or mention (a good sentence on it is found in [43, p.748], followed by, "This basic tenet is essential for the understanding of AC motor control"). This important concept is further investigated in Part II and we will revisit this discussion at that time.

One final connection will be made between the graphical and mathematical derivations. Equation (3.2) clearly shows the component MMF produced by each phase and the action of these standing waves is seen clearly in Figure 3.7 and Figure 3.8 where the instantaneous distributions are compared to their maximum unit values (the dashed lines). Equation (3.7) clearly shows the total MMF, and the action of this traveling wave is made clear by Figure 3.9. Each standing wave (component MMF) could be represented as an MMF phasor in the traditional manner, but abstracting to phasors just to have to project them back onto the real axis does nothing to aid the visualization. If instead the instantaneous value of each standing wave (component MMF) is drawn coincident with the axis along which it acts, it is possible to visualize that component's contribution to the total. This is shown in Figure 3.11, where the two figures correspond to current positions of zero and thirty electrical degrees—the same electrical position as in Figure 3.7 and Figure 3.8.

$$i_A = 1.0 \qquad f_A = 1.0$$
$$i_B = -0.5 \qquad f_B = -0.5$$
$$i_C = -0.5 \qquad f_C = -0.5$$
$$f = 1.5 \angle 0°$$

$$i_A = 0.866 \qquad f_A = 0.866$$
$$i_B = 0 \qquad f_B = 0$$
$$i_C = -0.866 \qquad f_C = -0.866$$
$$f = 1.5 \angle 30°$$
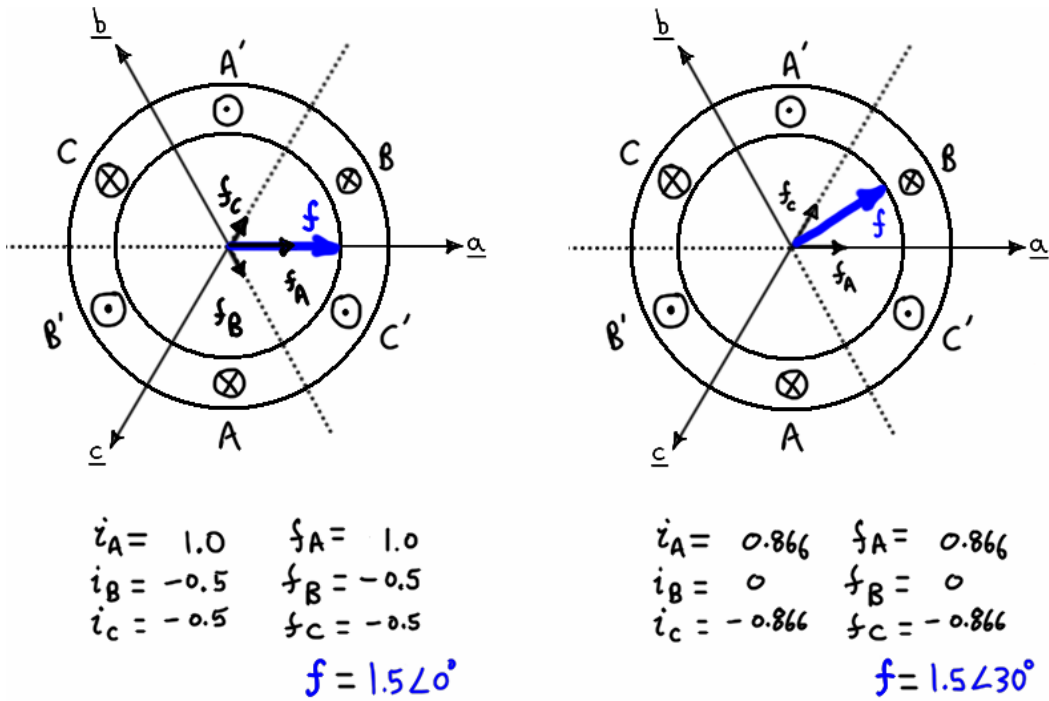
Figure 3.11 – Instantaneous values of component and total MMFs; (c.f. Figure 3.7, Figure 3.8).

Examining the component contributions shows the standing wave action—the contribution of each phase increases and decreases as a function of current but is always oriented in the same

direction. The contributions always add such that the total has a constant amplitude of $3/2$; this action will be discussed when space vectors are introduced.[14]
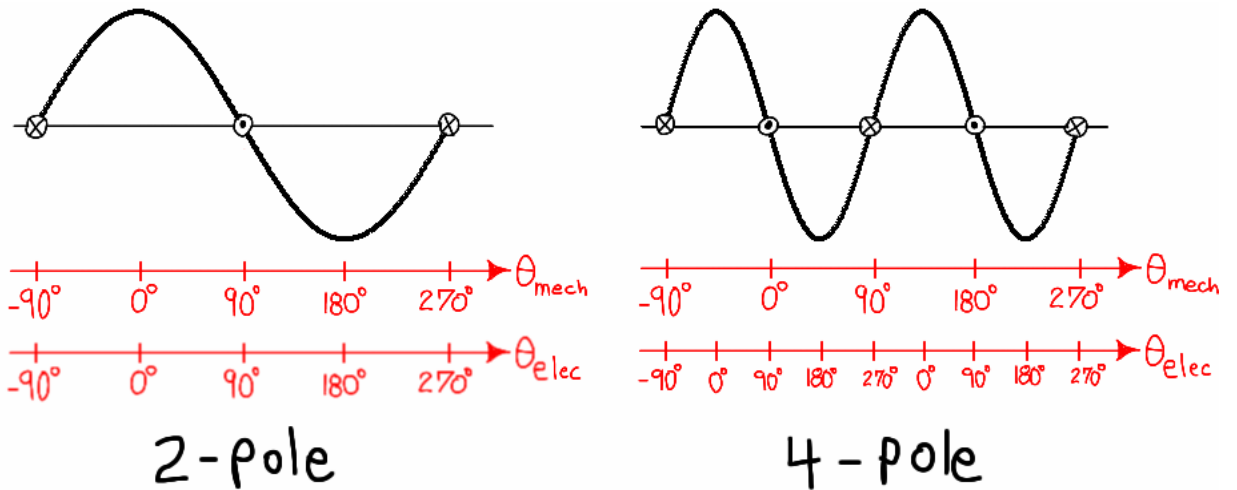
Electrical and Mechanical Measures

The speed at which the stator's traveling MMF wave moves around the stator is determined by the electrical frequency of the phase current and by the number of poles in the machine. Figure 3.1 showed a two pole machine in which the field rotates one mechanical revolution for every electrical cycle of the phase current. If the mechanical pitch of each coil is reduced by a factor of two, an identical set of coils are inserted into the stator and connected in series with the original coils, and a rotor with four magnets is used, four pole machine is created.[15] The developed view of a two-pole and four-pole motor are shown in Figure 3.12. After an entire electrical cycle has completed the plot will look exactly the same. Thus the two-pole motor will have advanced the space distribution of MMF through a full mechanical revolution but the four-pole motor will have advanced the space distribution of MMF by one-half a mechanical revolution. This action could be thought of as a magnetic "gear ratio."

---

[14] The factor of 3/2 in Equation (3.6)/(3.7) is interesting and shows up frequently in the analysis of three-phase machines. In each case the interpreted meaning and consequences will be different but it arises due to the same underlying cause which will be discussed throughout the report. In the case of Equation (3.6)/(3.7) the result it is a physical phenomenon. The spatial orientation of the windings, the isolated neutral, and the nature of three-phase quantities all act together in such a way that a set of balanced sinusoidal currents of unit amplitude produce a physically-existing MMF wave with a peak amplitude 3/2 larger than that which one phase would produce when excited by a current of unit amplitude; this is clear when examining Figure 3.7 and Figure 3.8. As a comparison, for example, a similar analysis of a symmetrical five-phase, isolated neutral stator winding subject to unit-amplitude five-phase sinusoidal current would yield a factor of 5/2.

[15] In synchronous machines the number of rotor poles is always equal to the number of stator poles (which will always be a multiple of 2. However, it is possible to make a three-phase motor with only three teeth (for an example cross section, see [68, p.232]); this is still a two-pole stator and would employ a two-pole rotor.

Figure 3.12 – Simplified developed view of a four pole motor.

This notion leads to the development of two systems of angular measure. The relationship between electrical and mechanical measurement is shown in Equation (3.8), where *P* indicates the number of poles.[16] Taking the time derivative yields Equation (3.9), which is the relationship between electrical and mechanical velocities; ω_e is usually called the synchronous speed. To avoid having to memorize the formulas, reconsider the gear ratio analogy, where P/2 is the ratio. A free rotating piece of steel or magnet situated inside the stator can do nothing other than follow the rotating field tied to the currents' electrical position and velocity, thus the mechanical velocity can never be faster than the electrical velocity. This means the ratio has a lower limit of unity, hence the ratio is always multiplied by the mechanical measure.

$$\theta_{elec} = \left(\frac{P}{2}\right)\theta_{mech} \tag{3.8}$$

$$\omega_{elec} = \left(\frac{P}{2}\right)\omega_{mech} \tag{3.9}$$

It is important to make the distinction between a mechanical or electrical angle (that is, an angle describing a mechanical or electrical displacement) and an angle measured in mechanical or electrical degrees. For example, in Equation (3.4) and Equation (3.6) ωt is an electrical angle and θ is a mechanical angle but both are measured in electrical degrees. The derivative of a

---

[16] Some texts use *P* to indicate pairs of poles to eliminate the factor of two in equations. However, industry specifies motors almost exclusively by the number of poles (not pole pairs) so this report uses P to indicate the number of poles. The reader is cautioned that many authors use a lowercase *p* to indicate poles (or pole pairs) which can also be used to denote the time derivative operator *d/dt*. The two are used interchangeably without distinction, often within the same formula. This is unfortunate, as the correct meaning in an equation cannot always be discerned from context without studying the derivation, which is often not given. This report uses rho (ρ) to denote the time derivative operator *d/dt*.

sinusoidal electrical variable will produce a factor of ω_e while the derivative of a rotor position will produce ω_r. In this report both electrical position and mechanical angles are generally specified in electrical degrees, thus the velocities would be $\omega_{e,elec}$ and $\omega_{r,elec}$. Since this report concerns only synchronous machines there would then be no difference between electrical and mechanical quantities so the notational distinction between ω_e & ω_r and the 'elec' & 'mech' subscripts are unnecessary.[17]

Reworking the units in Equation (3.9) yields Equation (3.10), where f_e is the electrical frequency expressed in [Hz] and N_m is the mechanical rotational speed expressed in [rpm]; solving for f_e yields Equation (3.11).

$$N_{rpm} = \frac{120 \cdot f_e}{P}, \ f_e \text{ in [Hz]} \tag{3.10}$$

$$f_e = \frac{P \cdot N_{rpm}}{120}, \ f_e \text{ in [Hz]} \tag{3.11}$$

Torque Production

As discussed in the previous chapter, non-salient machines produce torque through the interaction of the magnetic field associated with the stator and that associated with the rotor. Previously the airgap MMF due to stator current was developed. Now the magnetic field of the rotor will be introduced in order to examine torque production.
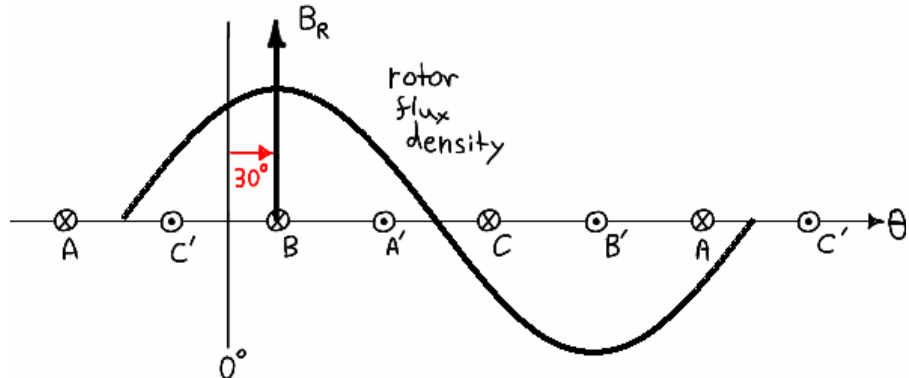
A magnetic field may be described by the distribution of its MMF, field strength, flux, or flux density. Using the assumptions presented earlier, all of these distributions are equivalent and only differ by constants. In reality this is not true due to several factors but it is a good enough approximation to explain motor operation [1, p.149], [27, p.117]. Therefore, the torque described by the interaction of stator and rotor fields may be expressed as various combinations of stator and rotor field quantities. The MMF produced by the stator is easily understood and is a reasonable choice because it is very simply related to the current by the winding function. But the influence of the rotor magnets is often thought of in terms of flux density rather than MMF. In

---

[17] An important consequence of doing this is that the factor $(P/2)$ or its inverse will not appear in formulas. This is fitting since for simplicity only 2-pole machines are considered thus the factor is also excluded from the derivations and discussions. The full formulas can be found in most machine texts.

this section torque production is examined in terms of the physical interaction of the space distributions of stator MMF (F_S) and rotor flux density (B_R).
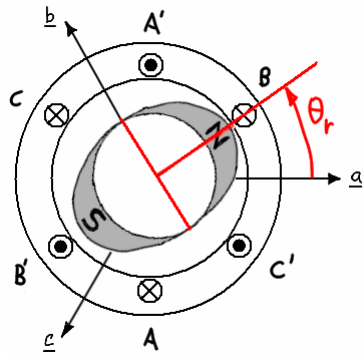
It is important to realize that the MMF produced by the stator and the MMF produced by the rotor will combine in the space of the airgap to produce a *resultant* MMF; the same can be said of the other magnetic quantities. Thus the torque can be described in terms of the stator and rotor components, the stator component and the resultant, or the rotor component and the resultant [27, p.121].

The developed view of a two pole three-phase motor is shown in Figure 3.13. Whereas the previous developed views have shown the stator MMF (e.g., Figure 3.7), this view shows only the rotor flux density distribution; the windings are shown only for positional reference. The rotor is positioned at 30° and this is only because it is a convenient number—the fact that the peak of the flux density is collocated with a coilside of phase-B is of no significance.
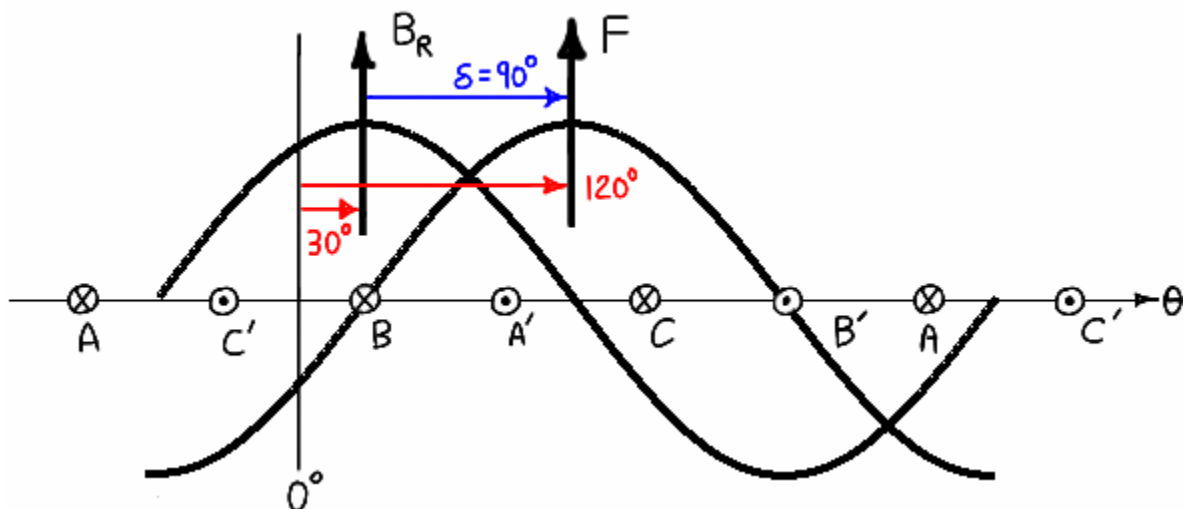
Figure 3.13 – Developed view of two pole motor showing rotor flux density.

$\mathbf{B}_R$ is a vector used to represent the peak of the space distribution of flux density due to the rotor. This vector ($\mathbf{B}_R$) and the vector $\mathbf{\Phi}_R$, which represents the peak of the space distribution of rotor flux, are always coincident with the rotor axis. Therefore any of these vectors can be used to denote the position of the rotor and its associated distributions. The cross section of the same motor with identical rotor position is shown in Figure 3.14.

Figure 3.14 – Cross section of two pole motor.

Now the stator and rotor quantities are shown together in the developed view of Figure 3.15. The rotor is still positioned at 30° and the stator MMF is that which would result if the stator currents were at 120° in *Figure* 3.6.

Figure 3.15 – Developed view showing rotor flux density and stator MMF.

There are a number of methods to derive the torque produced. Using coenergy it is possible to show that the torque produced in a non-salient machine with sinusoidally-distributed magnetic fields on the rotor and stator can be described in terms of the peaks of these distributions and the spatial angle between them [27, pp.117-121]. These cosine waves exist in space and can be described by phasors. Since this is a phasor analysis it only holds for sinusoidal quantities under steady-state.

It is easiest to begin with the MMF waves. In this case the torque is given by Equation (3.12), where c_1 is a constant, F_R and F_S are the amplitudes of the sinusoidal MMF waves of the rotor and stator, and δ is the angle (called the load angle or torque angle) measured *from* the peak of the

rotor MMF wave *to* the peak of the stator MMF wave.[18] The direction in which the angle δ is measured is a result of the convention that developed electromagnetic torque in a motor is taken to be positive. Equation (3.12) is recognized as the scalar equivalent of the vector cross product the vector quantities shown in Figure 3.15.

$$T = c_1 F_R F_S \sin(\delta) \tag{3.12}$$

In Equation (3.12) the constant c_1 is given by Equation (3.13), where D is the inside diameter of the stator steel laminations (or rotor diameter, assuming a negligible airgap), Y is the length of the rotor and stator lamination stack, and G is the airgap length.

$$c_1 = \left(D \cdot Y \frac{\pi}{2} \right) \cdot \left(\frac{\mu_0}{G} \right) \tag{3.13}$$

Since the rotor field has been introduced using flux density, the torque expression can be reformulated in terms of B_R as Equation (3.14) simply by rearranging the constant terms.

$$T = \left(D \cdot Y \frac{\pi}{2} \right) \cdot \left(\mu_0 \frac{F_R}{G} \right) F_S \sin(\delta)$$

$$T = \left(D \cdot Y \frac{\pi}{2} \right) \cdot \left(\mu_0 \cdot H_R \right) F_S \sin(\delta)$$

$$T = \left(D \cdot Y \frac{\pi}{2} \right) \cdot B_R F_S \sin(\delta) \tag{3.14}$$

Since the traditional symbol for flux density is always uppercase it is difficult to distinguish between peak and instantaneous values. For this reason B_R will now be replaced by B_p. Given that we typically think of rotor flux density and stator MMF, it will be understood that B_p refers to rotor flux density and Equation (3.14) is rewritten as Equation (3.15).

$$T = \left(D \cdot Y \frac{\pi}{2} \right) \cdot B_p F_S \sin(\delta) \tag{3.15}$$

Now the constants can be lumped together and torque is expressed by Equation (3.16) in terms of stator MMF and rotor flux density, as was desired.

$$T = c_2 B_p F_S \sin(\delta) \tag{3.16}$$

Since the stator MMF is created by the stator current it is useful to expand the F_S term to show this. Equation (3.6) gave the expression for stator MMF due to three sinusoidal balanced currents of amplitude I_p.

---

[18] The torque angle and load angle can refer to two different angles in the same machine but this distinction is not necessary for this report.

(3.6): $\quad f(\theta,t) = \dfrac{3}{2}\left(\dfrac{N_e}{2}\right)I_p \cos(\omega t - \theta)$

In the foregoing equations F_S represented the peak amplitude of the stator MMF cosine wave, which is given by the terms that multiply the cosine in Equation (3.6). Substituting this amplitude into Equation (3.16) gives Equation (3.17).

$$T = c_2 B_p \dfrac{3}{2}\left(\dfrac{N_e}{2}\right)I_p \sin(\delta) \qquad (3.17)$$

The angle δ was defined as the difference between the peaks of cosine waves, measured from the rotor wave to the stator wave (stator minus rotor). The angle of stator MMF in Equation (3.6) is equal to ωt when referenced to the magnetic axis of phase-A ($\theta = 0°$) and the rotor position is defined from the same reference. Thus the stator angle minus the rotor angle is equal to δ (in other words, $\theta = \theta_r$ in Equation 3.6). The stator MMF defined by Equation (3.6) and the rotor flux density defined by Figure 3.15 are cosine waves, thus the sine of δ in Equation (3.17) is still valid. The torque may then be written as Equation (3.18), where the constant c_3 is defined by Equation (3.19).

$$T = \dfrac{3}{2}c_3 B_p I_p \sin(\delta) \qquad (3.18)$$

$$c_3 = \left(D \cdot Y \dfrac{\pi}{2}\right)\cdot\left(\dfrac{N_e}{2}\right) \qquad (3.19)$$

For a given motor, B_p is fixed by the magnetic design thus Equation (3.18) shows that torque is proportional to the amplitude I_p of the sinusoidal three-phase currents and is scaled by the sine of the angle δ between the rotor and stator fields. For a given current it is obvious that the maximum torque is achieved when the fields are at $\delta = 90°$; this concept will form the basis of FOC discussed in Chapter 5. It is important to understand that torque is produced by the interaction of these two quantities as they maintain a fixed phase-relationship relative to one another while they both rotate at the synchronous frequency, ω. Equation (3.18) describes only the component of torque produced by fundamental stator and rotor quantities (the number of effective stator turns describes the fundamental MMF and B_p represents the amplitude of rotor flux density).

Note that if all else is held constant in Equation (3.12), torque is proportional to the magnitude of the stator MMF. Thus the factor of $3/2$ from the stator MMF expression comes through in the torque expression, as expected. This shows that a sinusoidal rotor flux will interact with the

fundamental of stator MMF (produced by any type of winding). The MMF created by balanced sinusoidal currents is in principle no different than that produced by a single winding save that it is $3/2$ larger *and* it rotates as a traveling wave whereas the per-phase MMF is a pulsating standing wave. In fact, with some manipulation (involving the removal of the factor $3/2$ and finding that $\delta = -\theta_r$) it could be shown that Equation (3.18) is essentially the same as the torque expression found in Chapter 2 for the simple sinusoidal motor and CFP winding:

$$T(\theta_r) = -N \cdot D \cdot Y \cdot B_p \cdot \sin(\theta_r) \cdot i(t) \quad .$$

Finally, Equations (3.18) and (3.19) can be written in terms of rotor-stator flux linkage. From Appendix C, the peak value of flux linkage of a sinusoidal winding with a sinusoidal rotor flux is given by Equation (3.20).

$$\Psi_R = \frac{\pi}{4} N_e \cdot D \cdot Y \cdot B_p \tag{3.20}$$

Comparing this with c_3 in Equation (3.18) (which is defined by Equation 3.19) it is seen that the torque can be rewritten as Equation (3.21). This version will be encountered in the SV model of Part III.

$$T = \frac{3}{2} \Psi_R I_p \sin(\delta) \tag{3.21}$$

Phasor Diagram and Single-Phase Equivalent (SPE) Circuit

Now that the rotating field and torque production have been discussed the electrical model for a synchronous machine will be developed in order to complete the standard treatment. Traditional analysis of the three-phase synchronous machine employs the use of phasors to describe the electrical circuit using the "single-phase equivalent" (SPE) concept.[19] In SPE a symmetrical sinusoidal machine is assumed, driven by balanced sinusoidal currents and operating in steady-state. Thus the machine can be sufficiently analyzed by examining a single phase (typically phase-A); all similar phase-B or phase-C quantities are thus unnecessary but may be found simply by adding a $-120°$ or $+120°$ phase shift to the phase-A quantities.

---

[19] Sometimes this is called the "per-phase equivalent" but that usage is avoided here because the three-phase "phase-variable" model can be analyzed on a per-phase basis and that is not the same as SPE.

In the previous chapter the per-phase model was expanded to produce the phase variable electromechanical model. That model explicitly accounts for the component torque produced by each phase; it is capable of describing motors with non-sinusoidal torque functions and it correctly accounts for transient conditions. Similarly, the applied voltage, winding current, and phase bEMF need not be sinusoidal functions; it is a general time-domain model. In contrast, Part I treats only the sinusoidal motor under balanced conditions; it is a phasor-domain model. The torque production was developed using phasors (albeit implicitly) and the SPE circuit developed in this section uses phasors as well. Whereas the phase-variable model is electromechanical, the single-phase equivalent model treats the circuit and torque production separately. Essentially, the torque expressions and electrical circuits of Part I (SPE) are a simplification of the phase-variable model that result when electrical quantities are restricted to sinusoids and the motor is operating in a mechanical steady-state condition. Since SPE assumes the motor is balanced and in steady-state, the electrical power and mechanical torque/power are found by multiplying a phase quantity by a factor of three. In contrast, the phase-variable model explicitly accounts for each phase, whether the quantities of the phases are equal or not. This is true for space vector analysis as well and in fact, space vector analysis is essentially a compact encapsulation of the phase-variable model with only one limitation: it cannot directly describe nonsinusoidal motors (but the currents may be arbitrary).

The SPE model represents one phase but it is known that there is mutual inductive coupling between phases. The SPE model accounts for this in the same way that the phase-variable model does: by modifying the simple self-inductance to include the mutual inductance due to current in the other phases (Appendix B). The resulting "effective" inductance is called the *synchronous inductance* L_s and is given by Equation (3.22), where L_ℓ is the phase leakage inductance and L_{mag} is the magnetizing inductance. *For simplicity the leakage inductance is ignored in these discussions*.

$$L_s = L_l + \frac{3}{2} L_{mag} \tag{3.22}$$

The factor $3/2$ is the same factor encountered in the MMF derivation of the previous chapter. The SPE circuit shown in Figure 3.16 is therefore similar to the per-phase circuit from the previous chapter (Figure 2.17) except it is in the phasor domain. The KVL equation is Equation (3.23). (The voltage $\widetilde{G}_a$ is the phasor representation of $g(t)$ from the previous chapter and will be discussed at the end of Part I.)
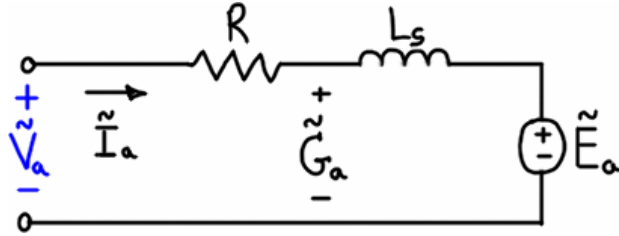
Figure 3.16 – Single-phase equivalent circuit.

$$\tilde{V}_a = R\tilde{I}_a + j\omega L_s \tilde{I}_a + \tilde{E}_a \tag{3.23}$$

The standard electrical phasor diagram for phase-A is shown in Figure 3.17 for an arbitrary lagging power factor. The current phasor is drawn with a hollow arrow head and the bEMF is always taken to be the reference phasor.
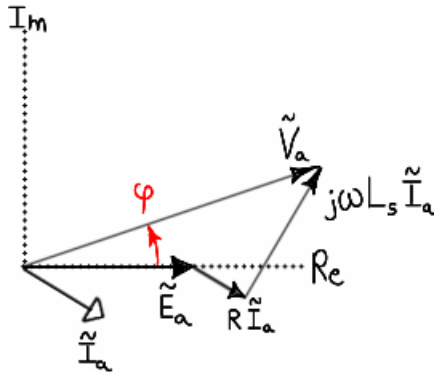
Figure 3.17 – Time phasor diagram of phase-A.

The other two phases have identical diagrams, except each is displaced by 120° to give the positive sequence rotation (A-B-C) as shown for the general phasor quantities $\tilde{X}$ in Figure 3.18. In the SPE analysis the phase designation (here, 'a') is not typically used but this report uses the subscript because it will help illustrate the connection between phasors and space vectors later on.
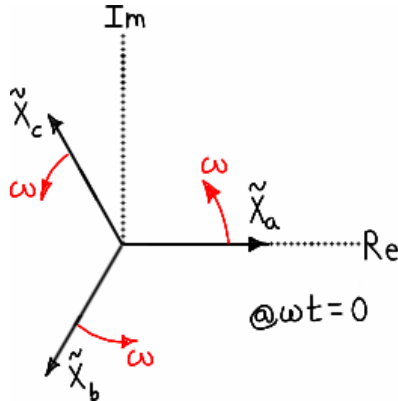
Figure 3.18 – Positive sequence phasor orientation.

Since there are several definitions of a phasor the definition used in this report is given here for clarity. The bEMF in Equation (3.24) is shown in its phasor representation in Equation (3.25); the

peak value is represented as an uppercase letter. Power system engineers use RMS-valued phasors exclusively but both peak- and RMS-valued space vectors are found in the motor control literature. Because peak space vectors are used in this report, peak phasors will also be used. Further, this report uses the cosine as reference; the sine reference is used in a portion of the literature but seems to complicate the math. The phasor is seen to represent a scalar quantity as the real part of a complex vector that is made to rotate at angular velocity ω.

$$e(t) = E_p \cos(\omega t) = \mathrm{Re}\left\{E_p e^{j\omega t}\right\} = \mathrm{Re}\left\{\tilde{E} \cdot e^{j\omega t}\right\} \tag{3.24}$$
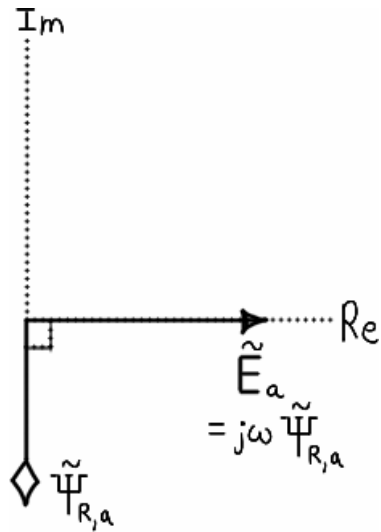
$$\tilde{E} \equiv E_p e^{j0°} = E_p \angle 0° \tag{3.25}$$

The phasor of Equation (3.25) is defined as the reference phasor because the scalar signal it represents has its peak value when $\omega t = 0$. By definition then, the reference line must be the real axis and the phasor diagram therefore represents the snapshot in time when $\omega t = 0$. The phasor diagram "captures" all phasors when at the reference signal peaks just like a digital storage oscilloscope set to trigger upon detection of a peak. Phasors for other sinusoids are defined with a phase measured relative to the reference phasor; traces on an oscillogram have a phase defined from the trigger point of the reference waveform. For example, the applied terminal voltage, Equation (3.26), is represented in phasor form as in Equation (3.27). Figure 3.17 shows clearly how the phase (φ) of $\tilde{V}_a$ is defined relative to $\tilde{E}_a$.

$$v(t) = V_p \cos(\omega t + \varphi) = \mathrm{Re}\left\{V_p e^{j\varphi} e^{j\omega t}\right\} = \mathrm{Re}\left\{\tilde{V} \cdot e^{j\omega t}\right\} \tag{3.26}$$
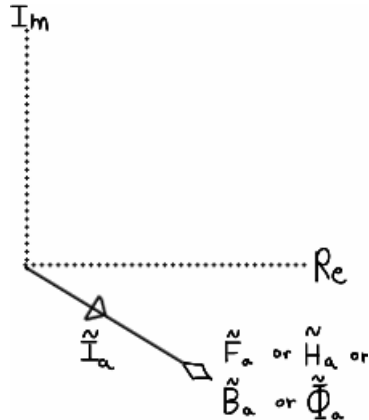
$$\tilde{V} \equiv V_p e^{j\varphi} = V_p \angle \varphi \tag{3.27}$$

According to the discussion in the previous chapter, the bEMF is the time derivative of the rotor-stator flux linkage, which is $\tilde{\Psi}_{R,a}$ for phase-A. In the phasor domain the time derivative corresponds to multiplication by $j\omega$. Therefore the bEMF $\tilde{E}_a$ will always lead $\tilde{\Psi}_{R,a}$ in phase by 90° and its amplitude will be proportional to rotor speed; this agrees with the development of the previous chapter and the relationship is shown in Figure 3.19. Following a convention used in [27], phasors of electromagnetic quantities are represented with a hollow diamond head.

Figure 3.19 – Time relationship between flux linkage due to rotor and bEMF.
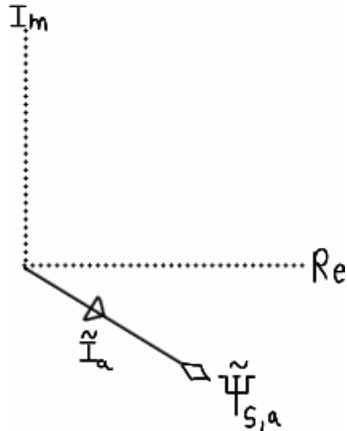
The magnetic quantity $\left(\tilde{F}_a, \tilde{H}_a, \tilde{B}_a, \tilde{\Phi}_a \right)$ produced by a phase current will be in time-phase with that current, as shown in Figure 3.20. (These are the components due to current in phase-A alone, not the total airgap quantities.)

Figure 3.20 – Time relationship between phase current and stator-produced magnetic quantities.
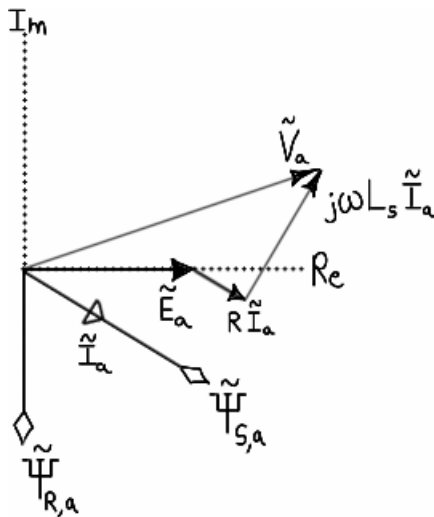
In addition, the self flux linkage of the stator is also in phase with the current, as shown in Figure 3.21. Unlike the magnetic quantities produced by phase-A current, the self flux linkage of phase-A is due to the *total* airgap flux produced by the stator. It is the synchronous inductance that enables the total airgap flux produced by the stator to be described by the phase-A current only, as shown in Equation (3.28).

$$\tilde{\Psi}_{S,a} = L_s \tilde{I}_a \tag{3.28}$$
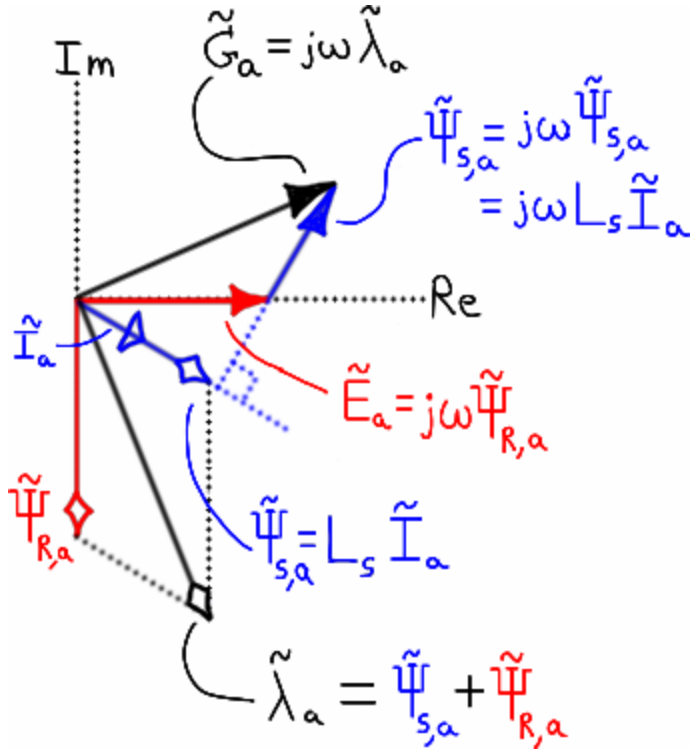
Figure 3.21 – Time relationship between phase-A current and stator self flux linkage.

To summarize the basic time relationships: the bEMF leads the rotor-stator flux linkage by 90°; the stator magnetic quantities and stator self flux linkage are both in phase with the current that produced them. The electrical and electromagnetic phasors of phase-A are combined onto a single diagram in Figure 3.22. Both sets of phasors rotate together in time.

Figure 3.22 – Time relationships between electrical and magnetic quantities.

The previous chapter elaborated on stator flux linkage and its components and made the distinction between the bEMF $e(t)$ and the total induced stator voltage $g(t)$. The results of that discussion are shown using the phasor diagram in Figure 3.23, where the applied terminal voltage and resistive voltage drop have been omitted for clarity. In other words, the phasor diagram shows only the flux linkages associated with field components in the airgap and the EMFs they induce.

87

Figure 3.23 – Time relationships between flux linkages and induced voltages; lagging PF.

These relationships in Figure 3.23 are given by Equations (3.29), (3.30), and (3.31).

$$\begin{aligned}
\tilde{\Lambda}_a &= \tilde{\Psi}_{S,a} + \tilde{\Psi}_{R,a} \\
&= L_s \tilde{I}_a + \tilde{\Psi}_{R,a}
\end{aligned}$$
(3.29)

$$\begin{aligned}
\tilde{G}_a &= j\omega\tilde{\Lambda}_a \\
&= j\omega L_s \tilde{I}_a + j\omega\tilde{\Psi}_{R,a} \\
&= j\omega L_s \tilde{I} + \tilde{E}_a
\end{aligned}$$
(3.30)

$$\tilde{E}_a = j\omega\tilde{\Psi}_{R,a}$$
(3.31)

Once again, the stator flux linkage is composed of two components: the rotor-stator flux linkage and the self flux linkage. The bEMF is the time derivative of the former and the inductive voltage drop is that of the latter. The total induced stator voltage is then the sum of the inductive voltage drop and the bEMF. In reality, the flux due to stator currents (which produces the self flux linkage) and the flux due to the rotor (which produces the bEMF) add together in the airgap to produce a resultant flux (with corresponding flux density, MMF, and field strength), and the time derivative of this resultant flux linkage is the total induced stator voltage ($\tilde{G}_a$). That the rotor-stator flux linkage induces the bEMF is familiar. That an inductor produces flux linkage with itself as a result of the current through it is familiar. That the two act independently of one

another and thus could be placed in series to model the circuit is reasonable and familiar. But the key to understanding this vital aspect is not evident in the circuit theory approach: the flux produced by the stator winding exists in the same airgap as the rotor flux. As natural as the rotor-produced airgap flux linkage induces the bEMF 90° ahead, the stator-produced airgap flux linkage induces a voltage 90°—the standard terminal characteristic of the inductor. This discussion should cement the meaning of flux linkage provided in the previous chapter: the flux linkage is the expression that describes the total flux linked by a winding (phase-A in this case). This should demonstrate why the inductor can be considered an electric circuit element separate from the bEMF, but both the inductance and bEMF are a result of the resultant *airgap* flux and for this reason there are the two distinct (but equivalent) circuit models. Finally, this reinforces the dependence of bEMF on rotor position.

Part II – Space Vectors

Part II introduces the space vector, which is a complex-valued quantity defined by a linear transformation of three-phase variables. The space vector is the basis of space vector analysis which can be used to analyze three-phase circuits and machines. There are some intuitive aspects of the space vector concept but other parts are more abstract and difficult to grasp upon first encountering them. The vector nature of the space vector is easy to understand, so it is developed first by using a simple example. Then the example is extended and the space vector's representation of distributed quantities is illustrated by building upon the understanding of stator MMF distributions presented in Part I. (The MMF space vector is the "connection point" between the familiar understanding of the machine and the more abstract representation by space vectors.) Finally the more abstract nature of the space vector transform is studied. The concept of reference frame theory will be encountered repeatedly and each time the understanding will be developed further.

A concise introductory statement regarding space vector analysis is given in the foreword to [88] by Dr. Donald Novotny, Professor Emeritus, University of Wisconsin–Madison:

> "Part way through my academic lifetime I was introduced to the next phase of unified theory, the use of complex notation to model the effective spatial orientation of quantities within a machine. This concept, often called space vector theory, provides a much clearer mathematical picture of what is happening in a machine, but at the expense of another level of abstraction in the model. However, the insights provided to one initiated in the method are so significant that today essentially all work in drive control is presented in this format. And therein lies a problem. To the uninitiated these presentations appear quite unintelligible. And a route to becoming initiated is generally hard to find and often harder to follow once found."

The author agrees heartily with these sentiments, particularly the last sentence. There are two extremes of space vector usage in the literature. In the popular literature space vector theory is used sparingly; many articles of popular literature incorrectly or inconsistently apply the theory. It seems as if the authors "copy and paste" from the academic literature and do not explain the equations they use. Perhaps this would be acceptable if space vector theory were a simpler and

more widely understood theory (such as single-phase equivalent analysis), but such is not the case (for students and engineers outside of the motor control field).

On the other end of the spectrum are works that rely entirely on the use of space vector theory. If connections between space vector theory and traditional theory are presented, they are usually based on the fully-general six-variable nonlinear time-varying coefficient models, which are difficult to grasp upon first encountering (these models absent in many undergraduate texts). Discussion of the meaning of the space vector and the nuances of its theory are generally minimal or absent entirely. It is the author's perception that most texts employing space vector theory are written above the graduate level. The application to the general machine is very generalized. Handling the rotor and stator quantities expressed in different reference frames requires bulky notation (such as variables laden with simultaneous superscripts and compound subscripts). It is time consuming and difficult to learn a notation and different texts use entirely different notation. The meaning and usefulness of the theory can be buried in the mathematics or it can be easily lost in the drudgery of keeping track of symbols. In addition, many texts are rooted in induction motor analysis and treat synchronous machines by issuing a statement along the lines of, "to be completely general, the theory has been developed in general terms of the induction motor but it is easily adapted for the synchronous machine." While this is a valid approach, it is very time consuming to work through induction motor literature in order to follow the specialization of an induction motor model to describe the synchronous machine.

Fortunately, references in between these extremes [42], [78], [88], [73] generally attempt (with varied success) to explain the theory in simple terms; these are of the most value to the newcomer. Nonetheless, it may still be difficult to bridge understanding between different resources, especially between works on opposite ends of the spectrum described above. The theory and its application are multifaceted and most unfortunately, while a particular reference may succeed at emphasizing a certain simplified understanding, other important aspects may be unintentionally minimized or ignored completely.

The author has found that the perspective most useful in learning space vector theory is found in the more theoretical texts (the perspective is called reference frame theory). Since they are written at an advanced level, it is necessary to have a fair grasp of traditional machine theory in order to understand them. The aim of Part II is to introduce and utilize space vector theory where necessary to develop the linear transformation of variables and the concept of reference frames,

which are required to understand modern motor control. An attempt has been made to provide explanations that are as simple as possible and easy to understand but are comprehensive enough to give the reader an understanding of space vector theory that can assist in migrating between references in the literature. If there is any one thing the reader should realize, it is that the theory can be approached from many different angles, all of which may be correct; therefore, one should not absorb or stick to one "interpretation" too rigidly (including the interpretation in this report).

Introduction

The meaning of the space vector and the nature of the application of its associated theory should become clear in reading this report. The theory and its application are intertwined and for this reason the material is difficult to organize and present; it is even more difficult to provide a concise overview. Oddly enough, when the details are correctly understood the application is easy to grasp and an overview is not *as* necessary as might be expected, but an attempt has been made to provide one here. A good starting point is to compare the space vector with the phasor (a more detailed comparison with the phasor is given in the last subsection of Part II).

Similar to the phasor, the space vector (SV) is simply a mathematical construct designed to ease analysis of machines and circuits; whereas the phasor exists to analyze sinusoidal quantities, the SV exists to analyze three-phase quantities. The phasor is a complex-valued representation of a scalar sinusoidal signal. The sinusoid is the basis of linear system analysis since it is the only signal that can pass through a linear time-invariant system without a change in shape. Further, a sinusoid is completely described by its amplitude, frequency, and phase; since the phasor contains this information, it is a convenient tool to represent a sinusoid. The phasor's vector nature is convenient for representing magnitude and phase, while its complex-exponential nature make it amenable to mathematical manipulation. If the voltages and currents in a circuit are represented using phasors, it is then possible to define a complex impedance and a complex power such that linear circuits may be analyzed using only complex numbers. This analysis is so compact and rapid that it might be termed an entirely new type of analysis, such as "complex AC analysis," to distinguish it from time-domain analysis. In addition to the speed and ease of use, the method provides a graphical presentation that helps visualize the magnitude and phase relationships between quantities. However, the entire analysis is built upon nothing more than a definition of the phasor and some supporting assumptions and conventions. In a similar way, the space vector is simply a mathematical contrivance with associated conventions, but an entire method of analysis has been built upon it; it might be called "space vector analysis" to distinguish it from

other methods, although it has close relationships to the other methods (phase-variable time-domain analysis and phasor analysis).

A phasor can describe any sinusoidal scalar quantity. Although the phasor is used in three-phase analysis, the phasor is used to describe the quantities associated with only one of the phases (the reference phase, often phase-A) with the understanding that the system is balanced, hence information about the other two phases can be found by adding or subtracting a 120° phase shift. The analysis of one phase is often called "single-phase equivalent" analysis [39, p.547] and it is almost always coupled with phasor analysis (that is, the single-phase equivalent circuit is analyzed using phasors). The phasor ($\tilde{X} = Xe^{j\varphi} = X\angle\varphi$) is a complex-valued entity and the real part represents the scalar quantity of interest; the complex entity does not necessarily have any physical interpretation as a vector, it is just a convenient mathematical form. In contrast, the SV ($\vec{x} = \hat{X}(t) \cdot e^{j\xi(t)}$) is a complex-valued notation that describes a vector quantity that exists in the complex space; the entire complex entity has a physical interpretation as a vector (as opposed to only the real part). Of course the complex plane has no physical meaning but it is mapped to a real polar coordinate system that does have physical meaning. Yet, like a phasor, there is also meaning in only the real part of the SV. The complex notation exists to aid in mathematical manipulation (as with a phasor) but in addition the complex notation carries information about quantities physically distributed in the machine.

Neither the SV nor the phasor can represent the zero-sequence component. Phasor analysis is only valid for circuits with balanced sinusoidal excitation in steady state whereas SV analysis is valid for arbitrary phase quantities and can describe transient behavior. When phasor analysis is coupled with the single-phase equivalent circuit the phasor "represents" all three phases working together, but only because the machine is balanced and the phase power can be multiplied by three to obtain total power. In contrast, the SV *directly* accounts for (contains information about) the total effect of each phase, even if the contributions of the phases are not equal.

It will be seen that there are several aspects of SV theory. (Compare this with the phasor. Depending on the analysis, it may be treated as a stationary vector, a rotating vector, or a complex number, yet these are all simply different ways of looking at the definition.) The vector nature of the SV allows for intuitive graphical presentations similar to phasor diagrams. The SV is a complex number that can be easily manipulated mathematically. The SV represents rotating

distributions that agree with the physical description of the motor's operation. Finally, the SV is a linear transformation of variables (LTV). Although the other aspects of the SV are obviously important, this LTV aspect could be said to be the most important and is the basis of the method. Simply stated, applying SV analysis consists of deriving the electrical model of a three-phase electrical or electromechanical system (expressed in terms of phase variables) and then transforming the phase variables to a different, two-dimensional orthogonal coordinate system (the stationary reference frame). As with any LTV, the SV transform can be expressed as a matrix. When the phase-variable model is expressed in matrix form, all of the standard linear algebra techniques apply. The SV is essentially the complex-valued representation of the traditional vector-matrix *two-axis*, *two-reaction*, or *dq* theories (though there are slight differences between these terms and these will be explained as they are encountered).

The most fundamental goal in motor control is the control of torque. The understanding of torque production requires a physical understanding of machine operation and SV theory can provide a graphical representation of this understanding. Since the transformation of variables is the basis of SV analysis and the motor control schemes that utilize it (such as FOC) it might make sense to begin with an examination of this transformation. But the interpretation of the LTV aspect is abstract compared to the physical aspect of the SV. Therefore the SV is developed using physical concepts before the more abstract portions are presented.

Organization

The SV theory presented here in Part II is voluminous enough to warrant its own chapter, and this may seem fitting since the theory is not specific to machine analysis. However, it is positioned at this point to aid in learning and integration. SV theory could be thought of as being purely mathematical (and this is the approach of some texts), but it seems to be best presented by building upon the physical description of the machine that was presented in Part I, thus this material should be located close to Part I. In this report, the primary purpose of using SV theory is to model the machine (to be compatible with the control system and inverter schemes that are likewise based on SV theory). Since the machine is modeled in Part I and SV theory is presented in Part II, the SV theory applied to the machine is presented in Part III. This makes for a long chapter but also facilitates integration that would be difficult otherwise. References in the literature take different approaches but several texts ([73], [78], [87]) begin with an approach similar to that used here. Some of the more technical references on SV math include [36], [84], [85], [86], [87], [89].

The SV as a Vector

The first facet of the SV to study is its simple vector nature. Both the SV and the phasor are complex-valued quantities but in the simplest sense it is their vector nature that makes them useful. The vector properties of the SV are similar to the familiar properties of regular vectors thus we begin by comparing the SV with linear algebra. This development will then be extended by introducing complex basis vectors. Finally, the manner in which MMF and current SVs add is examined.

Comparison with Linear Algebra

The space vector is like any other vector in that it describes a resultant vector quantity (in a vector space α) that is produced by a linear combination of products of a scalar quantity (belonging to a scalar field υ) multiplied by a basis vector in α. Consider the horizontal and vertical deflection plates of a CRT to which two scalar variables (voltages) are applied. This potential creates an electric field which imparts force on the electrons composing the beam. Looking into the electron gun, the Cartesian plane is the vector space α and can be described by the orthonormal unit vectors $\hat{\mathbf{x}}$ and $\hat{\mathbf{y}}$. The two scalar voltages applied to the plates belong to the field υ and have no meaning in the vector space α. But the voltage applied to each pair of plates produces an electric field that imparts a force whose direction can be described by some linear combination of the basis vectors ($\hat{\mathbf{x}}$ and $\hat{\mathbf{y}}$) and this result obviously does have meaning in α; this is the coupling mechanism found in space vector theory. The force on an electron is given by Equation (3.32), where c_1 is a constant of proportionality that relates electric potential v to electric field strength E and then to force F on an electron.[20] Since $\mathbf{F}$ is defined in the vector space α it could be called a space vector.[21]

$$\mathbf{F} = (c_1 \cdot v_x \hat{\mathbf{x}} + c_1 \cdot v_y \hat{\mathbf{y}}) = c_1 \cdot (v_x \hat{\mathbf{x}} + v_y \hat{\mathbf{y}}) \tag{3.32}$$

The net effect of the two voltages could be combined into a vector in the space α and this vector may be called the voltage space vector defined in Equation (3.33).

$$\mathbf{v} = \left(v_x \hat{\mathbf{x}} + v_y \hat{\mathbf{y}} \right) \tag{3.33}$$

The force could be written as Equation (3.34).

---
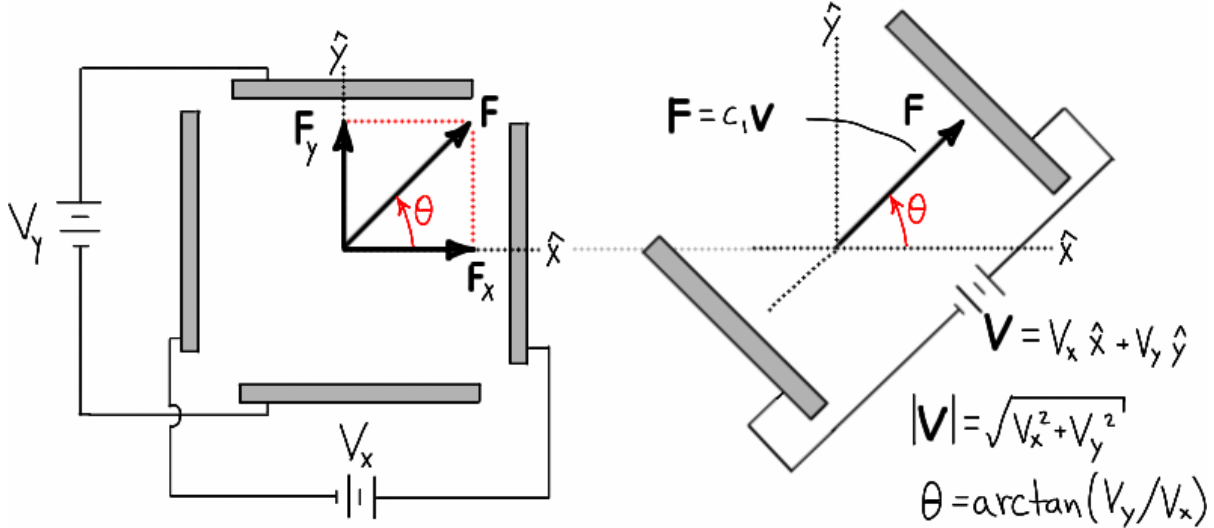
[20] The electric field would have a polarity opposite that of the applied voltage but the charge of the electron is negative.

[21] The simple vectors in space in this example ($\mathbf{v}$, $\mathbf{F}$) carry a slightly different meaning than the complex space vectors developed next. Hence the boldface notation is used in this example but all space vectors in the remainder of the report use the superscribed arrow notation listed in the beginning of the report.

$$\mathbf{F} = c_1 \cdot \mathbf{v} \tag{3.34}$$

The situation is shown graphically in Figure 3.24.

Figure 3.24 – Equivalent force produced by plates aligned with resultant force.

Per the above, the composition of the space vector is no different than a standard vector in linear algebra: any vector quantity is composed of a summation of the products of a basis vector with a scalar. In the simplest cases, such as the Cartesian plane, the two basis vectors ($\hat{\mathbf{x}}$ and $\hat{\mathbf{y}}$) are orthonormal and therefore linearly independent; in this case, the vector space $\boldsymbol{\alpha}$ is $\mathbb{R}^2$, as it is in the CRT example. In contrast, the space vector method uses complex exponentials as basis vectors and therefore the vector space is $\mathbb{C}$. Further, there is no restriction that the spanning set must be orthonormal. In fact the basis vectors are not even linearly independent (for three-phase systems without a grounded neutral) and this is part of the reason that that the factor $3/2$ arises in the analysis of three-phase machines, irregardless of whether traditional or space vector analysis is used.

Complex Basis Vectors

In three-phase systems there are three basis vectors, one aligned to each of the three electrical axes (A, B, C) which are 120 electrical degrees apart according to the convention established in Figure 3.1. Regardless of what type of quantity (voltage, current, flux, flux linkage) the space vector describes in a three-phase system, the basis vectors are the axes are given by several equivalent rectangular and polar forms in Equation (3.35). Note that $\gamma \triangleq 120° = 2\pi/3$, $e^{j240°} = e^{-j120°}$, and that by definition the phase-A axis is the real axis which corresponds to zero degrees.

$$\hat{\mathbf{a}} \triangleq 1 + j \cdot 0 \quad = e^{j0} \quad = e^{j0} \quad = e^{j0} \quad = 1$$

$$\hat{\mathbf{b}} \triangleq \frac{-1}{2} + j\frac{\sqrt{3}}{2} \quad = e^{j120°} \quad = e^{j2\pi/3} \quad = e^{j\gamma} \quad = a \tag{3.35}$$

$$\hat{\mathbf{c}} \triangleq \frac{-1}{2} + j\frac{-\sqrt{3}}{2} \quad = e^{-j120°} \quad = e^{-j2\pi/3} \quad = e^{-j\gamma} \quad = a^2$$

Similar to the CRT example presented earlier, the MMF produced due to the combined effect of current in the three windings could be represented by an MMF space vector. In the CRT example the relationship between voltage and the force it produces is a constant of proportionality and in a machine the relationship between current and the MMF it produces is also a constant of proportionality—the same as that in Equation (3.1). Using this constant, the concept of Equations (3.32)-(3.34) from the CRT example, and the directionality of the magnetic axes of windings shown in Figure 3.1, the MMF produced by current space vector could be described as Equation (3.36).[22]

$$\vec{f} = \left[\left(\frac{N_e}{2} \right) i_A(t)\hat{\mathbf{a}} + \left(\frac{N_e}{2} \right) i_B(t)\hat{\mathbf{b}} + \left(\frac{N_e}{2} \right) i_C(t)\hat{\mathbf{c}} \right] \tag{3.36}$$

Further, the CRT example showed that the constant of proportionality could be pulled out front and the force space vector could be described by defining a voltage space vector. The similar case here is to define the MMF space vector by defining a current space vector as shown in Equation (3.37), where the current space vector is given by Equation (3.38).

$$\vec{f} = \left(\frac{N_e}{2} \right) \left[i_A(t)\hat{\mathbf{a}} + i_B(t)\hat{\mathbf{b}} + i_C(t)\hat{\mathbf{c}} \right] \tag{3.37}$$

$$\vec{i} = \left[i_A(t)\hat{\mathbf{a}} + i_B(t)\hat{\mathbf{b}} + i_C(t)\hat{\mathbf{c}} \right] \tag{3.38}$$

The basis vectors in Equation (3.36)-(3.38) are typically represented by one of the rectangular or polar notations in Equation (3.35). Therefore the current space vector, for example, is typically written in the form of Equation (3.39) or Equation (3.40); this report will favor the form of Equation (3.40). In addition a very important transformation constant (k) has been added to scale the result to account for the fact that the basis vectors are not linearly independent; it will be discussed in detail later but for simplicity its importance will be minimized for now by selecting k=1 until further notice.

---

[22] Until the section titled "The SV as a Distribution," the reader is asked to ignore the idea of sinusoidally distributed quantities in a machine.

$$\vec{i} = k\left[i_A(t) \cdot 1 + a \cdot i_B(t) + a^2 \cdot i_C(t)\right] \tag{3.39}$$

$$\vec{i} = k\left[i_A(t) \cdot 1 + i_B(t) \cdot e^{j\gamma} + i_C(t) \cdot e^{-j\gamma}\right] \tag{3.40}$$

Using this notation the MMF space vector is written as Equation (3.41).

$$\vec{f} = \left(\frac{N_e}{2}\right) \cdot k\left[i_A(t) \cdot 1 + i_B(t) \cdot e^{j\gamma} + i_C(t) \cdot e^{-j\gamma}\right] \tag{3.41}$$

Recognizing that Equation (3.40) and Equation (3.41) differ by only a constant, the MMF space vector can be written directly in terms of the current space vector as shown in Equation (3.42). This corresponds to Equation (3.34) of the CRT example and should help solidify the understanding of mechanism by which a space vector in **α** (with units corresponding to υ) can be assigned units that correspond to **α** by means of a simple constant of proportionality.

$$\vec{f} = \left(\frac{N_e}{2}\right) \cdot \vec{i} \tag{3.42}$$

It was mentioned earlier that in the CRT example the vector space **α** was $\mathbb{R}^2$ but that the space vector uses the vector space $\mathbb{C}$. From the definition of the complex basis vectors in Equation (3.35) and the definition of the space vector it can be seen that the three phase variables (belonging to $\mathbb{R}^3$) are mapped onto the complex plane, hence the space vector is in $\mathbb{C}$. The important consequences of this mapping will be examined throughout this chapter.

Finally, it is clear that the magnitude and angle of the current SV will depend on the nature of the three phase currents in Equation (3.40). This concept is true for any SV and will be elaborated for the SV of the general quantity x whose SV is defined by Equation (3.43).

$$\vec{x} = k\left[x_A \cdot 1 + x_B \cdot e^{j\gamma} + x_C \cdot e^{-j\gamma}\right] \tag{3.43}$$

If the three phase quantities (x_A, x_B, x_C) form a balanced sinusoidal set (Equation 3.44) the SV will have a constant magnitude and its angle will be equal to ωt. This space vector is represented as Equation (3.46); this result is found by using the identity in Equation (3.45) to represent each phase quantity as its complex equivalent before substitution into Equation (3.43).

$$\{x\} = \begin{cases} x_A(t) = X_p \cos(\omega t) \\ x_B(t) = X_p \cos(\omega t - \gamma) \\ x_C(t) = X_p \cos(\omega t + \gamma) \end{cases} \tag{3.44}$$

$$\cos(\alpha) = \frac{1}{2}\left(e^{j\alpha} + e^{-j\alpha}\right) \tag{3.45}$$

$$\vec{x} = \frac{3}{2}k \cdot X_p e^{j\omega t} \tag{3.46}$$

If the three phase quantities do *not* form a balanced sinusoidal set then they are called *arbitrary*. Using the notation listed in the beginning of the report, the SV is represented as Equation (3.47).

$$\vec{x} = |\vec{x}|\exp\left[j\angle(\vec{x})\right] = \hat{X}e^{j\xi} \tag{3.47}$$

In other words, $\hat{X}$ and ξ are the magnitude and angle of any arbitrary SV; if the SV happens to represent sinusoidal quantities then we specifically know that $\hat{X} = \frac{3}{2}k \cdot X_p$ and $\xi = \omega t$. Note that the factor of $3/2$ is not present in the arbitrary case (Equation 3.47) as is for the sinusoidal case (Equation 3.46). The reason the factor $3/2$ appears in Equation (3.46) is that we have a known amplitude of the phase values which we can see as being scaled. Equation (3.47) lacks the factor because we do not have a phase amplitude that is fixed. In other words, the scaling apparent in the sinusoidal case is also present in the arbitrary case but is not so obvious. The topic of scaling is important but it will be played down until the end of Part II (and generally the scaling will be left as $k = 1$).

The take-away from this subsection is that the space vector is an instantaneous quantity that contains information from each phase variable and its orientation. Those variables do not need to be sinusoidal (but they cannot contain any zero-sequence component). As the values of the phase variables change the instantaneous magnitude and angle of the SV will change. If the phase variables happen to form a balanced sinusoidal set the magnitude and angle are easily related to the amplitude and phase of the variables.

Additivity of MMF and Current Space Vectors
When the rotating stator MMF wave was developed earlier in the chapter it was shown how the current in each phase creates a component MMF that is distributed cosinusoidally in space with the peak aligned with the magnetic axis of that phase. These component MMFs add to form a total MMF with the same distribution. The distributed nature of the MMF will continue to be ignored. Here we will assume that the SVs can be added as standard vectors and seek only to understand the basic vector nature of that addition. The MMF space vector (Equation 3.41) is

composed of three component space vectors corresponding to each phase as shown in Equation (3.48).[23]

$$\vec{f} = \left[\left(\frac{N_e}{2} \right) \cdot i_A(t) \cdot 1 + \left(\frac{N_e}{2} \right) \cdot i_B(t) \cdot e^{j\gamma} + \left(\frac{N_e}{2} \right) \cdot i_C(t) \cdot e^{-j\gamma} \right]$$

$$= \left[f_A(t) \cdot 1 + f_B(t) \cdot e^{j\gamma} + f_C(t) \cdot e^{-j\gamma} \right]$$

$$\vec{f} = \vec{f}_A + \vec{f}_B + \vec{f}_C \qquad\qquad (3.48)$$

It is clear that the magnitude of each component is proportional to the current in that phase and that each component acts in the direction of its magnetic axis. This matches the description of the MMF components given earlier in the chapter: the distribution is fixed in space, has a peak aligned to the magnetic axis, and has a magnitude that scales with the phase current. The definition of the MMF and current space vectors does not require the currents to be balanced sinusoids but for the moment we will consider this case. The instantaneous values of the component MMF SVs are shown directed along their respective axes in Figure 3.25 for three-phase currents at electrical positions of 0° and 30°. Figure 3.25 corresponds directly to Figure 3.11, and both figures correspond to Figure 3.7 and Figure 3.8.
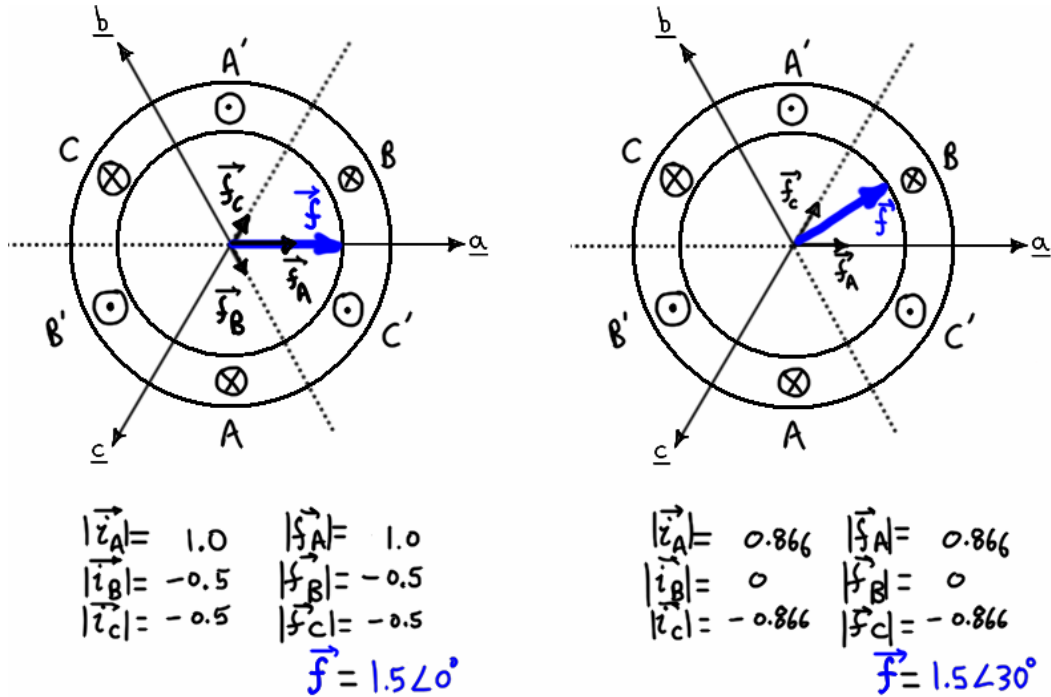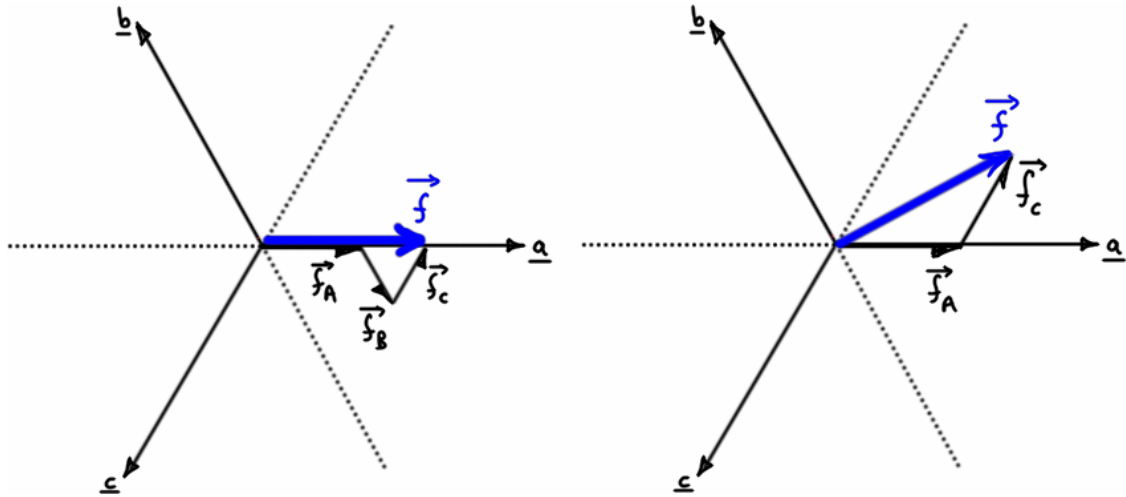
Figure 3.25 – Instantaneous values of component and total MMF space vectors; (c.f. Figure 3.11).

---

[23] Throughout this report it will be emphasized that the space vector describes the combined action of the phases. That emphasis cannot be placed on the space vectors associated with each phase and perhaps this terminology should not be used but it is found throughout the literature so it is adopted here.

Notice that the amplitude of the MMF SV seems to remain constant with the same amplitude of the sum of instantaneous values of component MMF phasors shown in Figure 3.11. This can be verified mathematically if the three-phase currents of Equation (3.3) are substituted into the definition of the MMF space vector, Equation (3.41). After simplification the resulting MMF SV is that given by Equation (3.49) and it is clear that the amplitude is indeed the same as that found earlier using real-valued arithmetic.

$$\vec{f} = \frac{3}{2}\left(\frac{N_e}{2}\right)I_p e^{j\omega t} \tag{3.49}$$

For simplicity the diagram in Figure 3.25 is usually drawn without showing the stator, as shown in Figure 3.26. The instantaneous values of the space vectors are shown added together for the two electrical positions used earlier.

Figure 3.26 – Addition of component MMF SVs to form total MMF SV (c.f. Figure 3.25).
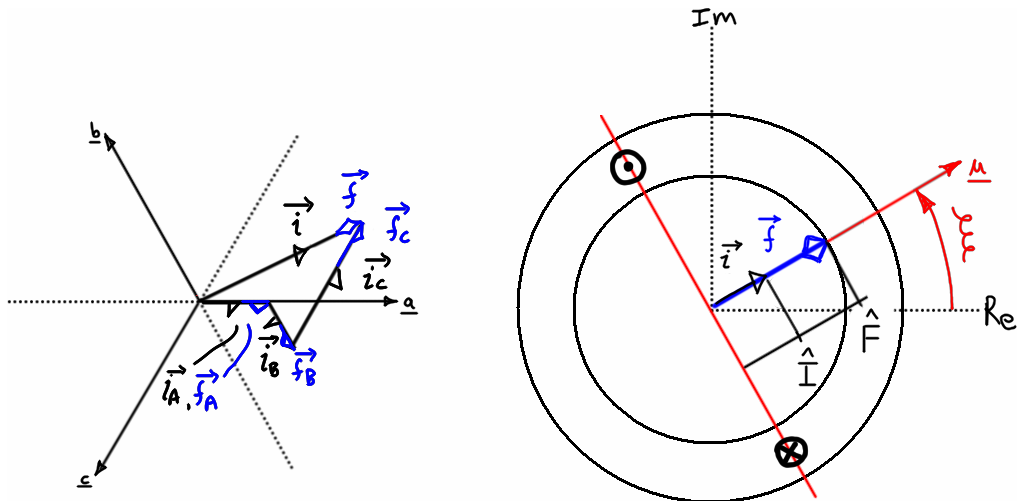
Given the relationship in Equation (3.42) it is clear that MMF space vector and current space vector are cophasal (they always have the same phase). This could also be seen if the three-phase currents are substituted into the current SV (instead of substituting them into the MMF SV equation). The resulting current SV would be the right-hand portion of Equation (3.49) and this result again agrees with Equation (3.42). And in comparing Equation (3.40) with the second line of Equation (3.48), it is seen that the component current space vectors add in the same way that the component MMF space vectors do.

So far the comparison with the CRT example has worked well to illustrate a physical interpretation of the space vector. It showed how each scalar quantity in υ (voltage, current) can be multiplied by a constant of proportionality and basis vector in **α** that when summed represent a vector with meaning in **α** (force in Cartesian space, MMF in complex space, Equation 3.32 and

Equation 3.36). It further showed how the scalar quantity in υ can itself be assigned a vector orientation in $\boldsymbol{\alpha}$ in its own units (the voltage and current SVs of Equation 3.33 and Equation 3.38) that when multiplied by the constant of proportionality produced the same result. The two versions differ only by how the constant of proportionality is distributed in the equation thus they are equivalent. The purpose of the discussion was to provide an interpretation for a voltage or current space vector in the space $\boldsymbol{\alpha}$ where they would otherwise not have a meaning, and this understanding is the basis on which we assume the voltage and current SVs may be added together.

In the case of voltage it isn't hard to understand that the electron experiences force in two orthogonal directions and that the sum of those forces *could* have been though of as being imparted by a certain voltage applied to two plates aligned in the direction of resultant force, as shown in Figure 3.24. This illustrates an important understanding of the space vector (voltage space vector in this case): the effect of the voltage SV has a physical interpretation but the voltage SV itself is an abstract quantity that does not exist and thus cannot be physically measured. The same applies to the MMF and current SVs. The resulting MMF SV *could* have been produced by a winding oriented along the axis of the resulting MMF. In that case, the MMF SV could be described by the constant of proportionality multiplied by the resulting current SV, as shown in Figure 3.27, for the general case of Equation (3.50).

$$\vec{f} = \left(\frac{N_e}{2} \right) \vec{i}$$
$$\vec{f} = \left(\frac{N_e}{2} \right) \hat{I} e^{j\xi} = \hat{F} e^{j\xi}$$

(3.50)

Figure 3.27 – Equivalent MMF produced by coil with axis aligned with resultant MMF (c.f. Figure 3.24).

This explains part of the meaning of the statement above that said the MMF and current SVs are cophasal (a fuller explanation is given in the next subsection). Figure 3.27 shows how the simple additivity of the force and voltage SVs of the CRT example directly applies to the MMF and current SVs of the machine.

The take-away from this subsection is that space vectors can be added and that the space vector itself is not a physically-existing quantity. Although a SV (such as $\vec{f}$) may represent a physically-distributed quantity, as SV (such as $\vec{i}$) may represent a quantity that cannot be understood in physical terms; this is discussed next and is the additional "level of abstraction" referred to in the quote that opened Part II.

The SV as a Distribution

The second facet of the SV to study is the manner in which it represents a distribution. The previous section concentrated on the vector nature of MMF but ignored distribution, which will be studied now. When a machine is modeled using SV theory all quantities (voltage, current, MMF, flux linkage) will be space vectors. Although each SV could be interpreted as representing a distribution, stator MMF is the only quantity whose physical distribution is equal to the distribution represented by the SV. For the other quantities, the "distribution" represented by the SV does not physically exist, or if it does, it is not exactly that described by the SV. This seems an unwelcome artifact of the theory but it will be shown to be the meaning of reference frame

theory and will be very useful. Since it is vital to understand reference frame theory, and since the distribution of the MMF SV coincides with the physical distribution, it is the author's opinion that studying the MMF's distribution is the only connection point between the familiar physical understanding of the machine and the abstract SV representation. With this opinion in mind it is first shown how the stator MMF SV represents the actual MMF distribution produced by the stator current. Then the previously-defined relationship between the stator current SV and the stator MMF SV is discussed to reveal the interpretation of the current SV.

MMF Space Vector and its Distribution

This subsection demonstrates how the MMF SV represents the actual MMF distribution in the machine. We will also gain a more solid understanding of reference frame theory.

In the CRT example the concept of a Cartesian voltage vector was reasonable because the force is a linear one which acts in the plane perpendicular to the electron beam. But in a synchronous machine the stator MMF does not simply act along a vector in a plane—it is a distribution about the stator periphery. It is obvious from the development of the MMF wave earlier in the chapter that the MMF distribution is cosinusoidal in θ, but this is perhaps not obvious from the math presented thus far. To show that the MMF SV represents a cosinusoidal MMF distribution, return to the real-valued expression of stator MMF developed earlier in the chapter (Equation 3.2) which is reproduced here as Equation (3.51). *Note that the currents are arbitrary and are not required to be sinusoidal.*

(3.2):
$$f(\theta,t) = f_A(\theta) + f_B(\theta) + f_C(\theta)$$
$$= \frac{N_e}{2}\left[i_A(t)\cdot\cos(\theta) + i_B(t)\cdot\cos(\theta-120°) + i_C(t)\cdot\cos(\theta+120°) \right]$$
(3.51)

The cosine terms can be expanded into their complex equivalents using the identity in Equation (3.52).

$$\cos(\alpha) = \frac{1}{2}\left(e^{j\alpha} + e^{-j\alpha} \right)$$
(3.52)

Substituting the resulting expressions into Equation (3.51) and simplifying yields Equation (3.53).

$$f(\theta,t) = \left(\frac{N_e}{2}\right)\frac{1}{2}\left[\left(i_A + i_B e^{j\gamma} + i_C e^{-j\gamma} \right)e^{-j\theta} + \left(i_A + i_B e^{-j\gamma} + i_C e^{j\gamma} \right)e^{j\theta} \right]$$
(3.53)

Recognizing that the first parenthesis contains definition of the current space vector ($k=1$) and the second parenthesis contains its complex conjugate, this can be rewritten as Equation (3.54).

$$f(\theta,t)=\left(\frac{N_e}{2}\right)\frac{1}{2}\left[\vec{i}\cdot e^{-j\theta}+\vec{i}*\cdot e^{j\theta}\right] \qquad (3.54)$$

Defining the first of the term in the square brackets as the complex number *z*, the identity in Equation (3.55) can be used to rewrite (3.54) as Equation (3.56).

$$\mathrm{Re}[z]=\frac{1}{2}\{z+z*\} \qquad (3.55)$$

$$f(\theta,t)=\left(\frac{N_e}{2}\right)\mathrm{Re}\{\vec{i}\cdot e^{-j\theta}\} \qquad (3.56)$$

According to Equation (3.46), the current SV (*k*=1) of three-phase balanced sinusoidal currents of amplitude I_p is given by Equation (3.57).

$$\vec{i}=\frac{3}{2}I_p e^{j\omega t} \qquad (3.57)$$

Substituting this into Equation (3.56) yields Equation (3.58).

$$f(\theta,t)=\left(\frac{N_e}{2}\right)\mathrm{Re}\left\{\frac{3}{2}I_p e^{j\omega t}\cdot e^{-j\theta}\right\}$$

$$f(\theta,t)=\frac{3}{2}\left(\frac{N_e}{2}\right)I_p\cos(\omega t-\theta) \qquad (3.58)$$

Equation (3.58) is identically Equation (3.6), the real-valued expression of stator MMF due to balanced sinusoidal currents developed in Part I of this chapter. To be clear, Equation (3.6) was developed without any knowledge of the space vector and it is written in terms of scalar currents. With some manipulation (by transforming it into complex form, but without making any changes) it was rewritten as the real part of a complex-valued expression in which the current space vector appeared along with a term that contained the angle about the stator periphery, θ. The space vector corresponding to balanced sinusoidal currents was substituted in and this resulted in the real-valued expression for the MMF that one would expect from those balanced sinusoidal currents. This roughly illustrates what this subsection set out to show: that the MMF SV represents a cosinusoidal MMF distribution.

Perhaps the result is questionable since we made the substitution of the current SV that represents *balanced sinusoidal currents*. That substitution was made in order to show the clear link to the result obtained earlier in the chapter but now we can treat the arbitrary current case. The current SV in Equation (3.56) can be expressed in terms of its magnitude and phase using the notation

given in Equation (3.47). The result is Equation (3.59), where $f\left(\theta,\xi(t)\right)=f(\theta,t)$ just as $f\left(\theta,\omega(t)\right)=f(\theta,t)$.

$$f(\theta,t)=\left(\frac{N_e}{2}\right)\mathrm{Re}\left\{\hat{I}e^{j\xi}\cdot e^{-j\theta}\right\}$$

$$f(\theta,t)=\left(\frac{N_e}{2}\right)\hat{I}\cos\left(\xi-\theta\right) \tag{3.59}$$

The current SV describes the combined effect of all three phase currents and the orientation of the windings. Regardless of the amplitude and angle of the current SV, it is seen that the MMF retains its cosinusoidal distribution; this matches the description from Part I.

It has been shown that the MMF SV represents a cosinusoidal distribution of the stator MMF regardless of the nature of the phase currents; for the special case of balanced sinusoidal currents the MMF SV is simply the complex representation of the same real-valued MMF expression from Part I. Now to further discuss the cosinusoidal distribution it would be useful to show how each *component* MMF SV represents a cosinusoidal MMF distribution about its basis vector. Then the special case of balanced sinusoidal currents will be examined again in this light. Returning to Equation (3.56), the current space vector can be expanded and the constant of proportionality can be redistributed as in previous discussions, such as those that developed Equation (3.36), Equation (3.37), and Equation (3.48).

$$f(\theta,t)=\left(\frac{N_e}{2}\right)\mathrm{Re}\left\{\vec{i}\cdot e^{-j\theta}\right\}$$

$$=\left(\frac{N_e}{2}\right)\mathrm{Re}\left\{\left[i_A(t)\cdot 1+i_B(t)\cdot e^{j\gamma}+i_C(t)\cdot e^{-j\gamma}\right]\cdot e^{-j\theta}\right\}$$

$$=\mathrm{Re}\left\{\underbrace{\overbrace{\left(\frac{N_e}{2}\right)i_A(t)\cdot 1\cdot e^{-j\theta}}^{f_A}}_{\vec{f}_A}+\underbrace{\overbrace{\left(\frac{N_e}{2}\right)i_B(t)\cdot e^{j\gamma}}^{f_B}\cdot e^{-j\theta}}_{\vec{f}_B}+\underbrace{\overbrace{\left(\frac{N_e}{2}\right)i_C(t)\cdot e^{-j\gamma}}^{f_C}\cdot e^{-j\theta}}_{\vec{f}_C}\right\}$$

$$=\left(\frac{N_e}{2}\right)i_A(t)\cdot\cos(0-\theta)+\left(\frac{N_e}{2}\right)i_B(t)\cdot\cos(120^\circ-\theta)+\left(\frac{N_e}{2}\right)i_C(t)\cdot\cos(-120^\circ-\theta)$$

$$f(\theta,t)=\frac{N_e}{2}\left[i_A(t)\cdot\cos(\theta)+i_B(t)\cdot\cos(\theta-120^\circ)+i_C(t)\cdot\cos(\theta+120^\circ)\right] \tag{3.60}$$

Equation (3.60) is seen to be the same as Equation (3.2). Comparison of the third and fifth lines that developed Equation (3.60) shows clearly that each component MMF SV represents an MMF

distribution that is cosinusoidal in θ with the peak located at the basis vector corresponding to the magnetic axis of that phase; this matches the physical understanding from Part I and is what we set out to show. Now we examine the special case of balanced sinusoidal currents by again considering Equation (3.56). Substituting the balanced sinusoidal currents of Equation (3.3) for the general currents (or equivalently, substituting Equation (3.57) in for the current SV) yields Equation (3.61), which is exactly Equation (3.4) found in the beginning of the chapter.

$$
\begin{aligned}
f(\theta,t) &= \left(\frac{N_e}{2}\right)\mathrm{Re}[\vec{i}\cdot e^{-j\theta}] \\[2mm]
&= \left(\frac{N_e}{2}\right)\mathrm{Re}\left\{\left[i_A(t)\cdot 1 + i_B(t)\cdot e^{j\gamma} + i_C(t)\cdot e^{-j\gamma}\right]\cdot e^{-j\theta}\right\} \\[2mm]
&= \mathrm{Re}\left\{\underbrace{\overbrace{\left(\frac{N_e}{2}\right)i_A(t)\cdot 1\cdot e^{-j\theta}}^{f_A}}_{\vec{f}_A} + \underbrace{\overbrace{\left(\frac{N_e}{2}\right)i_B(t)\cdot e^{j\gamma}\cdot e^{-j\theta}}^{f_B}}_{\vec{f}_B} + \underbrace{\overbrace{\left(\frac{N_e}{2}\right)i_C(t)\cdot e^{-j\gamma}\cdot e^{-j\theta}}^{f_C}}_{\vec{f}_C}\right\}
\end{aligned}
$$

$$
f(\theta,t) = \frac{N_e}{2}\left[\begin{array}{l} I_p\cos(\omega t)\cos(\theta) + I_p\cos(\omega t - 120°)\cos(\theta - 120°) \\ + I_p\cos(\omega t + 120°)\cos(\theta + 120°) \end{array}\right] \tag{3.61}
$$

Thus, not only does each component MMF SV represent a component distribution about its basis vector, but for the special case of balanced cosinusoidal currents, each one of those component distributions is a cosinusoidally-modulated standing wave cosinusoidally distributed in space, exactly as in Part I.

In summary, this section has shown that in SV theory the component MMF SV of each phase represents a cosinusoidally distributed MMF wave and these three component MMF SVs will sum to yield an MMF SV that also represents a cosinusoidally distributed MMF; this has direct correspondence to the real-valued descriptions of MMF developed earlier. That these SVs represent cosinusoidal distributions is true regardless of the nature of the currents. It was also shown that if the currents do form a balanced sinusoidal set, the distribution represented by the MMF SV is a traveling wave of constant amplitude whose peak aligns with the electrical position, just as the real-valued expressions developed in the beginning of the chapter. Since the MMF distributions can be described accurately by the SV, *SV theory can be used to analyze machines whose currents do not form a balanced sinusoidal set*. This stands in contrast to the single-phase equivalent approach and is one reason why SV theory is more useful.

107

However, if the per-phase MMF distributions are not cosinusoidally distributed, SV theory cannot be used as shown here to analyze the machine. (This is essentially the reason why many articles in the literature assume a sinusoidal machine, even if the article specifically concerns a trapezoidal machine.) The statement that SV theory applies only to sinusoidal machines is given without proof in [87, p.34], [43, p.223]. It does not mean that the theory cannot be augmented to describe nonsinusoidal machines [87, p.53]; it simply means that the theory *as presented here* cannot be used to describe them unless modifications are made. From Appendix C, when a nonsinusoidal machine is modeled using SV theory only the fundamental component of torque and bEMF will be represented. The reason this is important is that the expression for torque production involves the magnitude of the MMF (or flux, flux linkage, flux density, or field strength) of the stator. If the phase MMF distributions are not sinusoidal, they will not sum to a sinusoid of 3/2 amplitude, even for balanced sinusoidal current, thus the torque expression will be invalid.

Before moving on, one important observation will be made regarding the MMF space vector's representation of a distributed quantity. This section began with the real-valued expression of stator MMF, Equation (3.2), which was reproduced as Equation (3.51):

$$f(\theta,t) = \frac{N_e}{2}\left[i_A(t)\cdot\cos(\theta) + i_B(t)\cdot\cos(\theta - 120^\circ) + i_C(t)\cdot\cos(\theta + 120^\circ)\right] \ .$$

This was reworked to give an equivalent complex form, Equation (3.56):

$$f(\theta,t) = \left(\frac{N_e}{2}\right)\mathrm{Re}\left\{\vec{i}\cdot e^{-j\theta}\right\} \ ,$$

which has provided satisfactory results in this discussion. One of those results was the expression that describes the MMF resulting from balanced sinusoidal currents, Equation (3.58):

$$f(\theta,t) = \frac{3}{2}\left(\frac{N_e}{2}\right)I_p\cos(\omega t - \theta) \ .$$

But earlier (in the section "Additivity of MMF and Current Space Vectors"), balanced sinusoidal currents were substituted into the MMF SV definition, Equation (3.41):

$$\vec{f} = \left(\frac{N_e}{2}\right)\cdot k\left[i_A(t)\cdot 1 + i_B(t)\cdot e^{j\gamma} + i_C(t)\cdot e^{-j\gamma}\right]$$

and the result was the SV representation of MMF due to balanced sinusoidal currents, Equation (3.49):

$$\vec{f} = \frac{3}{2}\left(\frac{N_e}{2}\right)I_p e^{j\omega t} \quad .$$

This was an acceptable result because is the same as that produced when the current SV representing balanced sinusoidal currents, Equation (3.57):

$$\vec{i} = \frac{3}{2}I_p e^{j\omega t}$$

is substituted into the relationship between the MMF SV and the current SV, Equation (3.42):

$$\vec{f} = \left(\frac{N_e}{2}\right)\cdot\vec{i} \quad :$$

$$\vec{f} = \frac{3}{2}\left(\frac{N_e}{2}\right)I_p e^{j\omega t} \quad .$$

However, the real part of Equation (3.49) (which was derived using only space vectors) is:

$$f(\theta,t) = \frac{3}{2}\left(\frac{N_e}{2}\right)I_p \cos(\omega t) \quad ,$$

whereas Equation (3.58) (which was derived using only real-valued expressions) is:

$$f(\theta,t) = \frac{3}{2}\left(\frac{N_e}{2}\right)I_p \cos(\omega t - \theta) \quad .$$

Comparing the two it is seen that the result derived using SV analysis is missing the θ term that we have relied upon to prove that the MMF SV represents a distribution in θ. (To clarify, we began with a real-valued expression, rewrote it in terms of a SV, and found that *those* particular SV expressions (such as Equations 3.58 and 3.59) represent a cosinusoidal distribution. Per the above, we have not yet explicitly found that the particular MMF SV derived *solely* from SV equations represents this distribution and it appears that it does not since the θ term is missing.) The author's first encounter with this was met with much concern regarding the SV's representation of distributed quantities, but it turns out that any doubt is unfounded and the two forms are indeed equivalent. In fact, examining this potential discrepancy reveals the concept of reference frame theory that is requisite to understanding the space vector theory and FOC. Earlier in the chapter the MMF wave was given as Equations (3.6) and (3.7).

(3.6): $f(\theta,t) = \frac{3}{2}\left(\frac{N_e}{2}\right)I_p \cos(\omega t - \theta)$

(3.7): $\quad f(\theta,t) = \dfrac{3}{2}\left(\dfrac{N_e}{2}\right)I_p \cos(\theta - \omega t)$

At that time the argument of the cosine was briefly discussed and now we return to that discussion. It was shown that Equation (3.7) gives the traveling wave as expected, while Equations (3.6) is interpreted as giving the value of MMF at some observation point θ, as a function of time. In the simplest interpretation, taking the real part of Equation (3.49) yields Equation (3.6) for $\theta = 0$.

$$\mathrm{Re}\left\{\dfrac{3}{2}\left(\dfrac{N_e}{2}\right)I_p e^{j\omega t}\right\} = \dfrac{3}{2}\left(\dfrac{N_e}{2}\right)I_p \cos(\omega t - \theta),\ \theta = 0$$

Therefore, it can be interpreted that the real part of the MMF SV represents the value of MMF at the point of observation $\theta = 0$, ensuring us that the MMF SV does indeed represent the cosinusoidal distribution even if the θ terms is not present. But this might then raise questions as to how Equation (3.6) represents a cosinusoidal distribution in θ without having θ in the argument, or how it can remain cosinusoidal even if the currents are not. Assume the currents do not form a balanced sinusoidal set, but let the angle of this arbitrary current SV be defined as ξ as usual. Whatever it is, it will vary with time: $\xi(t)$. Substitution into Equation (3.6) and evaluating at $\theta = 0$ gives Equation (3.62).

$$f(\theta,t) = \dfrac{3}{2}\left(\dfrac{N_e}{2}\right)I_p \cos\left[\xi(t) - \theta\right]$$

$$f(\theta,t) = \dfrac{3}{2}\left(\dfrac{N_e}{2}\right)I_p \cos\left[\xi(t)\right]$$

(3.62)

As before, the MMF is known to exist in the airgap, thus Equation (3.62) must describe some function of the angle around the stator. This shows then that the currents can be arbitrary and the distribution is still cosinusoidal, although it is perhaps not immediately obvious unless the form of Equation (3.7) is used. Of course, we should certainly expect this to be the case since Equations (3.6) and (3.7) are equal to one another.

Now that the differences are resolved, an additional interpretation is presented. It was just shown that the equations with θ were the same as those without, simply because in the latter case, $\theta = 0$. Figure 3.9 shows the *distribution* in θ, but if we set $\theta = 0$ it is clear that the equations give the *peak* of the MMF wave, measured from $\theta = 0$. The reason that $\theta = 0$ in the SV equations is that the SV is defined in the *stationary reference frame* affixed to the stator. That means angles are defined as being measured from $\theta = 0$. The importance of this is that if we can set $\theta = 0$, we can

set θ to anything. Taking the real part of (a current SV multiplied by $e^{-j\theta}$) gave $\cos(\omega t - \theta)$ and θ disappears when it is set to zero. But in either the SV or real-valued equations, if we set θ to anything else, the equations define the peak of the MMF wave relative to that point θ, rather than relative to zero; this is the meaning of *reference frame theory*. While the use of the phase-A axis as a reference was declared in the beginning of the chapter (see Figure 3.1), this discussion provides a new insight into the MMF equation that relates the *position* of the peak of MMF to the *distribution* of the MMF. This discussion may fail to illuminate the concept, but as we revisit it throughout the remainder of Part II it should eventually become clear.

Current Space Vector and its Interpretation

The previous subsection demonstrated how the MMF SV $\vec{f}$ represents the actual MMF distribution in the machine; the MMF is the only true distribution represented by the space vector. In this section it is shown that the current SV $\vec{i}$ does not represent a distribution but that it does have close association with $\vec{f}$. This relationship is the connection between the physical understanding of the machine and the more abstract space vector model; in other words, the relationship is the basis for using SV theory to describe a machine (this basis will be finalized in Part III).

From Appendix C, the sinusoidal winding density for phase-A is given by Equation (3.63) and the number of ampere-turns for phase-A is given by Equation (3.64).

$$n_A(\theta) = \frac{N_e}{2}\sin(\theta) \tag{3.63}$$

$$d_A(\theta) = i_A \cdot n_A(\theta) = i_A \frac{N_e}{2}\sin(\theta) \tag{3.64}$$

For a single phase each function is fixed to the stator but when all phases are considered the total effect of current in those windings is the same as if an equivalent winding were rotating about the stator. This has direct similarity to the way the MMF component of each phase is fixed in space but together they produce a rotating MMF. This concept is sometimes referred to as the "rotating ampere-turn distribution" [69, p.6.8]. Similar to the way the MMF wave was developed we can find an expression for the overall amp-turn distribution due to the winding currents, Equation (3.65), where balanced sinusoidal currents are used.

$$d(\theta) = I_p \frac{N_e}{2} \left[\sin(\theta) \cdot \cos(\omega t) + \sin(\theta - \gamma) \cdot \cos(\omega t - \gamma) + \sin(\theta + \gamma) \cdot \cos(\omega t + \gamma) \right]$$

$$= I_p \frac{N_e}{2} \frac{1}{2} \left[\begin{array}{l} \sin(\theta + \omega t) + \sin(\theta - \omega t) + \sin(\theta + \omega t + \gamma) + \sin(\theta - \omega t) \\ + \sin(\theta + \omega t - \gamma) + \sin(\theta - \omega t) \end{array} \right]$$

$$d(\theta) = I_p \frac{3}{2} \frac{N_e}{2} \sin(\theta - \omega t) \tag{3.65}$$

It is clear that the effective number of amp-turns is a function around the stator and rotates according to the electrical position of the currents. Setting $\theta = 0$ the amp-turn distribution becomes Equation (3.66).

$$d(\theta) = -I_p \frac{3}{2} \frac{N_e}{2} \sin(\omega t) \tag{3.66}$$

This can be rewritten in terms of the current space vector as in Equation (3.67).

$$d(\theta) = -I_p \frac{3}{2} \frac{N_e}{2} \sin(\omega t)$$

$$= I_p \frac{3}{2} \frac{N_e}{2} \cos(\omega t + \pi / 2)$$

$$= \frac{N_e}{2} \mathrm{Re} \left\{ \frac{3}{2} I_p e^{j(\omega t + \pi/2)} \right\}$$

$$= \frac{N_e}{2} \mathrm{Re} \left\{ e^{j\pi/2} \cdot \frac{3}{2} I_p e^{j\omega t} \right\}$$

$$= \frac{N_e}{2} \mathrm{Re} \left\{ j \cdot \vec{i} \right\}$$

$$\vec{d} = \frac{N_e}{2} (j \cdot \vec{i}) \tag{3.67}$$

It is seen that if the rotating amp-turn distribution were described by a space vector it would be 90° ahead of the current SV ([42, p.181], [166]), and since we know that a sine-distributed winding produces a cosine-distributed MMF this should not come as a surprise. Likewise Equation (3.67) is very similar to the MMF expression (Equation 3.42), which is reproduced here as Equation (3.68).

$$(3.42): \quad \vec{f} = \left(\frac{N_e}{2} \right) \cdot \vec{i} \tag{3.68}$$

The MMF and current SVs are related by only a scalar constant of proportionality thus their "distributions" must be the same. But Equation (3.67) showed that the actual amp-turn (or current density) distribution is not equal to the "distribution" of the current SV (and we really should not expect this to be true anyway). This leads us to conclude that the current space vector does not

represent any physically-distributed quantity; this conclusion holds for all other space vectors except MMF. What its "distribution" instead represents is the meaning of reference frame theory discussed in the previous subsection; that interpretation is ultimately the most useful view of space vector theory. The meaning of the current SV will be further examined using Equation (3.68).

This direct phase relationship between current and MMF has already been encountered: the sinusoidal case was examined in Part I, and both the sinusoidal and arbitrary cases have been examined here in Part II. In Part I when the MMF wave was developed mathematically (Equation 3.6, θ=0), it was obvious that the angular position of the stator MMF is identical to the electrical position (ωt) of the balanced sinusoidal currents (refer again to Figure 3.9). In Part II when the SV was developed (for the case of balanced sinusoidal currents) it was shown that the MMF SV describes the same MMF with the peak again at ωt and that this is shown very clearly in the SV itself, as in Equation (3.49) for example.
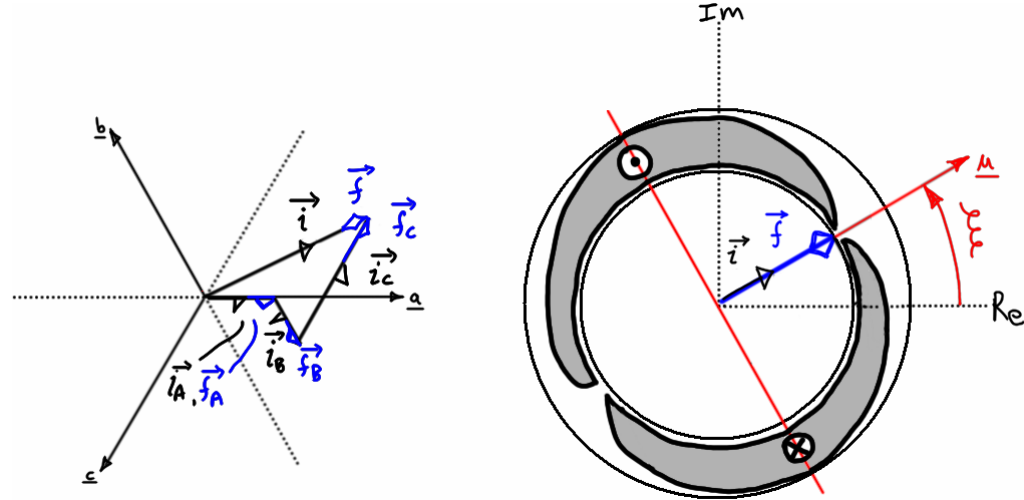
$$(3.49): \quad \vec{f} = \frac{3}{2}\left(\frac{N_e}{2}\right) I_p e^{j\omega t}$$

When the currents are arbitrary the SV theory gains an advantage over the real-valued descriptions of MMF since it is not restricted to balanced sinusoidal current. As discussed before, the MMF always retains its cosinusoidal distribution. Even in the arbitrary case, the SV of stator MMF is still cophasal with the SV of stator current, per Equation (3.42). Thus the angle ξ of the MMF SV represents the angular position of the peak of the MMF distribution, as measured from the phase-A axis and this is the same angle of the current SV. Further, the magnitude $\hat{F}$ of the physical MMF SV is proportional to the amplitude of the MMF wave and proportional to the magnitude of the current SV. Again from Part II, this was given by Equation (3.50).

$$(3.50): \quad \vec{f} = \left(\frac{N_e}{2}\right) \hat{I} e^{j\xi} = \hat{F} e^{j\xi}$$

When Equation (3.50) was developed it was shown that the stator MMF SV was cophasal with the current SV in Figure 3.27. But at that time the primary interest was the addition of the SVs and the distributions were ignored. The figure is now redrawn as Figure 3.28 and the equivalent sinusoidal amp-turn distribution is shown. This leads to a better interpretation of the current SV. When Figure 3.27 was discussed it was said that the resulting MMF could be thought of as being produced by a coil whose magnetic axis was oriented along the direction of the total MMF produced by the three phase currents; this was compared to the CRT example of Figure 3.24. The situation is the same here except now we can say that the MMF could be thought of as being

113

produced by an equivalent (N_e-turn) *sinusoidally-distributed* coil whose magnetic axis is aligned at the *angular position of the current SV* and driven by a current equal to the *magnitude of the current SV*.

Figure 3.28 – Axis of rotating amp-turn distribution cophasal with current and MMF SVs.

Torque production is of critical interest and torque production is directly related to the amplitudes and angular positions of the stator and rotor fields relative to one another, thus the stator MMF is of interest. Since the magnitude and angle of the stator MMF are directly related to the magnitude and angle of the current SV, *even for arbitrary currents*, it is clear that the current SV can be used to describe the torque of the machine; this will be developed in Part III.

The take-away from this subsection is that each SV represents a cosinusoidal distribution relative to the phase-A axis. For the MMF SV this distribution coincides with the actual distribution in the machine but for all other quantities the "distribution" is an abstract concept described by reference frame theory and this is the connection between the physical phenomena in the machine and its SV representation. Surprisingly, most texts offer only a mathematical treatment and make no distinction between the physical distribution represented by the MMF SV and the abstract distributions represented by the SVs of transformed quantities. However, one text [73]—which attempts (and does well) to look beyond the mathematical definition—explicitly states that no attempt will be made in the book to assign a physical meaning to the SVs of transformed quantities, indicating that only the MMF distribution is represented by the SV. Nonetheless, the discussion in this report is a simplification of the full theory (which is not often used to its fullest extent) in which the SV analysis treats a distributed-parameter machine [103] instead of the

lumped-parameter model in this report and in most references. [104] provides details and advanced theory regarding the interpretation of the SV, including the distribution aspect.

The SV as a Linear Transformation; Reference Frame Theory

The third and final facet of the SV to study is the fact that the definition of the SV is a linear transformation of variables (LTV). The transformed variables are the basis of reference frame theory thus the two are covered together. The previous two sections in Part II already touched on the LTV concept. The development of the vector aspect showed that the definition of the SV was a mapping (a LTV) from phase variables in $\mathbb{R}^3$ to a complex variable in $\mathbb{C}$ (the SV). The development of the distribution aspect mentioned the concept of reference frame theory in which quantities were defined with respect to the phase-A axis. Now the LTV aspect of the SV can be pursued further.

Clarke Transform
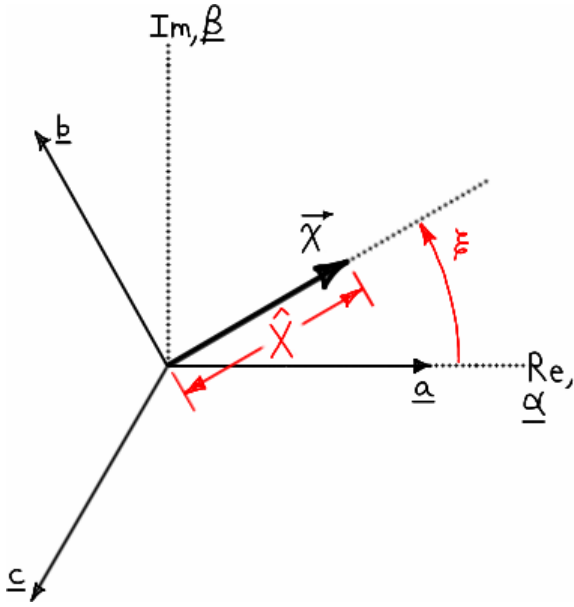
The complex SV is *defined* [42, p.396], [87, p.33], [88, p.84] as either the polar form of Equation (3.69) or the equivalent rectangular form of Equation (3.70).

$$\vec{x} \triangleq k \left[x_A \cdot 1 + x_B \cdot e^{j\gamma} + x_C \cdot e^{-j\gamma} \right] \tag{3.69}$$

$$\vec{x} = k \left[\left(x_A - \frac{1}{2} x_B - \frac{1}{2} x_C \right) + j \frac{\sqrt{3}}{2} \left(x_B - x_C \right) \right] \tag{3.70}$$

Regardless of the definition, an arbitrary SV (shown in Figure 3.29) can be described in terms of its magnitude and angle, Equation (3.71).

$$\vec{x} = \hat{X} e^{j\xi} \tag{3.71}$$

Figure 3.29 – Arbitrary space vector in the complex/αβ plane.

For convenience the real and imaginary axes could be relabeled as the α and β axes, respectively as shown in Figure 3.29. The component along the real axis is x_α and the component along the imaginary axis is x_β. The space vector can therefore be decomposed as shown in Equation (3.72), where both x_α and x_β are time varying—this is nothing but the standard parametric decomposition of a vector (the SV and its components are instantaneous quantities that are functions of time).

$$\vec{x} = \text{Re}\{\vec{x}\} + j \cdot \text{Im}\{\vec{x}\}$$
$$\vec{x} = x_\alpha + jx_\beta$$
(3.72)

Putting the α- and β- components into a vector would allow a SV quantity to be expressed as a real vector (Equation 3.73) and the SV transform itself to be expressed as a linear transformation matrix (as in Equation 3.74).

$$\mathbf{x}_{\alpha\beta} = \begin{bmatrix} x_\alpha \\ x_\beta \end{bmatrix}$$
(3.73)

$$\begin{bmatrix} x_\alpha \\ x_\beta \end{bmatrix} = k \begin{bmatrix} 1 & \dfrac{-1}{2} & \dfrac{-1}{2} \\ 0 & \dfrac{\sqrt{3}}{2} & \dfrac{-\sqrt{3}}{2} \end{bmatrix} \begin{bmatrix} x_A \\ x_B \\ x_C \end{bmatrix}$$
(3.74)

When the groups of variables are treated as vectors we can work with the complex SV by using standard linear algebra techniques and rewrite Equation (3.74) as Equation (3.75).

116

$$\mathbf{x}_{\alpha\beta} = k\mathbf{C}\mathbf{x}_{abc} \tag{3.75}$$

The set of variables defined by $\mathbf{x}_{abc}$ are the *phase variables*. When transformed by the matrix $\mathbf{C}$ they are written as $\mathbf{x}_{\alpha\beta}$, which is a vector defined in the *stationary reference frame*. Given Equation (3.72), $\vec{x}$ (which exists in the complex/αβ plane) could be said to be in the stationary reference frame as well. The matrix $\mathbf{C}$ goes by many names. In the popular literature and in this report, $\mathbf{C}$ is called the Clarke transform (after Edith Clarke), even though this is not the original transform (discussed in Appendix D).

From prior discussion is should be clear how the definition of Equation (3.69) came about: a vector is composed by summing the product of a scalar with a basis vector and in SV theory there are three complex basis vectors, one aligned to each phase axis. By simply substituting the rectangular form of the basis vectors into Equation (3.69), it is clear that Equation (3.70) is identical. Equation (3.70) makes sense from a cursory examination of projection as well. Using simple trigonometry, all of $\mathbf{a}$ projects onto $\boldsymbol{\alpha}$, $-1/2$ of $\mathbf{b}$ and $\mathbf{c}$ project onto $\boldsymbol{\alpha}$, $\sqrt{3}/2$ of $\mathbf{b}$ projects onto $\boldsymbol{\beta}$ and the same of $\mathbf{c}$ projects onto negative $\boldsymbol{\beta}$. Then when Equation (3.72) is considered, the real-valued matrix equivalent (Equation 3.74) is evident.[24] This shows that the SV definition is a transform (given by Equation 3.74) and that the SV is a complex-valued representation of a vector (Equations 3.72 and 3.73). This result is important because it is one point of connection (among several) between the traditional matrix-based analysis of polyphase circuits and machines ([11], [12], [32], [34]) (or tensor analysis [13]) and more modern "complex analysis" [78], [16], [15], [87].

Defining the phase basis vectors in αβ coordinates (Equation 3.76) allows Equation (3.74) to be written as Equation (3.77).

$$\mathbf{a} = \begin{bmatrix} 1 \\ 0 \end{bmatrix}; \quad \mathbf{b} = \begin{bmatrix} -1/2 \\ \sqrt{3}/2 \end{bmatrix}; \quad \mathbf{c} = \begin{bmatrix} -1/2 \\ -\sqrt{3}/2 \end{bmatrix} \tag{3.76}$$

---

[24] Historically the development proceeded in the opposite direction. A transform similar to the original Clarke transform was used as early as 1917 [11, p.310] and then around 1954 complex space vector theory was introduced [16], [15]. Finally, somewhere in that history was the interaction between matrix descriptions of machines and circuits and the application of tensor analysis (as early as 1938). The details are unimportant here. The best intuition can be had when the SV is viewed as a vector but the matrix case is easier to use to obtain key results.

$$\begin{bmatrix} x_\alpha \\ x_\beta \end{bmatrix} = k\begin{bmatrix} \mathbf{a} & \mathbf{b} & \mathbf{c} \end{bmatrix}\begin{bmatrix} x_A \\ x_B \\ x_C \end{bmatrix} \tag{3.77}$$

Equation (3.77) clearly shows how the α and β components are related to the value of the phase variables acting along their phase axes (basis vectors). Equations (3.75 or 3.77) clearly show a linear transformation in the form of $\mathbf{x}_{NEW} = \mathbf{T}\mathbf{x}_{OLD}$. The inverse of the transform is given by $\mathbf{x}_{OLD} = \mathbf{T}^{-1}\mathbf{x}_{NEW}$. A 2x3 matrix is singular but the inverse can be found several ways (Appendix D) and is given by Equation (3.78) and Equation (3.79).

$$\mathbf{x}_{abc} = \frac{1}{k}\mathbf{C}^{-1}\mathbf{x}_{\alpha\beta} \tag{3.78}$$

$$\begin{bmatrix} x_A \\ x_B \\ x_C \end{bmatrix} = \frac{1}{k}\begin{bmatrix} \dfrac{2}{3} & 0 \\ \dfrac{-1}{3} & \dfrac{1}{\sqrt{3}} \\ \dfrac{-1}{3} & \dfrac{-1}{\sqrt{3}} \end{bmatrix}\begin{bmatrix} x_\alpha \\ x_\beta \end{bmatrix} \tag{3.79}$$

As before, defining the columns of the matrix as basis vectors (Equation 3.80) allows the transformation (Equation 3.78) to be rewritten in terms of basis vectors (3.81).

$$\boldsymbol{\alpha} = \begin{bmatrix} \dfrac{2}{3} \\ \dfrac{-1}{3} \\ \dfrac{-1}{3} \end{bmatrix}; \quad \boldsymbol{\beta} = \begin{bmatrix} 0 \\ \dfrac{1}{\sqrt{3}} \\ \dfrac{-1}{\sqrt{3}} \end{bmatrix} \tag{3.80}$$

$$\begin{bmatrix} x_A \\ x_B \\ x_C \end{bmatrix} = \frac{1}{k}\begin{bmatrix} \boldsymbol{\alpha} & \boldsymbol{\beta} \end{bmatrix}\begin{bmatrix} x_\alpha \\ x_\beta \end{bmatrix} \tag{3.81}$$

As before, it is clear that the phase variable components are given by the values of the stationary variables along their axes, but these basis vectors are more difficult to visualize. The transformation matrix is singular thus its columns (the phase variable basis vectors) are not linearly dependent. Thus there is not a one-to-one mapping between the phase variables and the stationary reference frame. This should be exceptionally clear when examining Figure 3.29. Action along any phase variable axis has a component along the direction of each of the other two

phase variable axes; three axes in a plane cannot be independent of one another. Since this is the case it is difficult to use the Clarke transform and its pseudoinverse as defined—we must remove the linear dependence between the phase variable axes. To accomplish this we can first rewrite the $\Sigma = 0$ condition as Equation (3.82) and substitute it into the α-portion of Equation (3.74) to yield Equation (3.83). Then the complex form is given by Equation (3.84) and the inverse transformation is the given by Equation (3.85) (which is incidentally the same as Equation 3.79).

$$\frac{1}{2}x_A = -\frac{1}{2}x_B - \frac{1}{2}x_C \tag{3.82}$$

$$\begin{bmatrix} x_\alpha \\ x_\beta \end{bmatrix} = k \begin{bmatrix} \dfrac{3}{2} & 0 & 0 \\ 0 & \dfrac{\sqrt{3}}{2} & \dfrac{-\sqrt{3}}{2} \end{bmatrix} \begin{bmatrix} x_A \\ x_B \\ x_C \end{bmatrix} \tag{3.83}$$

$$\vec{x} = k \left[\left(\frac{3}{2}x_A \right) + j\frac{\sqrt{3}}{2}\left(x_B - x_C \right) \right] \tag{3.84}$$

$$\begin{bmatrix} x_A \\ x_B \\ x_C \end{bmatrix} = \frac{1}{k} \begin{bmatrix} \dfrac{2}{3} & 0 \\ \dfrac{-1}{3} & \dfrac{1}{\sqrt{3}} \\ \dfrac{-1}{3} & \dfrac{-1}{\sqrt{3}} \end{bmatrix} \begin{bmatrix} x_\alpha \\ x_\beta \end{bmatrix} \tag{3.85}$$

This makes the projection of the phase variable axes onto the **α** axis easier to see but it does not remove the ambiguity. To finish removing the dependence the $\Sigma = 0$ condition is rewritten as Equation (3.86) and substituted into the β-portion of Equation (3.83) to yield Equation (3.87). Then the complex form is given by Equation (3.88) and the inverse transformation is given by Equation (3.89) (which is now different from Equation 3.79).

$$\frac{-\sqrt{3}}{2}x_C = \frac{\sqrt{3}}{2}x_A + \frac{\sqrt{3}}{2}x_B \tag{3.86}$$

$$\begin{bmatrix} x_\alpha \\ x_\beta \end{bmatrix} = k \begin{bmatrix} \dfrac{3}{2} & 0 & 0 \\ \dfrac{\sqrt{3}}{2} & \sqrt{3} & 0 \end{bmatrix} \begin{bmatrix} x_A \\ x_B \\ x_C \end{bmatrix} \tag{3.87}$$

$$\vec{x} = k \left[\frac{3}{2}x_A + j\frac{\sqrt{3}}{2}\left(x_A + 2x_B \right) \right] \tag{3.88}$$

119

$$\begin{bmatrix} x_A \\ x_B \\ x_C \end{bmatrix} = \frac{1}{k} \begin{bmatrix} \dfrac{2}{3} & 0 \\ \dfrac{-1}{3} & \dfrac{1}{\sqrt{3}} \\ 0 & 0 \end{bmatrix} \begin{bmatrix} x_\alpha \\ x_\beta \end{bmatrix} \tag{3.89}$$

Now that we have removed the linear dependence the transformation matrix and its inverse are of rank 2 and each vector is only two-dimensional. However, phase-C's value cannot be directly obtained from Equation (3.89), thus we will use Equation (3.79 or 3.85) instead. Since the only difference between the two is the presence or absence of phase-C output there is no penalty for doing so. Our final forms of the Clarke transformation matrix and its inverse are then given by Equation (3.90).

$$\mathbf{C} = k \begin{bmatrix} \dfrac{3}{2} & 0 & 0 \\ \dfrac{\sqrt{3}}{2} & \sqrt{3} & 0 \end{bmatrix}; \qquad \mathbf{C}^{-1} = \frac{1}{k} \begin{bmatrix} \dfrac{2}{3} & 0 \\ \dfrac{-1}{3} & \dfrac{1}{\sqrt{3}} \\ \dfrac{-1}{3} & \dfrac{-1}{\sqrt{3}} \end{bmatrix} \tag{3.90}$$

Scaling & Trajectories

Comparing Equations (3.83) and (3.85), it is apparent that scaling occurs when transforming between coordinate systems. Since the purpose of the SV transformation is to work with the SV instead of the phase variables, it is important to understand this scaling, and that is best understood by studying the SV trajectory for balanced sinusoidal quantities.

The scaling has manifested itself several times already as the factor $3/2$. This factor arose even in real-valued expressions because the fields are described as a function of the angle around the stator (a cross-section)[25] but are created by three phase values. Regardless of whether that cross-sectional plane is described by the complex plane, the αβ plane, or a cylindrical coordinate system, the three phase axes "wrap around" as shown in Figure 3.29. Considering MMF for example, each axis' component MMF acts in a direction that has a component along the other phase axes. The other element that contributes to the scaling is the isolated neutral connection.

---

[25] The cross-section is sufficient for study because depth in the axial direction (rotor and stack length) has no effect on this phenomenon. But for a given magnitude of radial quantity, increasing motor length increases the flux linkage and hence the magnitudes of the torque and bEMF constants.

The component MMFs act away from the center of the machine thus they could possibly all cancel, but since the currents sum to zero their polarity is such that the component MMFs always sum to a nonzero value. This is seen clearly in Figure 3.7 and Figure 3.8 by examining the dashed lines which represent maximum MMF components—in each case at least one instantaneous component MMF had a polarity opposite the others.

We should expect the scaling to occur regardless of the nature of the currents. For the case of balanced sinusoidal currents the summation results in a constant amplitude traveling wave $3/2$ larger than the amplitude of a standing wave created by one phase alone. It turns out that this factor of $3/2$ does exist for nonsinusoidal currents but it is more difficult to see and more difficult to define, though it will be treated here.

From a linear algebra point of view we should expect the possibility of scaling in Equations (3.75) and (3.78). However the scaling is not easy to understand in terms of the traditional eigenvalues and eigenvectors for several reasons. Instead the scaling could be studied by examining the magnitude of the SV and the magnitude of its projections onto the **αβ** axes. It is easiest to begin with balanced sinusoidal phase variables; most of these results have already appeared earlier in the chapter but are collected here for clarity. Balanced sinusoidal phase variables are given by Equation (3.91).

$$\begin{cases} x_A = X_p \cos(\omega t) \\ x_B = X_p \cos(\omega t - \gamma) \\ x_C = X_p \cos(\omega t + \gamma) \end{cases} \tag{3.91}$$

The phase variables may be substituted into any of the SV transform definitions. It is easiest to rewrite the phase variables as their complex equivalents, Equation (3.92),

$$\begin{cases} x_A = \dfrac{1}{2}\left[e^{j\omega} + e^{-j\omega} \right] \\ x_B = \dfrac{1}{2}\left[e^{j(\omega-\gamma)} + e^{-j(\omega-\gamma)} \right] \\ x_C = \dfrac{1}{2}\left[e^{j(\omega+\gamma)} + e^{-j(\omega+\gamma)} \right] \end{cases} \tag{3.92}$$

and substitute them into the complex polar definition of the SV (Equation 3.69) and simplify to get Equation (3.93).

$$\vec{x} = k\frac{3}{2} X_p e^{j\omega t} \tag{3.93}$$

It is clear that the SV has a constant magnitude of $3k/2$ and its instantaneous angular position is ωt. As time increases it will trace a circular trajectory in time. Its projection (given by Equation 3.72) onto the **αβ** plane is Equation (3.94).

$$\begin{cases} x_\alpha = k\dfrac{3}{2}X_p\cos(\omega t) \\ x_\beta = k\dfrac{3}{2}X_p\sin(\omega t) \end{cases}$$

(3.94)

The phase variables, stationary variables, and SV trajectory in the **αβ** plane are all shown in Figure 3.30 for the case of balanced sinusoidal phase variables. The instantaneous position of the quantities is shown at $\omega t = 60°$.
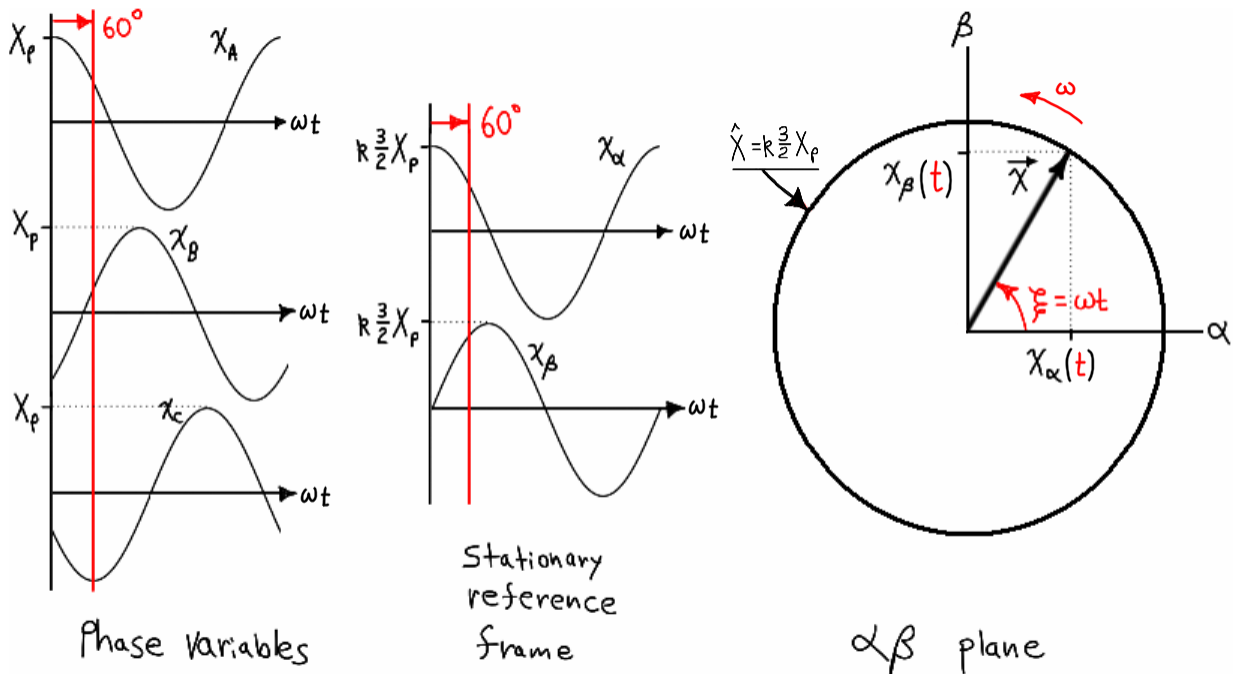
Figure 3.30 – Waveforms and SV trajectory for balanced sinusoidal phase variables.

It is clear that the magnitude of the SV (thus the amplitude of the α and β projections) is $k \cdot 3/2$ larger than the amplitude of the sinusoidal phase variables. The factor of $3/2$ is the same one that has been encountered before. The scaling coefficient k is artificially added to correct for the differences between the three-phase and two-phase models. k is rarely left explicit in formulae, rather a value is chosen to suit a particular purpose. The most obvious choice is $k=1$. This choice has appeal in dealing with torque and MMF because it yields SV equations that are similar to the traditional expressions (as seen throughout Part II). Choosing $k=2/3$ will yield a SV magnitude that is equal to the amplitude of the phase variables. Substituting this value into the Clarke and inverse Clarke matrices thus yields a *magnitude invariant* transformation. A third

common choice is to force the power in the equivalent two-phase network to match the power of the original three-phase network. For this to be true requires that $k = \sqrt{2/3}$; this yields a *power invariant* transformation [87, p.34], [88, p.87]. Different choices are made by different authors working in different areas. This report primarily uses $k = 1$ because using a value other than unity requires keeping track of the value of k used. The Clarke transformation matrices for these different choices are summarized below.

$$
\mathbf{C} = \begin{bmatrix} \dfrac{3}{2} & 0 & 0 \\ \dfrac{\sqrt{3}}{2} & \sqrt{3} & 0 \end{bmatrix}; \qquad \mathbf{C}^{-1} = \begin{bmatrix} \dfrac{2}{3} & 0 \\ \dfrac{-1}{3} & \dfrac{1}{\sqrt{3}} \\ \dfrac{-1}{3} & \dfrac{-1}{\sqrt{3}} \end{bmatrix} \qquad (k{=}1)
$$

$$
\mathbf{C}_m = \begin{bmatrix} 1 & 0 & 0 \\ \dfrac{1}{\sqrt{3}} & \dfrac{2}{\sqrt{3}} & 0 \end{bmatrix}; \qquad \mathbf{C}_m^{-1} = \begin{bmatrix} 1 & 0 \\ \dfrac{-1}{2} & \dfrac{\sqrt{3}}{2} \\ \dfrac{-1}{2} & \dfrac{-\sqrt{3}}{2} \end{bmatrix} \qquad (k{=}2/3 : \text{magnitude invariant})
$$

$$
\mathbf{C}_p = \begin{bmatrix} \sqrt{\dfrac{3}{2}} & 0 & 0 \\ \dfrac{1}{\sqrt{2}} & \sqrt{2} & 0 \end{bmatrix}; \qquad \mathbf{C}_p^{-1} = \begin{bmatrix} \sqrt{\dfrac{2}{3}} & 0 \\ \dfrac{-1}{\sqrt{6}} & \dfrac{1}{\sqrt{2}} \\ \dfrac{-1}{\sqrt{6}} & \dfrac{-1}{\sqrt{2}} \end{bmatrix} \qquad (k = \sqrt{2/3} : \text{power invariant})
$$

It should be noted that these various forms of $\mathbf{C}$ could have been derived such that only phase-B and phase-C (or only phase-A and phase-C) quantities were used. When only two phase variables are desired the choice most common in the literature is to use phase-A and phase-B as shown here.

Now to address the case when the phase variables are nonsinusoidal (even in this case they cannot have a zero-sequence component because the SV cannot represent it). In the sinusoidal case the phase variables have constant amplitudes and the SV trajectory has a constant radius—this allowed us to take the ratio and the factor $3/2$ was immediately obvious. When the phase variables contain harmonics the trajectory deviates from the circle. In this arbitrary case both the

phase variables and the SV trajectory are difficult to describe thus a ratio is impossible to define. The simples explanation is to examine the projection onto the **α** axis by using Equation (3.84) (or any $\Sigma = 0$ variant such as Equation 3.88).

$$(3.84): \quad \vec{x} = k\left[\left(\frac{3}{2}x_A\right) + j\frac{\sqrt{3}}{2}(x_B - x_C)\right]$$

$$(3.88): \quad \vec{x} = k\left[\frac{3}{2}x_A + j\frac{\sqrt{3}}{2}(x_A + 2x_B)\right]$$

In these particular forms it is clear that the projection onto **α** is affected by phase-A only. Therefore it does not matter what the instantaneous value of $x_A(t)$ is, the projection onto the **α** axis will be $3k/2$ larger than that instantaneous value. This demonstrates that the scaling is the same although the interpretation is not as clear. Or one could observe the results of Equation (3.95).

$$CC^T = \frac{3}{2}I$$

$$C_m C_m{}^T = \frac{2}{3}I \qquad\qquad (3.95)$$

$$C_p C_p{}^T = I$$

Inverse Clarke Transform

The inverse of the Clarke transformation has already been presented but will be elaborated briefly. Either Equation (3.79)/(3.85) or Equation (3.89) can be used to find phase variables corresponding to a SV represented by its α- and β- components.

$$(3.85): \quad \begin{bmatrix} x_A \\ x_B \\ x_C \end{bmatrix} = \frac{1}{k}\begin{bmatrix} \dfrac{2}{3} & 0 \\ \dfrac{-1}{3} & \dfrac{1}{\sqrt{3}} \\ \dfrac{-1}{3} & \dfrac{-1}{\sqrt{3}} \end{bmatrix}\begin{bmatrix} x_\alpha \\ x_\beta \end{bmatrix}$$

In Equation (3.85) the phase variables in $\mathbf{x}_{abc}$ are the result of the inverse of the Clarke transform. They are *NOT* the same values that would be obtained if the SV was simply projected onto the phase axes in Figure 3.29 because of the inherent scaling in the transformation.

As an example, find the SV that corresponds to unit-amplitude balanced sinusoidal quantities at an electrical position of zero. From Figure 3.6 or Equation (3.91), the values are given by Equation (3.96). Substituting them into the SV definition gives Equation (3.97), assuming $k = 1$ for simplicity.

$$\begin{cases} x_A = 1 \\ x_B = -1/2 \\ x_C = -1/2 \end{cases} \tag{3.96}$$

$$\vec{x} = \frac{3}{2}e^{j0} = \frac{3}{2} \tag{3.97}$$

Clearly the SV is aligned to the phase-A and α axes and the projection onto either is given by Equation (3.97). The scaling of $3/2$ is present as expected. But obtaining the value of x_A from Equation (3.85) gives $x_A = \frac{2}{3}x_\alpha = \frac{2}{3}\left(\frac{3}{2}\right) = 1$. This shows that the phase variables obtained using an inverse transform (such as Equation 3.85) are equal to the projected value reduced by a factor of $2/(3k)$. The Clark transformation (equivalently, SV transformation) maps $\mathbf{x}_{abc}$ to $\mathbf{x}_{\alpha\beta}$ thus any SV exists in the $\alpha\beta$ plane or $\mathbb{C}$ with scaling thus it makes sense that when we project back onto the phase axes we should have to reverse the scaling. The matrix in Equation (3.85) is the pseudoinverse of the Clarke transfomation matrix and it inherently scales the result back.

The issue of scaling and the difference between projection and the inverse transformation is not treated well in the popular literature. In most cases the "inverse Clarke" transform is presented as nothing other than a projection of a SV or an algorithm. Understanding the true inverse transformation provides much needed insight, especially when working with modulation techniques based on space vectors. Although the inverse transformation is the more rigorous perspective, the projection perspective is obviously useful and is correct when scaled properly. In fact, further studying the projections will provide further insight into reference frame theory.

Projections
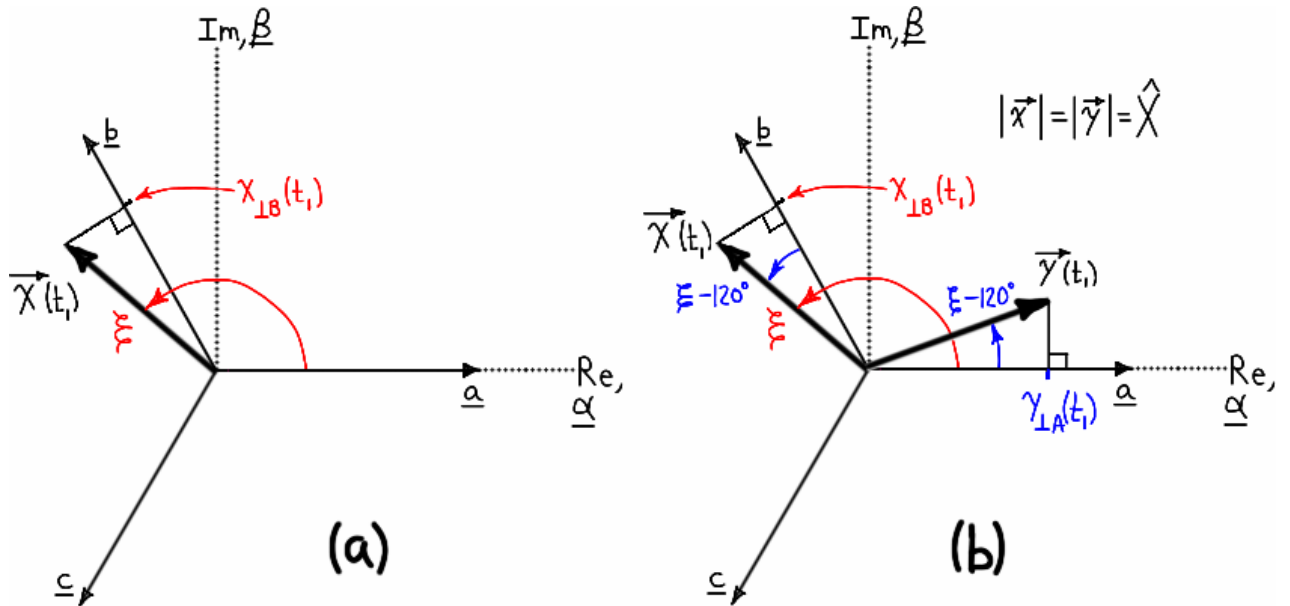
Projecting the SV onto the $\boldsymbol{\alpha}$ axis is simple because the projection is given by the real part of the SV. The projection onto the phase-A axis is given by the same. Similarly, projection onto the $\boldsymbol{\beta}$ axis is given by the imaginary part of the SV. However, projection onto the phase-B and phase-C axes is not that simple because they are not perpendicular to the real or imaginary axes. There are

a number of ways to project the SV onto these axes but only the commonly used method is discussed here. Since the projecting is done in the **αβ** plane it seems reasonable to find a way to make the phase-B and phase-C projections equal to the real part of a complex expression; this is exactly what the common method does.

If CCW rotation is to be defined to match the positive-sequence order (phase-A, phase-B, phase-C) with increasing ωt, arranging the phase axes as shown in Figure 3.29 forces the space vector to be defined as Equation (3.69). (There are various other combinations of definitions and conventions used in the literature; these obviously lead to different SV definitions.)

(3.69): $\vec{x} \triangleq k \left[x_A \cdot 1 + x_B \cdot e^{j\gamma} + x_C \cdot e^{-j\gamma} \right]$

A space vector $\vec{x}(t_1) = \hat{X} e^{j\xi}$ is at the position shown in Figure 3.31-a at some time t_1. Its projection onto the phase-B axis is also shown; the magnitude of the projection is denoted $x_{\perp B}(t_1)$, where the subscript indicates that it is a projection onto phase-B, not the actual value of the phase variable $x_B(t_1)$ that produced that SV.

Figure 3.31 – SV projection onto phase axes: (a) actual; (b) alternative.

At the same instant t_1 another SV $\vec{y}(t_1) = \hat{X} e^{j(\xi - 120°)}$ is shown in Figure 3.31-b that has a magnitude equal to that of $\vec{x}(t_1)$ but an angle that is 120° less. Its projection onto the phase-A axis is denoted $y_{\perp A}(t_1)$. Since the phase axes are 120° apart, the angle between $\vec{x}$ and the phase-B axis is the same as that between $\vec{y}$ and the phase-A axis. Therefore, because $\vec{x}$ and $\vec{y}$ have

126

the same magnitude, the projection $x_{\perp B}(t_1)$ must be identical to $y_{\perp A}(t_1)$. Comparing the definition for $\vec{x}$ and $\vec{y}$ shows they are related by $\vec{y} = \vec{x} \cdot e^{-j120^\circ}$. Thus, $\vec{y}$ was obtained by rotating $\vec{x}$ by -120°. The benefit is that the projection can then be obtained by simply taking the real part of the rotated vector as shown in Equation (3.98).

$$x_{\perp B} = \mathrm{Re}\left\{ \vec{x} \cdot e^{-j120^\circ} \right\} \tag{3.98}$$

However it must be understood that rotating the SV does nothing magic. For the moment we will say that we are not attempting to change or "control" the SV (this will be rectified shortly). Rather, we simply note that the projection of a SV onto the **phase-B** axis is *numerically equal* to the projection of (any *identical, separate* SV delayed by 120°) onto the **phase-A** axis. Since the phase-A axis is collinear with the real axis we can then take the real part to obtain the projection. The phase-C projection follows in a similar manner except the SV must be advanced by 120° (or equivalently, delayed by 240°). The projections are summarized in Equation (3.99).

$$\begin{cases} x_{\perp A} = \mathrm{Re}\left\{ \vec{x} \cdot 1 \right\} \\ x_{\perp B} = \mathrm{Re}\left\{ \vec{x} \cdot e^{-j\gamma} \right\} \\ x_{\perp C} = \mathrm{Re}\left\{ \vec{x} \cdot e^{j\gamma} \right\} \end{cases} \tag{3.99}$$

Finally, the relationship between projections and the phase variables obtained from the inverse Clarke transform is summarized in Equation (3.100). Note that by definition if the magnitude-invariant version of the Clarke transform and its inverse are used the coefficients in Equation (3.100) are unity thus the projection and inverse transformation are the same.

$$\begin{cases} x_A(t) = \dfrac{2}{3k} x_{\perp A} = \dfrac{2}{3k} \mathrm{Re}\left\{ \vec{x} \cdot 1 \right\} \\[2mm] x_B(t) = \dfrac{2}{3k} x_{\perp B} = \dfrac{2}{3k} \mathrm{Re}\left\{ \vec{x} \cdot e^{-j\gamma} \right\} \\[2mm] x_C(t) = \dfrac{2}{3k} x_{\perp C} = \dfrac{2}{3k} \mathrm{Re}\left\{ \vec{x} \cdot e^{j\gamma} \right\} \end{cases} \tag{3.100}$$

In Figure 3.31-a and Figure 3.31-b the phase axes are exactly the same because the SV $\vec{x}$ was fixed in place and the SV $\vec{y}$ was used for a demonstration. It must be understood that the projection was not onto the phase-A axis—it was the projection of the rotated SV onto the phase-A axis; that rotated SV would have been collinear with $\vec{y}$. Earlier it was said in pretense that in obtaining the projection we are not attempting to change the SV, even though we did rotate the

SV. This was done to obtain a similar SV ($\vec{y}$) that would be $\xi - 120°$ away from the phase-A axis and that interpretation is valid. But now the more-correct explanation can be provided. It was mentioned that given our choice of conventions the SV must be defined by Equation (3.69).

(3.69): $\vec{x} \triangleq k\left[x_A \cdot 1 + x_B \cdot e^{j\gamma} + x_C \cdot e^{-j\gamma}\right]$

Rotating the SV by $-120°$ to obtain the phase-B projection was accomplished by multiply the SV by $e^{-j120°} = e^{-j\gamma}$. Multiplying that factor through the SV definition yields Equation (3.101).

$$\vec{x} \cdot e^{-j\gamma} = k\left[x_A \cdot 1 + x_B \cdot e^{j\gamma} + x_C \cdot e^{-j\gamma}\right] \cdot e^{-j\gamma}$$

$$\vec{x} \cdot e^{-j\gamma} = k\left[x_A \cdot e^{-j\gamma} + x_B \cdot 1 + x_C \cdot e^{j\gamma}\right] \tag{3.101}$$

In Equation (3.101) we have done nothing to the definition of the complex plane (the Re/Im or α/β axes) but it is clear that the phase variable axes have been rotated by $-120°$; for example, x_A is no longer acting in a direction coincident with the real axis. Using Equation (3.100) it would be seen that in obtaining the phase-C projection, the phase axes are rotated another $-120°$ (for a total of $-240° = +120°$ from the original positions). The action of rotating the SV to align with the real axis is seen clearly below.

$$\begin{cases} x_{\perp A} = \mathrm{Re}\left\{\left[x_A \cdot 1 + x_B \cdot e^{j\gamma} + x_C \cdot e^{-j\gamma}\right] \cdot 1\right\} \\ x_{\perp B} = \mathrm{Re}\left\{\left[x_A \cdot 1 + x_B \cdot e^{j\gamma} + x_C \cdot e^{-j\gamma}\right] \cdot e^{-j\gamma}\right\} \\ x_{\perp C} = \mathrm{Re}\left\{\left[x_A \cdot 1 + x_B \cdot e^{j\gamma} + x_C \cdot e^{-j\gamma}\right] \cdot e^{j\gamma}\right\} \end{cases}$$

$$\begin{cases} x_{\perp A} = \mathrm{Re}\left\{\left[x_A \cdot \mathbf{1} + x_B \cdot e^{j\gamma} + x_C \cdot e^{-j\gamma}\right]\right\} \\ x_{\perp B} = \mathrm{Re}\left\{\left[x_A \cdot e^{-j\gamma} + x_B \cdot \mathbf{1} + x_C \cdot e^{j\gamma}\right]\right\} \\ x_{\perp C} = \mathrm{Re}\left\{\left[x_A \cdot e^{j\gamma} + x_B \cdot e^{-j\gamma} + x_C \cdot \mathbf{1}\right]\right\} \end{cases}$$

The apparent axes are shown in Figure 3.32 for the projection onto the phase –A, –B, and –C axes.
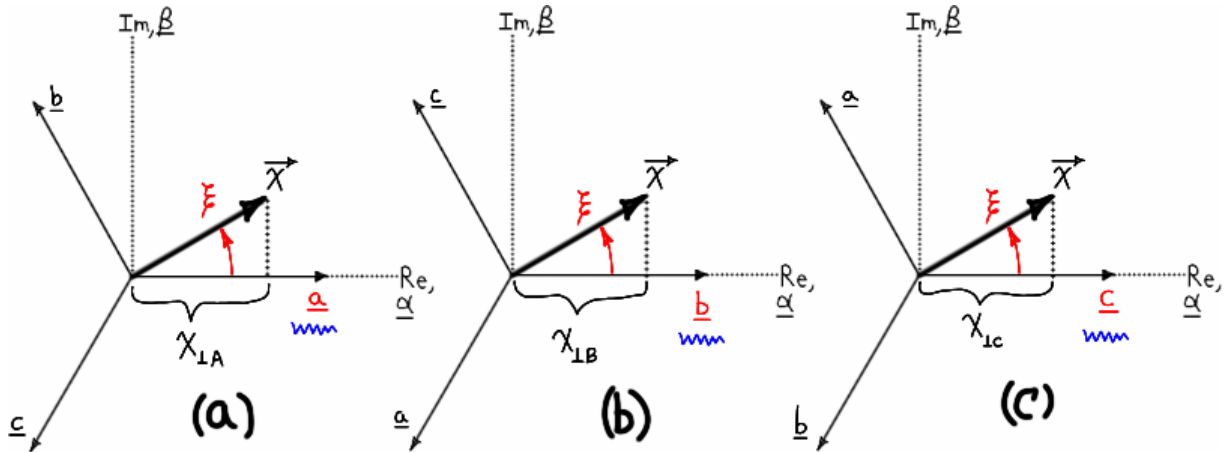
Figure 3.32 – Arbitrary SV referenced to axes of phases –A, -B, and –C.

It is seen that multiplying a SV by $e^{-j\gamma}$ rotated the SV (in the αβ plane) by $-120°$ while the phase axes remained in place (in Figure 3.31-b $\vec{x}$ was rotated to the position of $\vec{y}$). This result could also be interpreted as rotating the phase axes while leaving the SV in place (from the axes in Figure 3.32-a to the axes in Figure 3.32-b and Figure 3.32-c). This is an important result and is a demonstration of a change in reference frame. It has been presented here to aid the discussion of projections but will be shown in the next section in its more traditional and useful form.
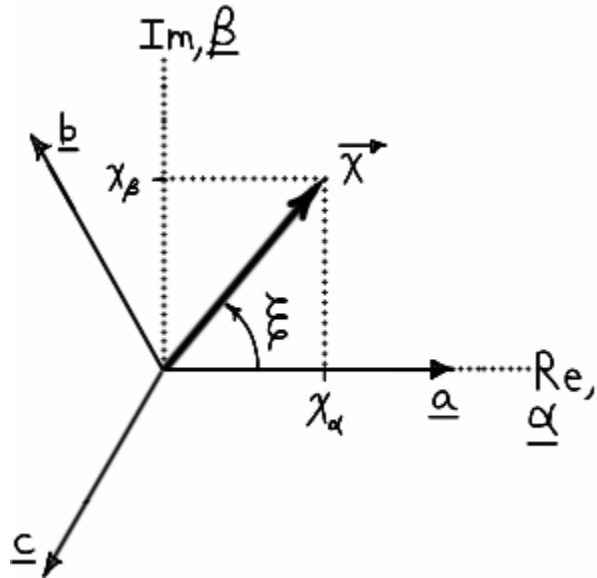
Before concluding this subsection it is worth verifying the action of the inverse Clarke transform on a SV that represents balanced sinusoidal phase variables. Substituting Equation (3.93) into Equation (3.100) yields Equation (3.102), as expected.

$$\begin{cases} x_A(t) = \dfrac{2}{3k}\text{Re}\left\{\dfrac{3k}{2}X_p e^{j\omega t} \cdot 1\right\} \\[2mm] x_B(t) = \dfrac{2}{3k}\text{Re}\left\{\dfrac{3k}{2}X_p e^{j\omega t} \cdot e^{-j\gamma}\right\} = \begin{cases} X_p\cos(\omega t) \\ X_p\cos(\omega t - \gamma) \\ X_p\cos(\omega t + \gamma) \end{cases} \\[2mm] x_C(t) = \dfrac{2}{3k}\text{Re}\left\{\dfrac{3k}{2}X_p e^{j\omega t} \cdot e^{j\gamma}\right\} \end{cases} \qquad (3.102)$$

Park Transform; Reference Frame Theory

As shown in the previous section, multiplying a SV by a complex exponential can be interpreted as rotating a SV in fixed coordinates or rotating the coordinates while the SV remains fixed. This concept applies to all regular vectors in linear algebra; it is not specific to the SV or to complex vectors. Previously the phase axes were studied to understand projections but now the same concept will be applied to coordinate systems of only two variables. (In the literature, *coordinate system* and *reference frame* are used synonymously.) The $\Sigma = 0$ condition means only two phase

variables are independent, but the resulting axes (A&B, A&C, or B&C) are not orthogonal. Thus the purpose of the Clarke transform is to form an orthogonal basis such that a SV is easily defined by components along the α and β axes as shown in Figure 3.33. This also allows other reference frames to be developed more easily as shown next.

Figure 3.33 – Space vector in stationary reference frame showing phase axes.

When a quantity is described as a SV ($\vec{x}$) or in terms of the αβ plane ($\mathbf{x}_{\alpha\beta}$) it is said to be in the *stationary* or *stator reference frame* because the angle of the SV is measured from the real (α) axis fixed to the stator. A vector can be described in different reference frames and there are a number of them defined in the literature. It has been seen that SV theory can be used to describe purely electrical quantities or physical quantities such as those present in a machine; it follows that a reference frame could be defined relative to an electrical or physical reference. Examples include the voltage at a power grid bus, the rotor position in a motor, the rotor flux (which is not coincident with the rotor position in induction motors), or a flux linkage. The only difference between these various reference frames is how they are defined with respect to the stationary reference frame, thus many texts base discussions on the *general reference frame*; the position of this frame (call it θ_Δ) could then be specialized to whatever frame is appropriate [87], [35]. Since in the synchronous machine the rotor flux and rotor-stator flux linkage SVs are aligned with the rotor position, only the stationary reference frame and the *rotor reference frame* will be used in this report. The rotor reference frame is defined using the position of the rotor ($\theta_\Delta = \theta_r$) as shown in Figure 3.34. The *direct axis* (**d**) is defined as being in the center of the rotor's North pole and the *quadrature axis* (**q**) axis is defined to be 90° electrical ahead of the direct axis in the positive direction of rotation. The rotor position is measured from **α** to **d**. These choices are not

universal and the choice of conventions is very important (see Appendix E). For clarity the phase axes will no longer be drawn but they are understood to be present.
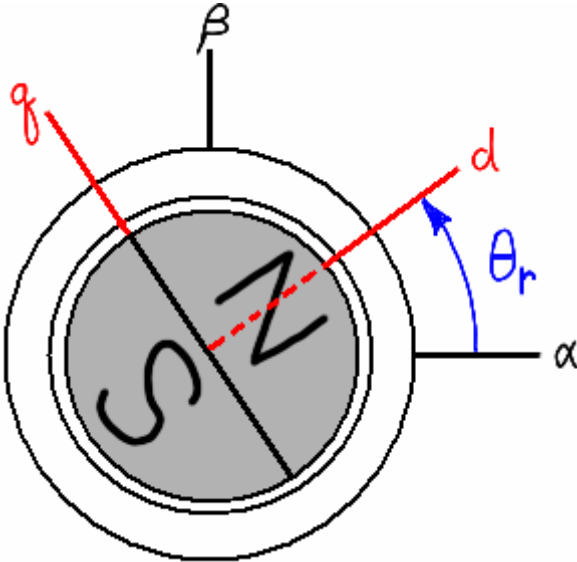
Figure 3.34 – Definition of rotor reference frame.

Figure 3.35 shows a SV and its projection onto the stator and rotor reference frames.
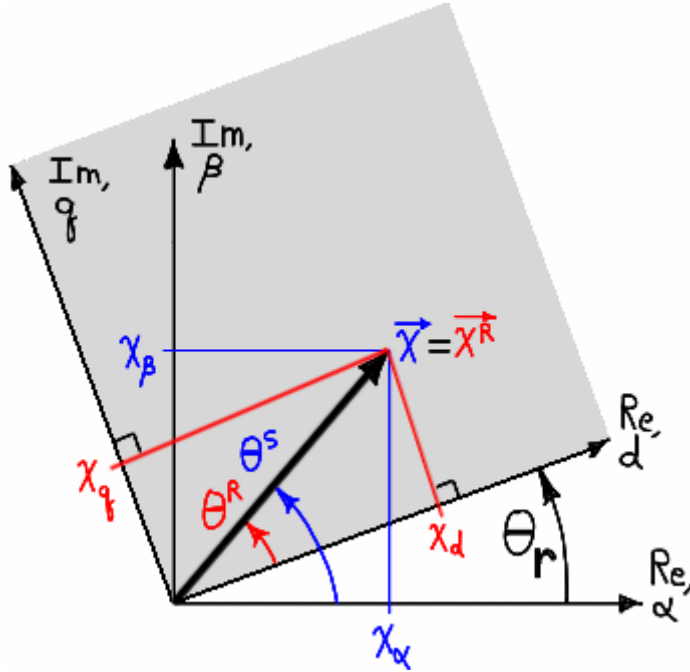
Figure 3.35 – SV in the stator and rotor reference frames.

The SV $\vec{x}$ is defined in the stator reference frame as $\vec{x} = \hat{X}e^{j\theta^S}$ or $\mathbf{x}_{\alpha\beta} = \begin{bmatrix} x_\alpha \\ x_\beta \end{bmatrix}$ as usual. There are several ways to obtain the components in the rotor reference frame but one of the easiest is to use a transformation matrix. Since we have a transform of the form $\mathbf{x}_{NEW} = \mathbf{T}\mathbf{x}_{OLD}$ the

131

transformation matrix must be composed of row vectors that are the basis vectors of the old coordinate system (αβ), which are found by inspection to be Equation (3.103). The transform is therefore defined by Equation (3.104).

$$\boldsymbol{\alpha} = \begin{bmatrix} \cos(\theta_r) \\ \sin(\theta_r) \end{bmatrix}; \qquad \boldsymbol{\beta} = \begin{bmatrix} -\sin(\theta_r) \\ \cos(\theta_r) \end{bmatrix} \tag{3.103}$$

$$\mathbf{T} = \begin{bmatrix} \boldsymbol{\alpha}^T \\ \boldsymbol{\beta}^T \end{bmatrix} = \begin{bmatrix} \cos(\theta_r) & \sin(\theta_r) \\ -\sin(\theta_r) & \cos(\theta_r) \end{bmatrix}$$

$$\begin{bmatrix} x_d \\ x_q \end{bmatrix} = \begin{bmatrix} \cos(\theta_r) & \sin(\theta_r) \\ -\sin(\theta_r) & \cos(\theta_r) \end{bmatrix} \begin{bmatrix} x_\alpha \\ x_\beta \end{bmatrix} \quad \Leftrightarrow \quad \mathbf{x}_{dq} = \mathbf{P}\mathbf{x}_{\alpha\beta} \tag{3.104}$$

The transformation matrix in Equation (3.104) is the same as Givens rotation and in the literature it goes by many names. In the popular literature and in this report it is called the Park transformation (after R.H. Park) even though this is not the original transformation (see Appendix E). It is clear that the complex equivalent of the Park transform is given by Equation (3.105), where the superscript R denotes that the SV is defined in the rotor reference frame (in this report any SV no so marked is understood to be in the stationary frame).
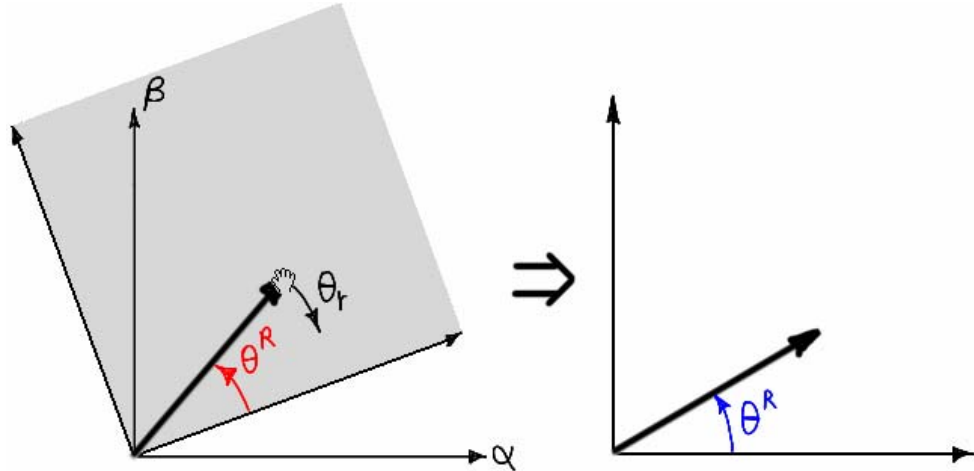
$$\vec{x}^R = \vec{x}e^{-j\theta_r} \tag{3.105}$$

It is worth showing how Equations (3.104) and (3.105) are equivalent.

$$\vec{x}^R = \vec{x}e^{-j\theta_r}$$

$$x_d + jx_q = \left(x_\alpha + jx_\beta\right)\cdot\left[\cos(-\theta_r) + j\sin(-\theta_r)\right]$$

$$x_d + jx_q = x_\alpha \cos(\theta_r) - jx_\alpha \sin(\theta_r) + jx_\beta \cos(\theta_r) + x_\beta \sin(\theta_r)$$

$$x_d + jx_q = \begin{bmatrix} x_\alpha \cos(\theta_r) + x_\beta \sin(\theta_r) \\ -jx_\alpha \sin(\theta_r) + jx_\beta \cos(\theta_r) \end{bmatrix}$$

$$\begin{bmatrix} x_d \\ x_q \end{bmatrix} = \begin{bmatrix} \cos(\theta_r) & \sin(\theta_r) \\ -\sin(\theta_r) & \cos(\theta_r) \end{bmatrix} \begin{bmatrix} x_\alpha \\ x_\beta \end{bmatrix}$$

$$\vec{x}^R = x_d + jx_q \tag{3.106}$$
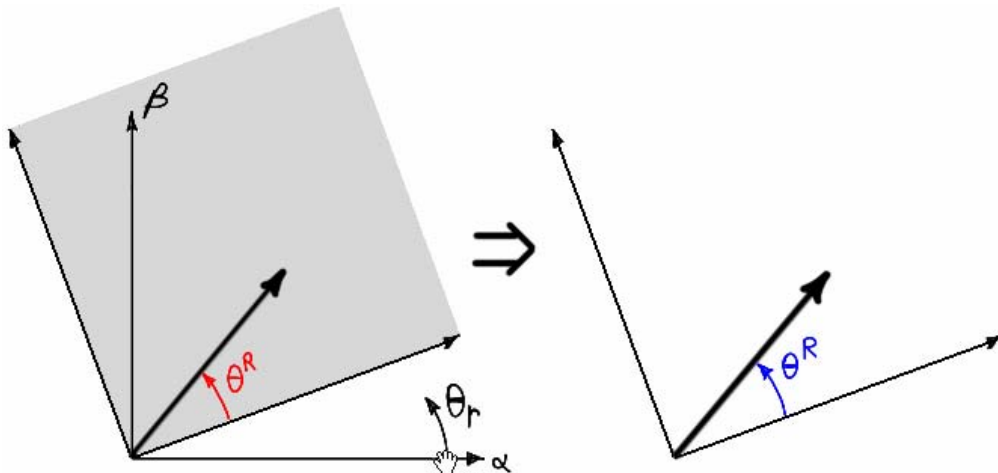
As previously discussed the transform can be interpreted as rotating the vector or rotating the coordinate system, but they are the same. However, a survey of the popular literature indicates that there is some general confusion on the subject and it is indeed easy to get "disoriented," therefore the different perspectives will be discussed. In Figure 3.35 the SV is at θ^S from the

132

stator's perspective and at θ^R from the rotor's perspective. The SV in the stator frame is $\theta^S - \theta^R = \theta_r$ ahead of the rotor frame, so if the SV in the stator frame is rotated by the negative of this angle, it is exactly the SV we would see from the rotor frame perspective. That is, if we rotate the SV by $-\theta_r$ we will see from the stator the exact SV the rotor sees (a SV at position θ^R). This is the vector rotation perspective and is illustrated in Figure 3.36, where the "grabbing hand" symbol indicates vector rotation.

Figure 3.36 – Park transform: vector rotation perspective.
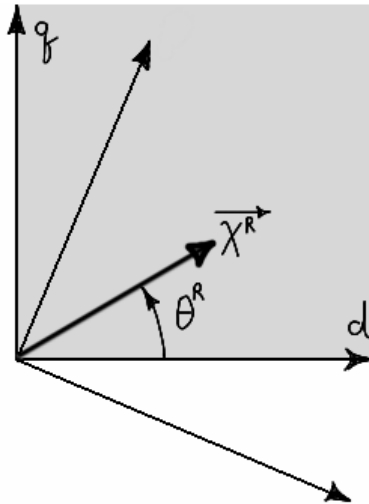
In coordinate rotation perspective the position of the SV is thought of as remaining fixed and the coordinate system is rotated by $+\theta_r$ instead of $-\theta_r$. This is shown in Figure 3.37, where the "grabbing hand" symbol indicates coordinate rotation.

Figure 3.37 – Park transform: coordinate rotation perspective.

Coordinate rotation is the better perspective because we are seeking to describe a SV from a different coordinate system, not control the position of the SV. In contrast, a vector controlled drive seeks to control the position of a SV (such as the stator current SV). An interpretation that is

more correct yet is to acknowledge that the components in the rotor reference frame are real and imaginary (Equation 3.106) just as they are in the αβ plane. Instead of thinking about *rotating* a space vector or *rotating* a coordinate system, simply think of the SV as existing in the rotor reference frame originally. Given Equation (3.106) and the definition of the complex plane, the rotor reference frame is always in the same position shown in Figure 3.38. The αβ axes (not labeled) would be rotating in the CW direction. In the rotor reference frame we are not concerned with where the SV may lie in the αβ plane; we look at the position of the SV relative to the rotor position only. Since this is the meaning of the rotor reference frame, it is also the best way to visualize the result of the Park transformation.

Figure 3.38 – Park transform: rotor reference frame perspective.

The Park transform allows us to continue to refine our understanding of SV- and reference frame theory. In Part I when the stator MMF was developed, the argument of the cosine was briefly discussed and it was said that the current position ωt (an electrical quantity) shares the same angular space as the MMF position (a mechanical quantity). Then in Part II (in the section "The SV as a Distribution") a potential discrepancy was examined to reveal the meaning of reference frame theory (and the Part I discussion was revisited in this light). Now the earlier Part II discussion will be revisited and finalized.

The potential discrepancy (p.108) will first be recounted. The real-valued stator MMF

$$f(\theta,t) = \frac{N_e}{2}\left[i_A(t)\cdot\cos(\theta) + i_B(t)\cdot\cos(\theta - 120^\circ) + i_C(t)\cdot\cos(\theta + 120^\circ)\right]$$

was put into complex form

(A): $f(\theta,t) = \left(\frac{N_e}{2}\right)\mathrm{Re}\left\{\vec{i}\cdot e^{-j\theta}\right\}$

and found to be equivalent to the real-valued MMF description found in the beginning of the chapter

(B): $f(\theta,t) = \frac{3}{2}\left(\frac{N_e}{2}\right)I_p\cos(\omega t - \theta)$.

Thus, all that had been done was to put the traditional real-valued result into complex form and check that it was correct. Then the stator MMF SV was derived using only SV analysis

$$\vec{f} = \left(\frac{N_e}{2}\right)\cdot\vec{i}$$

and when the SV corresponding to balanced sinusoidal currents

$$\vec{i} = \frac{3}{2}I_p e^{j\omega t}$$

was substituted in

$$\vec{f} = \frac{3}{2}\left(\frac{N_e}{2}\right)I_p e^{j\omega t}$$

it was found that when the real part (c.f. Equation A) was taken

(C): $f(\theta,t) = \mathrm{Re}\left\{\vec{f}\right\} = \left(\frac{N_e}{2}\right)\mathrm{Re}\left\{\vec{i}\right\} = \frac{3}{2}\left(\frac{N_e}{2}\right)I_p\cos(\omega t)$

the result did not match Equation (B).

First we should ask why $\mathrm{Re}\{\cdot\}$ is present in Equation (A). The reason is that we had an expression for MMF (Equation 3.53, p.104) which contained the sum of complex conjugates and an identity (Equation 3.55) was used to eliminate one conjugate. But we have seen that the SV $\vec{x} = \hat{X}e^{j\xi}$ is defined with respect to the phase-A axis (that is, ξ is measured CCW from 0° which is defined to be coincident with the phase-A axis). When the SV is one that represents balanced sinusoidal quantities, $\vec{x} = (3/2)X_p e^{j\omega t}$, the projection onto the real axis is

$x_\alpha = \mathrm{Re}\{\vec{x}\} = (3/2)X_p \cos(\omega t)$. There is an obvious connection between this projection and Equation (C). By taking the real part of a SV we are asking for the projection onto the real axis, which is a cosine (projection onto the imaginary axis would give a sine). The way to use a complex SV to represent the MMF (which we know to be real-valued and cosinusoidal) is to define $f(\theta,t) \triangleq \mathrm{Re}\{\vec{f}\}$. This principle is not much different than that of the phasor—we define the signal of interest to be associated with the real part of the inverse transform because that is what is mathematically valid: $x(t) = \mathrm{Re}\{\tilde{X} \cdot e^{j\omega t}\}$. This is the reason that the complex conjugates appeared in the identity (that identity is the same rearrangement of Euler's formula that gives us the complex-valued equivalents for the cosine and sine functions).

Thus, the $\mathrm{Re}\{\cdot\}$ in Equations (A) and Equation (C) are present for the same reason, though they were derived in different ways. With that out of the way we can then see that the discrepancy would boil down to the question as to why Equation (A) has $\mathrm{Re}\{\vec{i} \cdot e^{-j\theta}\}$ while Equation (C) has $\mathrm{Re}\{\vec{i}\}$. The simple answer is that $\mathrm{Re}\{\vec{i}\}$ is equal to $\mathrm{Re}\{\vec{i} \cdot e^{-j\theta}\}$ when $\theta = 0$. When Equation (A) was developed, θ was left explicit. Equation (C) was developed using SV theory and at that time only the stationary reference frame had been used, thus $\theta = 0$. The two equations are therefore equivalent. Finally, this shows that the multiplication by $e^{-j\theta}$ is the very same change of reference frame we have been working with in this subsection. In Part I the argument of Equation (B) was discussed and it was said that when we substitute a value for θ we are asking for the value of MMF at that angle about the stator. Further discussion revealed that it was the same as asking *where the peak is <u>in relationship to any position θ on the stator</u>*. This concept is exactly the reference frame change. That is, the relationship $\mathrm{Re}\{\vec{i} \cdot e^{-j\theta}\} = I_p \cos(\omega t - \theta)$ melds the physical understanding with the SV perspective. What is described here is the general reference frame (i.e., an arbitrary standpoint in θ from which we can observe something). When the MMF SV defined in the stator reference frame, $\vec{f}$, is multiplied by $e^{-j\theta}$, the MMF becomes described in whichever reference frame is defined as being displaced by θ from the phase-A. If $\theta = \theta_r$, the reference frame is the rotor frame.

Perhaps obviously, the inverse Park transform is found by inverting **P**. Since **P** is orthogonal the inverse is simply the transpose and the inverse transform is given by Equation (3.107).

$$\begin{bmatrix} x_\alpha \\ x_\beta \end{bmatrix} = \begin{bmatrix} \cos(\theta_r) & -\sin(\theta_r) \\ \sin(\theta_r) & \cos(\theta_r) \end{bmatrix} \begin{bmatrix} x_d \\ x_q \end{bmatrix} \quad \Leftrightarrow \quad \mathbf{x}_{\alpha\beta} = \mathbf{P}^{-1}\mathbf{x}_{dq} \tag{3.107}$$

In terms of the SV, since we rotated by $-\theta_r$ to transform *to* the rotor frame, we will now rotate by $+\theta_r$ to transform *from* the rotor frame, as shown in Equation (3.108).[26]

$$\vec{x} = \vec{x}^R e^{j\theta_r} \tag{3.108}$$

There are many other reference frames used and each is suited to a particular purpose. But since they only differ in the speed or position that they are referenced to, the math is always the same, hence the usefulness. Induction motor analysis is laden with several different frames because the rotor flux is not fixed to the rotor. These various reference frames are responsible in part for the wide variety of vector control schemes in the literature (rotor-flux-oriented, stator-flux-oriented, magnetizing-flux-oriented) and each serves its own purpose. Thankfully, only the rotor frame is required when working with the synchronous motor (again, other frames can be used).

---

[26] Per Equation (3.105), transforming *to* the rotor frame requires a multiplication by $\exp(-j\theta_r)$. Per Equation (3.108), transforming back *from* the rotor frame requires a multiplication by $\exp(+j\theta_r)$ as one would expect. Only transformation *to* the rotor frame was discussed from both the perspective of coordinate rotation and SV rotation. It was found that the former required $\exp(-j\theta_r)$ and the later required $\exp(+j\theta_r)$, but both were for transforming *to* the rotor. Yet we have just seen that transforming *from* the rotor also required $\exp(+j\theta_r)$. Thus we can correctly infer that Equation (3.108) is like Equation (3.105)—it is written for the coordinate rotation perspective. And also that if transformation *from* the rotor were performed from the perspective of SV rotation, it would require $\exp(-j\theta_r)$.

The transformations and the relationships between SV and matrix analyses are summarized below.

$$
\begin{aligned}
\mathbf{x}_{\alpha\beta} &= \mathbf{C}\mathbf{x}_{abc} &\Leftrightarrow& \quad \vec{x} = SV\{\mathbf{x}_{abc}\} \\
\mathbf{x}_{abc} &= \mathbf{C}^{-1}\mathbf{x}_{\alpha\beta} &\Leftrightarrow& \quad \{\mathbf{x}_{abc}\} = SV^{-1}\{\vec{x}\} \\
\hline
\mathbf{x}_{dq} &= \mathbf{P}\mathbf{x}_{\alpha\beta} &\Leftrightarrow& \quad \vec{x}^R = \vec{x}\cdot e^{-j\theta_r} \\
\mathbf{x}_{\alpha\beta} &= \mathbf{P}^{-1}\mathbf{x}_{dq} &\Leftrightarrow& \quad \vec{x} = \vec{x}^R\cdot e^{j\theta_r} \\
\hline
\mathbf{x}_{\alpha\beta} &= \begin{bmatrix} x_\alpha \\ x_\beta \end{bmatrix} &\Leftrightarrow& \quad \vec{x} = x_\alpha + jx_\beta \\
\mathbf{x}_{dq} &= \begin{bmatrix} x_d \\ x_q \end{bmatrix} &\Leftrightarrow& \quad \vec{x}^R = x_d + x_q
\end{aligned}
\tag{3.109}
$$

$$
\begin{aligned}
SV\{x_A, x_B, x_C\} &= k\left[\left(\frac{3}{2}x_A\right) + j\frac{\sqrt{3}}{2}(x_B - x_C)\right] \\
&= k\left[\frac{3}{2}x_A + j\frac{\sqrt{3}}{2}(x_A + 2x_B)\right] \\
&= \quad \text{other } \Sigma = 0 \text{ forms} \\
\hline
SV^{-1}\{\vec{x}\} &= \begin{cases} x_A = \dfrac{2}{3k}x_{\perp A} = \dfrac{2}{3k}\mathrm{Re}\{\vec{x}\cdot 1\} \\[2mm] x_B = \dfrac{2}{3k}x_{\perp B} = \dfrac{2}{3k}\mathrm{Re}\{\vec{x}\cdot e^{-j\gamma}\} \\[2mm] x_C = \dfrac{2}{3k}x_{\perp C} = \dfrac{2}{3k}\mathrm{Re}\{\vec{x}\cdot e^{j\gamma}\} \end{cases}
\end{aligned}
\tag{3.110}
$$

$$
\mathbf{C} = k\begin{bmatrix} \dfrac{3}{2} & 0 & 0 \\[2mm] \dfrac{\sqrt{3}}{2} & \sqrt{3} & 0 \end{bmatrix} \qquad \mathbf{C}^{-1} = \frac{1}{k}\begin{bmatrix} \dfrac{2}{3} & 0 \\[2mm] \dfrac{-1}{3} & \dfrac{1}{\sqrt{3}} \\[2mm] \dfrac{-1}{3} & \dfrac{-1}{\sqrt{3}} \end{bmatrix}
\tag{3.111}
$$

$$
\mathbf{P} = \begin{bmatrix} \cos(\theta_r) & \sin(\theta_r) \\ -\sin(\theta_r) & \cos(\theta_r) \end{bmatrix} \qquad \mathbf{P}^{-1} = \begin{bmatrix} \cos(\theta_r) & -\sin(\theta_r) \\ \sin(\theta_r) & \cos(\theta_r) \end{bmatrix}
\tag{3.112}
$$

It must be emphasized that we have thus far only dealt with stator quantities; these were expressed in the stator and rotor reference frames. It is also possible to talk about rotor quantities and these may be described in either frame. Thus the distinction must be made between a quantity *associated with* the stator or rotor and one *described in terms of the reference frame attached to* the stator or rotor. When a stator (rotor) SV is described in terms of the stator (rotor) reference frame it is said to be in the *natural reference frame* [87], [35]. For example, a stator quantity is represented as $\vec{x}_S$; a rotor quantity is represented as $\vec{x}_R$. But neither can be specified without a reference frame.

The stator and rotor quantities in the *stator frame* are $\vec{x}_S^{\mathbf{S}}$ and $\vec{x}_R^{\mathbf{S}}$, respectively.

The stator and rotor quantities in the *rotor frame* are $\vec{x}_S^{\mathbf{R}}$ and $\vec{x}_R^{\mathbf{R}}$, respectively. The transformations are given by Equation (3.113), where the boldface scripts correspond to the row and column labels.

$$
\begin{array}{c|c}
\text{stator frame} \quad \vec{x}_{\mathbf{S}}^{S} = \vec{x}_{S}^{R} \cdot e^{j\theta_r} & \vec{x}_{\mathbf{R}}^{S} = \vec{x}_{R}^{R} \cdot e^{j\theta_r} \\
\hline
\text{rotor frame} \quad \vec{x}_{\mathbf{S}}^{R} = \vec{x}_{S}^{S} \cdot e^{-j\theta_r} & \vec{x}_{\mathbf{R}}^{R} = \vec{x}_{R}^{S} \cdot e^{-j\theta_r} \\
\text{stator qtys} & \text{rotor qtys}
\end{array}
\tag{3.113}
$$

Although there is a difference between a rotor and stator quantity, it is obvious that for either, the transformation between reference frames is the same (which we should expect), thus Equation (3.114).

$$
\begin{aligned}
\vec{x}^{S} &= \vec{x}^{R} \cdot e^{j\theta_r} \\
\vec{x}^{R} &= \vec{x}^{S} \cdot e^{-j\theta_r}
\end{aligned}
\tag{3.114}
$$

It was earlier mentioned that the stator reference frame is assumed when no 'S' superscript is present, thus Equation (3.115), which was shown in the summary earlier.

$$
\begin{aligned}
\vec{x} &= \vec{x}^{R} \cdot e^{j\theta_r} \\
\vec{x}^{R} &= \vec{x} \cdot e^{-j\theta_r}
\end{aligned}
\tag{3.115}
$$

Comparison with Phasor

In concluding the presentation of space vectors it should be helpful to contrast it with the more familiar phasor analysis. Both the phasor and the SV map real quantities to the complex plane. The two largest differences between the two are that a phasor represents a single signal (a SV represents the combined action of all three phase variables) and that a phasor is technically a stationary variable in the phasor domain (a SV is an instantaneous variable in the complex domain; its magnitude and angle are functions of time).

The phasor transform, the phasor, and the inverse phasor transform are given by Equations (3.116), (3.117), and (3.118), respectively [39, p.418].

$$\tilde{X} = P\{x(t)\}; \quad x(t) = X_p \cos(\omega t + \varphi) \tag{3.116}$$

$$\tilde{X} = X_p e^{j\varphi} = X_p \angle \varphi \tag{3.117}$$
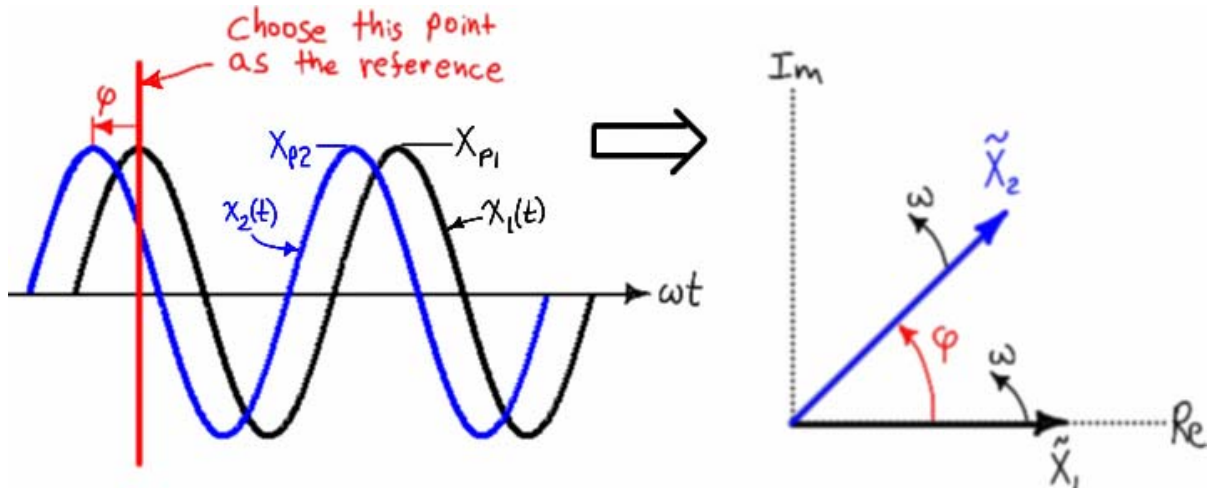
$$P^{-1}\{\tilde{X}\} = \text{Re}\{\tilde{X} \cdot e^{j\omega t}\} = \text{Re}\{X_p e^{j\varphi} \cdot e^{j\omega t}\} \tag{3.118}$$

In phasor analysis we are not concerned with the absolute position of signals in time—only the position relative to the reference signal—thus the reference point can be chosen at will. Since the cosine is used in the definition, the reference quantity is that which peaks at $\omega t = 0$. As an example consider the two signals given by Equations (3.119) and (3.120). The reference phasor is defined in Equation (3.119) and all other phasors would be defined with respect to this reference, such as the phasor in Equation (3.120). $x_2(t)$ leads $x_1(t)$ by φ/ω seconds; $\tilde{X}_2$ leads $\tilde{X}_1$ by φ degrees.

$$x_1(t) = \text{Re}\{X_{p1} e^{j\omega t}\} = \text{Re}\{\tilde{X}_1 e^{j\omega t}\} = X_{p1} \cos(\omega t) \tag{3.119}$$

$$x_2(t) = \text{Re}\{X_{p2} e^{j\varphi} e^{j\omega t}\} = \text{Re}\{\tilde{X}_2 e^{j\omega t}\} = X_{p2} \cos(\omega t + \varphi) \tag{3.120}$$

The phasor diagram of these two phasors is shown in Figure 3.39 along with their time-domain waveforms (plotted against ωt to make the angular displacement easier to see). This demonstrates how any phasor is defined with respect to the reference phasor.

Figure 3.39 – Time-domain waveform and corresponding phasor diagram.

By convention, the phasor diagram is drawn for the condition ωt=0, which forces the reference phasor to be aligned with the real axis as shown in Figure 3.18. The phasor diagram is a snapshot

in relative time like an oscillograph. Each sweep in an oscilloscope will the trigger on the same point in the periodic waveform and for the phasor diagram that trigger point is the peak of the reference signal. In contrast, SV diagrams are drawn with reference to the phase axes (or real/imaginary axes). For illustration two SVs are defined by Equations (3.121) and (3.122). These are shown on a SV diagram (Figure 3.40) for arbitrary values $\omega t=30°$ and $\delta=15°$.

$$\vec{x}_1 = \hat{X}_1 e^{j\xi_1} = X_{p1}e^{j\omega t} \tag{3.121}$$

$$\vec{x}_2 = \hat{X}_2 e^{j(\xi_2)} = X_{p1}e^{j(\omega t+\delta)} \tag{3.122}$$
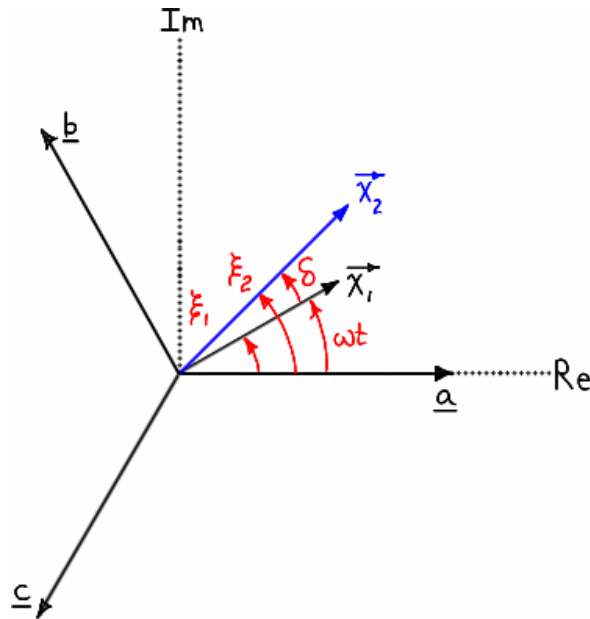
Figure 3.40 – Space vector diagram.

It is useful and appropriate to show the instantaneous SV relative to the phase axes for some value of ωt (such Figure 3.26) when showing the position of the SV at a particular instant. But often the steady-state SV diagram will be drawn at $t=0$ and the SV diagram will look like exactly like a phasor diagram. Comparing Equations (3.119)-(3.120) with Equations (3.121)-(3.122) it is seen that at $t=0$ the phasor is equal to the SV (with the exception of scaling). For sinusoidal quantities in steady state the phasors and SVs trace a circle and any imbalance transient condition causes the phasor trajectory to deviate from the circle. In contrast, nonsinusoidal quantities have a SV trajectory that is not circular in the steady state and these cannot be represented by phasors.

Returning to Equations (3.116)-(3.118) it is seen that the phasor transform takes a cosinusoidal quantity to a stationary vector in the complex plane; this is the phasor domain. It is common practice to say that the phasor rotates, but the phasor itself ($\tilde{X}$) does not rotate—rotation is

141

imparted by the definition of the inverse transform. This is made clear when an attempt is made to take the real part of the phasor only to find that it yields a stationary quantity:

$$\text{Re}\{\tilde{X}\} = \text{Re}\{X_p e^{j\varphi}\} = X_p \cos(\varphi) \quad .$$

In contrast, the inverse of the phasor transform is defined as

$$P^{-1}\{\tilde{X}\} = \text{Re}\{X_p e^{j\varphi} \cdot e^{j\omega t}\} = \text{Re}\{\tilde{X} \cdot e^{j\omega t}\}$$

and it is seen that the $e^{j\omega t}$ term is *appended* to the phasor as a part of the definition of the inverse transform—the phasor does not contain any "frequency" information itself. The trajectory of the phasor (coupled to $e^{j\omega t}$) is the same as the trajectory of the SV discussed above for the case of balanced sinusoidal quantities in steady-state. In contrast, the "frequency" information of the SV is contained in the SV itself. The SV can represent any $\Sigma = 0$ combination of the instantaneous phase variables, whether those variables are changing, stationary, or switching between discrete values. It is the instantaneous nature of the SV (along with its ability to capture each phase's contribution) that make it superior to the phasor for dynamic analysis.

Part III – SV Theory Applied to Sinusoidal BPMS Motor

In Part III the SV models of a sinusoidal BPMS motor are derived. In the first section, the phase-variable electrical model of the synchronous machine is reduced to the two-phase model in the stationary reference frame (both the real-valued vector-matrix version and the complex-valued space vector version are given). Then the model is transformed to the rotor reference frame. The second section examines torque production in both frames. Finally, the third section gives the electromechanical simulation model in both frames.

Electrical Models

The phase-variable model of the brushless permanent magnet motor will be transformed into the stationary and rotor reference frames.

Stationary Frame

From Chapter 2 and Appendix B, the stator voltage equations are given by Equation (3.123), where the voltages are the line-neutral voltages. Equation (3.124) is the vector-matrix form. Since the inverter can apply voltages that contain a ZS component, we should rewrite the equations using the pole voltages. Although, when the Clarke (or SV) transform is used to express the variables in the stationary frame, the ZS component cannot be represented anyhow and the ZS component cannot drive any current so it seems there is no problem. However, this also means that the three circuits represented by Equation (3.123) are *not independent,* and this is a problem. It turns out that the math takes care of this—performing the derivation in terms of pole voltages (which requires use of the phase interference matrix) will yield the same results as those given here. Since using the terminal voltages is simpler, it is presented here and the explanation is deferred to Appendix D.

$$
\begin{bmatrix} v_{AN} \\ v_{BN} \\ v_{CN} \end{bmatrix} = \begin{bmatrix} R & & \\ & R & \\ & & R \end{bmatrix} \begin{bmatrix} i_A \\ i_B \\ i_C \end{bmatrix} + \begin{bmatrix} L_s & & \\ & L_s & \\ & & L_s \end{bmatrix} \frac{d}{dt} \begin{bmatrix} i_A \\ i_B \\ i_C \end{bmatrix} + \begin{bmatrix} e_A \\ e_B \\ e_C \end{bmatrix} \tag{3.123}
$$

$$
\mathbf{v}_{abc} = \mathbf{R}\mathbf{i}_{abc} + \mathbf{L}_s \frac{d}{dt}\mathbf{i}_{abc} + \mathbf{e}_{abc} \tag{3.124}
$$

It is convenient to use the time derivative operator $\rho = d/dt$ to combine the resistance and inductance matrices and eliminate the derivative of the current vector. In traditional general

theory the time derivative operator operates on the inductance as well but only nonsalient machines are considered here thus it can be placed after the inductance, as shown in Equation (3.125).

$$\begin{bmatrix} v_A \\ v_B \\ v_C \end{bmatrix} = \begin{bmatrix} R+L_s\rho & & \\ & R+L_s\rho & \\ & & R+L_s\rho \end{bmatrix} \begin{bmatrix} i_A \\ i_B \\ i_C \end{bmatrix} + \begin{bmatrix} e_A \\ e_B \\ e_C \end{bmatrix} \qquad (3.125)$$

The resulting matrix is called the impedance matrix in the literature, thus Equation (3.126).

$$\mathbf{v}_{abc} = \mathbf{Z}_{abc}\mathbf{i}_{abc} + \mathbf{e}_{abc} \qquad (3.126)$$

Using any (Σ=0) Clarke transform (such as Equation 3.87) the three-phase voltages, currents, and bEMFs may be transformed to their two-phase equivalents in the stator reference frame, Equations (3.127)-(3.129).

$$(3.87): \quad \begin{bmatrix} x_\alpha \\ x_\beta \end{bmatrix} = k \begin{bmatrix} \dfrac{3}{2} & 0 & 0 \\ \dfrac{\sqrt{3}}{2} & \sqrt{3} & 0 \end{bmatrix} \begin{bmatrix} x_A \\ x_B \\ x_C \end{bmatrix} \qquad (\Sigma\text{=0, }k\text{=1})$$

$$\mathbf{v}_{\alpha\beta} = \mathbf{C}\mathbf{v}_{abc} \qquad (3.127)$$

$$\mathbf{i}_{\alpha\beta} = \mathbf{C}\mathbf{i}_{abc} \qquad (3.128)$$

$$\mathbf{e}_{\alpha\beta} = \mathbf{C}\mathbf{e}_{abc} \qquad (3.129)$$

Using the corresponding "inverse" of $\mathbf{C}$ given earlier, Equations (3.127)-(3.129) are rewritten as Equations (3.130)-(3.132).

$$\mathbf{v}_{abc} = \mathbf{C}^{-1}\mathbf{v}_{\alpha\beta} \qquad (3.130)$$

$$\mathbf{i}_{abc} = \mathbf{C}^{-1}\mathbf{i}_{\alpha\beta} \qquad (3.131)$$

$$\mathbf{e}_{abc} = \mathbf{C}^{-1}\mathbf{e}_{\alpha\beta} \qquad (3.132)$$

Substituting these into Equation (3.126) yields Equation (3.133).

$$\mathbf{C}^{-1}\mathbf{v}_{\alpha\beta} = \mathbf{Z}_{abc}\mathbf{C}^{-1}\mathbf{i}_{\alpha\beta} + \mathbf{C}^{-1}\mathbf{e}_{\alpha\beta} \qquad (3.133)$$

Premultiplying by $\mathbf{C}$ gives Equation (3.134) which simplifies to Equation (3.135) (the derivation is done by hand but is not worth repeating because it gives no additional information).

$$\mathbf{C}\mathbf{C}^{-1}\mathbf{v}_{\alpha\beta} = \mathbf{C}\mathbf{Z}_{abc}\mathbf{C}^{-1}\mathbf{i}_{\alpha\beta} + \mathbf{C}\mathbf{C}^{-1}\mathbf{e}_{\alpha\beta} \qquad (3.134)$$

$$\mathbf{I}_{2x2}\mathbf{v}_{\alpha\beta} = \mathbf{Z}_{\alpha\beta}\mathbf{i}_{\alpha\beta} + \mathbf{I}_{2x2}\mathbf{e}_{\alpha\beta}$$

$$\mathbf{v}_{\alpha\beta} = \mathbf{Z}_{\alpha\beta}\mathbf{i}_{\alpha\beta} + \mathbf{e}_{\alpha\beta} \qquad (3.135)$$
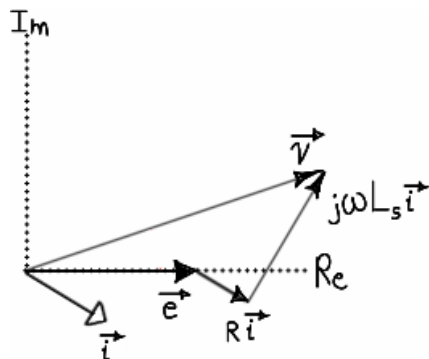
In Equation (3.135) $\mathbf{Z}_{\alpha\beta}$ has elements identical to those of $\mathbf{Z}_{abc}$ (eigenvalues are invariant under a linear transformation) but is only 2x2 (owing to the fact that we used the Clarke instead of αβ0 transform). This result means that the three-phase circuit can be modeled as a two-phase equivalent with the same values for the impedance elements (unlike the three-phase circuits, these two-phase circuits *are* independent). Expanding the impedance matrix yields Equation (3.136).

$$\mathbf{v}_{\alpha\beta} = R\mathbf{i}_{\alpha\beta} + L_s\rho\mathbf{i}_{\alpha\beta} + \mathbf{e}_{\alpha\beta} \tag{3.136}$$

By the relationship between matrix and SV representations (Equation 3.72), Equation (3.136) is equivalent to Equation (3.137).

$$\vec{v} = R\vec{i} + L_s\rho\vec{i} + \vec{e} \tag{3.137}$$

Figure 3.41 shows the steady-state $\left(\rho\vec{i} = j\omega\vec{i}\right)$ SV diagram for an arbitrary lagging power factor; the bEMF is used as the reference and the diagram is shown for $\omega t = 0$. This is similar to the phasor diagram of Figure 3.17 and all of the relationships that held for the SPE analysis (Figure 3.19 to Figure 3.23) hold for the SV analysis as well, giving the same clear picture of how the physical quantities relate to the electrical quantities. But since the phasors are replaced with space vectors which are instantaneous quantities that represent the contribution of all phase variables, the SV model is valid for nonsinusoidal and transient conditions. The two diagrams are the same only because we assumed balanced sinusoidal conditions at steady state, because we chose $\vec{e}$ as the reference, and because we drew the diagram at $\omega t = 0$. The alignment with the real axis actually has no meaning just as in phasor analysis—it simply shows the relationship between the SVs.

Figure 3.41 – SV diagram of synchronous motor in stationary frame (steady state).

In traditional analysis Equation (3.136) is used but its SV equivalent (Equation 3.137) is not used as often in SV analysis. Instead, the variant that incorporates the electromagnetic quantities is most common. Rewriting the stator flux linkage (as done in Chapter 2, in Appendix B, and in the

SPE model from Part I of this chapter), the stator voltage equations can be written as Equation (3.138), where the stator flux linkage is given by Equation (3.139).

$$\vec{v} = R\vec{i} + \frac{d}{dt}\vec{\lambda} \qquad (3.138)$$

$$\vec{\lambda} = L_s\vec{i} + \vec{\psi}_R \qquad (3.139)$$

In the phasor analysis each quantity is associated with one phase (such as phase-A in the SPE discussion). In SV analysis, the voltage, current, and bEMF for each phase are all taken into account for by the respective space vectors. This is easy to see because each is an electrical quantity and we've seen examples of them. What may not be so obvious is that the flux linkages (which had to be specified per-phase as $\tilde{\Lambda}_a$, $\tilde{\Psi}_{R,a}$, $\tilde{\Psi}_{S,a}$) are also accounted for by the space vector ($\vec{\lambda}$, $\vec{\psi}_R$, $\vec{\psi}_S$) and are thus not associated with any phase. For comparison, the SV equivalent of the phasor quantities in SPE analysis (Equations 3.29, 3.30, and 3.31) are given as Equations (3.140), (3.141), and (3.142).

$$\begin{aligned} \vec{\lambda} &= \vec{\psi}_S + \vec{\psi}_R \\ &= L_s\vec{i} + \vec{\psi}_R \end{aligned} \qquad (3.140)$$

$$\begin{aligned} \vec{g} &= \frac{d}{dt}\vec{\lambda} \\ &= \frac{d}{dt}L_s\vec{i} + \frac{d}{dt}\vec{\psi}_R \\ &= \frac{d}{dt}L_s\vec{i} + \vec{e} \end{aligned} \qquad (3.141)$$

$$\vec{e} = \frac{d}{dt}\vec{\psi}_R \qquad (3.142)$$

In the SPE analysis, Figure 3.23 showed the relationship between the flux linkages and the voltages induced by them. Just as Figure 3.17 from SPE was redrawn using SVs as Figure 3.41, Figure 3.23 could be redrawn using SVs and the same comments regarding their similarity would apply.

Rotor Frame

The phase-variable electrical model was transformed to an equivalent model in the stationary αβ reference frame. Now we can apply the concept of reference frame theory to derive an equivalent model in the *dq* reference frame of the rotor. In deriving the stationary model, the matrix form had to be used to reduce the size of the impedance matrix; in deriving the rotor model it is easier

to use SV theory. It may be helpful to review the relationships summarized in Equations (3.106) and (3.115) (which were summarized in Equation 3.109). An attempt is made to give the simplest derivation here. One alternate derivation is [87, pp.61-62,156-157], and another in terms of the general reference frame is [87, p.62-66].

(3.106): $\vec{x}^R = x_d + jx_q$

(3.115):
$$\vec{x} = \vec{x}^R \cdot e^{j\theta_r}$$
$$\vec{x}^R = \vec{x} \cdot e^{-j\theta_r}$$

As before, the voltage and stator flux linkage are given by Equations (3.138) and (3.139).

(3.138): $\vec{v} = R\vec{i} + \dfrac{d}{dt}\vec{\lambda}$

(3.139): $\vec{\lambda} = L_s\vec{i} + \vec{\psi}_R$

The rotor-stator flux linkage is given by Equation (3.143), where Ψ_R represents the peak value.

$$\vec{\psi}_R = \Psi_R e^{j\theta_r} \tag{3.143}$$

Similar to the stationary case, the voltage, current, and flux linkage are written in the stationary frame for direct substitution.

$$\vec{v} = \vec{v}^R e^{j\theta_r} \tag{3.144}$$

$$\vec{i} = \vec{i}^R e^{j\theta_r} \tag{3.145}$$

$$\vec{\lambda} = \vec{\lambda}^R e^{j\theta_r} \tag{3.146}$$

Substitution of Equations (3.144) – (3.146) into Equations (3.138) yields Equation (3.147).

$$\vec{v}^R e^{j\theta_r} = R\vec{i}^R e^{j\theta_r} + \frac{d}{dt}\left(\vec{\lambda}^R e^{j\theta_r}\right)$$

$$= R\vec{i}^R e^{j\theta_r} + \frac{d}{dt}\left(\vec{\lambda}^R\right)e^{j\theta_r} + \frac{d}{dt}\left(e^{j\theta_r}\right)\vec{\lambda}^R$$

$$= R\vec{i}^R e^{j\theta_r} + \frac{d}{dt}\left(\vec{\lambda}^R\right)e^{j\theta_r} + j\omega e^{j\theta_r}\vec{\lambda}^R$$

$$\vec{v}^R = R\vec{i}^R + \frac{d}{dt}\left(\vec{\lambda}^R\right) + j\omega\vec{\lambda}^R \tag{3.147}$$

At the same time, the stator flux linkage is written in the rotor frame, Equation (3.148). In the first line the variables are simply transformed to the rotor frame, as was done above. But it becomes clear that since the common exponential term cancels everywhere, we could have simply written the quantities expressed in the rotor frame. This is an advantage of the SV theory: an expression

can always be written directly in any reference frame. Once again, the fact that the rotor-stator flux linkage in the rotor frame is simply Ψ_R could have been recognized from the beginning.

$$\vec{\lambda}^R e^{j\theta_r} = L_s \vec{i}^R e^{j\theta_r} + \vec{\psi}_R^R e^{j\theta_r}$$

$$\vec{\lambda}^R = L_s \vec{i}^R + \vec{\psi}_R^R$$

$$\vec{\lambda}^R = L_s \vec{i}^R + \Psi_R \tag{3.148}$$

Thus, Equations (3.147) and (3.148) are simply Equations (3.138) and (3.139) expressed in the rotor frame. There is some similarity between Equations (3.138) and (3.147) in that each contains both a resistance multiplied by a current and the derivative of stator flux linkage. However, transformation into the rotor frame introduced a new term, $j\omega\vec{\psi}_R^R$. Although it is not obvious in the given form, this term represents a coupling between the d- and q- components of voltage. To see this, resolve Equations (3.147) and (3.148) into their *dq* components (in accordance with Equation 3.106) to yield Equations (3.149) and (3.150).

$$\begin{cases} v_d = R \cdot i_d + \dfrac{d}{dt}\lambda_d - \omega\lambda_q \\[2mm] v_q = R \cdot i_q + \dfrac{d}{dt}\lambda_q + \omega\lambda_d \end{cases} \tag{3.149}$$

$$\begin{cases} \lambda_d = L_s \cdot i_d + \Psi_R \\[1mm] \lambda_q = L_s \cdot i_q \end{cases} \tag{3.150}$$

In Equation (3.149) it is clear that the d-component voltage has a q-component of flux linkage and vice versa. These are *speed voltages* and they are the coupling mechanism. However, Equation (3.149) does not follow obviously from Equation (3.147). To see how it was derived, examine how the imaginary unit is represented in *dq* form, Equation (3.151), from which Equation (3.152) follows.

$$j = e^{j\pi/2} = \begin{bmatrix} \cos(\pi/2) & -\sin(\pi/2) \\ \sin(\pi/2) & \cos(\pi/2) \end{bmatrix} = \begin{bmatrix} 0 & -1 \\ 1 & 0 \end{bmatrix} \tag{3.151}$$

$$\therefore j\omega = \begin{bmatrix} 0 & -\omega \\ \omega & 0 \end{bmatrix} \tag{3.152}$$

This concept is illustrated in Figure 3.42.
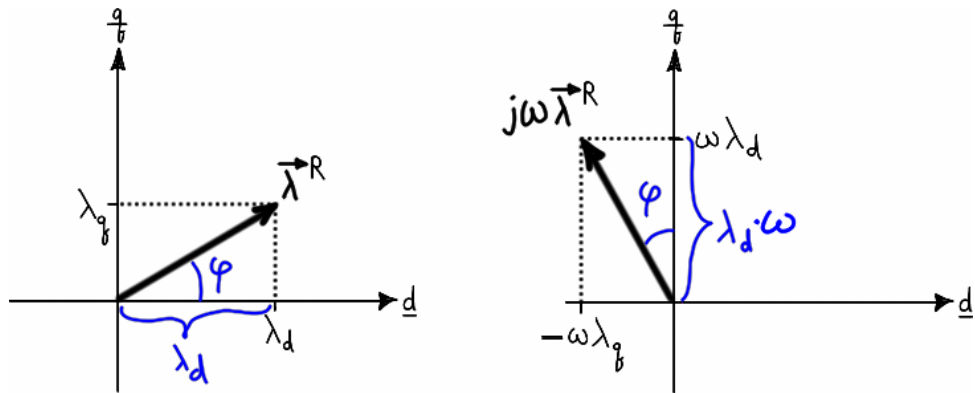
Figure 3.42 – Coupling between d- and q- axes in voltage equations.

From Chapter 2 onward we have routinely encountered the fact that the stator flux linkage is composed of its self flux linkage and the component due to the rotor (Equation 3.139). When expressed in the rotor frame (Equation 3.148) it is clear that the flux linkage the rotor contributes appears constant from the rotor's perspective. This is emphasized by Equation (3.150), which confirms what we already know: the **d** axis is *defined* as being aligned to the rotor flux, thus all of that flux (and its flux linkage) should be along the **d** axis. At this point it would be helpful to draw the SV diagram in the rotor frame. To do this we need the full voltage equations, which can be written either in SV for or *dq*-component form (which are equivalent via Equation 3.106). To get the SV form, substitute Equation (3.148) into (3.147); to get the component form, substitute Equation (3.150) into (3.149). Due to the coupling, the component form is simpler and the result is given by Equation (3.153). The peak value of the rotor-stator flux linkage is by definition constant thus its derivative is zero and the final result is rearranged as Equation (3.154).

$$\begin{cases} v_d = R \cdot i_d + L_s \dfrac{d}{dt} i_d + \dfrac{d}{dt} \Psi_R - \omega L_s \cdot i_q \\[2mm] v_q = R \cdot i_q + L_s \dfrac{d}{dt} i_q + \omega L_s \cdot i_d + \omega \Psi_R \end{cases} \tag{3.153}$$

$$\begin{cases} v_d = R \cdot i_d + L_s \dfrac{d}{dt} i_d - \omega L_s \cdot i_q \\[2mm] v_q = R \cdot i_q + L_s \dfrac{d}{dt} i_q + \omega L_s \cdot i_d + \omega \Psi_R \end{cases} \tag{3.154}$$

In Equation (3.154) the time derivative operates on the *dq* components of the current SV. As will be shown in the chapter on FOC, in the normal situation a BPMS motor drive will keep the stator current SV a fixed angular displacement ahead of the rotor flux, in which case these components are constant and only change during electrical or mechanical transients (electrical transients because a time-varying SV will have time-varying components; mechanical transients because

the components are defined *relative to the rotor*—if the stator current SV has *constant magnitude* but the *instantaneous rotor velocity changes*, so will the *dq* components). Therefore the voltages defined by the second terms in Equation (3.154) are transient components. On the other hand, the third terms in Equation (3.154) will be nonzero even in steady state operation. They are the *dq* embodiment of the inductive voltage drop (which is always 90° ahead of the current SV). Each component of that voltage drop will thus be 90° ahead of that component of current. A component that is 90° ahead of the **d** axis will lie along the **q** axis; a component that is 90° ahead of the **q** axis will lie along the –**d** axis. Hence, these third terms are responsible for the cross-coupling and the polarities (these polarities should be verified between Figure 3.42 and Equation 3.154). Finally, the q-component of voltage contains a fourth term, which is recognized to be the bEMF. By definition the **d** axis is along the rotor flux (which is cophasal with the rotor-stator flux linkage) so the bEMF must always lie along the **q** axis, and the equation confirms this. Further, the bEMF scales with velocity, as expected.

Now the SV diagram of the motor in the rotor frame can be drawn. A major difference from that in the stationary frame is that we do not have to pick a reference SV because the rotor flux (hence rotor-flux linkage and bEMF) are always along the said axes. As before, we will choose to enforce the steady-state condition $\rho = j\omega$, causing the second terms in the voltage equation above to vanish, thereby simplifying the diagram. The steady-state SV diagram is shown in Figure 3.43 and Figure 3.44, where the various SVs have been split between two diagrams to improve clarity.[27] (Usually BPMS motors are operated with the current being cophasal or leading the bEMF, as shown.)

For comparison with the stationary and SPE models, Equation (3.154) can be put into SV form as Equation (3.155), where only the steady-state terms have been kept in the final line.

---

[27] The direction (additivity) of SVs and phasors depends on how the polarity conventions are selected in the KVL equations. This report always assumes all circuit terms have the same polarity, defined to be the opposite of the applied voltage. The SVs in the figure still satisfy this rule. However, to avoid the pesky problem of distinguishing between a negative value and a negative projection direction, the components are always shown for positive values of current. In the figures, i_d is negative. Accordingly, reversing the i_d component directions will show that the components add to give the SVs, using the prior convention.

$$\vec{v}^R = R\vec{i}^R + \frac{d}{dt}\left(L_s\vec{i}^R + \Psi_R\right) + j\omega\left(L_s\vec{i}^R + \Psi_R\right)$$

$$= R\vec{i}^R + L_s\frac{d}{dt}\vec{i}^R + \frac{d}{dt}\Psi_R^{\,0} + j\omega L_s\vec{i}^R + j\omega\Psi_R$$

$$= R\vec{i}^R + L_s\frac{d}{dt}\vec{i}^{R\,S-S} + j\omega L_s\vec{i}^R + j\omega\Psi_R$$

$$\vec{v}^R = R\vec{i}^R + j\omega L_s\vec{i}^R + j\omega\Psi_R \qquad\qquad (3.155)$$
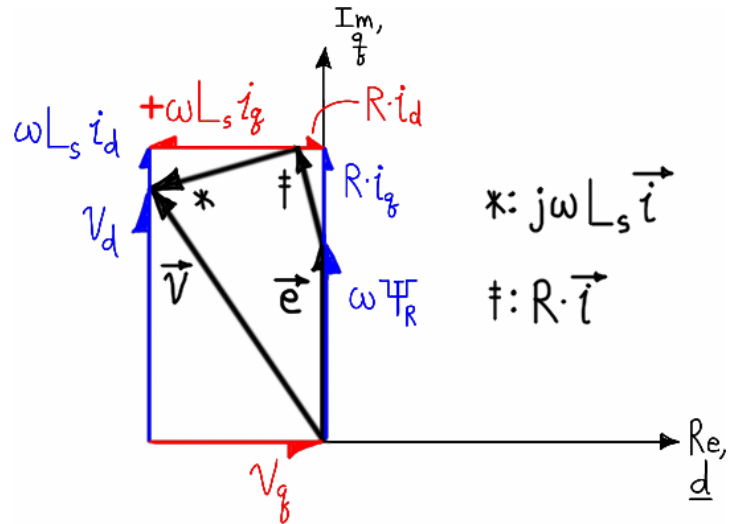
Figure 3.43 – Steady-state SV diagram in rotor frame; voltage and EMFs.
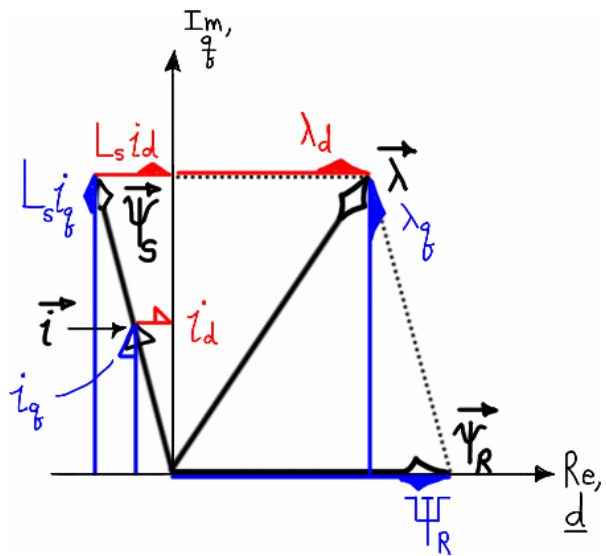
Figure 3.44 – Steady-state SV diagram in rotor frame; current and flux linkages.

151

Torque Production

As with all other forms of equations, the torque can be derived using numerous methods; only two are discussed here: the vector cross product in terms of space vectors and the cross product in terms of the *dq* components.

The torque of any nonsalient or singly-salient machine can be expressed as the cross product of the stator flux-linkage and the stator current [87, p.12], whether space vectors or scalar vectors are used. For simplicity the SV is chosen and the torque can be written as Equation (3.156).

$$T = c \cdot \vec{\lambda} \times \vec{i} \tag{3.156}$$

Substituting Equation (3.139) in for the flux linkage gives Equation (3.157), where the derivation has relied on the fact that a vector crossed with itself is zero.

$$T = c \cdot \left(L_s \vec{i} + \vec{\psi}_R \right) \times \vec{i}$$
$$= c \cdot L_s \vec{i} \times \vec{i} + c \cdot \vec{\psi}_R \times \vec{i}$$

$$T = c \cdot \vec{\psi}_R \times \vec{i} \tag{3.157}$$

Using the notation introduced earlier, the current SV is expressed as $\vec{i} = \hat{I} e^{j\xi}$ and the rotor-stator flux linkage SV as $\vec{\psi}_R = \Psi_R e^{j\theta_r}$. This corresponds to the situation shown in Figure 3.45, where the rotor is at position θ_r.
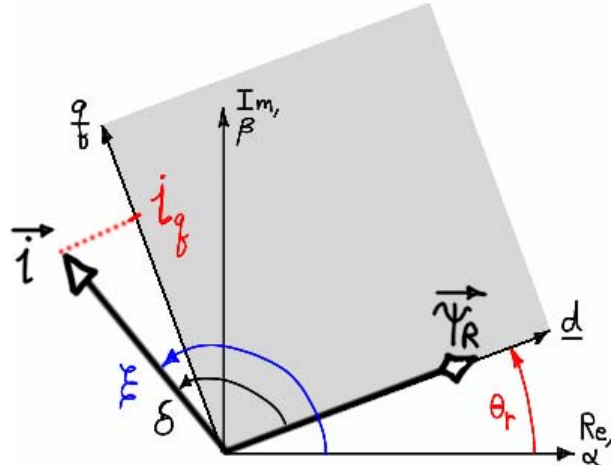
Figure 3.45 – Torque production; stationary reference frame.

The cross product can be defined as the product of the magnitude of each vector multiplied by the sine of the angle measured from the first toward the second vector. Using this definition the torque can be expressed as Equation (3.158). The angle δ is shown in Figure 3.45 as well and it is clearly the same torque angle defined in Part I. The equation is valid only as long as the stator

current does not influence the value of the rotor flux linkage (which is true when rare-earth magnets are used).

$$T = c \cdot |\vec{\psi}_R| \cdot |\vec{i}| \cdot \sin(\xi - \theta_r)$$

$$T = c \cdot |\vec{\psi}_R| \cdot |\vec{i}| \cdot \sin(\delta) \tag{3.158}$$

If this same procedure is followed in the rotor reference frame a great simplification results. Beginning again with Equation (3.156) and using the same technique yields Equation (3.159).

$$\begin{aligned} T &= c \cdot \vec{\lambda}^R \times \vec{i}^R \\ &= c \cdot \left(L_s \vec{i}^R + \vec{\psi}_R^{\ R} \right) \times \vec{i}^R \\ &= c \cdot L_s \vec{i}^R \times \vec{i}^R + c \cdot \vec{\psi}_R^{\ R} \times \vec{i}^R \end{aligned}$$

$$T = c \cdot \vec{\psi}_R^{\ R} \times \vec{i}^R \tag{3.159}$$

From the figure, $\vec{i}^R = \hat{I}e^{j\delta}$ and $\vec{\psi}_R^{\ R} = \Psi_R e^{j0} = \Psi_R$. Substituting these into the cross product yields Equation (3.160), where $c = (3/2)$ for a two-pole machine [87, p.68]. It is important to note that the derivation assumes a magnitude-invariant SV transform.

$$\begin{aligned} T &= c \cdot |\vec{\psi}_R^{\ R}| \cdot |\vec{i}^R| \sin(\delta - 0) \\ &= c \cdot \Psi_R \cdot |\vec{i}^R| \sin(\delta) \end{aligned}$$

$$T = \frac{3}{2} \Psi_R \hat{I} \sin(\delta) \tag{3.160}$$

It is seen that Equation (3.160) reduces to Equation (3.21) (which was developed in Part I for the SPE model) for the case of balanced sinusoidal currents. Continuing, if the angle between the **q** axis and the current SV is defined as Γ, $\sin(\delta) = \sin(\Gamma + \pi/2) = \cos(\Gamma)$. Then Equation (3.160) can be written as Equation (3.161).

$$T = \frac{3}{2} \cdot \Psi_R \cdot i_q \tag{3.161}$$

Ignoring temperature and saturation effects, Equation (3.161) shows that for a given machine torque is directly proportional to the q-axis component of stator current. (This is evident in Equation (3.158) as well.) By controlling the current SV to be completely along the **q** axis the maximum torque per current is produced. Another way to look at it is to realize that only the q-component of current generates torque. The rotor-oriented FOC discussed in Chapter 5 exploits this concept.

In addition to the forms above, the torque is often described in terms of *dq* components. As with the SV case, the *dq* derivation [80, p.678-688] is built up from first principles but we can begin at the cross product. (Normally the cross product is not shown and only Equation (3.162) is given—one must know the identity below to see how it is actually a cross product.)

$$T = \frac{3}{2}\boldsymbol{\lambda}_{dq} \times \mathbf{i}_{dq}$$

$$= \frac{3}{2}\det\left(\left[\boldsymbol{\lambda}_{dq},\mathbf{i}_{dq}\right]\right)$$

$$= \frac{3}{2}\begin{vmatrix} \lambda_d & i_d \\ \lambda_q & i_q \end{vmatrix}$$

$$T = \frac{3}{2}\left[\lambda_d i_q - \lambda_q i_d\right] \tag{3.162}$$

Substituting Equation (3.150) into Equation (3.162) and simplifying gives Equation (3.163).

$$T = \frac{3}{2}\Psi_R \cdot i_q \tag{3.163}$$

This result can also be arrived at using the conservation of energy equation [107].

Electromechanical Models

The equations required to construct the BPMS motor model in the stationary and rotor reference frames follow directly from the equations in the previous two sections. It should be noted that everything said here regarding the rotor frame applies to the general frame with only a modification of the rotor angle.

Stationary Frame

In the stationary frame the voltages are given by Equations (3.138) and (3.139).

(3.138): $\vec{v} = R\vec{i} + \dfrac{d}{dt}\vec{\lambda}$

(3.139): $\vec{\lambda} = L_s\vec{i} + \vec{\psi}_R$

Substitution of Equation (3.139) into (3.138) yields Equation (3.164), which can be split into its α- and β- components as Equation (3.165) and rearranged into state space variable as Equation (3.166).

$$\vec{v} = R\vec{i} + L_s\frac{d}{dt}\vec{i} + \frac{d}{dt}\vec{\psi}_R$$

$$\vec{v} = R\vec{i} + L_s\frac{d}{dt}\vec{i} + \vec{e} \tag{3.164}$$

$$\begin{cases} v_\alpha = R \cdot i_\alpha + L_s \dfrac{d}{dt} i_\alpha + e_\alpha \\[2mm] v_\beta = R \cdot i_\beta + L_s \dfrac{d}{dt} i_\beta + e_\beta \end{cases} \tag{3.165}$$

$$\begin{cases} \dfrac{d}{dt} i_\alpha = \dfrac{1}{L_s}\left[v_\alpha - R \cdot i_\alpha - e_\alpha \right] \\[2mm] \dfrac{d}{dt} i_\beta = \dfrac{1}{L_s}\left[v_\beta - R \cdot i_\beta - e_\beta \right] \end{cases} \tag{3.166}$$
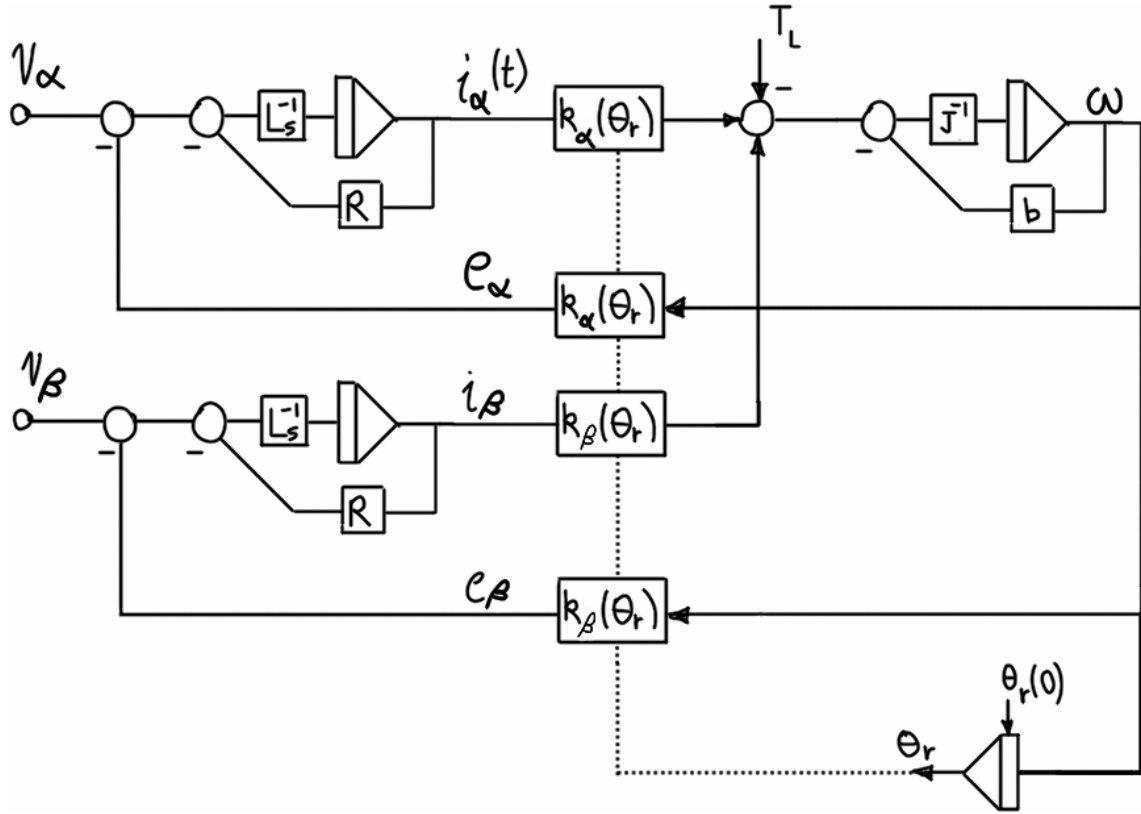
Using Equation (3.166) the simulation diagram is drawn as Figure 3.46. The rotor-stator flux linkage was given as Equation (3.143), where Ψ_R represents the peak value.

(3.143): $\vec{\psi}_R = \Psi_R e^{j\theta_r}$

The αβ components of Equation (3.143) are given by Equation (3.167). Since bEMF is the time-derivative of the rotor-stator flux linkage, the αβ components of the bEMF are given by Equation (3.168). By definition, the bEMF functions (i.e., those in Figure 3.46) are then simply Equation (3.168) divided by ω.

$$\begin{cases} \psi_\alpha = \Psi_R \cos(\theta_r) \\ \psi_\beta = \Psi_R \sin(\theta_r) \end{cases} \tag{3.167}$$

$$\begin{cases} e_\alpha = -\omega\Psi_R \sin(\theta_r) \\ e_\beta = +\omega\Psi_R \cos(\theta_r) \end{cases} \tag{3.168}$$

Figure 3.46 – Simulation diagram for BPMS motor in stationary reference frame.

The stationary model is essentially the same as the phase-variable model, less one phase. Since the SV (or αβ components) cannot contain a ZS component, it is clear that a wye-connected machine is modeled exactly as shown (since we do not have independent control of the third phase). This elimination of the redundant phase (and the orthogonalization of the coordinates) is the chief advantage of the stationary model, just as these were the chief advantages of using the SV. In addition, it was shown that the SV can be easily manipulated since it is a complex exponential. The additional benefit of the SV model (over the αβ model) then is that the (electrical or magnetic) quantities are all space vectors instead of components. This can be drawn as Figure 3.47, where the double lines indicate SV quantities. The applied voltage is shown as broken out into is αβ components (this idea was taken from [166]). There is no difference between this and the former model except it clearly emphasizes the SV as an entity (as opposed to treating its components separately).
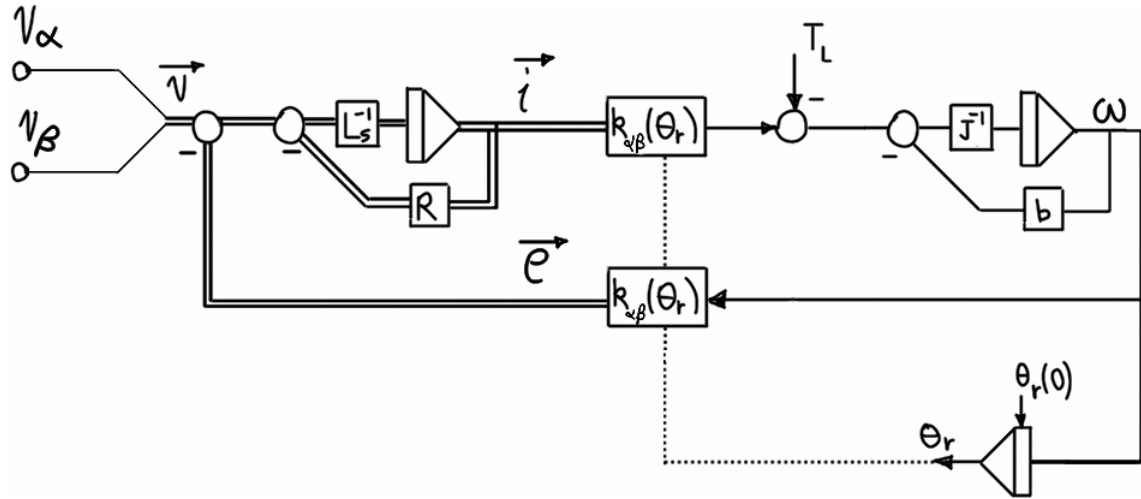
Figure 3.47 – Simulation diagram for BPMS motor in stationary frame (SV representation).

Rotor Frame

To obtain the model in the rotor frame, begin with the stator voltages in the rotor frame (Equation 3.154). Rearranging into state variable form gives Equation (3.169).
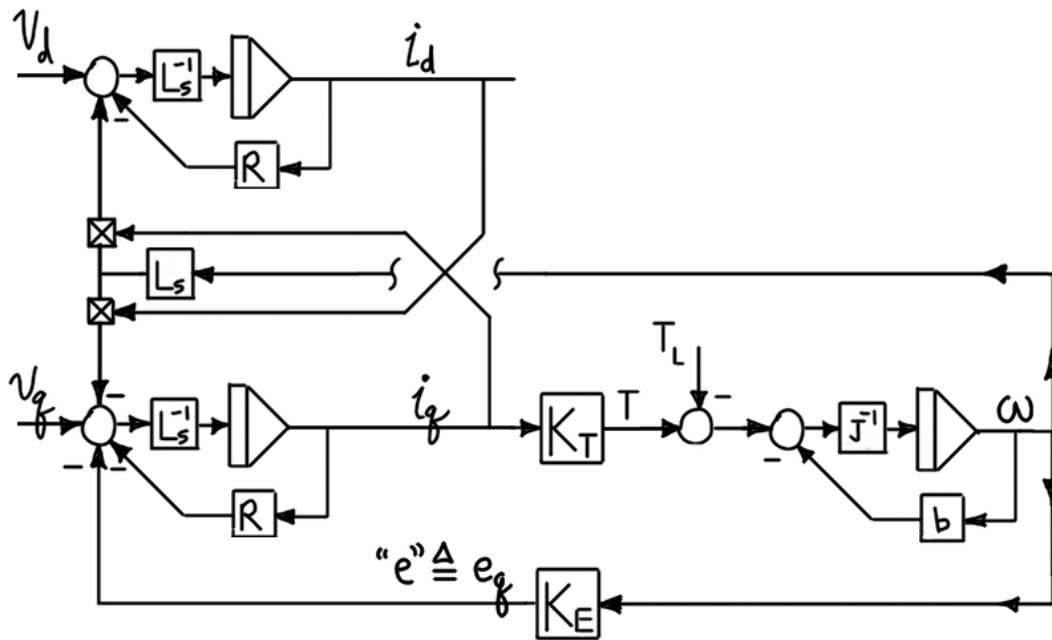
$$(3.154): \begin{cases} v_d = R \cdot i_d + L_s \dfrac{d}{dt} i_d - \omega L_s \cdot i_q \\[2mm] v_q = R \cdot i_q + L_s \dfrac{d}{dt} i_q + \omega L_s \cdot i_d + \omega \Psi_R \end{cases}$$

$$\begin{cases} \dfrac{d}{dt} i_d = \dfrac{1}{L_s} \left[v_d - R \cdot i_d + \omega L_s \cdot i_q \right] \\[3mm] \dfrac{d}{dt} i_q = \dfrac{1}{L_s} \left[v_q - R \cdot i_q - \omega L_s \cdot i_d - \omega \Psi_R \right] \end{cases} \tag{3.169}$$

Using Equation (3.169) the simulation diagram is drawn as Figure 3.48. The torque and bEMF constants given by Equations (3.170) and (3.171), although discussions in the literature of the *dq* model usually do not use this terminology (the constants are left as the right-hand side only); these follow directly from Equation 3.163 and 3.169.

$$K_T = \frac{3}{2} \Psi_R \tag{3.170}$$

$$K_E = \Psi_R \tag{3.171}$$

157

Figure 3.48 – Simulation diagram for BPMS motor in synchronous reference frame attached to rotor.

The stationary model was essentially a linearly independent, orthogonal version of the phase-variable model; clearly, the rotor frame model is more complex. The first thing to note is that the rotor angle θ_r has disappeared from the model. This is because the model is *in* the rotor reference frame, which is defined by θ_r. With that said, it is clear that this is the same model for the general reference frame (and in that case, the angular velocity ω would be that of the general frame). This model is often called the *synchronous reference frame* because it rotates synchronously with the stator electrical quantities (which are said to be at the synchronous frequency, ω).[28] The disappearance of θ_r can be further understood by recalling two facts presented earlier: (1) the bEMF is entirely in the q-circuit (that is, $\vec{e}$ is entirely along the **q** axis,

---

[28] Recall the discussion from Part I regarding electrical and mechanical measures. In the general case the electrical and mechanical speeds are *not* the same, even if they are expressed in the same measure. This is simply because the electrical (stator) and mechanical (rotor) quantities are separate dynamic subsystems—nothing forces them to be the same. In an induction motor, the rotor (at speed ω_r) slips past the stator electrical quantities (which are at the synchronous speed ω_e), but in a synchronous motor (ignoring transients) the electrical and mechanical speeds are the same by necessity. The importance of this discussion is that in Chapter 5, current regulation will be performed in the "synchronous frame" as a part of rotor-oriented FOC, but the properties of that current controller are applicable even to FOC that is not rotor-oriented, and to electrical circuits that are not motors. For this reason, the figure caption identifies the model as existing in a synchronous reference frame, which happens to be attached to the rotor.

$\vec{e} = je_q$), and (2) it was demonstrated that only the quadrature component of current contributed to torque production. Both of these features are seen clearly in the figure.

To further explore this model, return to the steady-state SV diagram in the rotor reference frame (presented in Figure 3.43 and Figure 3.44). The diagrams were split to improve clarity while introducing the d- and q- components. Now the electrical quantities will be combined and the components will be ignored in order to focus on circuit operation. The steady-state SV diagram of a BPMS motor in the rotor frame is shown in Figure 3.49.
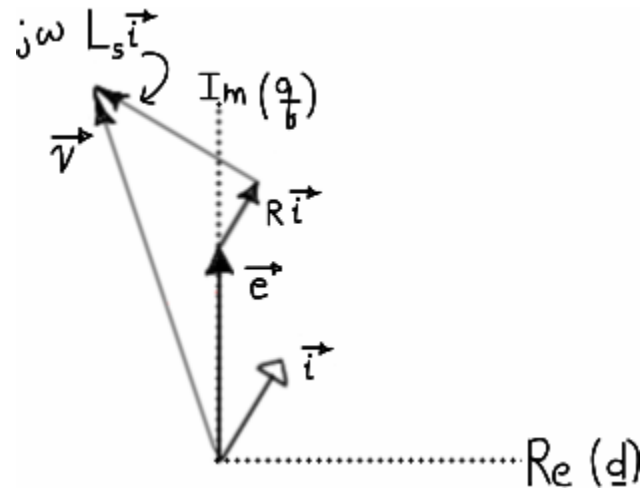
Figure 3.49 – Steady-state SV diagram in rotor frame.

In examining Figure 3.49 it becomes clear that the cross-coupling terms in Figure 3.48 are due to the inductances; the SV diagram and simulation diagram viewpoints are easily reconciled by comparing the two figures.

CHAPTER 4 - Inverters and Space Vector Modulation

In the subject of motor control there are three areas that can be very tightly integrated and hard to discuss separately: commutation or phasing (the synchronizing of the current waveforms with the shaft position), current control (controlling the shape and amplitude of current to produce the correct value of torque), and the motor control system structure (how references are generated, how commands are passed to the power converter, and how feedback is used). This chapter discusses inverters and space vector modulation. As a consequence it cannot avoid discussing current control, but the main discussion of current control must be delayed until the next chapter when FOC is presented.

This chapter begins by discussing the general structure common to all inverters. The common inverters will be divided into to classes (120° and 180°) and the control methods for each will be investigated. As the 120° class is discussed it will be natural to also discuss the 120° six-step commutation ("trapezoidal commutation") mentioned in Chapter 2; from that point on only 180° inverters will be treated.

The second section deals exclusively with SVM. It is first shown how SVM uses the 180° inverter. As a continuation of the space vector material from Chapter 3, the meaning of the magnitude and trajectories of space vectors is discussed. SVM overmodulation will be compared to PWM overmodulation and will reveal the concept of "maximum" inverter output. Finally, details regarding SVM implementation and relationships to PWM are discussed.

Overview of Voltage Source Inverters

There are many different inverter types reported in the literature, such as *matrix*, *multi-level*, *soft-switched*, and various *resonant* topologies. Only *hard-switched*, *two-level*, *three-phase* inverters are discussed here because they are the only common topologies in brushless permanent magnet motor control. The *current source inverter* (CSI) is only used in very large power ratings [75] thus the *voltage source* (or *stiff*) *inverter* (VSI) is the dominant topology, even though it is ultimately motor current that we desire to control. In a three-phase VSI there are three output terminals, each connected to a *leg* (also known as a *half-bridge*) that is connected across the DC *link* or *bus*. The bus could be supplied by a DC power supply or it could be created using a rectifier and a large bulk capacitor as shown in Figure 4.1. At no time can both transistors in one leg be ON otherwise they will short-circuit the bus (a *shoot-through fault*). Since each terminal can be connected to only two potentials (with respect to the bus midpoint) this is called a *two-level* inverter.
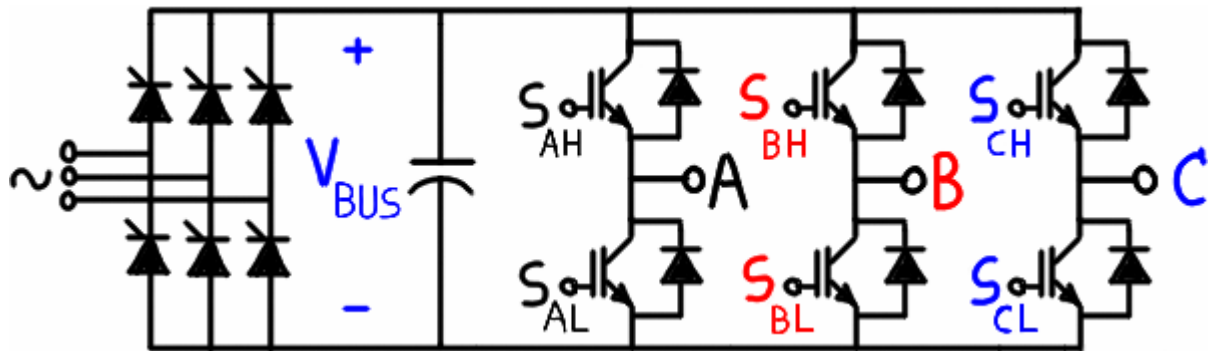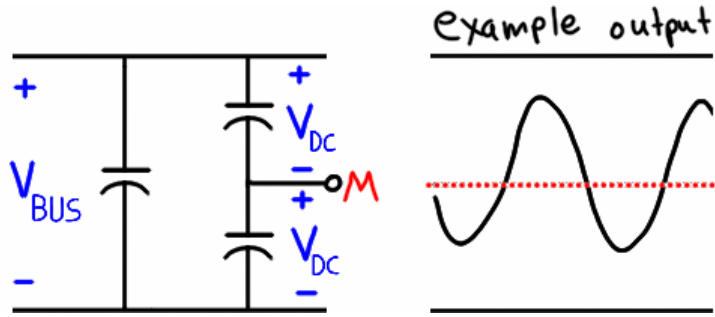
Figure 4.1 – VSI topology with controlled-rectifier front end.

In the VSI topology the output voltage waveform and frequency are controlled only by the transistor switching scheme (which will be called *commutation* regardless of whether a motor is considered). However, the magnitude of the voltage can be controlled using the transistors or by using the controlled rectifier at the input. (This is true even if the inverter is fed from a DC supply—the controlled rectifier is simply replaced with a chopper.)
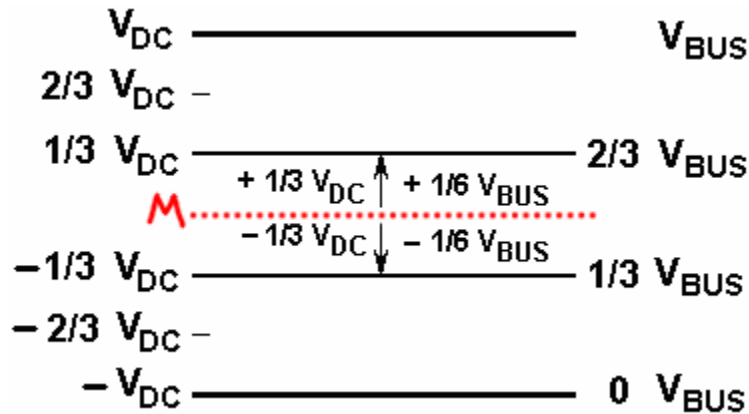
In order to get the largest possible amplitude, the output waveforms are synthesized about the midpoint of the DC bus, which is labeled M as shown in Figure 4.2. Many sources in the literature specify output voltages in terms of V_{BUS} because that it is the actual bus voltage. But the output waveforms are AC, thus it makes more sense to the author to specify them in terms of V_{DC} as shown (the output is at maximum when it reaches V_{DC}, as opposed to $V_{BUS}/2$). A

similar convention is to use V_{BUS} as shown but replace V_{DC} with $V_{BUS}/2$. This practice has a definite advantage in that it does not require the creation of an "artificial" voltage definition (V_{DC}) but it has the disadvantage that the factor of ½ will combine with other numerical factors in formulae. This leaves the voltages specified in terms of V_{BUS} which again loses the clear association with the midpoint shown in the figure and is not preferred in this report.
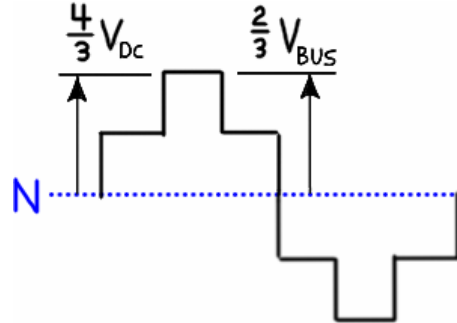
Figure 4.2 – Definitions of DC bus midpoint and voltage magnitudes.

Figure 4.3 shows a scale showing the two measures of voltage. On the left it is clear that the voltage scale is centered at the midpoint and bipolar voltages result (as we expect in an AC waveform). On the right the scale is referenced to the low side of the bus and is therefore unipolar. However, there is nothing to prevent us describing a bipolar voltage (relative to M) in terms of V_{BUS} or describing a unipolar voltage (relative to the low side of the bus) in terms of V_{DC}. It is difficult to use only one convention and references in the literature are testament to this. As much as possible, voltages in this report are referenced to the midpoint M and therefore, the measures V_{DC} and V_{BUS} refer to *magnitudes* of a bipolar voltage, as shown in the center of Figure 4.3.

Figure 4.3 – Voltage measurements.

In addition to measuring voltages with respect to the low side or the midpoint, the magnitudes of *differential* voltages (such as the voltage between a terminal and the load neutral) are also specified in terms of V_{DC} and V_{BUS} as shown in Figure 4.4.

Figure 4.4 – Differential voltage measurement.

The neutral point of the load is marked N and the midpoint of the DC bus is marked M. Voltage at the output of the inverter (which is the input to the load) is called *pole* (or *terminal*) *voltage*; voltage across the phase of the load is called the *line-neutral* (or *phase*) *voltage*; voltage between terminals is called the *line-line* (or *line*) *voltage*. Examples of notation are v_{AM}, v_{AN}, and v_{AB}, respectively. The neutral voltage is measured with respect to the midpoint: v_{NM}.

Gating and Leg Control Schemes

At the highest level we can classify any three-phase VSI as either a *120° inverter* or *180° inverter*. These definitions can be established according the way each leg is controlled or according to the period over which the transistors are not OFF. These definitions are essentially the same but both will be examined, in the order listed.

In a 180° inverter the top and bottom transistors in one leg are switched in a complementary fashion. Each pole voltage is equal to either high ($+V_{DC}$) or low ($-V_{DC}$). In a 120° inverter the top and bottom transistors in one leg are controlled separately, thus it is possible for both transistors to be OFF. Each pole voltage may be high ($+V_{DC}$), low ($-V_{DC}$) or undefined. (When both transistors in one leg are OFF the pole voltage will be determined by the current flowing trough that phase of the load into the clamping / free-wheeling diodes.) The allowable leg states for a 120° inverter are shown in Figure 4.5, where the transistors are symbolized by switches and phase-A is used as an example.
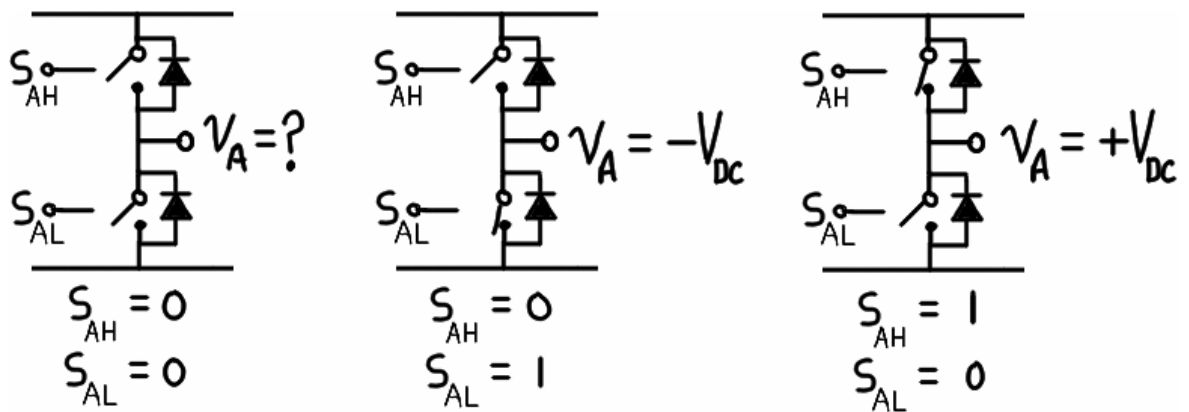
Figure 4.5 – Leg states for 120° inverter.

Since the leg of the 180° inverter is switched either high or low, the leg state to be represented by a single variable, resulting in the simplified diagram shown in Figure 4.6.
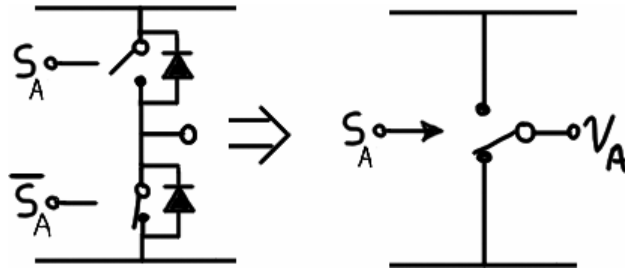
Figure 4.6 – Representation of leg in 180° inverter.

The allowable leg states for the 180° inverter are shown in Figure 4.7.
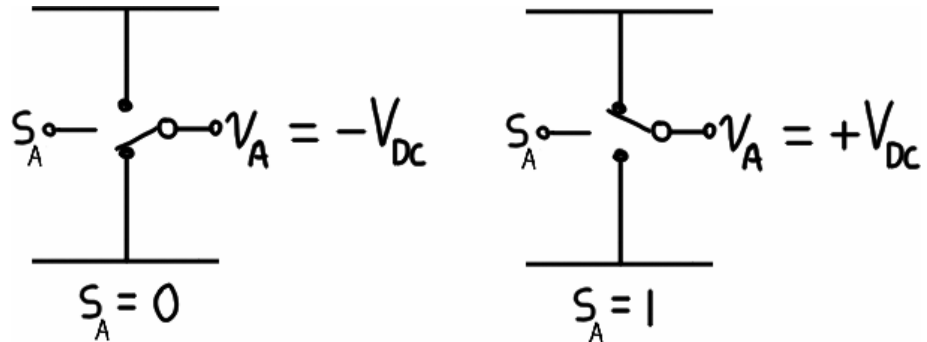
Figure 4.7 – Leg states for 180° inverter.

So far, the definition of the two types is based on the leg control scheme: either each leg must have one transistor on at any given time (180°) or there will be a period where both transistors are off (120°). These restrictions enforce a different restriction on the allowable gating period. Traditionally, these 120° and 180° were are derived from the full-on conduction periods of the transistors or thyristors in the 120° six-step inverter and the 180° six-step inverter [79], but it is apparent from the literature that these terms have been modified over the years to accommodate PWM inverters. 180° is one half-cycle so that is the maximum. If the duration was below 120°

then there would be periods during which only one phase would be connected to the bus (which results in zero potential since the neutral of the load is isolated), so that is the minimum. Perhaps there are schemes with gating durations between the two but these are not common. Therefore, in the 120° inverter at least one transistor per leg must be controlled (full-on or PWM) over 120° of the electrical half-cycle; during the remaining 60° both transistors must be OFF. In the 180° inverter both transistors in each leg must be controlled (full-on or PWM) at all times. The gating periods for 120° and 180° inverters are shown in Figure 4.8. The shaded blocks show the periods during which *either* transistor in one phase leg is controlled. In the 120° inverter it is seen that there are two 60° segments per electrical cycle (360°) where both transistors in a leg are OFF. This is true for each phase and the OFF periods are staggered between the phases, thus there will always be exactly two phase legs controlled at any given time. In the 180° inverter it is clear that the transistors in each leg are controlled at all times, thus all three legs are controlled at all times. Due to finite transistor turn-off times a small delay (called *dead-time* or a *blanking pulse*) must be separate the transistor switching in one leg, as discussed later.
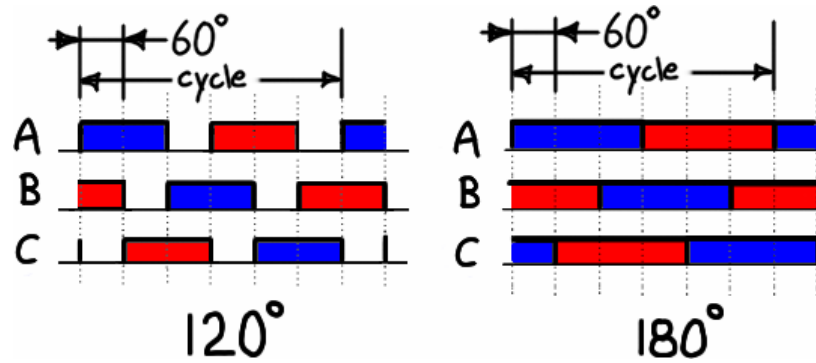
Figure 4.8 – Gating schemes for 120° and 180° inverters.

Inverter Control Methods

The 120° and 180° inverters can be controlled in many different ways. As one reference puts it, "…*the number and combination of permutations seem to be endless*" [128]. In another, "…*the enormous amount of material published makes it challenging for a user to identify basic modulation principles and apply them to particular implementations. Much reported research has presented "new" or "improved" PWM techniques, which are often only a straightforward variation of a previous approach. But it can at times be quite difficult to see how they are related*" [70, p.95]. These quotations were referring to PWM methods in general, but the problem is compounded in motor control because of the commutation/phasing and PWM are often inseparable from one another. Only the PWM methods commonly used in BPMS motor control will be discussed here. These are presented not only to give some perspective on motor control

but because they are the best basis for understanding the more advanced PWM techniques such as SVM.

The simplest method is to use a controlled front-end converter to control the voltage and switch (commutate) the transistors in a certain pattern to generate a fixed-shape output voltage waveform that varies in frequency. In both 120° and 180° inverters the simplest pattern involves six steps per electrical cycle and results in rectangular output voltage waveforms; this is called a *six-step squarewave inverter*. The second method uses the same six steps but eliminates the front-end converter by integrating the voltage control with the commutation; this is called a *six-step PWM* (or *squarewave PWM*) *inverter*. The third method does not use commutation. Instead, pulse width modulation is used to control directly the magnitude, waveshape, and frequency of the output voltage; this is called a *PWM inverter*. (There is a fourth method of control but since it is usually associated with SVM its presentation is delayed until that section.)[29]

Six-Step Squarewave

Both 120° and 180° inverters can be operated as a "six-step squarewave" inverter in which the output voltage is rectangular. In both inverters the voltage is controlled by the front-end converter and the rate of transistor commutation determines the frequency of the output. The gating and pole voltages are shown in Figure 4.9. (The full voltage waveforms are given in Figure 4.10 and Figure 4.11.) Because the 180° inverter always has three switches closed the neutral voltage will never be zero and therefore the line-neutral voltage will never be the same as the pole voltage. In the 120° inverter it appears that the line-neutral voltage is always the same as the pole voltage. However, this is true only for a resistive load [37, p.379]. The flat-top segments of the pole voltages will always be as shown since the transistors are ON. Contrarily, the zero-voltage segments of the pole voltage will not always be zero because current can flow through the diodes antiparallel to the transistors. This causes the neutral voltage to be nonzero, which causes the line-neutral voltages to deviate from the pole voltages. In addition, when the load is a motor it will have a bEMF that influences the pole and line-neutral voltages during these segments.

---

[29] In addition to these methods there are numerous "advanced" techniques for both overall inverter control and for control of the PWM specifically, such as on-line optimization techniques, selective harmonic elimination (SHE), delta modulation, sigma-delta modulation, random pulse width modulation (RPWM), sliding mode control (SMC), fuzzy methods, and innumerable artificial intelligence schemes (artificial neural networks, fuzzy-neural nets, and combinations of neutral control with most every other control method). For the most part each of these is a technique that exists to improve some specific aspect of operation or control and a comparison of the techniques would be a work in itself. Many are complicated enough or do not provide quantifiable benefits so they are still academic curiosities that are not implemented in industry; as such, they deserve no mention here.
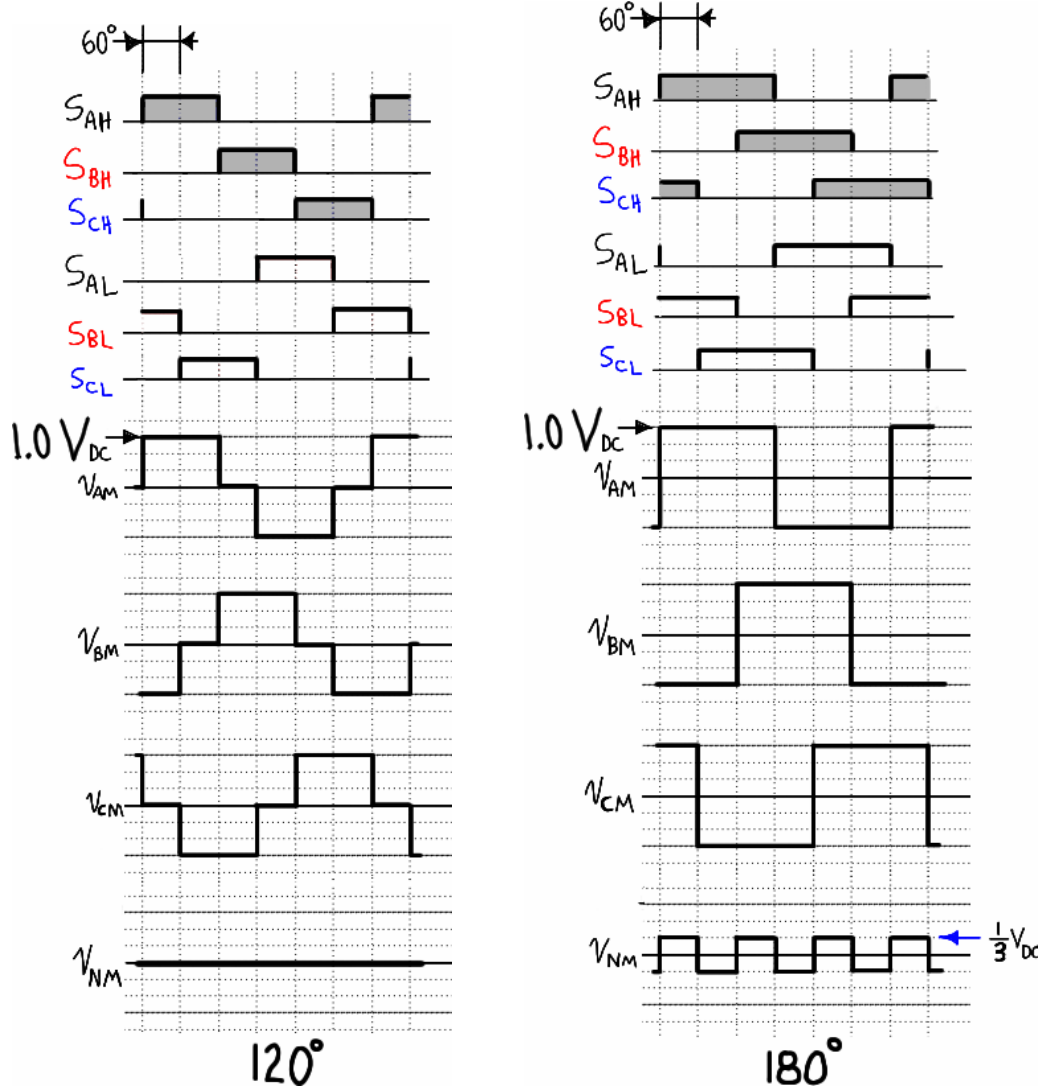
Figure 4.9 – Gating and POLE voltages for ideal 120° and 180° six-step inverters.

From a general power electronics perspective, both squarewave inverters can be used to approximate a sinewave output. It seems there is no sense in using the 120° inverter for this purpose because the fundamental would be lower than that of the 180° inverter; indeed it appears that only the 180° inverter is commonly used for this purpose. On the other hand, the squarewave 180° inverter was the basis of the original adjustable speed AC induction motor drives and these are still commonly used [73], [75]. In that application the frequency is adjusted in order to control motor speed and the bus voltage is adjusted proportionally (according to a "V/Hz" profile) to keep the flux constant [78], [77]. The same 180° inverter could be used to control sinusoidal synchronous machines but this is not common in brushless permanent magnet motors. From a motor control perspective, it is obvious that the 120° six-step inverter described here is exactly suited to driving the trapezoidal BPMS motor discussed in Chapter 2. However it seems that the

squarewave mode discussed here (where the voltage is controlled by the front-end converter) is not as common as the "six-step PWM" mode discussed next.
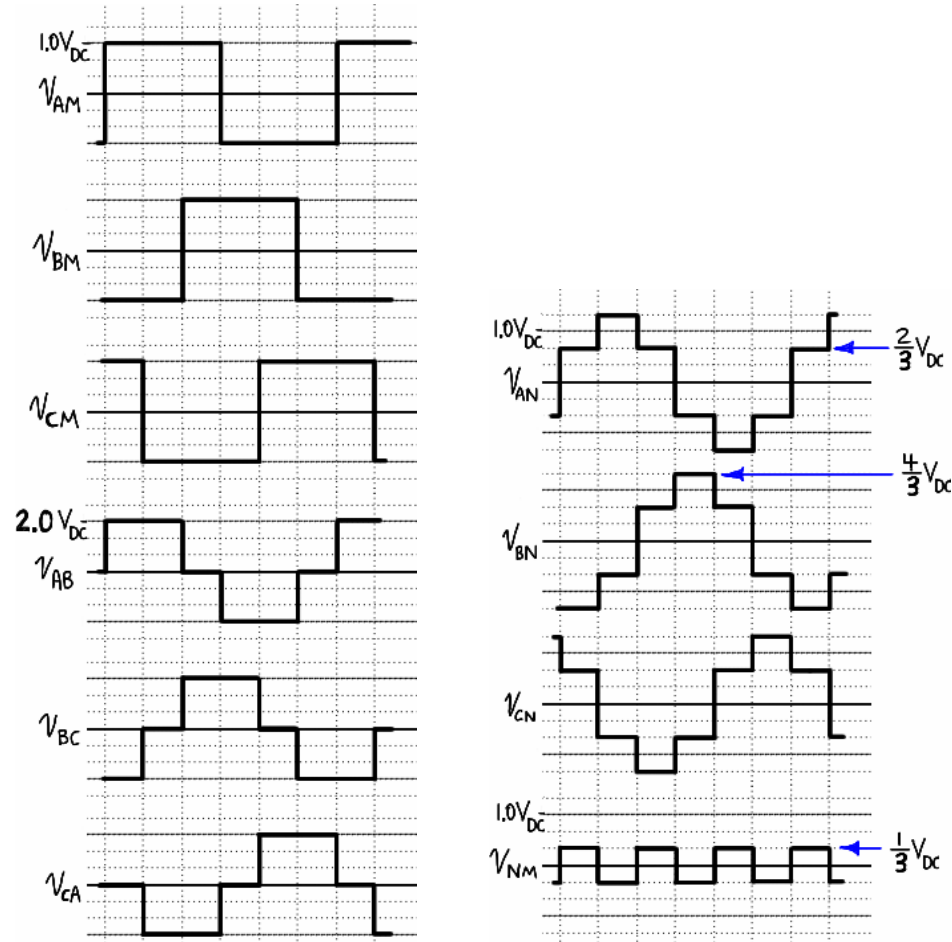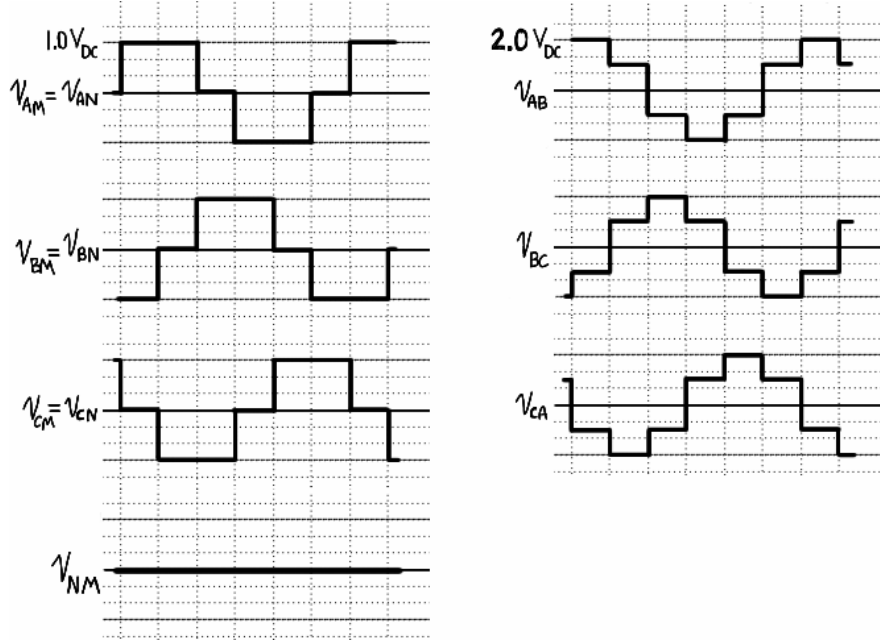
Figure 4.10 – Voltage waveforms for 180° six-step squarewave inverter.

Figure 4.11 – Ideal voltage waveforms for 120° six-step squarewave inverter with resistive load.

Six-Step PWM

The six-step PWM technique is essentially the same as the six-step squarewave except the voltage regulation is performed by the transistors using pulse width modulation. The commutation can be performed using the top transistors and the PWM can be performed using the bottom transistors. Or the opposite could be done. In addition to practical differences in implementation, these choices affect which quadrants the inverter can operate in [118]. PWM could be used on both top and bottom transistors, resulting in synchronous rectification, which affects current ripple. The basic varieties are shown in Figure 4.12 for a 120° inverter. Note that the PWM exists to maintain an average voltage—the duty cycle is essentially constant over a commutation period. If the duty cycle were 0% in Figure 4.12 it is clear that only one phase would be connected to the bus at any time thus the load voltage would be zero. If the duty cycle were 100%, during any 60° commutation period two phases would be connected across the bus (transistors full-on). Therefore the six-step PWM is the same as six-step squarewave mode when the duty cycle reaches 100%. It seems that the six-step PWM method is used primarily for trapezoidal BPMS motor control and the 120° inverter is the de facto implementation. A 180° variety of the six-step PWM inverter was at one time common in variable speed induction motor drives (sometimes it was called *block modulation*) but is no longer in common usage [78, p.19]. Information on 120° PWM in six-step commutation is presented in [117], [118].
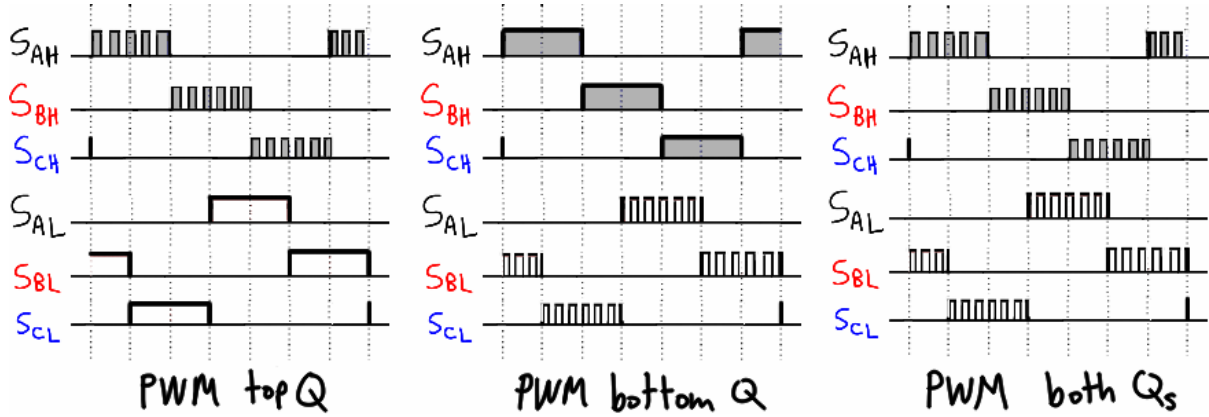
Figure 4.12 – Commutation and PWM configurations in 120° inverter.

PWM

The PWM inverter controls the magnitude, waveshape, and frequency of the output voltage at each terminal by adjusting the duty cycle of the gating signal for each leg—it is the familiar "standard" usage of PWM applied to three legs. Unlike the previous two methods, three-phase PWM inverters are only found in the 180° variety because the objective is to produce an output waveform whose average is continuous; it would not make sense to turn off both transistors in a leg at any time. The objective is to continuously adjust the duty cycle such that the <u>average</u> voltage follows some commanded value as shown in Figure 4.13. The waveform can be arbitrary (within limits) but this report only concerns *sinusoidal PWM* (SPWM). With this restriction we can then say the objective is to continuously adjust the duty cycle to produce an output voltage with a <u>fundamental</u> component of the desired amplitude and frequency.
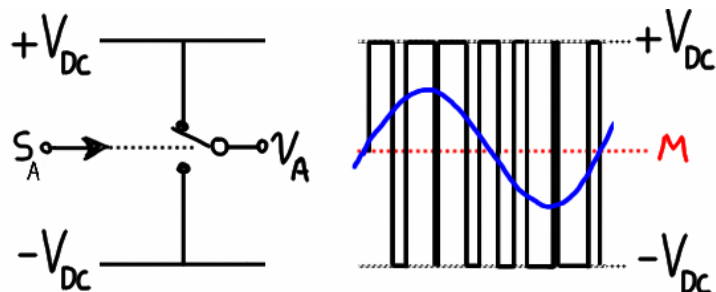
Figure 4.13 – Concept of PWM for one phase leg; not to scale.

It is the three-phase PWM inverter that is the subject of the remainder of this chapter, thus the 120° inverter will not be discussed further. The traditional method to control each leg of the

inverter is called sine-triangle comparison or the subharmonic method.[30] The method is illustrated

in Figure 4.14. The sinusoidal commands are compared with a carrier whose frequency (f_{tri}) is

several times greater than the frequency of the command (f_1, called the modulating frequency).

The error is fed to a zero- hysteresis comparator to generate the switching signal. The first

important characteristic is that the switching frequency is fixed by the carrier. The second is that

the amplitude of the fundamental output (V_1) is linearly proportional to the ratio of the amplitude

of the reference (V_{ref}) to the amplitude of the carrier (V_{tri}). The ratio is called the *amplitude*

modulation index (m_a) and is given by Equation (4.2). The maximum possible amplitude is

therefore equal to V_{DC}.

$$V_1 = m_a \cdot V_{DC} \tag{4.1}$$

$$m_a = \frac{V_{ref}}{V_{tri}} \tag{4.2}$$
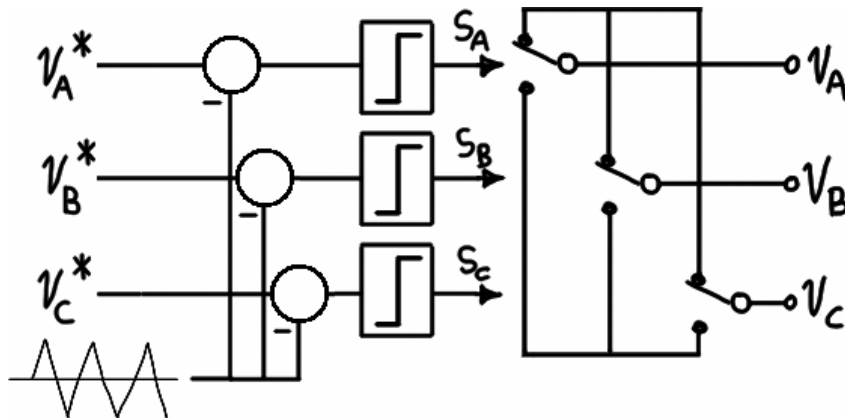
Figure 4.14 – Sine-triangle PWM.

Clearly the output will contain harmonics in addition to the desired fundamental frequency.

Harmonic components at multiples of the *modulating frequency* are called *baseband harmonics*

[70, p.103]. These are the low-order harmonics dealt with throughout this report that are

undesirable in normal sinusoidal operation because they produce the familiar *harmonic distortion*.

---
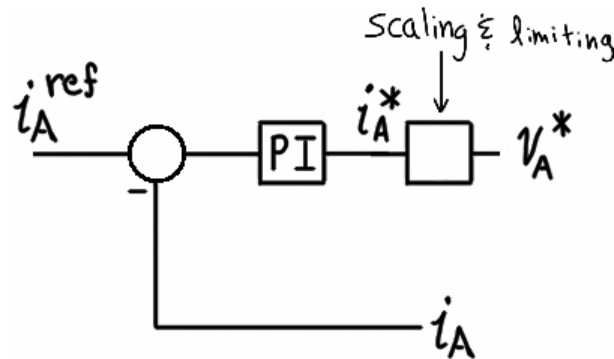
[30] The author does not claim any knowledge regarding the implementation of PWM in real designs. There are several fundamental aspects with which the author is unfamiliar, such as the distinctions between *naturally sampled* and *regularly sampled* PWM, triangle and sawtooth carriers, *symmetrical* and *asymmetrical sampling*, and *single-* and *double-edge modulation*, and the performance differences between analog and digital implementations, among others. The author does not claim that the version of sine-triangle PWM shown here is used in practice. (According to one reference, "The major [non-SV] modulation strategies for a VSI are analog natural sampled sine-triangle PWM [and] regular sampled PWM…" [70, p.337].) It is obvious that *some* form is used and the method given here is used only as an illustration of the concept and for comparison to SVM.

There are also the harmonics associated with the carrier frequency f_{tri}. These are the *carrier harmonics* and their *sidebands*, which we will lump together and call the *switching harmonics*. The spectrum of switching harmonics is governed by the frequency modulation ratio defined by Equation (4.3) [67], [75]. In this report, "harmonics" is generally used to refer to the baseband harmonics; switching harmonics are not discussed further.

$$m_f = \frac{f_{tri}}{f_1} \tag{4.3}$$
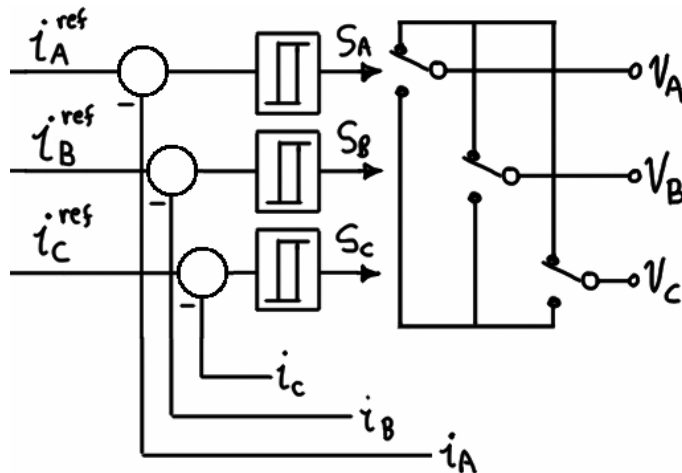
At the most basic level (shown in Figure 4.14) the sine-triangle PWM it is an open-loop scheme; in other words, it functions as a controlled voltage source. The usual way to make it closed-loop is to generate the voltage command by closing the loop around current; closed-loop current control of voltage converters is the most commonly used method [124]. The result is called a *current-regulated PWM* (CRPWM) *inverter* and it functions as a controlled current source. There are essentially three groups of methods that can be used to make a CRPWM [78, p.322]. The first method is to use some sort of ramp-comparison controller. The simplest example of this type is shown in Figure 4.15. When the reference and feedback signals are phase variables, this method has the disadvantage that the current ripple is fed back into the command [125] and usually use filtering [162] which would limit the bandwidth and stability [47]. Further the tuning of the regulator is dependent on the frequency of operation. However, these problems are limited can be eliminated by executing control in the synchronous reference frame (discussed in a later section).

Figure 4.15 – Ramp-comparison current regulator for one phase.

The second method to make a CRPWM is to use a bang-bang controller with hysteresis (also called *tolerance band* controller) [75, p.241], [61, p.243], [80, p.252]. In this method the carrier is eliminated and the switching signals are generated directly by feeding the current error to a comparator with hysteresis, as shown in Figure 4.16. The advantages of this method are that it is simple, it inherently compensates for dead-time distortion, it has excellent disturbance rejection,

and it offers the fastest dynamic response of any current controller [62, pp.30-31,93]. The chief disadvantage is that the switching frequency is not constant throughout an electrical cycle it varies depending on the load type and the shape of the reference waveform. Another disadvantage is that independent control of the three phases is not possible (Appendix D) thus "phase-interference minimization" control strategies are required to prevent errant behavior [132], which can include limit cycles [78, p.326]. There are methods to mitigate switching frequency variation ([62, p.31], [43, p.752]) or achieve constant switching frequency [132]. Hysteresis regulation is in use in some areas [78, p.324] but at this time hysteresis control is not widely in brushless motor control applications. A third class of CRPWMs are the *predictive* (and/or *dead-beat*) methods [43, p.751] that rely on a load model. As far as this report is concerned, those methods will be lumped with on-line optimization methods; neither are discussed here.
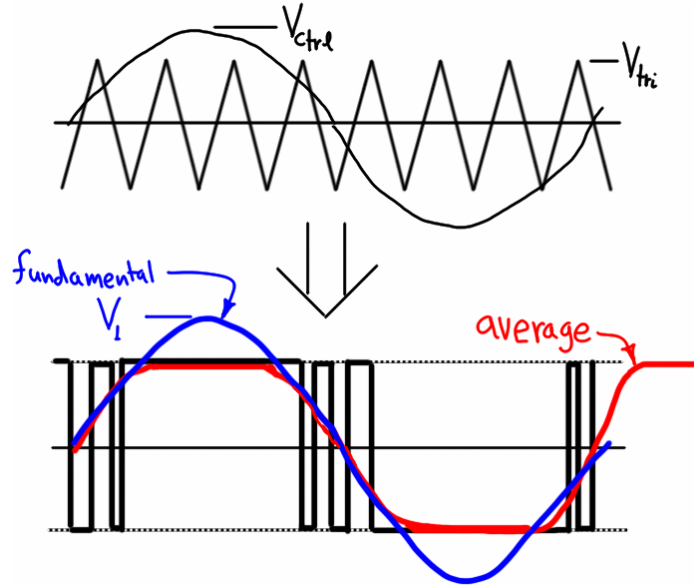
Figure 4.16 – Hysteresis CRPWM.

In the sine-triangle inverter it is possible for the reference value to be greater than peak value of the carrier; this causes the inverter to saturate over the peaks of the reference, as shown in Figure 4.17.[31] This causes harmonics to be produced as the average waveform deviates from sinusoidal. At the same time, the amplitude of the fundamental of the average waveform produced becomes larger than the amplitude of the sinusoidal output when no harmonics are generated (normal operation, when the reference amplitude is less than that of the carrier). In a properly designed SPWM controller the reference would be clamped so that saturation would not occur and harmonics would not be generated. However if the harmonics can be tolerated in exchange for the larger fundamental amplitude, the inverter could be designed to operate in this mode, which is

---
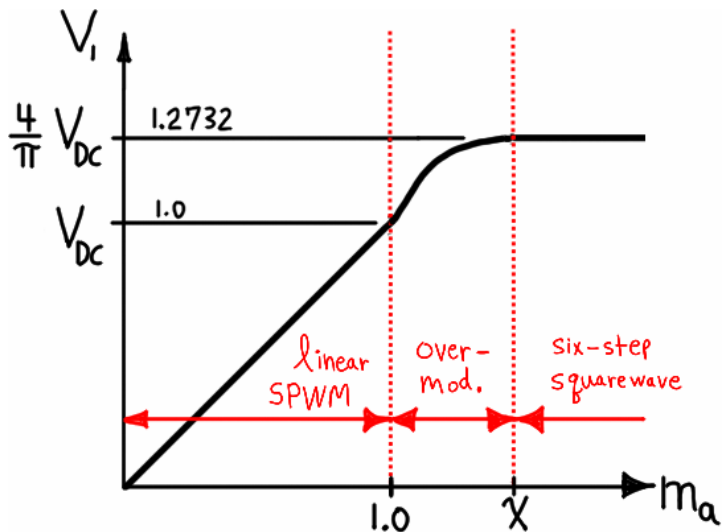
[31] This can happen in the hysteresis CRPWM as well but in that case it is an uncontrollable saturation, whereas the sine-triangle PWM the controller can prevent this from occurring, or command it to occur if desired.

called the *overmodulation region* (also called the *pulse-dropping region* because transitions that were previously present are "dropped" from the pulse train).

Figure 4.17 – Overmodulation in carrier-based SPWM; not to scale.

When operating in the overmodulation region the relationship between the reference amplitude and the fundamental of the output is no longer linear. Further, in examining Figure 4.17 it is clear that when the reference amplitude is made large enough the pole voltage will become a squarewave. In that case the inverter is operating exactly the same as the 180° six-step squarewave inverter presented earlier. Therefore the operation of the inverter can be divided into three regions or modes. These modes and a plot of the amplitude of the fundamental output voltage as a function of the modulation index are shown in Figure 4.18. The shape of the curve in the overmodulation region and the value of the modulation index (marked x) at which the inverter operates in six-step squarewave mode depend on the frequency modulation ratio m_f. The literature describes a host of different schemes to handle the nonlinearity of m_a in the overmodulation region and the transition between regions. In this report only the linear region of PWM inverters is of concern.

Figure 4.18 – Fundamental gain and operating modes of carrier-based SPWM.

It must be noted that the definition of the modulation index defined by Equation (4.2) (which is reflected in Figure 4.18) could be defined differently. If the inverter was restricted to the linear region of SPWM (no output harmonics) it would make the most sense to use the definition given because the maximum output of the inverter would correspond to a modulation index of unity. However, if operation in the overmodulation region is allowed (and only the fundamental component is of interest) then the modulation index could be defined to be unity at six-step operation by scaling it to the fundamental of the squarewave (SPWM would then correspond to $(\pi/4)V_{DC}$). Further, the modulation index could be defined by replacing V_{DC} in Equation (4.1) with V_{BUS} (SPWM would then correspond to $(1/2)V_{BUS}$). Or, the peak amplitude in Equation (4.1) could be replaced with the RMS value and either value could be described in terms of line-line voltage instead of line-neutral voltage. Obviously there are many possible definitions for the modulation index and a variety of these permutations are indeed found in the literature. For example, one common choice is to use line-line RMS values referenced to V_{BUS}; in this case, the SPWM linear limit is given by $1 \cdot \sqrt{3} \cdot (1/\sqrt{2}) \cdot (1/2) = 0.6124 V_{BUS,LL,RMS}$.

Triplen Harmonic Injection

Since the PWM inverter produces output signals centered about the DC bus midpoint, the maximum value of the terminal voltage is obviously limited to the voltage at the rail (V_{DC}), where the voltage drop across the switches is ignored for clarity. If harmonics cannot be tolerated (only a fundamental component is desired) the inverter restricted to SPWM operation and the maximum amplitude is V_{DC}; this is called the linear SPWM limit. If harmonics are allowed the inverter can be operated up to squarewave mode which gives a fundamental of amplitude

175

$(4/\pi)V_{DC} \approx 1.2732 V_{DC}$.[32] As with the harmonics involved in armature windings and rotor fluxes (Appendix C), the squarewave represents some type of physical maximum and if we cannot allow harmonics we must settle for a fundamental whose amplitude is less than this maximum. The "natural" limit for SPWM was thought to be $1.0 V_{DC}$ as shown. Then it was realized that this range could be extended for certain three-phase loads by intentionally introducing triplen harmonics into the reference signal. Most references claim this was first done by King in 1974 [129] or Buja in 1975 [130].

The method is based on the fact that adding an amount of the third harmonic to a fundamental sinusoid flattens the top significantly and lowers its *peak value*, as shown in Figure 4.19. The *fundamental* of this waveform is obviously unchanged, however. The $1.0 V_{DC}$ limit exists because the inverter cannot synthesize a waveform with a peak value greater than $1.0 V_{DC}$.
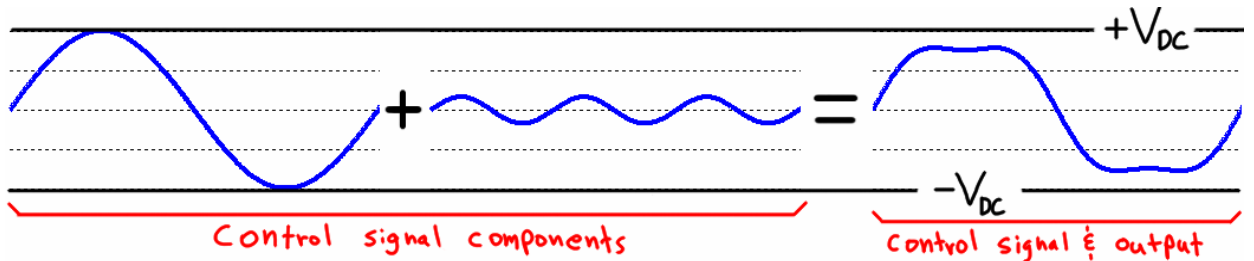
Figure 4.19 – Adding the third harmonic reduces peak amplitude.

If the same fundamental can be produced by a signal whose amplitude is less than $1.0 V_{DC}$, we could then increase the magnitude until this output signal is at the $1.0 V_{DC}$ limit of the inverter, as shown in Figure 4.20.
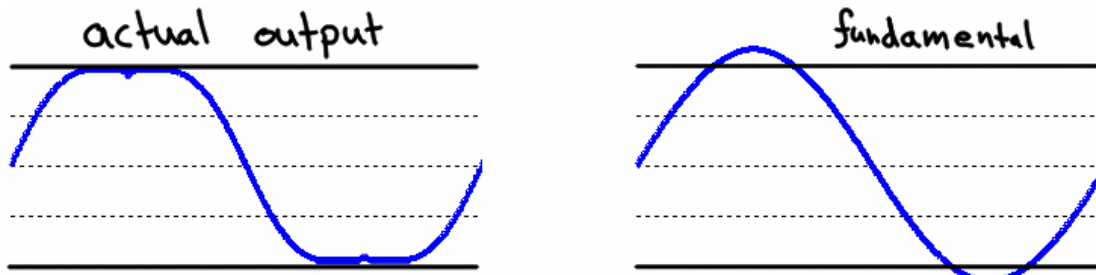
Figure 4.20 – Third harmonic injection can produce larger fundamental than SPWM.

---

[32] This is the fundamental of the pole voltage, which is a squarewave. The squarewave contains a ZS component and this component of the neutral voltage is absent in the phase voltage. Since only the phase voltage can drive a current through the load, we should compute the fundamental from the phase voltage waveform. In doing so one will find the same value.

In the literature this is called *third-harmonic injection* or *zero-sequence* injection; this report prefers the term *triplen harmonic injection* (THI). Only the third harmonic has been discussed so far but higher triplens are also used. THI produces a maximum fundamental voltage of $2/\sqrt{3}V_{DC} \approx 1.1547V_{DC}$. If the only advantage of THI was to obtain a larger fundamental component it would not be of much value because the largest fundamental component is produced by squarewave mode. The defining merit in THI is that only the triplen harmonics are used. As shown in Appendix D, the triplen voltage harmonics (which are zero-sequence) appear in the neutral of a wye-connected load. Therefore it does not matter what magnitude of which triplen harmonic we add, the line-neutral voltage of the load will not be affected. Similarly, the line-line voltage does not contain triplen harmonics so the technique is applicable to delta-connected loads as well, but it would cause a short circuit in a grounded-wye load.

The amplitude of the third harmonic that should be added is debated. Analytically the value is determined to be 1/6 [127], [70, pp.226-9], but a value of 1/4 is thought to have benefits [70, p.229]. The optimum value is not of interest here—we are only interested in the phenomenon. More importantly, there are numerous advanced modulation techniques that are capable of attaining this same $2/\sqrt{3}$ gain in fundamental amplitude (SVM is one of them) but each technique relies on the same principle (that triplen harmonics reduce the peak value but do not affect phase-neutral load voltages). It should be noted that *any* quarterwave symmetric signal with a fundamental frequency that is three times the modulating frequency (f_1) is a ZS signal; as such, it may be used to implement THI. For example, a squarewave has harmonics (1, 3, 5, 7, 9, 11, …) but since these are at triple-frequency the harmonics are (3, 9, 15, 21, 27, 33, …) which are all triplen harmonics.

Finally, in the same way that the modulation index could be referenced to the amplitude of the fundamental output in six-step squarewave mode, it could similarly be referenced to the maximum output of a THI inverter.

Space Vector Modulation (SVM)

The overview of VSIs discussed three common methods of controlling an inverter (six-step squarewave, six-step PWM, and PWM). The first two had an algorithm-like nature. In both cases the inverter could be in only one of six valid commutation states and operation of the inverter consisted of cycling through the states in order; the second case simply added PWM to control the magnitude. The third method (PWM) was somewhat different because it was concerned with producing arbitrary output voltages (usually sinusoidal) without any commutation states. SVM is somewhat of a combination of the first two methods' algorithm-like nature and the third method's ability to generate an arbitrary output voltage. SVM is simply a method of controlling the inverter as a whole. It seems to have been presented first by van der Broeck, et al. [133], though [131] is often cited as well.

States and Neutral Voltage

SVM is a 180° control method therefore it is best compared to the other 180° methods and the 120° methods are not discussed. In the 180° inverter each leg must have one transistor on at any given time (again ignoring the dead-time between leg transistor switching). Thus the pole voltage for each phase will be either high (H) at $+V_{DC}$ or low (L) at $-V_{DC}$. Since there are three legs and each can have only two states, the inverter will be in exactly one of $(2^3 = 8)$ discrete states at any given time. The states can be numbered and are given by Table 4.1.

Table 4.1 – States and corresponding pole voltages of 180° inverter.

inverter state	leg state			pole voltage		
	S_A	S_B	S_C	v_A	v_B	v_C
S0	L	L	L	$-V_{DC}$	$-V_{DC}$	$-V_{DC}$
S1	**H**	L	L	$\mathbf{+V_{DC}}$	$-V_{DC}$	$-V_{DC}$
S2	**H**	**H**	L	$\mathbf{+V_{DC}}$	$\mathbf{+V_{DC}}$	$-V_{DC}$
S3	L	**H**	L	$-V_{DC}$	$\mathbf{+V_{DC}}$	$-V_{DC}$
S4	L	**H**	**H**	$-V_{DC}$	$\mathbf{+V_{DC}}$	$\mathbf{+V_{DC}}$
S5	L	L	**H**	$-V_{DC}$	$-V_{DC}$	$\mathbf{+V_{DC}}$
S6	**H**	L	**H**	$\mathbf{+V_{DC}}$	$-V_{DC}$	$\mathbf{+V_{DC}}$
S7	**H**	**H**	**H**	$\mathbf{+V_{DC}}$	$\mathbf{+V_{DC}}$	$\mathbf{+V_{DC}}$

Of the eight states there are two states (S0 and S7) that result in zero voltage across any two phase terminals; these two states are called *null states* and the other six are the *active states*. In any active state one (two) phases will be high and two (one) will be low, therefore the neutral

voltage will be below (above) the bus midpoint by $(1/3)V_{DC}$. In the null states the neutral voltage will either be high or low $\left(+V_{DC} \text{ or } -V_{DC}\right)$. This is summarized in Figure 4.21.
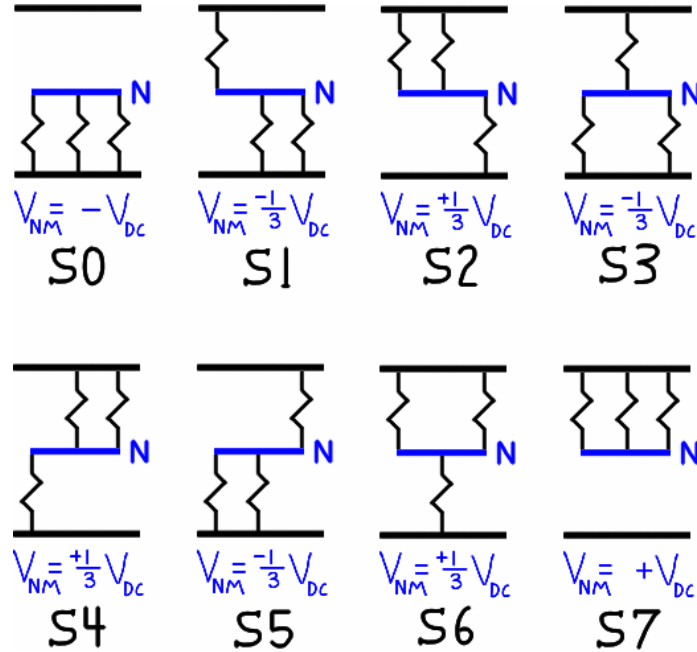
Figure 4.21 – Inverter states and neutral voltages.

The nonzero neutral voltage can be viewed from a bus perspective as being the result of voltage-divider action, or it can be viewed from the load neutral perspective as being the result of averaging the three terminal voltages. The latter viewpoint will be adopted because it emphasizes the fact that the neutral voltage is the common-mode voltage as shown by Equation (4.4).

$$v_{NM} = \frac{1}{3}\left(v_{AM} + v_{BM} + v_{CM}\right) \tag{4.4}$$

Recall the voltage relationships for an isolated neutral load connected to a three-phase source. This is given by Equation (4.5) and is summarized in Figure 4.22 (only phase-A is shown for clarity).

$$v_{AM} = v_{AN} + v_{NM} \quad \Leftrightarrow \quad v_{AN} = v_{AM} - v_{NM} \tag{4.5}$$
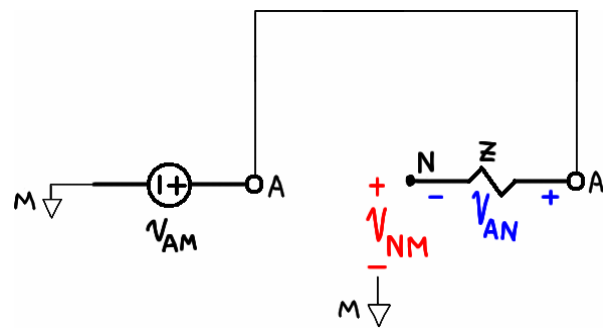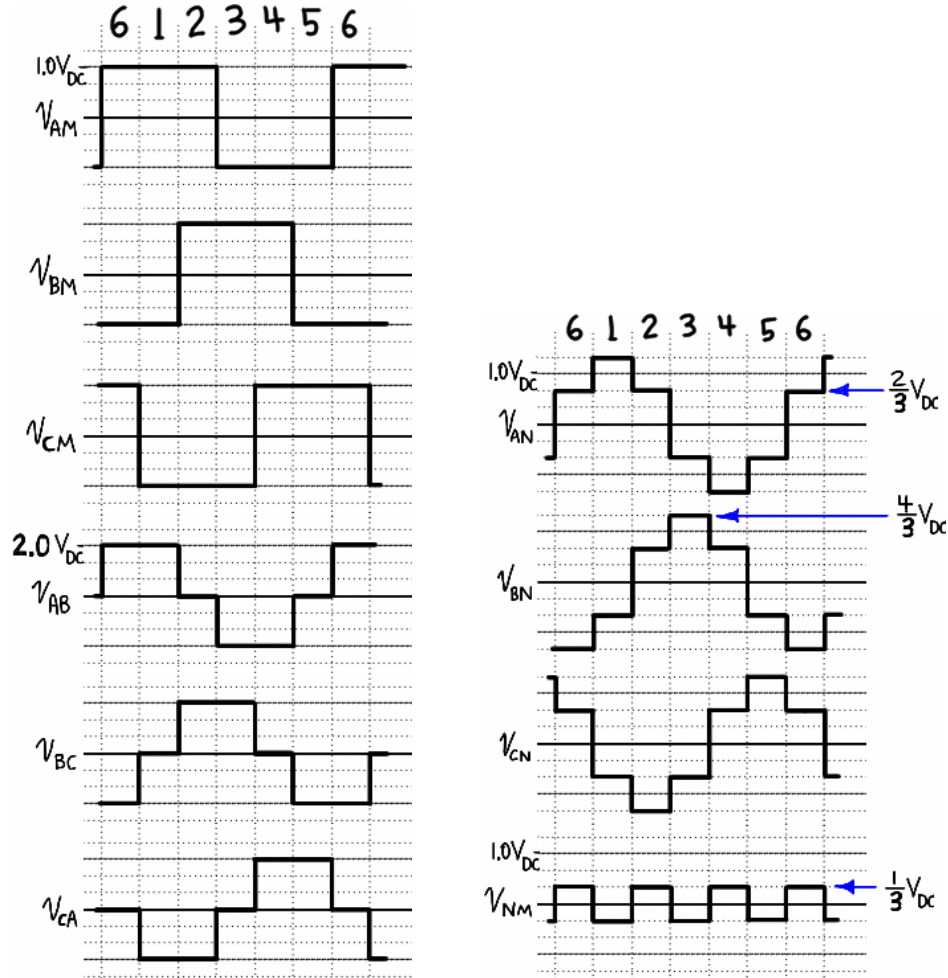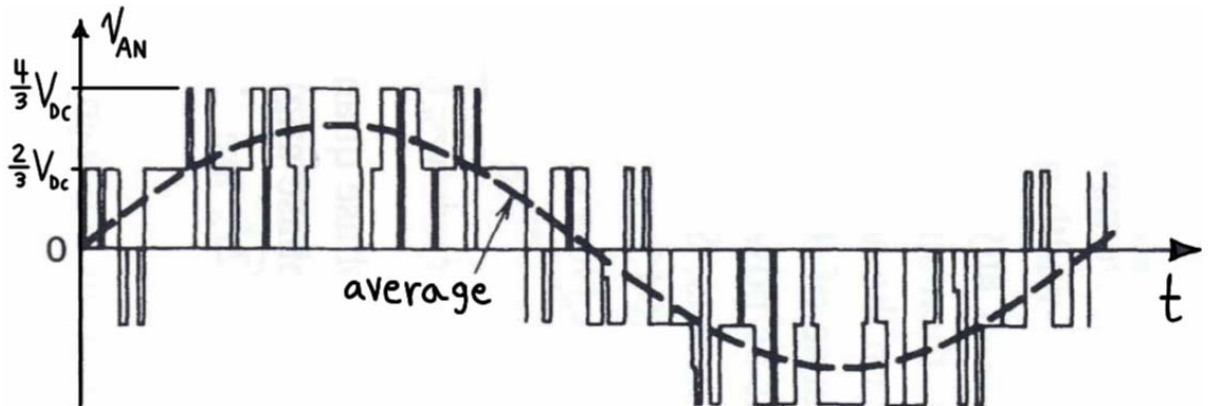
Figure 4.22 – Voltage relationships.

Return to the 180° six-step squarewave inverter. The voltage waveforms were given in an earlier figure that is now redrawn as Figure 4.23 with the states indicated.

Figure 4.23 – Voltage waveforms for 180° six-step squarewave inverter.
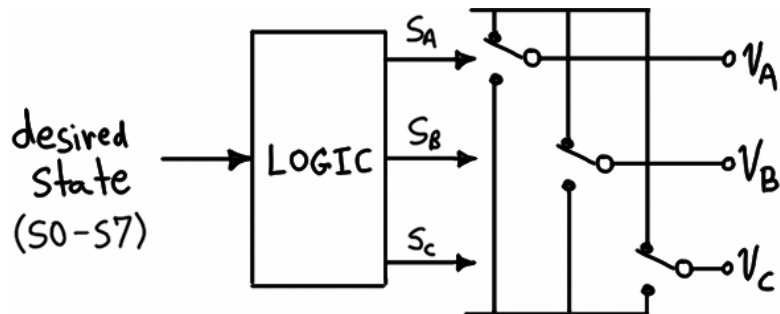
First, it is easily verifiable that the neutral voltage waveform is given by Equation (4.4). Next, it is clear that the phase (line-neutral) voltage waveforms are given by Equation (4.5). What is so interesting about the 180° inverter is that by definition the instantaneous neutral voltage is always nonzero (equivalently, the output voltages always contain an *instantaneous* common-mode component), yet the same inverter can naturally produce balanced three-phase sinusoids (which by definition have no ZS component and therefore, no neutral voltage). But the sinusoidal voltages (or any other $\Sigma = 0$ waveforms) only exist as an average (equivalently, the instantaneous voltages are integrated to produce a sinusoidal current). Therefore, the inverter synthesizes these waveforms by controlling the amount of time spent in each state such that the average neutral voltage is zero. Figure 4.24 shows the line-neutral voltage for phase-A.

Figure 4.24 – Instantaneous phase-A line-neutral voltage in SPWM inverter.

(Modified from [73, p.233].)

In the PWM inverter each phase leg was controlled separately by either reference-carrier comparison or hysteresis. A SVM inverter treats the inverter as one unit. Rather than controlling each leg in an attempt to command an average phase voltage, the SVM inverter is controlled simply by selecting which of the eight states is desired. This concept is symbolized in Figure 4.25.

Figure 4.25 – Direct selection of inverter state.

Obviously some high-level control will be necessary to determine how to time-average the correct states in order to synthesize the desired output waveforms; this will be developed in later subsections.

Space Vectors, Magnitudes, and Trajectories

The output of the inverter is usually studied by plotting the phase voltage as a function of time. Using SV theory allows a more compact representation of the inverter output. SV theory can also be used to control using the concept of Figure 4.25; the result is SVM. Before examining SVM it is necessary to study the inverter output voltages in terms of complex αβ0 components and to study the trajectories of various SVs.

Taking the αβ0 transform (Appendix D) of the pole voltages in Table 4.1 allows the inverter states to be written in terms of complex components as shown in Table 4.2, where $k = c = 2/3$ is used to achieve magnitude invariance. (The αβ0 transform (rather than the Clarke or SV transforms) must be used because the three-phase voltages produced by each inverter state contain a ZS component, as clearly evidenced by the 0-column in Table 4.2.)

Table 4.2 – Inverter states (pole voltages) expressed in complex components; k=c=2/3.

inverter state	pole voltage components		
	α	β	0
$\overrightarrow{S0}$	0	0	-1
$\overrightarrow{S1}$	$4/3$	0	$-1/3$
$\overrightarrow{S2}$	$2/3$	$2/\sqrt{3}$	$+1/3$
$\overrightarrow{S3}$	$-2/3$	$2/\sqrt{3}$	$-1/3$
$\overrightarrow{S4}$	$-4/3$	0	$+1/3$
$\overrightarrow{S5}$	$-2/3$	$-2/\sqrt{3}$	$-1/3$
$\overrightarrow{S6}$	$2/3$	$-2/\sqrt{3}$	$+1/3$
$\overrightarrow{S7}$	0	0	$+1$

The α- and β- components of the voltages in Table 4.2 are space vectors and may be plotted in the αβ plane, as shown in Figure 4.26. Since these are the only possible states of the inverter at any instant, they will be called the *base SVs*. As usual, any time we work with the SV we are working with its projection of the three phase variables onto the αβ plane and the ZS component (which is orthogonal to the αβ plane) thus cannot be seen in the figure.
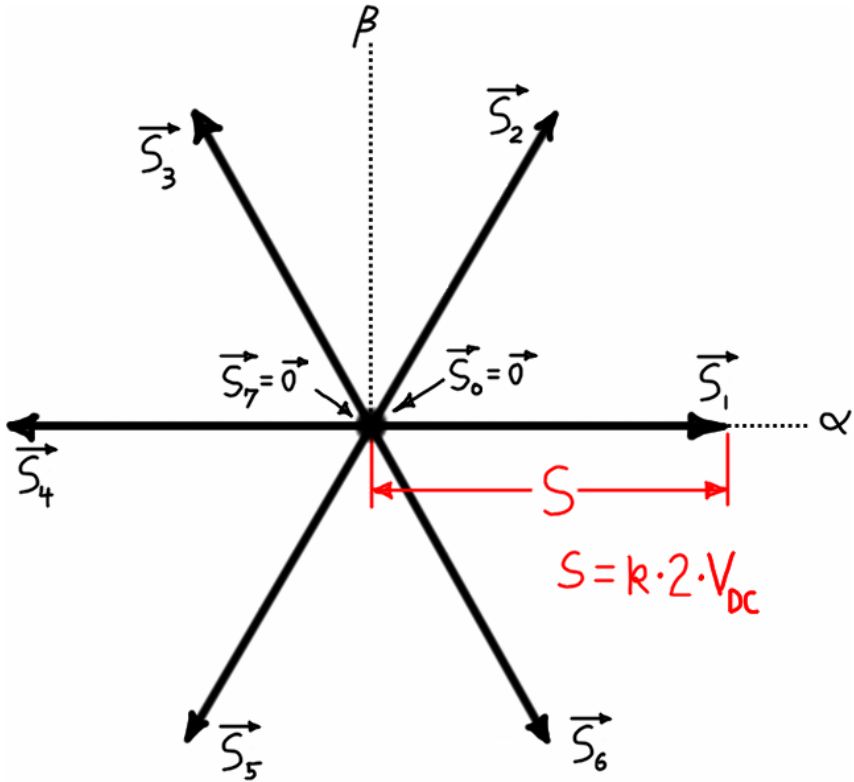
Figure 4.26 – Base SVs showing the states of a 180° inverter.

The values in Table 4.2 are for $k = 2/3$ such that they will be magnitude invariant. Since the values in Table 4.2 were computed from the voltages in Table 4.1 (which were peak line-neutral voltages specified in terms of V_{DC}), the SVs have magnitude $\left|\vec{S}_i\right| = (4/3)V_{DC}$. Now compare Figure 4.26 with Figure 4.23. For state S1, $\overrightarrow{S1}$ has a magnitude of $\left|\vec{S}_i\right| = (4/3)V_{DC}$ and it is seen that the phase-neutral voltage of phase-A has the same magnitude. This seems to make sense because $k = 2/3$ yields a magnitude-invariant SV. But the values in Table 4.2 (hence the magnitude of the SVs in Figure 4.26) were computed from the pole voltages in Table 4.1, not the phase voltages. Why then do the SV magnitudes match the phase voltages? The reason is that the SV (the α- and β- components) cannot contain a ZS component. By definition (Equation 4.5 and Appendix D) each pole voltage is composed of a phase voltage (which cannot contain a ZS component) and the neutral voltage (which consists of *only* the ZS component). Since the SV can only contain the non-ZS component, taking the SV transform of the pole voltages produces the same result as taking the SV transform of the phase voltages; *in either case, the resulting SV will represent the phase voltages*. Since the only difference is the ZS term, we should be able to see this using the αβ0 transform. The αβ0 transform of the *pole* voltages were given as Table 4.2; the ZS terms are clearly present. Now the αβ0 transform of the *phase* voltages is given below in
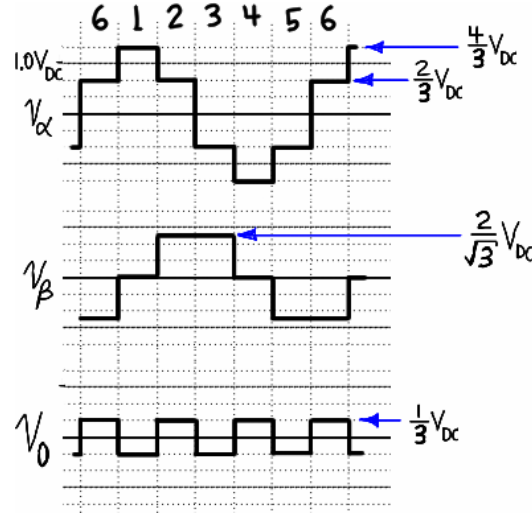
Table 4.3; there are no ZS terms present. There are a number of conclusions to be drawn, but the simplest is to recognize that by using the Clarke or SV transform, we are ignoring the ZS component, therefore it does not matter whether we transform the pole or phase voltages because they differ only by the ZS component.

Table 4.3 – Line-neutral voltages expressed in complex components.

Inverter state	voltage components		
	α	β	0
$\vec{S0}$	0	0	0
$\vec{S1}$	$4/3$	0	0
$\vec{S2}$	$2/3$	$2/\sqrt{3}$	0
$\vec{S3}$	$-2/3$	$2/\sqrt{3}$	0
$\vec{S4}$	$-4/3$	0	0
$\vec{S5}$	$-2/3$	$-2/\sqrt{3}$	0
$\vec{S6}$	$2/3$	$-2/\sqrt{3}$	0
$\vec{S7}$	0	0	0

In six-step squarewave operation (at a constant frequency) the inverter spends an equal amount of time in each of the states. The projection onto the **α-** and **β-** axes is plotted against time in Figure 4.27. Taking the inverse αβ0 transform of the waveforms in Figure 4.27 yields exactly the _pole_ voltage waveforms in Figure 4.23. Taking the inverse Clarke transform (i.e., the inverse αβ0 transform with empty 0-components) of the waveforms in Figure 4.27 yields exactly the _phase_ voltage waveforms in Figure 4.23. If the reader is uncertain as to why this is, consult Appendix D before re-reading this subsection.

Figure 4.27 – Transformed voltage waveforms for six-step 180° squarewave inverter.

From Appendix D we already know the SV cannot contain (encode) any ZS component; what has been illustrated here is that when the output of the inverter is represented as a SV, that SV is only showing us the non-ZS component—and for a wye-connected load, this is equal to the phase (line-neutral) voltages. Since the ZS component adds in the neutral and does not affect the load anyhow, this is particularly handy because it allows us to continue to use the two-dimensional SV plots we normally work with. However, when we need to examine the details (such as this discussion of the connection between SVM and six-step squarewave) it is obvious that we cannot ignore the ZS component. We will return to dealing with the ZS component in a later subsection; right now the study of the SV magnitude and trajectories will be resumed.

Chapter 3 derived the SV corresponding to balanced sinusoidal waveforms. Supposing those sinusoidal waveforms are produced by an inverter, the corresponding SV would be given by Equation (4.6). As with the above tables and SV diagram, our SV definition must take into account that the inverter output is given as a peak, line-neutral voltage specified in terms of V_{DC}.

$$\vec{v} = k\frac{3}{2}V_{DC}e^{j\omega t} \tag{4.6}$$

For $k = 2/3$ the SV has a constant magnitude of $\hat{V} = V_{DC}$, which is the maximum amplitude sinewave that can be generated using an SPWM inverter. Obviously the trajectory of this SV is a circle of radius V_{DC}; its projection will give **α**- and **β**- components that are sinusoidal; the inverse SV transform of those projections yield the original sinusoidal phase-variables, as we have already seen. If THI is used the maximum possible amplitude of the fundamental is $2/\sqrt{3}$ times

as large as that for regular SPWM, thus for $k = 2/3$ the SV would have a magnitude of $\hat{V} = (2/\sqrt{3})V_{DC}$ and trace a circle just as in SPWM. Finally, in six-step squarewave mode we saw that the "time history" of the SV consisted of discrete points (the SVs corresponding to the six active inverter states). When the projections onto the αβ plane are plotted against time and transformed back to phase variables the familiar six-step pattern appeared. But we know the *fundamental* of the output voltage in this mode has an amplitude of $(4/\pi)V_{DC}$ thus the SV representing this *fundamental* would have a magnitude of $\hat{V} = (4/\pi)V_{DC}$ for $k = 2/3$. The results of our investigation into magnitudes and trajectories are summarized by the diagram shown in Figure 4.28.
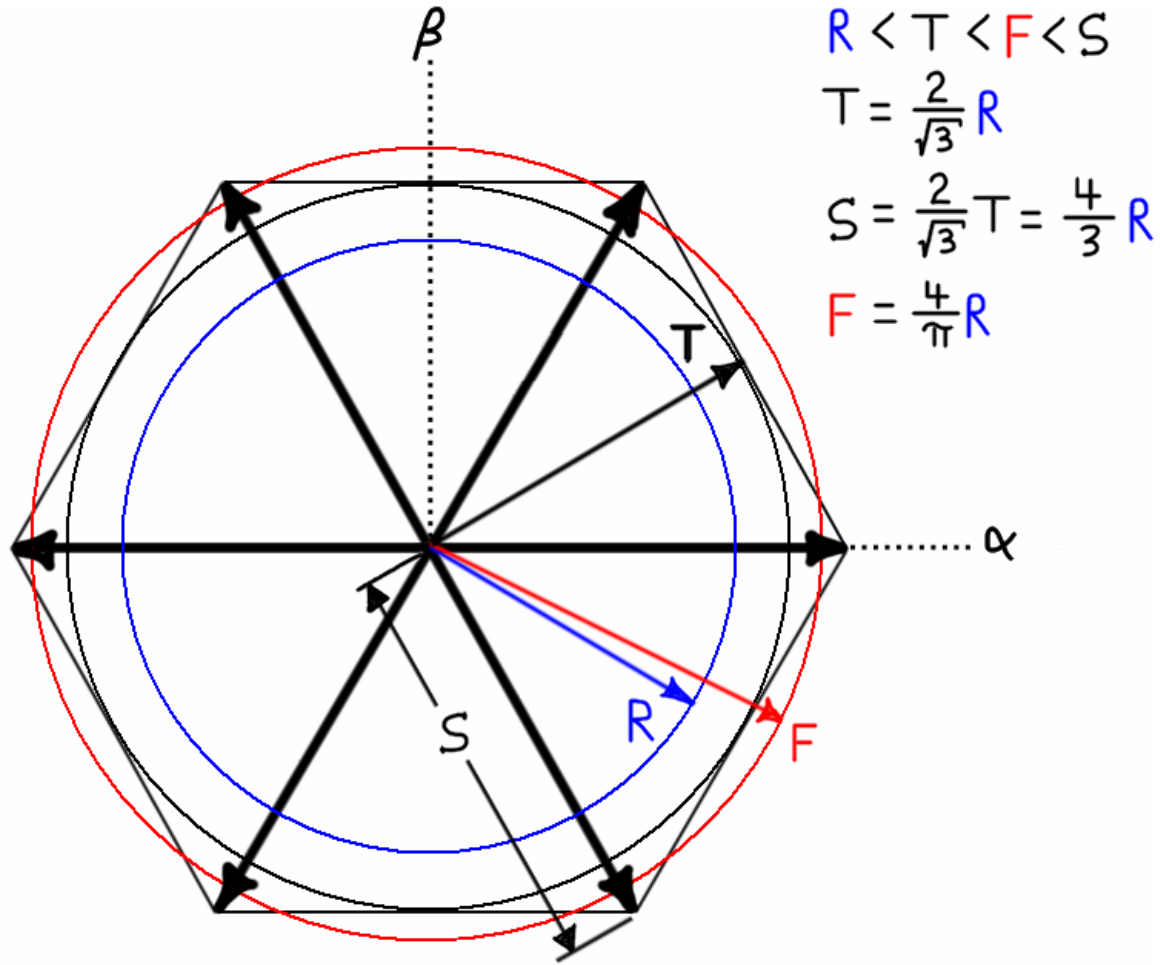
Figure 4.28 – Magnitudes and trajectories of some important SVs.

There are three circular trajectories shown: the SPWM linear limit (R, blue), the THI linear limit (T, black), and the maximum *fundamental* of six-step squarewave mode (F, red). In addition, the magnitude of the base SVs (corresponding to the six active states of the inverter) is shown (S); since six-step squarewave mode consists of stepping through these active states, the base SVs

also correspond to six-step squarewave operation. The relative magnitudes of the circular trajectories are given; these directly follow from the above discussion. It is crucial to understand that the only reason a comparison of these magnitudes makes any sense is that each space vector has been *defined* as describing the same type of quantity, relative to the same reference, in the same unit of measurement. In this case, the quantity is a peak voltage, the reference is the bus midpoint M (thus these are line-neutral voltages), and the unit of measurement is the fraction of V_{DC}. The relationships shown in the figure hold regardless of how we specify a SV, but it is clear that all SVs must be defined in exactly the same way in order to compare them on the same diagram. For this reason it is nearly impossible to decipher literature written in terms of space vectors unless this concept is understood well. One does not have to look far in the literature to find a surprising number of conventions used. Table 4.4 is provided to reconcile these different definitions. The boldface lines show the definition used in this report (peak, L-N, V_{DC}). In this report, k is often left explicit to aid understanding but when working with inverters, $k = 2/3$ is generally chosen.

Table 4.4 – Magnitude of space vectors of three-phase quantities.
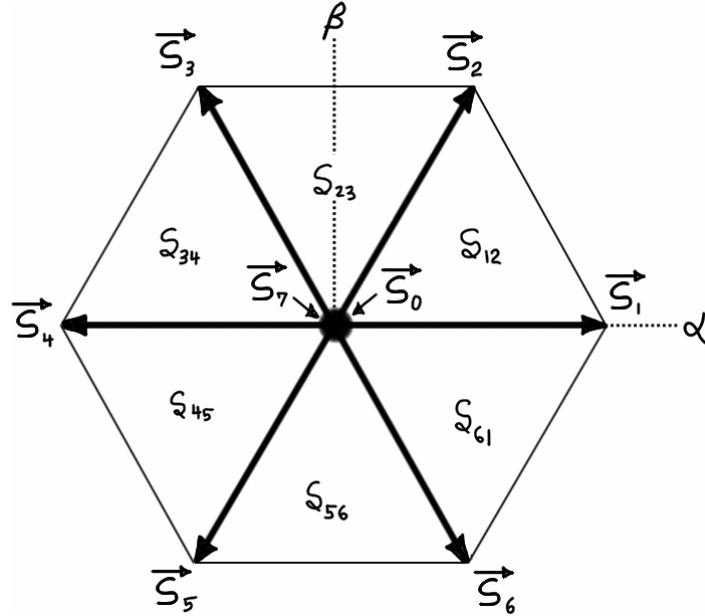
| | | | | maximum radius of SV trajectory for continuous balanced three-phase sinusoids in steady state | | | magnitude of discrete SV |
| | | | | Regular SPWM | Triplen harmonic injection (THI) | Fundamental of 180° six-step | 180° base SV |
				R	T	F	S
PEAK	L-N	V_{DC}	k=1	1.5000	1.7321	1.9099	2.0000
			k=2/3	**1.0000**	**1.1547**	**1.2732**	**1.3333**
			k=√(2/3)	1.2247	1.4142	1.5594	1.6330
		V_{BUS}	k=1	0.7500	0.8660	0.9549	1.0000
			k=2/3	0.5000	0.5774	0.6366	0.6667
			k=√(2/3)	0.6124	0.7071	0.7797	0.8165
	L-L	V_{DC}	k=1	2.5981	3.0000	3.3080	3.4641
			k=2/3	1.7321	2.0000	2.2053	2.3094
			k=√(2/3)	2.1213	2.4495	2.7009	2.8284
		V_{BUS}	k=1	1.2990	1.5000	1.6540	1.7321
			k=2/3	0.8660	1.0000	1.1027	1.1547
			k=√(2/3)	1.0607	1.2247	1.3505	1.4142
				R	T	F	S
RMS	L-N	V_{DC}	k=1	1.0607	1.2247	1.3505	1.4142
			k=2/3	0.7071	0.8165	0.9003	0.9428
			k=√(2/3)	0.8660	1.0000	1.1027	1.1547
		V_{BUS}	k=1	0.5303	0.6124	0.6752	0.7071
			k=2/3	0.3536	0.4082	0.4502	0.4714
			k=√(2/3)	0.4330	0.5000	0.5513	0.5774
	L-L	V_{DC}	k=1	1.8371	2.1213	2.3391	2.4495
			k=2/3	1.2247	1.4142	1.5594	1.6330
			k=√(2/3)	1.5000	1.7321	1.9099	2.0000
		V_{BUS}	k=1	0.9186	1.0607	1.1695	1.2247
			k=2/3	0.6124	0.7071	0.7797	0.8165
			k=√(2/3)	0.7500	0.8660	0.9549	1.0000

It should be pointed out that there is no such thing as an "RMS magnitude" of a SV, as shown in the lower right-hand corner of the table. However, once the choice for the SV definition is defined, *all* SVs must use the same reference, including the base SVs, thus it is listed in the table. It is not uncommon to see an RMS definition used in the literature (especially RMS, L-L, V_{BUS}, $k = \sqrt{2/3}$).

Space Vector Averaging and Overmodulation
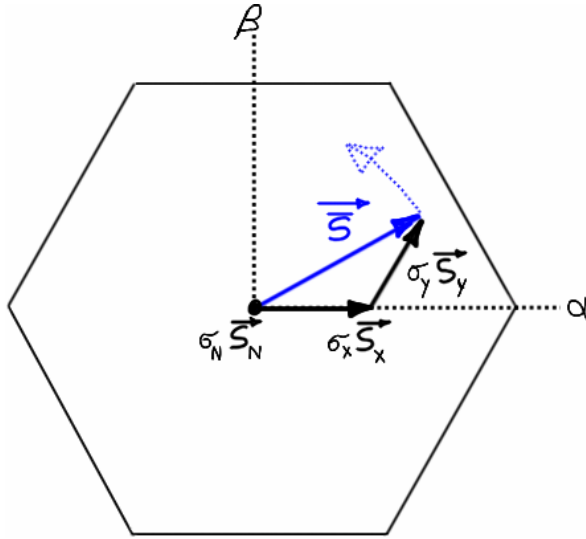
Three important points from before are now summarized: the 180° inverter can be in only one of eight states (represented base SVs) at any given time (Figure 4.26), there is a precise relationship between each base SV and the pole voltages it produces (Table 4.2), and it is possible to control the inverter by commanding which state it should be in (Figure 4.25). If the reader has not already deduced, a SVM inverter rapidly switches between different inverter states (base SVs) such that the vectorial time-average of the asserted base SVs is equal to the commanded voltage (which

was fed to the SVM inverter as a SV). The SVM inverter is a 180° inverter with the same allowable states as a PWM inverter. SVM is simply a method of controlling the inverter as a whole rather than controlling each phase leg independently. Even though the method of control is radically different, it is still a pulse width modulator and for this reason it is sometimes called space vector PWM (SVPWM). Figure 4.28 is redrawn as Figure 4.29 without the circular trajectories shown and the sextants have been labeled.

Figure 4.29 – Base SVs.

The figure shows all the possible SVs but of course, only one SV can be asserted at one time. In SVM, one base SV is asserted for a period of time, another for a different period of time, and so on. There are different implementations but there are two obvious minimum requirements. First, the only way to synthesize a time-average SV is to switch between two active base SVs. Second, the only way to control the magnitude of the synthesized time-average SV is to switch between null and active base SVs. Thus the general SVM algorithm is to switch between two active and at least one null base SVs during one switching period. Like regular PWM, the switching period may be selected arbitrarily, although there are many practical limits. The SVM synthesis of a time-average SV $\vec{\bar{S}}$ is shown in Figure 4.30. Simple as it is, the figure is somewhat deceiving. It shows the time-average SV $\vec{\bar{S}}$ as being composed of two vectors aligned with the base SVs. But the two shorter SVs do not exist—they are time-averages as well. In reality, one active base SV is asserted, then the other active base SV, then the null base SV, and the cycle repeats (as will be shown later). Thus, the magnitude of each shorter SV represents the duty cycle of that active SV.

189
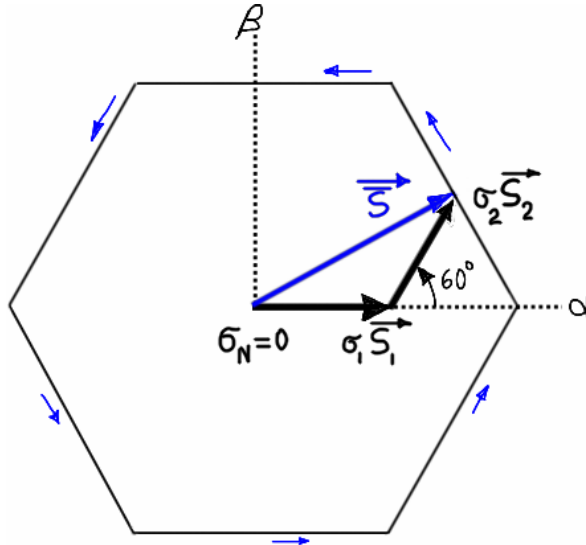
Figure 4.30 – Synthesis of SV by time-averaging base SVs.

Each base SV $\vec{S_i}$ is asserted for a certain fraction σ_i of the modulation period T. The time-average SV is the sum of these products and is given by Equation (4.7), where the subscripts 'x' and 'y' indicate active base SVs and the subscript 'N' represents a null base SV. (In Figure 4.30, the active base SVs are $\vec{S_1}$ and $\vec{S_2}$ and the null SV is arbitrary.)
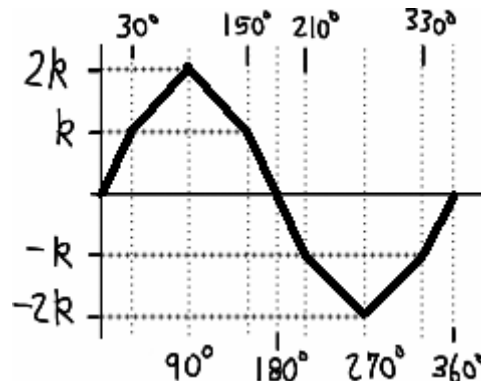
$$\vec{\vec{S}} = \sigma_x \vec{S_x} + \sigma_y \vec{S_y} + \sigma_N \vec{S_N} \tag{4.7}$$

Since σ_i is the *fraction* of the modulation period for which $\vec{S_i}$ is asserted, $\Sigma \sigma_i \overset{MUST}{=} 1$. The "maximum" static output would correspond to a single base SV being asserted continuously as we have already seen. The "maximum" output of a moving SV would be whatever SV is generated when only active base SVs are used ($\sigma_N = 0$). Using simple trigonometry it can be shown that the locus of all possible "maximum" ($\sigma_N = 0$) SVs is identically the hexagon that connects the tips of the base SVs, as shown in Figure 4.31.

190
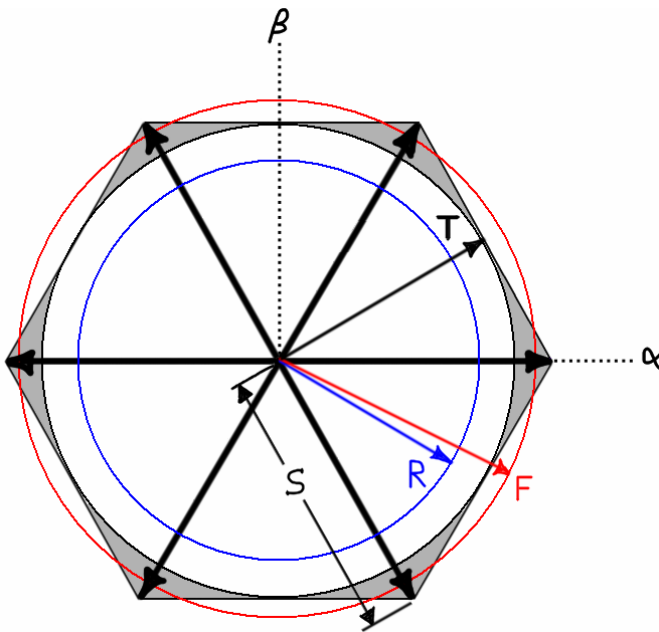
Figure 4.31 – Temporal limit of inverter output.

The α-projection of a SV tracing the hexagon is shown in Figure 4.32; it will be called the "gambrel" waveform. In the figure, the degree markings are nonstandard (they are measured from the negative imaginary axis).
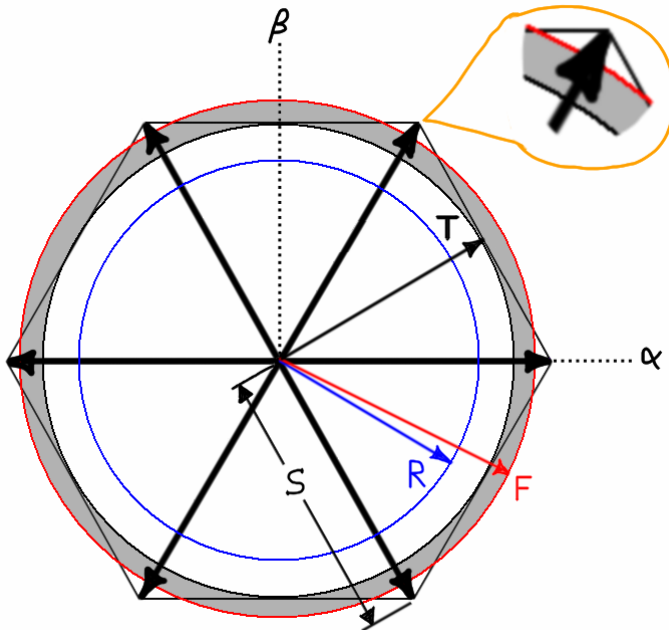
Figure 4.32 – α-projection of hexagon trajectory.

This is the "maximum" for a continuously-changing output. Recall that the THI limit was the circle inscribed in the hexagon (Figure 4.28). That limit is the maximum sinusoidal limit for any 180° inverter, whether it is an analog THI or a SVM implementation. Thus when the average SV is tracing the THI limit and the commanded magnitude is increased, the resulting SV will trace the THI limit tangentially but will enter the shaded regions shown in Figure 4.33 and harmonics will be produced since the trajectory is not circular. The relationship between the magnitude of the SV and the amplitude of its fundamental component becomes nonlinear. Operation in this region is similar to overmodulation in the SPWM inverter. Increasing the magnitude of the commanded SV to (S) will encounter the temporal hexagon limit and produce the gambrel waveform.

Figure 4.33 – SVM overmodulation region: SV locus.

Unlike the SPWM case, one cannot reach six-state squarewave operation by simply increasing the length of the commanded SV. Instead, the SV will have to be made to linger longer at the corners of the hexagon until finally it does not trace the hexagon but instead jumps between base SVs as in regular six-step squarewave mode. As in the SPWM case, there are numerous resources in the literature concerning the control of a SVM inverter through the overmodulation region and into six-step squarewave operation. Sometimes the literature will state that the shaded region in Figure 4.34 is what defines the SVM overmodulation region, but what they refer to is the *fundamental* produced in overmodulation. Notice that this shaded region in Figure 4.34 is outside the temporal limit; this shows that it is a representation of the *fundamental's* trajectory, not the actual output of the inverter.
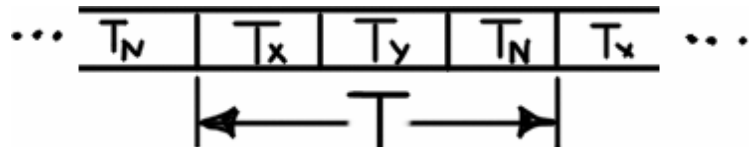
Figure 4.34 – SVM overmodulation region: locus of fundamental SV.

Comparing Figure 4.33 and Figure 4.34 should finalize the understanding that the hexagon is the "maximum" volt-second output and the circle (F) is the maximum of the fundamental of the output (for both pole and line-neutral voltages).

SVM Switching Schemes

The previous subsection explained how SVM synthesized a time-averaged SV by switching between at least two active SVs and at least one null SV. Since those are the only basic requirements, there are many different ways to realize a SVM inverter. This section will develop one of the common methods in order to illustrate some of the details involved in SVM implementation. Perhaps the most intuitive switching scheme would be to divide the modulation period into three parts corresponding to two active and one null SV, as shown in Figure 4.35. During the time T_X, $\overrightarrow{S_X}$ would be asserted, and so on.

Figure 4.35 – One period in a simple switching scheme.
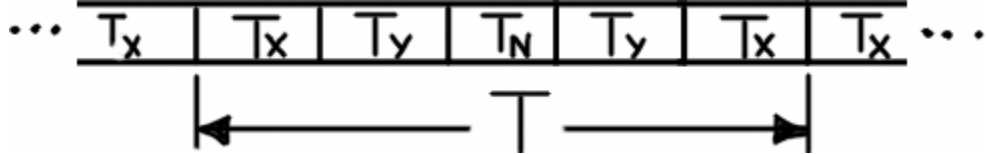
Similar to a single channel in a PWM inverter, the period consists of an 'on' segment (T_X+T_Y) and an 'off' segment (T_N). But instead of simply modulating a pulse width we are modulating the duration of a base SV, and there are two of them. There is a disadvantage to this simple scheme,

however. Assume for example that the commanded SV is in sextant s_{12} as shown in Figure 4.30. The obvious choice for the active base SVs would be $\overrightarrow{S_1}$ and $\overrightarrow{S_2}$; we could arbitrarily pick $\overrightarrow{S_7}$ as the null base SV. From Table 4.1, the switch states would progress as follows.
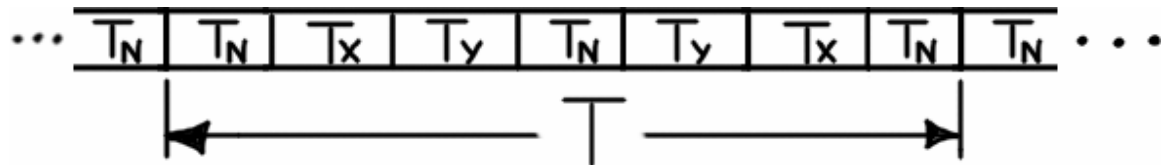
$$\cdots \rightarrow \quad S_1 \quad \rightarrow \quad S_2 \quad \rightarrow \quad S_7 \quad \rightarrow \quad \cdots$$
$$\cdots \rightarrow \left(HLL\right) \rightarrow \left(HHL\right) \rightarrow \left(HHH\right) \rightarrow \cdots$$

Each state transition within a period requires a change of only one leg state. However, the transition between periods requires two legs to switch states. Each time a leg changes states a switching loss is incurred, so this is not desirable. Selecting the null SV to be $\overrightarrow{S_0}$ does not solve the problem. Since inter-period transitions required only one transition, the period could be rearranged as shown in Figure 4.36, with appropriate changes to the durations of each base SV (dividing the previous T_x and T_y in half).

Figure 4.36 – One period in an improved switching scheme.

This solves the switch transition problem but there is another problem. Assume the commanded SV approaches $\overrightarrow{S_2}$ and crosses over into sextant s_{23}. $\overrightarrow{S_X} = \overrightarrow{S_1}$ and $\overrightarrow{S_Y} = \overrightarrow{S_2}$ would become $\overrightarrow{S_X} = \overrightarrow{S_2}$ and $\overrightarrow{S_Y} = \overrightarrow{S_3}$. As the SV crossed the boundary there would be extraneous switching between two periods and this could cause distortion. This problem can be solved by dividing the null time, adding a segment at the beginning and end of each period, as shown in Figure 4.37.

Figure 4.37 – One period on a second improved switching scheme.

But distributing the null SV as shown would cause the switch states would progress as follows.

$$S_7 \rightarrow S_1 \rightarrow S_2 \rightarrow S_7 \rightarrow S_2 \rightarrow S_1 \rightarrow S_7$$
$$\left(HHH\right) \rightarrow \left(HLL\right) \rightarrow \left(HHL\right) \rightarrow \left(HHH\right) \rightarrow \left(HHL\right) \rightarrow \left(HLL\right) \rightarrow \left(HHH\right)$$

The null state next to S_1 causes a double transition where previously there was none. The solution is to use S_0 for the beginning and end null states and S_7 for the center null state.

$$S_0 \rightarrow S_1 \rightarrow S_2 \rightarrow S_7 \rightarrow S_2 \rightarrow S_1 \rightarrow S_0$$
$$\left(LLL\right) \rightarrow \left(HLL\right) \rightarrow \left(HHL\right) \rightarrow \left(HHH\right) \rightarrow \left(HHL\right) \rightarrow \left(HLL\right) \rightarrow \left(LLL\right)$$

Checking sextant s_{23} again for this new scheme reveals that a double transition would occur.

$$S_0 \to S_2 \to S_3 \to S_7 \to S_3 \to S_2 \to S_0$$
$$(LLL) \to (HHL) \to (LHL) \to (HHH) \to (LHL) \to (HHL) \to (LLL)$$

The fix for that could be to reverse the null states for sextant s_{23}.

$$S_7 \to S_2 \to S_3 \to S_0 \to S_3 \to S_2 \to S_7$$
$$(HHH) \to (HHL) \to (LHL) \to (LLL) \to (LHL) \to (HHL) \to (HHH)$$
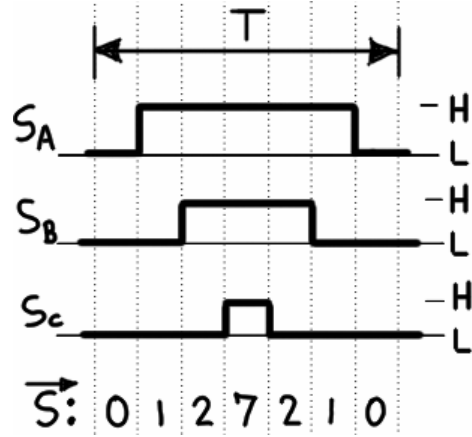
But then when the SV crosses a boundary, there would be a triple transition between the ending null state of the period for one sextant and the beginning null state of the period for the next sextant. Instead, the same null state order can be used for all sextants, but instead of always asserting $\overrightarrow{S_X}$ before $\overrightarrow{S_Y}$, the order could be reversed for alternate sextants.

$$S_0 \to S_X \to S_Y \to S_7 \to S_Y \to S_X \to S_0$$
$$S_0 \to S_Y \to S_X \to S_7 \to S_X \to S_Y \to S_0$$

For example, the sequences for sextant s_{12} and s_{23} would be as follows.
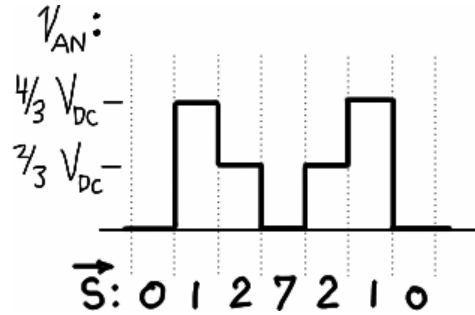
$$s_{12}: \begin{cases} S_0 \to S_X \to S_Y \to S_7 \to S_Y \to S_X \to S_0 \\ S_0 \to S_1 \to S_2 \to S_7 \to S_2 \to S_1 \to S_0 \\ (LLL) \to (HLL) \to (HHL) \to (HHH) \to (HHL) \to (HLL) \to (LLL) \end{cases}$$

$$s_{23}: \begin{cases} S_0 \to S_Y \to S_X \to S_7 \to S_X \to S_Y \to S_0 \\ S_0 \to S_3 \to S_2 \to S_7 \to S_2 \to S_3 \to S_0 \\ (LLL) \to (LHL) \to (HHL) \to (HHH) \to (HHL) \to (LHL) \to (LLL) \end{cases}$$

Sextants s_{12}, s_{34}, and s_{56} would be switched in the same order, and sextants s_{23}, s_{45}, and s_{61} would be switched using the alternate order. One reference calls this the "alternate reversing" sequence [83, p.260]. One SVM period is shown in Figure 4.38 for a commanded SV in sextants s_{12}. The periods are equal in the figure but as the magnitude and angle of the commanded SV change, the time spent in each state will change. The leg control signals are shown; the instantaneous pole voltage waveforms would look the same but would switch between $+V_{DC}$ and $-V_{DC}$ as usual.

Figure 4.38 – Leg control signals; commanded SV in sextant s$_{12}$.

Using the neutral voltages from Table 4.2, the line-neutral voltage of phase-A corresponding to Figure 4.38 can be plotted, as shown in Figure 4.39. For the SVM period in these figures, the SV would be at approximately 30° (equal time spent in S$_1$ and S$_2$). Examining the SPWM case shown in Figure 4.24, the 30° position is approximately above the letter "r" in the word average (cosine reference). Comparing the 30° position in Figure 4.24 with Figure 4.39 it is seen that around 30° both methods are switching between similar inverter states and produce similar instantaneous waveforms.
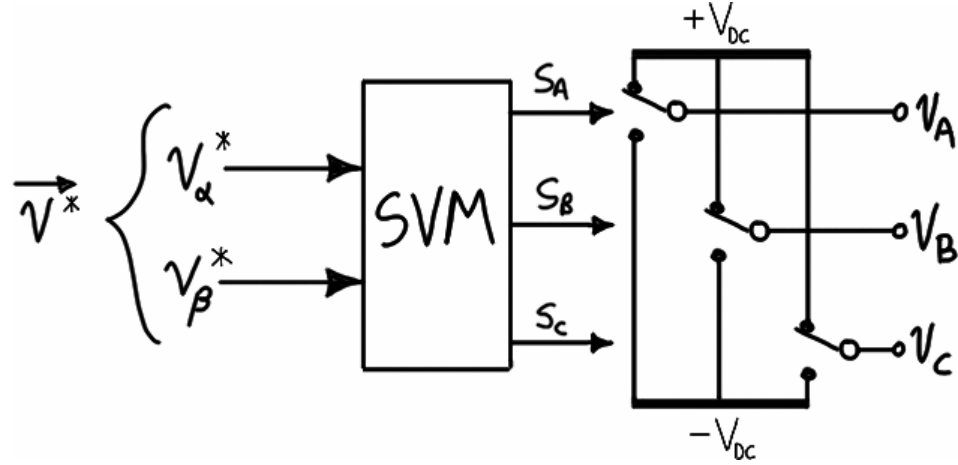
Figure 4.39 – Phase-A line-neutral voltage; commanded SV in sextant s$_{12}$.

It is apparent from the above discussion that selecting a switching scheme is not trivial. In addition to the issue of undesirable simultaneous leg transitions, the current measurement must be synchronized to the switching scheme, which adds additional requirements. The algorithm shown here is common in the popular literature but in the academic literature there are many others. In several variants, a phase is clamped to a rail during certain periods in order to minimize switching loss. These may be called *two phase SVM*, *bus-clamped SVM*, or *discontinuous SVM*, although the terms can carry different meanings. In addition to the issues discussed here, an important practical issue is the compatibility of the switching scheme with the gate drive circuitry [83, p.258]. These variants and practical issues are not discussed here.

SVM Implementation

The block diagram of the general SVM inverter is shown in Figure 4.40. The commanded voltage SV is passed to the SVM control unit as its α- and β- components.

Figure 4.40 – SVM inverter.

The switching scheme is a fixed set of rules that determines which active and null base SVs should be used to synthesize the commanded SV. There are many variations but it seems that most implementations have rules based on sextants similar to the previous discussion. Therefore, the first task of the SVM algorithm is to identify the sextant in which the commanded SV lies; this is fairly simple. After the sextant is identified the controller knows which base SVs it must modulate based on the switching rules. The second task of the SVM controller is therefore to determine the duration of each base SV (Figure 4.37); this is more difficult. The final task is to issue the leg control commands. Fortunately, this can be accomplished using the standard center-aligned PWM unit available in many microcontrollers [83, p.261] but there are other methods. This method is shown in Figure 4.41. The durations are computed as duty cycles which are converted to timer comparison values; these are updated every SVM period, although some PWM units are capable of half-cycle reloading. The change in each time-compare value at the update points has been greatly exaggerated.
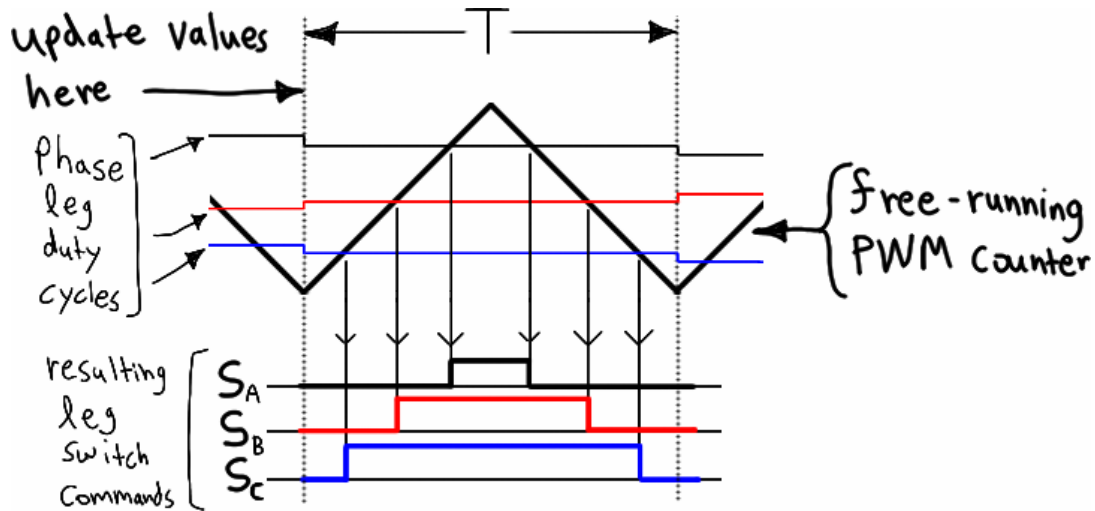
Figure 4.41 – Generating leg switch commands.

Only the leg switch commands are shown in Figure 4.41. Using phase-A as an example, the leg command (S_A) is translated to top (S_{AH}) and bottom (S_{AL}) signals. A dead-time delay of T_D is inserted as shown in Figure 4.42. The diodes antiparallel with the transistors conduct during this dead-time period (whereas in a 120° inverter they may conduct during the 60° period over which both transistors in a leg are OFF).
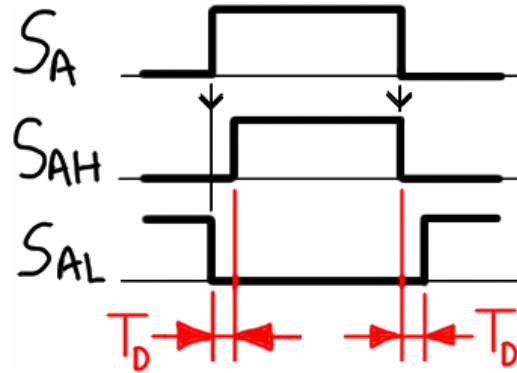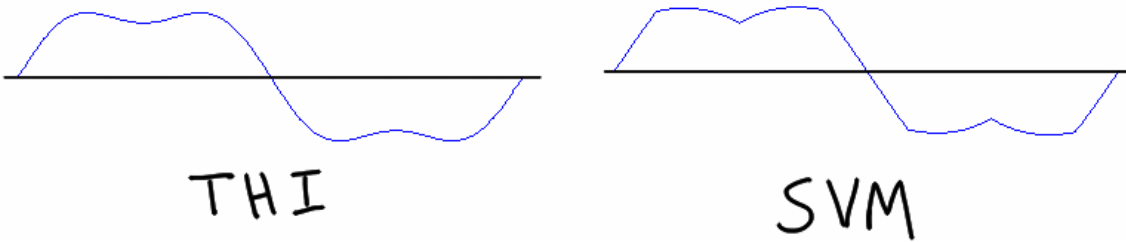
Figure 4.42 – Dead-time insertion.

The SVM algorithm (sector identification and duration calculation), the leg command generation, and the dead-time insertion can be realized by discrete units or in various combinations with one another. The implementation could be analog but is most commonly it is digital and uses a combination of hardware and software.

SVM Pole Voltage and ZS Component
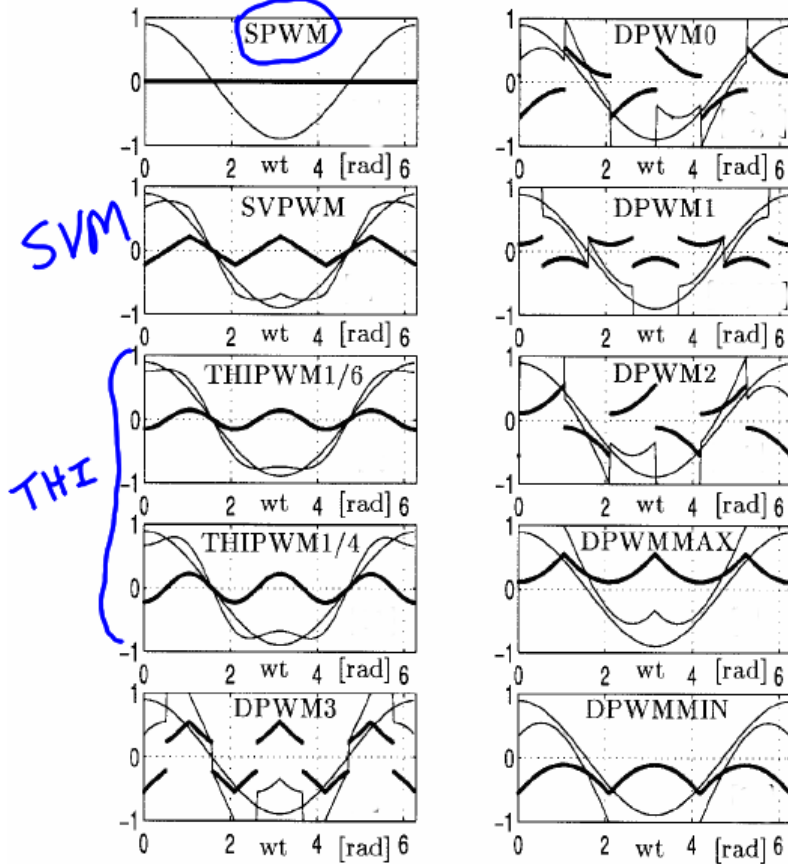
The discussion of the ZS component is no now resumed in order to finalize it. It was mentioned that the THI limit represents the maximum sinusoidal output of any 180° inverter but no mention

has been made of using THI in the SVM inverter. Indeed, one of the advantages of the SVM inverter is that it can produce an average SV anywhere inside the THI limit without having to "manually" inject any harmonics—it achieves this inherently, and not by injection but by "rearranging." Returning to the discussion that compared Table 4.2 with Table 4.3, we saw the instantaneous output of a 180° inverter always has a ZS component. This is true of SPWM as well, but it was distributed throughout the modulation period as to have a zero average (hence the output was limited to the SPWM limit, R). In SVM it is distributed throughout the modulation period so as to have a nonzero average (a very particular nonzero average that allows the output to reach the THI limit, T). We have not seen any evidence of this, however, because (per the previous discussion) the SV cannot contain this component. When we synthesize the SV using the base SVs and draw it on the two-dimensional diagram, we will never see it. This important understanding seems to be entirely absent in the popular literature. Plots of the phase voltage can indeed be found that show the phase voltage with the ZS component present (and the $2/\sqrt{3}$ gain in fundamental voltage is always touted) but there is no mention of how or why SVM generates such a waveform. Figure 4.43 shows the shape of the average pole voltage in a THI inverter and also shows the shape of the same for an SVM inverter. There is clearly a difference in shape; the former has rounded corners and a smooth dip, while the latter has steeper sides, sharp corners, and a pointed trough. This is because the ZS component in a THI inverter is a sinewave but in an SVM inverter it is a triangle wave.

Figure 4.43 – Average pole voltages for THI and SVM inverter.

The various SVM switching strategies mentioned earlier will produce a ZS component (and hence, pole voltages) that are very different from that shown above. Although they are not discussed here, a sample of these waveforms is shown in Figure 4.44, where the darker line is the ZS voltage generated. In each case there is a lighter line that is the line-neutral voltage and another line that is the pole voltage. In each case the line-neutral voltage is sinusoidal. This shows that the different modulation schemes produce radically different pole waveforms but in each case the ZS component generated is such that the phase voltage (pole minus ZS) is sinusoidal. The annotated graphs are those of the techniques discussed earlier in this report.

Figure 4.44 – ZS components of some popular PWM methods.

(Modified from [126].)

Clearly, since the ZS component adds in the neutral and since any triple-frequency waveform has spectra that are only ZS, there is a freedom to choose the ZS signal, as the figure has shown. This can be accomplished by "injecting" a ZS signal into the command of a ramp-comparison modulator, or it can be accomplished by using different switching rules in an SVM implementation. Since both methods use a 180° inverter, they are really only different ways of *controlling* the inverter. Thus, one should perhaps expect that there is a relationship between the control over the ZS signal in THI and SVM. Indeed there is: the freedom to choose the injected signal in THI corresponds to the placement of the $\vec{V_0}$ and $\vec{V_7}$ in SVM [72, p.151], [128], [70, ch.6]. The relationship of SPWM methods to those of SVM is described in [134], [135], [136].

The SVM inverter is often praised for its compatibility with digital implementation (since the switching rules and calculation of times can be done in software) and for its compatibility with a vector control structure (the commanded input is in the form of two SV components). However, "SVM" can be implemented using the exact same hardware as THI—the only difference is that a

different triplen signal would be injected. Such a scheme could obviously be implemented without a microprocessor, either in entirely in analog or as naturally-sampled PWM [128], [137]. However, the advantage of a SV-input command is lost and a switching algorithm is no longer used, thus it is different from the SVM discussed here. In other words, such a scheme produces pole and ZS waveforms that look like those produced using SVM but the control method is different. The reader is simply cautioned that "SVM" does not always indicate the modulation of base vectors as presented here.

Now, exactly why the switching algorithm discussed earlier produces a *triangular* ZS component is beyond the author's present understanding but that detail is not important here. On the contrary, it is important that the reader understand the discussion above. We should always be aware that any output produced by the SVM inverter will contain this average ZS component, which can only be represented as αβ0 components. However, the ZS component is not present in the phase voltages (indeed, we rely on this fact) and the SV cannot represent the ZS component. Therefore, we can *choose to ignore* the ZS component, draw the two-dimensional SV diagrams of the inverter output (such as Figure 4.26), and work with only the SV (only the αβ components) when we use a SVM inverter in a control system.

Modulation Index

The modulation index was previously developed for the SPWM inverter. It was mentioned that the modulation index could be defined with respect to the THI limit or to the fundamental produced in six-step squarewave mode. The modulation index of a SVM inverter can be defined in the same manner. Since SVM by definition uses SVs, it is also common to reference the SVM modulation index relative to the magnitude of the active base SVs. Therefore the modulation index may be referenced to three different SVs (representing the amplitudes of sinusoidal components) or to the magnitude of a SV. However, it was shown that the "magnitude" of a SV plotted in the αβ plane can be specified in different ways and it became apparent how important that definition is when examining inverter output. Thus, when the modulation index of a SVM inverter is discussed, the same considerations apply.

Recall that Table 4.4 gave the modulus of the space vector representation of different three-phase waveforms. The first column corresponds to the largest sinusoid produced via regular SPWM (R), the second column corresponds to the largest sinusoid produced via THI (T), and the third column corresponds to the amplitude of the fundamental produced in squarewave mode (F). Each of these

values could be interpreted as the maximum modulation index referenced to the SPWM linear limit, defined in terms of whichever row is selected. These values of maximum modulation indices are summarized in Table 4.5. (As mentioned, $k = 2/3$ is used in this report when working with inverters.) To be clear, these are the *maximum* values of the modulation indices.

Table 4.5 – Maximum m$_a$ referenced to SPWM linear limit (R).

	peak		RMS	
	L-N	L-L	L-N	L-L
	(R) SPWM linear limit			
V_{DC}	1.0000	1.7321	0.7071	1.2247
V_{BUS}	0.5000	0.8660	0.3536	0.6124
	(T) THI linear limit			
V_{DC}	1.1547	2.0000	0.8165	1.4142
V_{BUS}	0.5774	1.0000	0.4082	0.7071
	(F) fundamental of squarewave			
V_{DC}	1.2732	2.2053	0.9003	1.5594
V_{BUS}	0.6366	1.1027	0.4502	0.7797

Many of the values in Table 4.5 are used in the literature when discussing inverter performance but references often do not define the definition of the modulation index they use; in those cases the table can be used as a guide. For example, an article may state that the maximum modulation index corresponding to six-step square wave operation is 0.78. Searching the (F) entries for 0.78 will show that the modulation index was defined using line-line RMS quantities referenced to the full bus voltage V_{BUS}. When the modulation index is defined with reference to the THI linear limit the maximum modulation indices are those shown in Table 4.6.

Table 4.6 – Maximum m$_a$ referenced to THI linear limit (T).

	L-N		L-L	
	peak	RMS	peak	RMS
	(R) SPWM linear limit			
V_{DC}	0.8660	1.5000	0.6124	1.0607
V_{BUS}	0.4330	0.7500	0.3062	0.5303
	(T) THI linear limit			
V_{DC}	1.0000	1.7321	0.7071	1.2247
V_{BUS}	0.5000	0.8660	0.3536	0.6124
	(F) fundamental of squarewave			
V_{DC}	1.1027	1.9099	0.7797	1.3505
V_{BUS}	0.5513	0.9549	0.3898	0.6752

Similarly, when the modulation index is defined with reference to the fundamental obtained in squarewave mode the maximum modulation indices are those shown in Table 4.7.

Table 4.7 – Maximum m_a referenced to fundamental obtained in squarewave mode (F).

	L-N		L-L	
	peak	RMS	peak	RMS
	(R) SPWM linear limit			
V_{DC}	0.7854	1.3603	0.5554	0.9619
V_{BUS}	0.3927	0.6802	0.2777	0.4810
	(T) THI linear limit			
V_{DC}	0.9069	1.5708	0.6413	1.1107
V_{BUS}	0.4534	0.7854	0.3206	0.5554
	(F) fundamental of squarewave			
V_{DC}	1.0000	1.7321	0.7071	1.2247
V_{BUS}	0.5000	0.8660	0.3536	0.6124

Finally, when the modulation index is defined with reference to the magnitude of a base SV the maximum modulation indices are those shown in Table 4.8. This reference is used in the literature so it is presented here, but some caution is due in its interpretation. The modulation index is the ratio of [the amplitude of the fundamental component of the output voltage (equivalently, the magnitude of a magnitude-invariant SV that represents the combined action of the same)] to [the amplitude of the fundamental component of some other important waveform (or the magnitude of its SV)]. But the six-step basis space vector represents a fixed (and imbalanced) state of the inverter; it is not a space vector that represents a sinusoidal set, thus it is somewhat abstract to use its magnitude as the reference in the definition of modulation index. However, it is a valid concept and is frequently encountered in the literature.

Table 4.8 – Maximum m_a referenced to magnitude of six-step basis space vector (S).

	peak		RMS	
	L-N	L-L	L-N	L-L
	(R) SPWM linear limit			
V_{DC}	0.7500	1.2990	0.5303	0.9186
V_{BUS}	0.3750	0.6495	0.2652	0.4593
	(T) THI linear limit			
V_{DC}	0.8660	1.5000	0.6124	1.0607
V_{BUS}	0.4330	0.7500	0.3062	0.5303
	(F) fundamental of squarewave			
V_{DC}	0.9549	1.6540	0.6752	1.1695
V_{BUS}	0.4775	0.8270	0.3376	0.5848

While the information in Table 4.5 - Table 4.8 is helpful when interpreting the different modulation indices in the literature, this report specifies SVs in terms of peak L-N quantities referenced to V_{DC} (and for inverters, $k = 2/3$). Therefore it is helpful to summarize the maximum modulation indices defined in these terms, Table 4.9.

Table 4.9 –Maximum modulation indices defined using peak, L-N,V_{DC}, k=2/3.

| | | m_a of this limit $\cdots$ | | |
		R	T	F
$\cdots$ referenced to this magnitude	R	**1.0000**	1.1547	1.2732
	T	0.8660	**1.0000**	1.1027
	F	0.7854	0.9069	**1.0000**
	S	0.7500	0.8660	0.9549

If an inverter were to only operate using SPWM, it would make sense to use the modulation index defined with reference to (R). If an inverter were capable of operating using THI, it would make sense to use the modulation index defined with reference to (T). For inverters capable of THI, (T) is the limit of linear inverter operation. If the inverter can smoothly transition from THI to six-step squarewave mode and retain linear control over the fundamental of the output voltage (and if harmonics are acceptable in the output) it would make sense to use the modulation index defined with reference to (F). This report is concerned with SVM and attention is restricted to the linear region, thus the definition of the modulation index used is that referenced to (T). Explicitly, the modulation index used in this report is that given in Equation (4.8), where the space vector is amplitude invariant and represents the peak value of a line-neutral phase voltage; it is denoted as simply *m* to distinguish it from all other definitions.

$$m = \frac{\vec{v}\big|_{k=2/3}}{\frac{2}{\sqrt{3}}V_{DC}} = \frac{\vec{v}\big|_{k=2/3}}{1.1547 V_{DC}} \tag{4.8}$$

A final word of caution is that some references use one definition of space vector (for example, L-L RMS) and use a definition for the modulation index based on *different quantities* (for example, L-N peak). These conflicting usages can be confusing but are easily resolved using the above tables.

Summary and Conclusion

The two-level VSI is the dominant topology used in BPMS motor control. The six-step 120° commutation (in many different varieties) is used to control trapezoidal BPMS motors; it is also used to control any other type of BPMS motor, but torque ripple will be produced. For all other applications in low to medium power BPMS control, the 180° inverter is used. It can be controlled via traditional sinusoidal PWM methods or via SVM; the only differences lie in how the switch commands are generated and in the ZS signal produced. The ZS signal allows the maximum sinusoidal output of the inverter to be extended by $2/\sqrt{3}$ as compared to regular SPWM methods; there are any number of suitable ZS signals that accomplish this. Inverter control methods that produce a ZS signal can be used only with isolated neutral or delta-connected loads.

More information concerning PWM and VSIs is given in [60], [119], [120], [121], [122], [123].

In surveying the literature it seems that the most important measures of performance are those summarized below.

- bus utilization
- linearity of control
- ease of implementation
- control over the effects of dead-time
- switching loss
- voltage harmonic content
- current harmonic content

Bus utilization refers to the maximum fundamental amplitude achievable. For all properly-implemented inverters that use some form of ZS signal, this limit is as described above and cannot be made to be higher.

Linearity of control refers to the linearity of the modulation index over the operating range of the inverter. For SVM inverters this is naturally linear up to the THI limit. In all inverters, operation through the overmodulation mode into the six-step mode is not linear and requires a control algorithm to make it so. There are numerous overmodulation schemes but overmodulation is not

discussed in this report. Good references (which often contain useful information aside from overmodulation techniques) include [141], [142], [143], [144], [145], [146], [147].

The ease of implementation varies wildly with control methods, especially SVM because of the large number of implementation strategies. To review the innumerable varieties would be nearly impossible; surveying the latest articles in the literature would be a better starting point.

There are numerous articles regarding the effects of dead-time and their mitigation [138], [139], [140]. Although it is a fundamental issue that may bear much importance, it is nonetheless an entire subtopic (much like the optimal switching problem) and would require a literature review to gain an understanding of the nature and magnitude of the problem and its remedies. In addition to the simple blanking time the turn-off and turn-on characteristics differ between transistor types and may be a function of load. A similar and related problem is the compensation for non-constant DC link voltages (which can result from using too small a bulk capacitor, improper decoupling, commanding a very large step in torque, and so on).

The remaining three topics are somewhat different because they are more complicated and are influenced by many factors (although the switching algorithm seems to be the dominant one). Switching loss is proportional to the switching frequency and depends on the switching algorithm; it is also a function of loading. Voltage and current harmonics should be divided into the baseband and switching harmonics. Baseband voltage harmonics will cause baseband current harmonics, which produce torque ripple. They should not be encountered as long as operation is restricted to the linear region. Voltage switching harmonic content is determined by the switching scheme but may also vary with modulation index. It seems to be a concern associated primarily with EMI. Current switching harmonics are a function of the load inductance; the copper and core losses they induce are functions of the particular motor design. Of all the topics discussed here, these last three were investigated the least due to their complexity. References to begin with might include [70], [148], [149], [150], [151], [152].

CHAPTER 5 - Field Oriented Control of BPMS Motors

This chapter develops the concept of field oriented control as applied to the brushless permanent magnet synchronous motor.

In the first section some relevant terminology is discussed.

The next section returns to torque control in a synchronous machine. The concept of current phasing (from Chapter 2) is used to develop the concept of torque control from the perspective of the rotor frame using ideal current sources. The same concept is then developed again, first using a practical sine-triangle PWM inverter and then using an SVM inverter. The resulting system is precisely the rotor-flux-oriented FOC that is commonly used to control BPMS motors. Toque control of salient machines and field weakening are then briefly discussed.

The third section examines current control in FOC and to reveal the concept of the synchronous frame current regulator. This section will show how the synchronous regulator improves performance over the stationary regulator and will show how the motor under FOC can be modeled.

Terminology

The terms *field oriented control* and *vector control* are in general used synonymously, although some authors assign particular meaning to each. The first solid state three-phase induction motor drives were simply variable-voltage, variable-frequency (VVVF) three-phase voltage sources (also called a static inverter). The induction motor is asynchronous and the VVVF is all that is required to deliver variable speed operation. However, such a drive provides poor transient performance do to the induction motor dynamics. (The single phase equivalent model is only valid for steady state. Further, they express torque in relation to a frequency/slip-dependent circuit variable, not a spatial orientation [78, p.32].) Apparently one of the first successful analyses of controlled induction motor dynamics was given by Hasse in his now-classic 1969 dissertation [19]. Since the work emphasized that torque production in the induction motor is a spatial phenomenon (in contrast with the SPE tee circuit model) the name vector control was eventually adopted. Blaschke is also credited as being an early pioneer of the concept via his often-cited 1971 publication [20]. The title of his 1973 dissertation [21] contained the phrase "principle of field orientation." Since the original VVVFs only adjusted frequency and magnitude there were retroactively renamed *scalar drives*. These are still manufactured and used in variable speed applications that do not demand high dynamic performance, although at least one author [61, p.6] believes they will eventually displace the scalar drives. There is quite a difference between the approaches Hasse and Blaschke and hence, there are a large number of different FOC/vector control schemes for induction motors; these are not mentioned further.

[78, p.32] gives a good perspective from a machine standpoint: field oriented control may be used to describe distributed field quantities, whereas vector control may be used to describe the circuit variables. Given the relationship between the two (discussed in Part II of Chapter 3), they are essentially equivalent perspectives. However, the basic idea of controlling a vector quantity (e.g., a space vector) can be applied to stationary circuits as well, such as controlled rectifiers, inverters, and active filters. In these cases it seems that term vector control is the most appropriate (and most often used). On the contrary, vector control of a motor is called both that and FOC.

The ultimate objective in motor control is the control of torque. As hinted previously, FOC achieves linear torque control by adjusting the current SV to lie entirely along the **q** axis. To the extent that this instantaneous current control can be achieved, instantaneous torque control is achieved. Thus, unlike the VVVF drive, vector drives allow direct control of the instantaneous

torque production; this is called direct torque control. However, there is a specific method of motor control called "direct torque control" or DTC; this is not the FOC described here. DTC[33] is somewhat of a merger between FOC and SVM, in which the motor torque and inverter control scheme are integrated. Thus, the reader is alerted to the fact that many vector control schemes yield "direct torque control" but that the same is also used to refer to a particular control structure. An overview of the different types of DTC is given in [101].

Torque Control in the Rotor Reference Frame

In the literature one encounters the phrase "impressed stator currents;" this refers to the use of a controlled current source to generate phase currents that exactly follow the commanded currents. This assumption eliminates all disturbances to the current control loop and allows the underlying torque control to be examined. Impressed stator currents will be used to demonstrate torque control in the rotor frame and then the same will be demonstrated using practical CRPWM.

Using Impressed Stator Currents

When electronic commutation and phasing were introduced in Chapter 2, the concept was shown for a sinusoidal motor as the control system in Figure 5.1, where the reference currents were given by Equations (5.1) and (5.2).[34] The implementation of this concept will be developed first in the phase-variable form, then in the stationary reference frame, and finally in the rotor reference frame.

---

[33] Although DTC is found throughout the literature as a control concept, DTC is (or at least at one time was) a registered trademark of the Finnish company ABB Industry Oy.

[34] In this chapter cosine waves will be plotted as a function of ωt, where $\omega t = \theta_r + \pi / 2$. This allows the correct expressions (such as Equation 5.2) to be used while gaining the visual convenience of the cosine.
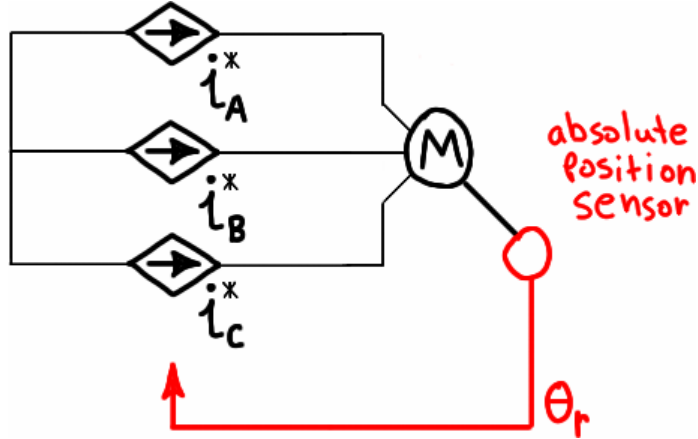
Figure 5.1 – Torque control of sinusoidal motor.

$$T = K_T I_p \quad \Rightarrow \quad I_p^{ref} = \frac{T^{ref}}{K_T} \tag{5.1}$$

$$\begin{cases} i_A^* = I_p^{ref} \cdot \left[-\sin(\theta_r) \right] \\ i_B^* = I_p^{ref} \cdot \left[-\sin(\theta_r - 120°) \right] \\ i_C^* = I_p^{ref} \cdot \left[-\sin(\theta_r + 120°) \right] \end{cases} \tag{5.2}$$

To impress the currents, an ideal hysteresis regulator will be used. It is shown in Figure 5.2 along with its simpler representation.
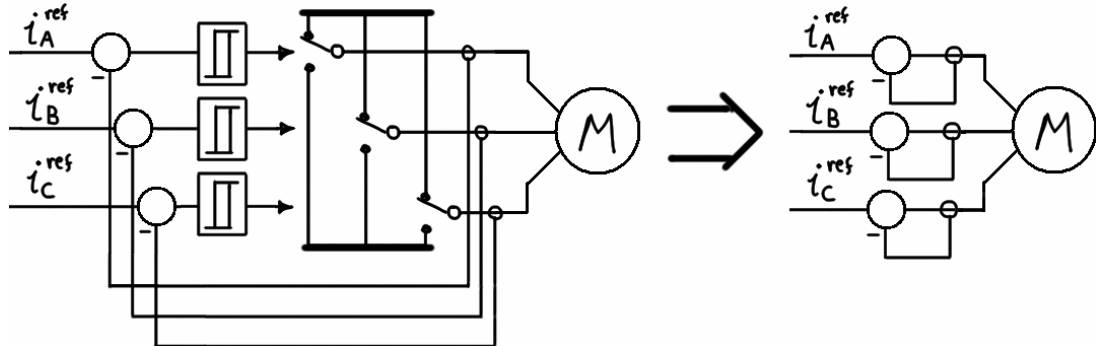
Figure 5.2 – Hysteresis CRPWM.

The torque control of Figure 5.1 is implemented using the hysteresis CRPWM by generating the appropriate current commands with reference to the rotor position, as shown in Figure 5.3. The "sinusoidal commutator"[35] generates three-phase sinusoidal reference values. If the absolute position sensor and the current regulators are assumed to be ideal this scheme provides perfect torque control. The current reference signals generated are those shown in Figure 5.8-c.

---

[35] The idea for using the term "sinusoidal commutator" in this fashion was taken from [99].
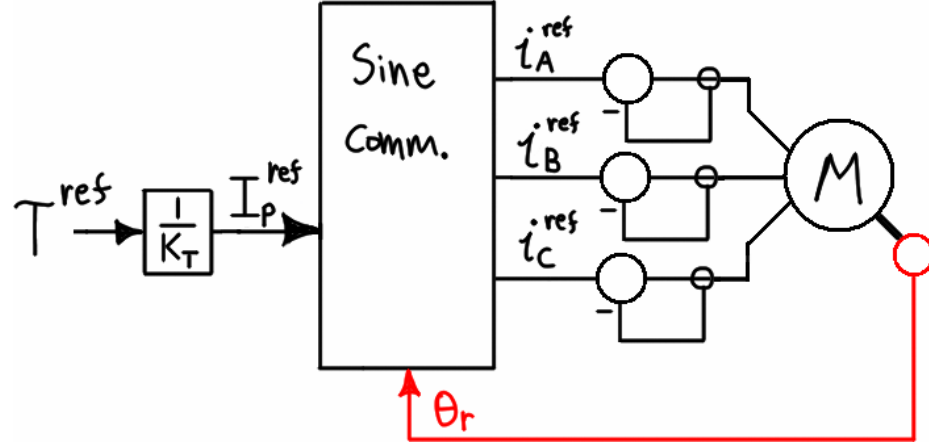
Figure 5.3 – Torque control of sinusoidal motor; phase variable form.

The next step is to employ the inverse Clarke transform to change the three-phase sinusoidal commutation block into an orthogonal two-phase one. This implements a controller in the stationary reference frame, as shown in Figure 5.4. The references are generated using Equation (5.3), where the factor of $3/2$ comes from the fact that just two windings must produce the same torque as the previous three. The current reference signals generated are those shown in Figure 5.8-b and Figure 5.8-c.
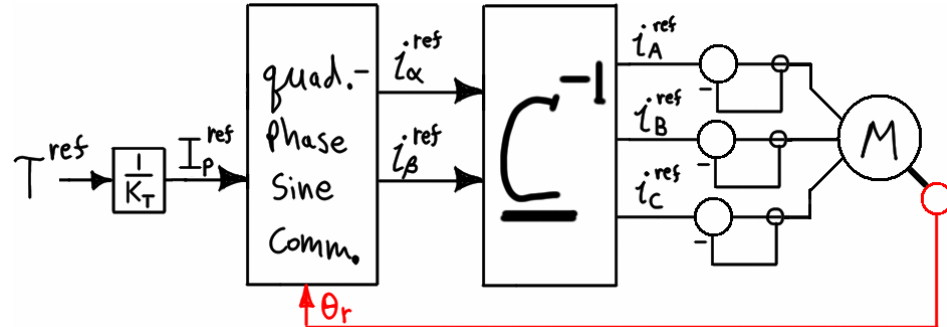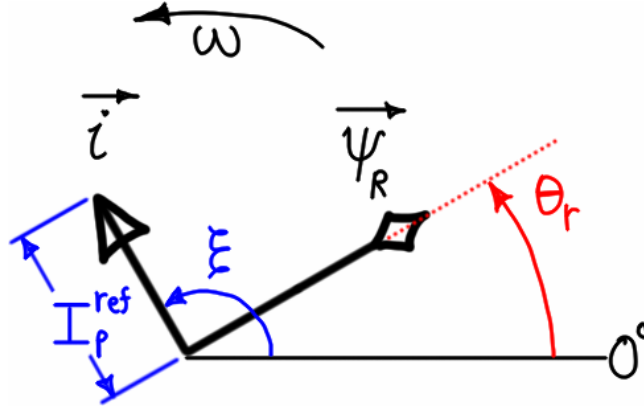
Figure 5.4 – Torque control in stationary reference frame.

$$\begin{cases} i_\alpha^{ref} = \dfrac{3}{2} I_p^{ref} \cdot \left[-\sin(\theta_r) \right] \\[2mm] i_\beta^{ref} = \dfrac{3}{2} I_p^{ref} \cdot \left[\cos(\theta_r) \right] \end{cases} \tag{5.3}$$

Although only the stationary reference frame controller operates using the SV directly, both versions *accomplish* the control shown in Figure 5.5, where the SVs are given by Equations (5.4)-(5.5). As the rotor rotates, θ_r increases and the sinusoidal commutator inherently produces three-phase (or two-phase) values corresponding to a SV with angle $\xi = \theta_r + \pi/2$ to ensure maximum torque per current. When the current SV is aligned as such, torque is directly proportional to the peak current.

211

Figure 5.5 – SV diagram for most efficient torque production; stationary frame.
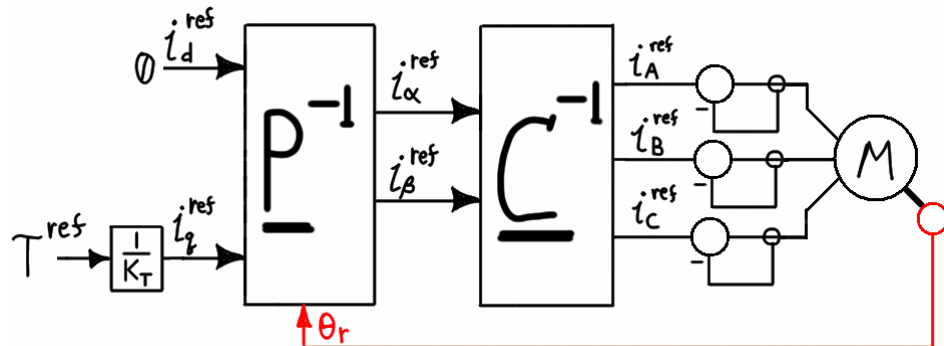
$$\vec{i} = \hat{I}e^{j\xi} = I_p^{ref}e^{j\left(\theta_r + \frac{\pi}{2}\right)} \tag{5.4}$$

$$\vec{\psi}_R = \Psi_R e^{j\theta_r} \tag{5.5}$$

All sinusoidal synchronous motor controllers must maintain a fixed space-phase relationship like this. Instead of using a sinusoidal commutator to generate reference signals using trigonometric functions, the reference could be generated in the rotor reference frame. A space vector is defined by its components and it is clear that for optimal torque generation, the direct-axis component should be zero. In that case torque is linearly proportional to the quadrature-axis component, thus the reference is generated using Equation (5.6).

$$i_q^{ref} = \frac{T^{ref}}{K_T} \tag{5.6}$$
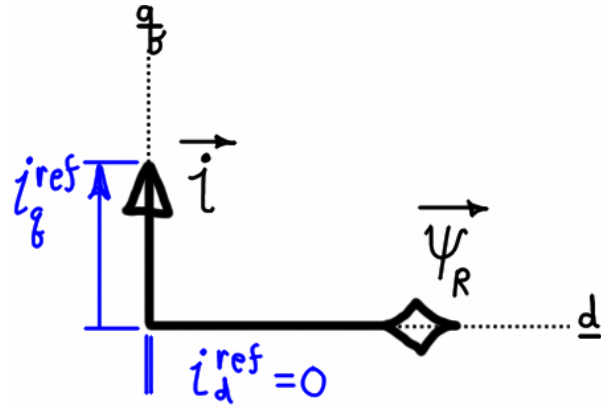
The torque controller in the rotor reference frame is shown in Figure 5.6, where the first block is the inverse Park transform. The current reference signals generated are those shown in Figure 5.8-a, Figure 5.8-b, and Figure 5.8-c.

Figure 5.6 – Torque control in rotor reference frame.
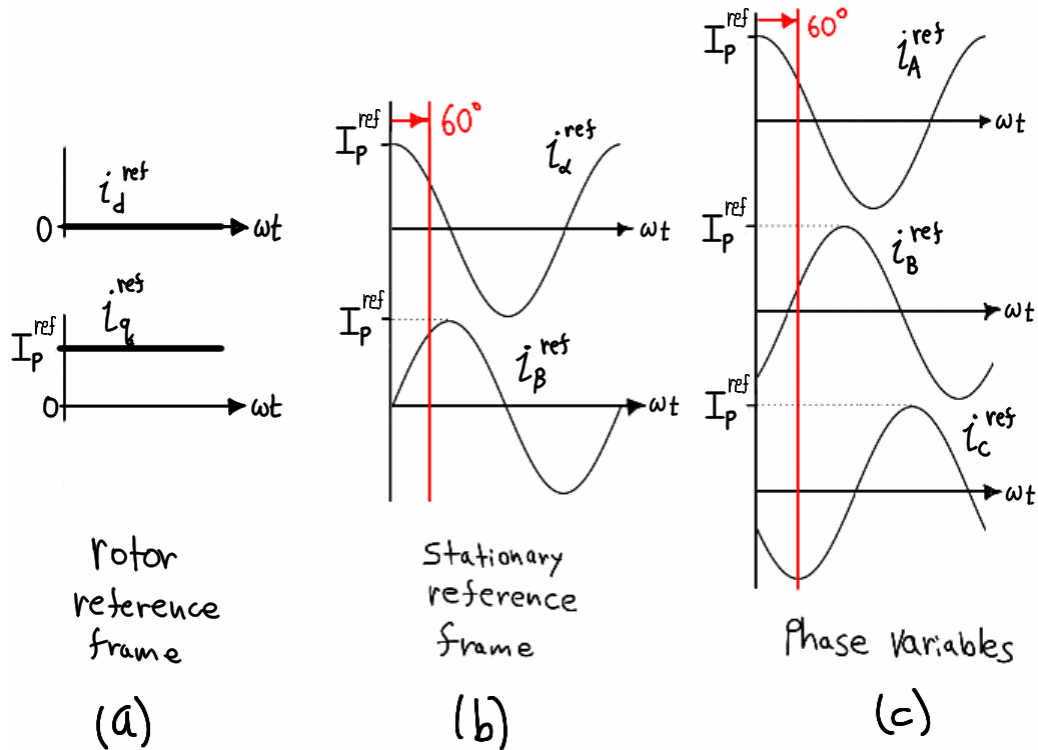
In the previous two schemes it was entirely obvious that rotor position was needed in order to properly phase the currents to produce torque. The same is true with this controller but there is

obviously a change in perspective. For the former controllers, one might imagine having a phase-locked loop keeping a set of sinusoidal currents locked 90° ahead of the rotor position. In the rotor frame controller the reference generated is a DC value. Figure 5.5 is now redrawn from the rotor reference frame perspective as Figure 5.7. There is no longer any attempt to create a rotating reference SV that is 90° ahead of another rotating quantity. In fact, although it is tempting to think about generating the current SV to be 90° of the rotor-stator flux linkage (which is stationary), it is better to think only about controlling the components of the SV in the rotor frame.

Figure 5.7 – SV diagram for most efficient torque production; rotor frame.

It is important to note that the signals in Figure 5.8-b and Figure 5.8-c have the relationship shown for all time (recall that since $\Sigma = 0$ one of the phase variable signals is simply a linear combination of the other two). On the contrary, the signals in Figure 5.8-a have no relationship to the others in the figure *unless* θ_r *is known*. The relationship between the signals of Figure 5.8-a and those of (Figure 5.8-b and Figure 5.8-c) is shown for a constant rotor speed.

Figure 5.8 – Comparison of reference signals under steady state operation.

The figure is now repeated as Figure 5.9 with the exact same commands in the rotor reference frame (Figure 5.8-a is identical to Figure 5.9-a). However, in Figure 5.9, the rotor was turning at constant speed as before, but at 60° the rotor was instantaneously locked by an external force that was applied. The same value of torque is still being produced and the current space vector is still orthogonal to the rotor flux (as enforced by the PI regulators in the rotor frame; any transient behavior is not shown). Since the rotor is frozen, the phase values that create the SV are frozen as well. This should help enforce the visualization that components in the rotor frame do not have any fixed relationship to those in the stationary frame. This is exactly the point of using the rotor frame to perform the regulation: the transformations will take care of producing the equivalent command in the stationary frame.
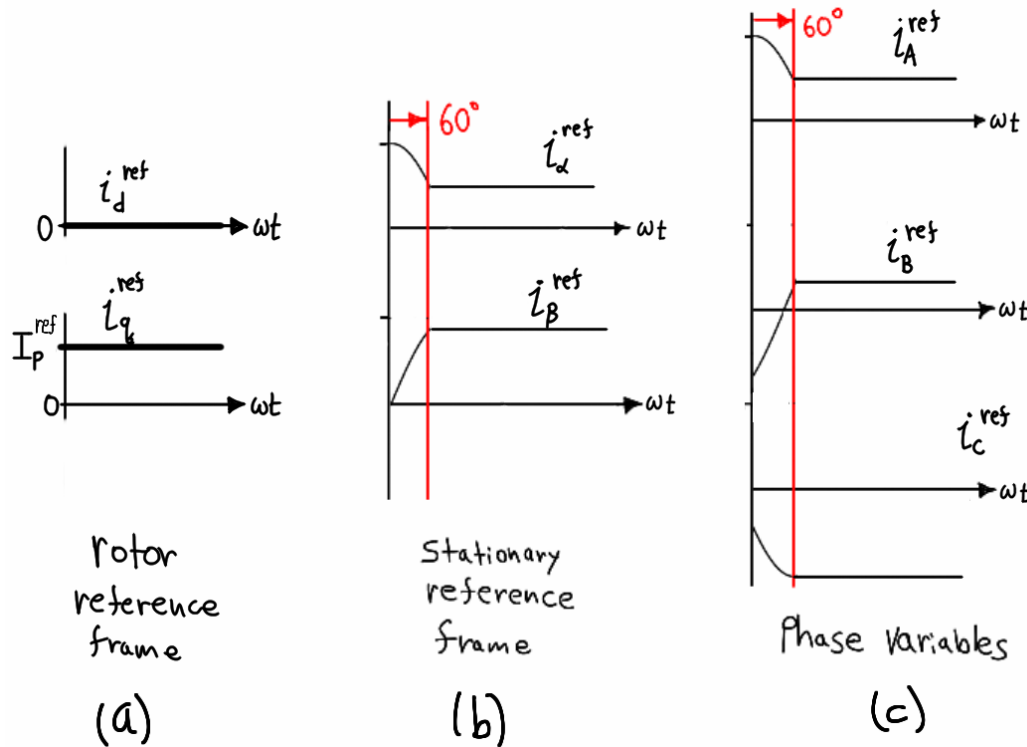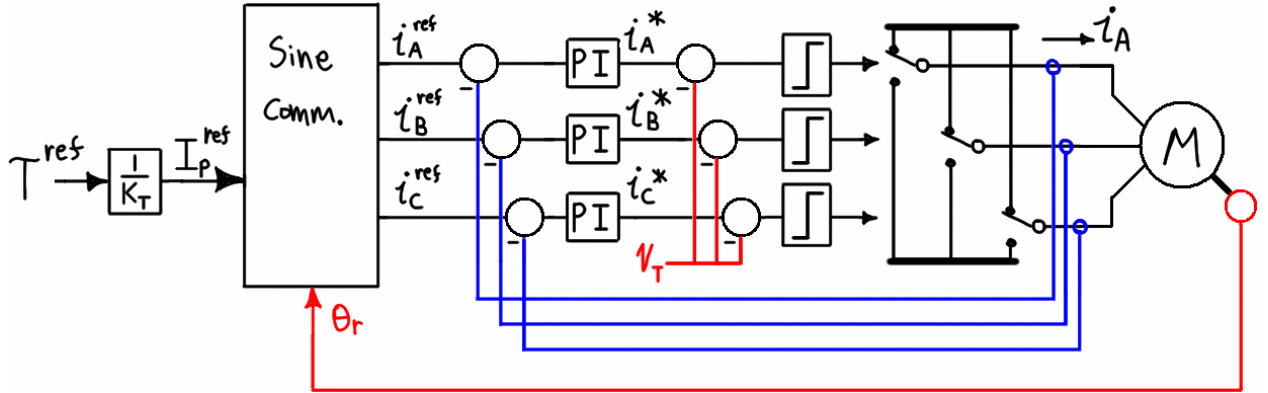
Figure 5.9 – Comparison of reference signals; rotor locked.

At this point a physical understanding of torque control in the rotor reference frame has been developed. However, it has relied on ideal controlled current sources. Now the torque controller will be developed with a more-realistic CRPWM.

Using CRPWM and SVM

The most familiar practical alternative to the hysteresis CRPWM is the sine-triangle CRPWM discussed in Chapter 4. To obtain a torque controller in the rotor reference frame using this type of CRPWM, the shortest path may be to replace the hysteresis CRPWM in Figure 5.6. However, the development will be clearer if we return to the beginning. Using the sine-triangle CRPWM,

the sinusoidal torque controller of Figure 5.3 is redrawn as Figure 5.10, where the triangle carrier is represented by v_T.[36] Filters on the phase current measurements are not shown.

Figure 5.10 – Torque control of sinusoidal motor; phase-variable form.
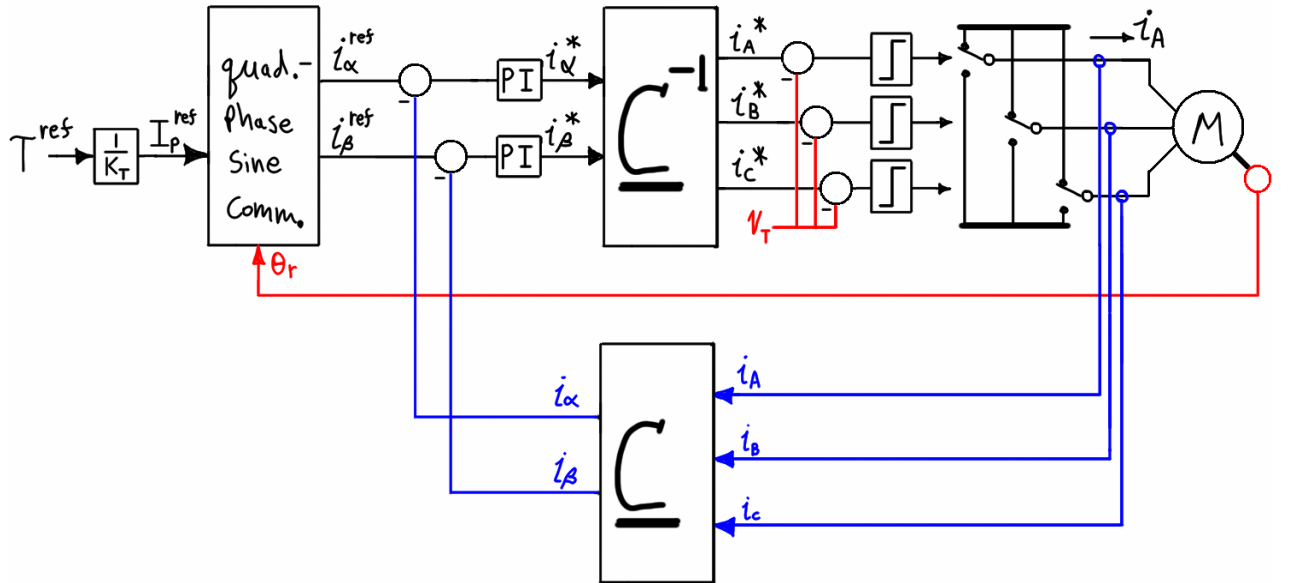
According to Figure 5.8-c, the PI controllers are required to regulate continuously-varying signals. In addition, if the control system diagram were drawn it would be seen that the bEMF acts as a periodic disturbance to the current loop. The primary limitation of this configuration is the phase shift associated with the PI controllers operating at synchronous frequency [154]. In steady state this phase shift causes the torque angle to decrease from the ideal 90° ($\delta = \xi - \theta_r$ in Figure 5.5). In this configuration the current loop is responsible for controlling both the amplitude and the phasing. In contrast the reference signal in Figure 5.6 is a DC quantity in steady state due to the Park transform. (The controller in Figure 5.6 had no current loop because impressed stator currents were assumed.) The way to fix the problem is to close the current loop around the stator currents transformed to the rotor frame.

The first step toward this is to use the inverse Clarke transform as before to replace the three-phase sinusoidal commutator with the two-phase one and move the current loops from the phase-

---

[36] In a wye-connected motor only two of the currents can be controlled independently. For this reason some references (primarily from the popular literature) claim that it does not make sense to use the third current loop (in that case the third PI compensator is not present and the phase-C current command is given by $i_C^* = -i_A^* - i_B^*$). The hysteresis controller has a phase interference problem because it does control all three phases [132]. The issue is that controlling the voltage at terminal-A can be accomplished only by pulling the terminal high or low. But each time this change is made to phase-A, it changes the state of the entire inverter, which changes the line-neutral voltages of phase-B and phase-C, thus the phases cannot be controlled independently. [78, p.335] confirms that it is not logical to use three regulators, and in addition to solving the problem by slaving the third as above, another option is to generate a ZS signal to be fed back to decouple the phase regulators. However, for some reason, the three-regulator variety seems most prevalent in the literature concerning CRPWM, perhaps indicating that the effect may not be as pronounced as in a hysteresis CRPWM. For simplicity all three regulators are shown here.

variables to the stationary reference frame.[37] The stationary regulators are just as they were before in the impressed-current (thus open-loop) case, but there is a problem: the α- and β- current components do not exist. The simple answer is to use the Clarke transform to obtain them, as shown in Figure 5.11.[38]

Figure 5.11 – Torque control of sinusoidal motor; stationary reference frame.

It is clear that the current regulators are still handling the AC quantities. In the impressed-current system, the next step was to generate the current reference in the rotor frame, thereby eliminating the quadrature-phase sinusoidal commutator and replacing it with the inverse Park transform. This is also the next step here. In addition, we will simultaneously move the current regulators to the rotor frame, as shown in Figure 5.12.

---

[37] The stationary reference frame is so called because it is fixed to the stator (it is also called the *stator reference frame*). When drawing SV diagrams this is a clear interpretation, as the 0° reference never moves. But in the control systems shown above, the control variables were "stationary" (unchanging DC quantities) in the *rotor* frame and the signals oscillate in the *stationary* reference frame. One might use caution in reading the popular literature, as sometimes the DC signals are referred to as "stationary signals" but this does not mean they are in the stationary frame.

[38] Notice that the problem mentioned in Footnote (36) is no longer of any concern because there are only two commands generated and these *dq* or αβ components cannot contain a ZS component. Further, the inverse Clarke transform is not capable of generating a ZS component!
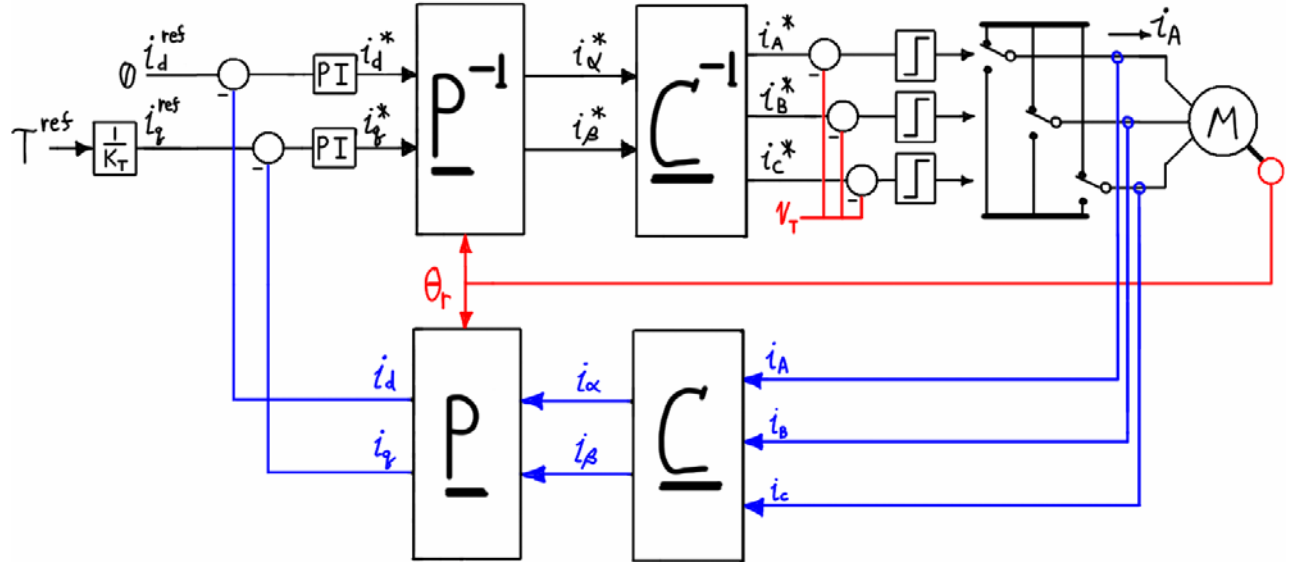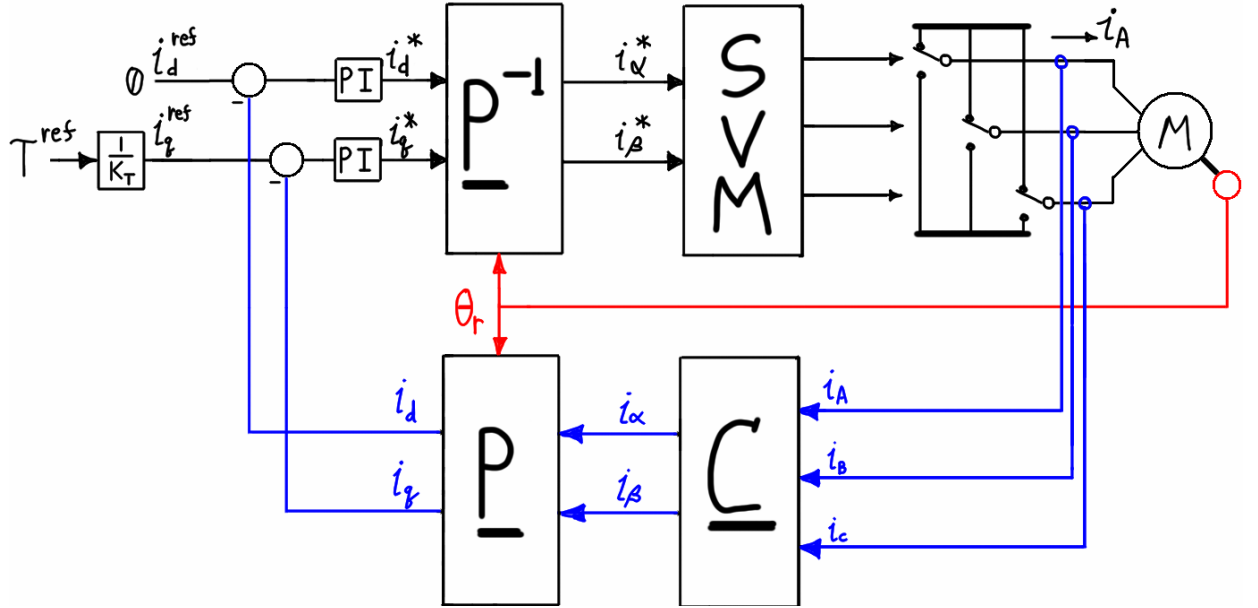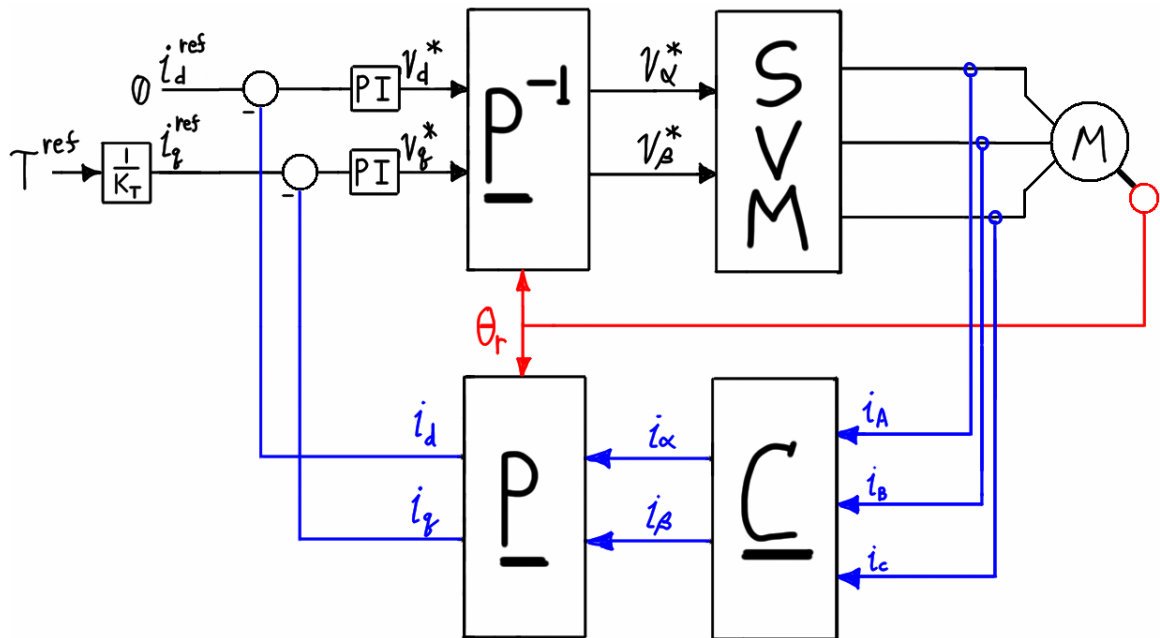
Figure 5.12 – Torque control of sinusoidal motor; rotor reference frame.

Now, according to Figure 5.8-a, the current loop compensators deal with DC quantities when the motor is in steady state (during transients the signals will have transients components). There are several things to note about Figure 5.12. First, since the current command exists (at some point in the control flow) in terms of αβ components, the SVM inverter would integrate well with this control system (SVM is an "open loop" inverter just as the sine-triangle PWM inverter in Figure 5.12). Second, a wye-connected motor can not have no ZS current, thus we can obtain the αβ components by measuring just two phase currents and by using one of the modified $\Sigma = 0$ Clarke transforms. (Practical implementations in SVM may require the third measurement, thus all three will continue to be shown.) Replacing the sine-triangle PWM the SVM inverter results in the system shown in Figure 5.13.

Figure 5.13 – Torque control of sinusoidal motor in rotor reference frame using SVM.

The diagram is often simplified further by not showing the DC link and inverter legs, as in Figure 5.14. In addition, the commanded currents have been changed to voltages for compatibility with later development.

Figure 5.14 – Field oriented control with SVM.

This control structure is generally called field oriented control. Because it both generates and servos the commands in the rotor reference frame (defined by θ_r) it is called rotor-oriented FOC.

In a nonsalient synchronous machine the rotor flux is also coincident with the rotor, thus it is also called rotor-flux-oriented FOC. When FOC is applied to other machines a variety of schemes are

common (such as stator-flux-oriented- or magnetizing-flux-oriented-). Each has various advantages and disadvantages but they are primarily used for machines other than the BPMS type. Useful references that discuss FOC of both the synchronous and induction motors include [78], [77], [87].

Field-Weakening and Salient Machines

For the most efficient production of torque in a nonsalient machine the stator current SV should be completely aligned with the **q** axis and this is accomplished simply by controlling the d-component to be zero. Clearly, if the d-component is nonzero the result is a space vector in the rotor frame that is not aligned with the **q** axis. In motor control, using a nonzero d-component may be more appropriately called "field angle control" [78, p.203] but oftentimes it is still called FOC. Field angle control can be used to control terminal power factor; this is required in high power ratings when a load-commutated inverter is used [78, p.212] (as opposed to the hard-switched inverters considered here). Angle control can also be used to optimize some parameter (such as the minimization of copper loss, which is essentially the power factor control mentioned earlier). In BPMS motor drives there are two common reasons to use a non-zero d-component of stator current: to control torque in a salient machine or to implement something akin to field (flux) weakening. This report does not concern either topic but both will be mentioned because they highlight some of the more subtle concepts of FOC. These topics are interrelated and the author does not possess a working knowledge of them; they are presented here in an effort to aid the reader in understanding just the very basic ideas. At the end of this subsection some further technicalities are mentioned, along with some references for further study.

Salient Machines

In Chapter 3 the torque was found to be given by Equation (3.160).

$$(3.160): T = \frac{3}{2}\left[\lambda_d i_q - \lambda_q i_d\right] \tag{5.7}$$

The regular expressions for the *dq* components of the stator flux linkage, Equation (5.8), were substituted in and the result simplified to Equation (5.9) as expected.

$$\begin{cases} \lambda_d = L_s \cdot i_d + \Psi_R \\ \lambda_q = L_s \cdot i_q \end{cases} \tag{5.8}$$

$$T = \frac{3}{2}\Psi_R \cdot i_q \tag{5.9}$$
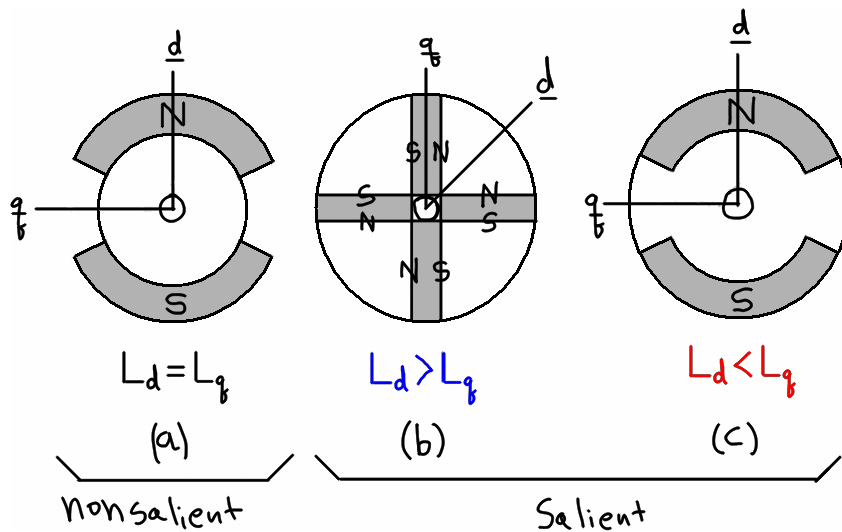
To analyze a salient machine one must employ the "full" *dq* theory (the two-reaction theory used by Park and those before him). In addition to separating vectors into their *dq* components (as we have seen), the full *dq* theory assumes the effects of rotor saliency can be represented by different inductances in the d- and q- directions (L_d and L_q) instead of the synchronous inductance L_s. In that case the simple SV analysis must be modified from what was shown in Chapter 3 to use these separate inductances. The only result of concern here is that Equation (5.8) must be modified to be Equation (5.10).

$$\begin{cases} \lambda_d = L_d \cdot i_d + \Psi_R \\ \lambda_q = L_q \cdot i_q \end{cases} \tag{5.10}$$

Substituting these flux linkages into Equation (3.160) yields the torque for a salient machine, Equation (5.11).

$$T = \frac{3}{2}\left[\lambda_d i_q - \lambda_q i_d \right]$$

$$= \frac{3}{2}\left[L_d i_d i_q + \Psi_R i_q - L_q i_q i_d \right]$$

$$T = \frac{3}{2}\left[\Psi_R i_q + \left(L_d - L_q \right) i_d i_q \right] \tag{5.11}$$

In Equation (5.11) the first term describes the mutual torque produced via interaction of the stator field with the magnets and the second term describes the reluctance torque produced as the salient rotor attempts to align with the stator field in order to minimize the reluctance of the magnetic circuit. The definitions of the inductances are not given here, but in a nonsalient machine they are equal to one another and to the synchronous inductance: $(L_d = L_q = L_s)$. Thus, for a nonsalient machine, Equation (5.11) simplifies to Equation (5.9) as expected. To investigate the meaning of the **d**- and **q**-axis inductances, examine the three types of rotors shown in Figure 5.15.

Figure 5.15 – Rotor types: (a) nonsalient (surface magnet); (b), (c) salient (interior magnet).

The amount of rotor steel along the **d** and **q** axes is different for each rotor type. High quality magnets have a relative permeability of approximately unity. Therefore the reluctances in the **d** and **q** directions are the same for the nonsalient rotor (Figure 5.15-a) which has been the subject of discussion throughout the report. Inductance is inversely proportional to reluctance, and the reluctance itself is directly proportional to length of the airgap through non-ferrous material. For the salient rotor where the **d** axis is through steel (Figure 5.15-b), the reluctance in the **d** direction is lower than that in the **q** direction, thus the **d**-axis inductance is larger than the than of the **q**-axis. The opposite is true for the other salient rotor (Figure 5.15-c), in which the **d** axis passes through less steel than the **q** axis. For the majority of interior magnet BPMS motors, $L_d < L_q$ [43, p.756].

If the magnetic material in each rotor was replaced with plastic, only the salient rotors would produce torque with the stator field; this is the reluctance torque mentioned above. The different ratios of these inductances cause the torque function (for a concentrated full-pitch winding) to be different. Figure 5.16-a shows the torque produced as a function of the torque angle. The black line indicates the mutual torque which varies as the sine of the torque angle [77, p.349]; it is the familiar torque-angle curve for a synchronous machine and is shown for both the braking and motoring directions. The two double-frequency components are those due to the different reluctances of the salient rotors; they are shown in only the motoring direction for clarity. The curves are combined in Figure 5.16-b. It is clear that for the rotor in Figure 5.15-b, the ideal torque angle is less than 90° [30, p.260], whereas for the rotor in Figure 5.15-c the ideal torque angle is greater than 90° [42, p.509].
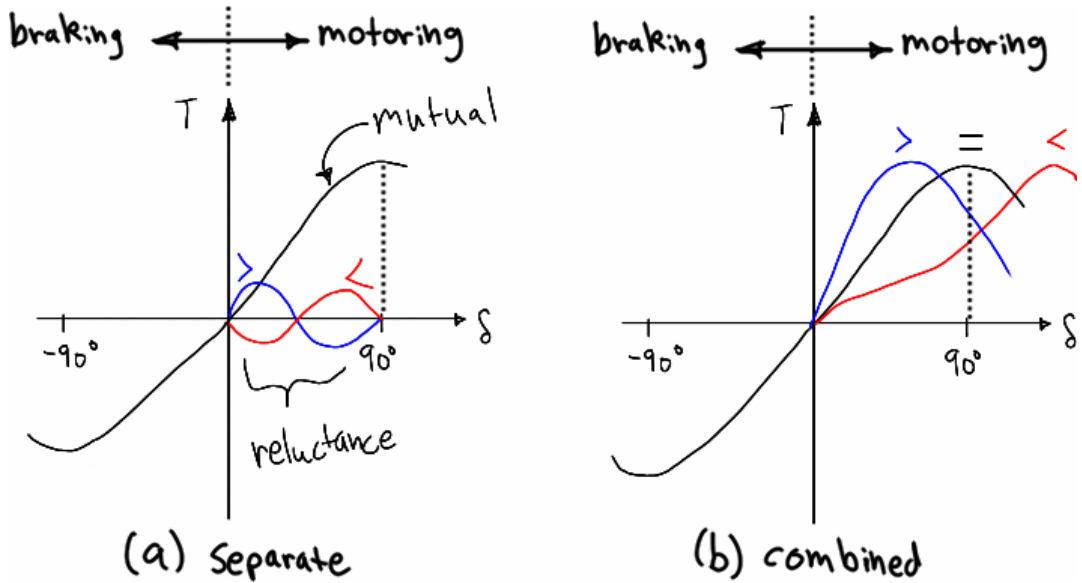
Figure 5.16 – Torque functions: (a) components; (b) combined.

This can also be seen by examining Equation (5.11). To produce positive mutual (magnet) torque, i_q should be positive as usual (for forward motoring operation). For the rotor of Figure 5.15-b, in which $L_d > L_q$, it is clear that i_d must have the same sign as i_q (positive) in order for the reluctance term to contribute positive torque. On the contrary, for the rotor of Figure 5.15-c, in which $L_d < L_q$, it is clear that i_d must have the opposite polarity as i_q in order for the reluctance term to contribute positive torque. In the *dq* rotor frame, when the current SV has a positive d-component, it is less than 90° ahead of the rotor flux; when the component is negative, its lead is greater than 90°. The relative location of the current SV required to produce maximum torque per current is shown in Figure 5.17. This should make clear the direct correspondence between Equation (5.11), Figure 5.15, Figure 5.16, and Figure 5.17.
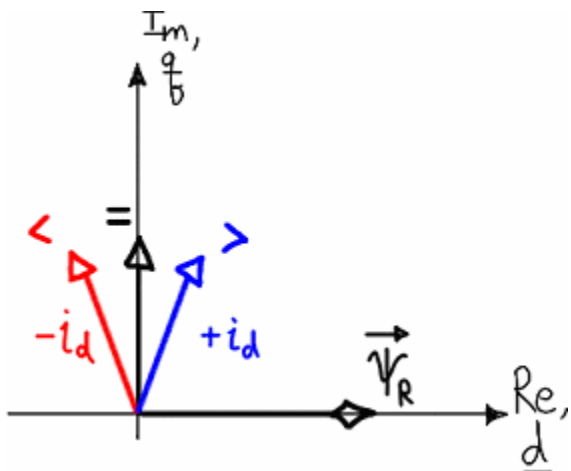
Figure 5.17 – Required position of stator current SV for maximum torque.

223

Therefore, to achieve linear control over torque in a nonsalient machine requires that the d-component of commanded current be controlled as well to the q-component. To control a salient machine with FOC, the torque constant K_T in the q-circuit must be replaced with the function block to control both d- and q- circuits, as shown in Figure 5.18. The type of motor and controller would determine the nature of the function block. In the simplest case it would be a simple function of fixed motor parameters, but in practice it may perhaps be a function of load (speed and current) or other variables.
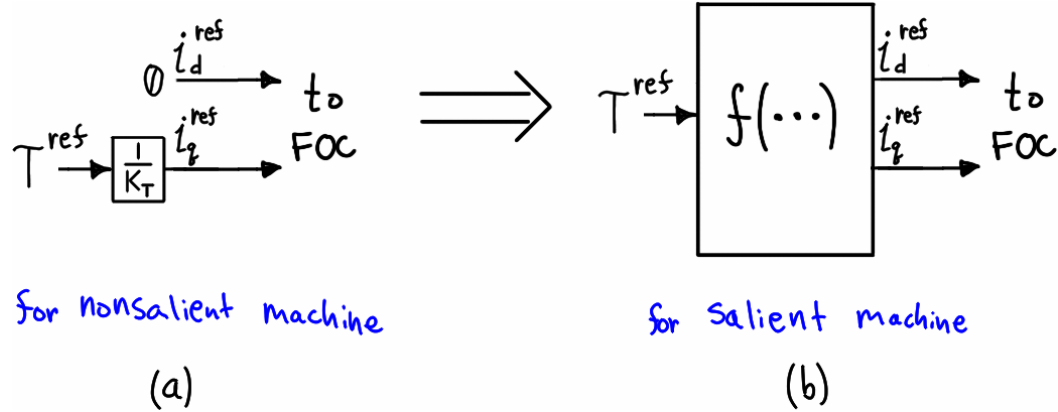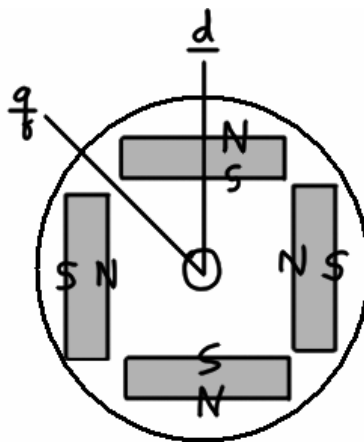
Figure 5.18 – Current command generator for FOC of salient motor.

Finally, it should be noted that there are many different (and conflicting) terms used to describe the rotors shown in Figure 5.15 [68], [69], [42], [41]. The magnets in Figure 5.15-a are nearly always called *surface mounted*; they can take on arbitrary shape, pitch, thickness, or magnetization profile. The magnets in Figure 5.15-b are called *circumferential*, *radial*, or *spoke*, magnets and those in Figure 5.15-c are called *inset magnets*; both are examples *interior magnets*. Many other types of rotors exist; the ones shown above were selected only to show the differences in saliency. However, one additional type of interior magnet rotor (often called a *buried permanent magnet* rotor) that appears quite often in the literature is shown in Figure 5.19. The magnets are completely contained in the rotor steel laminations and this allows the rotor to operate at very high speeds without the possibility of the magnets flying off (the other varieties shown may have a magnet that is bonded to the rotor or wrapped in a nonferrous retainer [69], [68]).
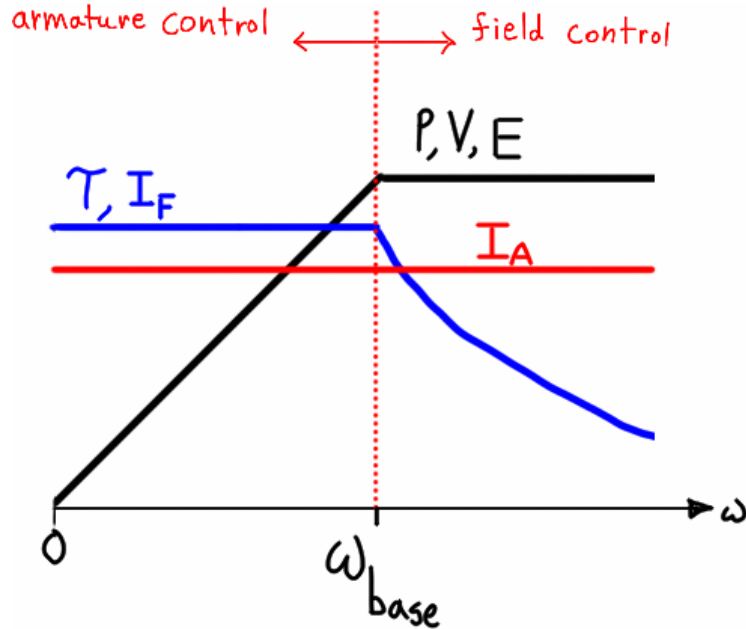
Figure 5.19 – Buried permanent magnet rotor.

Field Weakening

Field flux weakening (usually called *field weakening* or *flux weakening*) was originally a brushed DC motor concept and its purpose is simple to understand. Assume that a separately excited brush DC motor is loaded to maximum continuous rated torque at rated speed (known as *base speed* [25, p.405]); the armature and field currents will be at their maximum rated values. The magnitude of the bEMF is proportional to the rotational speed of the shaft, so at base speed it will be at a maximum value as well. In steady-state the terminal voltage is the sum of the bEMF and the resistive voltage drop (which is at maximum as well since the current is at maximum). The supply voltage under these conditions is the rated supply voltage which should not be exceeded; thus it can be though of as the maximum voltage available from the armature supply. Although the armature and field currents cannot be pushed beyond their limits, the motor can safely operate at speeds greater than base speed. With the armature voltage and current fixed, the only thing that can be changed is the field current. The bEMF constant K_E is proportional to field flux. If the field current is lowered, less flux will be produced, which raises the value of the bEMF "constant." Since the voltage "across the bEMF" (that is, the terminal voltage minus the fixed IR drop) is fixed, but K_E has been increased, a greater shaft speed results. However, torque is proportional to field flux[39] so this increase speed comes at the cost of a reduction in torque. Therefore, the region of operation below base speed is characterized by constant maximum torque at any speed; this is accomplished via armature current control. Operation above base speed is

---
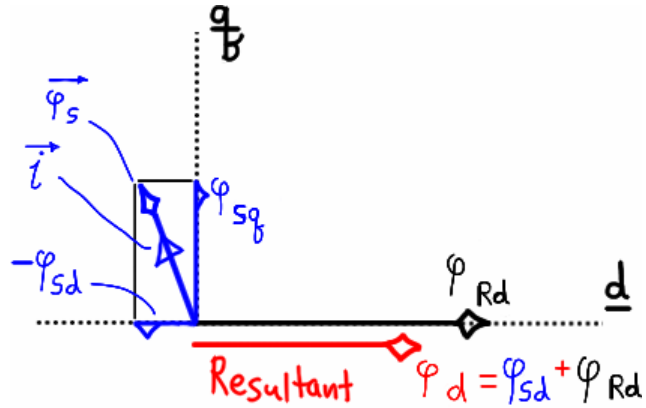
[39] Recall that $k_e(\theta_r) = k_t(\theta_r)$ and for a brush DC motor this simplifies to $K_E = K_T$, thus when K_E is lowered K_T will be lowered as well.

characterized by constant maximum power at any speed; this is accomplished via field current control. These regions are shown in Figure 5.20, where plots of maximum torque, armature current, field current, mechanical power, terminal voltage, and bEMF are shown. It is stressed that these are the *maximum* values and that only the shape of the plots is to be considered; in addition, the multiple variables assigned to each curve are not numerically equal.
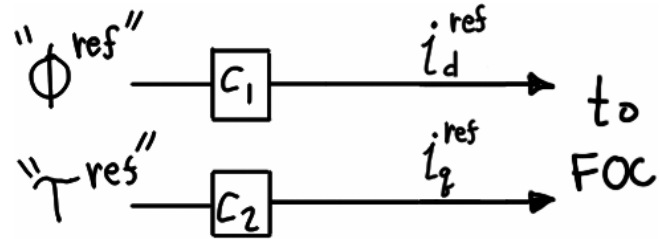
Figure 5.20 – Maximum values for operation below and above base speed.

"Field weakening" can be performed with the wound-field synchronous machine although it is not always called this name or used in the same way. In a motor the field current could be decreased to achieve constant power operation above base speed as explained above; in a grid generator or synchronous condenser it can be used to control the power factor. But in a BPMS motor, the field flux is due to the magnets instead of a controllable coil thus if the flux is to be weakened it must be accomplished via stator current; field weakening operation is therefore more complicated. Assuming rotor flux and stator flux are cosinusoidally distributed their airgap resultant could be resolved onto the *dq* axes as before. From the discussion of Figure 5.17 (and assuming a nonsalient machine) the q-component of current has been thought of as the torque-producing component (acting in quadrature to the rotor flux or rotor-stator flux linkage, as shown in Figure 5.7). Now, if the current SV is forced to be greater than 90° ahead of the **d** axis it will have a negative d-component. To the extent that the stator MMF creates flux in the airgap, this negative d-component (φ_{Sd}) would subtract from the rotor's flux (which is entirely along the **d** axis, $\varphi_{Rd} = \Phi_R$), yielding a lower value of airgap flux along the **d** axis (φ_d), as shown in Figure 5.21.

Figure 5.21 – Flux weakening in the rotor reference frame.

For this reason the q- and d- components of the current SV are sometimes called the torque-producing and flux-producing components, respectively, and this is drawn in the literature as Figure 5.22, where C_1 and C_2 are constants.[40]

Figure 5.22 – "Torque" and "flux" control.

For a salient machine the concept in Figure 5.22 would need to be modified in consideration of Figure 5.18-b. Continuing again with the assumption of a nonsalient machine, the bEMF is the derivative of the **d**-axis flux. Thus, advancing the current SV (by setting a negative reference value for flux in Figure 5.22) would achieve flux weakening that would allow operation above base speed. This could be implemented as shown in Figure 5.23, were "S.C." is a speed compensator and "F.C." is a flux controller. (For simplicity, both the flux loop is open, but using an estimator it could be made closed-loop.) As before, if a salient machine is used the flux weakening scheme of Figure 5.23 would likely need to be coordinated with the torque controller of Figure 5.18-b. [113] discusses concurrent flux weakening and torque control.

---

[40] In induction motor control (to achieve the most torque per current) the value of flux is held constant and in order to achieve this either the FOC control is used or the "volts per Hz" control (mentioned in Chapter 4) is used.
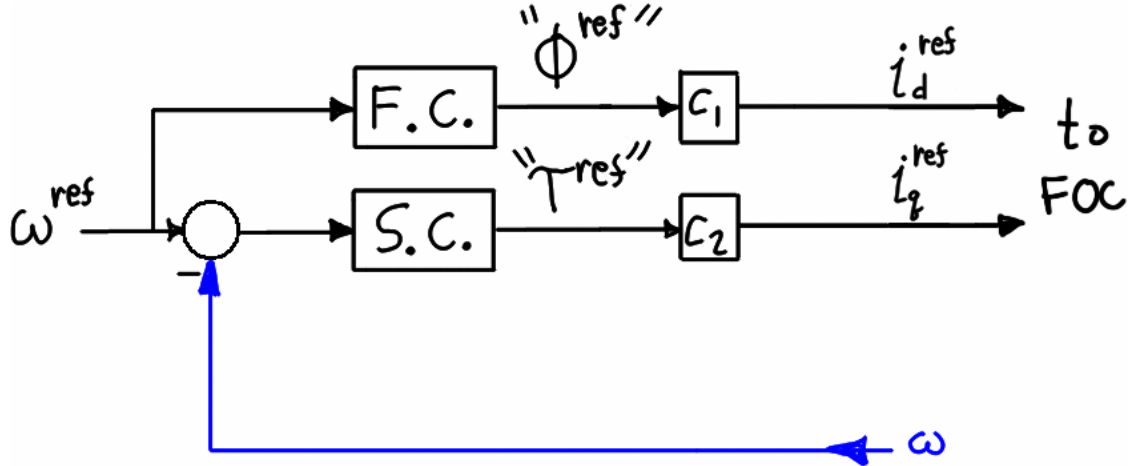
Figure 5.23 – Field weakening controller.

In summary, it has been shown that for a nonsalient rotor, torque control consists of setting $i_d = 0$ and controlling the torque according to $T = K_T \cdot i_q$. For a salient rotor both i_d and i_q must be controlled. Separate control of the "torque-producing" and "flux-producing" components of the stator current is possible using the FOC control structure, and this may be used to achieve flux weakening. However, for a salient rotor the torque control and the field-weakening control are not independent of one another. In addition to these fundamental ideas, several have been overlooked and the subject of flux weakening is far more complicated than presented here. Indeed, many of the details and interactions are beyond the author's present understanding.

First, it seems that the control of the two components of airgap flux is coupled in a synchronous machine (see [78, ch.5]) and it appears that this is the same as armature reaction flux [78, pp.249-250]. Second, as hinted by the key phrase above, "*to the extent* that the stator MMF creates flux in the airgap," the stator MMF is not always capable of truly weakening the magnet flux. This is because the magnet has a relative permeability of near unity, thus the airgap is effectively very large [78, pp.250], [87, p.96], [68, p.103]; in salient machines the effect is more pronounced [69, p. 4.18]. This also has something to do with the discussion of internal permeance of the magnet, as discussed in Chapter 2, and it is the same as saying the armature reaction is small or that the synchronous reactance/inductance (Appendix B) is small. The degree to which field weakening can occur thus depends on the motor's airgap, magnets, and saliency.

If a BPMS motor does not experience flux weakening with a negative d-component of stator current, the question arises as to what happens when the stator current SV is advanced like that. It

appears that this is very much related to the concept of "phase advance" in ECM motors but an investigation of the subject is beyond scope. Articles on field weakening show plots with many circles, ellipses, and hyperbolas indicating various limits. Understanding field weakening and/or current advancing would require a separate study. References that look to contain good information are [78, ch.9], [109], [110], [111], [112], [113], [114], [115], [116].

Synchronous Current Regulation

The FOC control structure has been developed by building upon the understanding of torque control (via phasing) because it is the most intuitive way to gain an understanding of how a space vector is regulated in the rotor frame. However, aside from the "motor control" aspect (determining the angle of $\vec{i}$ in accordance torque and field weakening) it is clear that the control structure is accomplishing current regulation in the rotor reference frame. Further, the same structure could be used to control any three-phase currents relative to some general reference frame (other than the rotor), such as the reference frame attached to a voltage space vector representing a bus on the grid. Whether it is the rotor frame in a synchronous motor, a grid voltage frame, or the reference frame of the magnetizing flux linkage in an induction motor, they will all be turning at the *synchronous frequency* as seen from the stationary frame (in the steady state). The idea of controlling a space vector in such a frame has come to be called *synchronous frame regulation*, or simply *synchronous regulation*.[41] The concept had been introduced previously by Schauder and Caddy [153] but it seems that Rowan and Kerkman were the ones who developed the concept in their widely-cited paper [154].

The main advantage of the synchronous regulator is that the compensators are in the synchronous frame. This removes them from the cyclic variation of the input error signal in order to prevent the increasing phase lag and magnitude droop that occurs with increasing frequency. In addition, the structure allows the bEMF to be offset and the decoupling of the motor's d- and q- circuits to be accomplished more easily [107]. In the first subsection the stationary and synchronous

---

[41] The terminology can be a bit confusing at times because the "synchronous" frame of an induction motor deals with the rotating excitation provided by the stator while the rotor slips by at an asynchronous speed. Therefore, various names could be used to refer to the "synchronous regulator" and its coordinates depending on the situation. Examples include: *dq-*, *synchronous-*, *rotor-*, or *excitation- frames/coordinates*. In other words, the rotor reference frame is a synchronous frame in a synchronous motor but it is not a synchronous frame in the induction motor (but the excitation frame is a synchronous frame).

regulators will be compared; in the second, the synchronous regulator will be developed further in order to show how the decoupling of the motor circuits can be achieved.

To better visualize the synchronous regulator, Figure 5.14 can be "bent" into a linear form and redrawn as Figure 5.24, where the loops and compensators are not shown. Previous diagrams have been schematic-like (for example, the output of a motor is a wire and current must be sensed with transducer). From now on they will be more transfer-function-like (where the output of a load *is* the current thus a transducer is unnecessary).
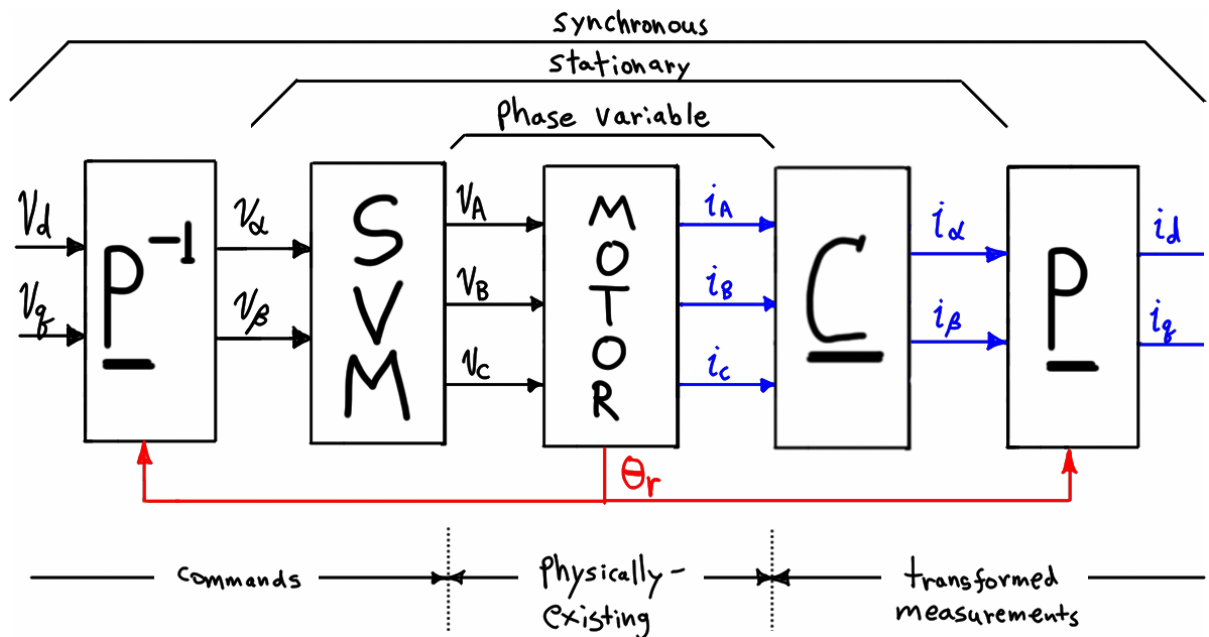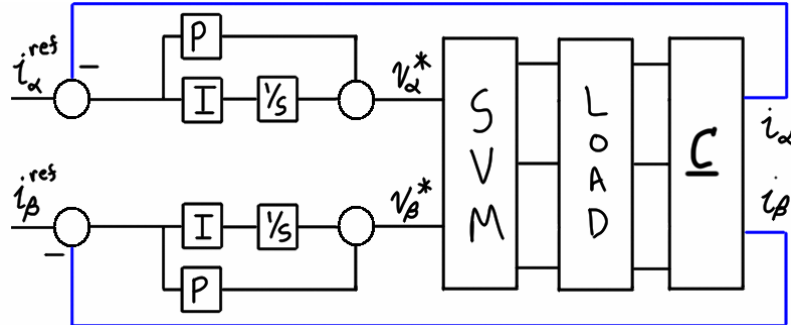
Figure 5.24 – Model of motor load (ideal inverter) viewed from three perspectives.

It should be realized that the motor and power converter are always three-phase. The two-phase stationary ($\alpha\beta$) and two-component synchronous (dq) voltages do not exist—they are only commands representative of the three-phase voltages applied to the motor. Likewise the $\alpha\beta$ and dq currents do not exist—they are transformed versions of the physical measurement of the three-phase currents. However, it has been shown that three-phase quantities may be represented as a SV in any arbitrary frame and that control can be carried out in that same frame. Since a controller in a frame "sees" the motor model from the perspective of that frame, it is as if the transformed voltages and currents existed and the motor can be modeled in the same frame, as shown in Part III of Chapter 3. This assumes the transformations and the SVM inverter are ideal. This assumption is not very practical because the SVM inverter has nonlinearities (dead-time distortion, transistor voltage drop, bus voltage drop), but it is good enough to introduce the concepts of three-phase current regulation and the synchronous regulator in particular.
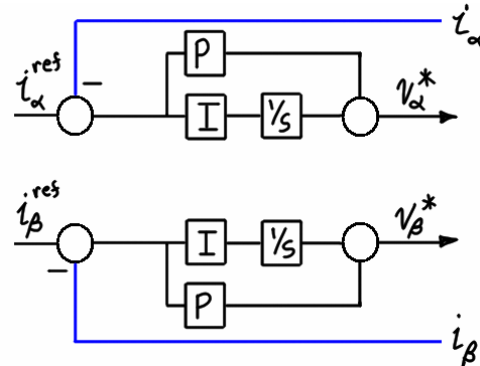
Stationary and Synchronous Regulators

The stationary regulator has already been encountered in Figure 5.11 where it was used in the development of FOC. As mentioned, FOC is the combination of a torque control scheme with a current regulation scheme; the torque control portion is ignored here and the stationary regulator is put into the same form as Figure 5.24. For compatibility with later developments, the d-loop is drawn on top of the figure, as shown in Figure 5.25.
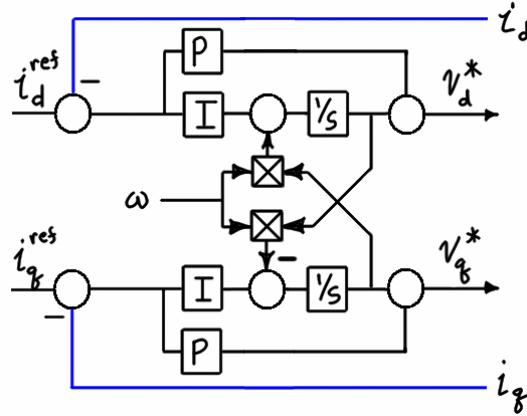
Figure 5.25 – Stationary current control.

To further simplify, the load can be omitted, as shown in Figure 5.26.

Figure 5.26 – Stationary regulator in stationary frame.
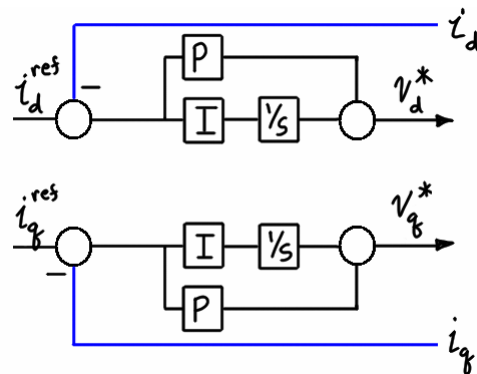
The stationary regulator is one that has a steady-state output that varies cyclically. However, any SV can be transformed to another frame. If each SV is transformed to the synchronous (rotor) frame, the stationary regulator can be viewed from the perspective of the synchronous frame. The derivation [78, p.341] is not reproduced here but the final result is shown in Figure 5.27.

Figure 5.27 – Stationary regulator in synchronous frame.

It must be emphasized that this is only a *representation* of the compensators that are physically operating in the stationary frame—control is not actually executed in the synchronous frame. Figure 5.27 shows that as the frequency of operation increases, the magnitude of the cross-coupling terms increases, causing phase lag in the output (the d-component is made larger while the q-component is made smaller). It is already known that the compensator will experience phase lag and a reduction of gain with increasing frequency—viewing the compensator in the synchronous frame simply exposes the fact in a different form. Finally, the cross coupling forms an oscillator but the oscillations are not present in steady state. However, they can be excited by transients and small-signal resonance is possible [78, pp.343-344]; this unwanted feature is not present in the synchronous regulator described next.
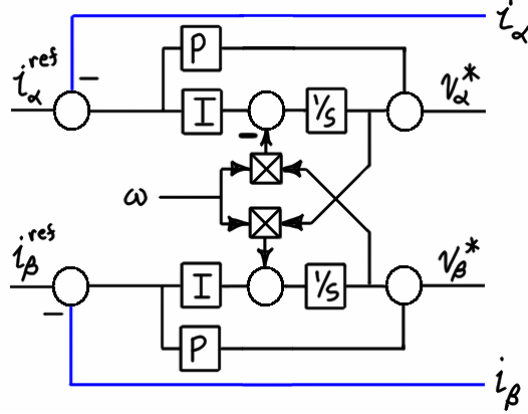
Now the same investigation can be repeated for the synchronous regulator. This was encountered as Figure 5.12 but again the current control will be isolated from the torque control. The simplified synchronous regulator in the synchronous frame is shown in Figure 5.28.

Figure 5.28 – Synchronous regulator in synchronous frame.

As with the stationary regulator in its native frame, the synchronous regulator in its native frame exhibits no cross coupling. This demonstrates that it will not have the phase lag problems the

stationary regulator had. For completeness the synchronous regulator can be transformed to the stationary frame. The math [154] is again omitted and the result is shown in Figure 5.29.

Figure 5.29 – Synchronous regulator in stationary frame.

Now the polarities of the cross-coupling terms are such that with increasing ω the α-component is decreased and the β-component is increased, resulting in a phase lead. As with the stationary regulator in the synchronous frame, examining the synchronous regulator in the stationary frame like this is simply a demonstration from a different viewpoint of what we already know to be true. In this case, the oscillator is active and is more complicated to analyze: it produces output signals even with zero error [78, p. 344] but of course errors are required to adjust the phase of the output to that of the command [158]. Figure 5.29 also demonstrates that a regulator with the performance benefits of the synchronous regulator can be implemented in the stationary frame; this was the original concept presented by Rowan and Kerkman [154]. It can be implemented more simply than a regulator in the synchronous frame (though with modern hardware this is no longer an issue).

In summary, the synchronous regulator is superior to the stationary regulator. It has become the standard for current regulation in polyphase AC machines [157]. Since FOC inherently implements synchronous (rotor) frame current regulation, it inherits the same benefits. Now current control of a motor under FOC will be investigated further.

FOC/Synchronous Current Regulation

Rotor-oriented FOC was shown in Figure 5.14. As before, the blocks in can be bent into the form of Figure 5.24. When the inverter is assumed ideal, then control system reduces to that shown in Figure 5.30. Notice that the rotor position is not relevant—the transformations autonomously handle the current phasing in both command and feedback signals.
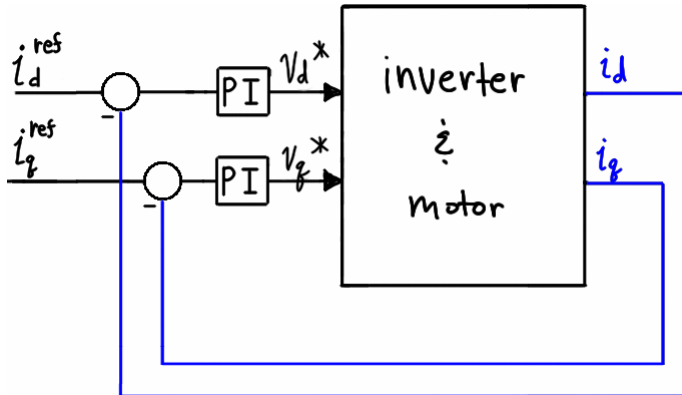
Figure 5.30 – Top-level model of rotor-oriented FOC.

In FOC the synchronous regulator operates in the rotor frame, thus the motor should be modeled in the same. From Chapter 3, the *dq* simulation diagram of the motor is given as Figure 5.31. The figure would normally also show the inverter gain but it is assumed to be unity here; the entire figure corresponds to the block in Figure 5.30.
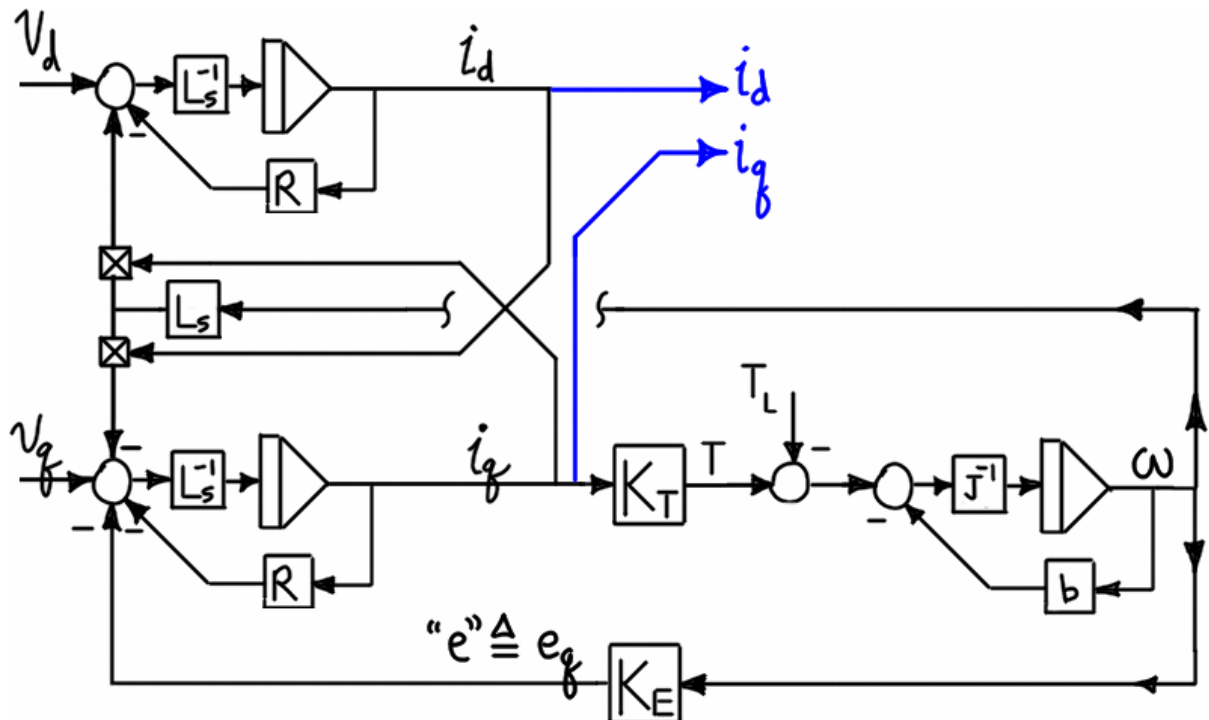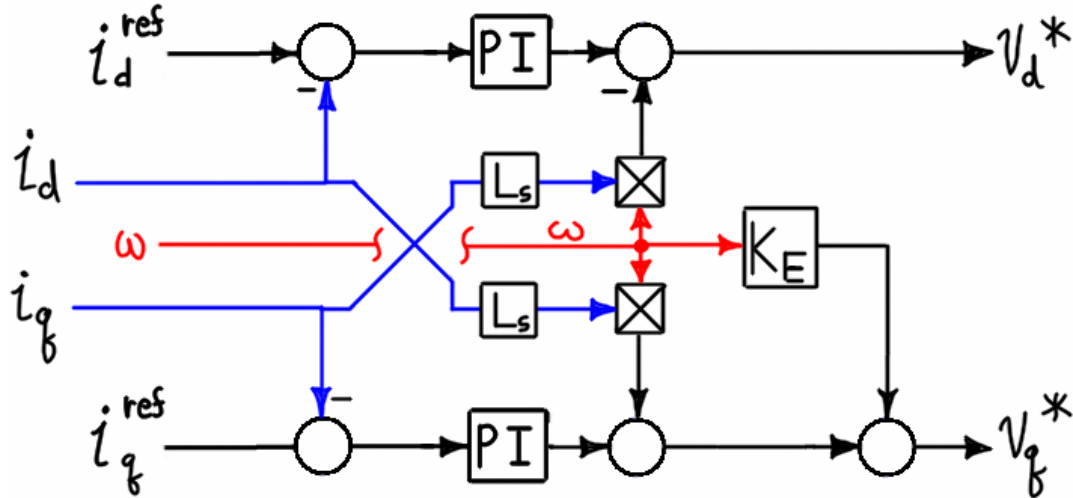
Figure 5.31 – Simulation diagram for BPMS motor in synchronous frame.

At this time the ability of FOC to separately control the *dq* components (as discussed in this chapter) should be contrasted with the coupling discussed in Chapter 3 and shown in Figure 5.31. The FOC *topology* is able to separately control the *dq* current components (because control is exercised in the rotor frame) and this allows direct torque control. However, the dynamics of the component currents are coupled inside the motor, thus it is not true that FOC offers "completely decoupled" control of the stator current components, as some references will insinuate.
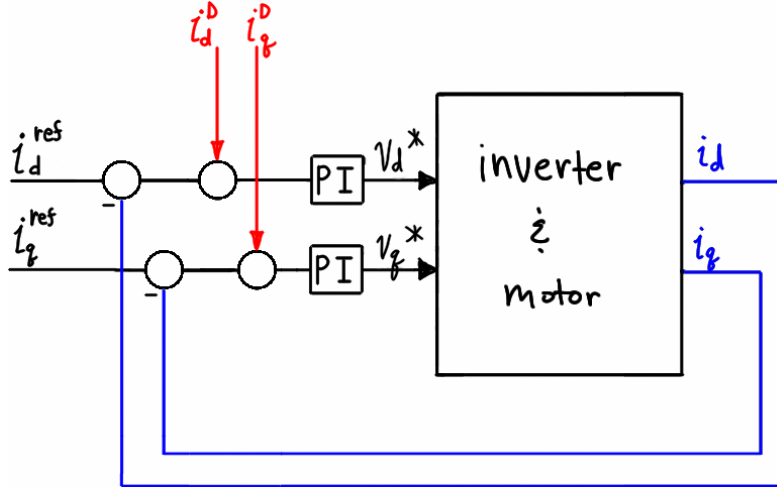
This coupling can be mitigated by modifying the voltage commands to include decoupling signals, as shown in Figure 5.32 (this figure replaces the error summing junctions and PI controllers in Figure 5.30). In addition to the decoupling terms, the q-circuit has a term to offset the effect of the bEMF. These terms are simply the negative of the corresponding terms in Figure 5.31. Usually when this decoupling controller is shown in the literature ([80, p.689], [107]) a salient machine is assumed and the inductances in both Figure 5.31 and Figure 5.32 are then L_d and L_q, but only a nonsalient machine is considered here, hence L_s.

Figure 5.32 – bEMF offset and d-q current decoupling controller in synchronous frame.

The decoupling controller of Figure 5.32 requires as an input the rotor frequency ω. FOC already requires the rotor position signal and the velocity can be estimated from this. (It should be noted that this structure is not the same as that in Figure 5.27 or Figure 5.29, wherein the cross-coupling was *internal to* the PI controller. Those figures showed the equivalent regulator viewed in different frames; Figure 5.32 shows a decoupling scheme implemented intentionally, and the cross-terms are external to the PI controller, as one would normally expect.) The decoupling can be represented more simply by Figure 5.33, where the signals i_d^D and i_q^D are the decoupling terms given by Equation (5.12); these are found directly from Figure 5.32.

$$\begin{cases} i_d^D = -\omega L_s i_q \\ i_q^D = +\omega L_s i_d + \omega K_E \end{cases} \tag{5.12}$$
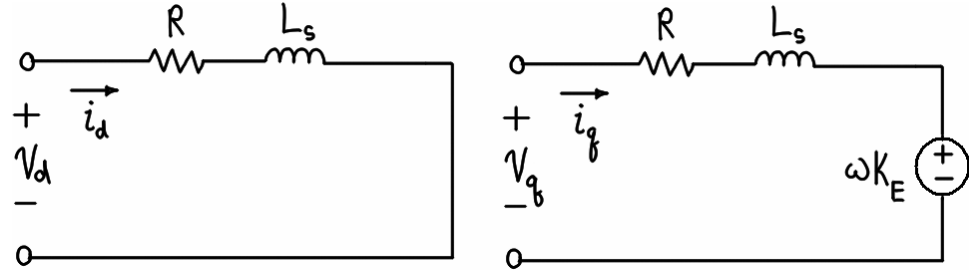
Figure 5.33 – Top-level model of rotor-oriented FOC (with decoupling).

The decoupling scheme is often presented without much discussion; the author's present understanding follows. Since the coupling exists because of the flux linkage, it is present in an R-L load as well (the bEMF offset term would not be present). Both the cross-coupling and the bEMF disturbance are multiplied by ω, which varies slowly compared to the possible rate of change of the currents (and in steady-state operation i_d and i_q are relatively constant). As far the as the steady-state cross-coupling of i_d and i_q is concerned (and as far as ω contributes to the bEMF offset), the disturbances are nearly steady-state quantities. It therefore appears that the decoupling serves to reduce the magnitude of the error (thus "unloading" the integrators) in order to improve transient response. On the other hand, transients in i_d and i_q feed straight through and are not steady-state disturbances, thus it appears that the decoupling also improves the transient response. At least one reference [118] seems to confirm this understanding.

It is curious that most diagrams of FOC controllers do not include these decoupling terms. It is certain that by injecting the bEMF offset term its disturbance on the current loop is eliminated [158]. Since ω varies slowly compared to the bandwidth of the current loop the regulators can handle the error, but as mentioned, [118] indicates that eliminating this offset does improve response. The cross-coupling in the model is clear as well. However, if the synchronous inductance is low the cross-coupling may not be significant enough to warrant the use of decoupling.

At any rate, when the decoupling is not performed and the coupling in the motor model is ignored, or when the decoupling is performed and assumed to be perfect, the BPMS model

reduces to two independent circuits, as shown in Figure 5.34. (Again, if the bEMF is offset as in Figure 5.32, it would not be present in the q-circuit.)

Figure 5.34 – Compensated or approximate model of BPMS motor in synchronous frame.

Since control is executed in the synchronous frame and we have a model of the motor in the same frame, this model could be used to tune the PI controllers. As stated earlier, the decoupling is usually presented without much discussion. However, it should be helpful to examine the decoupling in terms of state space design (both feedback and feedforward). This research has stopped short of a complete understanding. The following references concerning synchronous regulation, tuning, and current regulator design should be helpful starting points for building on the fundamentals presented here: [82], [155], [156], [157], [158], [159], [160], [161], [162]. In particular, examine [125].

CHAPTER 6 - Sensorless Techniques

It is evident that control of a brushless PM motor requires knowledge of the shaft position. For six-step 120° commutation, only six pulses per electrical revolution are required (hence three Hall-effect sensors are often used); for 180° commutation, position feedback of higher resolution is required (such as that provided by an encoder or resolver). This chapter discusses techniques that can be used to replace a physical shaft position sensor by indirectly determining the shaft position. Hence, in BPMS motor control, *sensorless* refers to the lack of a position sensor; voltage and/or current sensors are still required.

First, a brief overview of techniques is presented. Then the general structure of a sensorless FOC system is described and an open-loop estimation scheme is presented. Then the closed-loop topology (a Luenberger observer) is discussed further.

Overview of Techniques

As with BPMS motor types, PWM methods, and direct torque control schemes, there are a very large number of sensorless techniques reported in the literature. As before, there are many different approaches to classifying the sensorless methods. In this report the top-level distinction is between the techniques applicable when using a 120° inverter and those applicable when using either a 120° or a 180° inverter.

In the 120° inverter there is a 60° period per half-cycle when both switches in a phase leg are OFF. This gives a *chance* at monitoring the terminal voltage to detect the zero-crossing of the bEMF. These techniques are usually based on voltage measurement but not always. There are a number of ways to accomplish the task in practice. There are also a large number of practical issues that must be dealt with to ensure successful operation; the issues differ between methods and not all methods are applicable to all motors. For a given motor and drive, use of a sensorless control scheme may limit operation to an operating region that is only a subset of the capability of the same motor and drive under sensored control. All 120° voltage measurement techniques fail at low speed, some may fail with increasing speed or load, and none can achievable appreciable commutation advance unless a neutral connection is used in sensing. As discussed in Appendix

D, some of the 120° methods are applicable when using a 180° inverter, but these require a neutral connection which is not available on standard motors.

In contrast to the 120° inverter, a 180° inverter drives each phase high or low at all times thus there is no possibility of using the direct bEMF sensing techniques applicable with 120° inverters. Instead, an estimator of some sort must be used to determine rotor position. Many of these methods are applicable to 120° inverters as well (but as mentioned, the converse is not true). The estimation methods could be divided into two categories. The first consists of those that estimate variables (such as rotor-stator flux linkage, bEMF) based on principle (first-order) effects. The second consists of those that estimate variables based on second-order or parasitic effects. These include tracking inductance variation due to saliency (a second-order effect) or due to saturation (which is normally a parasitic effect but it can be intentionally exploited) [87, pp.167-176]. The latter methods are specialized to particular machine topologies; many require a salient machine but some are applicable to rotors with surface-mounted magnets. In addition, some of them exploit features that require analysis deeper than that presented in this report, including a detailed treatment of the leakage flux path and the consideration of the effects of slotting and tooth saturation. Some techniques require very accurate values of machine parameters. Finally, a variety of techniques require a high-frequency signal to be injected into the stator voltage commands to excite the variance they track (this requires a deeper understanding of the inverter) and the chosen frequency and magnitude can be critical to performance [168], [169], [170], [171]. Several methods require special techniques to remove ambiguity in position sensing. For these reasons, only the estimators of "normal" principle quantities will be discussed further. (As with all other areas of BPMS motor control, the sensorless literature is flooded with techniques that use artificial intelligence [87], [60], [61]. As before, many of these warrant their own field of study and are not mentioned here.)

Reviews of sensorless operation of AC motors have been published ([172], [167], [166]) as well as general articles reviewing AC motor control which include sections summarizing sensorless operation ([93], [102]). Many references address AC motors as a whole, thus care is required in discerning which general group of motors and inverters a technique is applicable to (induction or BPMS, nonsalient BPMS or salient BPMS, 120° or 180° inverters); this is very difficult to do when techniques for induction and BPMS motors are reviewed simultaneously.

Nature of Sensorless FOC

Chapter 3 gave the state-variable formulation of the motor model for both the stationary and synchronous frames and this was discussed in conjunction with the field oriented control in Chapter 5. In FOC, control is executed in the rotor frame; to transform into and out of this frame requires the rotor angle θ_r. This is true for a sensorless FOC scheme as well; the only difference is that the rotor angle is obtained without a physical sensor, as shown in Figure 6.1. As mentioned, the only sensorless schemes that estimate principle quantities will be discussed; these require knowledge of the motor voltage and/or current as shown.
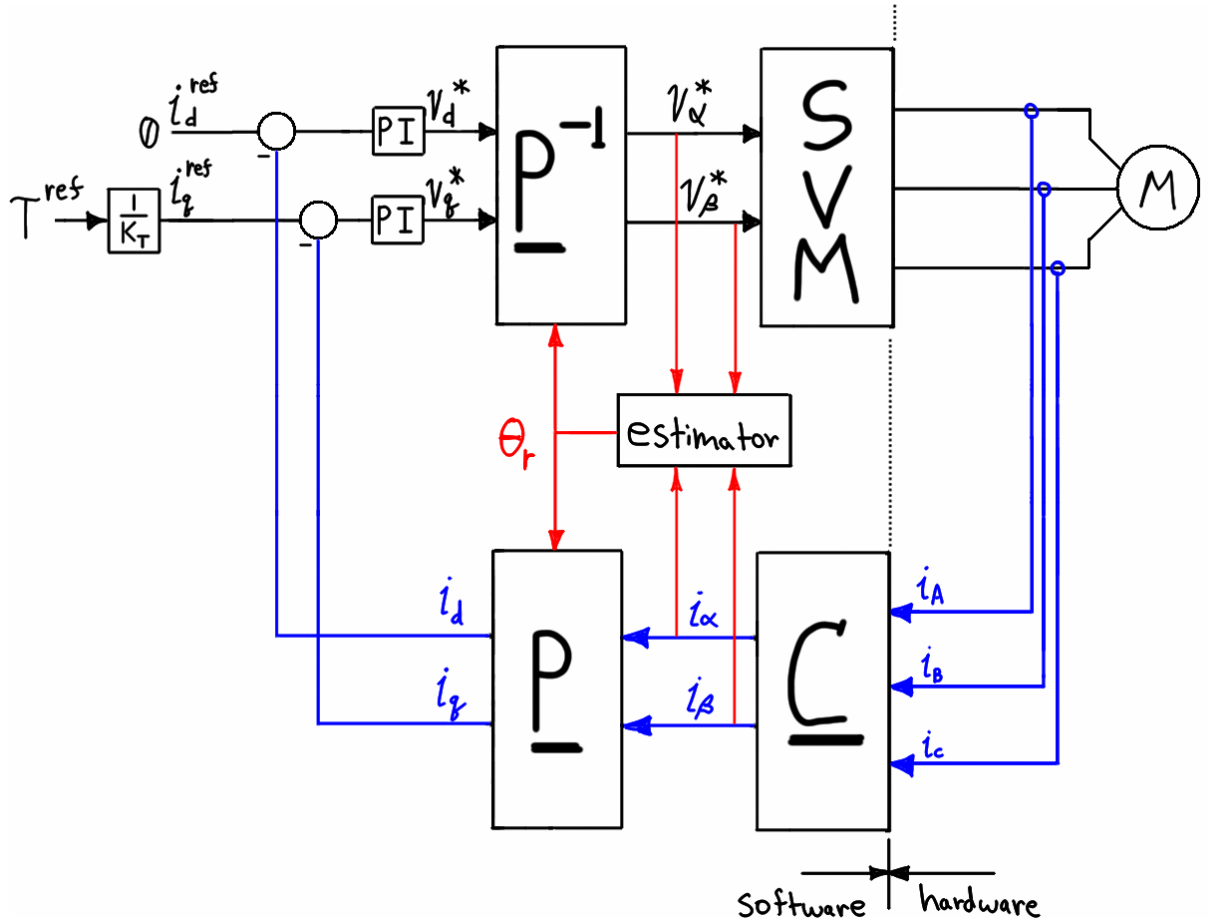
Figure 6.1 – General sensorless FOC structure.

Notice that the estimator requires values from the stationary frame (this can be either the two-phase variables shown or three-phase measurements could be used). This is because only the stationary variables contain information about the rotor position.

An example sensorless scheme is now presented (similar to the one in [173]). From Chapter 3 the voltage equation in the stationary frame is given by Equation (6.1).

$$\vec{v} = R\vec{i} + L_s \frac{d}{dt}\vec{i} + \frac{d}{dt}\vec{\psi}_R \tag{6.1}$$

The rotor-stator flux linkage is always cophasal with the rotor flux thus it contains the rotor position information. Solving for $\vec{\psi}_R$ and integrating both sides yields Equation (6.1).

$$\vec{\psi}_R = \int \left(\vec{v} - R\cdot\vec{i}\right)dt - L_s\vec{i} \tag{6.2}$$

To implement this in software the components would be treated separately as in Equations (6.3) and (6.4). The integration can be performed by any numerical method; each has its own benefits and disadvantages.
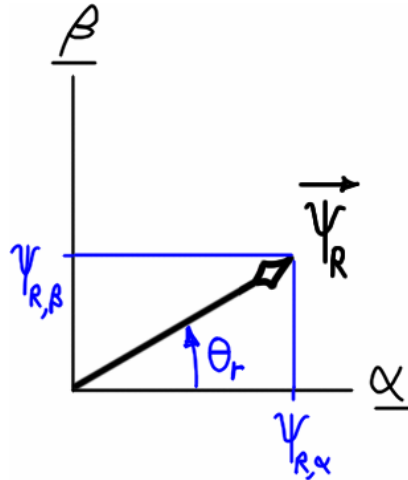
$$\psi_{R,\alpha} = \int \left(v_\alpha - R\cdot i_\alpha\right)dt - L_s i_\alpha \tag{6.3}$$

$$\psi_{R,\beta} = \int \left(v_\beta - R\cdot i_\beta\right)dt - L_s i_\beta \tag{6.4}$$

Finally, the angle of the rotor-stator flux linkage vector can be calculated using Equation (6.5), where the arctangent function is the "two-argument" (four-quadrant) type (so that the range of the rotor angle is $[-\pi, \pi]$).

$$\theta_r = \arctan\left(\frac{\psi_{R,\beta}}{\psi_{R,\alpha}}\right) \tag{6.5}$$

This scheme is summarized in Figure 6.2.

Figure 6.2 – Rotor position estimation via rotor-stator flux linkage estimation.

It is seen that the rotor position estimation consists of two distinct parts: estimating the variables related to the rotor position, and calculating the rotor position using those variables. This scheme estimates the rotor-stator flux linkage in the stationary frame and uses the arctangent function to calculate the rotor angle. This estimator is an open-loop scheme and does not appear to be widely used; most references use closed-loop estimators.

The number of closed-loop schemes is large. The methods differ primarily in the type of estimator and the type of correction used, although there are variations as to which signals are measured. A sizeable portion of the literature concerns the sensorless control of induction machines, which is a technical challenge that is very different in nature than the sensorless control of a BPMS motor. Due to different terminology in use is at times difficult to identify which type of estimator is used. For example, some references state a Luenberger observer is a structure applicable to only linear systems while other references claim otherwise. A full-order linear observer may be called a Luenberger observer, while a reduced-order linear observer may be called a Gopinath observer; another reference will reverse the names. Often an "extended" Luenberger observer is mentioned but the author has yet to find the subject treated in a control system text. Further, there are different structures identified as "extended" Luenberger or Kalman filters (ELO and EKF)—an EKF in one reference may simply estimate states, while an EKF in another reference may be used for simultaneous state estimation and parameter identification. In addition to the large variation in terminology and structure of the "simple" linear Luenberger and Kalman filters (and their extended varieties), nonlinear observers are reported, as is nonlinear compensation of a linear observer. It is also popular to combine adaptive schemes with the observers; there are simply too many possibilities to categorize.

A cursory examination of the literature on sensorless control will reveal that much of it requires a graduate- or post-graduate understanding of mathematical control theory to understand the operation of the system. Even if one had such training, conducting a literature review would be a formidable task. According to [93], "…for the two year period 2005-2006 over 120 papers featuring [sensorless control] were published in IEEE Transactions and Institution of Engineering and Technology Proceedings alone." Even if one were to read and comprehend all of them, it is difficult to make any performance comparisons because the different schemes are not evaluated according to a standard (though some have recently been proposed) [93]. For these reasons and others, this report presents only a simple linearized Luenberger-style observer (closed-loop, full order).

Luenberger Observer

The sensorless scheme just presented was given as a set of equations that could be solved numerically in software. Another popular alternative is to utilize the state-space form. In this

section a state-space model for the motor will be presented; two of the states will jointly contain to the rotor position information. Using a classical observer, the states can be estimated and the rotor position can be obtained. First a brief review of the state-space form is presented. Then a model of the BPMS motor is given. Finally, it will be shown how the said observer fits into a sensorless FOC control system.

Review of State-Space Structure

In modern control an nth-order linear system is described by a set of (n) simultaneous first-order differential equations in state-variable form. The inputs to the system are described by the input vector $\mathbf{u}$ ($r \times 1$), the outputs are described by the output vector $\mathbf{y}$ ($m \times 1$), and the states are described by the state vector $\mathbf{x}$ ($n \times 1$). The n states are related to one another by the state equations (Equation 6.6) and are related to the outputs by the output equations (Equation 6.7).

$$\dot{\mathbf{x}} = \mathbf{f}(\mathbf{x}, \mathbf{u}, t) \tag{6.6}$$

$$\mathbf{y} = \mathbf{h}(\mathbf{x}, \mathbf{u}, t) \tag{6.7}$$
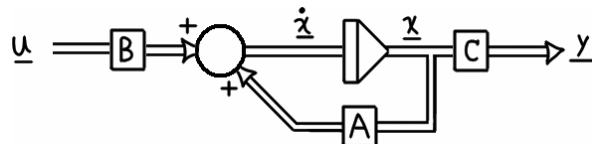
When the relationships are linear they can be described in vector-matrix format as Equations (6.8) and (6.9). $\mathbf{A}$ is the $n \times n$ system matrix, $\mathbf{B}$ is the $n \times r$ input matrix, and $\mathbf{C}$ is the $m \times n$ output matrix.

$$\dot{\mathbf{x}} = \mathbf{Ax} + \mathbf{Bu} \tag{6.8}$$

$$\mathbf{y} = \mathbf{Cx} \tag{6.9}$$
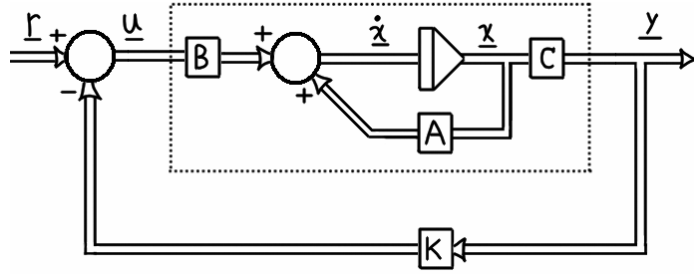
When the system is so described the relationships can be shown in a time-domain simulation diagram, Figure 6.3. The eigenvalues are given by the solution to the characteristic equation (Equation 6.10).

$$\Delta(s) = |s\mathbf{I} - \mathbf{A}| = 0 \tag{6.10}$$

Figure 6.3 – State-space representation of linear system.
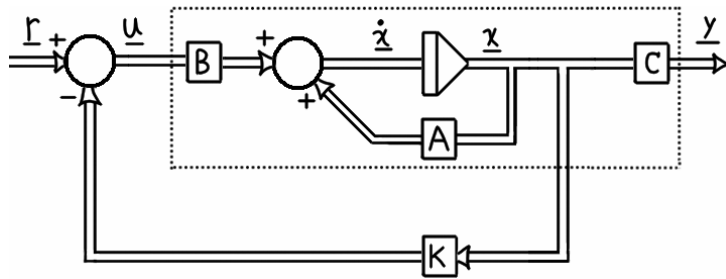
The system (plant) can be controlled by using output feedback as shown in Figure 6.4, where $\mathbf{r}$ is the setpoint and $\mathbf{K}$ is an ($r \times n$) matrix of gains. Output feedback has the limitation that not all eigenvalues can be placed and the setting of one may cause another to move.

Figure 6.4 – Output feedback controller.
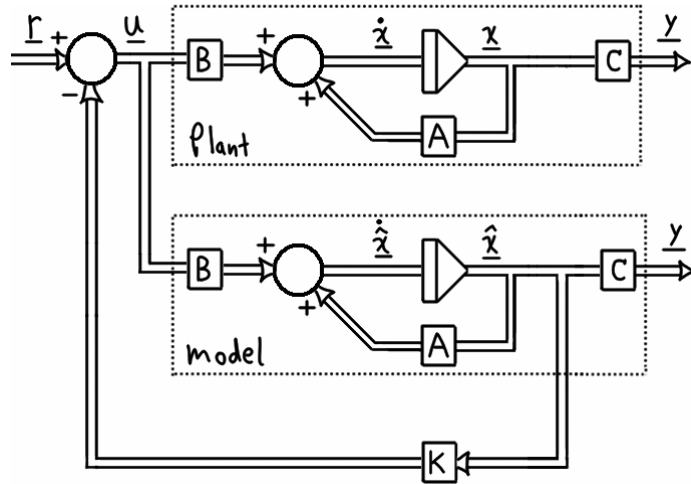
These limitations can be eliminated by using full state feedback as shown in Figure 6.5. If the system is completely controllable the closed-loop eigenvalues may be placed anywhere in the complex plane (subject to controller limitations) according to Equation (6.11).

$$\Delta(s) = \left| s\mathbf{I} - (\mathbf{A} - \mathbf{B}\mathbf{K}) \right| \tag{6.11}$$
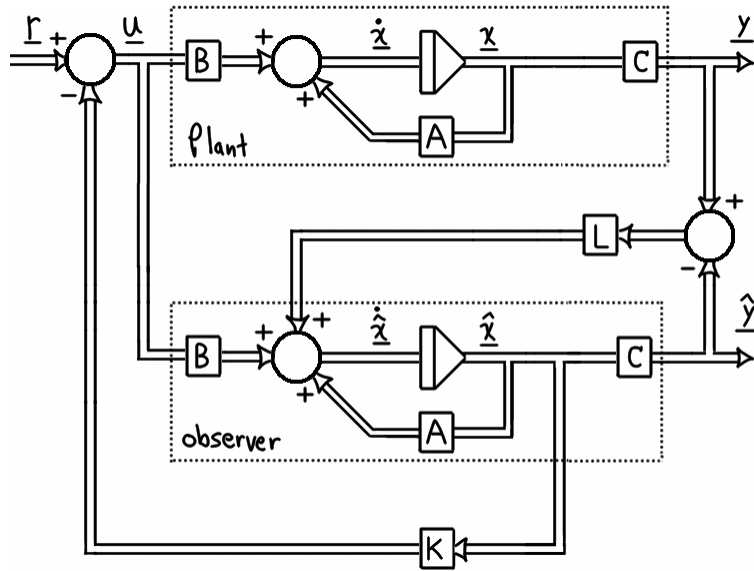
Figure 6.5 – Full state feedback controller.

Full state feedback is far superior to output feedback, but unfortunately the states may not be physically available to be measured (such as the rotor currents in a cage induction motor). To solve the problem another dynamic system (called an estimator) can be used to obtain an estimate of the states that can then be used in a state feedback controller. The simplest form would be to create a simulation model of the plant (an open-loop estimator) as shown in Figure 6.6, where the estimated quantities have hats.

Figure 6.6 – Full state feedback (open-loop estimator).

The estimated state would be in error if they were not initialized to the initial states of the plant or if the model was not exact (which it can never be). Further, the rate at which the error $\mathbf{e} = \mathbf{x} - \hat{\mathbf{x}}$ tends to zero is determined by the plant dynamics (thus the estimate could not be used for control); the math that shows this is found in any of the references cited at the end of this chapter. To solve these problems the estimator can be made to be closed-loop. There seems to be only one sensible way to do this and it is shown in Figure 6.7. The topology is generally called a *Luenberger observer* (named after its inventor, David Luenberger). The estimated output is compared with the actual output and the error is multiplied by a ($n \times m$) gain matrix $\mathbf{L}$. This allows the error dynamics to be controlled, eliminates the error due to incorrect initial state estimates, and should hedge against errors caused by the difference between the plant and the observer model.

Figure 6.7 – Full state feedback (Luenberger observer).

Observation and control of the states are somewhat duals of one another. If the original plant is completely controllable and observable, all *n* eigenvalues of the closed-loop system may be placed arbitrarily by selection of **K** and all *n* eigenvalues of the observer may be placed arbitrarily by selection of **L** ; this is called a separation principle. In sensorless FOC the motor is the plant and information about the rotor position is contained in the states. Although it is possible to control the motor using the full state feedback controller shown, this report uses FOC. Therefore the estimated state vector is *not* fed back into any type of controller. Its only purpose is to produce estimates of the two states that contain information about the rotor position which is required for FOC. According to Figure 6.7, the ability to arbitrarily set the eigenvalues of the observer is not dependent on the use of the state feedback controller, thus FOC may be used to control the plant and the observer can be used without modification. The eigenvalues of the observer may be placed anywhere in the complex plane (subject to digital system limitations) according to Equation (6.12).

$$\Delta(s) = \left| s\mathbf{I} - (\mathbf{A} - \mathbf{LC}) \right| \tag{6.12}$$
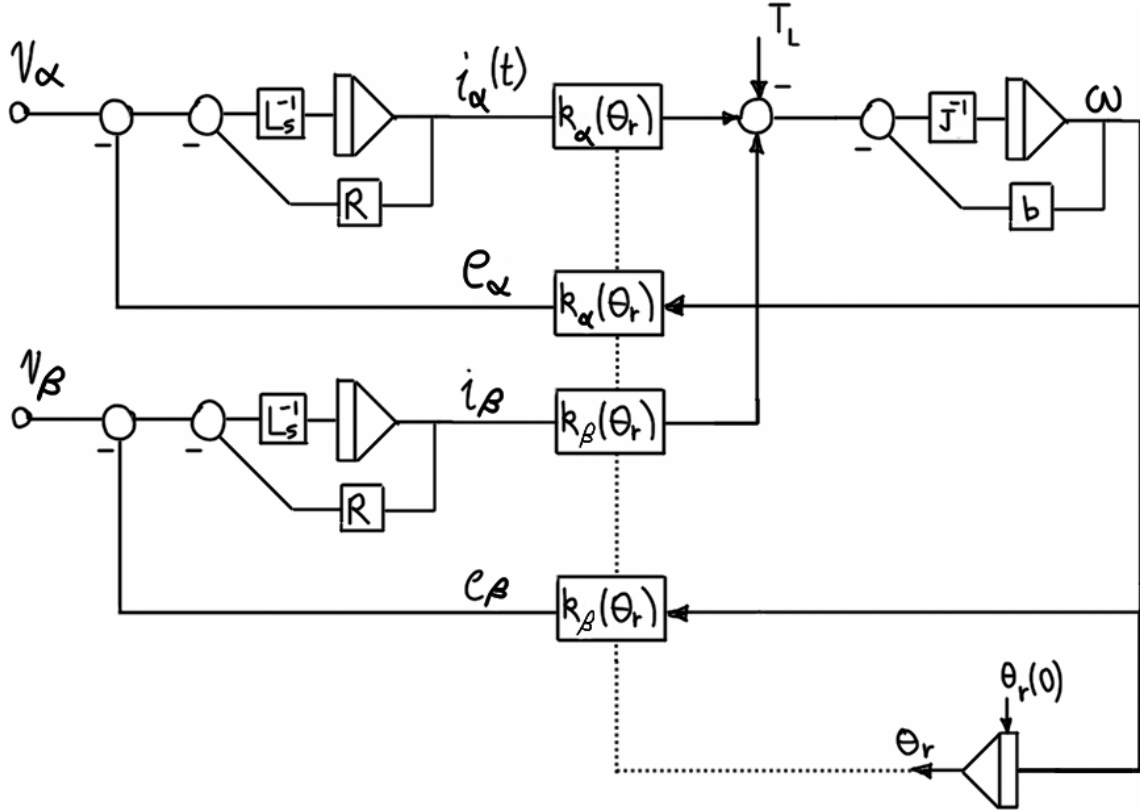
It can be shown that the error dynamics are those of the observer, hence Equation (6.13).

$$\dot{\mathbf{e}} = (\mathbf{A} - \mathbf{LC})\mathbf{e} \tag{6.13}$$

The placement of the observer poles should be sufficiently far into the left-half plane to yield a good state estimate, but there is the usual tradeoff between bandwidth and sensitivity to noise. Time has not allowed further reviewing the principles of modern control. References on observers and pole placement include [45], [46], [48], [49], [50], [51], [52], [53], [54], [55], [56], [57], [58], [59].

State-Space Model of BPMS Motor

A state-space model of a BPMS motor will now be developed. From Chapter 3 the simulation diagram in the stationary frame is given by Figure 6.8.

Figure 6.8 – BPMS motor model in stationary frame.

The most obvious choice of state variables would be $\mathbf{x} = [i_\alpha, i_\beta, \omega, \theta_r]^T$. This would require the mechanical parameters to be known (for use in setting the observer eigenvalues). Some sensorless techniques implement a full mechanical model but their performance suffers when the mechanical parameters change [172] thus it is beneficial to eliminate the mechanical state variables, especially if the mechanical parameters are not known to begin with. The bEMFs are tied to the position of the rotor and each is a function of both mechanical states, thus they are the natural choice to replace the speed and position states. The state vector is then $\mathbf{x} = [i_\alpha, i_\beta, e_\alpha, e_\beta]^T$. From Chapter 3 the state variable equations are given by Equation (6.14), where the bEMFs are given by Equation (6.15).

$$\begin{cases} \dfrac{d}{dt}i_\alpha = \dfrac{1}{L_s}\left[v_\alpha - R \cdot i_\alpha - e_\alpha\right] \\[4mm] \dfrac{d}{dt}i_\beta = \dfrac{1}{L_s}\left[v_\beta - R \cdot i_\beta - e_\beta\right] \end{cases} \tag{6.14}$$

247

$$\begin{cases} e_\alpha = -\omega \Psi_R \sin(\theta_r) \\ e_\beta = +\omega \Psi_R \cos(\theta_r) \end{cases} \qquad (6.15)$$

The model is nonlinear and cannot be described using Equations (6.8) and (6.9) unless it is linearized somehow. In [174] the authors rely on the assumption that the mechanical time constant is significantly less than the electrical time constant. Although this is not true for all motors, they claim that making the assumption allows the mechanical speed to be considered a relatively constant value as compared to the electrical quantities. Noting that the derivatives of the bEMFs are given by Equation (6.16), they can be written in terms of the states, Equation (6.17).

$$\begin{cases} \dot{e}_\alpha = -\omega \cdot \omega \Psi_R \cos(\theta_r) \\ \dot{e}_\beta = -\omega \cdot \omega \Psi_R \sin(\theta_r) \end{cases} \qquad (6.16)$$

$$\begin{cases} \dot{e}_\alpha = -\omega \cdot e_\beta \\ \dot{e}_\beta = +\omega \cdot e_\alpha \end{cases} \qquad (6.17)$$

Then the state and output equations may be written, Equations (6.18) and (6.19).

$$\frac{d}{dt}\begin{bmatrix} i_\alpha \\ i_\beta \\ e_\alpha \\ e_\beta \end{bmatrix} = \begin{bmatrix} -R/L_s & & -1/L_s & \\ & -R/L_s & & -1/L_s \\ & & & -\omega \\ & & \omega & \end{bmatrix}\begin{bmatrix} i_\alpha \\ i_\beta \\ e_\alpha \\ e_\beta \end{bmatrix} + \begin{bmatrix} 1/L_s & \\ & 1/L_s \\ & \\ & \end{bmatrix}\begin{bmatrix} v_\alpha \\ v_\beta \end{bmatrix} \qquad (6.18)$$

$$\begin{bmatrix} i_\alpha \\ i_\beta \end{bmatrix} = \begin{bmatrix} 1 & & & \\ & 1 & & \end{bmatrix}\begin{bmatrix} i_\alpha \\ i_\beta \\ e_\alpha \\ e_\beta \end{bmatrix} \qquad (6.19)$$

The authors implement a reduced-order observer which will not be further described.[42]

The observer that will be described in this report is full-order observer based on the linearized equations above. To see how an observer is used to implement sensorless FOC, recall the block diagram for FOC, Figure 6.9. The rotor angle must be measured by a suitable position transducer (resolver or encoder).

---

[42] Their observer achieved convergence within one mechanical revolution of starting, which is impressive. A plot of the error in rotor angle estimation was not given, but by visually comparing the plots of true versus estimated rotor position it appears the error is negligible. Finally, results are given that show negligible position error due to 130% detuning of parameters (R, Ls).
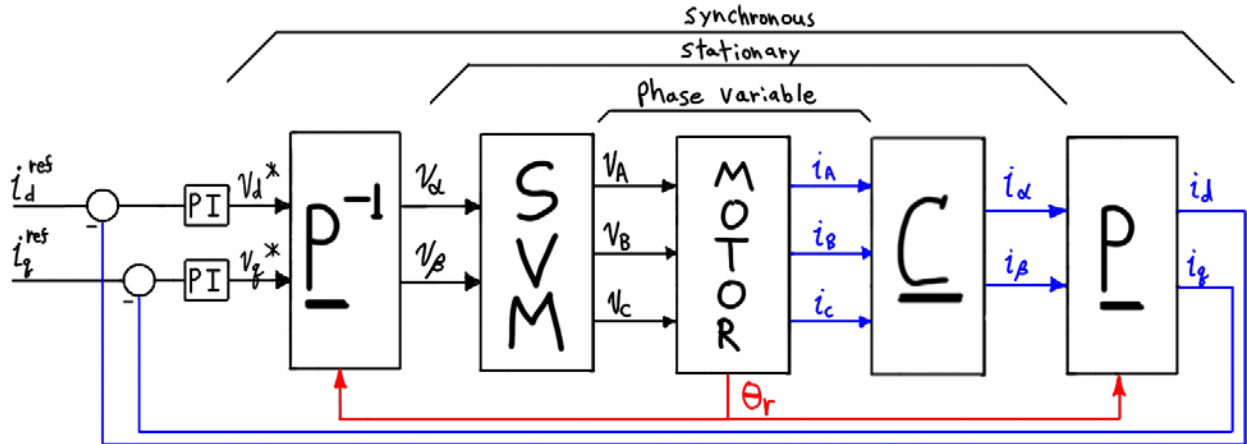
Figure 6.9 – FOC block diagram.

The motor and inverter (and Clarke transform) can be modeled in state-space as shown in Figure 6.10. This figure simply represents the way that the state-space model fits into FOC; it uses the non-linearized version of the model, thus the state vector is $\mathbf{x} = [i_\alpha, i_\beta, \omega, \theta_r]^T$. Therefore the function that gives rotor position in the model is simply $g(\mathbf{x}) = x_4 = \theta_r$.
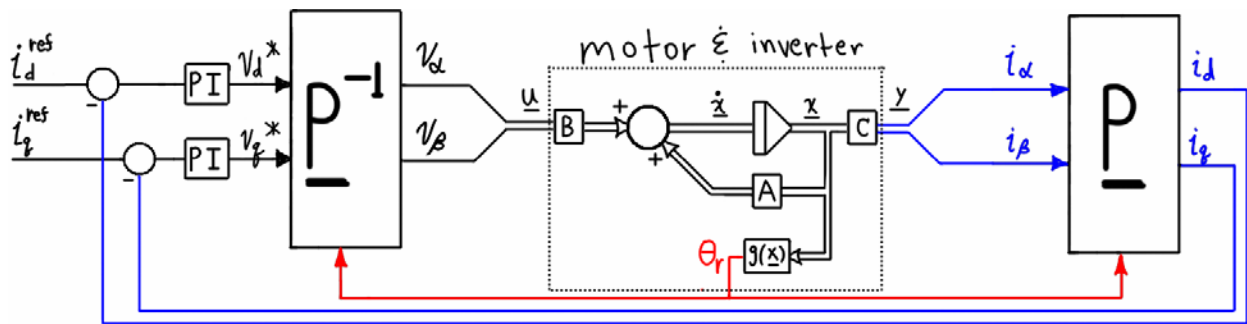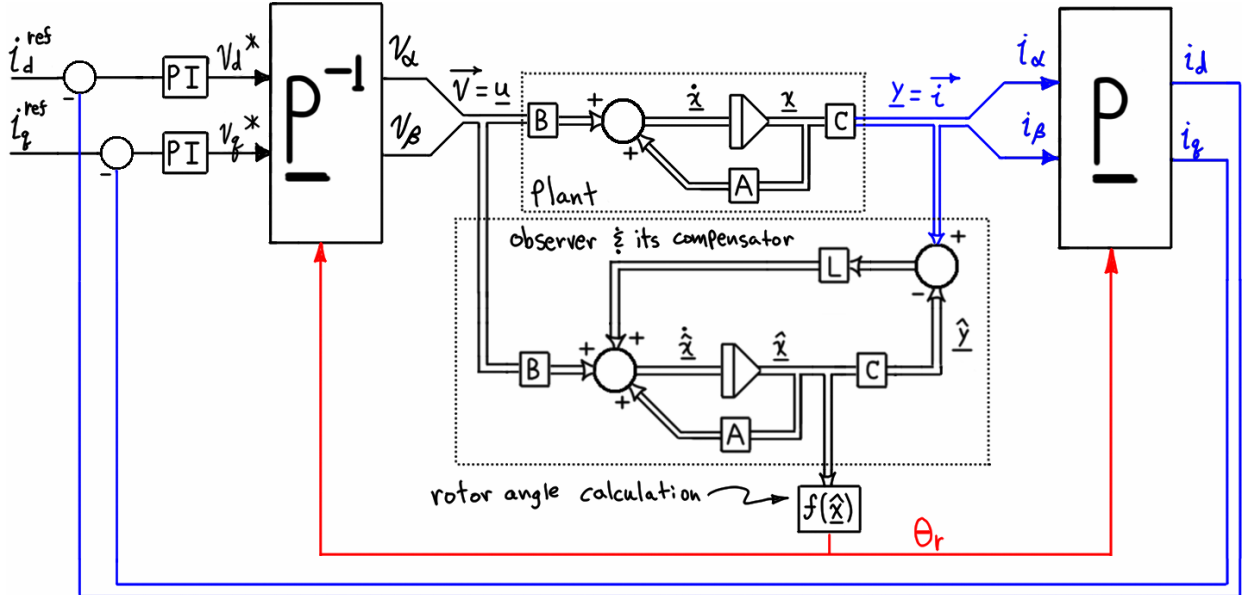
Figure 6.10 – State-space model of motor and inverter.

By definition, sensorless FOC cannot measure position or speed, thus the full state vector is not available. As mentioned, some observers do estimate the full state vector but that requires the mechanical parameters to be known. Instead, the pseudo state vector $\mathbf{x} = [i_\alpha, i_\beta, e_\alpha, e_\beta]^T$ is estimated as shown in Figure 6.11. From the last two estimated states the rotor angle may be calculated using the function $f(\hat{\mathbf{x}})$, which will be discussed shortly.

Figure 6.11 – Sensorless FOC using observer.

There are several things that must be understood about the diagram in Figure 6.11. The plant is representative of the motor, inverter, and Clarke transform. The plant is the only power-conversion part of the control system. However, it is modeled in the stationary (αβ) reference frame, which does not physically exist. This means that the input vector $\mathbf{u} = \vec{v}$ is a software variable. It could be the Clarke transform of the measured phase voltages but is often the αβ commands given to the SVM inverter.[43] This also means that the measured output vector $\mathbf{y} = \vec{i}$ is a software variable as well (the Clarke transform on phase-variable currents measured using a current transducer); since it is a measurement the vector is shown in blue. The current loops, PI compensators, Park and inverse-Park transforms, observer and its compensator, and the rotor angle calculation all exist in software. This is made clear by reexamining Figure 6.1.

In the simplest case, the function $f(\hat{\mathbf{x}})$ used to calculate the rotor angle could be the two-argument arctangent function mentioned earlier. A few articles in the popular literature insinuate that this function is only valid for sinusoidal motors but it is valid regardless of the waveshape—the arctangent is operating on the αβ components. One disadvantage of using the function is the required division. Another potential disadvantage may be the susceptibility to noise unless a digital filter is used (the observer states and rotor angle are calculated each cycle of the current

---

[43] The αβ commands will result in errors because they do not account for bus voltage variations, voltage drop in the transistors, and dead-time effects. There are any number of ways to correct for these deficiencies; the severity of the problem depends greatly on the power transistors, bus voltage, and load.

loop). A second way to implement the function $f\left(\hat{\mathbf{x}}\right)$ is to use a PLL technique that is used in resolver-to-digital conversion (sometimes called an *angle-tracking observer* or a *tracking demodulator*). This has inherent filtering action which could be beneficial, but of course that filtering action would also set an upper limit on observer bandwidth. More information on the technique can be found in [175], [176], [177], [178], [179].

CHAPTER 7 - Concluding Remarks

As stated in Chapter 1, this report summarizes a present state of understanding. As each topic was brought to a close, comments were given regarding the issues that deserve further study and lists of potentially-useful references were given. A few of the topics are mentioned again here, along with some addition ones.

The focus of this report has been the sinusoidal BPMS motor. Torque production was examined in Chapter 2, and Appendix C investigated the nature of the sinusoidal machine. However, the study of torque in that appendix concluded with the single-phase case. Thus the next step would be to study torque in terms of current harmonics for the three-phase machine.

As mentioned in Chapter 5, the coupling in the *dq* model is likely to be negligible because of the low synchronous reactance of BPMS motors, but it may be worth a more detailed look, especially in conjunction with the synchronous regulator. Similarly, the subject of current measurement needs further study, and this should be done in conjunction with the synchronous regulator or FOC topology as well. For example, it would be useful to understand why synchronous sampling of the current requires no filtering [62, p.34-40], [98]. There are many practical limitations to consider when using shunts in the legs of the inverter. It would be useful to determine if some of those limitations could be eliminated by inline current sensors (either shunt or Hall-effect) or if inline schemes have limitations of their own.

The area most lacking in this report is the sensorless operation of FOC. Unlike the other topics covered, the author has come across relatively little literature on the structure of observer presented here. There are many articles on the sensorless control of a BPMS motor but many require an advanced understanding of modern control techniques. Of considerable interest would be the sensitivity of observer's "DC" accuracy (steady-state error) to parameter changes.

Concerning sensorless operation, it would be useful to find a startup technique that is more robust than the "forced commutation" (open-loop) that is often used. Techniques exist to determine the initial position of the rotor, but that is only half of the problem—the other half of the problem is

knowing the rotor position from initialization to changeover to closed-loop operation. It seems that at the present time this can only be accomplished using signal injection techniques.

References

{·} gives additional information such as alternate printings or series titles. For references available through IEEE Xplore®, the 8-digit IEEE .pdf filename is given. (When searching IEEE Xplore®, users must omit leading zeros from the 8-digit number.)

[·]* indicates that a reference was not accessed by the author in preparing this report. Such references are cited to give credit where it is due, to provide historical background, and to provide the reader with a source of additional information. Therefore the author has not read these references and is relying on the citations of other authors for interpretation of the content.

Books (and some classic papers)

Of Historical Importance

[1]   André E. Blondel, <u>Synchronous motors and converters: theory and methods of calculation and testing</u>. McGraw-Hill Book Company, 1913. {Reprinted, Charleston, SC: BiblioBazaar, 2008.}

[2]*   R.E. Doherty, C.A. Nickle, "Synchronous machine I – an extension of Blondel's two-reaction theory," *AIEE Transactions*, vol. 45, pp. 912-926, 1926.

[3]*   R.E. Doherty, C.A. Nickle, "Synchronous machine II – steady power angle characteristics," *AIEE Transactions*, vol. 45, pp. 927-942, 1926.

[4]*   R.E. Doherty, C.A. Nickle, "Synchronous machine III – torque-angle characteristic," *AIEE Transactions*, vol. 46, pp. 1-18, 1927.

[5]*   R.E. Doherty, C.A. Nickle, "Synchronous machine IV – single-phase short circuits," *AIEE Transactions*, vol. 47, pp. 457-487, 1928.

[6]*   R.E. Doherty, C.A. Nickle, "Synchronous machine V – three-phase short circuit," *AIEE Transactions*, vol. 49, pp. 700-714, 1930.

[7]   R.H. Park, "Two reaction theory of synchronous machines, Part I," *AIEE Transactions*, vol. 48, pp. 716-727, 1929.

[8]*   R.H. Park, "Two reaction theory of synchronous machines, Part II," *AIEE Transactions*, vol. 52, pp. 352-354, 1933.

[9]*   C. Concordia, "Two reaction theory of synchronous machines with any balanced terminal impedance," *AIEE Transactions*, vol. 56, pp. 1124-1127, 1937.

[10]*   C. Concordia, <u>Synchronous machines – theory and performance</u>, New York: John Wiley, 1951.

[11]   E. Clarke, <u>Circuit analysis of A-C power systems, Volume I</u>, New York: John Wiley and Sons, 1943.

[12]   E. Clarke, <u>Circuit analysis of A-C power systems, Volume II</u>, New York: John Wiley and Sons, 1950.

[13]*   G. Kron, <u>The application of tensors to the analysis of rotating electrical machinery</u>, *General Electric Review*, 1938.

[14]   G. Kron, <u>Tensors for circuits</u>, Dover: New York, 1959. {Originally titled, <u>A short course in tensor analysis</u>, copyright 1942.}

[15]*   P.K. Kovács, I. Rácz, <u>Transiente vorgange in wechselstrommaschinen</u> (<u>Transient phenomena in electrical machines</u>), *Verlag der Ungarischen Akademie der Wissenschaften*, Budapest, 1959.

[16]*   W.V. Lyon, <u>Transient analysis of AC machinery</u>, New York: MIT & Wiley, 1954.

[17]*   D.C. White, H.H. Woodson, <u>Electromechanical energy conversion</u>, New York : Wiley, 1959.

[18]   A.J. Ellison, <u>Generalized electric machines</u>. London: Harrap, 1967.

[19]*   K. Hasse, "Zur Dynamik Drehzahlgeregelter Antriebe Mit Stromrichter gespeisten Asynchron-Kuzschlublaufermaschinen" (On the Dynamics of Speed Control of a Static AC Drive with a Squirrel Cage Induction Machine), Ph.D. Dissertation, Techn. Hochschule Darmstadt, 1969.

[20]*   F. Blaschke, "Das Prinzip der Feldorientierung, die Grundlage für die Transvektor-Regelung von Drehfeldmaschinen" ("The Principle of Field Orientation – the Basis for the Transvector Control of Three-Phase Machines"), *Siemens Zeitschrift*, Vol. 45, No. 10, pp. 757-760, 1971.

[21]*   F. Blaschke, "Das Verfahren der Feldorientierung zur Regelung der Drehfeldmaschine" ("The Method of Field Orientation for Control of Three Phase Machines"), Ph.D. Dissertation, University of Braunschweig, 1973.

Machines, Circuits, Electromagnetics

[22]   P.M. Anderson, A.A. Fouad, <u>Power system control and stability</u>. 2nd ed. Piscataway, NJ: IEEE Press, 2003.

[23]   N. Hawkins and staff, <u>Hawkins electrical guide – a practical treatise</u>, vols. 1-10, revised 2nd ed., 1917.

[24]   H.W. Beaty, D.G. Fink, <u>Standard handbook for electrical engineers</u>, 15th ed. New York: McGraw-Hill, 2007.

[25]   S.J. Chapman, <u>Electric machinery and power system fundamentals</u>. Boston: McGraw-Hill, 2002.

[26] V. Del Toro, <u>Electric machines and power systems</u>. Englewood Cliffs, NJ: Prentice-Hall, 1985.

[27] A.E. Fitzgerald, Charles Kingsley, Jr., <u>Electric machinery</u>, 2nd ed. New York: McGraw-Hill, 1961.

[28] A.E. Fitzgerald, Charles Kingsley Jr., S.D. Umans, <u>Electric machinery</u>, 6th ed. New York: McGraw-Hill, 2003.

[29] J.D. Glover, M.S. Sarma, <u>Power system analysis and design</u>, 3rd ed. Pacific Grove, CA: Wadsworth/Thomson Learning, 2002.

[30] C. Gross, <u>Electric machines</u>. Boca Ratone: CRC Press, 2007.

[31] D. Halliday, R. Resnick, J. Walker, <u>Fundamentals of physics</u>, 6th ed. New York: John Wiley & Sons, 2001.

[32] N.N. Hancock, <u>Matrix analysis of electrical machinery</u>, 2nd ed. New York: Pergamon Press, 1974.

[33] A. Hughes, <u>Electric motors and drives: fundamentals, types, and applications</u>, 3rd ed. Boston: Newnes, 2006.

[34] C.V. Jones, <u>The unified theory of electrical machines</u>. London: Butterworths, 1967.

[35] P.C. Krause, O. Wasynczuk, S.D. Sudhoff, <u>Analysis of electric machinery</u>. New York: IEEE Press, 1995.

[36] Werner Leonhard, <u>Control of electrical drives</u>. New York: Springer, 2001.

[37] S.A. Nasar, L.E. Unnewehr, <u>Electromechanics and electric machines</u>. New York: John Wiley & Sons, 1979.

[38] S.A. Nasar, <u>Electric machines and power systems</u>. New York: McGraw-Hill, 1995.

[39] J.W. Nilsson, S.A. Riedel, <u>Electric circuits</u>, 6th ed. Upper Saddle River, NJ: Prentice-Hall, 2001.

[40] D.H. Braymer, A.C. Roe, <u>Rewinding small motors</u>, 3rd ed. New York: McGraw-Hill, 1949.

[41] P.C. Sen, <u>Principles of electric machines and power electronics</u>, 2nd ed. New York: John Wiley & Sons, 1997.

[42] Gordon R. Slemon, <u>Electric machines and drives</u>. Reading, MA: Addison-Wesley, 1992.

[43] H.A. Toliyat, G.B. Kliman, eds., <u>Handbook of electric motors</u>, 2nd ed. New York: Marcel Dekker, 2004.

[44] F.T. Ulaby, <u>Fundamentals of applied electromagnetics</u>, 2004 media ed. Upper Saddle River, NJ: Pearson Prentice Hall, 2004.

Control Systems, Linear Analysis

[45]   W.L. Brogan, <u>Modern control theory</u>, 3rd ed. Upper Saddle River, NJ: Prentice Hall, 1991.

[46]   P.M. DeRusso, R.J. Roy, C.M. Close, A.A. Desrochers, <u>State variables for engineers</u>, 2nd ed. New York: Wiley-Interscience, 1998.

[47]   George Ellis, <u>Control system design guide: a practical guide</u>. 3rd ed. Amsterdam: Elsevier Academic Press, 2004.

[48]   George Ellis, <u>Observers in control systems: a practical guide</u>. San Diego, CA: Academic Press, 2002.

[49]   Bernard Friedland, <u>Control system design: an introduction to state-space methods</u>. Mineola, NY: Dover Publications, 1986.

[50]   M. Gopal, <u>Digital control and state variable methods</u>, 2nd ed. New Delhi: Tata McGraw-Hill, 2003.

[51]   B.P. Lathi, <u>Signal processing & linear systems</u>. New York: Oxford University Press, 1998.

[52]   N.E. Leonard, W.S. Levine, <u>Using Matlab to analyze and design control systems</u>, 2nd ed. Redwood City, CA: Addison-Wesley, 1995.

[53]   W.S. Levine, ed, <u>The control handbook</u>. Boca Ratone, FL; Piscataway, NJ: CRC Press; IEEE Press, 1996.

[54]   B. Shahian, M. Hassul, <u>Control system design using MATLAB</u>. Englewood Cliffs, NJ: Prentice-Hall, 1993.

[55]   R.L. Williams, II, D.A. Lawrence, <u>Linear state-space control systems</u>. Hoboken, NJ: John Wiley & Sons, 2007.

[56]   K. Ogata, <u>State space analysis of control systems</u>. Englewood Cliffs, NJ: Prentice-Hall, 1967.

[57]   K. Ogata, <u>Modern control engineering</u>, 4th ed. Upper Saddle River, NJ: Prentice Hall, 2002.

[58]   M.S. Santina, A.R. Stubberud, G.H. Hostetter, <u>Digital control system design</u>, 2nd ed. Fort Worth: Saunders College Publishing, 1994.

[59]   G.F. Franklin, J.D. Powell, M. Workman, <u>Digital control of dynamic systems</u>, 3rd ed. Menlo Park, CA: Addison-Wesley, 1998.

Drives, Control, Power Electronics, PM & Servo Motors, Modeling

[60]   B.K. Bose, <u>Power electronics and motor drives: advances and trends</u>. Boston: Academic Press, 2006.

[61]   B.K. Bose, ed., <u>Power electronics and variable frequency drives: technology and applications</u>. Piscataway, NJ: IEEE Press, 1997.

[62]   S. Buso, P. Mattavelli, <u>Digital control in power electronics</u>. San Rafael, CA: Morgan & Claypool Publishers, 2006.

[63]   Y. Dote, S. Kinoshita, eds., <u>Brushless servomotors: fundamentals and applications</u>. New York: Oxford University Press, 1990. {Monographs in Electrical & Electronic Engineering #23}

[64]   Bill Drury, <u>The Control Techniques Drives and Controls Handbook</u>. London: Institution of Electrical Engineers, 2001.

[65]   *DC motors, speed controls, servo systems*, 5th ed., an engineering handbook by Electro-Craft Corporation, Hopkins, MN, 1980.

[66]   J.F. Gieras, R-J Wang, M.J. Kamper, <u>Axial flux permanent magnet brushless machines</u>. Boston: Kluwer, 2004.

[67]   D.W. Hart, <u>Introduction to power electronics</u>. Upper Saddle River, NJ: Prentice Hall, 1997.

[68]   D. Hanselman, Brushless <u>Permanent Magnet Motor Design</u>, 2nd ed. Lebanon, OH: Magna Physics Publishing, 2006.

[69]   J.R. Hendershot, T.J.E. Miller, <u>Design of brushless permanent-magnet motors</u>. Hillsboro, OH: Magna Physics Publications; Oxford: Clarendon Press, 1994. {Monographs in Electrical & Electronic Engineering #37}

[70]   D. Grahame Holmes, Thomas A. Lipo, <u>Pulse width modulation for power converters: principles and practice</u>. Hoboken, NJ: Wiley-Interscience, 2003.

[71]   R. Krishnan, <u>Electric motor drives: modeling, analysis, and control</u>. Upper Saddle River, N.J.: Prentice Hall, 2001.

[72]   M.P. Kazmierkowski, R. Krishnan, F. Blaabjerg, <u>Control in power electronics: selected problems</u>. New York: Academic Press, 2002.

[73]   N. Mohan, <u>Electric drives: an integrative approach</u>. Minneapolis: MNPERE, 2003.

[74]   N. Mohan, <u>Advanced electric drives: analysis, control and modeling using Simulink</u>. Minneapolis: MNPERE, 2001.

[75]   N. Mohan, T. Undeland, W.P. Robbins, <u>Power electronics: converters, applications, and design</u>, 3rd ed. Hoboken, NJ: John Wiley & Sons, 2003.

[76]   Peter Moreton, <u>Industrial brushless servomotors</u>. Oxford: Newnes, 2000.

[77]   J.M.D. Murphy, F.G. Turnbull, <u>Power electronic control of AC motors</u>. New York: Pergamon Press, 1988.

[78]   D.W. Novotny, T.A. Lipo, <u>Vector control and dynamics of AC drives</u>. Oxford: Clarendon Press; New York: Oxford University Press, 1996. {Monographs in Electrical & Electronic Engineering #41}

[79]   Muhammad H. Rashid, <u>Power electronics: circuits, devices, and applications</u>, 2nd ed. Upper Saddle River, NJ: Prentice-Hall, 1993.

[80]   Muhammad H. Rashid, editor, <u>Power electronics handbook</u>. San Diego, CA: Academic Press, 2001.

[81]   S.B. Dewan, G.R. Slemon, A. Straughen, <u>Power semiconductor drives</u>. New York: Wiley-Interscience, 1984.

[82]   V. Subrahmanyam, <u>Electric drives: concepts and applications</u>. New York: McGraw-Hill, 1994.

[83]   Richard Valentine, ed., <u>Motor control electronics handbook</u>. New York: McGraw-Hill, 1998.

[84]   Peter Vas, <u>Vector control of AC machines</u>. Oxford: Clarendon Press; New York: Oxford University Press, 1990. {Monographs in Electrical & Electronic Engineering #22}

[85]   Peter Vas, <u>Electrical machines & drives: a space-vector theory approach</u>. Oxford: Clarendon Press; New York: Oxford University Press, 1992. {Monographs in Electrical & Electronic Engineering #25}

[86]   Peter Vas, <u>Parameter estimation, condition monitoring, and diagnosis of electrical machines</u>. Oxford: Clarendon Press; New York: Oxford University Press, 1993. {Monographs in Electrical & Electronic Engineering #27}

[87]   Peter Vas, <u>Sensorless Vector and Direct Torque Control</u>. New York: Oxford University Press, 1998. {Monographs in Electrical & Electronic Engineering #42; this book is an updated version of #22}

[88]   A. Veltman, D.W.J. Pulle, R.W. De Doncker, <u>Fundamentals of electrical drives</u>. Springer, 2007.

[89]   Ion Boldea, S.A. Nasar, <u>Vector control of AC drives</u>. Boca Raton: CRC Press, 1992.

Articles, Conference Proceedings, Transactions

AC Drives

[90]   E.L. Owen, M.M. Morack, C.C. Herskind, A.S. Grimes, "AC adjustable-speed drives with electronic power converters—the early days," *IEEE Transactions on Industry Applications*, vol. IA-20, no. 2, pp. 298-308, Mar./Apr. 1984. {04504412}

[91]   E.L. Owen, T.M. Jahns, "AC adjustable-speed drives at the millennium: how did we get here?" *IEEE Transactions on Power Electronics*, vol. 16, no. 1, pp. 17-25, Jan. 2001. {00903985}

[92]   R.J. Kerkman, G.L. Skibinski, D.W. Schlegel, "AC drives: Year 2000 (Y2K) and beyond," *Fourteenth Annual Applied Power Electronics Conference and Exposition (APEC)*, 1999, vol. 1, pp. 28-39. {00749486}

[93]   J.W. Finch, D.Giaouris, "Controlled AC electrical drives," *IEEE Transactions on Industrial Electronics*, vol. 55, no. 2, pp. 481-491, Feb. 2008. {04401131}

[94]   J. Bocker, S. Mathapati, "State of the art of induction motor control," *IEEE International Electric Machines & Drives Conference*, 2007, vol. 2, pp. 1459-1464. {04270863}

[95]   W. Drury, "Electrical variable speed drives: mature consumable or radical infant?" *Power Engineering Journal*, vol. 13, no. 2, pp. 65-78, Apr. 1999. {00765690}

[96]   V. Vučković, "Interpretation of a discovery," *Serbian Journal of Electrical Engineering*, vol. 3, no. 2, pp. 177-202, Nov. 2006. [Online]. Available: `http://www.journal.tfc.kg.ac.yu/Vol_3-2/06-Vuckovic.pdf`

[97]   W. Leonhard, "30 years space vectors, 20 years field orientation, 10 years digital signal processing with controlled AC-drives, a review, Part I," *EPE Journal*, vol. 1, no. 1, Jul. 1991.

[98]   W. Leonhard, "30 years space vectors, 20 years field orientation, 10 years digital signal processing with controlled AC-drives, a review, Part II," *EPE Journal*, vol. 1, no. 2, Oct. 1991.

[99]   "What is field oriented control and what good is it?" Copley Controls Corp. [Online]. Available: `http://www.maccon.de/FTPROOT/Field-Oriented-Control.pdf`

[100]   F.J. Bartos, "Got Field-Oriented Control in Your Servos?" *Control Engineering*, 01 Feb 2004. [Online]. Available: `http://www.controleng.com/article/CA379359.html`

[101]   G.S. Buja, M.P. Kazmierkowski, "Direct torque control of PWM inverter-fed AC motors—a survey," *IEEE Transactions on Industrial Electronics*, vol. 51, no. 4, pp. 744-757. {01318735}

[102]   W. Leonhard, "Adjustable speed AC drives," *Proceedings of the IEEE*, vol. 76, no. 4, pp. 455-471, Apr. 1988. {00004430}

Machine Modeling, Analysis

[103] J. Holtz, "The representation of AC machine dynamics by complex signal flow graphs" (invited paper), *IEEE Transactions on Industrial Electronics*, vol. 42, no. 3, pp.263-271, 1995. {00382137}

[104] J. Holtz, "On the spatial propagation of transient magnetic fields in AC machines," *IEEE Transactions on Industry Applications*, vol. 32, no. 4, pp. 927-937, Jul./Aug. 1996. {00511561}

[105] T.A. Lipo, *Reference frame theory*, Chapter 2 of course notes for ECE511 - Theory and Control of Synchronous Machines, Department of Electrical and Computer Engineering, College of Engineering, University of Wisconsin-Madison, draft date 12 Oct. 2007. [Online]. Available:
`http://ecow.engr.wisc.edu/cgi-bin/getbig/ece/511/lipo/notes/511ch2.pdf`

[106] T.A. Lipo, "A Cartesian vector approach to reference frame theory of AC machines," Wisconsin Electric Machines and Power Electronics Consortium (WEMPEC), Madison, WI, Research Report 84-2, Apr. 1984. [Online]. Available:
`http://www.ece.wisc.edu/~lipo/1980s%20pubs/84-02.pdf`

[107] D.Y. Ohm, "Dynamic model of PM synchronous motors," Drivetech, Inc., 16 May 2000. [Online]. Available: `www.drivetechinc.com/articles/IM97PM_Rev1forPDF.pdf`

[108] T.M. Jahns, "Motion control with permanent magnet AC machines," *Proceedings of the IEEE*, vol. 82, no. 8, pp. 1241-1252, Aug. 1994. {00301686}

Field Weakening, Interior Magnet Motors

[109] T. Sebastian, G.R. Slemon, "Operating limits of inverter-driven permanent magnet motor drives," *IEEE Transactions on Industry Applications*, vol. IA-23, no. 2, pp. 327-333, Mar./Apr. 1987. {04504909}

[110] B. Sneyers, D.W. Novotny, T.A. Lipo, "Field weakening in buried permanent magnet AC motor drives," *IEEE Transactions on Industry Applications*, vol. IA-21, no. 2, pp. 398-407, Mar./Apr. 1985. {04157998}

[111] A.M. EL-Refaie, T.M. Jahns, "Comparison of synchronous PM machine types for wide constant-power speed operation: converter performance," *IET Electric Power Applications*, vol. 1, no. 2, pp. 217–222, Mar. 2007. {04145269}

[112] S. Morimoto, et al., "Expansion of operating limits for permanent magnet motor by current vector control considering inverter capacity," *IEEE Transactions on Industry Applications*, vol. 26, no. 5, pp. 866-871, Sep./Oct. 1990. {00060058}

[113] R. Monajemy, R. Krishnan, "Implementation strategies for concurrent flux weakening and torque control of the PM synchronous motor," *Conference Record of the IEEE Industry Applications Annual Meeting*, 1995, pp. 238-245. {00530307}

[114] W.L. Soong, T.J.E. Miller, "Field-weakening performance of brushless synchronous AC motor drives," *IEE Proceedings of Electric Power Applications*, vol. 141, no. 6, pp. 331-340, Nov. 1994. {00336343}

[115] R.F. Schiferl, T.A. Lipo, "Power capability of salient pole permanent magnet synchronous motors in variable speed drive applications," *IEEE Transactions on Industry Applications*, vol. 26, no. 1, pp. 115-123, Jan./Feb. 1990. {00052682}

[116] M. Bilewski, et al., "Control of high performance interior permanent magnet synchronous drives," *Conference Record of the IEEE Industry Applications Society Annual Meeting*, 1990, pp. 531-538. {00152236}

Inverters (CRPWM, VSI, SVM)

Summary, overview

[117] D.Y. Ohm, R.J. Oleksuk, "Influence of PWM schemes and commutation methods for DC and brushless motors and drives," Drivetech, Inc., presented at *P.E. Technology 2002 Conference*, Stephens Convention Center (Rosemont, IL), Oct. 27-31, 2002. [Online]. Available: `www.drivetechinc.com/articles/SW_BLDCAC5.pdf`

[118] D.Y. Ohm, J.H. Park, "About commutation and current control methods for brushless motors," Drivetech, Inc., presented at the *29th annual IMCSD symposium*, San Jose, July 26-29, 1999. [Online]. Available: `www.drivetechinc.com/articles/curbldc3.pdf`

[119] J. Holtz, "Pulsewidth modulation for electronic power converters," *Proceedings of the IEEE*, vol. 82, no. 8, pp. 1194-1214, Aug. 1994. {00301684}

[120] J. Holtz, "Pulsewidth modulation—a survey," *IEEE Transactions on Industrial Electronics*, vol. 39, no. 5, pp. 410-420, Dec. 1992. {00161472}

[121] L. Malesani, P. Tomasin, "PWM current control techniques of voltage source converters—a survey," *Proceedings of the International Conference on Industrial Electronics, Control, and Instrumentation*, 1993, vol. 2, pp. 670-675. {00339000}

[122] D.M. Brod, D.W. Novotny, "Current control of VSI-PWM inverters," *IEEE Transactions on Industry Applications*, vol. IA-21, no. 4, pp. 562-570, May/Jun. 1985. {04158027}

[123] A.M. Trzynadlowski, "An overview of modern PWM techniques for three-phase, voltage-controlled, voltage-source inverters," *Proceedings of the IEEE International Symposium on Industrial Electronics*, 1996, pp. 25-39. {00548389}

[124] M.P. Kazmierkowski, L. Malesani, Guest editorial - special section on PWM converter current control, *IEEE Transactions on Industrial Electronics*, vol. 45, no. 5, pp. 689-690, Oct. 1998. {00720324}

[125] M.P. Kazmierkowski, L. Malesani, "Current control techniques for three-phase voltage-source PWM converters: a survey," *IEEE Transactions on Industrial Electronics*, vol. 45, no. 5, pp. 691-703, Oct. 1998. {00720325}

[126] A.M. Hava, R.J. Kerkman, T.A. Lipo, "Simple analytical and graphical methods for carrier-based PWM-VSI drives," *IEEE Transactions on Power Electronics*, vol. 14, no. 1, pp. 49-61, Jan. 1999. {00737592}

THI, SVM, SPWM

[127] J.A. Houldsworth, D.A. Grant, "The use of harmonic distortion to increase the output voltage of a three-phase PWM inverter," *IEEE Transactions on Industry Applications*, vol. IA-20, no. 5, pp.1224-1228, Sep./Oct. 1984. {04504587}

[128] D.G. Holmes, "The significance of zero space vector placement for carrier-based PWM schemes," *IEEE Transactions on Industry Applications*, vol. 32, no. 5, pp. 1122-1129, Sep./Oct. 1996. {00536874}

[129] K.G. King, "A three phase transistor class B inverter with sinewave output and high efficiency," *Institution of Electrical Engineers (IEE) Conference Publication l23, Power Electronics, Power Semiconductors and Their Applications*, pp. 204-209, 1974.

[130]* G. Buja, G. Indri, "Improvement of pulse width modulation techniques," *Archiv fur Elektrotechnik*, vol. 57, pp.281-289, 1975.

[131]* J. Holtz, S. Stadtfeld, "A predictive controller for the stator current vector of AC machines fed from a switched voltage source", *Conference Record IPEC*, Tokyo, 1983, Vol. 2, pp. 1665-1675.

[132] L. Malesani, P. Tenti, E. Gaio, R. Piovan, "Improved Current Control Technique of VSI PWM Inverters with Constant Modulation Frequency and Extended Voltage Range," *IEEE Transactions on Industry Applications*, vol. 27, no. 2, pp. 365-369, Mar./Apr. 1991. {00073627}

[133] H.W. Van Der Broeck, H-C Skudelny, G.V. Stanke, "Analysis and realization of a pulsewidth modulator based on space vectors," *IEEE Transactions on Industry Applications*, vol. 24, no. 1, pp. 142-150, Jan./Feb. 1988. {00087265}

[134] K. Zhou, D. Wang, "Relationship between space-vector modulation and three-phase carrier-based PWM: a comprehensive analysis," *IEEE Transactions on Industrial Electronics*, vol. 49, no. 1, pp. 186-196, Feb 2002. {00982262}

[135] S.R. Bowes, Y-S Lai, "The relationship between space-vector modulation and regular-sampled PWM," *IEEE Transactions on Industrial Electronics*, vol. 44, no. 5, pp.670-679, Oct. 1997. {00633469}

[136] D.G. Holmes, "The general relationship between regular-sampled pulse-width-modulation and space vector modulation for hard switched converters," *Conference Record of the 1992 IEEE Industry Applications Society Annual Meeting*, vol. 1, pp. 1002-1009. {00244437}

[137] G-M Lee, D-C Lee, "Implementation of naturally sampled space vector modulation eliminating microprocessors," *Proceedings of the Third International Power Electronics and Motion Control Conference (IPEMC) 2000*, vol. 2, pp. 803-807. {00884606}

Dead-Time Effects & Compensation

[138] D. Leggate, R.J. Kerkman, "Pulse based dead time compensator for PWM voltage inverters," *Proceedings of the International Conference on Industrial Electronics, Control, and Instrumentation*, 1995, pp. 474-481. {00483455}

[139] A.R. Munoz, T.A. Lipo, "On-line dead-time compensation technique for open-loop PWM-VSI drives," *IEEE Transactions on Power Electronics*, vol. 14, no. 4, pp. 683-689, Jul. 1999. {00774205}

[140] Y. Murai, T. Watanabe, H. Iwasaki, "Waveform distortion and correction circuit for PWM inverters with switching lag-times," *IEEE Transactions on Industry Applications*, vol. IA-23, no. 5, pp. 881-886, Sep./Oct. 1987. {04504998}

Overmodulation

[141] J. Holtz, W. Lotzkat, A.M. Khambadkone, "On continuous control of PWM inverters in the overmodulation range including the six-step mode," *IEEE Transactions on Power Electronics*, vol. 8, no. 4, pp. 546-553, Oct. 1993. {00261026}

[142] R.J. Kerkman, D. Leggate, B.J. Seibel, T.M. Rowan, An overmodulation strategy for PWM voltage inverters," *Proceedings of the International Conference on Industrial Electronics, Control, and Instrumentation*, 1993, vol. 2, pp. 1215-1221. {00339240}

[143] R.J. Kerkman, T.M. Rowan, D. Leggate, B.J. Seibel, "Control of PWM voltage inverters in the pulse dropping region," *IEEE Transactions on Power Electronics*, vol. 10, no. 5, pp. 559-565, Sep. 1995. {00406843}

[144] R.J. Kerkman, D. Leggate, B.J. Seibel, T.M. Rowan, "Operation of PWM voltage source-inverters in the overmodulation region," *IEEE Transactions on Industrial Electronics*, vol. 43, no. 1, pp. 132-141, Feb. 1996. {00481418}

[145] A.M. Hava, R.J. Kerkman, T.A. Lipo, "Carrier-based PWM-VSI overmodulation strategies: analysis, comparison, and design," *IEEE Transactions on Power Electronics*, vol. 13, no. 4, pp. 674-689, Jul. 1998. {00704136}

[146] A.M. Hava, S-K Sul, R.J. Kerkman, T.A. Lipo, "Dynamic overmodulation characteristics of triangle intersection PWM methods," *IEEE Transactions on Industry Applications*, vol. 35, no. 4, pp. 896-907, Jul./Aug. 1999. {00777199}

[147] A.R. Bakhshai, et al., "Incorporating the overmodulation range in space vector pattern generators using a classification algorithm," *IEEE Transactions on Power Electronics*, vol. 15, no. 1, pp. 83-91, Jan. 2000. {00817366}

SVM Harmonics, Losses

[148] J.F. Moynihan, M.G. Egan, J.M.D. Murphy, "Theoretical spectra of space-vector-modulated waveforms," *IEE Proceedings on Electric Power Applications*, vol. 145, no. 1, pp. 17-24, Jan. 1998. {00655168}

[149] R.H Ahmad, et al., "Comparison of space vector modulation techniques based on performance indexes and hardware implementation," *Proceedings of the International Conference on Industrial Electronics, Control, and Instrumentation*, 1997, vol. 2, pp. 682-687. {00671816}

[150] J. Vining, "Harmonic effects of space vector modulation on induction motor performance," Department of Electrical and Computer Engineering, University of

Wisconsin-Madison. [Online]. Available:
`http://homepages.cae.wisc.edu/~vining/JVining_SpaceVectorModulation.pdf`

[151]   J.W. Kolar, H. Ertl, F.C. Zach, "Influence of the modulation method on the conduction and switching losses of a PWM converter system," *Conference record of the IEEE Industry Applications Society Annual Meeting*, 1990, pp. 502-512. {00152232}

[152]   F. Jenni, D. Wueest, "The optimization parameters of space vector modulation," *Fifth European Conference on Power Electronics and Applications*, 1993, vol. 4, pp. 376-381. {00264822}

Synchronous Regulation, Tuning, Performance, Decoupling, (FOC)

[153]   C.D. Schauder, R. Caddy, "Current control of voltage-source inverters for fast four-quadrant drive performance," *IEEE Transactions on Industry Applications*, vol. IA-18, no. 2, pp.163-171, Mar./Apr. 1982. {04504051}

[154]   T.M. Rowan, R.J. Kerkman, "A new synchronous current regulator and an analysis of current-regulated PWM inverters," *IEEE Transactions on Industry Applications*, vol. IA-22, no. 4, pp. 678-690, Jul./Aug. 1986. {04504778}

[155]   R.D. Lorenz, "Synthesis of state variable controllers for industrial servo drives," *Proceedings of the Conference on Applied Motion Control*, 1986, pp. 247-251.

[156]   R.D. Lorenz, D.W. Novotny, "A control systems perspective of field oriented control for AC servo drives," *Proceedings of the Seventh Annual Control Engineering Conference*, 1988.

[157]   F. Briz, M.W. Degner, R.D. Lorenz, "Analysis and design of current regulators using complex vectors," *IEEE Transactions on Industry Applications*, vol. 36, no. 3, pp. 817-825, May/Jun. 2000. {00845057}

[158]   R.D. Lorenz, D.B. Lawson, "Performance of feedforward current regulators for field-oriented induction machine controllers," *IEEE Transactions on Industry Applications*, vol. IA-23, no. 4, pp. 597-602. {04504956}

[159]   J. Holtz, et al. "Design of fast and robust current regulators for high-power drives based on complex state variables," *IEEE Transactions on Industry Applications*, vol. 40, no. 5, pp. 1388-1397, Sep./Oct. 1994. {01337067}

[160]   S. Bolognani, M. Zigliotto, "A space-vector approach to the analysis and design of three-phase current controllers," *Proceedings of the IEEE International Symposium on Industrial Electronics*, 2002, vol. 2, pp. 645-650. {01026367}

[161]   D. Jouve, J.P. Rognon, D. Roye, "Effective current and speed controllers for permanent magnet machines—a survey," *Proceedings of the Applied Power Electronics Conference and Exposition (APEC)*, 1990, pp. 384-393. {00066439}

[162]   D.Y. Ohm, R.J. Oleksuk, "On practical digital current regulator design for PM synchronous motor drives," *Conference Proceedings of the Applied Power Electronics Conference and Exposition (APEC)*, 1998, pp. 56-63. {00647669}

Sensorless Control

[163]   J.C. Moreira, "Indirect sensing for rotor flux position of permanent magnet AC motors operating over a wide speed range," *IEEE Transactions on Industry Applications*, vol. 32, no. 6, pp. 1394-1401, Nov./Dec. 1996. {00556643}

[164]   F. Profumo, et al., "Universal field oriented controller based on air gap flux sensing via third harmonic stator voltage," *Conference Record of the IEEE Industry Applications Society Annual Meeting*, 1992, pp. 515-523. {00244352}

[165]   L. Kreindler, et al., "Direct field orientation controller using the stator phase voltage third harmonic," *IEEE Transactions on Industry Applications*, vol. 30, no. 2, pp. 441-447, Mar./Apr. 1994. {00287511}

[166]   J. Holtz, "Sensorless control of induction motor drives," *Proceedings of the IEEE*, vol. 90, no. 8, pp. 1359-1394, Aug. 2002. {01037566}

[167]   J. Holtz, "Speed estimation and sensorless control of AC drives," *Proceedings of the International Conference on Industrial Electronics, Control, and Instrumentation*, 1993, vol. 2, pp. 649-654. {00339003}

[168]   M.J. Corley, R.D. Lorenz, "Rotor position and velocity estimation for a permanent magnet synchronous machine at standstill and high speeds," *Conference Record of the IEEE Industry Applications Conference Annual Meeting*, 1996, pp. 36-41. {00556994}

[169]   J. Holtz, "Sensorless control of induction machines—with or without signal injection?" *IEEE Transactions on Industrial Electronics*, vol. 53, no. 1, pp. 7-30, Feb. 2006. {01589362}

[170]   M. Linke, R. Kennel, J. Holtz, "Sensorless speed and position control of synchronous machines using alternating carrier injection," *Conference Record of the IEEE International Electric Machines and Drives Conference*, 2003, vol. 2, pp. 1211-1217. {01210394}

[171]   H. Kim, R.D. Lorenz, "Carrier signal injection based sensorless control methods for IPM synchronous machine drives," *Conference Record of the IEEE Industry Applications Annual Meeting*, 2004, vol. 2, pp. 977-984. {01348532}

[172]   P.P. Acarnley, J.F. Watson, "Review of position-sensorless operation of brushless permanent-magnet machines," *IEEE Transactions on Industrial Electronics*, vol. 53, no. 2, pp. 352-362, Apr. 2006. {01614117}

[173]   R. Wu, G.R. Slemon, "A permanent magnet motor drive without a shaft sensor," *IEEE Transactions on Industry Applications*, vol. 27, no. 5, pp. 1005-1011, Sep./Oct. 1991. {00090359}

[174]   J-S Kim, S-K Sul, "High performance PMSM drives without rotational position sensors using reduced order observer," *Conference Record of the IEEE Industry Applications Society Annual Meeting*, 1995, pp. 75-82. {00530286}

Angle Tracking

[175] D. Morgan, "Tracking demodulation," *Embedded System Design*, 26 Feb 2001. [Online].
       Available: `http://www.embedded.com/story/OEG20010221S0089`

[176] Motorola, "DSP56F80x resolver driver and hardware interface," application note
       AN1942/D, Mar. 2002. [Online]. Available:
       `http://www.iele.polsl.pl/elenota/Freescale/an1942_d.pdf`

[177] D. Dujic, D. Ostojic, "Rotor angular position and speed estimation with use of
       electromagnetic resolvers for motor drives." [Online]. Available:
       `www.ljmu.ac.uk/geri/geri_docs/GARS2006papers_S3P3.pdf`

[178] G. Ellis, J.O. Krah, "Observer-based resolver conversion in industrial servo systems,"
       PCIM 2001 Conference, Nurnberg. [Online]. Available: `http://www.f07.fh-`
       `koeln.de/imperia/md/content/personen/krah_jens/pcim2001.pdf`

[179] Analog Devices, "Resolver-to-digital conversion with the ADMC401," application note
       AN401-22, Jan. 2000. [Online]. Available:
       `http://www.analog.com/Analog_Root/static/marketSolutions/motorControl/`
       `applicationCode/admc401/pdf/res2digi401.pdf`

Bibliography

[1]   J.E. Brittain, "From computor to electrical engineer: the remarkable career of Edith Clarke," *IEEE Transactions on Education*, vol. E-28, no. 4, pp. 184-189, Nov. 1985.

[2]   G-A Capolino, "André Blondel (1863–1938) French Scientist and Engineer," *IEEE Industry Applications Magazine*, pp. 12-15, May/Jun. 2004.

[3]   Andrzej Trzynadlowski, The field orientation principle in control of induction motors. Boston: Kluwer Academic, 1994.

[4]   J.F. Gieras, M. Wing, Permanent Magnet Motor Technology, 2nd ed. New York: Marcel Dekker, 2002.

[5]   M. Barnes, Practical variable speed drives and power electronics. Oxford: Newnes, 2003.

[6]   Ion Boldea, S.A. Nasar, Electric drives. 2nd ed. Boca Raton: CRC, 2006.

[7]   D. Hanselman, "Figure of merit: motor constant indicates brushless motor performance," *PCIM*, vol. 24, no.12, pp.32-39, 1998.

[8]   Irving Gottlieb, Practical Electric Motor Handbook. Oxford: Newnes, 1997.

[9]   T.J.E. Miller, Brushless permanent-magnet and reluctance motor drives. Oxford: Clarendon Press; New York: Oxford University Press, 1989. {Monographs in Electrical & Electronic Engineering #21}

[10]   K. Rajashekara, A. Kawamura, K. Matsuse, Eds., Sensorless control of AC motor drives: speed and position sensorless operation. New York: IEEE Press, 1996.

[11]   Texas Instruments Europe, "Field-oriented control of 3-phase AC-motors," application note, Literature Number BPRA073, Feb. 1998.

[12]   V. Utkin, J. Gulder, J. Shi, Sliding mode control in electromechanical systems. London: Taylor & Francis, 1999.

[13]   S. Yamamura, Spiral vector theory of AC circuits and machines. Oxford: Clarendon Press, 1992.

Appendix A - Elementary Electromagnetics

This appendix reviews some basic electromagnetic concepts of a general machine in order to clarify terms that are sometimes incorrectly defined in the literature. Then the general case is specialized for the brushless permanent magnet motor in order to define the terminology used in the report.

Figure A.1 shows a motor with general windings on the stator and rotor. The variables may all be functions of rotor position or time but for clarity this is not shown explicitly. Leakage flux is ignored (see Appendix B).
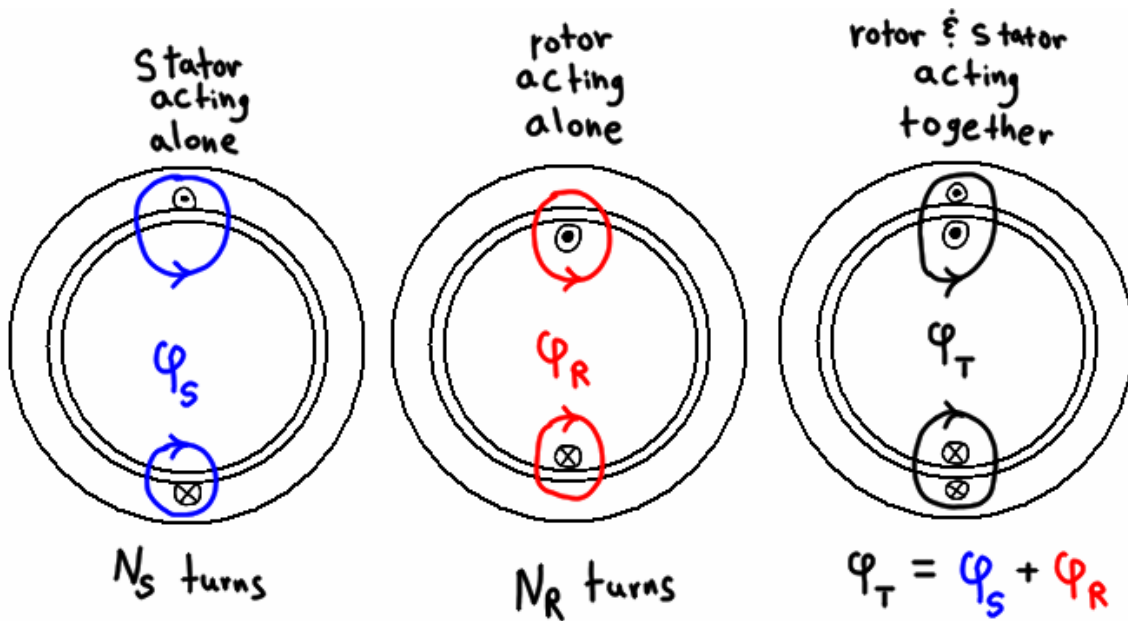
Figure A.1 – Stator, rotor, and total flux linkage.

The fluxes involved are as follows:

φ_S flux produced as a result of current i_S flowing in N_S turns of stator

φ_R flux produced as a result of current i_R flowing in N_R turns of rotor

φ_T total airgap flux produced by stator and rotor

If R is the airgap reluctance then the fluxes are defined by Equations (A.1)-(A.3).

$$\varphi_S = \frac{F_S}{R} i_S = \frac{N_S i_S}{R} \tag{A.1}$$

$$\varphi_R = \frac{F_R}{R} i_R = \frac{N_R i_R}{R} \qquad\qquad\qquad\qquad (A.2)$$

$$\varphi_T = \varphi_S + \varphi_R = \frac{N_S i_S}{R} + \frac{N_R i_R}{R} \qquad\qquad\qquad (A.3)$$

The total flux linked by the stator and rotor winding is given by Equations (A.4) and (A.5).

$$\lambda_S = N_S \varphi_T = N_S \left[\frac{N_S}{R} i_S + \frac{N_R}{R} i_R \right]$$

$$= \frac{N_S N_S}{R} i_S + \frac{N_S N_R}{R} i_R \qquad\qquad\qquad (A.4)$$

$$\lambda_R = N_R \varphi_T = N_R \left[\frac{N_S}{R} i_S + \frac{N_R}{R} i_R \right]$$

$$= \frac{N_R N_S}{R} i_S + \frac{N_R N_R}{R} i_R \qquad\qquad\qquad (A.5)$$

Inductance is defined as the amount of flux linked by a winding per amount of current, thus the terms that multiply the currents in Equations (A.4)-(A.5) are inductances. The inductances $(N_S N_S / R)$ and $(N_R N_R / R)$ are self inductances because they describe flux linkage in a circuit due to current in the same circuit. The inductances $(N_S N_R / R)$ and $(N_R N_S / R)$ are mutual inductances because they describe flux linkage in a circuit due to current in another circuit. The total flux linkage equations can be written in terms of self and mutual inductances in matrix form as Equation (A.6).

$$\begin{bmatrix} \lambda_S \\ \lambda_R \end{bmatrix} = \begin{bmatrix} L_{SS} & L_{SR} \\ L_{RS} & L_{RR} \end{bmatrix} \begin{bmatrix} i_S \\ i_R \end{bmatrix} \qquad\qquad (A.6)$$

Recognizing that the product of inductance and current is flux linkage, the total flux linkage equations can be written in terms of self and mutual flux linkages as Equation (A.7).

$$\begin{bmatrix} \lambda_S \\ \lambda_R \end{bmatrix} = \begin{bmatrix} \psi_{SS} & \psi_{SR} \\ \psi_{RS} & \psi_{RR} \end{bmatrix} \qquad\qquad (A.7)$$

In a permanent magnet brushless motor flux passes through the rotor but there is no winding on the rotor. Therefore there is no rotor current and there is no rotor flux linkage λ_R, so Equations (A.6) and (A.7) simplify to Equations (A.8) and (A.9), respectively.

$$\lambda_S = L_{SS} i_S + \psi_{SR} \tag{A.8}$$

$$\lambda_S = \psi_{SS} + \psi_{SR} \tag{A.9}$$

Since there is only one winding and it is understood to be on the stator, the subscript 'S' can be dropped from the total flux linkage and current. Similarly the first subscript can be dropped from the self and mutual flux linkages and the two equations simplify to Equations (A.10) and (A.11).

$$\lambda = L_{SS} \cdot i + \psi_R \tag{A.10}$$

$$\lambda = \psi_S + \psi_R \tag{A.11}$$

In Equation (A.11) λ is the total flux linkage of the stator and it has two components: ψ_S is the stator's self flux linkage due to stator current (shown clearly by Equation A.10) and ψ_R is the stator's flux linkage due to the flux from the rotor magnets. Each of the components might be called the stator flux linkage but this would clearly be ambiguous. In this report the total stator flux linkage will be called the *flux linkage*. The stator flux linkage due to rotor flux will be called the *rotor-stator flux linkage*. Finally, the only inductance of concern is the stator self inductance. In a wye-connected machine this is the "effective" inductance of the entire machine in operation (Appendix B) and it is called the *synchronous inductance* L_s. (The 's' subscript stands for *synchronous*, whereas the 'S' subscript stands for *stator*.) With these changes, Equation (A.10) is written as Equation (A.12).

$$\lambda = L_s i + \psi_R \tag{A.12}$$

To more clearly show that the rotor flux is responsible for the rotor-stator flux linkage, Equation (A.4) can be rewritten using Equation (A.3).

$$\lambda = N_S \left[\varphi_S + \varphi_R \right]$$
$$\lambda = \varphi_S + N_S \varphi_R$$

$$\lambda = L_s i + N_S \Phi_R \tag{A.13}$$

Only nonsalient machines are considered, thus L_s is not a function of rotor position. However, the stator winding may be a distribution and the rotor flux (as seen from the stator) will always be a function of rotor position. The interaction of these two to produce the rotor-stator flux linkage and may require an integral evaluation (Appendix C). Further, as far as motor operation is concerned, the details of the two are not important—only the rotor-stator flux linkage is required. Therefore this report will use Equation (A.11) or Equation (A.12).

$$\boxed{\lambda = L_s i + \psi_R = \psi_S + \psi_R}$$

Appendix B - Phase-Variable BPMS Motor Model

This appendix derives the phase-variable model of a BPMS motor. Particular attention is given to the concepts of magnetizing, leakage, and synchronous inductance of a three-phase machine and the influence wye connection on the phase-variable model.

Appendix A considered the total flux produced as having two components: that produced by the rotor and that produced by the stator. This separation is still considered but the stator-produced flux is studied more carefully. Figure B.1 shows the general paths taken by flux produced by the stator.
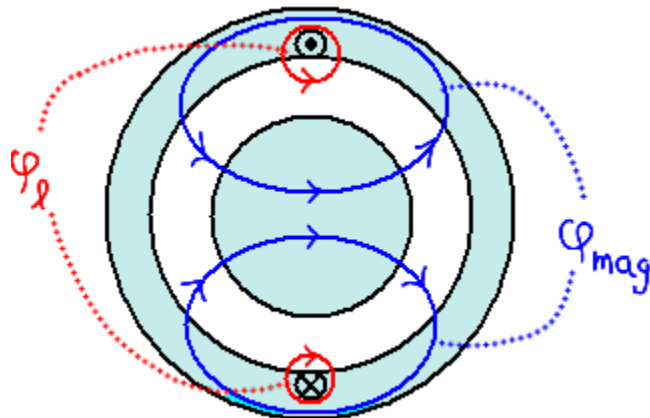
Figure B.1 – Magnetizing and leakage paths of stator flux.

Magnetizing flux (φ_{mag}) is that which crosses the airgap and links both the rotor and stator steel (shaded regions). The leakage flux (φ_ℓ) shown is produced by stator current but it does not link the rotor. In addition additional leakage flux is associated with end turns and harmonic slot leakage, but there is no disadvantage to grouping them together. The leakage flux cannot contribute to torque production but it does contribute to the electrical inductance of the winding. There is also rotor leakage but the only consequence of it is that the rotor flux profile will not be ideal; the rotor-stator flux linkage ψ_R already takes this into account. In other words the formulae cannot distinguish between the ideal and actual rotor flux, whereas we can always separate those two components in the stator.

First the self-flux-linkage of an individual winding is considered. The total flux is given by Equation (B.1). We know the total flux produced splits between the magnetizing and leakage paths as represented by Equation (B.2).

$$\varphi = \frac{f}{R} = \frac{N \cdot i}{R} \tag{B.1}$$

$$\varphi = \varphi_{mag} + \varphi_{\ell} \tag{B.2}$$

Since the number of turns and the current are the same, the only difference must be the reluctance. This is shown by combining these two results into Equation (B.3).

$$\varphi = \frac{N \cdot i}{R_{mag}} + \frac{N \cdot i}{R_{\ell}} \tag{B.3}$$

Now the flux linkage can be found as shown in Equation (B.4).

$$\lambda = N\varphi = \frac{N^2 \cdot i}{R_{mag}} + \frac{N^2 \cdot i}{R_{\ell}} \tag{B.4}$$

A self inductance is defined as the amount of flux linked per unit current, which for a simple inductor is equal to the number of turns squared divided by the reluctance as shown by Equation (B.4). These inductances are shown explicitly in Equation (B.5) and are called the *magnetizing inductance* (or *airgap inductance*) and the *leakage inductance*.

$$\lambda = \left(\frac{N^2}{R_{mag}} \right) i + \left(\frac{N^2}{R_{\ell}} \right) i \tag{B.5}$$
$$\lambda = L_{mag} i + L_{\ell} i$$

Although they are separate components they are both a part of the self inductance of a winding. Thus the self inductance could be defined as Equation (B.6) and each phase in a motor would have this same self inductance.

$$L = L_{mag} + L_{\ell} \tag{B.6}$$

Now the total flux linkage of a winding is considered. The flux linkage of a phase winding consists of its own self flux linkage, mutual flux linkage between other windings, and the flux linked by the rotor. In general terms these are given for each phase by Equation (B.7).

$$\begin{aligned} \lambda_A &= L_{AA} i_A + L_{AB} i_B + L_{AC} i_C + \psi_{AR} \\ \lambda_B &= L_{BA} i_A + L_{BB} i_B + L_{BC} i_C + \psi_{BR} \\ \lambda_C &= L_{CA} i_A + L_{CB} i_B + L_{CC} i_C + \psi_{CR} \end{aligned} \tag{B.7}$$

In a symmetrical machine the self inductance of each phase is equal and the mutual inductance between any two phases is equal,

$$L_{AA} = L_{BB} = L_{CC} = L$$

$$L_{AB} = L_{BA} = L_{AC} = L_{CA} = L_{BC} = L_{CB} = M$$

thus the set of flux linkages can be written as Equation (B.8).

$$\lambda_A = Li_A + Mi_B + Mi_C + \psi_{AR}$$
$$\lambda_B = Mi_A + Li_B + Mi_C + \psi_{BR} \tag{B.8}$$
$$\lambda_C = Mi_A + Mi_B + Li_C + \psi_{CR}$$

When the phase resistance is considered the voltage equation can be written for each phase as Equation (B.9).

$$v_{AN} = R \cdot i_A + \frac{d}{dt}\lambda_A$$

$$v_{BN} = R \cdot i_B + \frac{d}{dt}\lambda_B \tag{B.9}$$

$$v_{CN} = R \cdot i_C + \frac{d}{dt}\lambda_C$$

Substituting in Equation (B.8) yields the full voltage equations, Equation (B.10). Using the bEMF and matrix form this is given as Equation (B.11).

$$v_{AN} = R \cdot i_A + Li_A + M\dot{i}_B + M\dot{i}_C + \dot{\psi}_{AR}$$
$$v_{BN} = R \cdot i_B + M\dot{i}_A + Li_B + M\dot{i}_C + \dot{\psi}_{BR} \tag{B.10}$$
$$v_{CN} = R \cdot i_C + M\dot{i}_A + M\dot{i}_B + Li_C + \dot{\psi}_{CR}$$

$$\begin{bmatrix} v_{AN} \\ v_{BN} \\ v_{CN} \end{bmatrix} = \begin{bmatrix} R & & \\ & R & \\ & & R \end{bmatrix}\begin{bmatrix} i_A \\ i_B \\ i_C \end{bmatrix} + \begin{bmatrix} L & M & M \\ M & L & M \\ M & M & L \end{bmatrix}\frac{d}{dt}\begin{bmatrix} i_A \\ i_B \\ i_C \end{bmatrix} + \begin{bmatrix} e_A \\ e_B \\ e_C \end{bmatrix} \tag{B.11}$$

This report considers only isolated neutral motors thus the currents must sum to zero. The linear dependence of the currents is expressed by $\Sigma = 0$ the expression; this can be arranged in the three different ways shown in Equation (B.12).

$$i_B + i_C = -i_A$$
$$i_A + i_C = -i_B \tag{B.12}$$
$$i_A + i_B = -i_C$$

Writing out Equation (B.11) by hand, substituting Equation (B.12) and simplifying gives Equation (B.13). The result is that although the mutual inductances still exists, the isolation of the neutral decouples the circuits.

274

$$\begin{bmatrix} v_{AN} \\ v_{BN} \\ v_{CN} \end{bmatrix} = \begin{bmatrix} R & & \\ & R & \\ & & R \end{bmatrix} \begin{bmatrix} i_A \\ i_B \\ i_C \end{bmatrix} + \begin{bmatrix} L-M & & \\ & L-M & \\ & & L-M \end{bmatrix} \frac{d}{dt} \begin{bmatrix} i_A \\ i_B \\ i_C \end{bmatrix} + \begin{bmatrix} e_A \\ e_B \\ e_C \end{bmatrix} \tag{B.13}$$

However, the voltages are true line-neutral voltages (by definition). If a grounded neutral were used these voltages would simply be the terminal voltages (v_{AM}, v_{BM}, v_{CM}) because the neutral would be at zero potential. The same is true when common-mode/zero-sequence component is not present in the applied voltages (see Appendix D). However, if ZS components are present the terminal voltages must be used instead of the line-neutral voltages by using the "phase interference matrix" (Appendix D).

Now this result will be specialized for the sinusoidally distributed winding which this report assumes. From this point on only the matrix of inductances will be manipulated to save space. Including the magnetizing inductance (Equation B.6) yields Equation (B.14).

$$\begin{bmatrix} (L_{mag}+L_\ell)-M & & \\ & (L_{mag}+L_\ell)-M & \\ & & (L_{mag}+L_\ell)-M \end{bmatrix} \tag{B.14}$$

If the windings are sinusoidally distributed the mutual inductance between is given by Equation (B.15) [28, pp.251,654], [69, p.6.8].

$$M = L_{mag} \cos(\beta) \tag{B.15}$$

For a three-phase machine $\beta = 120°$ thus the mutual inductance is given by Equation (B.16).

$$M = L_{mag} \cos(-120°)$$
$$M = \frac{-1}{2} L_{mag} \tag{B.16}$$

It is worth noting that using $\beta = 0$ in Equation (B.15) gives the airgap portion of the self inductance of a winding. This emphasizes that the mutual inductance is a result of magnetizing flux.[44] Substituting the result of Equation (B.16) into Equation (B.14) yields Equation (B.17).

---

[44] There is also a slot leakage component of mutual inductance but it is usually negligible [28, p.251].

$$
\begin{bmatrix}
\dfrac{3}{2}L_{mag} + L_{\ell} & & \\
& \dfrac{3}{2}L_{mag} + L_{\ell} & \\
& & \dfrac{3}{2}L_{mag} + L_{\ell}
\end{bmatrix}
\tag{B.17}
$$

It is seen that the "effective inductance" seen by each phase is larger than the self inductance of that phase and is called the *synchronous inductance* L_S.

$$
L_S = \frac{3}{2}L_{mag} + L_{\ell}
\tag{B.18}
$$

The synchronous inductance is therefore a result of the fundamental airgap flux produced by one winding, the fundamental airgap flux produced by current in the other two windings, and the leakage flux [69], [75], [28]. This is roughly symbolized by Figure B.2 and Figure B.3, which again emphasize that leakage and airgap components exist in the self inductance but the mutual inductance is due to the airgap component alone. Figure B.3 emphasizes that the reluctance paths are the same for the magnetizing and mutual components are the same (because we neglect the reluctance of the steel). The only difference is the displacement in coil axes, hence Equation (B.16).
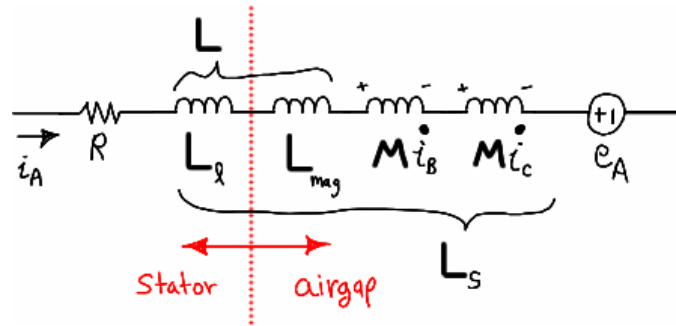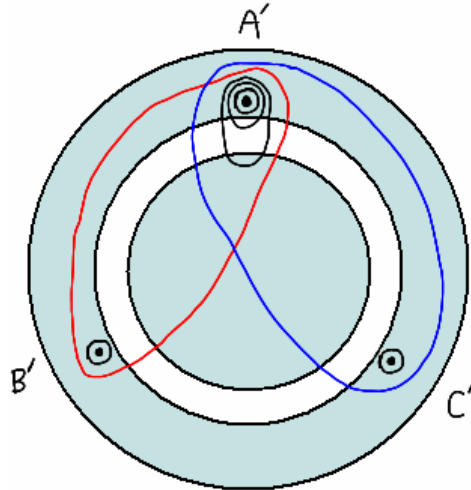
Figure B.2 – Relationship of inductances for phase-A.

Figure B.3 – One-half of the flux paths linking phase-A.

The full voltage equations written in terms of the synchronous inductance are given by Equation (B.19) or Equation (B.20).

$$
\begin{bmatrix} v_{AN} \\ v_{BN} \\ v_{CN} \end{bmatrix} = \begin{bmatrix} R & & \\ & R & \\ & & R \end{bmatrix} \begin{bmatrix} i_A \\ i_B \\ i_C \end{bmatrix} + \begin{bmatrix} \frac{3}{2}L_{mag} + L_\ell & & \\ & \frac{3}{2}L_{mag} + L_\ell & \\ & & \frac{3}{2}L_{mag} + L_\ell \end{bmatrix} \frac{d}{dt}\begin{bmatrix} i_A \\ i_B \\ i_C \end{bmatrix} + \begin{bmatrix} e_A \\ e_B \\ e_C \end{bmatrix}
$$

(B.19)

$$
\begin{bmatrix} v_{AN} \\ v_{BN} \\ v_{CN} \end{bmatrix} = \begin{bmatrix} R & & \\ & R & \\ & & R \end{bmatrix} \begin{bmatrix} i_A \\ i_B \\ i_C \end{bmatrix} + \begin{bmatrix} L_S & & \\ & L_S & \\ & & L_S \end{bmatrix} \frac{d}{dt}\begin{bmatrix} i_A \\ i_B \\ i_C \end{bmatrix} + \begin{bmatrix} e_A \\ e_B \\ e_C \end{bmatrix}
$$

(B.20)

There are many variations of voltage equations presented in the literature but often no explanation is given as to the significance of the choice of variation. The differences lie in which substitutions are made and whether the leakage inductance is ignored or not. To assist in reading the literature the most common variants are shown below; only the matrix of inductances is given for clarity. The variations are shown groups of two equations: the first does not assume the wye connection whereas the second does.

Equations (B.21) and (B.22) are for general windings.

$$\begin{bmatrix} L_{mag} + L_\ell & M & M \\ M & L_{mag} + L_\ell & M \\ M & M & L_{mag} + L_\ell \end{bmatrix} \tag{B.21}$$

wye:
$$\begin{bmatrix} L_{mag} + L_\ell - M & & \\ & L_{mag} + L_\ell - M & \\ & & L_{mag} + L_\ell - M \end{bmatrix} \tag{B.22}$$

Equations (B.23) and (B.24) are for general windings, ignoring leakage.

$$\begin{bmatrix} L & M & M \\ M & L & M \\ M & M & L \end{bmatrix} \tag{B.23}$$

wye:
$$\begin{bmatrix} L - M & & \\ & L - M & \\ & & L - M \end{bmatrix} \tag{B.24}$$

Equations (B.25) and (B.26) are for sinusoidal windings.

$$\begin{bmatrix} L_{mag} + L_\ell & \dfrac{-1}{2} L_{mag} & \dfrac{-1}{2} L_{mag} \\[2mm] \dfrac{-1}{2} L_{mag} & L_{mag} + L_\ell & \dfrac{-1}{2} L_{mag} \\[2mm] \dfrac{-1}{2} L_{mag} & \dfrac{-1}{2} L_{mag} & L_{mag} + L_\ell \end{bmatrix} \tag{B.25}$$

wye:
$$\begin{bmatrix} \dfrac{3}{2} L_{mag} + L_\ell & & \\[2mm] & \dfrac{3}{2} L_{mag} + L_\ell & \\[2mm] & & \dfrac{3}{2} L_{mag} + L_\ell \end{bmatrix} = \begin{bmatrix} L_S & & \\ & L_S & \\ & & L_S \end{bmatrix} \tag{B.26}$$

Equations (B.27) and (B.28) are for sinusoidal windings, ignoring leakage.

$$\begin{bmatrix} L & \dfrac{-1}{2}L & \dfrac{-1}{2}L \\ \dfrac{-1}{2}L & L & \dfrac{-1}{2}L \\ \dfrac{-1}{2}L & \dfrac{-1}{2}L & L \end{bmatrix} \tag{B.27}$$

wye:
$$\begin{bmatrix} \dfrac{3}{2}L & & \\ & \dfrac{3}{2}L & \\ & & \dfrac{3}{2}L \end{bmatrix} \tag{B.28}$$

This report will use the voltage equations for sinusoidal windings with an isolated neutral where the synchronous inductance is written explicitly (Equation B.20).

$$(\text{B.20}):\ \begin{bmatrix} v_{AN} \\ v_{BN} \\ v_{CN} \end{bmatrix} = \begin{bmatrix} R & & \\ & R & \\ & & R \end{bmatrix} \begin{bmatrix} i_A \\ i_B \\ i_C \end{bmatrix} + \begin{bmatrix} L_S & & \\ & L_S & \\ & & L_S \end{bmatrix} \frac{d}{dt} \begin{bmatrix} i_A \\ i_B \\ i_C \end{bmatrix} + \begin{bmatrix} e_A \\ e_B \\ e_C \end{bmatrix}$$

Appendix C - Sinusoidal and Nonsinusoidal Motors

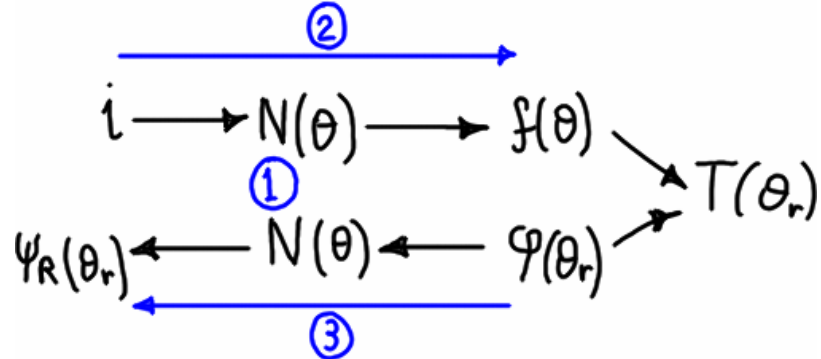This appendix elaborates the distinction between sinusoidal and nonsinusoidal motors.

Chapter 2 introduced the important concept of flux linkage. It was shown that the interaction between the distributions of the rotor flux and the stator winding requires a spatial analysis but that the end result (the rotor-stator flux linkage, ψ_R) is a function of rotor position θ_r. It was mentioned that the physical details of motor construction were irrelevant in elementary analysis since the bEMF/torque functions are derived from the rotor-stator flux linkage. The emphasis was thus placed on ψ_R in order to see how it related to torque and bEMF. Simple motors were studied to introduce the concept of sinusoidal and trapezoidal motors. Now that the basics have been presented, these same concepts can be studied in greater detail.

Chapter 2 discussed the difference between sinusoidal and trapezoidal motors; that material is relevant to understanding their operation and control. But it was mentioned that the trapezoidal motor is not well defined. Similarly, although a sinusoidal motor was said to have a sinusoidal $\psi_R(\theta_r)$ this can be achieved in various ways. The purpose of this appendix is to present a better understanding of the constructional features that determine the shape of the rotor-stator flux linkage. While this material is not directly useful from a motor control perspective it is required to be able to define "sinusoidal" and "nonsinusoidal" motors. Eventually this information will aid in the understanding of what happens when a model (space vector theory) or control scheme (FOC)—both of which stipulate a sinusoidal motor—are used with a nonsinusoidal motor.

The first section discusses the fundamental relationships. The different types of windings are discussed and their influence on MMF and rotor-stator flux linkage is investigated. Thus the first section provides the link between motor construction and $\psi_R(\theta_r)$. The second section reexamines the how $\psi_R(\theta_r)$ influences torque and bEMF. Finally, the third section provides a practical summary that defines the "sinusoidal" motor and the *effective number of turns* (N_e) that are used throughout this report.

Fundamental Relationships

Figure C.1 shows the basic relationships in a motor. They hold for the machine as a whole but this section concerns only a per-phase analysis.

Figure C.1 – Fundamental relationships in a motor.

For a <u>fixed current</u>, the space distribution of MMF $f(\theta)$ produced by the stator winding is obviously a function of how that winding is wound on the stator; this is described by the *winding function n*(θ) (also known as a *winding density*- or *distribution- function*). The rotor flux $\varphi_R(\theta_r)$ interacts with the stator MMF to produce torque that is a function of rotor position. The rotor flux also interacts with the winding distribution to produce the rotor-stator flux linkage $\psi_R(\theta_r)$ which is a function of rotor position. Since the winding function affects both torque production and bEMF generation, it will be studied first. Then the MMF and rotor-stator flux linkage will be discussed in the order indicated in the figure.
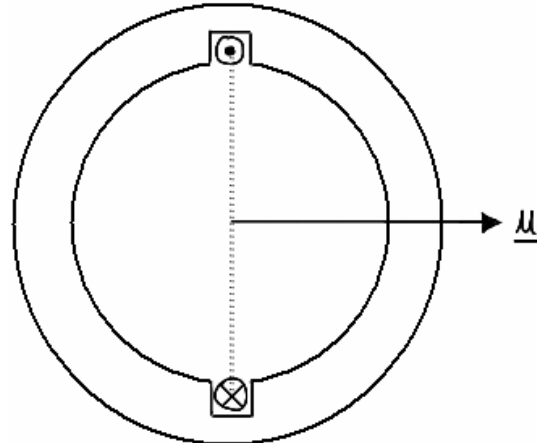
Only the rotor-stator flux linkage has been mentioned as being affected by the winding function but the stator self flux linkage is also affected. However, the result is that distributing the winding simply reduces the self flux linkage (by a factor up to ½) [69, p.6.6]. This does not affect torque or bEMF so it is not discussed here.

Windings

A winding may be either concentrated or distributed. In a concentrated winding all N turns are placed into two stator slots (per pole per phase), thus each slot then has N conductors. In a distributed winding the N turns of are distributed into different slots around the stator. Concentrated windings are simpler and will be discussed first.

Concentrated Full-Pitch (CFP)
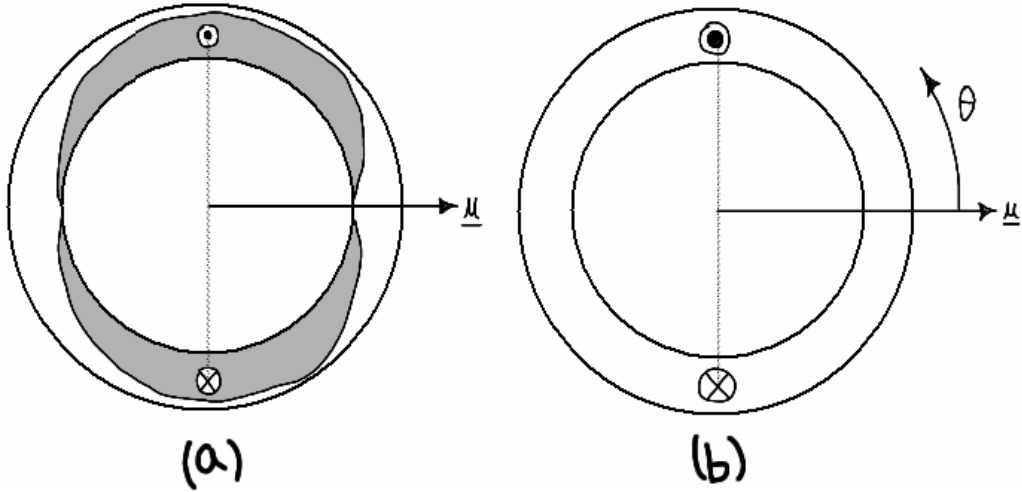
The simplest concentrated winding is the concentrated full-pitch (CFP) winding shown in Figure C.2. (The span/throw of a coil is the angular distance between the centers of the winding, thus the largest possible span 180° (though there are exceptions). When the coil span is expressed as a fraction of 180° is often called the coil pitch. A full-pitch coil thus spans 180° while a 2/3-pitch coil would span 120°.)

Figure C.2 – Concentrated full-pitch (CFP) winding.

Ideal Sinusoidal

A distributed winding can be formed any number of ways. The only distributed windings of interest here are the ideal sinusoidal winding (covered in this section) and those that serve to approximate it (covered in the next section). The sinusoidal winding distribution is defined as having a density that is a function of the sine of the angle around the rotor. By assuming that each conductor has negligible diameter the radial thickness of the winding would define the density of the winding, thus it can be visualized as shown in Figure C.3-a. Since this is impossible to draw when all three phases are considered the shading is generally not drawn, as shown in Figure C.3-b. The convention used in this report is that a concentrated winding (of any variety) will be indicated by coilsides in the stator slots (such as in Figure C.2) and a sinusoidal winding will be indicated by coilsides buried in the stator with no slots shown (such as in Figure C.3-b).

Figure C.3 – Sinusoidal winding density.

To derive the ideal sinusoidal winding function, assume that the radial winding density (which is always nonnegative) is sinusoidal about the stator as shown in Equation (C.1); [26, p.460], [78, p.37], [42, p.173], [73, p.9.2].

$$n(\theta) = N_p \sin(\theta) \tag{C.1}$$

N_p is the peak value of this distribution and it clearly must be less than N because the N turns are distributed around one-half the stator. To determine the value of N_p, the winding density can be integrated over one side of the stator to obtain the total number of windings. Since we stipulate that there be N total turns, the result is set equal to N.

$$N \overset{set}{=} \int_0^\pi N_p \sin(\theta) d\theta$$
$$= N_p \left[-\cos(\theta) \right]_0^\pi$$
$$N = 2N_p$$
$$\therefore N_p = \frac{N}{2}$$

Therefore the winding density is given by Equation (C.2). The density is negative from π to 2π and this may be interpreted as indicating that the direction of the winding on that side of the stator is opposite that of the top [42, p.173].[45]
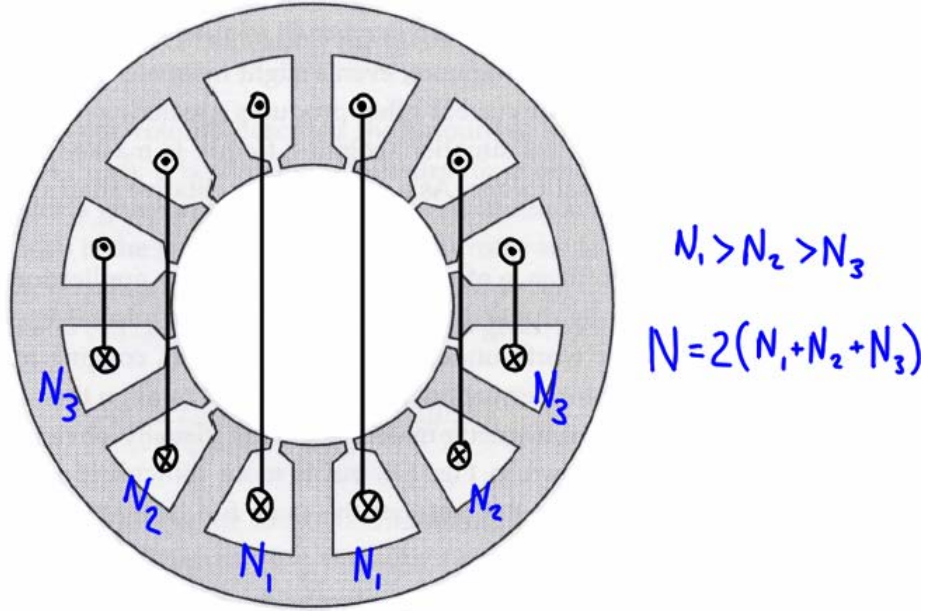
$$n(\theta) = \left(\frac{N}{2} \right) \sin(\theta) \tag{C.2}$$

---

[45] The reader is alerted to a conflict in the literature for which the author has no explanation. The majority of references surveyed agree with the MMF expression given here. However, there are several authoritative references whose expression lacks the factor ½, such as [87] and [36].

Sinusoidal Approximations

There are several ways a winding can be made to approximate a sinusoidal distribution. Perhaps the most intuitive is to allocate a number of conductors per slot in a stepped approximation to a sinewave, as shown in Figure C.4, where all coils are connected in series. The end turns curve around the stator but are shown straight for clarity.

$$N_1 > N_2 > N_3$$

$$N = 2(N_1 + N_2 + N_3)$$

Figure C.4 – Stepped approximation.

A particular example is given in [42, p.175] where the optimal values were determined and were as follows. Assuming impractical ideal conditions, this stepped winding did not produce any MMF harmonics below the 11th (which was 18% of the fundamental).

$N_1 = 250$ turns
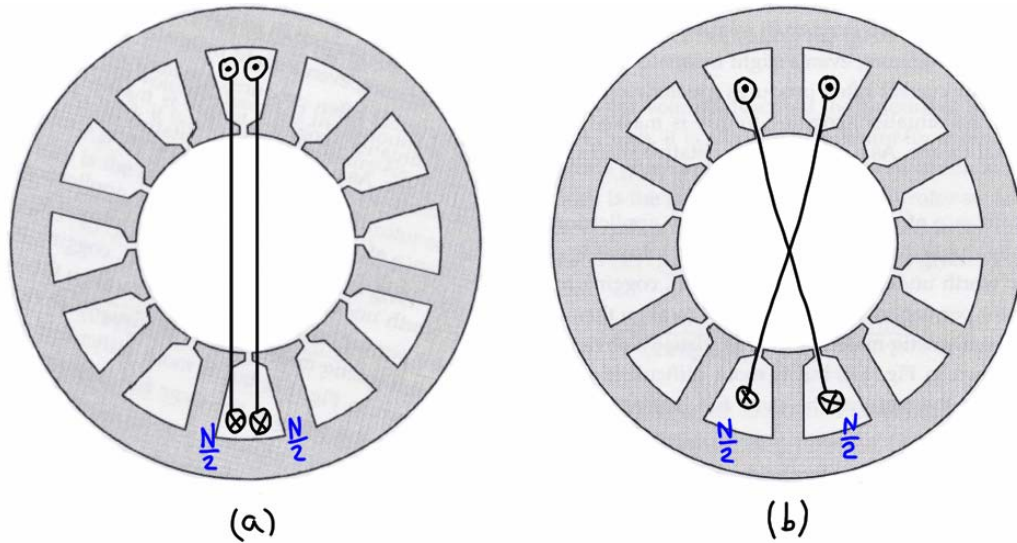
$N_2 = 183$ turns

$N_3 = 67$ turns

Such a stepped winding can only be wound if the motor has a large number of slots per pole (six in this case if the motor had two poles). In addition, this winding would force conductors from all three phases to occupy each slot which increases the manufacturing complexity and cost of the winding [68, p.180]. The least intuitive method is to build a *fractional slot motor*, which is one with a non-integral number of slots per pole per phase [68, p.87]. In this type of motor the coils are connected in series as usual and each individual coil has the same span, but the coils are *not* placed symmetrically about the stator. While not all fractional slot motors approximate sinusoidal windings they can be made to do so. Apparently the factional slot motor is more easily
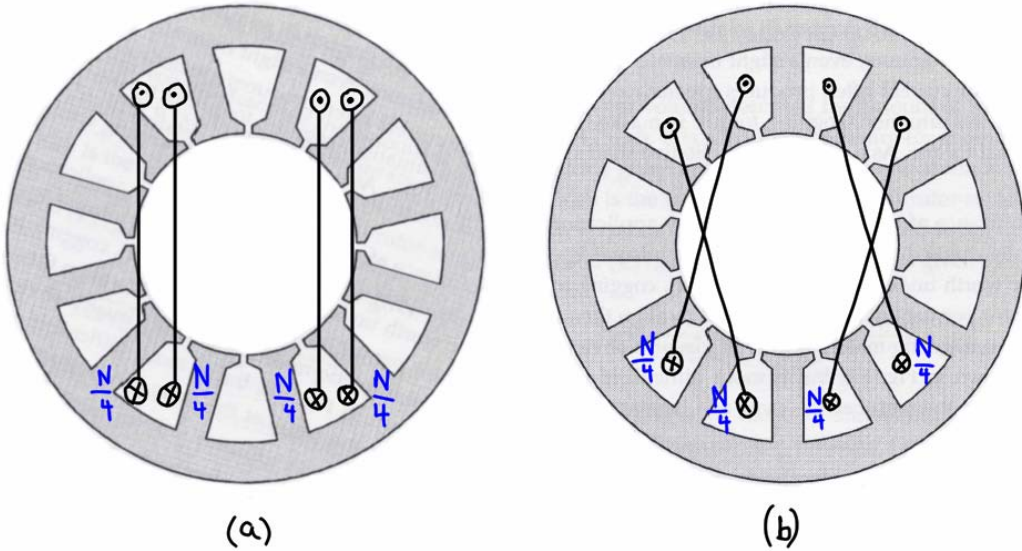
manufactured compared to the stepped winding, but do to its complexity in analysis it is not further discussed.

The traditional methods used to approximate a sinusoidal winding in induction motors and grid-tied synchronous machines are to use full pitch windings that are distributed, short-pitched (chorded) windings, or a combination of the two. In all techniques, the winding is symmetrical about the phase axis, all coils have the same span and number of turns, and all coils are connected in series. The CFP winding is shown in Figure C.5-a. The distributed full-pitch winding is shown in Figure C.5-b. It consists of the same two coils as the CFP but the coil axes have been offset from zero by plus-and-minus one slot pitch. For symmetry, each coil has N/2 turns.
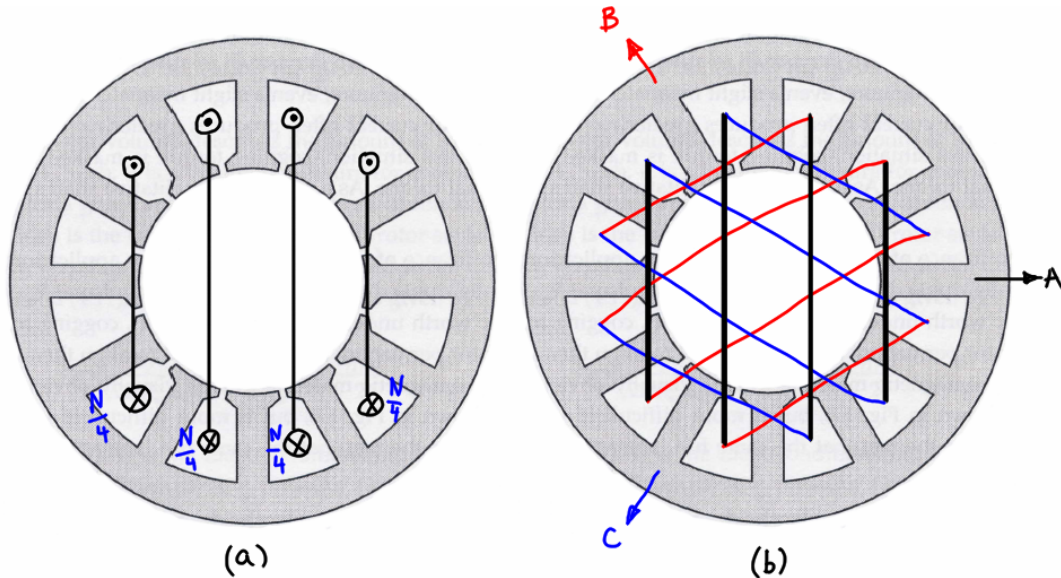
Figure C.5 – Full-pitch windings: (a) concentrated; (b) distributed.

The fundamental coil does not have to span a full pole pitch. In the case that it does not it is called a short-pitched or chorded winding (it may also be called a fractional pitch winding but that terminology is avoid here to avoid confusion with fractional *slot* construction). A short-pitched winding is shown in Figure C.6-a. Each coil is one slot pitch less in span than those in Figure C.5. In Figure C.6-b are the same four coils but their axes have been offset from one another. For symmetry, each coil has N/4 turns.

Figure C.6 –Short-pitched windings: (a) concentrated; (b) distributed.

Each of the four windings shown above is a different approximation to a sinusoidal winding. But, an additional degree of freedom exists because the interconnection of the windings does not matter so long as it is additive (the only sensible choice) [27, p.552]. This is essentially the difference between the traditional lap and concentric windings. For example, Figure C.6-b is a lap winding but would yield the same result as the concentric winding shown in Figure C.7-a.

Figure C.7 – Concentric winding of Figure C.6-b: (a) phase-A only; (b) all phases.

It might be noted that the winding of Figure C.7-a looks somewhat like the stepped winding of Figure C.4 that was said to be more difficult and expensive to manufacture. The difference (each phase does not have coilsides in each slot) is revealed when the other phases are drawn in, as shown in Figure C.7-b. Each slot contains the coilsides of only two phases, whereas the three-

phase winding of Figure C.4 will have coilsides of all three phases in each slot. When a slot is occupied by coilsides from only two phases—such as in Figure C.7-b—the winding is said to be a *double-layer winding*. According to one motor designer, the double-layer lap winding is the most common winding in brushless permanent magnet motors [68, p.130]. The other windings can be similarly checked for practicality by adding the other phases. The windings of Figure C.5-a and Figure C.6-a would be double-layer but not all slots would be filled thus these configurations are not practical. The winding in Figure C.5-b would fill all slots but it would only be a *single-layer winding*. These results are particular to the slot and pole configuration of the example. They do not indicate, for example, that the CFP winding of Figure C.5 always leads to a single-layer winding with some empty slots. These are all motor design considerations and are not relevant here but have been pointed out to show how a sinusoidal winding can be approximated by the use of chorded and distributed windings.
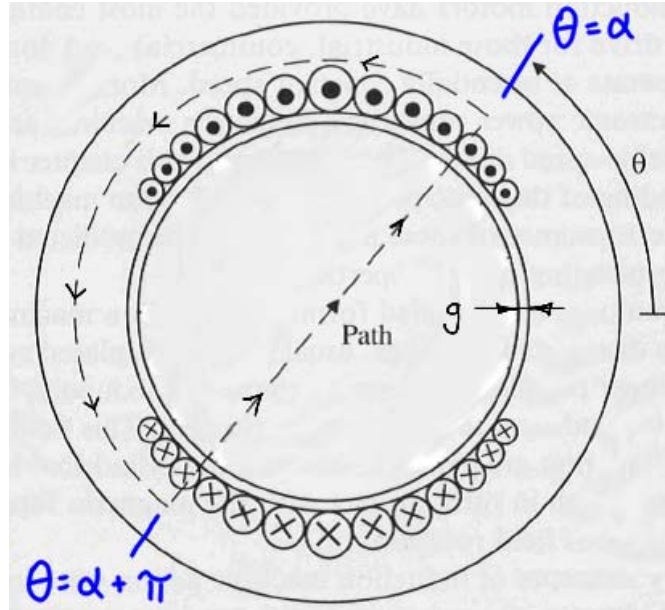
Stator MMF

Per Figure C.1, the impact of the winding function on MMF production is to be studied next. The total MMF produced by stator current is found by using Ampère's law which is defined by Equation (C.3) [44, p.202].

$$\oint_{path} \mathbf{H} \bullet d\mathbf{l} = I_{enclosed} \tag{C.3}$$

Assuming the stator and rotor steel have infinite permeability, the magnetic field is confined to the airgap. Assuming the field is radial and taking advantage of stator symmetry, the integral reduces to a scalar multiplication of product of H and total airgap length 2·G. A suitable Ampèrian loop is shown in Figure C.8 with an arbitrary, symmetric conductor distribution; c.f. [42, p.172], [73, p.9.5].

Figure C.8 – Ampèrian loop; modified from [42, p.172].

The total enclosed current can be written in terms of the winding density function and the winding current i, as shown in Equation (C.4).

$$H \cdot (2G) = I_{enclosed} = \int_{\alpha}^{\alpha+\pi} N(\theta) \cdot i \cdot d\theta \tag{C.4}$$

The winding density function in Equation (C.4) is responsible for ensuring the correct polarity of current in each conductor. The convention established earlier is that positive current flow in a winding is out of the page for conductors marked with $\odot$. Given that hole flow is considered positive current, it is required that the path of integration be traversed in the counterclockwise direction per the right-hand rule in order to yield a positive value of field strength for current out of the page [31, p.695], [44, p.203]. The sign convention used in this report is that an airgap magnetic quantity (B, Φ, H, F) is positive when traveling from the rotor to the stator. When used with the current polarity convention, the right hand rule also produces a positive value of MMF thus all of these conventions agree. Finally, the airgap MMF can be found by evaluating Equation (C.4), where it is recognized that the definition of field strength is MMF-per-length (which is 2G since there are two airgaps across which the MMF acts).

CFP

The MMF of the CFP winding (Figure C.5-a) can be found visually with the help of Figure C.8 and the integral is unnecessary. The total MMF (across two airgaps) is found to be equal to the product N·i over the interval $(-\pi/2, \pi/2)$. The MMF across each gap plotted in developed form in Figure C.9, where the peak value is given by Equation (C.5).

$$F_p = \left(\frac{N}{2}\right)i \tag{C.5}$$
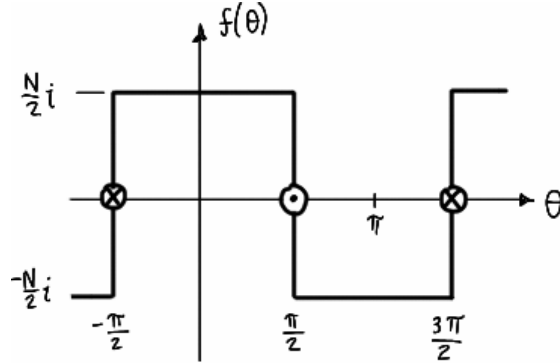
Figure C.9 – MMF of CFP winding.

Distributed

The effect of distributing and chording the winding can be visualized by plotting the MMF created by such windings. For example, the MMF of the windings in Figure C.5-b and Figure C.6-b are shown in Figure C.10-a and Figure C.10-b, respectively.
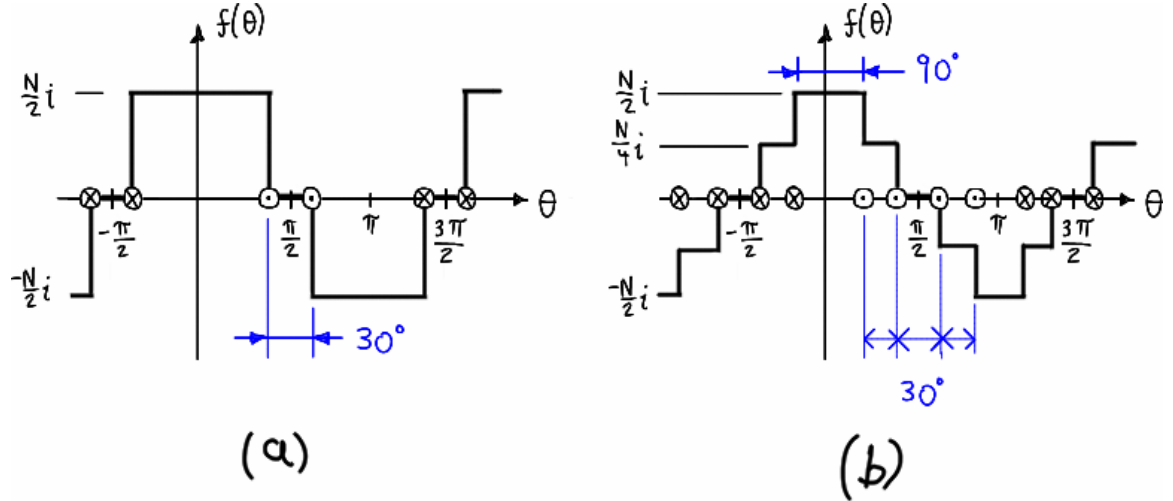
Figure C.10 – MMF of (a) distributed full-pitch winding; (b) distributed short-pitched winding.

It is seen that as the winding is distributed away from the CFP case, the MMF will take on a different shape. In each case the peak value will remain at $F_p = (N/2)i$ but the amplitudes of the harmonic components will decrease and the winding becomes a better approximation to an ideal sinusoidal winding. However, the amplitude of the fundamental will also decrease from its maximum value (given by Equation C.6) so there is a tradeoff.

$$F_1 = \frac{4}{\pi}\left(\frac{N}{2}\right)i \tag{C.6}$$

Historically, AC machines were designed to produce sinusoidal electrical quantities so the fundamental component was of greatest concern. The winding's effect on fundamental amplitude was determined by accounting for the distribution (breadth) and pitch by defining reduction factors whose values could be found for each particular winding. These were called the *distribution-* (or *breadth-*) *factor* k_d (or k_b) and the *pitch factor* k_p. Then to obtain the value of fundamental MMF amplitude, the maximum value (produced by the CFP winding) could be multiplied by these reduction factors per Equation (C.7).

$$F_1 = \frac{4}{\pi} \cdot k_b \cdot k_p \cdot \left(\frac{N}{2}\right) i \tag{C.7}$$

The effects of the breadth and pitch factors are often combined to form the *winding factor*: $k_w = k_b \cdot k_p$.[46] There are a variety of ways to define these factors ([27], [69], [40]) but the definitions are not required here.[47] We are not concerned with the winding specifics (k_b, k_p) so we will only use the overall winding factor k_w. The important point is that deviation from the CFP winding will reduce the value of the amplitude of the fundamental component of MMF by a certain fraction (k_w) for a particular winding configuration. The amplitude of fundamental MMF is thus given by Equation (C.8).

$$F_1 = \frac{4}{\pi} k_w \left(\frac{N}{2}\right) i \tag{C.8}$$

It may be that traditionally the winding factor was defined for only the fundamental component. But it is clear that distributing the winding reduces the amplitudes of other harmonics as well and modern texts [68], [69] also define a harmonic winding factor for each harmonic (though in a

---

[46] In addition to breadth and pitch factors, a *skew factor* is required for skewed rotor magnets or stator slots [69, p.6-21]. This advanced topic is not considered here.

[47] Traditional texts do a fair job explaining the winding factor, its usage, and its derivation. A typical key result is that a shortening the winding or magnet pitch by 1/n of a pole pitch will eliminate the nth harmonic from flux linkage so long as fringing and slotting is ignored [69, p.5-28]. It seems that this was a good rule for traditional synchronous machines which had a steel rotor; the airgap was small and the assumption could be made that the field was radial in the airgap [27, p.117]. However, since the effective airgap of a permanent magnet machine is larger (because the relative permeability of the magnet is close to that of air), fringing is more pronounced and the former rule cannot be used reliably. (For example a 5/6 pitch coil and full-pitch magnet should create a 150° flat top bEMF but in practice it is closer to 120° and is significantly rounded [69, p.5-5].) Indeed, one designer states that the traditional breadth and pitch factors are no longer used in motor design—design is done on a computer and the Fourier series components of various key waveforms can be adjusted directly [68, p.140]. Further, basic magnetic analysis (such as using the short-pitch rule described) cannot accurately predict the flux linkage in a brushless permanent magnet motor and more advanced techniques must be used [68, p.151]. As with all other construction-specific details, this result is not of concern here but the author feels it is worth pointing that not all standard results found in traditional machine texts are directly applicable to understanding brushless permanent magnet motors.

balanced machine only odd harmonics need be considered). When k_w is written it is understood to refer to the fundamental component. The *harmonic winding factor* for the nth harmonic would be written $k_{w,n}$ and the amplitude of each harmonic of MMF would be given by Equation (C.9), which follows directly from the Fourier series of a squarewave (see Figure C.9 and Equation C.5).[48]

$$F_n = \frac{4}{\pi}\left(\frac{1}{n}\right)k_{w,n}\left(\frac{N}{2}\right)i \tag{C.9}$$

Sinusoidal

Finally the MMF produced by a sinusoidal winding can be investigated. The MMF can be found by using Equation (C.4) and the sinusoidal winding function given by Equation (C.2). θ' is used as a dummy variable of integration so that we can integrate beginning at an arbitrary angle θ.

$$
\begin{aligned}
H \cdot (2g) &= \int_{\theta}^{\theta+\pi} N(\theta') \cdot i \cdot d\theta' \\
&= \int_{\theta}^{\theta+\pi} \left(\frac{N}{2}\right) \sin(\theta') \cdot i \cdot d\theta' \\
&= \left(\frac{N}{2}\right)\left[-\cos(\theta')\right]_{\theta}^{\theta+\pi} \cdot i \\
&= \left(\frac{N}{2}\right)\left[-\cos(\theta+\pi)+\cos(\theta)\right] \cdot i \\
&= f(\theta) = N \cdot i \cdot \cos(\theta)
\end{aligned}
\tag{C.10}
$$

Equation (C.10) is the total MMF along the path and due to symmetry it is split equally between the two airgaps. The MMF per airgap is found by dividing each side by two, Equation (C.11). By associating half the MMF with one airgap we get the traditional bipolar result that agrees with the sign convention for magnetic quantities in the airgap.

$$f(\theta) = \left(\frac{N}{2}\right)i \cdot \cos(\theta) \tag{C.11}$$

As expected, the sinusoidal winding produces a cosinusoidal MMF with no other harmonics (the harmonic winding factor $k_{w,n}$ is zero for all harmonics). Also as expected, the amplitude is not as large as the fundamental amplitude produced by the CFP winding. It is in fact less by a factor of $(\pi/4)$, canceling the $(4/\pi)$ in Equation (C.6). In comparing Equation (C.11) with Equation (C.8), it is clear that the value of k_w for an ideal sinusoidal winding is $(\pi/4)$.

---

[48] There are several possible definitions for the winding factors; those used here are just one example.

In summary, the CFP winding produces a squarewave MMF with the largest possible amplitude of all harmonics. Distributing the winding away from the CFP case will reduce the harmonic content. Different winding configurations will decrease each harmonic by different amounts. The amount of reduction of each harmonic is indicated by the winding factor for that harmonic, thus there is a set of harmonic winding factors associated with each winding. The CFP winding produces the most harmonics; the sinusoidal winding produces the least harmonics. In the ideal case only the fundamental of MMF is produced but it comes at a cost of reduction in amplitude. This concept is summarized in Figure C.11.
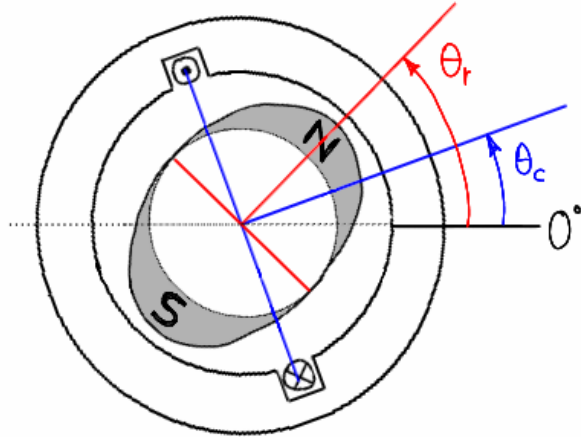
Figure C.11 – Summary of MMF Fourier series amplitudes.

Rotor-Stator Flux Linkage

Proceeding according to Figure C.1, this section discusses the interaction of the rotor flux with the winding distribution. In examining the stator MMF it was found that the CFP and sinusoidal windings are the two natural extrema—the former produces a squarewave with maximum harmonic content and the latter produces a sinewave. Any winding in between those two can be analyzed using harmonic winding factors. A similar approach could be taken in discussing rotors except the situation is more complicated because in addition to the range of windings discussed we can have a range of rotor flux profiles. A reasonable approach would be to study the CFP and

sinusoidal windings with a sinusoidal rotor and then study the same windings with the squarewave rotor.[49] Example rotor flux distributions were given in Chapter 2 for the sinusoidal rotor and an arbitrary trapezoidal rotor. The sinusoidal rotor flux varied as the cosine away from the rotor axis and the trapezoidal rotor flux had the positive portion centered on the rotor axis; the only change here is that the magnets span a full pitch, as shown later by Figure C.14.

In order to study both windings with a sinusoidal rotor it is useful to derive an expression that gives the flux linked by a single-turn coil whose axis is at an arbitrary position. The full-pitch coil's axis and the rotor position are defined as shown in Figure C.12.

Figure C.12 – Full-pitch coil axis at θc and sinusoidal rotor at position θr.
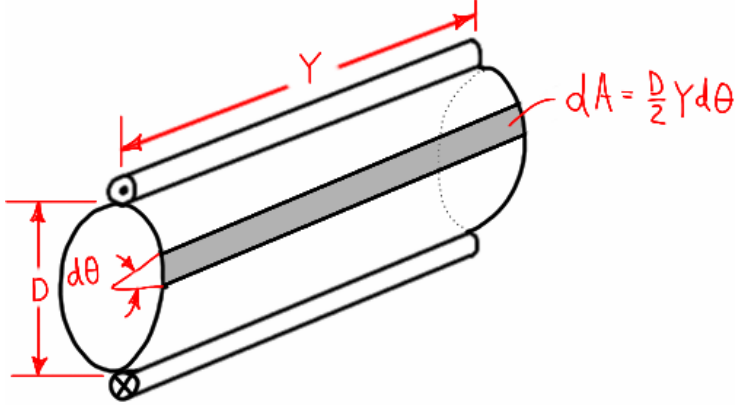
The rotor's flux density profile is a cosine about the rotor's axis. When the rotor's axis is at θ_r (as measured from zero) the value of flux density at some arbitrary angle θ around the stator given by Equation (C.12).

$$B(\theta,\theta_r) = B_p \cos(\theta - \theta_r) \tag{C.12}$$

The flux through the single-turn coil is found by integrating the flux density over a differential area defined in Figure C.13.

---

[49] A rotor can never produce airgap flux that is a squarewave. The rotor would need to have a continuous magnet and if this was manufactured as a cylinder and then magnetized, it would seem impossible to perfectly magnetize the poles where they met; a dead spot would be expected. If the magnets were made separately and attached to the rotor, one would expect flux leakage that would produce a transition from North to South that was not sharp but somewhat rounded. Even with this limitation studying an ideal squarewave profile will illuminate the concepts this appendix is to demonstrate.

Figure C.13 – Single-turn full-pitch winding.

The integral is taken from the $\otimes$ side of the coil to the $\odot$ side, as shown below.

$$\varphi(\theta_c,\theta_r) = \int_{\theta_c-\pi/2}^{\theta_c+\pi/2} B(\theta,\theta_r)dA$$

$$= \int_{\theta_c-\pi/2}^{\theta_c+\pi/2} B_p \cos(\theta-\theta_r)\frac{D}{2}Yd\theta$$

$$= \frac{D}{2}Y \cdot B_p \left[\sin(\theta-\theta_r)\right]_{\theta_c-\pi/2}^{\theta_c+\pi/2}$$

$$= \frac{D}{2}Y \cdot B_p \left[\sin(\theta_c+\pi/2-\theta_r)-\sin(\theta_c-\pi/2-\theta_r)\right]$$

$$= \frac{D}{2}Y \cdot B_p \left[\cos(\theta_c-\theta_r)+\cos(\theta_c-\theta_r)\right]$$

$$\varphi(\theta_c,\theta_r) = D \cdot Y \cdot B_p \cos(\theta_c-\theta_r) \qquad (C.13)$$

Equation (C.13) gives the flux (from a sinusoidal rotor at θ_r) through the single-turn winding with axis at θ_c. Now finding the rotor-stator flux linkage for an entire winding consists of defining the winding distribution, computing the flux through each elemental coil, and summing or integrating over the distribution. For the CFP winding this is simple. There are N total turns and they are all located at the same place. Each turn thus links the same amount of flux so integration is unnecessary. The total rotor-stator flux linkage is thus given by Equation (C.14).

$$\psi_R(\theta_r) = N \cdot \varphi(\theta_c,\theta_r)\big|_{\theta_c=0}$$

$$\psi_R(\theta_r) = N \cdot D \cdot Y \cdot B_p \cos(\theta_r) \qquad \text{(CFP winding, sine rotor flux)} \qquad (C.14)$$

This is the same result found in Chapter 2; the setup was exactly the same (CFP winding and sine rotor). Now the sine rotor will be evaluated with the sine winding. The procedure is the same but since the winding is distributed, integration must be used and the range must be carefully defined. Equation (C.2) gives the ideal sinusoidal winding distribution. Since it is positive over the range

$[0, \pi]$ and since the direction of integration used to get Equation (C.13) was from $\otimes$ to $\odot$, the rotor-stator flux linkage integral will have to be taken over the span of conductors from only one side ($\otimes$). This means the coil axis must swing from $-\pi/2$ to $\pi/2$. The total rotor-stator flux linkage would be given by Equation (C.15).

$$\psi_R(\theta_r) = \int_{-\pi/2}^{\pi/2} n(\theta) \cdot \varphi(\theta, \theta_r) d\theta \tag{C.15}$$

However, the winding density of Equation (C.2) gives the density of conductors at θ as a function of θ, not the density at $\theta_c \mp \pi/2$ as a function of coil axis angle θ_c. This can be corrected by modifying the density function to be Equation (C.16), which can be verified visually via Figure C.12. It should be understood that the math is not changed—the winding density is simply defined by the coil axis instead of the coilsides.
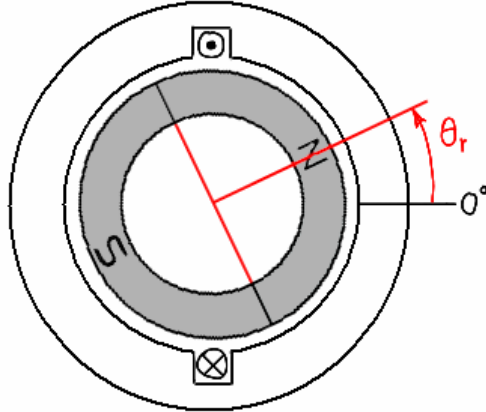
$$n(\theta_c) = \frac{N}{2} \cos(\theta_c) \tag{C.16}$$

Now the rotor-stator flux linkage can be found as planned.

$$\psi_R(\theta_r) = \int_{\theta_c=-\pi/2}^{\pi/2} n(\theta_c) \cdot \varphi(\theta_c, \theta_r) d\theta_c$$

$$= \int_{\theta_c=-\pi/2}^{\pi/2} \frac{N}{2} \cos(\theta_c) \cdot D \cdot Y \cdot B_p \cos(\theta_c - \theta_r) d\theta_c$$

$$= \frac{N}{2} D \cdot Y \cdot B_p \int_{\theta_c=-\pi/2}^{\pi/2} \frac{1}{2} \left[\cos(\theta_r) + \cos(2\theta_c - \theta_r) \right] d\theta_c$$

$$= \frac{N}{2} D \cdot Y \cdot B_p \frac{1}{2} \left[\theta_c \cos(\theta_r) + \frac{1}{2} \sin(2\theta_c - \theta_r) \right]\Big|_{\theta_c=-\pi/2}^{\pi/2}$$

$$= \frac{N}{2} D \cdot Y \cdot B_p \frac{1}{2} \left[\left(\frac{\pi}{2}\right) \cos(\theta_r) + \frac{1}{2} \sin(\pi - \theta_r) - \left(\frac{-\pi}{2}\right) \cos(\theta_r) - \frac{1}{2} \sin(-\pi - \theta_r) \right]$$

$$= \frac{N}{2} D \cdot Y \cdot B_p \frac{1}{2} \left[\frac{\pi}{2} \cos(\theta_r) + \frac{1}{2} \sin(\theta_r) + \frac{\pi}{2} \cos(\theta_r) - \frac{1}{2} \sin(\theta_r) \right]$$

$$\psi_R(\theta_r) = \frac{\pi}{4} N \cdot D \cdot Y \cdot B_p \cos(\theta_r) \quad \text{(sine winding, sine rotor flux)} \tag{C.17}$$

Comparing Equation (C.17) with Equation (C.14) shows that the sinusoidal winding linked the sinusoidal rotor flux but the amplitude was only $\pi/4$ of the flux linked by the CFP.

Examining the two windings with a squarewave motor would be more difficult because of the discontinuous function describing rotor flux but fortunately the analysis may be done intuitively, beginning again with the CFP winding. When the rotor is at zero degrees all the flux would be linked by all N turns, as shown in Figure C.14.
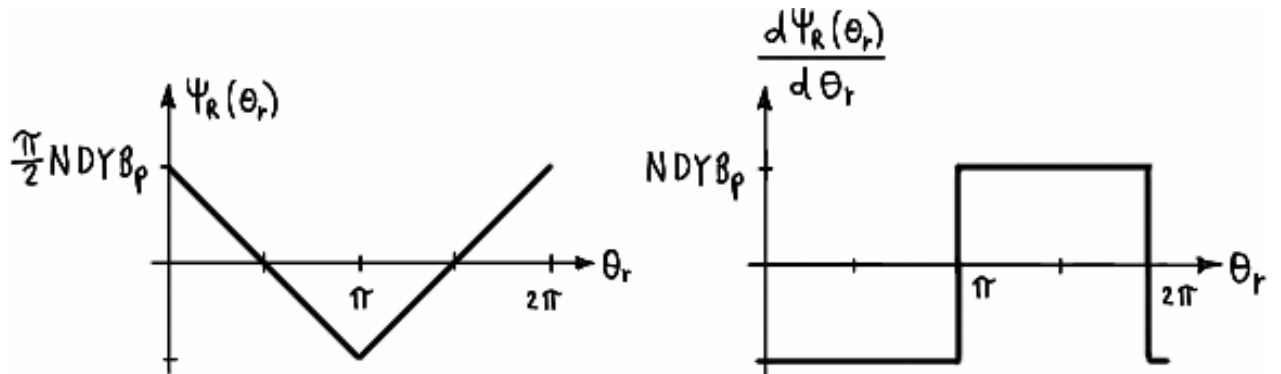
Figure C.14 – CFP winding with ideal squarewave rotor.

The peak rotor-stator flux linkage is thus found by multiplying the total flux by N.

$$\Psi_R = N \cdot \Phi$$
$$= N \cdot B_p \cdot Area$$
$$= N \cdot B_p \left(\frac{D}{2} \pi Y \right)$$
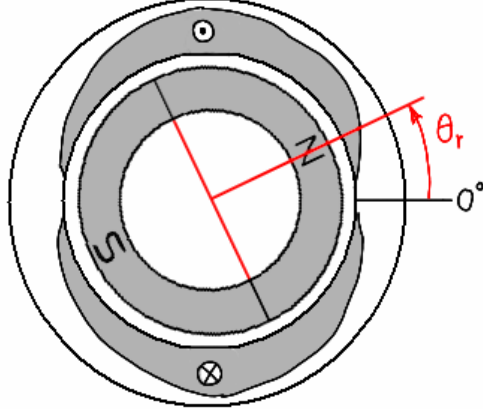
$$\Psi_R = \frac{\pi}{2} N \cdot D \cdot Y \cdot B_p \qquad \text{(CFP winding, squarewave rotor flux)} \qquad (C.18)$$

As the rotor rotates CCW the rotor-stator flux linkage changes linearly with negative slope over $[0, \pi]$ and with positive slope over $[\pi, 2\pi]$ as shown in Figure C.15-a. (The position-derivative is shown as well but will not be discussed until later.)

Figure C.15 – CFP winding with squarewave rotor: (a) rotor-stator flux linkage, and (b) its position-derivative.

296

That the rotor-stator flux linkage is triangular is certainly intuitive and in agreement with Figure C.14 but it seems a bit out of place, considering all of the other results (including the next case) have been squarewaves or sinusoids. An explanation will be given soon but first the sinusoidal winding with the squarewave rotor is investigated. The sinusoidal winding and squarewave rotor are shown in Figure C.16.

Figure C.16 – Sinusoidal winding and squarewave rotor.

There are several ways to proceed but they are all very similar to the previous derivations. Different authors take different approaches; in approximate order of formulae complexity: [69, p.6.8], [68, p.180], [26, p.462]. These proofs are not recreated here. The result is simple: the sinusoidal winding does not link any harmonics of rotor flux and the fundamental of rotor flux that it does link is only $\pi/4$ of that linked by the CFP, as found earlier in the MMF section and after Equation (C.17) was derived. Since the fundamental of the squarewave is $4/\pi$ the two factors cancel and the rotor-stator flux linkage is that given by Equation (C.19).

$$\psi_R(\theta_r) = N \cdot D \cdot Y \cdot B_p \cos(\theta_r) \quad \text{(sine winding, squarewave rotor flux)} \qquad \text{(C.19)}$$

The rotor-stator flux linkages (or peak value) are summarized below for the four winding and rotor combinations studied.

(C.14): $\psi_R(\theta_r) = N \cdot D \cdot Y \cdot B_p \cos(\theta_r)$ (CFP winding, sine rotor flux)

(C.17): $\psi_R(\theta_r) = \dfrac{\pi}{4} N \cdot D \cdot Y \cdot B_p \cos(\theta_r)$ (sine winding, sine rotor flux)

(C.18): $\Psi_R = \dfrac{\pi}{2} N \cdot D \cdot Y \cdot B_p$ (CFP winding, squarewave rotor flux)

(C.19): $\psi_R(\theta_r) = N \cdot D \cdot Y \cdot B_p \cos(\theta_r)$ (sine winding, squarewave rotor flux)

For the sine rotor it is clear to see that the sine winding linked only $\pi/4$ the flux that did the CFP winding as expected, but since there were no rotor flux harmonics we do not see any harmonic filtering action. For the sine winding and squarewave rotor it is seen that all harmonics are filtered, and per the above discussion above we see that the fundamental is again reduced by $\pi/4$. The result that is not obvious is that the CFP winding "passes" all harmonics of rotor flux (that is, it links all harmonics) but each is attenuated.

In other words, we saw that the CFP winding generated *unit-amplitude fundamental* MMF and the maximum possible MMF amplitude of each harmonic (*but these were less than unit amplitude*); the sine winding did not generate the MMF harmonics but produced a *lower-amplitude fundamental MMF*. The similar situation here is that the CFP winding links the *full value fundamental of rotor flux* and links to the fullest extent all harmonics present in the rotor flux (*but these linkages are less than unit amplitude*); the sine winding did not link the rotor flux harmonics but links a *reduced amount of the fundamental of rotor flux*. The parallel statements for MMF and rotor-stator flux linkage indicate that the winding distribution influences MMF production and rotor-stator flux linkage in similar ways. It turns out that the effect on each is identical and is thus described in terms of the fundamental and harmonic winding factors. Whereas the winding restricts harmonics from the CFP in the case of MMF (Figure C.11), it restricts the harmonics from the rotor flux in the case of rotor-stator flux linkage (Figure C.17). It should now be very clear that the rotor flux and winding distribution interact in space to produce the rotor-stator flux linkage and Figure C.1 should be reviewed in comparison with Figure C.11 and Figure C.17.

Winding factors for arbitrary winding

$$\Phi_1 \cdot k_w = \Psi_1$$

$$\Phi_3 \cdot k_{w,3} = \Psi_3$$

$$\Phi_5 \cdot k_{w,5} = \Psi_5$$

$$\cdots$$

$$\Phi_n \cdot k_{w,n} = \Psi_n$$

amplitudes of rotor flux harmonics

flux linkage amplitudes for this particular winding-rotor combination
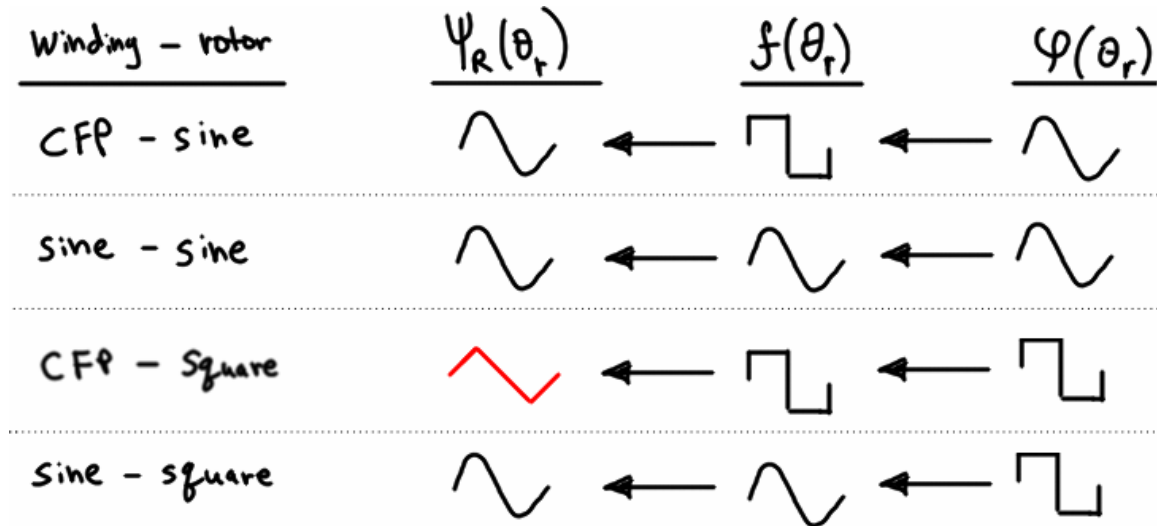
Figure C.17 – Summary of rotor-stator flux linkage Fourier series amplitudes.

Earlier it was observed that the rotor-stator flux linkage for the CFP winding and squarewave rotor was triangular and that it was the only waveform involved that wasn't a squarewave or sinusoid. This result is of no consequence but investigating it further should present a clearer visualization of the winding function. Instead of visualizing the CFP and sinusoidal windings as physically constructed, as shown in Figure C.2 and Figure C.3-a, respectively, the windings could be thought of in terms of some function. The winding density function comes to mind, but it is not a continuous function in the case of a CFP winding. An alternative would be to plot the MMF produced, as it is intimately tied to the winding's distribution and is at least piecewise continuous. For the CFP and sinusoidal windings, the MMF waveforms are a squarewave centered about zero and a cosine.[50]

---

[50] The graphical representations in these figures are the author's own work. While the procedure and discussion are derived from the results in the literature, the results have been pieced together from several sources and from some original derivations. Thus the reader should not expect to find identical discussion in the literature and should use caution in leaning on the results.

The four winding-rotor combinations studied are shown in Figure C.18. Keeping with the directionality used in Figure C.1, Figure C.18 shows the rotor flux interacting with the winding function (which is "represented" by the MMF) to produce the rotor-stator flux linkage for each winding-rotor combination. Since there is a one-to-one relationship between the winding and its MMF, the MMF can be used to graphically depict the "effect" of the winding rather than its physical distribution.

Figure C.18 – Summary of MMF and rotor-stator flux linkage results.

Figure C.18 simply summarizes the qualitative observations so far, but a quantitative look is required to gain a complete understanding. Figure C.19 shows the amplitudes of the components of Figure C.18. Some shorthand notation is used: $1 + \frac{1}{3} + \cdots$ represents $1\cos(\theta_r) + \frac{1}{3}\cos(3\theta_r) + \cdots$ (the Fourier series of a squarewave); any single digit is thus associated with the fundamental $\cos(\theta_r)$; and only the numerical portion of the amplitude is shown because the parameter constants are always the same ($N \cdot D \cdot Y \cdot B_p$).

Winding – rotor	$\psi_R(\theta_r)$	$f(\theta_r)$	$\varphi(\theta_r)$
CFP – sine	1	$\leftarrow \left[1+\frac{1}{3}+\frac{1}{5}+\frac{1}{7}\cdots\right] \leftarrow$	1
sine – sine	$\frac{\pi}{4}$	$\leftarrow \frac{\pi}{4}\left[1\right] \leftarrow$	1
CFP – square	$\frac{4}{\pi}\left[1+\frac{1}{3^2}+\frac{1}{5^2}+\frac{1}{7^2}\cdots\right]$	$\leftarrow \left[1+\frac{1}{3}+\frac{1}{5}+\frac{1}{7}\cdots\right] \leftarrow$	$\frac{4}{\pi}\left[1+\frac{1}{3}+\frac{1}{5}+\frac{1}{7}\cdots\right]$
Sine – square	1	$\leftarrow \frac{\pi}{4}\left[1\right] \leftarrow$	$\frac{4}{\pi}\left[1+\frac{1}{3}+\frac{1}{5}+\frac{1}{7}\cdots\right]$

Figure C.19 – Amplitudes of harmonic components.

Figure C.18 and Figure C.19 should be compared to understand the harmonic content. The rotor-stator flux linkages (or peak) are again reproduced below.

(C.14): $\psi_R(\theta_r) = N \cdot D \cdot Y \cdot B_p \cos(\theta_r)$ (CFP winding, sine rotor flux)

(C.17): $\psi_R(\theta_r) = \frac{\pi}{4} N \cdot D \cdot Y \cdot B_p \cos(\theta_r)$ (sine winding, sine rotor flux)

(C.18): $\Psi_R = \frac{\pi}{2} N \cdot D \cdot Y \cdot B_p$ (CFP winding, squarewave rotor flux)

(C.19): $\psi_R(\theta_r) = N \cdot D \cdot Y \cdot B_p \cos(\theta_r)$ (sine winding, squarewave rotor flux)

Looking at the amplitudes of rotor flux, the sinusoidal rotor flux profile has only the fundamental; its amplitude is unity because the definition of the rotor flux is given by the peak value B_p. Since the squarewave rotor flux was also defined by the peak value (of the squarewave) B_p, it's fundamental component is $4/\pi$ larger and the harmonics are given by the Fourier series of a squarewave.

Now looking at the MMF (which is used here to "represent" the winding) we recall that the CFP winding generated the maximum achievable amplitude for each MMF harmonic and that it did not attenuate the fundamental. Therefore we use the Fourier series of a squarewave, *but note well: since "unity gain" is defined by normalizing the fundamental (as opposed to the squarewave amplitude like usual) the expressions is scaled by $\pi/4$ and the $4/\pi$ coefficient is eliminated.* Looking at the sinusoidal winding it is seen that its fundamental (and only) component is $\pi/4$ of unity; this directly follows from the previous statement and shows clearly the $\pi/4$ attenuation of

the fundamental we had observed in the sinusoidal winding (both in MMF and rotor-stator flux linkage). The factor $4/\pi$ is written in red and the factor $\pi/4$ is written in blue to signify that they stem from different constraints (B_p describing maximums that are a fundamental or peak value; unity gain set by a fundamental).

Finally, looking at the rotor-stator flux linkage produced, it is first interesting to note that the first and last combinations produce the same result. That is, a "sinusoidal motor" could be built by using a CFP winding and sinusoidal rotor, or by using a sinusoidal winding and a squarewave rotor. In the first combination the fundamental of rotor flux has unit amplitude but is not attenuated whereas in the second combination the amplitude of fundamental rotor flux is greater than unity but is attenuated by the sinusoidal winding. Examining the sine-sine combination, we see that only the fundamental of rotor flux is present and it gets attenuated by $\pi/4$ as expected. The last combination (CFP-square) is the one for which an explanation was promised and is the most interesting. If the reader has not yet deduced it, the factors shown in the MMF column [$f(\theta_r)$] of Figure C.19 are indeed the fundamental- and harmonic- winding factors. As stated earlier and as shown by Figure C.1, the role of the winding distribution (described by winding factors) is two-way in nature (MMF and rotor-stator flux linkage). The results described here are all consistent with Figure C.17. That is, the amplitude of each flux harmonic is multiplied by that harmonic's winding factor to yield the amplitude of rotor-stator flux linkage for that particular winding-rotor combination.

This is best exemplified by discussing this last winding-rotor combination. We know that for the CFP winding and squarewave rotor the rotor-stator flux linkage is given by Figure C.15-a and the peak value is given by Equation (C.18).

(C.18): $\Psi_R = \dfrac{\pi}{2} N \cdot D \cdot Y \cdot B_p$ (CFP winding, squarewave rotor flux)

First, amplitudes of $\varphi(\theta_r)$ are those of the squarewave rotor flux and are known to be correct. Next, the winding factors are those of the CFP winding, which have also given correct results. The term-by-term multiplication yields the amplitudes given for $\psi_R(\theta_r)$. Earlier, Equation (C.18) was taken directly from Figure C.15-a which was derived graphically based on Figure C.14 and it is consistent will all of Chapter 2. The Fourier coefficients given for $\psi_R(\theta_r)$ are those of a triangle wave (which is why the rotor-stator flux linkage is triangular) but the multiplier is not correct—it should be $8/\pi^2$. Per Equation (C.18), we already know the rotor-stator flux linkage to be a

triangle with an amplitude whose numerical portion is $\pi/2$. Thus, the Fourier coefficients are given by Equation (C.20). This confirms the value given in Figure C.19.

$$\left(\frac{\pi}{2}\right)\cdot\left(\frac{8}{\pi^2}\right)\left[1+\frac{1}{3^2}+\frac{1}{5^2}+\frac{1}{7^2}+\cdots\right]$$

$$=\left(\frac{4}{\pi}\right)\left[1+\frac{1}{3^2}+\frac{1}{5^2}+\frac{1}{7^2}+\cdots\right] \tag{C.20}$$

This combination allows us to finally see how the CFP passes all of the harmonic content of the rotor flux but attenuates each harmonic. It is the interaction of the flux harmonics and harmonic winding factor that defines the shape of the rotor-stator flux linkage. Although each harmonic is attenuated, the CFP winding still achieves the maximum possible amplitude of each component rotor-stator flux linkage in the same way that it produced the maximum possible amplitude of each component of MMF. As before, the sinusoidal winding is the minimum in both regards and all other distributed windings will fall somewhere in between the CFP and sinusoidal windings. Obviously, the winding factors can only "filter" out a harmonic of rotor flux if that harmonic is present in the rotor flux.

Torque and Back-EMF

An expanded version of Figure C.1 is shown in Figure C.20. It is clear that torque is produced via the interaction of the stator and rotor fields and an expression could be found in terms of these. But the stator field is directly related to the current by the winding function thus an expression for torque could also be found in terms of the rotor field and the stator current; this is desirable since it is the stator current that we can control.
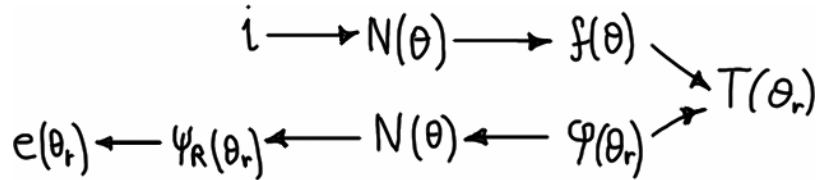
Figure C.20 – 'Natural' torque and bEMF relationships.

As discussed in Chapter 2, the torque produced by a winding in a nonsalient brushless permanent magnet motor (found via coenergy) is given by Equation (C.21). Also, bEMF can be found (using Faraday's law and some manipulation) to be given by Equation (C.22).

$$T(t) = \frac{d}{d\theta_r} \psi_R(\theta_r) \cdot i(t) \tag{C.21}$$

$$e(t) = \frac{d}{d\theta_r} \psi_R(\theta_r) \cdot \omega(t) \tag{C.22}$$

Using this information the relationships can be redrawn as Figure C.21.
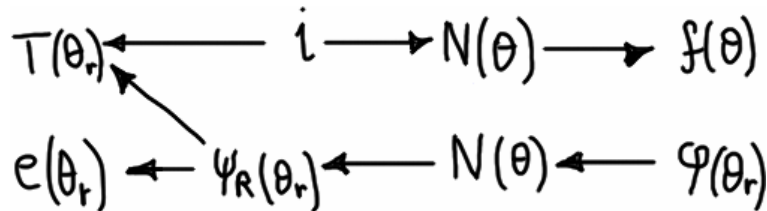
Figure C.21 – Torque and bEMF in terms of rotor-stator flux linkage.

It was also found in Chapter 2 that the torque and bEMF functions were the same as the position derivative of rotor-stator flux linkage, Equation (C.23).

$$\frac{d}{d\theta_r} \psi_R(\theta_r) = k_e(\theta_r) = k_t(\theta_r) \tag{C.23}$$

Torque and bEMF are determined by the derivative of rotor-stator flux linkage. Since all three functions in Equation (C.23) are easily visualized and are equivalent it is easy to see how the motor construction affects torque production and bEMF generation. The previous discussion showed how the fundamental and harmonic winding factors affect MMF and rotor-stator flux linkage. The same affects apply to torque and bEMF.

Returning to Figure C.18 it is clear that a sinusoidal torque function can be obtained using any of three basic winding-rotor combinations:

1. CFP winding, sinusoidal rotor
2. sinusoidal winding, sinusoidal rotor
3. sinusoidal winding, squarewave rotor

We know the CFP winding passes all harmonics of rotor flux thus combination (1) works because the rotor flux has no harmonic content. Combinations (2) and (3) both use a sine winding and we know a sine winding does not link flux harmonics, *thus flux harmonics do not produce torque in a sine winding*. Examining the coefficients for these three combinations (Figure C.19) shows that combination (2) links less flux than combination (3) because the fundamental of rotor flux for the squarewave is larger than unity. As long as a sinusoidal winding is used the rotor-stator flux linkage will be sinusoidal—the rotor flux profile is does not affect the shape of $\psi_R(\theta_r)$ but the amplitude of its fundamental does. Since the torque and bEMF functions are equal to the derivative of $\psi_R(\theta_r)$ they are sinusoidal as well (and have a +90° phase shift).

In the CFP winding with squarewave rotor flux the amplitudes of rotor flux harmonics are multiplied by the harmonic winding factors to produce a $\psi_R(\theta_r)$ that is triangular. But the derivative of a triangle wave is a squarewave therefore the torque and bEMF functions are as shown in Figure C.15-b. If the MMF and rotor flux harmonic content were not exactly equal the shape of the flux linkage would not have been "recovered" in the rotor-stator flux linkage. This combination shows that nonsinusoidal motors are essentially sinusoidal motors with harmonic content in their rotor-stator flux linkage.

Using this information the torque production in a sinusoidal motor will be discussed. Torque is given by Equation (C.21).

(C.21): $\quad T(t) = \dfrac{d}{d\theta_r} \psi_R(\theta_r) \cdot i(t)$

For the CFP winding and sinusoidal rotor $\psi_R(\theta_r)$ was given by Equation (C.14).

(C.14): $\quad \psi_R(\theta_r) = N \cdot D \cdot Y \cdot B_p \cos(\theta_r)$ $\qquad$ (CFP winding, sine rotor flux)

This expression can be reduced by the winding factor and substituted to give the torque as Equation (C.24), where B_1 is the fundamental of rotor flux.

$$T(\theta_r) = -k_w N \cdot D \cdot Y \cdot B_1 \sin(\theta_r) \cdot i(t) \qquad\qquad (C.24)$$

This expression gives the torque produced by the fundamental of stator MMF interacting with the fundamental of rotor flux. Substituting in the appropriate winding factor for CFP (k_w=1) and sinusoidal ($k_w = \pi / 4$) windings yields the torque produced in each case.

$$T(\theta_r) = -N \cdot D \cdot Y \cdot B_1 \sin(\theta_r) \cdot i(t) \qquad \text{(CFP winding, sine rotor flux)} \qquad (C.25)$$

$$T(\theta_r) = -\frac{\pi}{4} N \cdot D \cdot Y \cdot B_1 \sin(\theta_r) \cdot i(t) \quad \text{(sine winding, sine rotor flux)} \qquad (C.26)$$

Equation (C.25) is identical to the expression for torque found in Chapter 2 for the same motor. It must be emphasized that Equation (C.25) describes only that torque produced by the fundamental of rotor flux. If the rotor flux has harmonics, torque ripple will be produced. Equation (C.26) correctly describes the torque regardless of rotor flux because the sinusoidal winding filters the harmonics. Since any practical winding will function somewhere between the two it would be possible to use the harmonic winding factor (in Equation C.24) to compute the torque produced by each harmonic. (The harmonic winding factors can be obtained from spectral analysis of the bEMF.)

Conclusions

It is clear that the shape of the rotor-stator flux linkage is determined by the winding function and the rotor flux profile. Several simple windings and two simple rotor profiles have been presented to demonstrate how $\psi_R(\theta_r)$ can be changed. In addition there are numerous ways to manipulate the harmonic content of the rotor flux [69], [68]. These include varying the magnet thickness, magnetization strength function, magnetization direction, and span/pitch of the magnet (among others). Sinusoidal motors do not typically have full-pitch windings [69, ch.6], [68, p.78] and often have fractional pitch magnets or may be of fractional-slot design [68, p.180].

The focus of this report is on sinusoidal motors. A sinusoidal motor could be defined as one in which $\psi_R(\theta_r)$ (and consequently the torque and bEMF functions) have a sinusoidal shape. By this definition a sinusoidal motor is not required to have sinusoidal windings. However, space vector theory can only describe the MMF produced by a sinusoidal winding. For this reason most of the academic literature concerning FOC makes the assumption of a sinusoidal winding and a sinusoidal rotor flux. This report will use the same assumptions and the resulting expression for

torque will describe the torque produced by the fundamental components of stator MMF and rotor-stator flux linkage.

Making these assumptions greatly simplifies the presentation and understanding of FOC but leaves questions as to how a nonsinusoidal motor should be handled, but the answer is simple. A motor with nonsinusoidal windings can be modeled using space vectors but the model will only represent the fundamental components. Therefore the torque and bEMF space vector equations will not be correct (there will be torque ripple even with sinusoidal current and there will be bEMF harmonics).

Traditional texts work with the winding factor but to streamline the equations, modern texts replace the number of turns N with the number of *effective turns* as defined by Equation (C.27) [69, p.6.22], [42, pp.177,448].

$$N_e = \frac{4}{\pi} k_w N \tag{C.27}$$

The effective number of turns represents the number of turns used to produce fundamental MMF. Using the effective number of turns allows the consideration of the fundamental MMF produced by a nonsinusoidal winding. Although [87] states the space vector can only describe windings that produce sinusoidal MMF, all references in the literature surveyed use something akin to Equation (C.27).

NOTE

This appendix has analyzed the single-winding case only in order to show the mechanisms at work. Every result is valid for a three phase machine. However, there is no point in computing anything related to the third or triplen harmonics if the machine is wye-connected. Meaning that even if a the third harmonic winding factor $k_{w,3}$ is found to be nonzero, it would not contribute to torque or bEMF [69, p.6.16]. As shown, the harmonic winding factor affects the rotor-stator flux linkage, which affects both bEMF and torque. As far as bEMF is concerned, the triplen components in the bEMF will simply appear at the isolated motor neutral, not affecting operation. As far as torque is concerned, it is impossible for the third harmonic of flux to produce torque without the third harmonic of current, which cannot be driven into a wye winding. Two cases where the triplen harmonics are important are grid-connected generators (usually wye-connected with a grounded neutral) and delta-connected machines (in which the third harmonic of bEMF would cause circulating current).

Appendix D - Three-Phase Concepts & Transformations

This appendix is a collection of various "basic" and "advanced" topics related to three-phase systems that appear throughout the report. Although all readers are assumed to have an electrical engineering degree, many of these basic concepts are not taught in courses outside the power systems emphasis. In addition, many modern machines and power electronics texts are nearly half a century out of date, thus many graduating students (the author included) are likely to have not been exposed to the more advanced topics.

Harmonic Analysis

Any periodic signal can be described in terms of a Fourier series. All ideal steady-state waveforms in nonsalient machines possess quarterwave symmetry so they can be represented using only cosine or sine terms; here, the cosine is selected in order to match the conventions for the phasor and space vector reference. Since waveforms with quarterwave symmetry also have halfwave symmetry only odd terms are present. The standard harmonic components are therefore defined by Equation (D.1).

$$x_n(t) = X_n \cos(n \cdot \omega t); \quad n = 1, 3, 5, 7, 9, \cdots \tag{D.1}$$

As remarked earlier, this report only considers symmetric three-phase systems. For loads, this condition means that the self impedance of each phase must be identical and the mutual impedance between any two phases must be the same regardless of which pair is considered. From Chapter 3 and Appendix B, the impedance matrix for a three-phase sinusoidal motor satisfies this requirement. For sources (a controlled three-phase source or a bEMF in a load) the restriction means that each harmonic component of the phase-neutral voltage is identical to that of the other phases but is displaced by 120°.

The harmonic components defined in Equation (D.1) are for a single phase only (and since phase-A is always taken as the reference, they are for phase-A). Extending the definition to phase-B and phase-C would appear to be given by Equation (D.2).

$$\begin{cases} x_{nA}(t) = X_n \cos(n \cdot \omega t) \\ x_{nB}(t) = X_n \cos(n \cdot \omega t - \gamma) \\ x_{nC}(t) = X_n \cos(n \cdot \omega t + \gamma) \end{cases} \quad \begin{matrix} n = 1, 3, 5, 7, 9, \cdots \\ \gamma = 120° \end{matrix} \tag{D.2}$$

However, Equation (D.2) is incorrect. Since the fundamental component of phase-B and phase-C are displaced by $\mp 120°$ from the fundamental component of phase-A, the harmonic components in phase-B and phase-C must be similarly displaced. That is, for each harmonic set the nth component in each phase must be displaced by $(120° / 360°) = 2/3$ of a *fundamental* electrical cycle from the nth component in the other phases, not 120° of that *harmonic* electrical cycle as Equation (D.2) would imply. The period of the nth harmonic is $360° / n$, thus the angle corresponding to a 120° delay in harmonic measure is equal to a $120° / n$ delay in fundamental measure. Therefore to make the phase-B and phase-C $\mp 120°$ harmonic delays equal to the phase-B and phase-C $\mp 120°$ fundamental delays, the $\mp 120°$ harmonic delay must be multiplied by n, as shown in Equation (D.3). In other words, there is noting special about the harmonic components themselves. If they were indeed defined by Equation (D.2) their phase offsets would all be $(0, -\gamma, +\gamma)$, exactly like those of the fundamental, and they would all sum to zero just the same. It is the fact that harmonics are 120 *fundamental*-degrees apart that gives them different properties in a three-phase system. (Again, the reason that the harmonic components are *defined* to be 120 fundamental degrees apart, instead of 120 harmonic degrees, is because the harmonics of each phase are given by Equation (D.1), thus the entire set of harmonics in a phase are displaced by 120 fundamental degrees from the set of each other phase.)

$$
\begin{cases}
x_{nA}(t) = X_n \cos(n \cdot \omega t) \\
x_{nB}(t) = X_n \cos(n \cdot \omega t - n \cdot \gamma) \\
x_{nC}(t) = X_n \cos(n \cdot \omega t + n \cdot \gamma)
\end{cases}
$$

$$
= \begin{cases}
x_{nA}(t) = X_n \cos(n \cdot [\omega t]) \\
x_{nB}(t) = X_n \cos(n \cdot [\omega t - \gamma]) \\
x_{nC}(t) = X_n \cos(n \cdot [\omega t + \gamma])
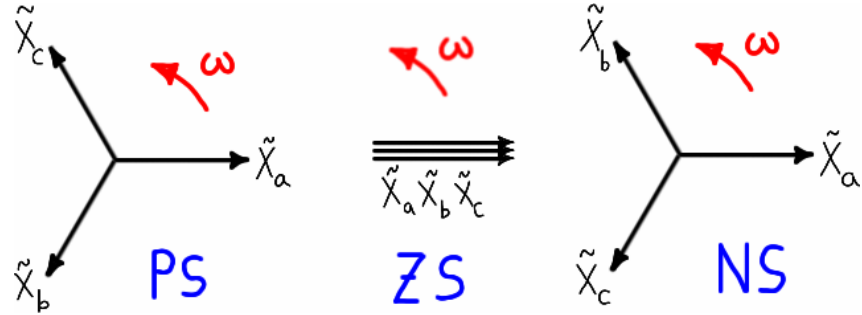\end{cases} \tag{D.3}
$$

Equation (D.3) is now evaluated for the fundamental and the first two harmonics.

$$n=1: \quad \begin{cases} x_{1A}(t) = X_1 \cos\left(1\cdot[\omega t]\right) \\ x_{1B}(t) = X_1 \cos\left(1\cdot[\omega t - \gamma]\right) \\ x_{1C}(t) = X_1 \cos\left(1\cdot[\omega t + \gamma]\right) \end{cases} = \begin{cases} x_{1A}(t) = X_1 \cos\left(\omega t\right) \\ x_{1B}(t) = X_1 \cos\left(\omega t - \gamma\right) \\ x_{1C}(t) = X_1 \cos\left(\omega t + \gamma\right) \end{cases} \tag{D.4}$$

$$n=3: \quad \begin{cases} x_{3A}(t) = X_3 \cos\left(3\cdot[\omega t]\right) \\ x_{3B}(t) = X_3 \cos\left(3\cdot[\omega t - \gamma]\right) \\ x_{3C}(t) = X_3 \cos\left(3\cdot[\omega t + \gamma]\right) \end{cases} = \begin{cases} x_{3A}(t) = X_3 \cos\left(3\omega t\right) \\ x_{3B}(t) = X_3 \cos\left(3\omega t\right) \\ x_{3C}(t) = X_3 \cos\left(3\omega t\right) \end{cases} \tag{D.5}$$

$$n=5: \quad \begin{cases} x_{5A}(t) = X_5 \cos\left(5\cdot[\omega t]\right) \\ x_{5B}(t) = X_5 \cos\left(5\cdot[\omega t - \gamma]\right) \\ x_{5C}(t) = X_5 \cos\left(5\cdot[\omega t + \gamma]\right) \end{cases} = \begin{cases} x_{5A}(t) = X_5 \cos\left(5\omega t\right) \\ x_{5B}(t) = X_5 \cos\left(5\omega t + \gamma\right) \\ x_{5C}(t) = X_5 \cos\left(5\omega t - \gamma\right) \end{cases} \tag{D.6}$$

It is seen that the phase offsets follow the pattern $(0, -\gamma, +\gamma)$, $(0, 0, 0)$, $(0, +\gamma, -\gamma)$. Only the fundamental and the first two harmonics need be evaluated because the pattern repeats. If a set of balanced phasors were used to describe the sets in Equations (D.4)-(D.6) they would look like those in Figure D.1.[51] Note that the order of the phasors differs between the PS and NS diagrams.
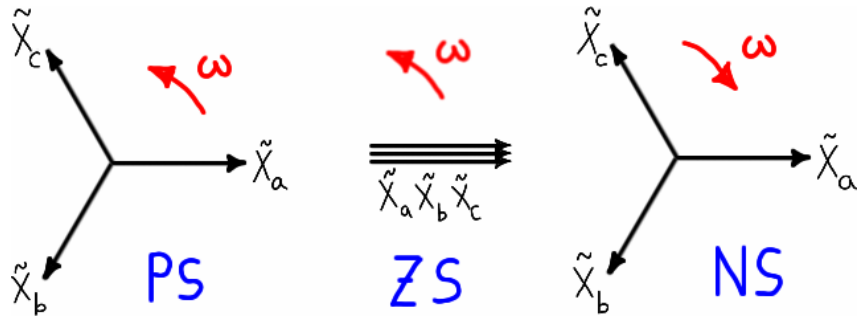
Figure D.1 – Phasor diagrams for positive-, zero-, and negative- sequence sets.

Projecting the phasors of each set onto the real axis would show that the order in which the phase variables peak. In the first set the order is ($A - B - C$), in the second set the variables are all cophasal, and in the third set the order is ($A - C - B$). The first set is called a *positive-sequence* (PS) set, the second a *zero-sequence* (ZS) set, and the third a *negative-sequence* (NS) set. Sometimes the argument of the cosines in Equation (D.6) is negated, yielding phasors that have

---

[51] Each phasor would be defined using a different ω (namely, $n\cdot\omega$) but this fact is not shown because the emphasis is on the sequence rotation.

the same *order* as the PS set (arranged A-C-B in the CCW direction) but rotate in the opposite *direction*, as shown in Figure D.2.[52]

Figure D.2 – An alternate (but equivalent) interpretation of sequence sets.

The sequence order of some low-order harmonics are summarized in Figure D.3.

Figure D.3 – Sequence order of some low-order harmonics.

The component of MMF that a current harmonic produces in a machine will rotate according to its sequence. To see this it is not necessary to use SV theory but doing eases understanding. The SVs corresponding to the harmonics of Equations (D.4)-(D.6) are given by Equations (D.7)-(D.9), respectively, where $k = 2/3$ has been used to achieve magnitude-invariance (a derivation is given later in this appendix).

$$\vec{x}_1 = X_1 e^{j\omega t} \tag{D.7}$$

$$\vec{x}_3 = 0 \tag{D.8}$$

$$\vec{x}_5 = X_5 e^{-j5\omega t} \tag{D.9}$$

It is clear that PS harmonics would cause a positive rotation, NS harmonics would cause negative rotation, and ZS harmonics do not cause any rotation.[53] More importantly the phasor diagrams in

---

[52] In the method of symmetrical components (MSC) all phasors are at the fundamental frequency. These sets discussed here are *similar* to those of MSC but since they have different frequencies they are *not* the same. Therefore when "PS," "NS," and "ZS" are used in this report, they refer to general sets that have PS, NS, and ZS rotation, not those sets particular to the MSC.

[53] There are several simultaneous "reasons" why the third-harmonic SV is zero. First, we cannot force ZS current into a winding when the neutral is isolated (KCL). Second, even if the neutral were grounded so

Figure D.1 show that the PS and NS phasors vectorially sum to zero but the ZS phasors sum to a cophasal phasor whose magnitude is three times that of the ZS phasors. Since the PS and NS components sum to zero we will call them $\Sigma = 0$ components. Since the ZS component does not sum to zero it could be called the $\Sigma \neq 0$ component but since only the ZS component has this property it will be called the ZS component. The consequence of this is that in analyzing symmetrical three-phase systems we can group the harmonic components into $\Sigma = 0$ components and a ZS component. As will be shown, the reason for the separate treatment is that ZS component affects three-phase systems differently than do $\Sigma = 0$ components.

The ZS component has been defined in the traditional manner using phasors. From Figure D.3 it is seen that in three-phase systems the ZS component is composed of the odd multiples of three; these are called the *triplen harmonics*. But also, any common-mode component among the phase variables in a set is a ZS component. If a common mode component were plotted against time it would be found to have a spectra consisting of only triplens and/or a DC component. Thus, *this report defines the ZS component to be the common-mode component*; this is commonly implied in the literature but is often unstated.
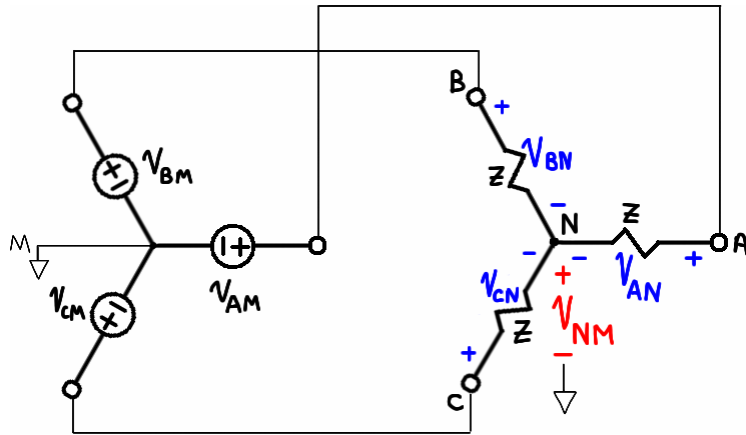
---

that ZS current would flow, the current would produce zero net MMF, which obviously cannot rotate. Third, the SV cannot capture ZS terms even if they were present (this is true for any space vector).

Implications of the ZS Component

There are many aspects of circuit and machine operation that are affected by the ZS component. First we will examine the passive impedance load and then the motor load. Then the results will then be summarized.

Passive Impedance Load

An impedance load driven by a source is shown in Figure D.4.

Figure D.4 – Passive impedance load driven by source.

The supply neutral is called the midpoint (M) and is used as the reference; the load neutral (N) is floating. Using KVL on each phase loop results in Equation (D.10).

$$\begin{cases} v_{AM} = v_{AN} + v_{NM} \\ v_{BM} = v_{BN} + v_{NM} \\ v_{CM} = v_{CN} + v_{NM} \end{cases} \tag{D.10}$$

The sum of these equations is given by Equation (D.11).

$$\left(v_{AM} + v_{BM} + v_{CM} \right) = \left(v_{AN} + v_{BN} + v_{CN} \right) + 3v_{NM} \tag{D.11}$$

The source voltages can be written as Equation (D.12) where we assume there is a ZS component v_{ZS} present in each source voltage in addition to the $\Sigma = 0$ components v'_{xM}.

$$\begin{cases} v_{AM} = v'_{AM} + v_{ZS} \\ v_{BM} = v'_{BM} + v_{ZS} \\ v_{CM} = v'_{CM} + v_{ZS} \end{cases} \tag{D.12}$$

The sum of the source voltages will be equal to three times the ZS component (Equation D.13) and the $\Sigma = 0$ components sum to zero.

$$\left(v_{AM} + v_{BM} + v_{CM}\right) = \left(v'_{AM} + v'_{BM} + v'_{BM}\right) + 3v_{ZS}$$

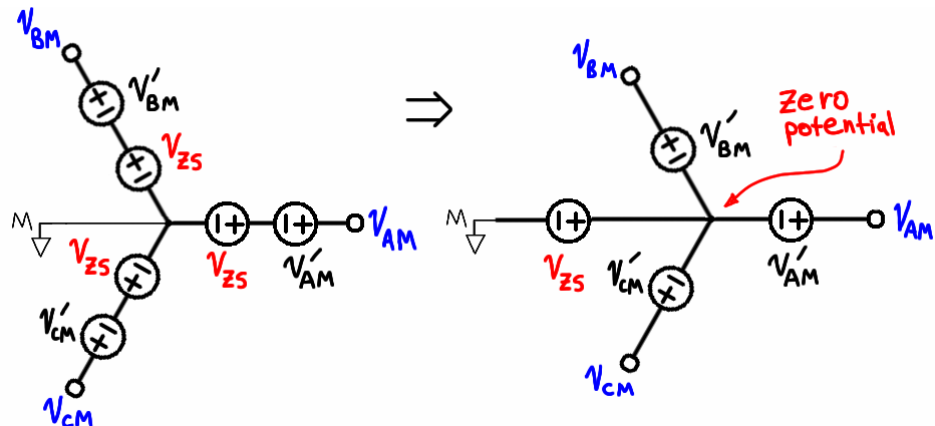$$\left(v_{AM} + v_{BM} + v_{CM}\right) = 3v_{ZS} \tag{D.13}$$

The currents in the load must sum to zero. Since there are no voltage sources in the load, the sum of the line-neutral load voltages must also sum to zero (Equation D.14).

$$Z(s)\left[I_A(s) + I_B(s) + I_C(s)\right] = 0$$
$$\left[V_{AN}(s) + V_{BN}(s) + V_{CN}(s)\right] = 0$$

$$\therefore \left(v_{AN} + v_{BN} + v_{CN}\right) = 0 \tag{D.14}$$

Applying the results of Equations (D.13)-(D.14) to Equation (D.11) gives Equation (D.15).
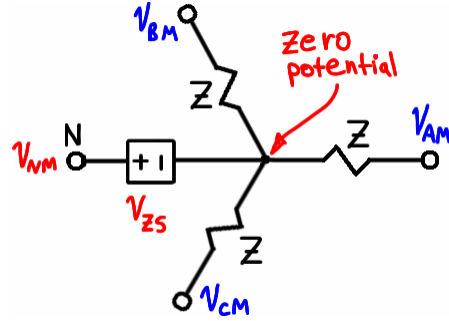
$$\left(3v_{ZS}\right) = \left(0\right) + 3v_{NM}$$

$$v_{NM} = v_{ZS} \tag{D.15}$$

Thus the ZS component of source voltage will always appear at the neutral in a passive load with an isolated neutral. That v_{NM} is a common-mode voltage should have already been clear from Equation (D.10) and that the neutral voltage is exactly the common-mode voltage should be clear from a general knowledge of circuit theory. To emphasize the latter, examine Figure D.5 in light of Equation (D.12). There is no difference between the two circuits in Figure D.5 and it is seen that the "balanced portion" of the source is v_{ZS} above ground.

Figure D.5 – Equivalent source showing that ZS is common-mode.

By using Equation (D.15) the same perspective can be used to examine the load, as shown in Figure D.6. The voltage v_{ZS} is drawn as a square because it is not a real source (just as the point of zero potential does not physically exist); the v_{ZS} voltage against the zero potential simply represents the effect of v_{ZS} on the load; no current can be driven through it.

Figure D.6 – Neutral voltage of load is common mode voltage of source.
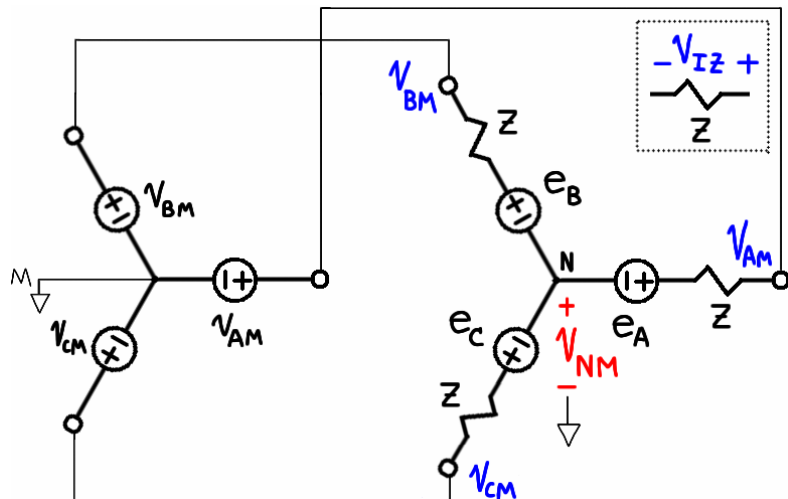
The common-mode voltage seen by the three-phase load is defined by Equation (D.16).

$$v_{common} = \frac{1}{3}\left(v_{AM} + v_{BM} + v_{CM}\right) \tag{D.16}$$

Substituting Equation (D.12) into Equation (D.16) yields Equation (D.15), as before. Finally, comparing Equation (D.10) and Equation (D.12) in light of Equation (D.15) makes it exceptionally clear that since the ZS component of source voltage appears in the neutral, only the PS and NS components voltage appear across the load impedance. Since the ZS component does not appear across the load it cannot drive a current, thus from a current-control perspective it does not matter if a ZS component is present or not.

Motor Load

Most of the results for the passive load apply here, except the load's line-neutral voltages are not required to sum to zero as they were in Equation (D.14) (several articles in the literature make grave mistakes regarding this). Each phase of the motor load is the bEMF in series with an impedance, Figure D.7.

Figure D.7 – Motor load driven by source.

The load line-neutral voltages are given by Equation (D.17), where $\left(v_{IZ,A}, v_{IZ,C}, v_{IZ,C}\right)$ are the voltage drops across the impedances.

$$\begin{cases} v_{AN} = e_A + v_{IZ,A} \\ v_{BN} = e_B + v_{IZ,B} \\ v_{CN} = e_C + v_{IZ,C} \end{cases} \tag{D.17}$$

Similar to Equation (D.14), the drops across the impedances must sum to zero, thus Equation (D.18).

$$Z(s)\left[I_A(s) + I_B(s) + I_C(s)\right] = 0$$
$$\left[V_{IZ,A}(s) + V_{IZ,B}(s) + (s)V_{IZ,C}(s)\right] = 0$$
$$\therefore \left(v_{IZ,A} + v_{IZ,B} + v_{IZ,C}\right) = 0 \tag{D.18}$$

Summing Equation (D.17) and substituting Equation (D.18) gives Equation (D.19).

$$\left(v_{AN} + v_{BN} + v_{CN}\right) = \left(v_{IZ,A} + v_{IZ,B} + v_{IZ,C}\right) + \left(e_A + e_B + e_C\right)$$
$$\left(v_{AN} + v_{BN} + v_{CN}\right) = \left(e_A + e_B + e_C\right) \tag{D.19}$$

In order to examine the impact of a ZS component in the bEMF, the assumptions in Equation (D.12) for source voltage are now applied to the bEMF. We assume (Equation D.20) that there is a ZS component e_{ZS} in addition to the $\Sigma = 0$ components e'_{xM}.

$$\begin{cases} e_A = e'_A + e_{ZS} \\ e_B = e'_B + e_{ZS} \\ e_C = e'_C + e_{ZS} \end{cases} \tag{D.20}$$

Substituting the result into Equation (D.19) gives Equation (D.21).

$$\left(v_{AN} + v_{BN} + v_{CN}\right) = \left(e'_A + e'_B + e'_C + 3e_{ZS}\right)$$
$$\left(v_{AN} + v_{BN} + v_{CN}\right) = 3e_{ZS} \tag{D.21}$$

The KVL result is the same as before (Equation D.10) and since we still make the assumptions of Equation (D.12) for the source voltages, Equation (D.13) still holds.

$$(D.10): \begin{cases} v_{AM} = v_{AN} + v_{NM} \\ v_{BM} = v_{BN} + v_{NM} \\ v_{CM} = v_{CN} + v_{NM} \end{cases}$$

$$(D.13): \left(v_{AM} + v_{BM} + v_{CM}\right) = 3v_{ZS}$$
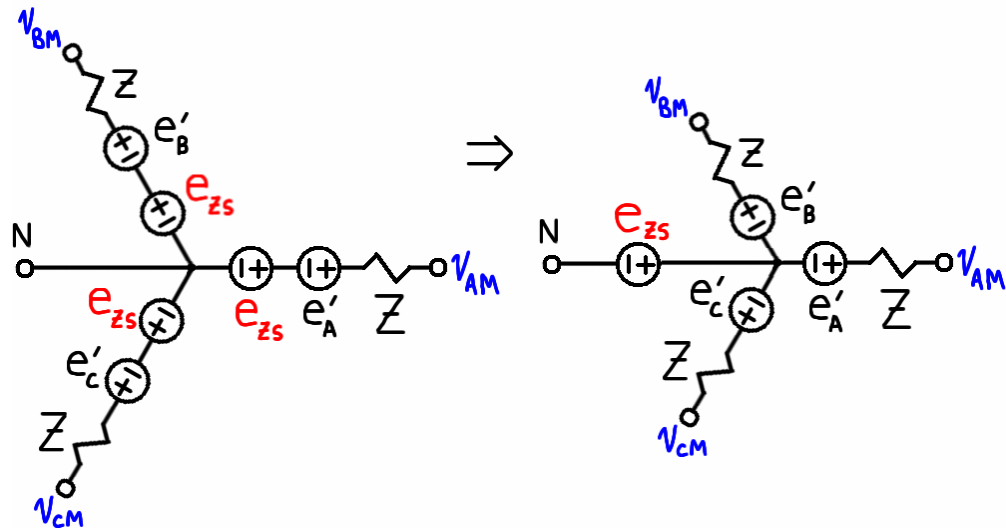
Summing Equation (D.10) and substituting Equations (D.13) and (D.21) gives Equation (D.22).

316

$$\left(v_{AM} + v_{BM} + v_{CM}\right) = \left(v_{AN} + v_{BN} + v_{CN}\right) + 3v_{NM}$$

$$\left(3v_{ZS}\right) = \left(3e_{ZS}\right) + 3v_{NM}$$

$$v_{NM} = v_{ZS} - e_{ZS} \tag{D.22}$$

For the impedance load it was concluded that the ZS component in the source had no ability to drive currents in the load and Equation (D.22) shows that this is true for the motor load as well. In addition Equation (D.22) shows the same comments apply to the ZS component of the bEMF. The motor load may be redrawn by using the concept in Figure D.5, as shown in Figure D.8.[54]
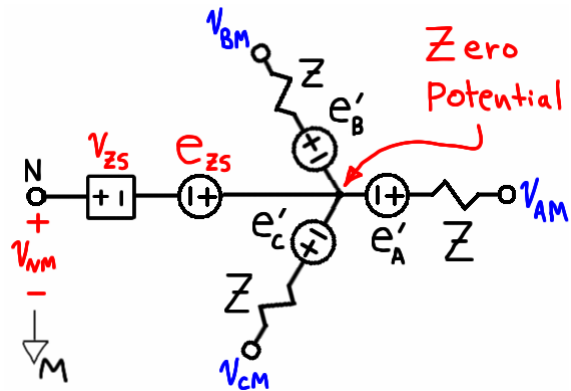
Figure D.8 – Equivalent motor bEMF arrangement.

Figure D.8 shows the rearranging of the bEMF only. To show the total influence on the neutral voltage, the concept used in Figure D.6 (which was found to be valid for the motor as well) is combined with the concept shown in Figure D.8 to yield Figure D.9.

---

[54] In Figure D.7 the lines connecting source and load are thin to emphasize that the source and load are separate parts; the connection of the source to the midpoint M is likewise a lightweight line. In contrast, in Figure D.6 and Figure D.8 the "connection" to the neutral point is a heavyweight line, indicating that it is an integral part of the load.

Figure D.9 – Load neutral voltage influence by ZS of source and bEMF.

Figure D.9 clearly confirms Equation (D.22). Setting $e_{ZS} = 0$ confirms that the ZS source voltage would appear in the neutral as before; similarly setting $e_A = e_B = e_C = 0$ reduces the circuit to that in Figure D.6. Or, if the source had no ZS component but the bEMF did have, the neutral voltage would be the negative of the bEMF ZS component (the negative is the result of the "source opposing load" sign convention). Given any combination of amplitudes of source and bEMF ZS components, it is clear that both affect the neutral voltage but neither affects the flow of current.

Summary

In a passive load that is wye-connected with isolated neutral, the ZS component in the source voltage will appear as a neutral voltage. If the load has a bEMF source, the bEMF ZS component will combine with the source ZS component to influence the neutral voltage according to Equation (D.22). In either case it is impossible for ZS current to flow. PS and NS components of voltage do not appear in the isolated neutral because they sum to zero; they are the only components that can drive current through an isolated-neutral-wye load.

If the neutral of the wye-connected load is grounded then the ZS components of voltage and bEMF will drive a ZS current through the neutral and the neutral point potential will be zero (in reality, it would be determined by the impedance of the conductor that grounds the neutral point). Most BPM motors have an isolated neutral; if it were available it would NOT normally be connected to ground (the bus midpoint). In PWM schemes that produce a ZS component, or with a motor that had a ZS bEMF component, grounding the neutral would cause a short circuit for the ZS component and likely trip the overcurrent protection and possibly damage the inverter (or overheat the windings if the fault level was below the trip point). Since the PS and NS

components of source voltage sum to zero (produce no net neutral voltage) they would not cause any current to flow in a grounded neutral (the menial result presented in circuit theory texts).

If the load is delta-connected the ZS component of the source voltage would be present at each terminal by definition, thus ZS current cannot flow in this case either and the delta connection can be used with PWM schemes that produce a ZS component. However, if the bEMF contains ZS components they will drive current around the delta, restricted only by the impedance of the winding, thus delta motors must be designed to have minimal ZS components in the bEMF.

A final note of interest concerns sensorless control techniques that use a three-phase resistor network to create an "artificial neutral" connected to the three motor/inverter terminals, such as [163], [87, p.148]. The network is used to collect triplen harmonics of the bEMF, from which the third is filtered out and used for rotor position detection. Per the above, in a 180° system the *artificial* neutral will contain the triplens of the source but not the triplens of the bEMF that are required. The method works only when a 120° inverter is used (because this causes the zero-sequence network of the load to become coupled to the phase network, which allows the triplens to be measured at the terminals). It seems that articles presenting these types of methods (and especially the references that cite them) leave unmentioned that the technique works only for 120° inverters. Other sensorless methods that utilize the third harmonic do employ a 180° inverter (such as [164], [165]) but these require a connection to the motor neutral or a specially-wound armature.

Method of Symmetrical Components

The method of symmetrical components (MSC) [29], [32], [26] is a linear transformation of variables that is used to study unbalanced three-phase circuits. A discussion is beyond scope but because it bears much similarity to the αβ0 transform and space vector it is mentioned briefly. The MSC (phasor) transforms the three-phase variables $\left(\tilde{X}_a, \tilde{X}_b, \tilde{X}_c \right)$ into three *sequence components* $\left(\tilde{X}_0, \tilde{X}_1, \tilde{X}_2 \right)$ (ZS, PS, and NS, respectively). The transformation is defined by Equation (D.23) and the inverse transform by Equation (D.24).

$$
\begin{bmatrix} \tilde{X}_a \\ \tilde{X}_b \\ \tilde{X}_c \end{bmatrix} = \begin{bmatrix} 1 & 1 & 1 \\ 1 & a^2 & a \\ 1 & a & a^2 \end{bmatrix} \begin{bmatrix} \tilde{X}_0 \\ \tilde{X}_1 \\ \tilde{X}_2 \end{bmatrix} \quad \Leftrightarrow \quad \mathbf{x}_{abc} = \mathbf{A}\mathbf{x}_{012}
\tag{D.23}
$$

$$
\begin{bmatrix} \tilde{X}_0 \\ \tilde{X}_1 \\ \tilde{X}_2 \end{bmatrix} = \frac{1}{3} \begin{bmatrix} 1 & 1 & 1 \\ 1 & a & a^2 \\ 1 & a^2 & a \end{bmatrix} \begin{bmatrix} \tilde{X}_a \\ \tilde{X}_b \\ \tilde{X}_c \end{bmatrix} \quad \Leftrightarrow \quad \mathbf{x}_{012} = \mathbf{A}^{-1}\mathbf{x}_{abc}
\tag{D.24}
$$

In single-phase equivalent (SPE) analysis we analyze the phasor diagram for phase-A only; phase-B and phase-C have diagrams of identical magnitude and phase but are displaced by 120°. Unlike SPE analysis, the MSC is concerned with only *one* quantity (such as a load voltage) but all three phasors $\left(\tilde{X}_a, \tilde{X}_b, \tilde{X}_c \right)$ of that quantity are considered because they are unbalanced (and SPE is not applicable). Each sequence component $\left(\tilde{X}_0, \tilde{X}_1, \tilde{X}_2 \right)$ is a single phasor for only one phase (phase-A) but there is also a phase-B and a phase-C phasor for each component. Thus the phasors are

$$
\left(\tilde{X}_{a0}, \tilde{X}_{a1}, \tilde{X}_{a2}, \tilde{X}_{b0}, \tilde{X}_{b1}, \tilde{X}_{b2}, \tilde{X}_{c0}, \tilde{X}_{c1}, \tilde{X}_{c2} \right)
$$

but we choose to only work with the ones for phase-A. Like any set of phasors, those for a sequence component (such as $\tilde{X}_0$) are displaced by 120°.[55] The PS phasors are made to have the PS order, the NS the NS order, and the ZS order as was shown in Figure D.1. This is the purpose of the **A** matrix—it creates the various sequence phasors from those of phase-A simply by rotating each by 0 or $\pm 120°$. For illustration, the PS row in Equation (D.24) is broken out as

---

[55] Since each of the three phasors for a sequence component are of equal magnitude but displaced by 120° they are not linearly dependent. Thus the MSC takes three variables to three variables, not three-to-nine.

Equation (D.25) and instantaneous quantities have replaced the phasors. (Recall that $a = e^{j120^\circ} = e^{j\gamma}$.)

$$X_1 = \frac{1}{3}\left[x_A \cdot 1 + x_B \cdot e^{j\gamma} + x_C \cdot e^{-j\gamma} \right] \tag{D.25}$$

Equation (D.25) is seen to be the definition of the SV (with an inconsequential scaling factor). Therefore the SV transform gives *essentially* the same result as the *instantaneous* PS component in MSC. The second item of interest is that the ZS component defined in Equation (D.24) is the same as that of Equation (D.16), showing that the ZS component in MSC has essentially the same meaning as the common-mode component.

Clarke & αβ0 Transforms

The matrix transformations used in electrical circuit and machine analysis ([32], [34], [22], [35]) have evolved over the years, becoming rearranged, scaled, expanded, reduced, and reordered to serve various purposes; in the process they also acquire various names. The Clarke, Park, and MSC transformations given in this report are just one particular form of each. To compare the various versions is important for several reasons: to understand the significance of the ZS (0) term, to get an idea of the varieties in use, and to understand that there are so many variants that one should never take a sentence at its word—such as, "the Park transform accomplishes…"— until the matrix transformation in question is verified. This section examines the Clarke and αβ0 transforms; the "Park," "original Park," and *dq0* transforms are investigated in Appendix E.

The primary difference between the Clarke and αβ0 transforms is the presence or absence of the ZS component. It has been shown numerous times that the SV transform is the complex-valued version of the Clarke transform, and that neither can contain the ZS component. This is very much worth a closer look. In the simplest case when we know the ABC components do not contain a ZS component (such as the measurement of currents in a wye connection with isolated neutral), we are free to not have to calculate it, as in Equation (D.26). This is the "raw" Clarke transformation matrix defined in Chapter 3. It is sometimes called a *phase transformation matrix*, which is a fitting name because it implies a stationary transform that effectively functions as a 3-to-2-phase "Scott-T" transformer connection.

$$\begin{bmatrix} x_\alpha \\ x_\beta \end{bmatrix} = k \begin{bmatrix} 1 & -1/2 & -1/2 \\ 0 & \sqrt{3}/2 & -\sqrt{3}/2 \end{bmatrix} \begin{bmatrix} x_A \\ x_B \\ x_C \end{bmatrix} \tag{D.26}$$

We previously acknowledged that since $\Sigma = 0$ it would be more convenient if we made that simplification in order to obtain more direct relationships between the components. Rearranging the $\Sigma = 0$ condition and substituting gives the form of either Equation (D.27) or (D.28).

$$\begin{bmatrix} x_\alpha \\ x_\beta \end{bmatrix} = k \begin{bmatrix} 3/2 & 0 & 0 \\ 0 & \sqrt{3}/2 & -\sqrt{3}/2 \end{bmatrix} \begin{bmatrix} x_A \\ x_B \\ x_C \end{bmatrix} \tag{D.27}$$

$$\begin{bmatrix} x_\alpha \\ x_\beta \end{bmatrix} = k \begin{bmatrix} 3/2 & 0 & 0 \\ \sqrt{3}/2 & \sqrt{3} & 0 \end{bmatrix} \begin{bmatrix} x_A \\ x_B \\ x_C \end{bmatrix} \tag{D.28}$$

If a ZS component could possibly be present in the ABC quantities (such as the measurement of voltages in a three-phase system), it could be calculated by adding a row to the matrix in Equation (D.26), as in Equation (D.29). This is the original transformation used by Edith Clarke [11, p.308], although it had been presented and used by different authors prior to that, at least as early as 1917 [11, p.310]. The transform was used in a fashion similar to that in the MSC (which is not what we have been using it for here). More information about the original Clarke transform and its application to synchronous machines can be found in [11], [12].

$$
\begin{bmatrix} x_\alpha \\ x_\beta \\ x_0 \end{bmatrix} = k \begin{bmatrix} 1 & -1/2 & -1/2 \\ 0 & \sqrt{3}/2 & -\sqrt{3}/2 \\ 1 & 1 & 1 \end{bmatrix} \begin{bmatrix} x_A \\ x_B \\ x_C \end{bmatrix}
\tag{D.29}
$$

In the popular literature it is common to call Equation (D.26) (or any of its $\Sigma = 0$ variants) the *Clarke transform* and this report adopts that usage. The academic literature is more technical and generalized, studying circuits in which a ZS component is assumed to be present. Equation (D.29) or a variant (discussed below) is used, which in this report is called the *αβ0 transform*. These names are used interchangeably in the literature and it may also be called a *Concordia transform* (after the pioneer Charles Concordia ([9], [10]). In addition, the axis along which the ZS component acts may be called the γ- or Z- axis. Some variations will now be discussed.

We have seen the usage of the scaling constant k in regards to the αβ components. The same remarks apply to the ZS component, meaning that there is a choice of k to make the ZS part of the transform in Equation (D.29) be magnitude- or power- invariant just like the αβ part. Since the ZS coefficients are scaled by k, one would expect to find three matrices that match the three varieties of the Clarke transform. However, no such standardization exists because authors often choose scaling between the αβ and 0 components to be different. This is handled in this report by introducing a separate constant c to describe the ZS component scaling. The general αβ0 transform is given by Equation (D.30) (hence, the original Clarke transform used $c = 2$).

$$
\begin{bmatrix} x_\alpha \\ x_\beta \\ x_0 \end{bmatrix} = \begin{bmatrix} k & & \\ & k & \\ & & c \end{bmatrix} \begin{bmatrix} 1 & -1/2 & -1/2 \\ 0 & \sqrt{3}/2 & -\sqrt{3}/2 \\ 1/2 & 1/2 & 1/2 \end{bmatrix} \begin{bmatrix} x_A \\ x_B \\ x_C \end{bmatrix}
\tag{D.30}
$$

Since the αβ0 transform is the Clarke transform plus the ZS (0) component, the matrix will be denoted $\mathbf{C}_0$. The "raw," magnitude-invariant, and power-invariant αβ0 transform matrices are given by Equations (D.31), (D.32), and (D.33), respectively [87, p.34], [88, p.87]. Note that in the

power invariant form, $k \neq c$. In this report the αβ0 transform is primarily used when studying inverters so the magnitude-invariant variety is used.

$$\mathbf{C}_0 = \begin{bmatrix} 1 & -1/2 & -1/2 \\ 0 & \sqrt{3}/2 & -\sqrt{3}/2 \\ 1/2 & 1/2 & 1/2 \end{bmatrix}; \quad k = c = 1 \tag{D.31}$$

$$\mathbf{C}_{0m} = \begin{bmatrix} 2/3 & -1/3 & -1/3 \\ 0 & 1/\sqrt{3} & -1/\sqrt{3} \\ 1/3 & 1/3 & 1/3 \end{bmatrix}; \quad \begin{matrix} k = c = 2/3 \\ \text{(magnitude-invariant)} \end{matrix} \tag{D.32}$$

$$\mathbf{C}_{0p} = \begin{bmatrix} \sqrt{2/3} & -1/\sqrt{6} & -1/\sqrt{6} \\ 0 & 1/\sqrt{2} & -1/\sqrt{2} \\ 1/\sqrt{6} & 1/\sqrt{6} & 1/\sqrt{6} \end{bmatrix}; \quad \begin{matrix} k = \sqrt{2/3} \\ c = 2/\sqrt{3} \\ \text{(power-invariant)} \end{matrix} \tag{D.33}$$

The **α** axis has been defined to be coincident with the real axis and the **β** with the imaginary axis. However, for some reason a sizeable portion of the literature aligns the **β** axis in the *negative* direction of the imaginary axis. The order of the variables in the vector are also sometimes rearranged (for example, the 0αβ transform uses the order 0,α,β). Both of these changes affect the way the SV and Clarke transform are defined and this change obviously propagates to other definitions and expressions, thus care is required in interpreting the literature. Finally, it should be noted that that **α** and **β** axes may be labeled D,Q or d,q.

The Zero Sequence Component

The chapter on inverters shows that the magnitude-invariant form of the Clarke transform has direct correlation to the physical values (such as voltage). The interpretation is the same for the ZS component of the magnitude-invariant αβ0 transform. Clearly, if Equation (D.32) were used on a set of voltages, v_0 would be the same term defined by Equation (D.16). If the voltages were across an isolated-neutral wye load, the v_0 term would be the neutral voltage, in agreement with Equation (D.15). Thus the 0-component is the same as the general ZS component encountered throughout this appendix. As mentioned throughout the report, the SV (or αβ components) simply cannot encode the ZS component; this is now shown. Consider the example of phase variables (Equation D.34) that contain the first PS, ZS, and NS harmonics (which were defined by Equations D.4–D.6). Writing the phase variables in complex form (Equation D.35) and substituting them into the SV definition (Equation D.36, where $k = 2/3$ to achieve magnitude invariance) yields Equation (D.37) which simplifies to Equation (D.38).

324

$$\begin{cases} x_A = & X_1 \cos(\omega t) & +X_3 \cos(3\omega t) & +X_5 \cos(5\omega t) \\ x_B = & X_1 \cos(\omega t - \gamma) & +X_3 \cos(3\omega t) & +X_5 \cos(5\omega t + \gamma) \\ x_C = & X_1 \cos(\omega t + \gamma) & +X_3 \cos(3\omega t) & +X_5 \cos(5\omega t - \gamma) \end{cases} \tag{D.34}$$

$$\begin{cases} x_A = \begin{bmatrix} \dfrac{1}{2}X_1 e^{j\omega t} + \dfrac{1}{2}X_1 e^{-j\omega t} + \dfrac{1}{2}X_3 e^{j3\omega t} + \dfrac{1}{2}X_3 e^{-j3\omega t} \\ +\dfrac{1}{2}X_5 e^{j5\omega t} + \dfrac{1}{2}X_5 e^{-j5\omega t} \end{bmatrix} \\[2em] x_B = \begin{bmatrix} \dfrac{1}{2}X_1 e^{j(\omega t - \gamma)} + \dfrac{1}{2}X_1 e^{-j(\omega t - \gamma)} + \dfrac{1}{2}X_3 e^{j(3\omega t)} + \dfrac{1}{2}X_3 e^{-j(3\omega t)} \\ +\dfrac{1}{2}X_5 e^{j(5\omega t + \gamma)} + \dfrac{1}{2}X_5 e^{-j(5\omega t + \gamma)} \end{bmatrix} \\[2em] x_C = \begin{bmatrix} \dfrac{1}{2}X_1 e^{j(\omega t + \gamma)} + \dfrac{1}{2}X_1 e^{-j(\omega t + \gamma)} + \dfrac{1}{2}X_3 e^{j(3\omega t)} + \dfrac{1}{2}X_3 e^{-j(3\omega t)} \\ +\dfrac{1}{2}X_5 e^{j(5\omega t - \gamma)} + \dfrac{1}{2}X_5 e^{-j(5\omega t - \gamma)} \end{bmatrix} \end{cases} \tag{D.35}$$

$$\vec{x} = \frac{2}{3}\left[x_A \cdot 1 + x_B \cdot e^{j\gamma} + x_C \cdot e^{-j\gamma} \right] \tag{D.36}$$

$$\vec{x} = \frac{1}{3}\begin{bmatrix} X_1 e^{j\omega t} + X_1 e^{-j\omega t} & + X_3 e^{j3\omega t} & + X_3 e^{-j3\omega t} & + X_5 e^{j5\omega t} & + X_5 e^{-j5\omega t} \\ +X_1 e^{j\omega t} + X_1 e^{-j(\omega t + \gamma)} & + X_3 e^{j(3\omega t + \gamma)} & + X_3 e^{-j(3\omega t - \gamma)} & + X_5 e^{j(5\omega t - \gamma)} & + X_5 e^{-j5\omega t} \\ +\underbrace{X_1 e^{j\omega t}}_{PS} + \underbrace{X_1 e^{-j(\omega t - \gamma)}}_{0} & + \underbrace{X_3 e^{j(3\omega t - \gamma)}}_{ZS=0} & + \underbrace{X_3 e^{-j(3\omega t + \gamma)}}_{0} & + \underbrace{X_5 e^{j(5\omega t + \gamma)}}_{0} & + \underbrace{X_5 e^{-j5\omega t}}_{NS} \end{bmatrix}$$
$$\tag{D.37}$$

$$\vec{x} = X_1 e^{j\omega t} + X_5 e^{-j5\omega t} \tag{D.38}$$

Equation (D.37) has six vertical columns indicated by brackets. The terms in the three columns marked "0" are often encountered when SV equations are simplified by hand and they sum to zero. For each such column there is normally a corresponding column (marked PS, ZS, and NS) that does *not* sum to zero. However in this case it is clear that the ZS column *does* sum to zero. Equation (D.38) demonstrates that the SV contains the PS and NS components present in the phase variables but does *not* contain the ZS component. Given that the SV is of dimension two it simply *cannot* contain all of the information in $\mathbf{x}_{abc}$ (which is of dimension three) unless $\Sigma = 0$ is true (in which case $\mathbf{x}_{abc}$ can always be rewritten as dimension two). This does not mean that some quantity $\mathbf{q}$ of dimension two can never contain common-mode components; the basis of $\mathbf{q}$ could be defined such that it does. What is instead true is that the MSC and SV transforms *are*

indeed __defined__ such that common-mode components are simply not contained in the PS & NS or α & β components; there is obviously good reason for defining the transforms this way. There is a very meaningful graphical understanding of the ZS component that the interested reader can pursue [106], [105], [62, p.83], [70, p.25] but for brevity it is not presented here. However, a simplified and insightful result is shown: if the **0** axis is taken to be orthogonal to the **α** and **β** axes, we can draw a three-dimensional vector (although this does not fit our technical definition of an SV since it only has two components). From the inverter chapter, the eight base SVs of a 180° inverter were projected onto the αβ plane as shown in Figure D.10. The magnitude of each SV is $k \cdot 2 \cdot V_{DC}$, which for $k = 2/3$ is equal to $\left| \vec{S} \right| = \dfrac{4}{3} V_{DC}$.
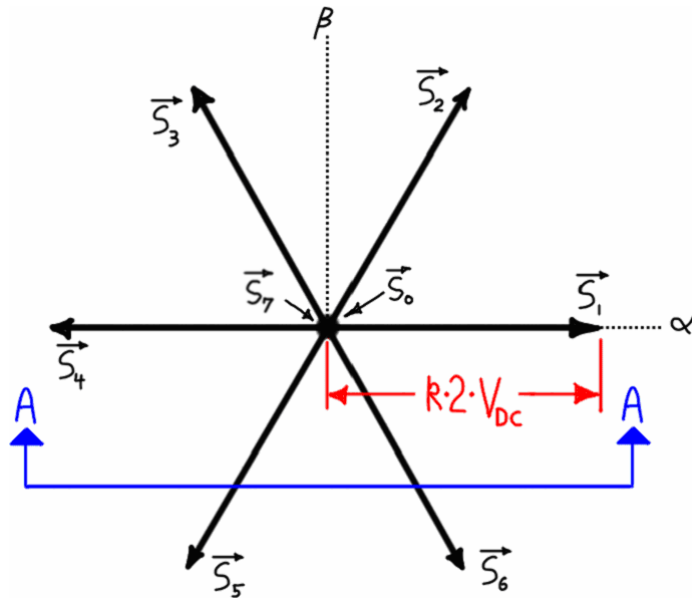

Figure D.10 – Projection of base SVs of 180° inverter onto AB plane.

If the thee-dimensional vectors were plotted they would be as shown in Figure D.11 ($k = 2/3$), where the cross section is that shown in Figure D.10. This shows a graphical interpretation of the ZS component of the output voltage. (Be aware that in Figure D.11, only $\overrightarrow{S_0}$, $\overrightarrow{S_1}$, $\overrightarrow{S_4}$, and $\overrightarrow{S_7}$ are in the **αγ** plane; $\overrightarrow{S_2}$ and $\overrightarrow{S_3}$ are behind the plane in the **+β** direction. The cross-section should show a truncated portion of $\overrightarrow{S_5}$ and $\overrightarrow{S_6}$ but these are omitted for clarity.)
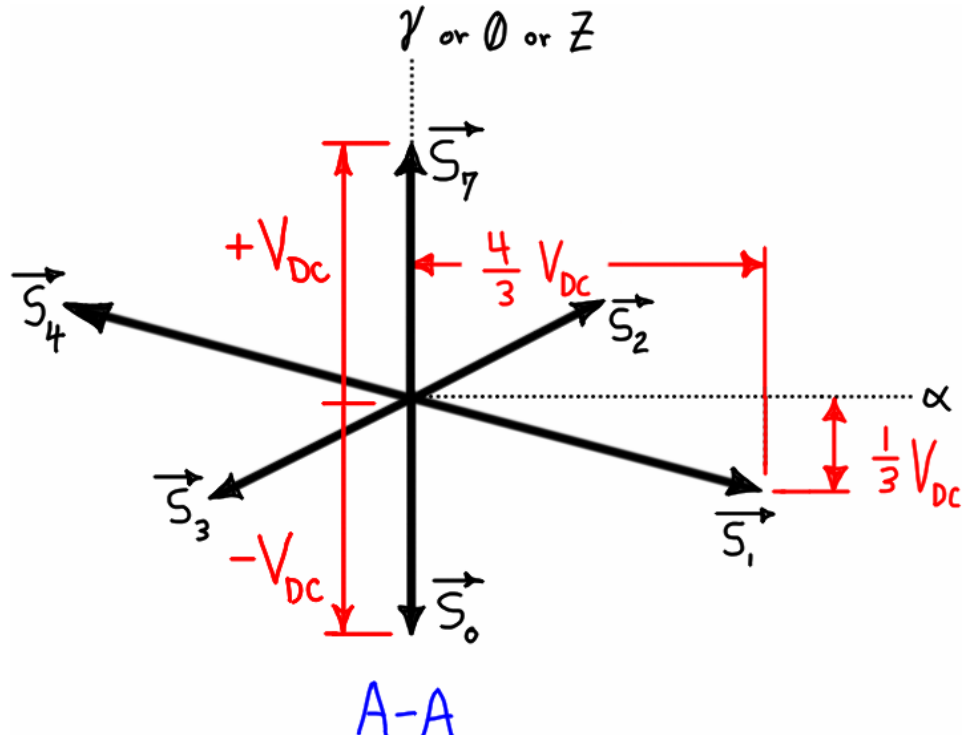
Figure D.11 – 3-D base vectors of 180° inverter.

In inverter state S_0 all legs are low and the neutral is at $-V_{DC}$; in S_7 all legs are high and the neutral is at $+V_{DC}$. In S_1, A is high, B and C are low, and the neutral voltage is therefore $-(1/3)V_{DC}$. Since the pole voltage of phase-A is $1.0V_{DC}$, the line-neutral voltage is $1-(-1/3)V_{DC} = (4/3)V_{DC}$. Figure D.10 had already shown that fact but as discussed in the inverter chapter, the SV transform of either the pole or phase voltage gives the same result (namely, Figure D.10). Figure D.11 shows graphically what was explained in the inverter chapter—that the SV (Figure D.10) could not capture the ZS component (which is shown in Figure D.11). It is known that in the active states the neutral voltage alternates between $\mp(1/3)V_{DC}$. This means the 3-D vector would alternately be $(1/3)V_{DC}$ below and above the αβ plane; this is evident in Figure D.11. Visualizing the ZS component in this way proves that the projection of the ABC phase variables onto the αβ plane is unique *only* when no ZS component is present. Likewise it clearly shows that unless the αβ0 transform is used, the ZS component will be lost when transforming back.

Finally, a brief warning will be issued. It has been shown that the αβ0 transform is simply the Clarke transform (Equation D.26), augmented with terms for the ZS component. If we are working with a system in which no ZS component can possibly be present (such as current in an

isolated-neutral wye load) there is no reason to use the full αβ0 transform and we can delete the ZS row without consequence. In that case (where we know that $\Sigma = 0$, which means ZS components are <u>not present</u>) we can then make the simplifications in Equation (D.27) or (D.28). But, if we have a system where ZS components <u>are or could be present</u>, and we choose to ignore that ZS component (that is, we are only interested in the αβ components), we may use Equation (D.26), but we <u>may not</u> use Equation (D.27) or (D.28). The reason is that ($\Sigma = 0$) was assumed in deriving those forms, thus they are not valid if $\Sigma \neq 0$. As an example, the voltages in state S_1 are given by Equation (D.39).

$$\begin{cases} x_{AM} = +V_{DC} \\ x_{BM} = -V_{DC} \\ x_{CM} = -V_{DC} \end{cases} \tag{D.39}$$

Using the αβ0 transform (Equation D.32) (where $k = 2/3$), they are equivalent to Equation (D.40).

$$\begin{cases} x_\alpha = (4/3)V_{DC} \\ x_\beta = 0 \\ x_0 = -(1/3)V_{DC} \end{cases} \tag{D.40}$$

Using the Clarke transform (Equation D.26) with $k = 2/3$, the αβ components are given by Equation (D.41), which of course match the αβ components in Equation (D.40).

$$\begin{cases} x_\alpha = (4/3)V_{DC} \\ x_\beta = 0 \end{cases} \tag{D.41}$$

Now using Equation (D.27) with $k = 2/3$, the αβ components are given by Equation (D.42), which is clearly incorrect.

$$\begin{cases} x_\alpha = V_{DC} \\ x_\beta = 0 \end{cases} \tag{D.42}$$

The set in Equation (D.39) does not satisfy $\Sigma = 0$ (that is, it is known to contain a ZS component). This does not mean, however, that the α- and β- components have somehow been encoded the ZS component. It means that Equation (D.27) relies on $\Sigma = 0$ to account for the contributions of phase-B and phase-C in determining the α- component, and since that does not hold, it cannot properly reconstruct them.

The practical consequence is that for the motor control aspects (current measurement, space vector regulation, and SVM inverter) the ZS component cannot exist, it is never mentioned, and

the Clarke transform is used. However, the SVM inverter physically produces voltages with a ZS component so to understand its operation the αβ0 transform is required. Still, the detailed aspects of the SVM inverter can be ignored from a high-level perspective if one does not care *how* the inverter works or *why* the output waveforms look as they do.

Inverse Clarke Transform

The inverse of the αβ0 transform is simply given by the matrix inverse, which is known to exist because the transform matrix is not singular (it takes three linearly dependent variables to three linearly dependent variables). But the inverse of the Clarke transform does not exist because it is not square. The simplest way to obtain it is to substitute in a symbolic variable in the place of the ZS coefficients in the matrix of the αβ0 transform, as in Equation (D.43).

$$\begin{bmatrix} x_\alpha \\ x_\beta \\ x_0 \end{bmatrix} = \begin{bmatrix} 1 & -1/2 & -1/2 \\ 0 & \sqrt{3}/2 & -\sqrt{3}/2 \\ c & c & c \end{bmatrix} \begin{bmatrix} x_A \\ x_B \\ x_C \end{bmatrix} \tag{D.43}$$

Upon taking its inverse (Equation D.44) it is clear that the ZS coefficients only multiple the x_0 and since the Clarke transform does not use x_0, the column can be deleted.

$$\begin{bmatrix} x_A \\ x_B \\ x_C \end{bmatrix} = \frac{2}{3} \begin{bmatrix} 1 & 0 & 1/2c \\ -1/2 & \sqrt{3}/2 & 1/2c \\ -1/2 & -\sqrt{3}/2 & 1/2c \end{bmatrix} \begin{bmatrix} x_\alpha \\ x_\beta \\ x_0 \end{bmatrix} \tag{D.44}$$

Once again, the matrix in Equation (D.44) agrees with the understanding presented in the discussion of Figure D.11: the phase-variable components consist of the αβ projection (given by the first two columns of the matrix in Equation D.44) *plus* the ZS component. Of course, the same ZS component x_0 is added to each phase.

Phase Interference Matrix

It is clear that there is a relationship between the terminal voltages and the neutral voltage of an impedance load. Thus, a change in one terminal's voltage will affect the neutral voltage, which will change the other phases' line-neutral voltages. This effect is known as "phase interference" [62, p.93] and it does not seem to be treated well in the literature. In this report, the effect is represented using the matrix **Q**. The derivation follows simply from the results already presented and the final result is given by Equation (D.45).

$$\begin{cases} v_{AM} = v_{AN} + v_{NM} \\ v_{BM} = v_{BN} + v_{NM} \\ v_{CM} = v_{CN} + v_{NM} \end{cases}$$

$$v_{NM} = \frac{1}{3}\left(v_{AM} + v_{BM} + v_{CM}\right) \implies 3v_{NM} = v_{AM} + v_{BM} + v_{CM}$$

$$\begin{cases} v_{AM} = 3v_{NM} - v_{BM} - v_{CM} \\ v_{BM} = 3v_{NM} - v_{AM} - v_{CM} \\ v_{CM} = 3v_{NM} - v_{AM} - v_{BM} \end{cases}$$

$$\begin{cases} v_{AN} = v_{AM} - v_{NM} \\ v_{BN} = v_{BM} - v_{NM} \\ v_{CN} = v_{CM} - v_{NM} \end{cases}$$

$$\begin{cases} v_{AN} = \dfrac{2}{3}\left[v_{AM} - \dfrac{1}{2}v_{BM} - \dfrac{1}{2}v_{CM} \right] \\[2mm] v_{BN} = \dfrac{2}{3}\left[-\dfrac{1}{2}v_{AM} + v_{BM} - \dfrac{1}{2}v_{CM} \right] \\[2mm] v_{CN} = \dfrac{2}{3}\left[-\dfrac{1}{2}v_{AM} - \dfrac{1}{2}v_{BM} + v_{CM} \right] \end{cases}$$

$$\begin{bmatrix} v_{AN} \\ v_{BN} \\ v_{CN} \end{bmatrix} = \frac{1}{3}\begin{bmatrix} 2 & -1 & -1 \\ -1 & 2 & -1 \\ -1 & -1 & 2 \end{bmatrix}\begin{bmatrix} v_{AM} \\ v_{BM} \\ v_{CM} \end{bmatrix} \iff v_{abcN} = \mathbf{Q}v_{abcM} \tag{D.45}$$

When there is no ZS component present, $v_{NM} = 0$ and it can be verified that the phase voltage vector in Equation (D.45) is the same as the pole voltage vector. An interesting result is that the phase interference matrix relates the Clarke and αβ0 transforms as shown by Equation (D.46).

$$\mathbf{C}_0 \cdot \mathbf{Q} = \mathbf{C}$$

$$\begin{bmatrix} 1 & -1/2 & -1/2 \\ 0 & \sqrt{3}/2 & -\sqrt{3}/2 \\ 1/2 & 1/2 & 1/2 \end{bmatrix} \cdot \frac{1}{3}\begin{bmatrix} 2 & -1 & -1 \\ -1 & 2 & -1 \\ -1 & -1 & 2 \end{bmatrix} = \begin{bmatrix} 1 & -1/2 & -1/2 \\ 0 & \sqrt{3}/2 & -\sqrt{3}/2 \\ 0 & 0 & 0 \end{bmatrix} \tag{D.46}$$

As a consequence, when the phase-variable model is reduced to the stationary reference frame, the αβ0 transform can be used on the pole voltages, or, using the results of Equation (D.46), the Clarke transform can be used on the phase voltages.

Appendix E - Park Transforms

This appendix discusses a few forms of the Park transform and the issues related to their axis and angle conventions.

In Chapter 3 and Appendix D it was explained that the Clarke transform defined in this report (and found in the popular literature) is not the original Clarke transform. The original more closely resembles the αβ0 transform which contained an extra row in the matrix to give the zero-sequence component. Similarly, the Park transform can be defined to transform the zero-sequence component as well. This zero-sequence form is shown in Equation (E.1).

$$\begin{bmatrix} x_d \\ x_q \\ x_0 \end{bmatrix} = \begin{bmatrix} \cos(\theta_r) & \sin(\theta_r) & 0 \\ -\sin(\theta_r) & \cos(\theta_r) & 0 \\ 0 & 0 & 1 \end{bmatrix} \begin{bmatrix} x_\alpha \\ x_\beta \\ x_0 \end{bmatrix} \tag{E.1}$$

By definition, the ZS component remains unchanged in the transformation.

Unlike the Clarke and αβ0 transforms, there is not only a ZS and non-ZS version, but also a completely different version of the Park transform, which is a combination of the Park and αβ0 transforms. This is the "original" Park transform is the one used by Park and those before him (although like the Clarke transform, the scaling and ordering of variables may be different) [22], [30], [32], [34], [87]. It is obtained by multiplying the ZS-Park and αβ0 transforms. After simplification the result is given by Equation (E.2).

$$\begin{bmatrix} x_d \\ x_q \\ x_0 \end{bmatrix} = \begin{bmatrix} \cos(\theta_r) & \sin(\theta_r) & 0 \\ -\sin(\theta_r) & \cos(\theta_r) & 0 \\ 0 & 0 & 1 \end{bmatrix} \cdot k \begin{bmatrix} 1 & -1/2 & -1/2 \\ 0 & \sqrt{3}/2 & -\sqrt{3}/2 \\ 1/2 & 1/2 & 1/2 \end{bmatrix} \cdot \begin{bmatrix} x_\alpha \\ x_\beta \\ x_0 \end{bmatrix}$$

$$\begin{bmatrix} x_d \\ x_q \\ x_0 \end{bmatrix} = k \begin{bmatrix} \cos(\theta_r) & \cos(\theta_r - \gamma) & \cos(\theta_r + \gamma) \\ -\sin(\theta_r) & -\sin(\theta_r - \gamma) & -\sin(\theta_r + \gamma) \\ 1/2 & 1/2 & 1/2 \end{bmatrix} \cdot \begin{bmatrix} x_\alpha \\ x_\beta \\ x_0 \end{bmatrix} \tag{E.2}$$

An easier derivation that avoids the algebraic simplification can be had by using SV notation. When the real and imaginary parts of Equation (E.3) are taken and put into matrix form as usual, the result is the same as Equation (E.2) (since the SV does not transform the ZS component it must be manually added, as in the case of the αβ0 transform above.

$$k\left(x_A + x_B \cdot e^{j\gamma} + x_C \cdot e^{-j\gamma}\right) \cdot e^{-j\theta_r}$$

$$k\left(x_A \cdot e^{-j\theta_r} + x_B \cdot e^{-j(\theta_r - \gamma)} + x_C \cdot e^{-j(\theta_r + \gamma)}\right) \qquad\qquad \text{(E.3)}$$

Like the Clarke transform, the Park transform goes by many names, such as the *dq0 transform*, *Blondel transform*, and *commutator transform*. The names most generally refer to Equation (E.2), not Equation (E.1), but this is not always true. In Appendix D, when the Clarke transform was discussed it was mentioned there are two primary axis conventions, and that the vector is commonly ordered as either αβ0 or 0αβ. Unfortunately, with the Park transform comes a large number of choices for conventions, and many are in use. Like the Clarke transform, one axis can be defined in the negative direction, and the vector can be arranged as dq0 or 0dq. However, if the axes directions for the αβ and *dq* axes are different this can lead to arrangements, such as qd0 or 0qd. Finally, the rotor position may be measured to the **d** or **q** axis (these are the two different "correct" absolute rotor positions mentioned in Footnote (8) in Chapter 2). Finally, the rotor flux may be defined to be coincident with either the **d** or **q** axis. Of course, all of these varieties have different orderings of the elements of the transform matrix and the convention choice affects many other aspects. There is again the issue of scaling constants, both for the *dq* components and the ZS component. Since only the 2x2 Park transform is used in this report it is not necessary to elaborate further, however some common variations are shown in Figure E.1 to illustrate the issue. In most varieties the **q** axis leads the **d** axis in the direction of rotation, but this is not always so.
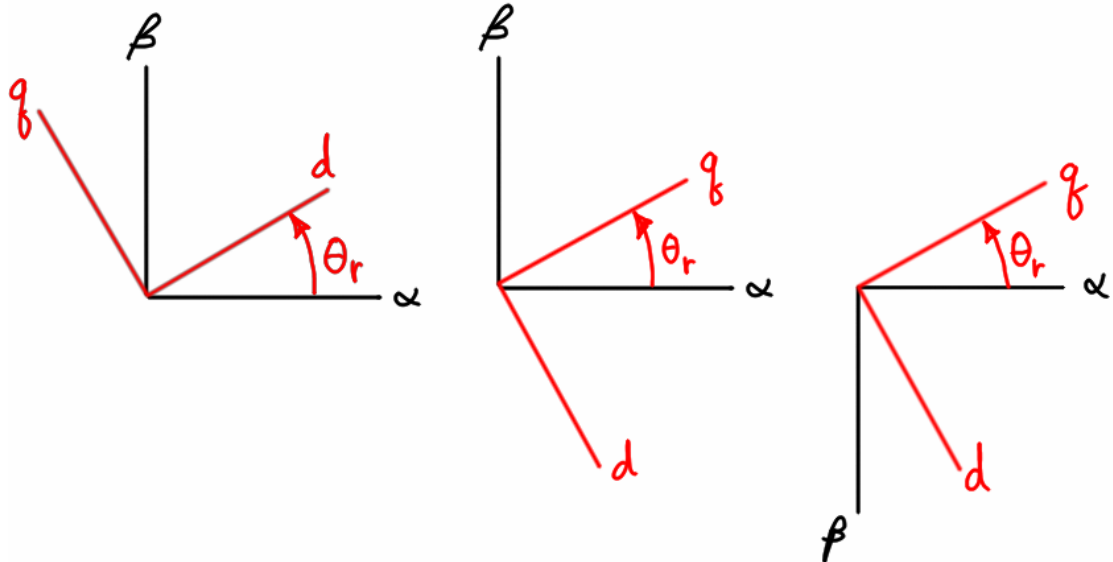

Figure E.1 – Some common axes and rotor angle conventions.

Appendix F - Useful Mathematical Results

This appendix lists some useful mathematical identities and provides a table of the Fourier series coefficients for some waveforms commonly encountered when working with brushless permanent magnet motors.

$$\text{Re}[w \cdot z] = \text{Re}[w] \cdot \text{Re}[z] - \text{Im}[w] \cdot \text{Im}[z]$$

$$(w \cdot z)^* = w^* \cdot z^*$$

$$\text{Re}[z] = \frac{1}{2}\text{Re}[z + z^*] \quad \therefore \quad \cos(\theta) = \frac{1}{2}\left[e^{j\theta} + e^{-j\theta}\right]$$

$$\text{Im}[z] = \frac{1}{j2}\text{Im}[z - z^*] \quad \therefore \quad \sin(\theta) = \frac{1}{j2}\left[e^{j\theta} - e^{-j\theta}\right]$$

$$\cos(A)\cos(B) = \frac{1}{2}\left[\cos(A - B) + \cos(A + B)\right]$$

$$\sin(A)\cos(B) = \frac{1}{2}\left[\cos(A + B) + \cos(A - B)\right]$$

$$\sin\left(\frac{\pi}{2} - \theta\right) = \cos(\theta)$$

$$\cos\left(\frac{\pi}{2} - \theta\right) = \sin(\theta)$$

$$\sin\left(\theta - \frac{\pi}{2}\right) = -\cos(\theta)$$

$$\cos\left(\theta + \frac{\pi}{2}\right) = -\sin(\theta)$$

$$\sin\left(\theta + \frac{\pi}{2}\right) = \cos(\theta)$$

$$\cos\left(\theta - \frac{\pi}{2}\right) = \sin(\theta)$$

As discussed in Appendix D, only odd harmonics are considered and the waveforms may be represented using only cosine terms. Each harmonic is represented in the general form

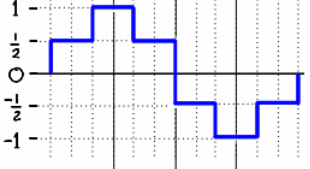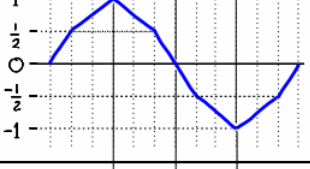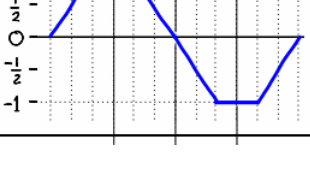$$x_n(t) = X_n \cos(n \cdot \omega t); \quad n = 1, 3, 5, 7, 9, \cdots \quad .$$

Therefore a waveform is represented by the series

$$x(t) = X_1 \cos(\omega t) + X_3 \cos(3\omega t) + X_5 \cos(5\omega t) + \cdots \quad .$$

To ease comparison, a multiplying factor M is introduced to allow the amplitude of the fundamental component to be set to unity for each waveform ($A_1 = 1.0$). The waveform is then represented by the series

$$x(t) = M\left[A_1 \cos(\omega t) + A_3 \cos(3\omega t) + A_5 \cos(5\omega t) + \cdots\right] \quad .$$

The multiplying factor M and the amplitudes A_n are given in the following table. M is given in rational form and to four decimal places. Amplitudes of zero are left blank to emphasize the pattern for each waveform and the similarity between waveforms.

		Sequence: +	0	−	+	0	−	+
Waveform	30° multiplier	fund.	3rd	5th	7th	9th	11th	13th
180° Square	$\dfrac{4}{\pi}$ 1.2732	1	$\dfrac{1}{3}$	$\dfrac{1}{5}$	$\dfrac{1}{7}$	$\dfrac{1}{9}$	$\dfrac{1}{11}$	$\dfrac{1}{13}$
120° rectangle	$\dfrac{2\sqrt{3}}{\pi}$ 1.1027	1		$\dfrac{-1}{5}$	$\dfrac{-1}{7}$		$\dfrac{1}{11}$	$\dfrac{1}{13}$
180° six-step	$\dfrac{3}{\pi}$ 0.9549	1		$\dfrac{1}{5}$	$\dfrac{1}{7}$		$\dfrac{1}{11}$	$\dfrac{1}{13}$
"gambrel"	$\dfrac{9}{\pi^2}$ 0.9119	1		$\dfrac{1}{5^2}$	$\dfrac{-1}{7^2}$		$\dfrac{1}{11^2}$	$\dfrac{-1}{13^2}$
triangle	$\dfrac{8}{\pi^2}$ 0.8106	1	$\dfrac{-1}{3^2}$	$\dfrac{1}{5^2}$	$\dfrac{-1}{7^2}$	$\dfrac{1}{9^2}$	$\dfrac{-1}{11^2}$	$\dfrac{1}{13^2}$
trapezoid 120° flat-top	$\dfrac{12}{\pi^2}$ 1.2159	1	$\dfrac{1}{3^2}$	$\dfrac{1}{5^2}$	$\dfrac{-1}{7^2}$	$\dfrac{1}{9^2}$	$\dfrac{-1}{11^2}$	$\dfrac{1}{13^2}$
trapezoid 60° flat-top	$\dfrac{6\sqrt{3}}{\pi^2}$ 1.0530	1		$\dfrac{-1}{5^2}$	$\dfrac{1}{7^2}$		$\dfrac{-1}{11^2}$	$\dfrac{1}{13^2}$